

**The Potential of *in vitro* Pharmacokinetic Profiling  
to Predict Oral Bioavailability of  
Carbohydrate Mimetics and Cyclic Hexapeptides**

**Inauguraldissertation**

zur

Erlangung der Würde eines Doktors der Philosophie

vorgelegt der

Philosophisch-Naturwissenschaftlichen Fakultät

der Universität Basel

von

**Jacqueline Bezençon**

aus Goumoëns, VD, Schweiz

Basel, 2017

Genehmigt von der Philosophisch-Naturwissenschaftlichen Fakultät

auf Antrag von

Prof. Dr. Beat Ernst, Institut für Molekulare Pharmazie, Universität Basel

Prof. Dr. med. Jürgen Drewe, Max Zeller Söhne AG, Romanshorn

Basel, den 13. Oktober 2015

Prof. Dr. Jörg Schibler  
Dekan



*“Tell me and I’ll forget.  
Show me and I might remember.  
Involve me and I will understand.”*

Benjamin Franklin



---

## Acknowledgments

---

This thesis would not have been possible without the support and help of many people to whom I am sincerely grateful.

First, I would like to thank Prof. Dr. Beat Ernst for giving me the opportunity to work in his group. I appreciate his work, his knowledge, and I am very grateful that he shared his experiences with me. I am very thankful that he gave me the freedom to explore my own ideas throughout my work, to collaborate and meet with other scientists, and for sharing a passion for Swedish Daim chocolate.

I would like to thank Prof. Dr. Jürgen Drewe for being my co-referee in this thesis-committee and for his supporting words.

A special thank you goes to Prof. Henriette Meyer zu Schwabedissen for giving me the opportunity to gain insight into the transporter systems, and for allowing me to work in her lab at the University of Basel, where I was introduced to the transport experiments. I am very thankful for her ideas, the discussions we had, and for her supporting words during the last period of my Ph.D.

Furthermore, I would like to thank Prof. Dr. Horst Kessler for giving me the opportunity to work with him on the cyclic hexapeptides project.

Several people from the laboratory deserve special thanks: I am particularly grateful to Dr. Matthias Wittwer for introducing me into the fantastic world of *in vitro* pharmacokinetics. Dr. Simon Kleeb for his supporting words and his help with the LC-MS: whenever I had a question, he was there, and many thanks also for being a good and patient friend. In addition, I would like to thank Philipp Dätwyler for his support on the pharmacokinetic team and for sharing a passion for music.

## Acknowledgments

---

Furthermore, I would like to express my gratitude to Bea Wagner, Dr. Oliver Schwardt, Dr. Tobias Klein, Dr. Xiaohua Jiang, Dr. Katharina Mayer, Dr. Lijuan Pang, Dr. Wojciech Schönemann, Margrit Hartmann, Philip Dätwyler, Priska Frei, Marcel Lindegger, Sophie Boschung, Hülya Süyün, Martina Haug, and Janno Herold for synthesizing all the FimH antagonists – an essential prerequisite for all my analysis during my thesis.

A special thank you goes to Bea, Deniz, Adam, Oya, Rachel, Anja, Janine, and Marleen for the motivating chats and exchanges not only about work, but also about life, which helped me a lot to generate new ideas. Moreover, I would like to thank all of the IMP members for making the work environment comfortable.

I would like to thank Gabi Lichtenhahn and Claudia Huber for their support with applications, contracts, and other administrative work. I would also like to thank Marina Kuhn and Roger Sauder for their great support with ordering and defect devices.

Many thanks goes to the master students Kaja Maier, Stefania Cigardi, Karen Bamberger, Timothy Sprenger, and the internship student Aleksandra Djekic, for their support and patience during their work and in contributing generating all of the results that I have today.

Many thanks go to Dr. Roland Preston, Dr. Rachel Hevey, Dr. Brigitte Fiege, Dr. Katharina Mayer, and Dr. Remo Schmidt for proofreading language.

In particular, I would like to thank the group at Roche (especially Dr. Manfred Kansy, Björn Wagner, and Severin Wendelspiess) for sharing their knowledge and expertise in their field. I am thankful to Georgius Stikas from Agilent Technologies AG, who has helped me with all of the LC-MS troubles we have had, and who has made me familiar with the technical challenges of the LC-MS. Many thanks go to Dr. Brian Cutting for his help with the NMR.

Finally, I would like to thank my family and best friends: my mom Ruth for being my Mom; Michel for being my Dad; my brother Nicolas for making me smile again and again in hard times; my boyfriend Benz for all of the love, happiness, and joy he has brought into my life, and for his help and patience with drawing the images in the introduction part of my thesis; my best friends Katharina, Sibylle, and Maïssa for believing in me and my goals, for their encouraging words, and their constant help and support not only during my Ph.D. thesis.

Thank you! Merci viu mau! Vielen Dank! Grazie mille! Muchas gracias! Merci beaucoup!

---

# Contents

---

Preface .....	9
List of Abbreviations.....	11
Abstract and Aim of This Thesis .....	15
<b>1 Introduction to Urinary Tract Infection .....</b>	<b>17</b>
1.1 Pathogens and Infection Cycle.....	18
1.2 Type I Pili and the Bacterial Lectin FimH.....	19
1.3 Prevention and Therapy of Urinary Tract Infection .....	20
1.3.1 FimH Antagonists.....	21
1.4 References .....	23
<b>2 Introduction to Oral Bioavailability: How to Overcome Multiple Barriers?.....</b>	<b>27</b>
2.1 Intestinal Tract – Oral Absorption.....	29
2.1.1 Stability.....	30
2.1.2 Solubility .....	31
2.1.3 Passive and Active Permeability .....	34
2.2 Blood and Tissue Binding – Distribution .....	40
2.2.1 Plasma Protein Binding.....	40
2.3 Liver Passage – Metabolism.....	41
2.3.1 Metabolic Stability.....	41
2.3.2 Enterohepatic Circulation .....	42
2.4 Kidney – Renal Elimination.....	44
2.4.1 Reabsorption and Secretion .....	45
2.5 References .....	46

<b>3</b>	<b>Materials and Methods – PADMET-Profiling</b> .....	53
3.1	Paper 1 – A Method in Detail:	
	pK <sub>a</sub> Determination by <sup>1</sup> H NMR Spectroscopy – An Old Methodology Revisited .....	57
3.2	Preformulation Studies .....	67
3.3	Carrier-Mediated Transport Studies .....	69
3.4	Cell Toxicity Studies.....	73
3.5	References .....	74
<b>4</b>	<b>Results and Discussion: FimH Antagonists</b> .....	75
4.1	Trends to Predict Potential Oral Bioavailability of FimH Antagonists .....	76
4.2	Improved Permeability of FimH Antagonists .....	87
	4.2.1 Carrier-Mediated Transport Studies with FimH Antagonists.....	87
	4.2.2 Paper 2 – Prodrug Approach:	
	FimH Antagonists for the Oral Treatment of Urinary Tract Infections:	
	From Design and Synthesis to <i>in Vitro</i> and <i>in Vivo</i> Evaluation.....	107
4.3	Improved Solubility of FimH Antagonists.....	123
	4.3.1 Approaches to Improve Solubility of FimH Antagonists .....	123
	4.3.2 Paper 3 – Structural and Solvent Modifications:	
	FimH Antagonists - Bioisosteres to Improve the PK/PD Profile .....	133
	4.3.3 Paper 4 – Structural Modifications:	
	FimH Antagonists: Phosphate Prodrugs Improve Oral Bioavailability .....	153
	4.3.4 Paper 5 – Structural and Solvent Modifications:	
	FimH Antagonists – Solubility vs. Permeability.....	189
4.4	Stability of FimH Antagonists in Gastrointestinal Fluids .....	217
<b>5</b>	<b>Results and Discussion: Cyclic Hexapeptides</b> .....	225
5.1	<i>In Vitro</i> Permeability Evaluation of Cyclic Hexapeptides .....	226
	5.1.1 Paper 6: Enantiomeric Cyclic Peptides with Different Caco-2 Permeability	
	Suggest Carrier-Mediated Transport .....	237
<b>6</b>	<b>Summary and Outlook</b> .....	253

---

## Preface

---

Jacqueline Bezençon performed the work described in this thesis from May 2011 until October 2015 at the Institute of Molecular Pharmacy, University of Basel, under the supervision of Prof. Dr. Beat Ernst. In addition, published work is included in this thesis, which contributes to the FimH antagonists project and was conducted during her master thesis in 2009 under the supervision of Dr. Matthias Wittwer.

Parts of the thesis have been published in peer-reviewed journals and are included in the thesis, termed as *Papers*. These *Papers* are included in the respective subchapter, where the specific contribution of Jacqueline Bezençon is mentioned.

References are listed at the end of each chapter (Introduction, Materials and Methods) and the end of each subchapter (Results and Discussion).

### Article Published in Peer-Reviewed Journals:

S. Kleeb, X. Jiang, P. Frei, A. Sigl, **J. Bezençon**, K. Bamberger, O. Schwaradt, B. Ernst, FimH Antagonists: Phosphate Prodrugs Improve Oral Bioavailability. *J. Med. Chem.* **2016**, *59*, 3163-3182.

U. K. Marelli, **J. Bezençon**, E. Puig, B. Ernst, H. Kessler, Enantiomeric cyclic peptides with different Caco-2 permeability suggest carrier-mediated transport. *Chem. Eur. J.* **2015**, *21*, 8023-8027.

S. Kleeb, L. Pang, K. Mayer, D. Eris, A. Sigl, R. C. Preston, P. Zhilman, T. Sharpe, R. P. Jakob, D. Abgottspon, A. S. Hutter, M. Scharenberg, X. Jiang, G. Navarra, S. Rabbani, M. Smiesko, N. Lüdin, **J. Bezençon**, O. Schwaradt, T. Maier, B. Ernst, FimH Antagonists: Bioisosteres To Improve the *in Vitro* and *in Vivo* PK/PD Profile. *J. Med. Chem.* **2015**, *58*, 2221-2239.

**J. Bezençon**, M. B. Wittwer, B. Cutting, M. Smiesko, B. Wagner, M. Kansy, B. Ernst, pK<sub>a</sub> determination by <sup>1</sup>H NMR spectroscopy - an old methodology revisited. *J. Pharm. Biomed. Anal.* **2014**, *93*, 147-155.

T. Klein, D. Abgottspon, M. Wittwer, S. Rabbani, J. Herold, X. Jiang, S. Kleeb, C. Luethi, M. Scharenberg, **J. Bezençon**, E. Gubler, L. Pang, M. Smiesko, B. Cutting, O. Schwaradt, B. Ernst, FimH Antagonists for the Oral Treatment of Urinary Tract Infections: From Design and Synthesis to *in Vitro* and *in Vivo* Evaluation. *J. Med. Chem.* **2010**, *53*, 8627-8641.

#### Article Published in Books:

L. Pang, **J. Bezençon**, S. Kleeb, S. Rabbani, A. Sigl, M. Smiesko, C.P. Sager, D. Eris, O. Schwaradt, B. Ernst, FimH Antagonists – Solubility vs. Permeability. *Carbohydrate Chemistry*, **2017**, *42*, 248-273.

#### Poster Presented at Scientific Meetings:

**J. Bezençon**, J. Hussner, B. Ernst, H. Meyer zu Schwabedissen, Identification of FimH Antagonist Interactions with OATP2B1 Transporter:

- Drug Metabolism Gordon Research Conference: *The Precision Medicine Revolution: New Frontiers for Scientists in Drug Metabolism, Transport and Pharmacokinetics*, **2016**, Holderness, NH, USA

**J. Bezençon**, U.K. Marelli, E. Puig, B. Ernst, H. Kessler, Carrier-Mediated Transport of Enantiomeric Cyclic Peptides?:

- BioMedical Transporters: *Membrane Transporters - from Basic Science to Drug Discovery*, **2015**, Lugano, Switzerland

**J. Bezençon**, S. Kleeb, B. Ernst, Treatment of Urinary Tract Infections - Optimized Drug Delivery of FimH Antagonists:

- World Pharma Congress: *Formulation & Drug Delivery*, **2014**, Boston, USA.
- *Swiss Pharma Science Day* **2014**, Bern, Switzerland.

**J. Bezençon**, S. Kleeb, B. Ernst, How to Make Carbohydrate Mimetics Orally Available for the Treatment of Urinary Tract Infections?:

- Drug Absorption, Transport and Delivery (WCDATD): *Responding to Challenging Situations* **2013**, Uppsala, Sweden.

**J. Bezençon**, S. Kleeb, L. Pang, D. Abgottspon, B. Ernst, Development of Orally Available FimH Antagonists for the Treatment of Urinary Tract Infections:

- *Annual Research Meeting of the Department of Pharm. Sci.* **2013**, Basel, Switzerland.

**J. Bezençon**, M. B. Wittwer, S. Kleeb, B. Cutting, B. Ernst, pK<sub>a</sub> determination of polyprotic acids and bases by <sup>1</sup>H-NMR:

- *Swiss Pharma Science Day* **2011**, Bern, Switzerland.
- *fiP world congress: Towards a future vision for complex patients* **2013** Dublin, Ireland.

---

## List of Abbreviations

---

A	atorvastatin
$\alpha$ -AGP	$\alpha_1$ -acid glycoprotein
ABC-transporter	ATP-binding cassette transporter
ALP	alkaline phosphatase
ASBT	apical sodium/bile acid co-transporter
ATP	adenosine 5'-triphosphate
AUC	area under the curve
BCRP	breast cancer resistance protein
BCS	biopharmaceutical classification system
BNPP	bis(4-nitrophenyl) phosphate
BSEP	bile-salt export pump
Caco-2 cells	human colorectal adenocarcinoma cells
CE	carboxylesterase
$CL'_{int}$	intrinsic clearance
CRD	carbohydrate recognition domain
CYP450	cytochrome P450
<i>D</i>	distribution coefficient
Da	dalton
DCM	dichloromethane
DDI	drug-drug interactions
DMEM	Dulbecco's Modified Eagle's Medium

## List of Abbreviations

---

DMSO	dimethyl sulfoxide
DPBS	Dulbecco's Phosphate Buffered Saline
E <sub>1</sub> S	estrone 3-sulfate
E <sub>2</sub> G	estradiol-17 $\beta$ -glucuronide
EDTA	ethylenediaminetetraacetic acid
FaSSGF	fasted state simulated gastric fluids
FaSSIF	fasted state simulated intestinal fluids
FeSSGF	fed state simulated gastric fluids
FeSSIF	fed state simulated intestinal fluids
FBS	fetal bovine serum
FCS	fetal calf serum
FDA	U.S. Food and Drug Administration
GIT	gastro intestinal tract
HEPES	4-(2-hydroxyethyl)-1-piperazineethanesulfonic acid
HLM	human liver microsomes
HP $\beta$ CD	hydroxypropyl- $\beta$ -cyclodextrin
HSA	human serum albumin
IBCs	intracellular bacterial communities
IC <sub>50</sub>	half maximal inhibitory concentration
K <sub>a</sub>	acid dissociation constant
K <sub>m</sub>	michaelis-menten constant
LC-MS	liquid chromatography-mass spectrometry
MATE	multidrug and toxin extrusion protein
MCT	monocarboxylic acid transporter
MDCK cells	Madin Darby Canine Kidney cells
MeCN	acetonitrile
MeOH	methanol
MP	melting point
MRD	multidrug resistance
MRP	multidrug resistance protein
MPP	1-methyl-4-phenylpyridinium
MTT	3-[4,5-dimethylthiazol-2-yl]-2,5-diphenyltetrazolium bromide



MTX	methotrexate
NADPH	nicotinamide adenine dinucleotide phosphate
NMR	nuclear magnetic resonance
NRB	number of rotatable bonds
NTCP	sodium/taurocholate co-transporting peptide
OAT	organic anion transporter
OATP	organic anion transporting polypeptide
OCT	organic cation transporter
OCTN	organic cation/ergothioneine transporter
OD	optical density
OST	heteromeric organic solute transporter
<i>P</i>	partition coefficient
PADMET	physicochemical properties, absorption, distribution, metabolism, excretion, toxicity
PAH	para-aminohippuric acid
$P_{app}$	apparent permeability
PAMPA	parallel artificial membrane permeability assay
$P_e$	effective permeability
PEG	polyethylene glycol
PEPT	peptide transporter
pfu	plaque forming units
PG	propylglycol
P-gp	P-glycoprotein
PLP	permeable lipophilic peptide
PPB	plasma protein binding
PSA	polar surface area
$r^2$	coefficient of determination
SDS	sodium dodecyl sulfate
sGF	simulated gastric fluids
sIF	simulated intestinal fluids
S9 fraction	supernatant obtained from differential centrifugation at 9000g
SGA	spectral gradient analysis

## List of Abbreviations

---

SLC	solute carrier
SPR	structure property relationship
T	testosterone
$t_{1/2}$	half-life
TEER	transepithelial electrical resistance
TRIS	tris(hydroxymethyl)aminomethane
UDP	uridine 5'-diphosphate
UDPGA	uridine 5'-diphosphoglucuronic acid
URAT	urate transporter
UPEC	uropathogenic <i>Escherichia coli</i>
UPIa	uroplakin Ia
UTI	urinary tract infection
UV/Vis spectroscopy	ultraviolet-visible spectroscopy
VHP	Veber-Hirschmann peptide

---

## Abstract and Aim of This Thesis

---

Urinary tract infection (UTI) is one of the most prevalent infectious diseases and is mainly caused by uropathogenic *Escherichia coli* (UPEC). The first step of the infection cycle, the adhesion of UPEC to urothelial cells, is mediated by the lectin FimH, which is located at the tip of bacterial type 1 pili. Its interaction with the mannosylated glycoprotein uroplakin Ia (UPIa) on urothelial cells can be prevented by glycomimetic antagonists. Thus,  $\alpha$ -D-mannopyranosides derivatives with nanomolar affinity offer a potential therapeutic approach for prevention and treatment of UTI.

To achieve oral availability as well as a therapeutic concentration in the bladder over an extended period of time, a number of key issues have to be fulfilled.

- Stability of the antagonist against various gastrointestinal conditions (pH, enzymatic activity) is required.
- Sufficient solubility is a prerequisite for successful absorption.
- To reach circulation, the intestinal mucosa has to be permeated.
- In case of a prodrug approach, hepatic first pass metabolism is requested.
- To reach the therapeutic target in the bladder, renal excretion is required.

These various properties can be predicted based on lipophilicity ( $\log D_{7.4}$ ), stability in different gastrointestinal fluids, kinetic and thermodynamic solubility, metabolic stability (liver microsomes), and permeability (parallel artificial membrane permeability assay and Caco-2 cells assay), methods implemented in the PADMET platform (physicochemical properties, absorption, distribution, metabolism, elimination and toxicity) of our research group.

The aim of this thesis is to develop *in vitro* assays to provide information regarding the factors influencing the pharmacokinetic properties of glycomimetics and to predict their oral bioavailability. For this purpose, we developed our PADMET platform.

The focus was on glycomimetic FimH antagonists and the evaluation of their structural, physicochemical, and biochemical properties. Besides *in vitro* assays to determine their solubility and potential passive permeability, assays predictive for  $pK_a$  (Paper 1, page 57), stability in gastrointestinal fluids, and carrier-mediated permeability were implemented into our PADMET platform.

As a result, low passive membrane permeability constraint oral absorption of mannosidic FimH antagonists with *para*-carboxy-biphenyl aglycone. With ester prodrugs permeability could be improved and the hydrolysis by carboxylesterase released the active principle within minutes (Paper 2, page 107). Unfortunately, the ester prodrugs suffer from low solubility. For early *in vivo* trials, the solubility issue was addressed with phosphate prodrugs (Paper 4, page 153) or with appropriate preformulations using co-solvents, surfactants, and complexing agents (chapter 4.3.1, page 123; Paper 3, page 133; and Paper 5, page 189). In addition, phosphate and ester prodrugs were stable in gastrointestinal fluids, whereas a prodrug with acylation in the C-6 position of the mannose moiety showed instability in intestinal fluids due to the enzyme pancreatin (chapter 4.4, page 217). Furthermore, interactions of FimH antagonists with carrier-mediated transporters were observed and require further investigations (chapter 4.2.1, page 87).

In a collaborative project with the research group of Prof. Horst Kessler (Technical University of Munich, Institute for Advanced Study) the *in vitro* permeability of cyclic hexapeptides was evaluated with  $\log D_{7.4}$ , PAMPA, and Caco-2 cells. The cyclic hexapeptides were synthesized in the research group of Prof. Dr. Horst Kessler and permeability experiments were performed in our laboratory.

As a result, di-*N*-pentyl alkylation of cyclic hexapeptides improved passive permeability (chapter 5.1, page 226). In addition, differential Caco-2 permeability was measured for enantiomers suggesting the involvement of carrier-mediated transporters (Paper 6, page 237).

---

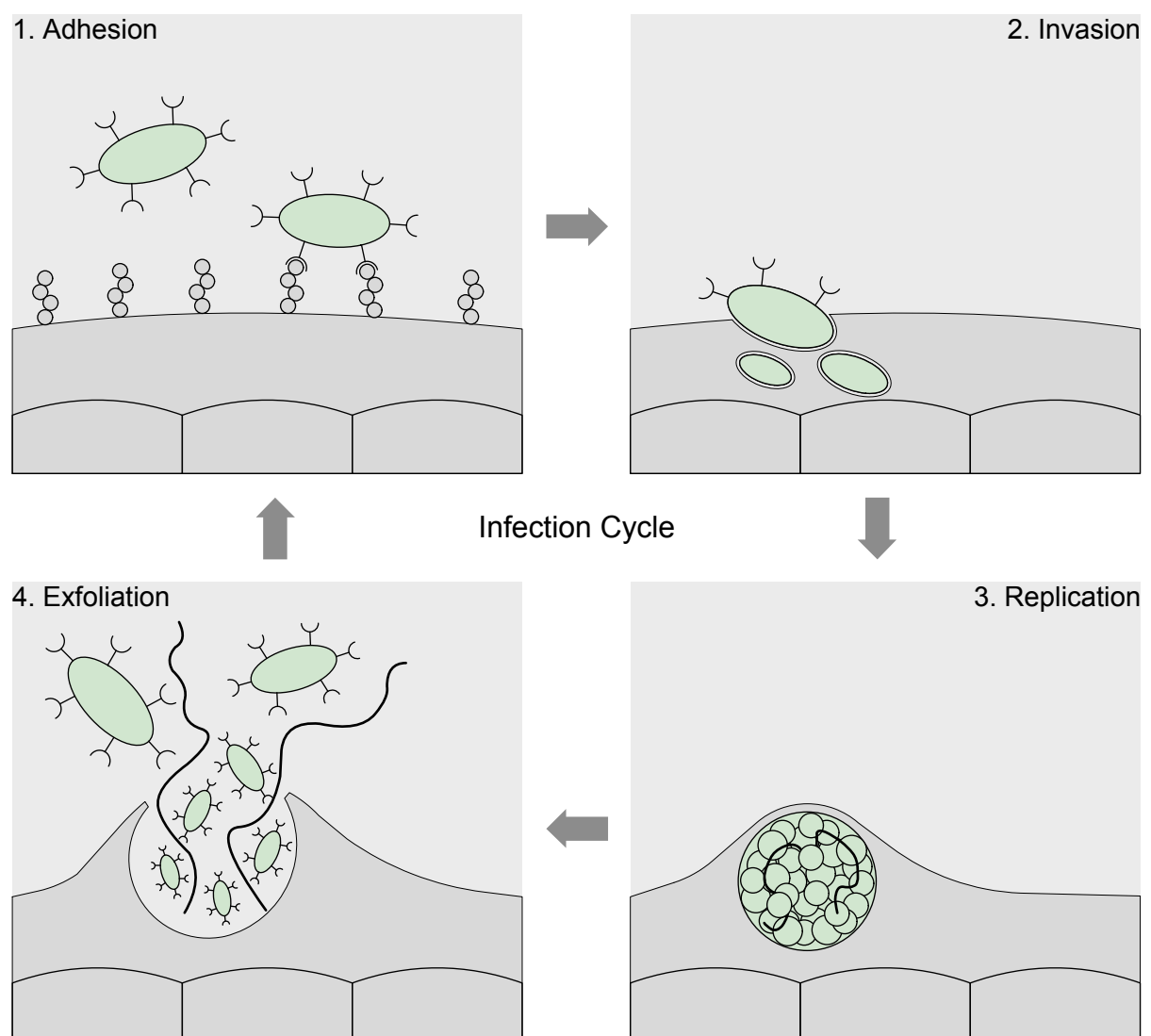
# 1 Introduction to Urinary Tract Infection

---

The first step of urinary tract infections (UTI) is the invasion of bacteria into epithelial cells of the bladder, the urethra, the ureter, or even the kidneys. Each year, millions of people suffer from UTI, which makes this infection one of the most prevalent infectious diseases worldwide and is causing major costs in diagnosis and treatment.<sup>1</sup> With a prevalence of 40-50%, women are at high risk to experience a symptomatic UTI once during their lifetime, whereas 60% thereof will experience a recurrent infection within six months.<sup>2</sup> Anatomical differences between females and males are the reason why women are more prone to UTI. Due to a shorter urethra, the proximity to rectal and vaginal bacteria increase the risk for an infection.<sup>3</sup> Additional risk factors are diabetes,<sup>4,5</sup> spinal cord injuries and/or catheters,<sup>6</sup> pregnancy,<sup>7</sup> age (infants<sup>8</sup> or elderly,<sup>9</sup> or women in menopause<sup>10</sup>), a suppressed immune system,<sup>11</sup> multiple sclerosis,<sup>12</sup> the use of contraception (diaphragm, condoms and/or spermicides), and frequency of sexual intercourse.<sup>13,14</sup> Symptoms of an acute, uncomplicated lower UTI (termed cystitis or bladder infection) are pain during micturition (dysuria), frequent and urgent urination (polyuria), and in some cases blood traces in the urine (hematuria). In addition, there are cases in subpopulation showing asymptomatic bacteriuria<sup>15</sup> (e.g. elderly<sup>16</sup>, infants<sup>17</sup>). If not treated, bacteria can ascend and infect the upper urinary tract, i.e. the ureter and the kidney, which can lead to more complicated infections (pyelonephritis or urosepsis) with the risk of sepsis, kidney failure, and finally death.<sup>18</sup>

## 1.1 Pathogens and Infection Cycle

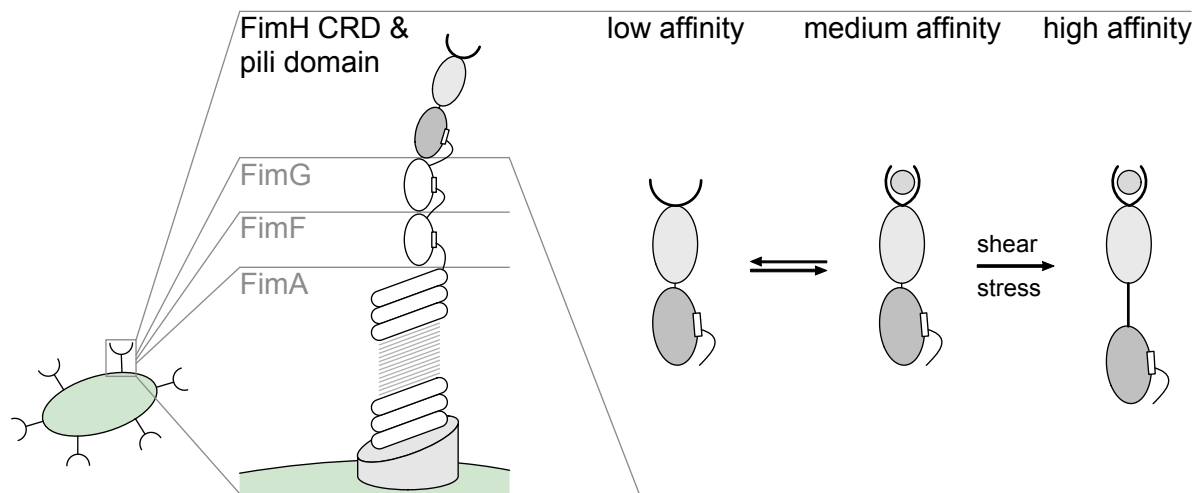
In over 70% of the cases, the cause of uncomplicated UTI is *Escherichia coli* (*E. coli*), in 5-15% *Staphylococcus saprophyticus*, and in less than 10% of the cases *klebsiella* or *proteus* species.<sup>18-21</sup> The infection cycle of uropathogenic *E. coli* (UPEC) as illustrated in Figure 1.1 is highlighted in this introduction. Once UPEC reach the bladder, the infection cycle is initiated by their adhesion to the high-mannose glycoprotein uroplakin Ia (UPIa), located on human urothelial cells. Then, invasion and replication within the urothelial cells take place. In a next step, bacteria form biofilm-like intracellular bacterial communities (IBCs), adopt a filamentous morphology and finally escape and re-enter the infectious cycle by spreading to new cells, resulting in a bladder infection (cystitis).<sup>22,23,24</sup>



**Figure 1.1.** Infection cycle of uropathogenic *E. coli* (UPEC). Figure modified from Ref.<sup>22,24</sup> and pictured by Benz Hubler.

## 1.2 Type I Pili and The Bacterial Lectin FimH

The first and most important step of UTI is mediated by filamentous surface-adhesive organelles of the bacteria, termed type 1 pili or fimbriae (Figure 1.2). These pili are composed of a helical rod formed by 500 to 3000 copies of the main structural subunit FimA and a linear tip fibrillum formed by the subunits FimF, FimG, and FimH at the very tip of the pili.<sup>25-27</sup> FimH subunit is composed of two domains, namely the C-terminal pilin domain and the N-terminal lectin domain. The former connects the FimH subunit with FimG and regulates the switch between the low- and medium-affinity states. When mechanical force (shear stress) is induced, the lectin domain is locked in a high affinity state, which explains the strong adhesion of the bacteria under shear stress (Figure 1.2).<sup>28,29</sup> The lectin domain, also termed the carbohydrate-recognizing domain (CRD), contains the binding site for oligomannosides presented by the urothelial cells (Figure 1.2).<sup>28,30</sup> The binding site consists of a deep, negatively charged pocket. The entrance to the binding site is composed of three hydrophobic amino acids (Tyr48, Tyr137, and Ile52) and is therefore referred as the “tyrosine gate”.<sup>31-33</sup> Terminal mannose residues are present in many mammalian carbohydrate structures and thus the bacteria are capable to bind to a wide range of host cells.<sup>26, 34</sup> The target of the bacteria in the bladder is UPIa, a glycoprotein located on the urothelial cells.<sup>35,36</sup> The adhesion mechanism to the target cells enables bacteria to evade from the natural clearing mechanism, with the result that UPEC cannot be washed out by the bulk flow of urine.<sup>23,37</sup> It is known that UPECs are capable of expressing various adhesins with different binding phenotypes. For initial colonization in the lower urinary tract, UPECs rely on type 1 pili bearing the mannose-specific adhesin FimH, as described above. In ascending infections, however, P-pili, which bind to glycolipids of the globoseries, take over the role as primary adhesive factor. Therefore, P-pili play an important role in the development of pyelonephritis, an infection of the upper urinary tract and the kidneys.<sup>38</sup> This Ph.D. thesis is focused on the type 1 pili presented by UPEC with the lower urinary tract as target organ.



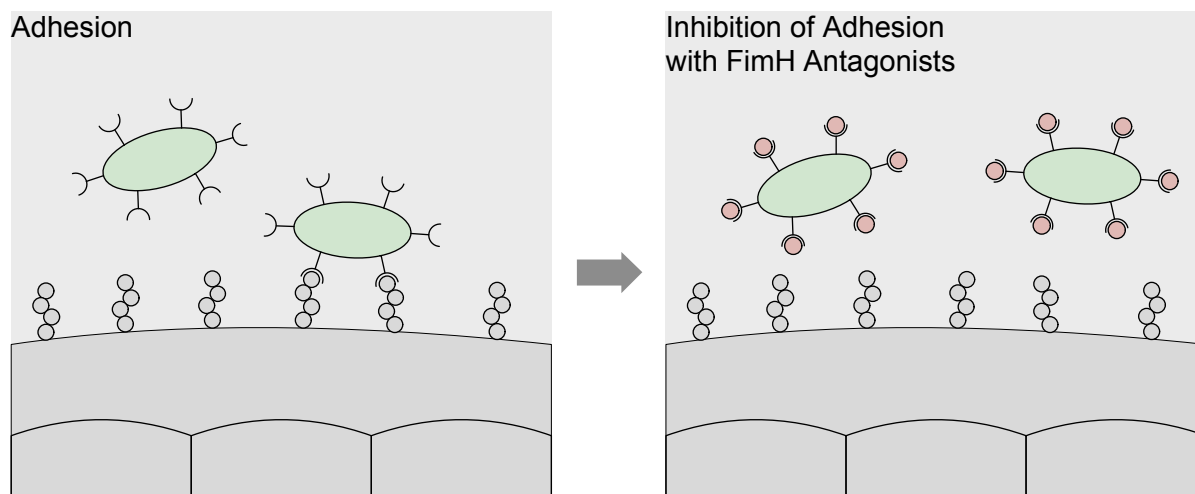
**Figure 1.2.** Structure of *E. coli*, its fimbriae and of FimH low-, medium-, and high-affinity state. Figure modified from Ref.<sup>26,39</sup> and pictured by Benz Hubler.

### 1.3 Prevention and Therapy of Urinary Tract Infection

Current therapies of UTI involve antibiotics as the first-line treatment. Such therapies alleviate the acute symptoms and prevent potentially life threatening complications such as kidney infections (pyelonephritis). Nevertheless, treatment of asymptomatic bacteriuria with antibiotics,<sup>15</sup> increases the emergence of a multi-drug resistant microbial flora and are therefore not recommended.<sup>40</sup> Exceptions for treatment of asymptomatic bacteriuria with antibiotics are pregnant women in the first trimester to avoid complication during pregnancy.<sup>15</sup> Several guidelines were published to avoid overtreatment by frequent and repeated use of antibiotics.<sup>41,42</sup> Non-antibiotic prophylactic treatments for recurrent UTI (e.g. cranberry) can be used by young and middle-aged women, however, their clinical use in prevention is not statistically validated and the evidence for other population groups remains an open question.<sup>43,44</sup> To avoid treatment failure because of increasing resistance,<sup>40</sup> new approaches are still needed for prevention and treatment of UTI. Numerous studies demonstrated the usefulness of D-mannose for the prevention of UTI.<sup>45,46</sup> The D-mannose moiety, the major component of the UPIa glycan, is the minimal binding epitope recognized by the CRD of FimH. Blocking the CRD by suitable mannosides prevents FimH from adhering to the epithelial cells, ultimately resulting in clearance of the bacteria by the bulk flow of urine and consequently in prevention of infection (Figure 1.3). This approach is a promising alternative to the generally used antibiotic treatments of UTI. However, carbohydrates have pharmacokinetic drawbacks, as they are too hydrophilic to permeate through the intestinal membrane when dosed orally.<sup>47</sup>



In addition, once reached systemic circulation, they suffer from rapid renal elimination. An alternative would be a prodrug approach, as successfully applied in case of the glycomimetic oseltamivir.<sup>48</sup>

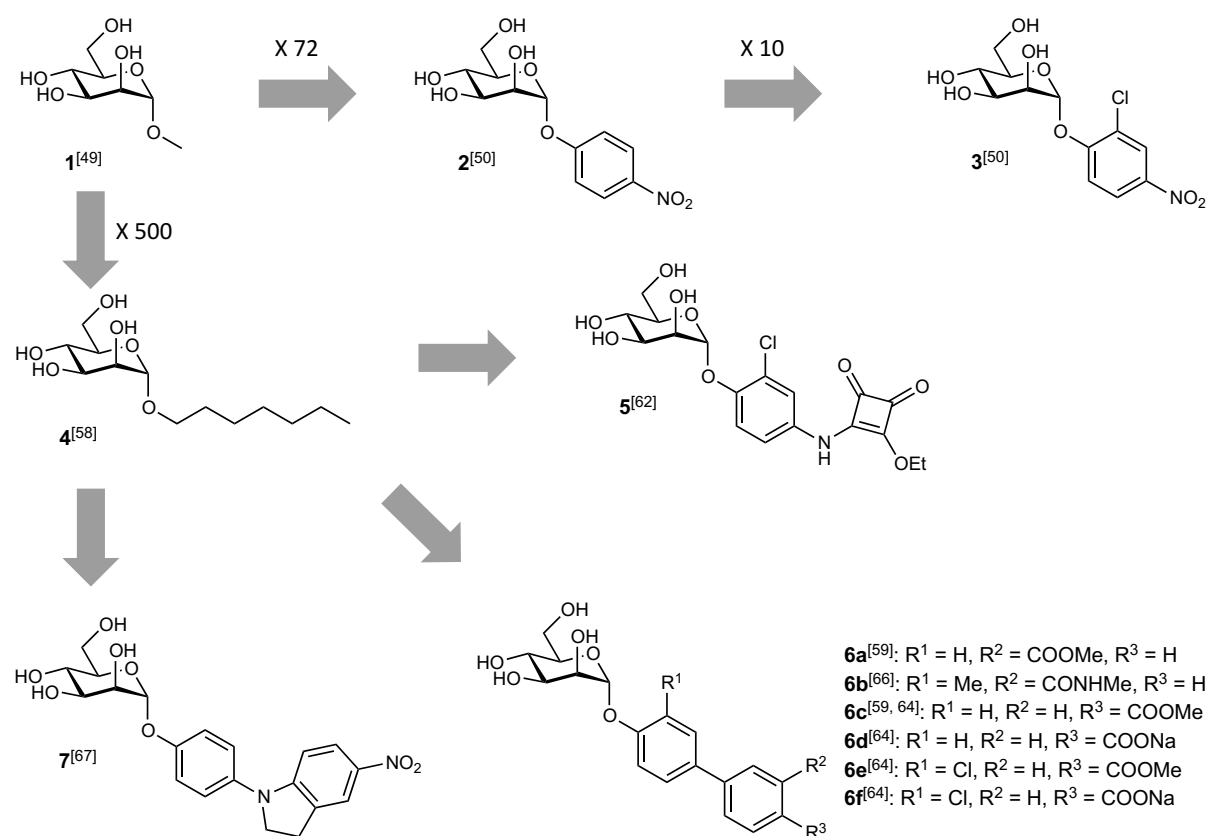


**Figure 1.3.** Inhibition of the adhesion of the bacteria UPEC to the urothelial cells with FimH antagonists and therefore, interruption of the infection cycle. Figure modified from Ref.<sup>24</sup> and pictured by Benz Hubler.

### 1.3.1 FimH Antagonists

More than three decades ago, Sharon and coworkers analyzed various mannosides and oligomannosides and identified methyl  $\alpha$ -D-mannopyranoside (**1**, Figure 1.4) as antagonist for type I fimbriae-mediated bacterial adhesion.<sup>49-52</sup> Furthermore, aromatic glycosides such as *p*-nitrophenyl  $\alpha$ -D-mannopyranoside (**2**, Figure 1.4) exhibited a 72-fold stronger affinity compared to methyl  $\alpha$ -D-mannopyranoside (**1**). In addition, affinity could be improved by a factor of ten by adding a chloro substituent in *ortho* position ( $\rightarrow$ **3**, Figure 1.4).<sup>50,51,53</sup> To further improve affinity, two approaches were investigated. First, multivalent mannosides were synthesized,<sup>54</sup> for which nanomolar affinities to the CRD were obtained<sup>55-57</sup>. However, due their drawbacks regarding oral availability, multivalent FimH antagonists are not further discussed in this thesis. Second, monovalent  $\alpha$ -D-mannopyranosides with modifications of the aglycone were designed considering the information obtained from the crystal structure of the CRD of FimH co-crystallized with FimH antagonists.<sup>30,58-60</sup> In the course of these studies, alkyl  $\alpha$ -D-mannopyranosides were analyzed and revealed *n*-heptyl- $\alpha$ -D-mannopyranoside (**4**, Figure 1.4) as an optimal FimH antagonist with a 500-fold stronger affinity than methyl- $\alpha$ -D-mannopyranoside.<sup>58,61</sup> Extension of the aromatic aglycone led to squaric acid monoamide derivatives (e.g. **5**, Figure 1.4),<sup>62,63</sup> biphenyl mannosides modified with a carboxylic acid substituent (e.g. **6a-f**, Figure 1.4),<sup>59,64-66</sup> and indolinyl phenyl mannosides (e.g. **7**, Figure 1.4).<sup>67</sup>

In these structures additional hydrophobic interactions of the aglycone with the aromatic residues of the tyrosine gate are provided and therefore a further increase in affinity to the low nanomolar range was realized. Substituents on the terminal ring of the biaryl aglycone, such as the carboxylic acid present in the biphenyl derivatives **6a-f**<sup>59,64,66</sup> (Figure 1.4) or the nitro group in antagonist **7** (Figure 1.4),<sup>67</sup> further enforce the  $\pi$ - $\pi$  stacking interactions with the electron rich Tyr48.<sup>68</sup> Once high affinity FimH antagonists were identified, the focus was set on physicochemical and pharmacokinetic properties of the FimH antagonists to enable oral bioavailability. An ester prodrug approach allowed an oral application in an animal disease model, however, insufficient solubility was observed.<sup>69</sup>



**Figure 1.4.** Structures of identified potent FimH antagonists with the affinity enhancement indicated over the arrows (if > 5). Structures and values are taken from Ref.<sup>49,50,58,59,62,64,67</sup>.

## 1.4 References

1. Foxman, B.; Barlow, R.; D'Arcy, H.; Gillespie, B.; Sobel, J. D. Urinary tract infection: self-reported incidence and associated costs. *Ann. Epidemiol.* **2000**, *10*, 509-15.
2. Fihn, S. D. Clinical practice. Acute uncomplicated urinary tract infection in women. *The New England Journal of medicine* **2003**, *349*, 259-266.
3. Dielubanza, E. J.; Schaeffer, A. J. Urinary tract infections in women. *Med. Clin. North Am.* **2011**, *95*, 27-41.
4. Ronald, A.; Ludwig, E. Urinary tract infections in adults with diabetes. *Int. J. Antimicrob. Agents* **2001**, *17*, 287-92.
5. Patterson, J. E.; Andriole, V. T. Bacterial urinary tract infections in diabetes. *Infect. Dis. Clin. North Am.* **1997**, *11*, 735-50.
6. Cardenas, D. D.; Hooton, T. M. Urinary tract infection in persons with spinal cord injury. *Arch. Phys. Med. Rehabil.* **1995**, *76*, 272-80.
7. Cunningham, F. G.; Lucas, M. J. Urinary tract infections complicating pregnancy. *Baillieres Clin. Obstet. Gynaecol.* **1994**, *8*, 353-73.
8. Winberg, J.; Bergstrom, T.; Jacobsson, B. Morbidity, age and sex distribution, recurrences and renal scarring in symptomatic urinary tract infection in childhood. *Kidney Int. Suppl.* **1975**, *4*, S101-6.
9. Ruben, F. L.; Dearwater, S. R.; Norden, C. W.; Kuller, L. H.; Gartner, K.; Shalley, A.; Warshafsky, G.; Kelsey, S. F.; O'Donnell, C.; Means, E.; *et al.* Clinical infections in the noninstitutionalized geriatric age group: methods utilized and incidence of infections. The Pittsburgh Good Health Study. *Am. J. Epidemiol.* **1995**, *141*, 145-57.
10. Foxman, B.; Somsel, P.; Tallman, P.; Gillespie, B.; Raz, R.; Colodner, R.; Kandula, D.; Sobel, J. D. Urinary tract infection among women aged 40 to 65: behavioral and sexual risk factors. *J. Clin. Epidemiol.* **2001**, *54*, 710-8.
11. Tolkoff-Rubin, N. E.; Rubin, R. H. Urinary tract infection in the immunocompromised host. Lessons from kidney transplantation and the AIDS epidemic. *Infect. Dis. Clin. North Am.* **1997**, *11*, 707-17.
12. Metz, L. M.; McGuinness, S. D.; Harris, C. Urinary tract infections may trigger relapse in multiple sclerosis. *Axone* **1998**, *19*, 67-70.
13. Foxman, B. Epidemiology of urinary tract infections: incidence, morbidity, and economic costs. *Disease-a-month: DM* **2003**, *49*, 53-70.
14. Foxman, B. Recurring urinary tract infection: incidence and risk factors. *Am. J. Public Health* **1990**, *80*, 331-3.
15. Colgan, R.; Nicolle, L. E.; McGlone, A.; Hooton, T. M. Asymptomatic bacteriuria in adults. *Am. Fam. Physician* **2006**, *74*, 985-90.
16. Woodford, H. J.; George, J. Diagnosis and management of urinary infections in older people. *Clin. Med.* **2011**, *11*, 80-3.
17. Robinson, J. L.; Finlay, J. C.; Lang, M. E.; Bortolussi, R.; Canadian Paediatric Society, I. D.; Immunization Committee, C. P. C. Urinary tract infections in infants and children: Diagnosis and management. *Paediatr. Child Health* **2014**, *19*, 315-25.
18. Hooton, T. M.; Besser, R.; Foxman, B.; Fritsche, T. R.; Nicolle, L. E. Acute uncomplicated cystitis in an era of increasing antibiotic resistance: a proposed approach to empirical therapy. *Clin. Infect. Dis.* **2004**, *39*, 75-80.
19. Gupta, K.; Hooton, T. M.; Stamm, W. E. Increasing antimicrobial resistance and the management of uncomplicated community-acquired urinary tract infections. *Ann. Intern Med.* **2001**, *135*, 41-50.
20. Ronald, A. The etiology of urinary tract infection: traditional and emerging pathogens. *Am. J. Med.* **2002**, *113 Suppl 1A*, 14S-19S.
21. Nicolle, L.; Anderson, P. A.; Conly, J.; Mainprize, T. C.; Meuser, J.; Nickel, J. C.; Senikas, V. M.; Zhanel, G. G. Uncomplicated urinary tract infection in women. Current practice and the effect of antibiotic resistance on empiric treatment. *Can. Fam. Physician* **2006**, *52*, 612-8.
22. Mulvey, M. A.; Schilling, J. D.; Martinez, J. J.; Hultgren, S. J. Bad bugs and beleaguered bladders: interplay between uropathogenic *Escherichia coli* and innate host defenses. *Proc. Natl. Acad. Sci. U S A* **2000**, *97*, 8829-35.

23. Wiles, T. J.; Kulesus, R. R.; Mulvey, M. A. Origins and virulence mechanisms of uropathogenic *Escherichia coli*. *Exp. Mol. Pathol.* **2008**, *85*, 11-9.
24. Abgottsson, D.; Ernst, B. *In vivo* evaluation of FimH antagonists - a novel class of antimicrobials for the treatment of urinary tract infection. *Chimia (Aarau)* **2012**, *66*, 166-9.
25. Capitani, G.; Eidam, O.; Glockshuber, R.; Grütter, M. G. Structural and functional insights into the assembly of type 1 pili from *Escherichia coli*. *Microbes and infection / Institut Pasteur* **2006**, *8*, 2284-2290.
26. Thomas, W. Catch bonds in adhesion. *Ann. Rev. Biomed. Engin.* **2008**, *10*, 39-57.
27. Schilling, J. D.; Mulvey, M. A.; Hultgren, S. J. Structure and function of *Escherichia coli* type 1 pili: new insight into the pathogenesis of urinary tract infections. *J. Infect. Dis.* **2001**, *183 Suppl. 1*, S36-40.
28. Le Trong, I.; Aprikian, P.; Kidd, B. A.; Forero-Shelton, M.; Tchesnokova, V.; Rajagopal, P.; Rodriguez, V.; Interlandi, G.; Klevit, R.; Vogel, V.; Stenkamp, R. E.; Sokurenko, E. V.; Thomas, W. E. Structural basis for mechanical force regulation of the adhesin FimH via finger trap-like beta sheet twisting. *Cell* **2010**, *141*, 645-55.
29. Rodriguez, V. B.; Kidd, B. A.; Interlandi, G.; Tchesnokova, V.; Sokurenko, E. V.; Thomas, W. E. Allosteric coupling in the bacterial adhesive protein FimH. *J. Biol. Chem.* **2013**, *288*, 24128-39.
30. Choudhury, D.; Thompson, A.; Stojanoff, V.; Langermann, S.; Pinkner, J.; Hultgren, S. J.; Knight, S. D. X-ray structure of the FimC-FimH chaperone-adhesin complex from uropathogenic *Escherichia coli*. *Science* **1999**, *285*, 1061-6.
31. Hung, C. S.; Bouckaert, J.; Hung, D.; Pinkner, J.; Widberg, C.; DeFusco, A.; Auguste, C. G.; Strouse, R.; Langermann, S.; Waksman, G.; Hultgren, S. J. Structural basis of tropism of *Escherichia coli* to the bladder during urinary tract infection. *Mol. Microbiol.* **2002**, *44*, 903-15.
32. Wellens, A.; Garofalo, C.; Nguyen, H.; Van Gerven, N.; Slattegard, R.; Hernalsteens, J. P.; Wyns, L.; Oscarson, S.; De Greve, H.; Hultgren, S.; Bouckaert, J. Intervening with urinary tract infections using anti-adhesives based on the crystal structure of the FimH-oligomannose-3 complex. *PLoS One* **2008**, *3*, e2040.
33. Wellens, A.; Lahmann, M.; Touaibia, M.; Vaucher, J.; Oscarson, S.; Roy, R.; Remaut, H.; Bouckaert, J. The tyrosine gate as a potential entropic lever in the receptor-binding site of the bacterial adhesin FimH. *Biochemistry* **2012**, *51*, 4790-9.
34. Aprikian, P.; Tchesnokova, V.; Kidd, B.; Yakovenko, O.; Yarov-Yarovoy, V.; Trinchina, E.; Vogel, V.; Thomas, W.; Sokurenko, E. Interdomain interaction in the FimH adhesin of *Escherichia coli* regulates the affinity to mannose. *J. Biologic. Chem.* **2007**, *282*, 23437-23446.
35. Berglund, J.; Knight, S. D. Structural basis for bacterial adhesion in the urinary tract. *Adv. Experim. Med. Biol.* **2003**, *535*, 33-52.
36. Westerlund-Wikström, B.; Korhonen, T. K. Molecular structure of adhesin domains in *Escherichia coli* fimbriae. *Int. J. Med. Microbiol.* **2005**, *295*, 479-486.
37. Mulvey, M. A. Adhesion and entry of uropathogenic *Escherichia coli*. *Cellular Microbiology* **2002**, *4*, 257-271.
38. Melican, K.; Sandoval, R. M.; Kader, A.; Josefsson, L.; Tanner, G. A.; Molitoris, B. A.; Richter-Dahlfors, A. Uropathogenic *Escherichia coli* P and Type 1 fimbriae act in synergy in a living host to facilitate renal colonization leading to nephron obstruction. *PLoS Pathog* **2011**, *7*, e1001298.
39. Yakovenko, O.; Sharma, S.; Forero, M.; Tchesnokova, V.; Aprikian, P.; Kidd, B.; Mach, A.; Vogel, V.; Sokurenko, E.; Thomas, W. E. FimH forms catch bonds that are enhanced by mechanical force due to allosteric regulation. *J. Biol. Chem.* **2008**, *283*, 11596-11605.
40. Sanchez, G. V.; Master, R. N.; Karlowsky, J. A.; Bordon, J. M. In vitro antimicrobial resistance of urinary *Escherichia coli* isolates among U.S. outpatients from 2000 to 2010. *Antimicrob. Agents Chemother.* **2012**, *56*, 2181-3.
41. Warren, J. W.; Abrutyn, E.; Hebel, J. R.; Johnson, J. R.; Schaeffer, A. J.; Stamm, W. E. Guidelines for antimicrobial treatment of uncomplicated acute bacterial cystitis and acute pyelonephritis in women. Infectious Diseases Society of America (IDSA). *Clin. Infect. Dis.* **1999**, *29*, 745-58.
42. Nicolle, L. E.; Bradley, S.; Colgan, R.; Rice, J. C.; Schaeffer, A.; Hooton, T. M.; Infectious Diseases Society of, A.; American Society of, N.; American Geriatric, S. Infectious Diseases Society of America guidelines for the diagnosis and treatment of asymptomatic bacteriuria in adults. *Clin. Infect. Dis.* **2005**, *40*, 643-54.

43. Mansour, A.; Hariri, E.; Shelh, S.; Irani, R.; Mroueh, M. Efficient and cost-effective alternative treatment for recurrent urinary tract infections and interstitial cystitis in women: a two-case report. *Case Rep. Med.* **2014**.
44. Aydin, A.; Ahmed, K.; Zaman, I.; Khan, M. S.; Dasgupta, P. Recurrent urinary tract infections in women. *Int. Urogynecol. J.* **2014**.
45. Duran, J. M.; Cano, M.; Peral, M. J.; Ilundain, A. A. D-mannose transport and metabolism in isolated enterocytes. *Glycobiology* **2004**, *14*, 495-500.
46. Kranjcec, B.; Papes, D.; Altarac, S. D-mannose powder for prophylaxis of recurrent urinary tract infections in women: a randomized clinical trial. *World J. Urol.* **2014**, *32*, 79-84.
47. Ernst, B.; Magnani, J. L. From carbohydrate leads to glycomimetic drugs. *Nat. Rev. Drug Discov.* **2009**, *8*, 661-77.
48. Kim, C. U.; Lew, W.; Williams, M. A.; Liu, H.; Zhang, L.; Swaminathan, S.; Bischofberger, N.; Chen, M. S.; Mendel, D. B.; Tai, C. Y.; Laver, W. G.; Stevens, R. C. Influenza neuraminidase inhibitors possessing a novel hydrophobic interaction in the enzyme active site: design, synthesis, and structural analysis of carbocyclic sialic acid analogues with potent anti-influenza activity. *J. Am. Chem. Soc.* **1997**, *119*, 681-90.
49. Ofek, I.; Mirelman, D.; Sharon, N. Adherence of *Escherichia coli* to human mucosal cells mediated by mannose receptors. *Nature* **1977**, *265*, 623-5.
50. Firon, N.; Ofek, I.; Sharon, N. Interaction of mannose-containing oligosaccharides with the fimbrial lectin of *Escherichia coli*. *Biochem. Biophys. Res. Commun.* **1982**, *105*, 1426-32.
51. Firon, N.; Ofek, I.; Sharon, N. Carbohydrate specificity of the surface lectins of *Escherichia coli*, *Klebsiella pneumoniae*, and *Salmonella typhimurium*. *Carbohydr. Res.* **1983**, *120*, 235-49.
52. Sharon, N. Bacterial lectins, cell-cell recognition and infectious disease. *FEBS Lett* **1987**, *217*, 145-57.
53. Firon, N.; Ashkenazi, S.; Mirelman, D.; Ofek, I.; Sharon, N. Aromatic alpha-glycosides of mannose are powerful inhibitors of the adherence of type 1 fimbriated *Escherichia coli* to yeast and intestinal epithelial cells. *Infect. Immun.* **1987**, *55*, 472-6.
54. Lindhorst, T. K.; Kieburg, C.; Krallmann-Wenzel, U. Inhibition of the type 1 fimbriae-mediated adhesion of *Escherichia coli* to erythrocytes by multiantennary alpha-mannosyl clusters: the effect of multivalency. *Glycoconj. J.* **1998**, *15*, 605-13.
55. Pieters, R. J. Maximising multivalency effects in protein-carbohydrate interactions. *Org. Biomol. Chem.* **2009**, *7*, 2013-25.
56. Imberty, A.; Chabre, Y. M.; Roy, R. Glycomimetics and glycodendrimers as high affinity microbial anti-adhesins. *Chemistry* **2008**, *14*, 7490-9.
57. Hartmann, M.; Lindhorst, T. K. The Bacterial Lectin FimH, a Target for Drug Discovery - Carbohydrate Inhibitors of Type 1 Fimbriae-Mediated Bacterial Adhesion. *Eur. J. Org. Chem.* **2011**, *20-21*, 3583-3609.
58. Bouckaert, J.; Berglund, J.; Schembri, M.; De Genst, E.; Cools, L.; Wuhrer, M.; Hung, C. S.; Pinkner, J.; Slattegard, R.; Zavialov, A.; Choudhury, D.; Langermann, S.; Hultgren, S. J.; Wyns, L.; Klemm, P.; Oscarson, S.; Knight, S. D.; De Greve, H. Receptor binding studies disclose a novel class of high-affinity inhibitors of the *Escherichia coli* FimH adhesin. *Mol. Microbiol.* **2005**, *55*, 441-55.
59. Han, Z.; Pinkner, J. S.; Ford, B.; Obermann, R.; Nolan, W.; Wildman, S. A.; Hobbs, D.; Ellenberger, T.; Cusumano, C. K.; Hultgren, S. J.; Janetka, J. W. Structure-based drug design and optimization of mannoside bacterial FimH antagonists. *J. Med. Chem.* **2010**, *53*, 4779-92.
60. Wellens, A.; Garofalo, C.; Nguyen, H.; Van Gerven, N.; Slattegard, R.; Hernalsteens, J. P.; Wyns, L.; Oscarson, S.; De Greve, H.; Hultgren, S.; Bouckaert, J. Intervening with Urinary Tract Infections Using Anti-Adhesives Based on the Crystal Structure of the FimH-Oligomannose-3 Complex. *Plos One* **2008**, *4*, 1-13.
61. Sharon, N. Carbohydrates as future anti-adhesion drugs for infectious diseases. *Biochim. Biophys. Acta* **2006**, *1760*, 527-37.
62. Sperling, O.; Fuchs, A.; Lindhorst, T. K. Evaluation of the carbohydrate recognition domain of the bacterial adhesin FimH: Design, synthesis and binding properties of mannoside ligands. *Org. Biomol. Chem.* **2006**, *4*, 3913-22.
63. Grabosch, C.; Hartmann, M.; Schmidt-Lassen, J.; Lindhorst, T. K. Squaric acid monoamide mannosides as ligands for the bacterial lectin FimH: covalent inhibition or not? *ChemBioChem* **2011**, *12*, 1066-74.

64. Klein, T.; Abgottspon, D.; Wittwer, M.; Rabbani, S.; Herold, J.; Jiang, X.; Kleeb, S.; Luethi, C.; Scharenberg, M.; Bezencon, J.; Gubler, E.; Pang, L.; Smiesko, M.; Cutting, B.; Schwardt, O.; Ernst, B. FimH Antagonists for the Oral Treatment of Urinary Tract Infections: From Design and Synthesis to *in Vitro* and *in Vivo* Evaluation. *J. Med. Chem.* **2010**, *53*, 8627-8641.
65. Cusumano, C. K.; Pinkner, J. S.; Han, Z.; Greene, S. E.; Ford, B. A.; Crowley, J. R.; Henderson, J. P.; Janetka, J. W.; Hultgren, S. J. Treatment and Prevention of Urinary Tract Infection with Orally Active FimH Inhibitors. *Sci. Transl. Med.* **2011**, *109*, 1-10.
66. Han, Z.; Pinkner, J. S.; Ford, B.; Chorell, E.; Crowley, J. M.; Cusumano, C. K.; Campbell, S.; Henderson, J. P.; Hultgren, S. J.; Janetka, J. W. Lead optimization studies on FimH antagonists: discovery of potent and orally bioavailable ortho-substituted biphenyl mannosides. *J. Med. Chem.* **2012**, *55*, 3945-59.
67. Jiang, X.; Abgottspon, D.; Kleeb, S.; Rabbani, S.; Scharenberg, M.; Wittwer, M.; Haug, M.; Schwardt, O.; Ernst, B. Antiadhesion therapy for urinary tract infections--a balanced PK/PD profile proved to be key for success. *J. Med. Chem.* **2012**, *55*, 4700-13.
68. Kleeb, S.; Pang, L.; Mayer, K.; Eris, D.; Sigl, A.; Preston, R. C.; Zihlmann, P.; Sharpe, T.; Jakob, R. P.; Abgottspon, D.; Hutter, A. S.; Scharenberg, M.; Jiang, X.; Navarra, G.; Rabbani, S.; Smiesko, M.; Ludin, N.; Bezencon, J.; Schwardt, O.; Maier, T.; Ernst, B. FimH Antagonists: Bioisosteres To Improve the *in Vitro* and *in Vivo* PK/PD Profile. *J. Med. Chem.* **2015**, *58*, 2221-39.
69. Pang, L.; Kleeb, S.; Lemme, K.; Rabbani, S.; Scharenberg, M.; Zalewski, A.; Schadler, F.; Schwardt, O.; Ernst, B. FimH antagonists: structure-activity and structure-property relationships for biphenyl alpha-D-mannopyranosides. *ChemMedChem* **2012**, *7*, 1404-22.

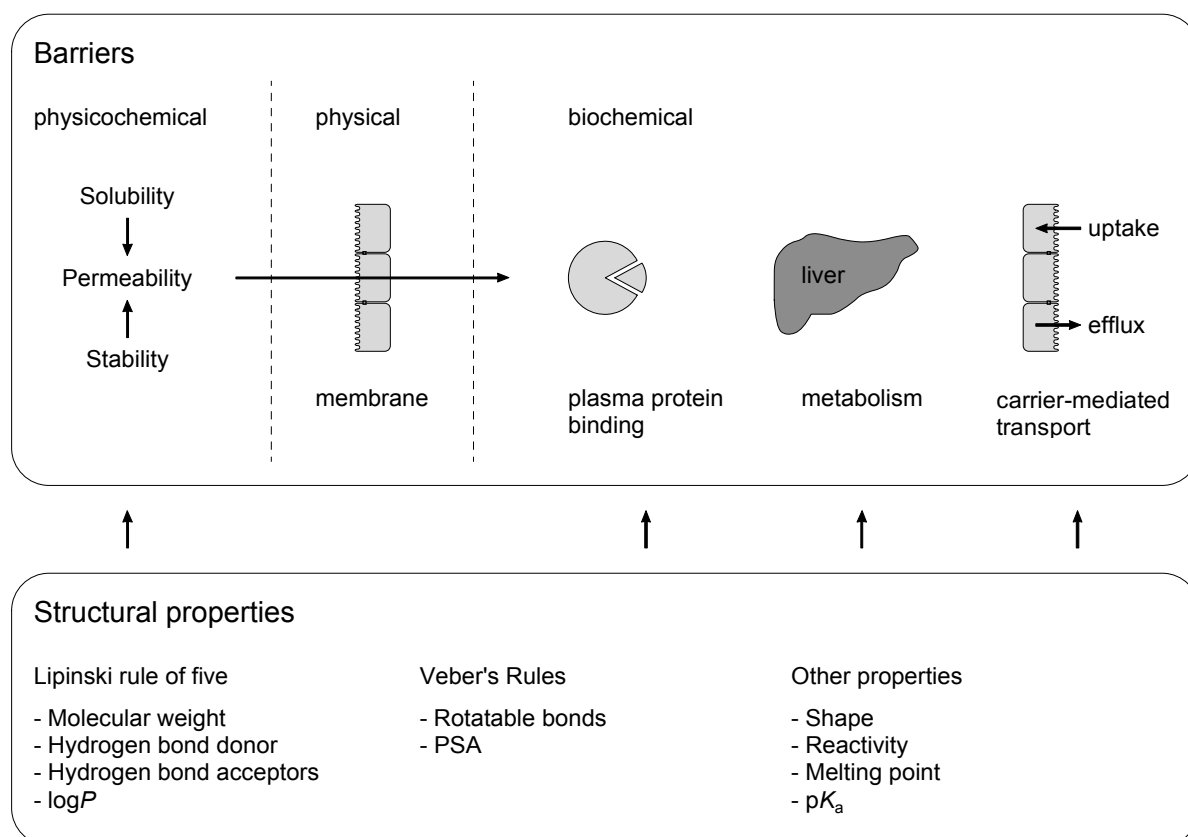
---

## 2 Introduction to Oral Bioavailability: How to Overcome Multiple Barriers?

---

60% of the marketed drugs are administered via the oral route. Oral application is not only the preferential and most convenient drug administration and therefore results in higher patient compliance, but also exhibits benefits in respect to variability in design and dosage forms.<sup>1,2</sup> Therefore, we are aiming in our FimH project for an orally available antagonist for prevention and/or treatment of UTI. FDA (U.S. Food and Drug Administration) defines bioavailability as “the rate and extent to which the active ingredient or active moiety is absorbed from a drug product and becomes available at the site of action.”<sup>3,4</sup> Overcoming the barriers of an orally administered drug in order to reach high oral bioavailability is challenging.<sup>5</sup> Barriers can be physical (e.g. membrane), physicochemical (e.g. stability, solubility, permeability), or biochemical (e.g. metabolism, transporters).<sup>6</sup> It was shown, that the early *in vitro* evaluation of pharmacokinetic properties dramatically decreased the attrition rate from 40% in 1991 to less than 10% in 2000.<sup>7</sup> Hence, it is important to evaluate as many compound properties (*i.e.* structural, physicochemical, and biochemical) as possible to reliably predict the *in vivo* behavior.<sup>8,9</sup> Additionally, the number of barriers depends on the place of action, *i.e.* on the location of the target protein. For the herein described prevention or/and treatment of UTI, FimH antagonists have to reach the bladder where they meet their target located on bacterial pili. Therefore, the drug has to be dissolved in the stomach, absorbed in the small intestines to reach the portal vein, stable against first pass metabolism in the liver (unless there is a prodrug approach<sup>10</sup>), and finally has to be eliminated by the kidney.<sup>11,12</sup>

The ability of a molecule to overcome these multiple barriers is depending on its structural (Lipinski rule of five,<sup>13</sup> Veber's rules,<sup>14</sup>  $pK_a$ ), physicochemical (stability, solubility, permeability), and biochemical (metabolism, plasma protein binding, and transporter) properties (Figure 2.1). However, the environment in the body, i.e. gastro and intestinal fluids, plasma proteins, tissue, enzymes, and transporters can interact with the molecule and can change physicochemical and biochemical properties of a compound.<sup>15</sup>

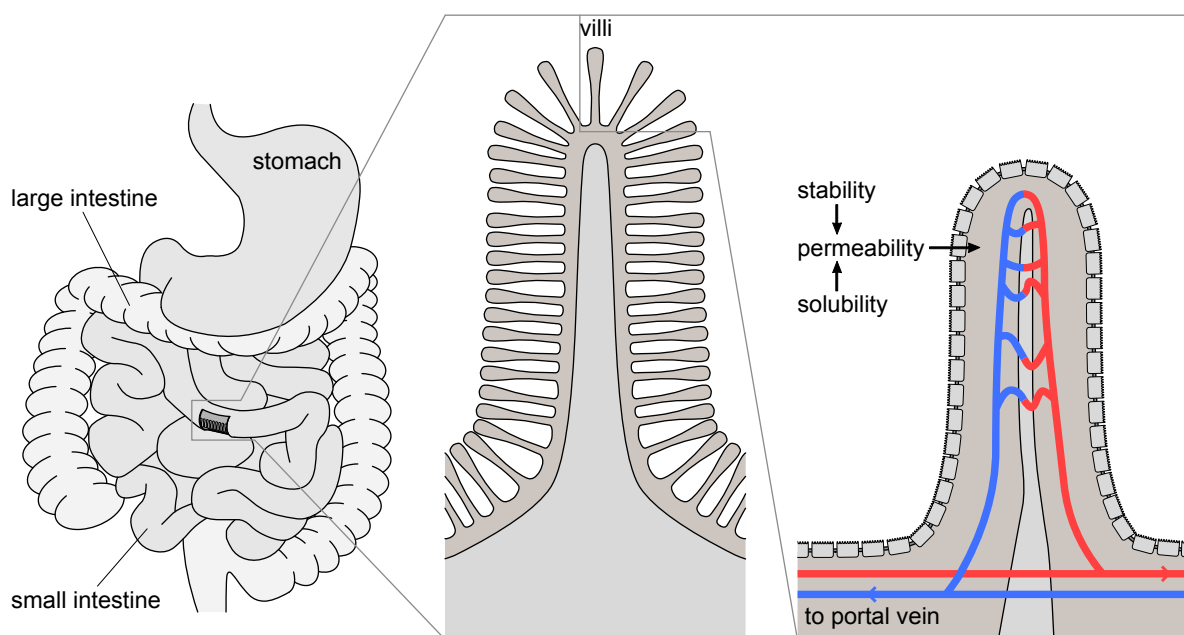


**Figure 2.1.** Key structural, physicochemical, and biochemical properties influencing the compound to overcome the various barriers in the body. PSA = polar surface area. Pictured by Benz Hubler.



## 2.1 Intestinal Tract – Oral Absorption

After oral administration of a drug, the gastrointestinal tract (GIT) is the first barrier to overcome. Gastrointestinal fluids with their large  $pH$  range and enzymatic activity impair the stability of the drug.<sup>16</sup> In addition, sufficient solubility in the gastrointestinal fluids has to be ensured.<sup>17</sup> And finally, permeability across intestinal membranes by passive diffusion or carrier-mediated transport is required.<sup>11</sup> Several physiological factors, such as  $pH$ , surface areas of the GIT, activity of enzymes, transit time, and specific transport mechanisms within the enterocytes (e.g. uptake and efflux-transporters), can influence physicochemical properties.<sup>18</sup> Acidity in the GIT varies from  $pH$  1.4 (stomach) to  $pH$  8 (small and large intestine) and differs for the fasted and fed state. Furthermore, interactions with food can lead to negative food effects, as longer retention times, longer gastric exposure and higher enzyme secretion, higher luminal degradation or complexation.<sup>19-21</sup> In contrast, gastric intestinal motility increases concentration of bile salts and lipid digestion and was shown to improve dissolution and solubilization of drugs and are therefore called positive food effects.<sup>22,23</sup> Since the surface area of the stomach is much smaller than the intestinal, drugs will be absorbed predominantly in the upper small intestine.<sup>24-26</sup> Figure 2.2 illustrates the structure of the villi and the enterocytes in the small intestines.



**Figure 2.2.** Illustration of the stomach and intestine, the schematic structure of the inner small intestinal wall and the villi in more detail with its enterocyte and the influence of stability, solubility, and permeability of a compound on oral absorption. Figure modified from Ref.<sup>18,27</sup> and pictured by Benz Hubler.

The protective function of the GIT, leading to a reduced absorption of a drug, is realized by enzymes, such as cytochrome P450 (CYP450),<sup>28</sup> pancreatin,<sup>29</sup> esterases,<sup>30</sup> and phosphatases,<sup>31,32</sup> and efflux transporters (e.g. P-glycoprotein; P-gp) located on the apical site of the endothelial cells.<sup>33-35</sup>

### 2.1.1 Stability

pH instability can occur due to large pH differences from stomach to colon.<sup>18</sup> A variety of fluids are secreted from the saliva, pancreas, stomach and gallbladder, into the intestinal lumen, including peptidases (pepsin) and hydrolytic enzymes such as proteases, lipases, and amylases (pancreatin).<sup>36</sup> The degradation of a drug is also called the first pass metabolism in the gut wall.<sup>37</sup> Accordingly, for testing stability, biorelevant media including components from the intestine (e.g. enzymes and surfactants) are applied next to simple aqueous buffer systems at different pH ranges in order to provide more accurate information for the prediction of the *in vivo* performance of a drug.<sup>37-40</sup> Many of the metabolic enzymes, such as UDP-glucuronyltransferases, sulfotransferases, esterases and CYP450 expressed in the liver are as well found in the small intestine, however, with much lower protein level and catalytic activity.<sup>41,42</sup> In addition, enzymes in the intestine can be easily saturated, unless a very small dose is given.<sup>41</sup> CYP450 3A4 (CYP3A4) shows the largest contribution in the intestine and exhibited large interindividual variation.<sup>28,43</sup>

For phosphate prodrugs, where a hydrolytic step is required before uptake, cleavage by the intestinal alkaline phosphatase (ALP) is needed. The half-life of phosphate prodrugs can be determined with Caco-2 cells, which provide phosphatase activity similar to that of normal human intestine.<sup>44,45</sup> Obviously, when a drug exhibits low stability in the stomach, the amount available for permeation through the intestinal membrane is reduced. In these cases, a possible solution is a gastro-resistant formulation (e.g. for proton pump inhibitors<sup>46,47</sup>). Advantages of ester prodrugs are possible shielding from food interaction as complexation, when the active compound contains charged groups, e.g. carboxylic acid.<sup>16</sup>

### 2.1.2 Solubility

For the permeation through the intestinal membrane, a drug must be dissolved. Solubility depends on numerous factors. It is determined by the solvent, i.e. solvent composition (e.g. salts, co-solvents, surfactants, ions, proteins) and by physicochemical conditions (e.g.  $pH$ , temperature).<sup>15</sup> The gallbladder secretes bile salts acting as detergents and therefore enhancing solubility of lipophilic compounds.  $pH$  differences can have an influence on the ionization state of ionizable groups ( $pK_a$  in the range of 1 to 11). Thus, charged compounds show higher solubility, whereas neutral compounds improved permeability.<sup>15</sup> On the other hand solubility is influenced by the compound's physical state (e.g. crystalline or amorphous) or its structural properties as lipophilicity ( $\log P$ ) and melting point (MP).<sup>15,48</sup>  $\log P$  is accounting for the interaction of the solute with the water and the MP is a descriptor of the lattice energy lost in the dissolution process.<sup>48</sup> Because solubility can affect results of other *in vitro* screenings, it should be determined early in the drug discovery process.<sup>17,49</sup>

#### Importance of $pK_a$

The  $pK_a$  (the negative logarithm of the acid dissociation constant  $K_a$ ) defines the ionized and neutral fractions of an acid or a base in aqueous solution at a given  $pH$ . When the  $pH$  is equal to the  $pK_a$ , 50% of both species are present. Since ionized molecules are more polar than neutral molecules,<sup>15</sup> the  $pK_a$  of a drug affects various properties, such as aqueous solubility at a given  $pH$ , permeability through biological membranes, plasma protein binding, or excretion via the bile or the kidney.<sup>50</sup> In our group, we revisited an old methodology, namely the determination of  $pK_a$  by  $^1H$ -NMR spectroscopy. A comparison with two *in silico* (Epik and Marvin) and two experimental approaches (electropotentiometric and UV-spectroscopic approaches) confirmed the validity of the method. (Paper 1, page 57).<sup>51</sup>

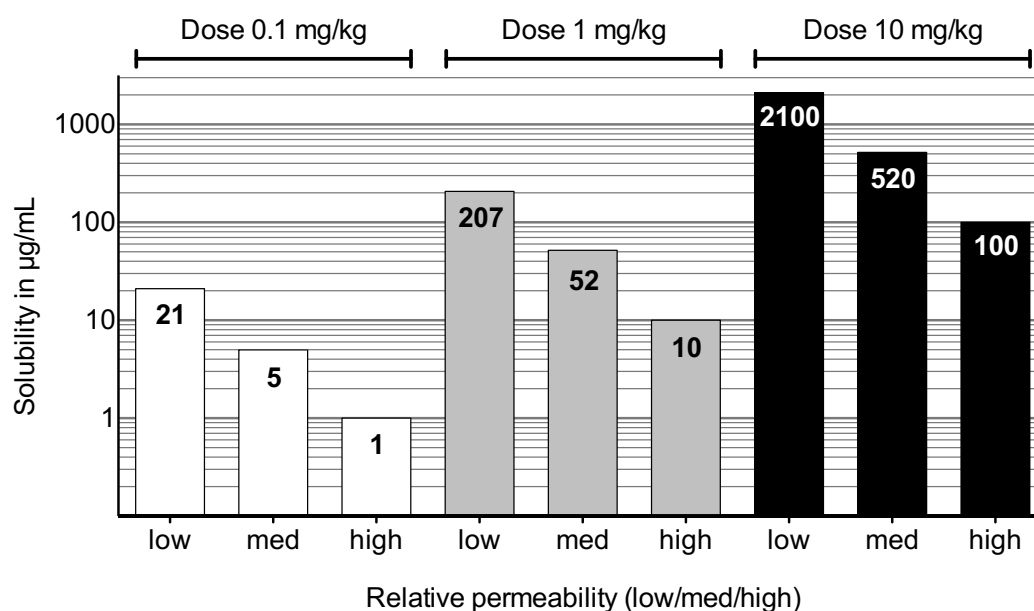
#### Methods to Measure Solubility

We can differentiate between thermodynamic and kinetic solubility. For *thermodynamic solubility*, the compound is solved in the solvent of interest until the solution is saturated and precipitation becomes visible. It is defined as the equilibrium of the saturated solution with the thermodynamically stable polymorph.<sup>40</sup> *Thermodynamic solubility* is often used in drug development, due to its small scale methodology and single tubes format.<sup>52</sup> For the determination of the *kinetic solubility*, the compound is first pre-solved in an organic solvent (e.g. DMSO) at a known concentration and then added to a solvent of interest (5% < DMSO) until precipitation. In contrast to the *thermodynamic solubility*, the tendency to overestimate solubility often occurs, due to

oversaturation.<sup>53</sup> However, because of the high throughput of this approach and the small amount of test compound required, *kinetic solubilities* are preferably used in drug discovery.<sup>52</sup>

### Solubility Requirements

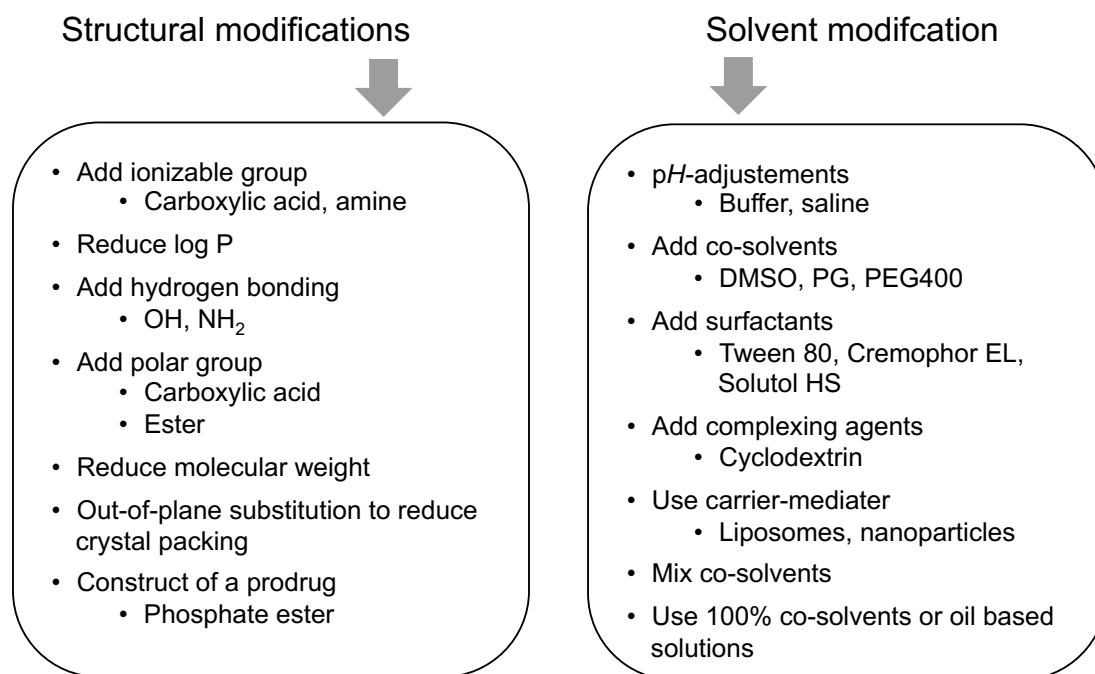
The required minimal solubility varies depending on the route of administration. For an intravenously applied drug, a solution is required, because the injection of a precipitate can lead to embolism,<sup>54,55</sup> whereas for an oral application a suspension is tolerated. As discussed by Lipinski<sup>17</sup> and Curatolo,<sup>56</sup> dose and permeability define the required minimum aqueous solubility for oral administration. Thus, a dose of 1 mg/kg of a compound with moderate permeability requires a solubility of at least 52  $\mu\text{g/mL}$  (Figure 2.3).<sup>17,56</sup>



**Figure 2.3.** Minimum acceptable solubility in  $\mu\text{g/mL}$ . Bars show the minimum solubility for low, medium, and high permeability at a clinical dose of 0.1 mg/kg (white), 1 mg/kg (grey), and 10 mg/kg (black). Figure modified from Ref.<sup>17</sup>.

### Approaches to Improve Solubility

To improve solubility, two main approaches can be applied, namely structural and solvent modifications (Figure 2.4).<sup>57</sup>



**Figure 2.4.** Approaches to improve solubility by structural and solvent modifications. PG = propylene glycol, PEG = polyethylene glycol. Figure modified from Ref.<sup>15</sup>.

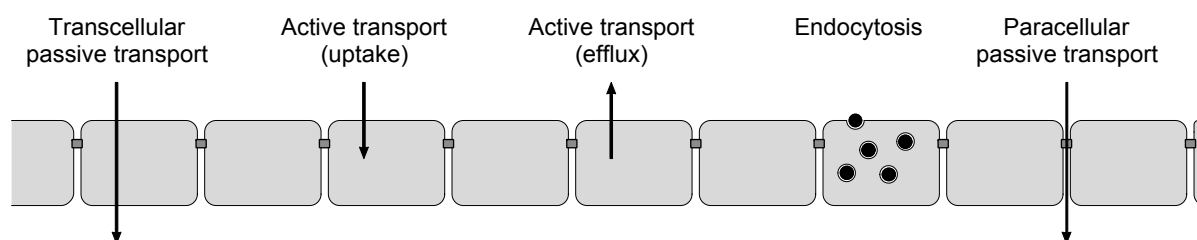
*Structural modifications.* The first choice to improve solubility of a compound is to modify its structure without affecting the affinity to its target.<sup>15</sup> Ishikawa *et al.* demonstrated strategies to improve aqueous solubility: (i) disruption of molecular planarity and symmetry due to their influence on crystal packing and the melting point<sup>58</sup> and (ii) introduction of ionizable groups, i.e. the more charges a compound has the better is its solubility<sup>15</sup> Another approach to increase solubility is the introduction of phosphate moiety to the active principle (prodrug approach).<sup>10</sup>

*Solvent modifications.* Adapting the solvent of oral administered form by pH-adjustment (buffer, saline), by adding solubilizer (co-solvents, surfactants, complexing agents), or by using carrier-mediators (e.g. liposomes or nanoparticles) is considered as a second approach to improve solubility.<sup>59</sup> Its advantage is that there is no requirement for a chemical modification of the drug.<sup>60</sup> pH-adjustment can help weak bases or acids, which contain a ionizable group with  $pK_a$  2-9. Co-solvents, such as propylene glycol (PG) or polyethylene glycol (PEG) have a solubilizing capacity. Surfactants reduce surface tension, avoid precipitation of the drug and are used for particle wetting

and dispersing.<sup>61,62</sup> In addition, surfactants (e.g. Tween 80, cremophor EL, solutol HS) can inhibit efflux transporter and improve permeability of compounds with slow permeability.<sup>63-66</sup> Complexing agents such as cyclodextrins with a hydrophilic surface and a lipophilic cavity can build water-soluble drug-cyclodextrin complexes and improve solubility. However, it should be noted that complexation can reduce the amount of free drug and therefore its permeability.<sup>61,67</sup> Also, systemic toxicity of the surfactants has to be taken into account.<sup>61</sup>

### 2.1.3 Passive and Active Permeability

To reach intracellular targets, intestinal drug absorption, the passage through blood-organ boundaries (e.g. brain barrier) as well as hepatic and renal clearance permeation processes play a crucial role.<sup>68</sup> Besides from other transport pathways illustrated in Figure 2.5, transcellular passive diffusion is the major route to achieve drug permeability.<sup>69</sup> Cumulative effects of structural properties of a molecule<sup>69</sup> as well as biochemical features of the intestinal layers influence passive permeability.<sup>70</sup>



**Figure 2.5.** Overview of various transport pathways through membranes. Figure modified from Ref.<sup>69</sup> and pictured by Benz Hubler.

### Importance of Lipophilicity

Lipophilicity is quantified by the octanol-water partition coefficient ( $\log P$ ), which considers only non-charged compounds, or the distribution coefficient ( $\log D$ ), which describes lipophilicity of ionizable compounds at a specific  $pH$ .<sup>18</sup> Therefore, the lipophilicity of ionizable compounds depends on the  $pH$  of the aqueous buffer and on the  $pK_a$  of the acid or base.<sup>71</sup> Approximately 70% of orally available marketed drugs are rather lipophilic with  $\log D$  values between 0.5 and 3.0.<sup>69,72</sup> Lipophilicity can be correlated to various drug properties.<sup>72</sup> Lipophilicity supports the transfer of a drug from the extracellular phase into cells<sup>73</sup> and further into the blood stream (permeability), where the drug undergoes binding to plasma protein or distribution into the tissue (distribution).<sup>74</sup> Furthermore, lipophilicity influences the permeability into hepatocytes where the drug is prone to metabolism,<sup>75-77</sup> and in case of renal elimination the reabsorption from the proximal tubuli back into circulation.<sup>11</sup>

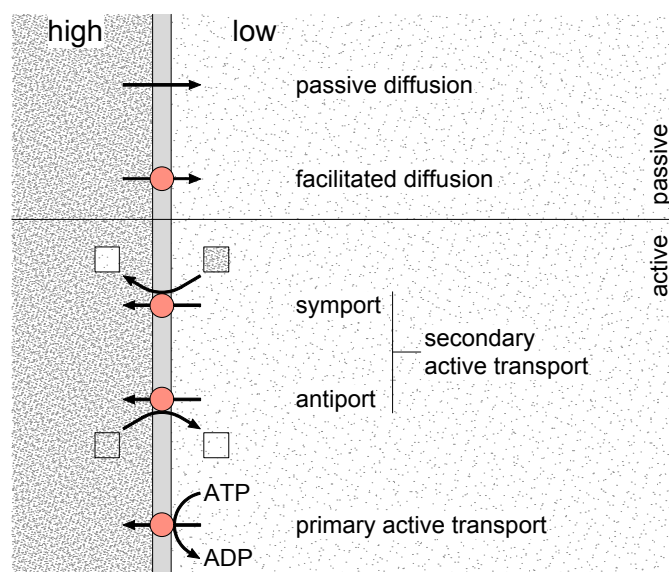
Several *in silico* tools have been developed for predicting log *P* values.<sup>78</sup> Moriguchi log *P* is calculated from a model consisting of a regression equation based on 13 parameters available from the structure of the compound of interest.<sup>79</sup> For *in vitro* determination of log *D* the shake flask approach is used as gold standard.<sup>80</sup>

### Passive Permeability

Passive permeability is driven by the concentration gradient, is not saturable, cannot be inhibited, and is less sensitive than carrier-mediated transport to the stereochemical effects.<sup>69</sup> It can be classified into two alternative mechanisms, namely the transcellular, the route through the cells, and the paracellular pathway, the route through the tight junctions at the interface of the cells.<sup>6,69</sup> Passive permeation depends on structural properties of compounds. Lipinski developed his famous rule of five for predicting passive transcellular permeability based on key structural properties of a compound, namely molecular weight ( $\leq 500$  Da), number of hydrogen bond donors ( $\leq 5$ ) and acceptors ( $\leq 10$ ), and lipophilicity ( $\log P \leq 5$ ).<sup>13</sup> Additionally, Veber's rule account for the negative influence of rotatable bonds ( $\text{NRB} \leq 10$ ) and large polar surface area ( $\text{PSA} \leq 140 \text{ \AA}^2$ ) on permeability.<sup>14</sup> In general, neutral compounds permeate more easily through the membrane than charged compounds,<sup>6</sup> and properties such as  $\text{pK}_a$  values influence permeability *pH*-dependent. Finally, the paracellular pathway is mainly reserved for small ( $< 250$  Da) and hydrophilic compounds.<sup>11</sup>

### Active Permeability

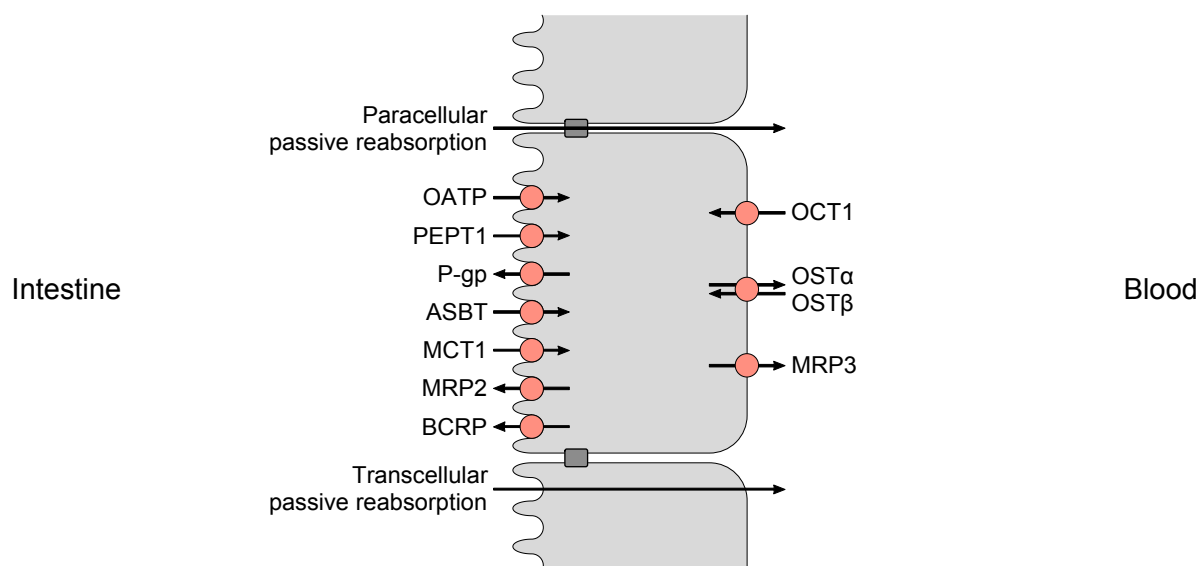
Active permeability describes the interaction of a drug with a carrier with the aim to overcome a membrane.<sup>69</sup> This pathway is of interest for compounds with low lipophilicity or for charged compounds that do not permeate passively through the intestinal membrane. Carrier-mediated transports are substrate specific, are saturable, and can be inhibited.<sup>81</sup> They can be divided into facilitated and active transport. Facilitated diffusion does not require energy and is driven by a concentration gradient. For active transport, we can distinguish between primary active transporter, which are directly coupled to adenosine-5'-triphosphate (ATP) and secondary active transport (e.g. uniport, symport, and antiport), which are not directly coupled to ATP and are synonymous to co-transporter.<sup>81</sup> Figure 2.6 illustrates these different transport mechanisms. The solute carrier (SLC) superfamily of the membrane transport proteins represents mostly cases of secondary active transporters, whereas the ATP-binding cassette (ABC) transporters are primary active transporters.<sup>82</sup>



**Figure 2.6.** Classification of membrane transport mechanisms. Black points depict the substrate (the more points the higher the concentration). Arrows show the direction of flux. Points in black squares represent the ion that supplies the driving force for transport (the more points the higher the concentration). Red points depict carrier-mediated proteins. Figure modified from Ref.<sup>81</sup> and pictured by Benz Hubler.

Figure 2.7 gives an overview on the different active transporters involved in the uptake or efflux in the small intestines. Members of the organic anion transporting polypeptide (OATP) family and the peptide transporter 1 (PEPT1) are assumed to be determinants of the uptake of organic anions and di- and tripeptides, respectively.<sup>83,84</sup> Efflux transporters, e.g. the ABC transporter P-glycoprotein (P-gp), have protective functions and can have a huge influence on oral absorption.<sup>16,63,85</sup> Especially in the case of low passive permeability, substrates of efflux transporters are transported back into the intestines. This mechanism can be hampered when the efflux transporter is saturated with a high concentration (high dose) of the compound.<sup>86</sup> To reach high concentrations, solubility becomes an important parameter.<sup>87</sup> In addition, P-gp expression increases from the jejunum to the distal ileum,<sup>88</sup> leading to a decrease in permeation for compounds with low solubility and slow permeation.

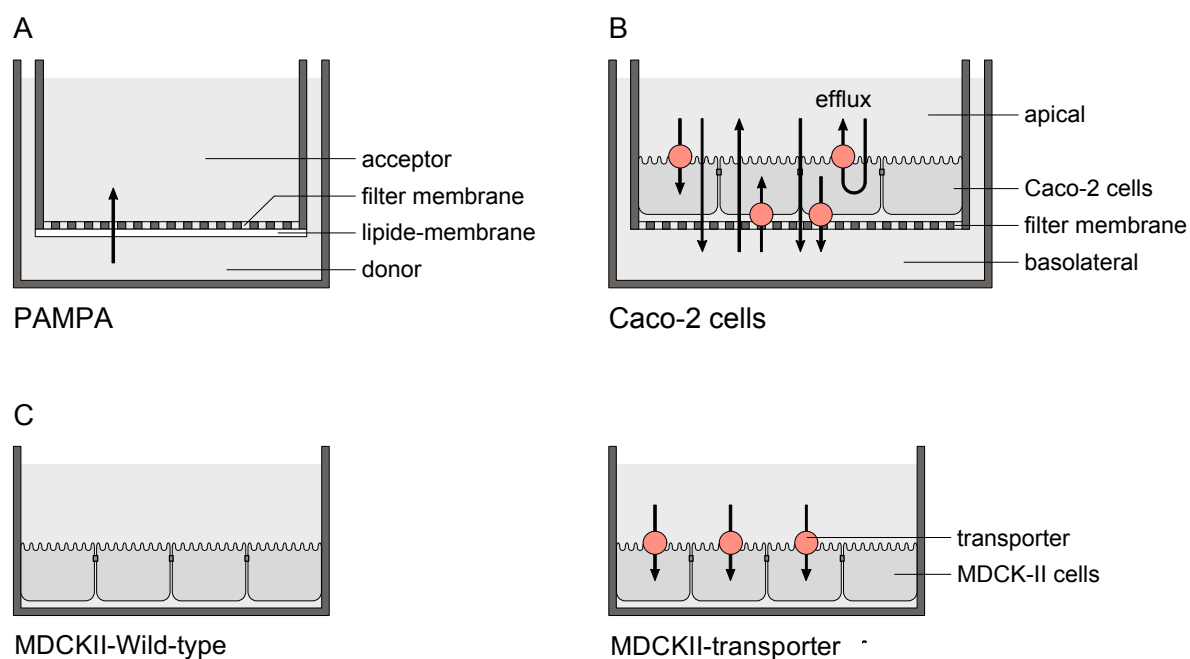




**Figure 2.7.** Intestinal epithelial cell with its apical (luminal) membrane uptake transporter including OATP, PEPT1 (SLC15A1), apical sodium/bile acid co-transporter (ASBT; SLC10A2), and monocarboxylic acid transporter 1 (MCT1; SLC16A1), their apical ATP-dependent efflux pumps including multidrug resistance protein 2 (MRP2; ABCC2), breast cancer resistance protein (BCRP; ABCG2), and P-glycoprotein (P-gp; MDR1, ABCB1). On the basolateral membrane, organic cation transporter 1 (OCT1; SLC22A1), heteromeric organic solute transporter (OST $\alpha$ –OST $\beta$ ), and MRP3 (ABCC3) are located. Figure modified from Ref.<sup>82</sup> and pictured by Benz Hubler.

### Methods to Measure Permeability

*Passive permeability.* The Parallel Artificial Membrane Permeability Assay (PAMPA) is a high throughput assay, first introduced by Kansy *et al.* in 1998.<sup>89</sup> It consists of a donor and receiver compartment separated by a microfilter coated with a lipid mixture (Figure 2.8A). This barrier mimics the membrane of cells. By measuring the flux of a compound across this artificial membrane, the intestinal transcellular permeation by passive diffusion can be estimated and classified into high ( $\log P_e > -5.7$  cm/s), moderate ( $-5.7$  cm/s  $> \log P_e > -6.3$  cm/s), and low ( $\log P_e < -6.3$  cm/s) effective permeability.<sup>90</sup> One drawback is the fact that carrier-mediated and paracellular pathways are not covered and have to be evaluated separately by cell-based assays.<sup>8,89</sup> Progress is being made in evolving 3D human small intestine microenvironment with more-reliable preclinical results.<sup>27</sup>



**Figure 2.8.** Construct of permeability assay A) Parallel Artificial Membrane Permeability Assay (PAMPA), B) Caco-2 cell assay, and C) MDCK-II transporter overexpressing cell assay. Figure pictured by Benz Hubler.

*Carrier-mediated permeability.* Cell-based assays have a similar set up as the PAMPA assay, consisting of a donor and receiver compartment, which are separated by a permeable filter on which cells (e.g. Caco-2<sup>87,91-96</sup>) are cultivated. The cells grow to polarized cell monolayers with an apical side forming microvilli and a basolateral side (Figure 2.8B).<sup>15</sup> Across this monolayer the compound flux is measured.

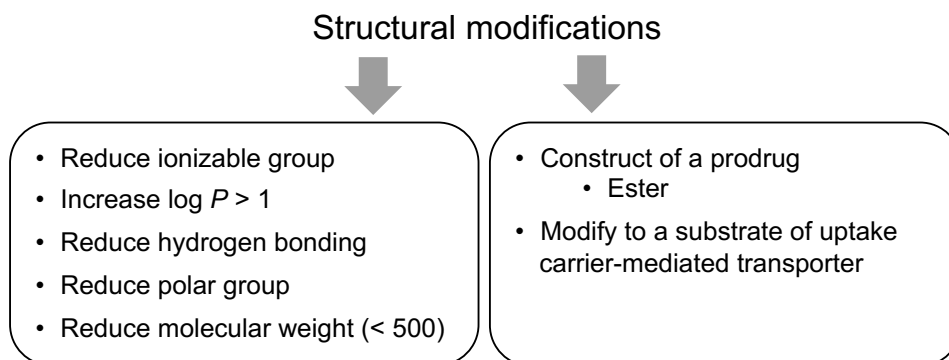
Since it takes 21 days until Caco-2 cells grow confluent, develop the microvilli and express the transporters, the model is very laborious, time-consuming and expensive.<sup>91</sup> Furthermore, reproducibility of results gained using the model across different laboratories is small.<sup>97</sup> Nevertheless, Caco-2 cells express several transport systems on their apical and basolateral sides and shares some similarities to enterocytes in the human intestine (jejunum).<sup>98</sup> A good correlation of oral bioavailability and Caco-2 permeability  $P_{app}$  values has been demonstrated and allows the determination of thresholds for Caco-2 results.<sup>99,100</sup>

To evaluate individual transporters, transfected cell lines (e.g. MDCK-II, HeLa, HEK293) are used and compared to their wild-type counterparts (Figure 2.8C). The advantages of these cell lines are the low expression level of membrane transporters in wild-type cells, their high transporter expression after transfection, and their convenience for *in vitro* studies (e.g. MDCK-II cell are ready in three days

compared to 21 days of cultivation for the Caco-2 cells).<sup>15</sup> For simple uptake studies, membrane based assay systems (i.e. ATPase assay, inverted vesicle assay) or oocytes can be used.<sup>82</sup>

### Approaches to Improve Permeability

Figure 2.9 lists the main various approaches to modify structures for improving permeability.



**Figure 2.9.** Approaches to improve permeability of a compound.

One guideline is offered by Lipinski rule of five.<sup>13</sup> A second approach to improve structural properties to be fulfilled for oral availability is the prodrug approach as demonstrated by e.g. enalapril, oseltamivir. A prerequisite for success is the cleavage of the prodrug into the active principle once it has arrived in the portal vein.<sup>10,101</sup> A third approach to improve permeability is the transformation of a drug into a substrate of an uptake transporter (e.g. for PEPT) as done for valacyclovir and captopril.<sup>102,103</sup> However, when structural modifications other than prodrug approaches are applied, changes in pharmacodynamics or in other pharmacokinetic properties have to be considered.<sup>104</sup> Finally, solvent modifications to improve paracellular permeability, by opening the tight junction or to improve transcellular permeability are rare due to their cell toxicity.<sup>15,57,105</sup>

### 2.2 Blood and Tissue Binding – Distribution

Once in circulation, drugs are either bound to plasma or tissue components or remain unbound in the aqueous environment. Only free drug can interact with its target. Nevertheless, efforts are rather undergone to improve oral bioavailability, i.e. by improving solubility, permeability, and metabolic stability than to increase the unbound drug concentration, because a higher free drug concentration will lead to a greater availability for metabolism or elimination.<sup>106,107</sup> Furthermore, studies show that in most of the cases changes in free drug concentration do not lead to pharmacological or toxicological responses.<sup>108-110</sup>

#### 2.2.1 Plasma Protein Binding

Plasma proteins interacting with drugs are mainly human serum albumin (HSA),  $\alpha_1$ -acid glycoprotein ( $\alpha$ -AGP), and lipoproteins.<sup>15</sup> Plasma protein binding (PPB) reduces the volume of distribution between plasma and the rest of the body, renal excretion, liver metabolism, and increases half-lives.<sup>6</sup> Structural properties such as  $pK_a$  and  $\log P$  can have an influence on plasma protein binding.<sup>111,112</sup> For 50% of 222 analyzed marketed drugs plasma protein binding was between 90% and 100%.<sup>111</sup>

#### Methods to Measure PPB

PPB can be determined with several methods, namely equilibrium dialysis, ultrafiltration, ultracentrifugation, microdialysis, or surface plasmon resonance.<sup>8,113</sup>

*Equilibrium dialysis* is generally accepted as “gold standard”.<sup>114</sup> The principle of this method is a two-chamber system, where one is filled with plasma and the compound of interest and the other is filled with buffer. The chambers are separated by a dialysis membrane which is permeable for free drug but impermeable for plasma proteins due to the molecular weight cut-off of the membrane. When an equilibrium of the free- and bound state is reached, samples are drawn from both chambers and analyzed. For determining the unbound fraction in the plasma, the concentration measured in the chamber containing buffer is divided by the concentration in the plasma chamber. High throughput is achieved by transferring this method to a 96-well format.<sup>114</sup>

## 2.3 Liver Passage – Metabolism

When the drug after oral absorption has reached the portal vein, it encounters the first pass metabolism in the liver before reaching circulation and other organs. Enzymes responsible for phase I modifications (hydrolysis, oxidation, or reduction) and phase II conjugations are present in the liver and can lead to the formation of metabolites. Drug-metabolizing enzymes are also found extracellular, e.g. in blood plasma, in membranes, and intracellular, e.g. in mitochondria, organelles as lysosomes, and the cytoplasm.<sup>115</sup> These enzymes support the transformation of the generally lipophilic xenobiotic into more water-soluble compounds exhibiting an improved elimination.<sup>16</sup> Furthermore, involvement of active transporters in the hepatocytes can ensure the enterohepatic circulation pathway.<sup>116</sup>

### 2.3.1 Metabolic Stability

A high metabolic stability is required to achieve drug levels required for the therapeutic effect. In contrast, a fast metabolic cleavage is a prerequisite for a prodrug approach.<sup>10</sup> Next to metabolic activity in the gut<sup>117</sup> and in the plasma<sup>118</sup>, the liver is the main organ with high expression levels of metabolic enzymes.<sup>41</sup> CYP450 as the most important enzyme superfamily in phase I drug metabolism catalyze mono-oxygenase reactions.<sup>119</sup> In addition, esterases as carboxylesterases CE1 and in lower amounts CE2 are involved in the metabolic cleavage of esters in the liver. In addition, CE2 is expressed also in the intestines.<sup>120,121</sup> CE1 and CE2 exhibit different substrate specificity, with CE1 is mainly hydrolyzing substrates with a small alcohol group and large acyl group and CE2 is recognizing substrates with large alcohol and small acyl groups.<sup>121</sup> In the case of an ester prodrug approach, cleavage with the CE2 in the gut would oppose permeation into the portal vein. However, cleavage into the active principle in the liver with CE1 is a necessity to regain activity.<sup>10,117</sup>

Phase II conjugations are mediated by uridine 5`-diphospho (UDP)-glucuronosyltransferases forming glucuronide metabolites,<sup>122</sup> by sulfotransferases forming sulfate metabolites,<sup>123</sup> and by glutathione-S-transferases forming glutathione metabolites.<sup>124</sup> These metabolites can be inactive, active or even have toxic effects.<sup>125</sup>

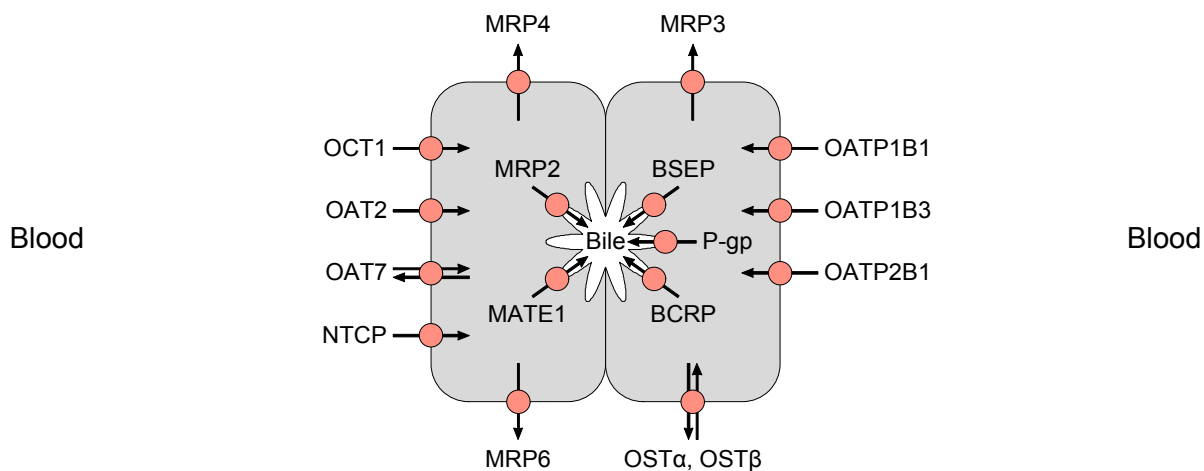
### Methods to Measure Metabolic Stability

Several *in silico* tools have been developed for predicting biotransformation mediated by CYP450. The interest is not only focused on substrate specificity, but also on the inhibition and induction potential to predict drug-drug interactions.<sup>126</sup> The most common metabolic stability studies *in vitro* are conducted with liver microsomes (mouse, rat, or human), S9 fraction, hepatocytes, liver slices, or plasma.<sup>8,113,127</sup>

*Liver microsomes* are the most common way to evaluate metabolic stability *in vitro*.<sup>77,128</sup> They contain the metabolizing enzymes that are bound to the endoplasmic reticulum, e.g. the CYP450 oxidizing enzymes, the carboxylesterases superfamily, or phase II conjugating enzymes as the UDP-glucuronosyltransferases.<sup>15</sup> Co-factors such as nicotinamide adenine dinucleotide phosphate (NADPH) or uridine 5'-diphospho-glucuronic acid (UDPGA) need to be added for the assessment of CYP-mediated monooxygenation or glucuronidation, respectively.<sup>122,129</sup> To test metabolic stability, a test compound is added to a buffered aqueous solution containing microsomes. By adding the respective co-factor the reaction is started. Samples are then drawn at specific time points to determine the remaining parent compound. The metabolic stability is usually reported as metabolic half-life ( $t_{1/2}$ ) or intrinsic clearance ( $CL'_{int}$ ).<sup>129</sup> In addition, to relate the instability to specific enzymes, inhibitors can be applied. Liver microsomes are also used for screening of drug-drug interactions, especially for CYP450 interactions.<sup>130,131</sup>

### 2.3.2 Enterohepatic Circulation

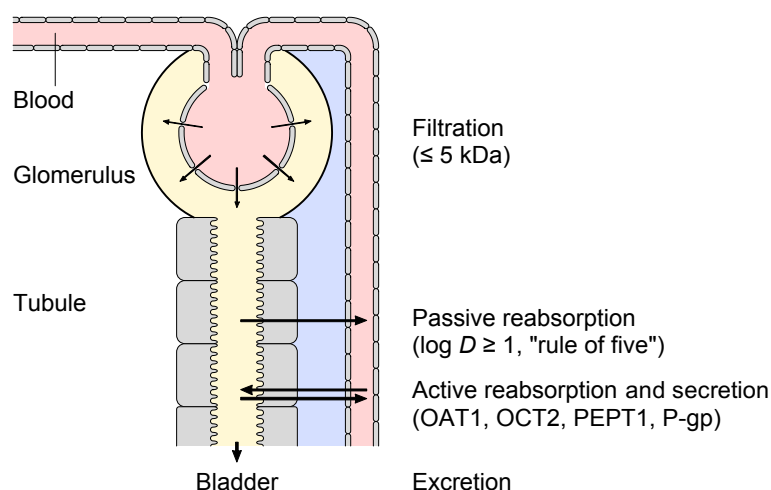
The enterohepatic circulation is initiated by the intestinal uptake into the portal vein, passive or active transport into hepatocytes, further transport into the gall bladder and finally intestinal reabsorption back to the duodenum, where the drug can be reabsorbed into the portal vein by the same mechanism by which bile salts are recycled.<sup>116,132</sup> Enterohepatic recycling can result in multiple plasma concentration peaks, longer apparent half-life in a plasma concentration-time profile, and therefore may prolong the pharmacological effect of a drug,<sup>116</sup> as e.g. for indomethacin<sup>133</sup> and ezetimibe<sup>134</sup>. Figure 2.10 illustrates the carrier-mediated transporters involved in the enterohepatic circulation. OATP are involved in the transport into the liver, whereas efflux transporter, e.g. P-gp and Breast Cancer Resistance Protein (BCRP) are involved in the transport into the bile.<sup>82</sup> Finally, the drug can be reabsorbed from the gall bladder via the sphincter of Oddi back into the intestine.<sup>116</sup> Nevertheless, active transporters such as the multiple resistance-associated proteins (MRP) 3, 4, and 6 can transport the drug in the hepatocytes back into the blood.<sup>82</sup>



**Figure 2.10.** Human hepatocyte cells with its uptake transporters in the basolateral (sinusoidal) membrane including sodium/taurocholate co-transporting peptide (NTCP; SLC10A1), three members of the OATP family (OATP1B1; SLCO1B1, OATP1B3; SLCO1B3, and OATP2B1; SLCO2B1), two members of the organic anion transporter family (OAT2; SLC22A7 and OAT7; SLC22A9), and OCT1. Efflux pumps in the hepatocyte basolateral membrane include three members of the MRP family (MRP3; ABCC3, MRP4; ABCC4, and MRP6; ABCC6). Apical (canalicular) efflux pumps of the hepatocyte comprise P-gp, bile-salt export pump (BSEP or SPGP; ABCB11), BCRP, and MRP2. In addition, multidrug and toxin extrusion protein 1 (MATE1; SLC47A1) is located in the apical hepatocyte membrane. Figure modified from Ref.<sup>82</sup> and pictured by Benz Hubler.

## 2.4 Kidney – Renal Elimination

Finally, a drug, which is absorbed in the intestine and is stable in the plasma and in the liver, will be eliminated either through the bile or the kidney. Hydrophilic and polar drugs are predominantly excreted renally and lipophilic apolar drugs, which are not prone to bioconversion, prefer the hepatobiliary route.<sup>135,136</sup> For FimH antagonists to reach their target in the bladder, renal elimination is of major importance. Next to the secretion of toxins into the urine, the kidney's functions are reabsorption of glucose, amino acids, salts and other nutrients. The physiological units of the kidney are the approx. 1 million nephrons, each consisting of a glomerulus, and the renal tubules, which are formed by the proximal tubule, the loop of Henle, and the distal tubule.<sup>137</sup> The rate of renal excretion depends on the rate of glomerular filtration and the propensity to tubular secretion and reabsorption of a drug (Figure 2.11).<sup>136</sup>



**Figure 2.11.** Renal excretion including glomerular filtration, tubular reabsorption and tubular secretion. Pictured by Benz Hubler.

The glomerular filtration is size and charge dependent. Size restriction starts with molecular weights larger than approx. 5 kDa and is complete for molecules with the size of serum albumin (>68 kDa).<sup>138,139</sup> Therefore, only unbound drugs are expected to undergo glomerular filtration.<sup>140</sup> Once the proximal tubuli is reached, lipophilic compounds will mainly be passively reabsorbed back into circulation, due to the high concentration gradient created by water reuptake throughout the whole tubule.<sup>11,135,141</sup> Furthermore, compounds can be secreted into the tubuli by active transporter systems.<sup>136</sup> Approximately 32% of the top 200 prescribed drugs in 2010 undergo renal elimination (i.e. ≥ 25% of their absorbed dose is excreted unchanged in the urine). 92% thereof exceed their filtration clearances and showed net secretion.<sup>142</sup>

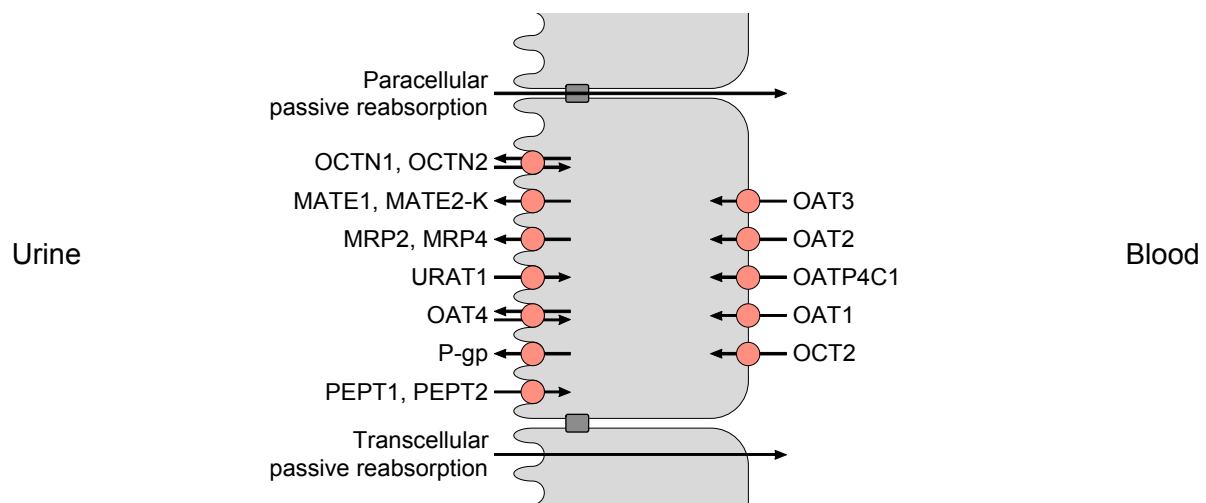


Together with drug-metabolizing enzymes, transporters in the liver and predominantly in the proximal tubule<sup>142</sup> are the major determinants of both hepatic and renal drug elimination.

### 2.4.1 Renal Secretion and Reabsorption

Renal reabsorption mainly depends on passive permeability and is influenced by urine flow and pH. Lipophilicity ( $\log D$ ) is a key determinant for tubular reabsorption and renal elimination is correlated with increasing lipophilicity.<sup>11,135,143</sup> In contrast, hydrophilic and charged compounds are poorly reabsorbed and thus rapidly renally eliminated, leading to high initial levels in the urine.<sup>136</sup> For active secretion into the urine (without additional possible passive permeation) at least two carrier-mediated transporters are needed, one at the basolateral membrane for drug transport from the blood into the cell and one on the apical membrane for drug transport into the urine.<sup>136</sup> Figure 2.12 illustrates the different important transporters involved in the secretion and reabsorption process in the proximal tubulus cells. Due to transport against the electrochemical gradient, secretion is mainly controlled by active transporters of SLC and ABC superfamilies.

Transporter located on the basolateral (urine) side as organic anion transporter 1 (OAT1) and organic cation transporter 2 (OCT2) are mainly contributing to the secretion. Other transporters that facilitate secretion or hinder reabsorption into the blood are efflux transporters, e.g. P-gp and the multidrug resistant proteins MRP2 and MRP4.<sup>82</sup>



**Figure 2.12.** Kidney proximal tubuli cells with its transporters in the apical (luminal) membrane including OAT4 (SLC22A11), urate transporter 1 (URAT1; SLC22A12), PEPT1, PEPT2 (SLC15A2), MRP2, MRP4, MATE1, MATE2-K (SLC47A2), P-gp, organic cation/ergothioneine transporter (OCTN1; SLC22A4), and organic cation/carnitine transporter (OCTN2; SLC22A5). Basolateral uptake transporters in proximal tubule epithelia include OATP4C1 (SLCO4C1), OCT2, OAT1, OAT2 and OAT3 (SLC22A8). Figure modified from Ref.<sup>82</sup> and pictured by Benz Hubler.

## 2.5 References

1. Masaoka, Y.; Tanaka, Y.; Kataoka, M.; Sakuma, S.; Yamashita, S. Site of drug absorption after oral administration: assessment of membrane permeability and luminal concentration of drugs in each segment of gastrointestinal tract. *Eur. J. Pharm. Sci.* **2006**, *29*, 240-50.
2. Krishnaiah, Y.S.R. Pharmaceutical Technologies for Enhancing Oral Bioavailability of Poorly Soluble Drugs. *J. Bioequiv. Bioavail.* **2010**, *2*, 28-36.
3. Guidance for industry, bioavailability and bioequivalence studies for orally administered drug products - general considerations. U.S. Department of Health and Human Services, Food and Drug Administration, Center for Drug Evaluation and Research (CDER). In 2003.
4. Chen, M. L.; Shah, V.; Patnaik, R.; Adams, W.; Hussain, A.; Conner, D.; Mehta, M.; Malinowski, H.; Lazor, J.; Huang, S. M.; Hare, D.; Lesko, L.; Sporn, D.; Williams, R. Bioavailability and bioequivalence: an FDA regulatory overview. *Pharm. Res.* **2001**, *18*, 1645-50.
5. Hamman, J. H.; Demana, P. H.; Olivier, E. I. Targeting receptors, transporters and site of absorption to improve oral drug delivery. *Drug Target Insights* **2007**, *2*, 71-81.
6. Kerns, E. H.; Di, L. Pharmaceutical profiling in drug discovery. *Drug Discov. Today* **2003**, *8*, 316-323.
7. Kola, I.; Landis, J. Can the pharmaceutical industry reduce attrition rates? *Nat. Rev. Drug Discov.* **2004**, *3*, 711-5.
8. Ruiz-Garcia, A.; Bermejo, M.; Moss, A.; Casabo, V. G. Pharmacokinetics in drug discovery. *J. Pharm. Sci.* **2008**, *97*, 654-690.
9. Hodgson, J. ADMET--turning chemicals into drugs. *Nat. Biotechnol.* **2001**, *19*, 722-6.
10. Rautio, J.; Kumpulainen, H.; Heimbach, T.; Oliyai, R.; Oh, D.; Jarvinen, T.; Savolainen, J. Prodrugs: design and clinical applications. *Nat. Rev. Drug Discov.* **2008**, *7*, 255-70.
11. van de Waterbeemd, H.; Smith, D. A.; Beaumont, K.; Walker, D. K. Property-based design: Optimization of drug absorption and pharmacokinetics. *J. Med. Chem.* **2001**, *44*, 1313-1333.
12. Burton, P. S. Predicting Drug Absorption: How Nature Made It a Difficult Problem. *J. Pharmacol. Exp. Therap.* **2002**, *303*, 889-895.
13. Lipinski, C. A.; Lombardo, F.; Dominy, B. W.; Feeney, P. J. Experimental and computational approaches to estimate solubility and permeability in drug discovery and development settings. *Adv. Drug Deliv. Rev.* **1997**, *23*, 3-25.
14. Veber, D. F.; Johnson, S. R.; Cheng, H. Y.; Smith, B. R.; Ward, K. W.; Kopple, K. D. Molecular properties that influence the oral bioavailability of drug candidates. *J. Med. Chem.* **2002**, *45*, 2615-23.
15. Kerns, E., H.; Di, L. *Drug-like Properties: Concepts, Structure Design and Methods, from ADME to Toxicity Optimization*. 1st ed.; Elsevier: London, 2008; p 526.
16. Hu, M.; Li, X. *Oral bioavailability : basic principles, advanced concepts, and applications*. John Wiley & Sons: Hoboken, N.J., 2011; p xvii, 540 p.
17. Lipinski, C. A. Drug-like properties and the causes of poor solubility and poor permeability. *J. Pharmacol. Toxicolog. Methods* **2000**, *44*, 235-249.
18. Avdeef, A. *Absorption and drug development : solubility, permeability, and charge state*. 2nd ed.; John Wiley & Sons: Hoboken, N.J., 2012; p xli, 698 p.
19. Welling, P. G. Effects of food on drug absorption. *Annu. Rev. Nutr.* **1996**, *16*, 383-415.
20. Schmidt, L. E.; Dalhoff, K. Food-drug interactions. *Drugs* **2002**, *62*, 1481-502.
21. Drabant, S.; Nemes, K. B.; Horvath, V.; Tolokan, A.; Grezal, G.; Anttila, M.; Gachalyi, B.; Kanerva, H.; Al-Behaisi, S.; Horvai, G.; Klebovich, I. Influence of food on the oral bioavailability of deramciclane from film-coated tablet in healthy male volunteers. *Eur J. Pharm. Biopharm.* **2004**, *58*, 689-95.
22. Rolan, P. E.; Mercer, A. J.; Weatherley, B. C.; Holdich, T.; Meire, H.; Peck, R. W.; Ridout, G.; Posner, J. Examination of some factors responsible for a food-induced increase in absorption of atovaquone. *Br. J. Clin. Pharmacol.* **1994**, *37*, 13-20.
23. Humberstone, A. J.; Porter, C. J.; Charman, W. N. A physicochemical basis for the effect of food on the absolute oral bioavailability of halofantrine. *J. Pharm. Sci.* **1996**, *85*, 525-9.
24. Dressman, J. B.; Amidon, G. L.; Reppas, C.; Shah, V. P. Dissolution testing as a prognostic tool for oral drug absorption: immediate release dosage forms. *Pharm. Res.* **1998**, *15*, 11-22.

25. Wilson, J. P. Surface area of the small intestine in man. *Gut* **1967**, *8*, 618-21.
26. Shen, D. D.; Kunze, K. L.; Thummel, K. E. Enzyme-catalyzed processes of first-pass hepatic and intestinal drug extraction. *Adv. Drug Deliv. Rev.* **1997**, *27*, 99-127.
27. Yu, J.; Carrier, R. L.; March, J. C.; Griffith, L. G. Three dimensional human small intestine models for ADME-Tox studies. *Drug Discov. Today* **2014**, *19*, 1587-94.
28. Paine, M. F.; Hart, H. L.; Ludington, S. S.; Haining, R. L.; Rettie, A. E.; Zeldin, D. C. The human intestinal cytochrome P450 "pie". *Drug Metab. Dispos.* **2006**, *34*, 880-6.
29. Whitcomb, D. C.; Lowe, M. E. Human Pancreatic Digestive Enzymes. In 2007; Vol. 52, pp 1-17.
30. Satoh, T.; Taylor, P.; Bosron, W. F.; Sanghani, S. P.; Hosokawa, M.; La Du, B. N. Current progress on esterases: from molecular structure to function. *Drug Metab. Dispos.* **2002**, *30*, 488-93.
31. Harris, H. The human alkaline phosphatases: what we know and what we don't know. *Clin. Chim. Acta* **1990**, *186*, 133-50.
32. Lalles, J. P. Intestinal alkaline phosphatase: multiple biological roles in maintenance of intestinal homeostasis and modulation by diet. *Nutr. Rev.* **2010**, *68*, 323-32.
33. Benet, L. Z.; Wu, C. Y.; Hebert, M. F.; Wachter, V. J. Intestinal drug metabolism and antitransport processes: A potential paradigm shift in oral drug delivery. *J. Contr. Rel.* **1996**, *39*, 139-143.
34. Sharom, F. J. The P-glycoprotein multidrug transporter. *Essays in Biochem.* **2011**, *50*, 161-178.
35. Suzuki, H.; Sugiyama, Y. Role of metabolic enzymes and efflux transporters in the absorption of drugs from the small intestine. *Eur. J. Pharm. Sci.* **2000**, *12*, 3-12.
36. Di, L.; Kerns, E. H.; Carter, G. T. Drug-Like Property Concepts in Pharmaceutical Design. *Curr. Pharm. Design* **2009**, *15*, 2184-2194.
37. Dressman, J. B.; Thelen, K.; Jantratid, E. Towards quantitative prediction of oral drug absorption. *Clin. Pharmacokinet.* **2008**, *47*, 655-67.
38. Takano, R.; Sugano, K.; Higashida, A.; Hayashi, Y.; Machida, M.; Aso, Y.; Yamashita, S. Oral absorption of poorly water-soluble drugs: computer simulation of fraction absorbed in humans from a miniscale dissolution test. *Pharm. Res.* **2006**, *23*, 1144-1156.
39. Jantratid, E.; Janssen, N.; Reppas, C.; Dressman, J. B. Dissolution media simulating conditions in the proximal human gastrointestinal tract: an update. *Pharm. Res.* **2008**, *25*, 1663-76.
40. Bergstrom, C. A.; Holm, R.; Jorgensen, S. A.; Andersson, S. B.; Artursson, P.; Beato, S.; Borde, A.; Box, K.; Brewster, M.; Dressman, J.; Feng, K. I.; Halbert, G.; Kostewicz, E.; McAllister, M.; Muenster, U.; Thinnis, J.; Taylor, R.; Mullertz, A. Early pharmaceutical profiling to predict oral drug absorption: Current status and unmet needs. *Eur. J. Pharm. Sci.* **2013**, *57*, 173-199.
41. Lin, J. H.; Chiba, M.; Baillie, T. A. Is the role of the small intestine in first-pass metabolism overemphasized? *Pharmacol. Rev.* **1999**, *51*, 135-58.
42. Waterbeemd, H. v. d.; Lennernäs, H.; Artursson, P. *Drug bioavailability : estimation of solubility, permeability, absorption, and bioavailability*. Wiley-VCH: Weinheim, 2003; p xxiv, 579 p.
43. van Herwaarden, A. E.; van Waterschoot, R. A. B.; Schinkel, A. H. How important is intestinal cytochrome P450 3A metabolism? *Trends in Pharma. Sci.* **2009**, *30*, 223-227.
44. Heimbach, T.; Oh, D. M.; Li, L. Y.; Forsberg, M.; Savolainen, J.; Leppanen, J.; Matsunaga, Y.; Flynn, G.; Fleisher, D. Absorption rate limit considerations for oral phosphate prodrugs. *Pharm. Res.* **2003**, *20*, 848-56.
45. Pinto, M.; Robineleon, S.; Appay, M. D.; Kedinger, M.; Triadou, N.; Dussaulx, E.; Lacroix, B.; Simonassmann, P.; Haffen, K.; Fogh, J.; Zweibaum, A. Enterocyte-Like Differentiation and Polarization of the Human-Colon Carcinoma Cell-Line Caco-2 in Culture. *Biol. of the Cell* **1983**, *47*, 323-330.
46. Shin, J. M.; Cho, Y. M.; Sachs, G. Chemistry of covalent inhibition of the gastric (H<sup>+</sup>, K<sup>+</sup>)-ATPase by proton pump inhibitors. *J. Am. Chem. Soc.* **2004**, *126*, 7800-11.
47. Lindberg, P.; Brandstrom, A.; Wallmark, B.; Mattsson, H.; Rikner, L.; Hoffmann, K. J. Omeprazole: the first proton pump inhibitor. *Med. Res. Rev.* **1990**, *10*, 1-54.
48. Jain, N.; Yalkowsky, S. H. Estimation of the aqueous solubility I: application to organic nonelectrolytes. *J. Pharm. Sci.* **2001**, *90*, 234-52.
49. Di, L.; Kerns, E. H. Biological assay challenges from compound solubility: strategies for bioassay optimization. *Drug Discov. Today* **2006**, *11*, 446-51.

50. Kerns, E. H.; Di, L. Physicochemical profiling: overview of the screens. *Drug Discov. Today Technol.* **2004**, *1*, 343-8.
51. Bezencon, J.; Wittwer, M. B.; Cutting, B.; Smiesko, M.; Wagner, B.; Kansy, M.; Ernst, B. pKa determination by (1)H NMR spectroscopy - an old methodology revisited. *J. Pharm. Biomed. Anal.* **2014**, *93*, 147-55.
52. Alsenz, J.; Kansy, M. High throughput solubility measurement in drug discovery and development. *Adv. Drug Deliv. Rev.* **2007**, *59*, 546-67.
53. Saal, C.; Petereit, A. C. Optimizing solubility: kinetic versus thermodynamic solubility temptations and risks. *Eur. J. Pharm. Sci.* **2012**, *47*, 589-95.
54. Hedrich, H. J.; Bullock, G. R. *The laboratory mouse*. Elsevier Academic Press: Amsterdam ; Boston, 2004; p xvi, 600 p.
55. Woodard, G. *Methods of Animals Experimentation*. Academic Press: New York, 1965; Vol. 1.
56. Curatolo, W. Physical chemical properties of oral drug candidates in the discovery and exploratory development settings. *Pharm. Sci. Technol. Today* **1998**, *1*, 387-393.
57. Majumdar, S.; Mitra, A. K. Chemical modification and formulation approaches to elevated drug transport across cell membranes. *Expert Opin. Drug Deliv.* **2006**, *3*, 511-27.
58. Ishikawa, M.; Hashimoto, Y. Improvement in aqueous solubility in small molecule drug discovery programs by disruption of molecular planarity and symmetry. *J. Med. Chem.* **2011**, *54*, 1539-54.
59. Pouton, C. W. Formulation of poorly water-soluble drugs for oral administration: physicochemical and physiological issues and the lipid formulation classification system. *Eur. J. Pharm. Sci.* **2006**, *29*, 278-87.
60. Gomez-Orellana, I. Strategies to improve oral drug bioavailability. *Expert Opin. Drug Deliv.* **2005**, *2*, 419-33.
61. Li, P.; Zhao, L. Developing early formulations: practice and perspective. *Int. J. Pharm.* **2007**, *341*, 1-19.
62. Savjani, K. T.; Gajjar, A. K.; Savjani, J. K. Drug solubility: importance and enhancement techniques. *ISRN pharmaceuticals* **2012**, *2012*, 1-10.
63. Cornaire, G.; Woodley, J.; Hermann, P.; Cloarec, A.; Arellano, C.; Houin, G. Impact of excipients on the absorption of P-glycoprotein substrates in vitro and in vivo. *Int. J. Pharm.* **2004**, *278*, 119-31.
64. Katneni, K.; Charman, S. A.; Porter, C. J. Impact of cremophor-EL and polysorbate-80 on digoxin permeability across rat jejunum: delineation of thermodynamic and transporter related events using the reciprocal permeability approach. *J. Pharm. Sci.* **2007**, *96*, 280-93.
65. Yamagata, T.; Kusuvara, H.; Morishita, M.; Takayama, K.; Benameur, H.; Sugiyama, Y. Improvement of the oral drug absorption of topotecan through the inhibition of intestinal xenobiotic efflux transporter, breast cancer resistance protein, by excipients. *Drug Metab. Dispos.* **2007**, *35*, 1142-8.
66. Nerurkar, M. M.; Burton, P. S.; Borchardt, R. T. The use of surfactants to enhance the permeability of peptides through Caco-2 cells by inhibition of an apically polarized efflux system. *Pharm. Res.* **1996**, *13*, 528-34.
67. Dahan, A.; Miller, J. M.; Hoffman, A.; Amidon, G. E.; Amidon, G. L. The solubility-permeability interplay in using cyclodextrins as pharmaceutical solubilizers: mechanistic modeling and application to progesterone. *J. Pharm. Sci.* **2010**, *99*, 2739-49.
68. Fagerholm, U. The role of permeability in drug ADME/PK, interactions and toxicity--presentation of a permeability-based classification system (PCS) for prediction of ADME/PK in humans. *Pharm. Res.* **2008**, *25*, 625-38.
69. Sugano, K.; Kansy, M.; Artursson, P.; Avdeef, A.; Bendels, S.; Di, L.; Ecker, G. F.; Faller, B.; Fischer, H.; Gerebtzoff, G.; Lennernaes, H.; Senner, F. Coexistence of passive and carrier-mediated processes in drug transport. *Nat. Rev. Drug Discov.* **2010**, *9*, 597-614.
70. Boegh, M.; Nielsen, H. M. Mucus as a Barrier to Drug Delivery - Understanding and Mimicking the Barrier Properties. *Basic Clin. Pharmacol. Toxicol.* **2014**.
71. Kerns, E. H. High throughput physicochemical profiling for drug discovery. *J. Pharm. Sci.* **2001**, *90*, 1838-58.
72. Waring, M. J. Lipophilicity in drug discovery. *Expert Opin. Drug Discov.* **2010**, *5*, 235-48.
73. Guimaraes, C. R.; Mathiowetz, A. M.; Shalaeva, M.; Goetz, G.; Liras, S. Use of 3D properties to characterize beyond rule-of-5 property space for passive permeation. *J. Chem. Inf. Model.* **2012**, *52*, 882-90.

74. Valko, K.; Nunhuck, S.; Bevan, C.; Abraham, M. H.; Reynolds, D. P. Fast gradient HPLC method to determine compounds binding to human serum albumin. Relationships with octanol/water and immobilized artificial membrane lipophilicity. *J. Pharm. Sci.* **2003**, *92*, 2236-48.
75. Lewis, D. F.; Dickins, M. Baseline lipophilicity relationships in human cytochromes P450 associated with drug metabolism. *Drug Metab. Rev.* **2003**, *35*, 1-18.
76. Johnson, T. W.; Dress, K. R.; Edwards, M. Using the Golden Triangle to optimize clearance and oral absorption. *Bioorg. Med. Chem. Lett.* **2009**, *19*, 5560-4.
77. Nassar, A. E.; Kamel, A. M.; Clarimont, C. Improving the decision-making process in the structural modification of drug candidates: enhancing metabolic stability. *Drug Discov. Today* **2004**, *9*, 1020-8.
78. Mannhold, R.; van de Waterbeemd, H. Substructure and whole molecule approaches for calculating log P. *J. Comput. Aided Mol. Des.* **2001**, *15*, 337-54.
79. Moriguchi, I.; Hirono, S.; Liu, Q.; Nakagome, I.; Matsushita, Y. Simple Method of Calculating Octanol Water Partition-Coefficient. *Chemical & Pharmaceutical Bulletin* **1992**, *40*, 127-130.
80. Dearden, J. C.; Bresnen, G. M. The Measurement of Partition-Coefficients. *Quant. Structure-Activity Relationships* **1988**, *7*, 133-144.
81. Goodman, L. S.; Brunton, L. L.; Chabner, B.; Knollmann, B. r. C. *Goodman & Gilman's pharmacological basis of therapeutics*. 12th ed.; McGraw-Hill: New York, 2011; p 2084
82. Giacomini, K. M.; Huang, S.-M.; Tweedie, D. J.; Benet, L. Z.; Brouwer, K. L. R.; Chu, X.; Dahlin, A.; Evers, R.; Fischer, V.; Hillgren, K. M.; Hoffmaster, K. A.; Ishikawa, T.; Keppler, D.; Kim, R. B.; Lee, C. A.; Niemi, M.; Polli, J. W.; Sugiyama, Y.; Swaan, P. W.; Ware, J. A.; Wright, S. H.; Yee, S. W.; Zamek-Gliszczynski, M. J.; Zhang, L.; International, T. Membrane transporters in drug development. *Nat. Rev. Drug Discov.* **2010**, *9*, 215-236.
83. Varma, M. V.; Rotter, C. J.; Chupka, J.; Whalen, K. M.; Duignan, D. B.; Feng, B.; Litchfield, J.; Goosen, T. C.; El-Kattan, A. F. pH-sensitive interaction of HMG-CoA reductase inhibitors (statins) with organic anion transporting polypeptide 2B1. *Mol. Pharm.* **2011**, *8*, 1303-13.
84. Grube, M.; Kock, K.; Oswald, S.; Draber, K.; Meissner, K.; Eckel, L.; Bohm, M.; Felix, S. B.; Vogelgesang, S.; Jedlitschky, G.; Siegmund, W.; Warzok, R.; Kroemer, H. K. Organic anion transporting polypeptide 2B1 is a high-affinity transporter for atorvastatin and is expressed in the human heart. *Clin. Pharmacol. Ther.* **2006**, *80*, 607-20.
85. Kwon, H.; Lionberger, R. A.; Yu, L. X. Impact of P-glycoprotein-mediated intestinal efflux kinetics on oral bioavailability of P-glycoprotein substrates. *Mol. Pharm.* **2004**, *1*, 455-65.
86. Shugarts, S.; Benet, L. Z. The role of transporters in the pharmacokinetics of orally administered drugs. *Pharm. Res.* **2009**, *26*, 2039-54.
87. Artursson, P.; Palm, K.; Luthman, K. Caco-2 monolayers in experimental and theoretical predictions of drug transport. *Adv. Drug Deliv. Rev.* **2001**, *46*, 27-43.
88. Takano, M.; Yumoto, R.; Murakami, T. Expression and function of efflux drug transporters in the intestine. *Pharmacol. Ther.* **2006**, *109*, 137-61.
89. Kansy, M.; Senner, F.; Gubernator, K. Physicochemical high throughput screening: Parallel artificial membrane permeation assay in the description of passive absorption processes. *J. Med. Chem.* **1998**, *41*, 1007-1010.
90. Avdeef, A.; Bendels, S.; Di, L.; Faller, B.; Kansy, M.; Sugano, K.; Yamauchi, Y. PAMPA - Critical factors for better predictions of absorption. *J. Pharm. Sci.* **2007**, *96*, 2893-2909.
91. Hubatsch, I.; Ragnarsson, E. G. E.; Artursson, P. Determination of drug permeability and prediction of drug absorption in Caco-2 monolayers. *Nat. prot.* **2007**, *2*, 2111-2119.
92. Artursson, P.; Karlsson, J. Correlation between oral drug absorption in humans and apparent drug permeability coefficients in human intestinal epithelial (Caco-2) cells. *Biochem. Biophys. Res. Commun.* **1991**, *175*, 880-5.
93. Press, B.; Di Grandi, D. Permeability for intestinal absorption: Caco-2 assay and related issues. *Curr. Drug Metab.* **2008**, *9*, 893-900.
94. Volpe, D. A. Drug-permeability and transporter assays in Caco-2 and MDCK cell lines. *Future Med. Chem.* **2011**, *3*, 2063-77.

95. Rubas, W.; Cromwell, M. E.; Shahrokh, Z.; Villagran, J.; Nguyen, T. N.; Wellton, M.; Nguyen, T. H.; Mrsny, R. J. Flux measurements across Caco-2 monolayers may predict transport in human large intestinal tissue. *J. Pharm. Sci.* **1996**, *85*, 165-9.
96. Barthe, L.; Woodley, J.; Houin, G. Gastrointestinal absorption of drugs: methods and studies. *Fundam. Clin. Pharmacol.* **1999**, *13*, 154-68.
97. Hayeshi, R.; Hilgendorf, C.; Artursson, P.; Augustijns, P.; Brodin, B.; Dehertogh, P.; Fisher, K.; Fossati, L.; Hovenkamp, E.; Korjamo, T.; Masungi, C.; Maubon, N.; Mols, R.; Mullertz, A.; Monkkonen, J.; O'Driscoll, C.; Oppers-Tiemissen, H. M.; Ragnarsson, E. G.; Rooseboom, M.; Ungell, A. L. Comparison of drug transporter gene expression and functionality in Caco-2 cells from 10 different laboratories. *Eur. J. Pharm. Sci.* **2008**, *35*, 383-96.
98. Hilgendorf, C.; Ahlin, G.; Seithel, A.; Artursson, P.; Ungell, A. L.; Karlsson, J. Expression of thirty-six drug transporter genes in human intestine, liver, kidney, and organotypic cell lines. *Drug Metab. Dispos.* **2007**, *35*, 1333-40.
99. Gres, M. C.; Julian, B.; Bourrie, M.; Meunier, V.; Roques, C.; Berger, M.; Boulenc, X.; Berger, Y.; Fabre, G. Correlation between oral drug absorption in humans, and apparent drug permeability in TC-7 cells, a human epithelial intestinal cell line: comparison with the parental Caco-2 cell line. *Pharm. Res.* **1998**, *15*, 726-33.
100. Hou, T.; Wang, J.; Zhang, W.; Xu, X. ADME evaluation in drug discovery. 7. Prediction of oral absorption by correlation and classification. *J. Chem. Inf. Model* **2007**, *47*, 208-18.
101. Kim, C. U.; Lew, W.; Williams, M. A.; Liu, H.; Zhang, L.; Swaminathan, S.; Bischofberger, N.; Chen, M. S.; Mendel, D. B.; Tai, C. Y.; Laver, W. G.; Stevens, R. C. Influenza neuraminidase inhibitors possessing a novel hydrophobic interaction in the enzyme active site: design, synthesis, and structural analysis of carbocyclic sialic acid analogues with potent anti-influenza activity. *J. Am. Chem. Soc.* **1997**, *119*, 681-90.
102. Rubio-Aliaga, I.; Daniel, H. Mammalian peptide transporters as targets for drug delivery. *Trends Pharmacol. Sci.* **2002**, *23*, 434-40.
103. Ganapathy, M. E.; Huang, W.; Wang, H.; Ganapathy, V.; Leibach, F. H. Valacyclovir: a substrate for the intestinal and renal peptide transporters PEPT1 and PEPT2. *Biochem Biophys. Res. Commun.* **1998**, *246*, 470-5.
104. Mandagere, A. K.; Thompson, T. N.; Hwang, K. K. Graphical model for estimating oral bioavailability of drugs in humans and other species from their Caco-2 permeability and in vitro liver enzyme metabolic stability rates. *J. Med. Chem.* **2002**, *45*, 304-11.
105. Ward, P. D.; Tippin, T. K.; Thakker, D. R. Enhancing paracellular permeability by modulating epithelial tight junctions. *Pharm. Sci. Technol. Today* **2000**, *3*, 346-358.
106. Smith, D. A.; Di, L.; Kerns, E. H. The effect of plasma protein binding on *in vivo* efficacy: misconceptions in drug discovery. *Nat. Rev. Drug Discov.* **2010**, *9*, 929-39.
107. Trainor, G. L. The importance of plasma protein binding in drug discovery. *Expert Opin. Drug Discov.* **2007**, *2*, 51-64.
108. Benet, L. Z.; Hoener, B. A. Changes in plasma protein binding have little clinical relevance. *Clin. Pharmacol. Ther.* **2002**, *71*, 115-21.
109. Rolan, P. E. Plasma protein binding displacement interactions--why are they still regarded as clinically important? *Br. J. Clin. Pharmacol.* **1994**, *37*, 125-8.
110. Sansom, L. N.; Evans, A. M. What is the true clinical significance of plasma protein binding displacement interactions? *Drug Saf.* **1995**, *12*, 227-33.
111. Zhang, F.; Xue, J.; Shao, J.; Jia, L. Compilation of 222 drugs' plasma protein binding data and guidance for study designs. *Drug Discov. Today* **2012**, *17*, 475-85.
112. Lombardo, F.; Obach, R. S.; Shalaeva, M. Y.; Gao, F. Prediction of volume of distribution values in humans for neutral and basic drugs using physicochemical measurements and plasma protein binding data. *J. Med. Chem.* **2002**, *45*, 2867-76.
113. Singh, S. S.; Mehta, J. Measurement of drug-protein binding by immobilized human serum albumin-HPLC and comparison with ultrafiltration. *J. Chromatogr. B Analyt. Technol. Biomed. Life Sci.* **2006**, *834*, 108-16.
114. Kariv, I.; Cao, H.; Oldenburg, K. R. Development of a high throughput equilibrium dialysis method. *J. Pharm. Sci.* **2001**, *90*, 580-87.

115. Testa, B.; Krämer, S. D. *The biochemistry of drug metabolism : principles, redox reactions, hydrolyses*. Wiley-VCH: Weinheim ; Chichester, 2008; p xiii, 319 p.
116. Roberts, M. S.; Magnusson, B. M.; Burczynski, F. J.; Weiss, M. Enterohepatic circulation: physiological, pharmacokinetic and clinical implications. *Clin. Pharmacokinet.* **2002**, *41*, 751-90.
117. Doherty, M. M.; Charman, W. N. The mucosa of the small intestine: how clinically relevant as an organ of drug metabolism? *Clin. Pharmacokinet.* **2002**, *41*, 235-53.
118. Li, B.; Sedlacek, M.; Manoharan, I.; Boopathy, R.; Duysen, E. G.; Masson, P.; Lockridge, O. Butyrylcholinesterase, paraoxonase, and albumin esterase, but not carboxylesterase, are present in human plasma. *Biochem. Pharmacol.* **2005**, *70*, 1673-84.
119. Guengerich, F. P. Cytochrome P450s and other enzymes in drug metabolism and toxicity. *AAPS J* **2006**, *8*, E101-11.
120. Testa, B.; Krämer, S. D. *The biochemistry of drug metabolism : conjugations, consequences of metabolism, influencing factors*. Wiley-VCH: Weinheim ; Chichester, 2010; p xiii, 588 p.
121. Imai, T. Human carboxylesterase isozymes: catalytic properties and rational drug design. *Drug Metab. Pharmacokinet.* **2006**, *21*, 173-185.
122. Kilford, P. J.; Stringer, R.; Sohal, B.; Houston, J. B.; Galetin, A. Prediction of drug clearance by glucuronidation from in vitro data: use of combined cytochrome P450 and UDP-glucuronosyltransferase cofactors in alamethicin-activated human liver microsomes. *Drug Metab. Dispos.* **2009**, *37*, 82-9.
123. Gamage, N.; Barnett, A.; Hempel, N.; Duggleby, R. G.; Windmill, K. F.; Martin, J. L.; McManus, M. E. Human sulfotransferases and their role in chemical metabolism. *Toxicol. Sci.* **2006**, *90*, 5-22.
124. de Waziers, I.; Cugnenc, P. H.; Yang, C. S.; Leroux, J. P.; Beaune, P. H. Cytochrome P 450 isoenzymes, epoxide hydrolase and glutathione transferases in rat and human hepatic and extrahepatic tissues. *J. Pharmacol. Exp. Ther.* **1990**, *253*, 387-94.
125. Drayer, D. E. Pharmacologically active drug metabolites: therapeutic and toxic activities, plasma and urine data in man, accumulation in renal failure. *Clin. Pharmacokinet.* **1976**, *1*, 426-43.
126. Crivori, P.; Poggesi, I. Computational approaches for predicting CYP-related metabolism properties in the screening of new drugs. *Eur. J. Med. Chem.* **2006**, *41*, 795-808.
127. Di, L.; Kerns, E. H.; Hong, Y.; Chen, H. Development and application of high throughput plasma stability assay for drug discovery. *Int. J. Pharm.* **2005**, *297*, 110-9.
128. Li, A. P. Screening for human ADME/Tox drug properties in drug discovery. *Drug Discov. Today* **2001**, *6*, 357-366.
129. Obach, R. S. Prediction of human clearance of twenty-nine drugs from hepatic microsomal intrinsic clearance data: An examination of in vitro half-life approach and nonspecific binding to microsomes. *Drug Metab. Dispos.* **1999**, *27*, 1350-9.
130. Rodrigues, A. D.; Lin, J. H. Screening of drug candidates for their drug--drug interaction potential. *Curr. Opin. Chem. Biol.* **2001**, *5*, 396-401.
131. Spaggiari, D.; Geiser, L.; Daali, Y.; Rudaz, S. Phenotyping of CYP450 in human liver microsomes using the cocktail approach. *Anal. Bioanal. Chem.* **2014**, *406*, 4875-87.
132. Sievanen, E. Exploitation of bile acid transport systems in prodrug design. *Molecules* **2007**, *12*, 1859-89.
133. Kwan, K. C.; Breault, G. O.; Umbenhauer, E. R.; McMahon, F. G.; Duggan, D. E. Kinetics of indomethacin absorption, elimination, and enterohepatic circulation in man. *J. Pharmacokinet. Biopharm.* **1976**, *4*, 255-80.
134. Ezzet, F.; Krishna, G.; Wexler, D. B.; Statkevich, P.; Kosoglou, T.; Batra, V. K. A population pharmacokinetic model that describes multiple peaks due to enterohepatic recirculation of ezetimibe. *Clin. Ther.* **2001**, *23*, 871-85.
135. Varma, M. V. S.; Feng, B.; Obach, R. S.; Troutman, M. D.; Chupka, J.; Miller, H. R.; El-Kattan, A. Physicochemical Determinants of Human Renal Clearance. *J. Med. Chem.* **2009**, *52*, 4844-4852.
136. Feng, B.; LaPerle, J. L.; Chang, G.; Varma, M. V. S. Renal clearance in drug discovery and development: molecular descriptors, drug transporters and disease state. *Expert Opin. Drug Metab. Toxicol.* **2010**, *6*, 939-952.
137. Lote, C. J. *Principles of renal physiology*. 5th ed.; Springer: New York, 2012; p xv, 204 p.

138. Chang, R. L.; Ueki, I. F.; Troy, J. L.; Deen, W. M.; Robertson, C. R.; Brenner, B. M. Permeability of the glomerular capillary wall to macromolecules. II. Experimental studies in rats using neutral dextran. *Biophys. J.* **1975**, *15*, 887-906.
139. Tencer, J.; Frick, I. M.; Oquist, B. W.; Alm, P.; Rippe, B. Size-selectivity of the glomerular barrier to high molecular weight proteins: upper size limitations of shunt pathways. *Kidney Int.* **1998**, *53*, 709-15.
140. Schmidt, S.; Gonzalez, D.; Derendorf, H. Significance of protein binding in pharmacokinetics and pharmacodynamics. *J. Pharm. Sci.* **2010**, *99*, 1107-22.
141. Fagerholm, U. Prediction of human pharmacokinetics - renal metabolic and excretion clearance. *J. Pharm. Pharmacol.* **2007**, *59*, 1463-71.
142. Morrissey, K. M.; Stocker, S. L.; Wittwer, M. B.; Xu, L.; Giacomini, K. M. Renal transporters in drug development. *Annu. Rev. Pharmacol. Toxicol.* **2013**, *53*, 503-29.
143. Smith, D. A.; Jones, B. C.; Walker, D. K. Design of drugs involving the concepts and theories of drug metabolism and pharmacokinetics. *Med. Res. Rev.* **1996**, *16*, 243-66.



---

## 3 Materials and Methods – PADMET-Profiling

---

ADME-Tox profiling *in vitro* gained a lot of importance in the last two decades, since in 1991 40% of drug-attribution were due to pharmacokinetic failure.<sup>1</sup> Therefore, during his Ph.D. studies, Matthias Wittwer started in 2007 to establish the PADMET platform (**p**hysico-chemical properties, **a**bsorption, **d**istribution, **m**etabolism, **e**limination, **t**oxicity) for carbohydrate mimetics. Dr. Simon Kleeb and myself continued his work and complemented the platform establishing additional assays. Table 3.1 summarizes the currently available assays on the PADMET platform, supporting the drug discovery programs in the laboratory of Molecular Pharmacy providing information on structural, physicochemical and biochemical properties. Several of the applied methods have already been described in our publications<sup>2-5</sup> and will therefore not be discussed in detail herein.

**Table 3.1.** ADME-Tox assays applied in the PADMET platform.

Properties	Assays	Where to find in this thesis?
<b>Structural properties</b>		
pK <sub>a</sub>	<sup>1</sup> H-NMR spectroscopy <sup>6</sup>	3.1. Paper 1, page 57
<b>Physicochemical properties</b>		
log <i>D</i> <sub>7,4</sub>	Miniaturized shake flask procedure <sup>2, 4, 7, 8</sup>	4.2.2 Paper 2, page 107 4.3.2 Paper 3, page 133 4.3.4 Paper 5, page 189 5.1.1 Paper 6, page 237
Stability	Gastrointestinal fluids <sup>5, 9, 10</sup>	4.3.3 Paper 4, page 153 4.4 Stability of FimH Antagonists, page 217
Solubility	Kinetic <sup>3, 4, 11</sup>	4.3.2 Paper 3, page 133 4.3.4 Paper 5, page 189
	Thermodynamic <sup>2, 5, 11</sup>	4.2.2 Paper 2, page 107 4.3.3 Paper 4, page 153
	Preformulations <sup>12</sup>	3.2 Preformulation Studies, page 67 4.3.1 Approaches to Improve Solubility of FimH Antagonists, page 123
Permeability	Parallel artificial membrane permeability assay (PAMPA) <sup>13</sup>	4.2.2 Paper 2, page 107 4.3.2 Paper 3, page 133
	Caco-2, cell-based permeability assay <sup>14, 15</sup>	4.3.3 Paper 4, page 153 4.3.4 Paper 5, page 189 5.1.1 Paper 6, page 237
<b>Biochemical properties</b>		
Metabolism	Liver microsomes (human, mouse, rat) <sup>16, 17</sup>	4.2.2 Paper 2, page 107
Plasma protein binding	Equilibrium dialysis <sup>18</sup>	4.2.2 Paper 2, page 107
Carrier-mediated Transport	OATP2B1, <sup>19</sup> OATP1B3, OAT1, OCT2	3.3 Carrier-Mediated Transport, page 69 4.2.1 Carrier-Mediated Transport Studies with FimH Antagonists, page 87
<b>Toxicity</b>		
Cell toxicity	MTT-assay <sup>20</sup>	3.4 Cell Toxicity studies, page 73 4.1 Trends to Predict Potential Oral Bioavailability, page 76

## Materials

Polysorbate 80 (Tween 80), Solutol HS 15, Cremophor EL, (2-hydroxypropyl)- $\beta$ -cyclodextrin (HP $\beta$ CD), poly(ethyleneglycol) 400 (PEG400), propylene glycol (PG), dimethyl sulfoxide (DMSO), Dulbecco's modified Eagle's medium (DMEM) high glucose with phenol red, L-glutamine 200 mM, penicillin-streptomycin solution with 10'000 units/ml penicillin and 10 mg/ml streptomycin, Dulbecco's phosphate buffered saline (DPBS), and trypsin-EDTA (1x) solution, thiazolyl blue tetrazolium bromide (MTT), hydrochloric acid  $\geq$  37% (HCl), terfenadine, potassium chloride (KCl), magnesium sulfate (MgSO<sub>4</sub>), potassium phosphate (K<sub>2</sub>HPO<sub>4</sub>), calcium chloride (CaCl<sub>2</sub>), glucose, 2-(4-(2-hydroxyethyl)-1-piperazinyl)-ethansulfonsäure (HEPES), sodium butyrat, blastidicin S hydrochloride, rifampicin, probenecid, atorvastatin, and estrone-3-sulfat (E<sub>3</sub>S) were purchased from Sigma–Aldrich (Sigma-Aldrich, St. Louis, MA, USA). Ethylenediaminetetraacetic acid (EDTA)-Na and Rotiszint were purchased from Carl Roth AG (Karlsruhe, Germany). Tritium-labeled estrone-3-sulfate (E<sub>1</sub>S<sup>+</sup>, specific activity, 40-60 Ci/mmol), [glycyl-2-3H]-4-aminohippuric acid (PAH<sup>+</sup>, 40-60 Ci/mmol), methyl-4-phenyl-pyridinium acetate [3-H] (MPP<sup>+</sup>, specific activity 80-85 Ci/mmol), and estradiol 17 $\beta$ -D-glucoronide [3H] (E<sub>2</sub>G<sup>+</sup>, specific activity 30-60 Ci/mmol) were obtained from Hartmann Analytic (Braunschweig, Germany). Heat inactivated fetal bovine serum (FBS), MEM non-essential amino acids (MEM-NEAA) solution, glutaMAX, G418 (Geneticin), and trypan blue stain 0.4% were ordered from Invitrogen (Carlsbad, CA, USA). Fetal calf serum was obtained from BioConcept AG (Allschwil, BL, Switzerland). Hygromycin B solution was purchased from Roche Diagnostics (Basel, Switzerland). Sodium dodecyl sulfate (SDS) was obtained from Bio-Rad Laboratories Inc. (Hercules, CA, USA). Monopotassium phosphate (KH<sub>2</sub>PO<sub>4</sub>) and sodium hydroxide (NaOH) were bought from Merck (Merck KGaA, Darmstadt, Germany). Tris(hydroxymethyl)aminomethane (TRIS) ultrapure and sodium bicarbonate (NaHCO<sub>3</sub>) were purchased from AppliChem (AppliChem GmbH, Darmstadt, Germany). Sodium chloride (NaCl) was purchased from Hanseler (Hanseler AG, AR, Switzerland). Long-life, heat-treated and homogenized milk (UHTmilk) containing 3.5% fat was bought from Coop (Coop Qualite & Prix). Methanol (MeOH), acetonitrile (MeCN), and dichloromethane (DCM) were obtained from Acros Organics (Geel, Belgium). Testosterone was purchased from P.H. Stehelin & Co (Basel, Switzerland). The FimH antagonists were synthesized in-house.

#### **Cell Lines and Microsomes**

The human epithelial colorectal carcinoma cell line (Caco-2) was kindly provided by Prof. G. Imanidis, FHNW (Muttens, Switzerland) and originated from the American Type Culture Collection ATCC (Rockville, MD, USA). The human hepatoma cell line (HepG2) was purchased from DSMZ (Deutsche Sammlung von Mikroorganismen und Zellkulturen GmbH, Braunschweig, Germany). The wild-type Madin-Darby canine kidney II (MDCK-II) cell line, originally obtained from ATCC, and the established OATP2B1-,<sup>19</sup> OCT2-, and OATP1B3-overexpressing MDCK-II cell lines, HeLa cell line and the OAT1 adenovirus were kindly provided by Prof. H. Meyer zu Schwabedissen, Department of Pharmaceutical Sciences, University of Basel.

#### **LC-MS Detection**

Analyses were performed using an 1100/1200 Series HPLC System coupled to a 6410 Triple Quadrupole mass detector (Agilent Technologies, Inc., Santa Clara, CA, USA) equipped with electrospray ionization. The system was controlled with the Agilent Mass Hunter Workstation Data Acquisition software (version B.01.04 and B.03.01). The column used was an Atlantis<sup>®</sup> T3 C18 column (2.1 x 50 mm) with a 3 µm particle size (Waters Corp., Milford, MA, USA). The mobile phase consisted of two eluents: eluent A (H<sub>2</sub>O, containing 0.1% formic acid, v/v, or ammonium acetate buffer, 10 mM, pH 5, or formiate buffer, 10 mM, pH 3) and eluent B (MeCN, containing 0.1% formic acid, v/v), delivered at 0.6 mL/min. The gradient was ramped from 95% A/5% B to 5% A/95% B over 1 min, and then held at 5% A/95% B for 0.1 min. The system was then brought back to 95% A/5% B, resulting in a total duration of 4 min. MS parameters such as fragmentor voltage, collision energy, polarity were optimized individually for each analyte, and the molecular ion was followed for each compound in the multiple reaction monitoring mode. The concentrations of the analytes were quantified by the Agilent Mass Hunter Quantitative Analysis software (version B.01.04 and B.04.00).

#### **Synthesis of FimH Antagonists**

FimH antagonists mentioned in this thesis were synthesized in-house by Dr. Tobias Klein, Dr. Oliver Schwardt, Dr. Katharina Mayer, Dr. Lijuan Pang, Dr. Xiaohua Jiang, Bea Wagner, Dr. Wojciech Schönemann, Margrit Hartmann, Philip Dätwyler, Priska Frei, Marcel Lindegger, Sophie Boschung, Hülya Süyün, Martina Haug, and Janno Herold.

### 3.1. Paper 1 – A Method in Detail:

#### **pK<sub>a</sub> Determination by <sup>1</sup>H-NMR Spectroscopy - An Old Methodology Revisited**

This publication revisits an old methodology for pK<sub>a</sub> determination by <sup>1</sup>H-NMR spectroscopy and compares the results with two *in silico* (Epik and Marvin) and well-established experimental approaches (electropotentiometric and UV-spectroscopic approaches). Even though the methodology is not new, it is the first time that its scope and limitations were explored. The numerous advantages of this approach make it a valid tool for pK<sub>a</sub> determination in an academic environment.

#### **Contribution to the Project:**

Jacqueline Bezençon was responsible for the pK<sub>a</sub> determination by <sup>1</sup>H-NMR, first during her master thesis under the supervision of Dr. Matthias Wittwer and then during her Ph.D. she was responsible for the collaboration with Roche for the determination of pK<sub>a</sub> by UV-spectroscopy and furthermore contributed to the revision of the manuscript.

The paper was published in the peer-reviewed *Journal of Pharmaceutical and Biomedical Analysis* in 2014:

**J. Bezençon**,\* M. B. Wittwer,\* B. Cutting, M. Smiesko, B. Wagner, M. Kansy, B. Ernst, pK<sub>a</sub> Determination by <sup>1</sup>H-NMR Spectroscopy - An Old Methodology Revisited. *J. Pharm. Biomed. Anal.* **2014**, *93*, 147-155.

\*contributed equally.



Contents lists available at ScienceDirect

Journal of Pharmaceutical and Biomedical Analysis

journal homepage: [www.elsevier.com/locate/jpba](http://www.elsevier.com/locate/jpba)

## pK<sub>a</sub> determination by <sup>1</sup>H NMR spectroscopy – An old methodology revisited



Jacqueline Bezençon<sup>a,1</sup>, Matthias B. Wittwer<sup>a,1</sup>, Brian Cutting<sup>a</sup>, Martin Smieško<sup>a</sup>, Bjoern Wagner<sup>b</sup>, Manfred Kansy<sup>b</sup>, Beat Ernst<sup>a,\*</sup>

<sup>a</sup> Institute of Molecular Pharmacy, Pharmacenter, University of Basel, Klingelbergstrasse 50, CH-4056 Basel, Switzerland

<sup>b</sup> Pharmaceuticals Division, Non-Clinical Safety, F. Hoffmann-La Roche Ltd., 4070 Basel, Switzerland

### ARTICLE INFO

#### Article history:

Received 20 September 2013

Received in revised form

12 December 2013

Accepted 16 December 2013

Available online 24 December 2013

#### Keywords:

pK<sub>a</sub> determination

<sup>1</sup>H NMR spectroscopy

Physicochemical properties

Dissociation constant

Site of protonation

### ABSTRACT

pK<sub>a</sub> values of acids and protonated bases have an essential impact on organic synthesis, medicinal chemistry, and material and food sciences. In drug discovery and development, they are of utmost importance for the prediction of pharmacokinetic and pharmacodynamic properties. To date, various methods for the determination of pK<sub>a</sub> values are available, including UV-spectroscopic, potentiometric, and capillary electrophoretic techniques. An additional option is provided by nuclear magnetic resonance (NMR) spectroscopy. The underlying principle is the alteration of chemical shifts of NMR-active nuclei (e.g., <sup>13</sup>C and <sup>1</sup>H) depending on the protonation state of adjacent acidic or basic sites. When these chemical shifts are plotted against the pH, the inflection point of the resulting sigmoidal curve defines the pK<sub>a</sub> value. Although pK<sub>a</sub> determinations by <sup>1</sup>H NMR spectroscopy are reported for numerous cases, the potential of this approach is not yet fully evaluated. We therefore revisited this method with a diverse set of test compounds covering a broad range of pK<sub>a</sub> values (pK<sub>a</sub> 0.9–13.8) and made a comparison with four commonly used approaches. The methodology revealed excellent correlations ( $R^2 = 0.99$  and  $0.97$ ) with electropotentiometric and UV spectroscopic methods. Moreover, the comparison with *in silico* results (Epik and Marvin) also showed high correlations ( $R^2 = 0.92$  and  $0.94$ ), further confirming the reliability and utility of this approach.

© 2014 Elsevier B.V. All rights reserved.

### 1. Introduction

pK<sub>a</sub> values of acids and protonated bases have an essential impact on organic synthesis, medicinal chemistry, and material and food sciences. In drug discovery and development, they are of utmost importance for the prediction of pharmacokinetic and pharmacodynamic properties such as permeation through biological barriers, interactions with targets, or induction of side effects [1]. It is therefore indispensable to have access to this parameter at an early stage of a medicinal chemistry program.

For the determination of pK<sub>a</sub> values, various experimental approaches are commonly used. First, protonation and deprotonation can be followed by UV-spectroscopy [2]. Second potentiometric measurements, also called the pH-metric approach, enable the determination of pK<sub>a</sub> values [3]. Third, with capillary electrophoresis, an additional method is available. As the migration time of a compound through a capillary depends on the fraction of charged compound, the pK<sub>a</sub> value is derived from the inflection

point of the sigmoidal curve obtained when the retention times are plotted against the pH of various buffers [4]. Finally, *in silico* pK<sub>a</sub> prediction offers an alternative to experimental methods [5].

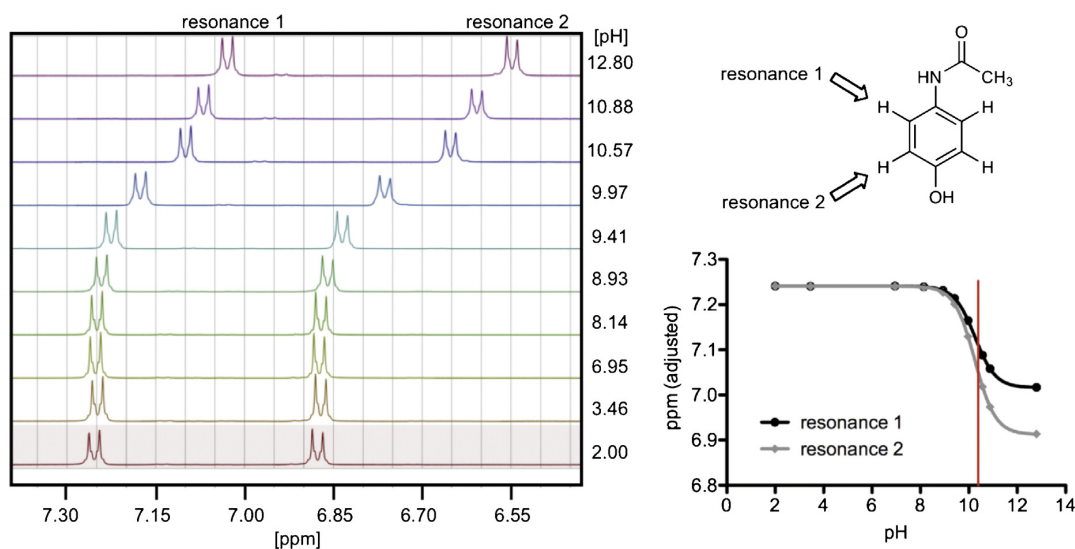
NMR spectroscopy offers a valuable alternative, since the protonation state of adjacent centers relates to the chemical shifts of NMR-active nuclei [6] and an NMR spectrometer is available in most chemists' laboratories. Although specific approaches based on <sup>15</sup>N, <sup>11</sup>B, <sup>19</sup>F or <sup>31</sup>P NMR spectroscopy are reported [7–10], the pH-dependence of chemical shifts of <sup>13</sup>C nuclei adjacent to ionizable groups is a more general approach [11] and has successfully been employed for the determination of pK<sub>a</sub> values of both acids [6,12] and protonated bases [13]. Additionally, <sup>13</sup>C NMR spectroscopy (often in combination with <sup>1</sup>H or <sup>15</sup>N NMR) allows the determination of pK<sub>a</sub> values in isotopically enriched proteins. The applicability has been demonstrated with, e.g., calmodulin [14]. Furthermore, pH-implications on structure (see e.g. [15]) and functionality (see e.g. [16]) of peptides and proteins can be investigated as well. If no isotope enrichment is available, the low natural abundance of <sup>13</sup>C nuclei (1.11%) results in prolonged recording times, representing a substantial drawback.

In contrast, <sup>1</sup>H nuclei have a higher natural abundance, which leads to a sensitivity improvement by a factor of 5600 compared to <sup>13</sup>C, enabling the use of smaller amounts of sample as well

\* Corresponding author. Tel.: +41 61 267 1551; fax: +41 61 267 1552.

E-mail address: [beat.ernst@unibas.ch](mailto:beat.ernst@unibas.ch) (B. Ernst).

<sup>1</sup> These authors contributed equally to this work.



**Fig. 1.**  $^1\text{H}$  chemical shift dependence on the ionization state of the analyte paracetamol. When plotted against the corresponding pH values, the  $\text{pK}_a$  value corresponds to the inflection point of the resulting sigmoidal curve. The downfield doublet (resonance 1) corresponds to the two protons in *meta*-position to the hydroxy-group, whereas the upfield resonance 2 represents those at the *ortho*-position. The  $\text{pK}_a$  derived from both resonances is 9.80 after correction for  $\text{D}_2\text{O}$ , compared to 9.63 determined by an electrometric measurement [22].

as shorter recording times. The first applications were published in 1973 using a 60 MHz continuous wave spectrometer [17], and an adapted procedure to FT-NMR spectrometers was published in 2012 [18]. Moreover, an automated NMR controlled titration was described in 1995 [19]. The approach has found broad application in biology, i.e., for the  $\text{pK}_a$  determination of amino acids [20], or whole proteins such as human thioredoxin [21].

In summary, despite its occasional use the broad applicability of  $^1\text{H}$  NMR for  $\text{pK}_a$  determinations in drug discovery has not been fully demonstrated. Furthermore, the method has not been extensively validated against other approaches. We therefore explored its scope and limitation and compared the results with two experimental methods, namely potentiometric [22] and UV-spectroscopic (measured by Sirius SGA, spectral gradient analysis, according to [23])  $\text{pK}_a$  determinations. In addition, a comparison with two *in silico* tools (Epik [24], based on the Hammett and Taft empirical equations and Marvin [25], based on the calculation of partial charge of atoms) completed the validation process.

## 2. Materials and methods

### 2.1. Instrument and chemicals

NMR experiments were performed on a Bruker Avance III 500 MHz spectrometer equipped with a 5 mm PABBO probe with Z gradients at a temperature of 298 K. Spectra were recorded and processed with Topspin 2.1 (Bruker, Switzerland). Chemical shifts are given in ppm. 1D  $^1\text{H}$  NMR experiments were performed with presaturation in order to suppress the residual HDO signal.

Deuterium oxide and deuterated  $\text{d}_6$ -dimethyl sulfoxide were purchased from Armar Chemicals (Switzerland). Dimethyl sulfoxide, *N*-acetylneuraminic acid, diazepam, glycine, L-arginine, L-cysteine, L-lysine, phenol, papaverine, propranolol, paracetamol, neocuproine, 5-nitro-1,10-phenanthroline, 4,7-dimethoxy-1,10-phenanthroline, 4-phenylbutylamine, serotonin, benzoic acid, aniline, phenobarbital, diltiazem, promethazine, sucrose, 2,6-dimethylaniline, 2,6-dimethylphenol, 2,2-dichloropropionic acid and uracil were purchased from Sigma. Imidazole was purchased from Acros Organics. Dioxane was obtained from Fluka.

1,10-phenanthroline and 2,2'-bipyridine were purchased from Riedel-de Haën. Codeine phosphate, acetylsalicylic acid, benzocaine, and phenazone were purchased from Siegfried AG. 4-aminopyridine-2-carboxylic acid was purchased from Apollo Scientific. 2-amino-1,10-phenanthroline was purchased from Specs. 3'-( $\alpha$ -D-mannopyranosyloxy)-biphenyl-4-carboxylate and 3'-chloro-4'-( $\alpha$ -D-mannopyranosyloxy)-biphenyl-4-carboxylate were synthesized in house [26]. 2-Naphthacencarboxamide was obtained from F. Hoffmann-La Roche (Basel, Switzerland).

### 2.2. Principle of $\text{pK}_a$ determination by $^1\text{H}$ NMR

Chemical shifts of NMR-active nuclei (e.g.,  $^{13}\text{C}$  and  $^1\text{H}$ ) depend on the chemical environment, including the protonation state of adjacent acidic or basic sites. Therefore, gradual alteration of the pH causes changes in the chemical shifts that can be plotted against the pH. The  $\text{pK}_a$  of the corresponding protonation site can then be extracted from the inflection point of the resulting sigmoidal curves (see Fig. 1).

### 2.3. $\text{pK}_a$ determination by $^1\text{H}$ NMR

A 100  $\mu\text{M}$  solution of the analyte in  $\text{D}_2\text{O}$  was prepared and dioxane (50  $\mu\text{M}$ ) was added as an internal standard (at 3.75 ppm [27]). For compounds which were pre-dissolved in DMSO, DMSO was taken as the internal standard (at 2.71 ppm [27]). The solution of 100  $\mu\text{M}$  was aliquoted into 9–15 samples and the pH values of the samples were adjusted with 0.5 M or 8 M NaOH and 0.5 M or 4 M HCl, respectively. The pH values were chosen close to the predicted  $\text{pK}_a$  (software CS ChemBioDraw<sup>®</sup> Ultra, version 11.0.1), at the  $\text{pK}_a$  itself, and at two extreme pH values, e.g. 1 and 13.5. Aliquots (500  $\mu\text{l}$ ) of samples at each pH value were transferred to 5 mm NMR tubes (Armar Chemicals, Switzerland) and the recorded spectra were analyzed with MestReNova (Mestrelab research, version 5.2.5-4119). The chemical shifts of the reporter proton close to the ionizable center were plotted against the pH of the solution. The resulting sigmoidal curve was subjected to nonlinear curve fitting using Prism<sup>®</sup> (GraphPad, version 5.0b and 5.0f). The  $\text{pK}_a$  was obtained as the inflection point of the fitted curve. Since the

measurements were performed in D<sub>2</sub>O, 0.45 pH units were subtracted to yield the corrected pK<sub>a</sub> values for a nondeuterated environment [28].

When sample consumption is critical, the titration is done progressively in a single NMR sample, lowering the compound consumption to as little as 25 µg for an analyte with a molecular weight of 500 g/mol. Furthermore, when small volume NMR tubes (200 µL compared to 500 µL of a standard tube of 5 mm diameter) are used, compound consumption can be further lowered to 10 µg. As a consequence, the pK<sub>a</sub> value of compounds with a solubility of as little as 50 µg/mL can still be analyzed. Lower solubility can be improved by using different solvents (e.g., CD<sub>3</sub>OD, CD<sub>3</sub>CN), allowing the determination of pK<sub>a</sub> values of sparsely soluble compounds. When water/organic solvent mixtures are used, the influence of the organic solvent on the pK<sub>a</sub> value can be corrected by applying Yasuda–Shedlovsky extrapolations [29,30]. Furthermore, since NMR is a non-destructive method, the analyte can be recovered provided that no pH-dependent decomposition occurred.

The overall recording time is typically in the range of less than 5 min per data point and thereby reduced by a factor of 10 compared to <sup>13</sup>C NMR spectroscopy. A further advantage of the <sup>1</sup>H NMR method is the possibility to start from a DMSO stock solution as usually prepared for biological testing. In contrast to methods in earlier publications (see e.g. [28]) HCl and NaOH were used instead of DCl and NaOD for the pH-adjustment of the samples. The small amounts of added base or acid did not generate spectral disturbances when the H<sub>2</sub>O signal was suppressed (see e.g. [20]).

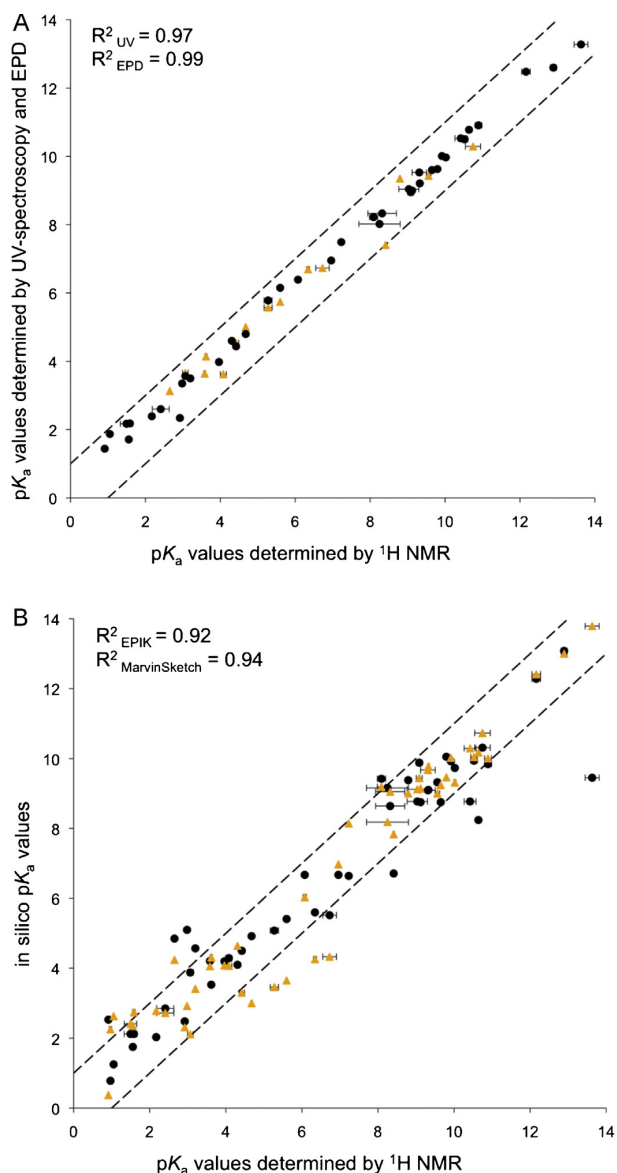
### 3. Results and discussion

For the determination of pK<sub>a</sub> values various methods are available, namely UV-spectroscopic [2], potentiometric [3], and capillary electrophoretic [4] techniques. These experimental methods offer the advantage of being highly compatible with automation, and therefore, are promising candidates for medium- to high-throughput applications. Moreover, overlapping pK<sub>a</sub> values for compounds can be determined and, with an appropriate co-solvent, pK<sub>a</sub> values for compounds with low solubility can be determined as well.

Major drawbacks of these three approaches for pK<sub>a</sub> determination are the inaccessibility of information on the sites of protonation and the requirement of expensive, automated instrumentation, or laborious and time-consuming manual titration experiments. In addition, the required amount of sample is often critical. Typically, only milligram amounts of a test compound are available and the investment in expensive equipment is not always justified for single pK<sub>a</sub> determinations. Furthermore, sample impurities can lead to distorted results, with the exception of capillary electrophoresis due to its separation technique. Additionally, the UV-spectroscopic approach relies on chromophores located in proximity to the ionizable centers.

In contrast to the experimental approach, *in silico* pK<sub>a</sub> predictions are fast and inexpensive. Nevertheless, commercial software needs to be trained and validated when applied to a new class of compounds [5].

For the evaluation of the <sup>1</sup>H NMR approach a diverse set of test compounds covering a broad range of pK<sub>a</sub> values (pK<sub>a</sub> 0.9–13.8) was selected (Table 1). Furthermore, pK<sub>a</sub> values were measured for compounds with up to three ionizable centers. The excellent correlation of pK<sub>a</sub> values over a range of 12 orders of magnitude with reference values determined by electrochemistry [22] and UV-spectroscopy (measured by Sirius SGA according to [23]) is reflected by R<sup>2</sup> values of 0.99 and 0.97, respectively (Fig. 2A). In addition, the absolute average deviation of <sup>1</sup>H NMR pK<sub>a</sub> values compared to UV-spectroscopic and EPD were ±0.37 and ±0.25, respectively.



**Fig. 2.** (A) Comparison of published data from electrochemistry [22] (black dots) and data obtained from UV-spectroscopic (orange triangles) measurements with values obtained by the presented <sup>1</sup>H NMR method; (B) comparison of <sup>1</sup>H NMR determined pK<sub>a</sub> values with computed values calculated with EpiK [24] (black dots) and Marvin [25] (orange triangle) (cf. Table 1). pK<sub>a</sub> values determined by <sup>1</sup>H NMR are indicated as an average of the inflection points deduced from the detectable chemical shifts.

Moreover, the comparison with *in silico* results also exhibits a high correlation ( $R^2_{\text{EpiK}} = 0.92$ ,  $R^2_{\text{Marvin}} = 0.94$ ) (Fig. 2B).

A major advantage of this approach is the accessibility of pK<sub>a</sub>s of different sites of protonation, since the chemical shift differences of the reporter protons depend on the distance from the ionizable center. For example, for serotonin (Table 1, entry 34, Fig. 3B and C) two pK<sub>a</sub> values can be allocated (pK<sub>a</sub><sup>1</sup>: 10.02 ± 0.03 for the NH<sub>2</sub> group, based on the chemical shifts of the protons H<sup>8</sup> and H<sup>9</sup> and pK<sub>a</sub><sup>2</sup>: 10.89 ± 0.09 for the phenolic OH, based on the chemical shifts of the protons H<sup>2</sup>, H<sup>4</sup>, H<sup>6</sup>, and H<sup>7</sup>). As demonstrated with the examples of codeine (Table 1, entry 22), paracetamol (entry 26 and Fig. 1),



**Table 1**

$pK_a$  values obtained by  $^1\text{H}$  NMR spectroscopy compared to published data obtained by potentiometric determination (EPD) (values are taken from one source [22], unless indicated otherwise); values from UV-spectroscopic determinations were measured with a Sirius SGA according to [23]. Furthermore, in silico data (Epik [24] and Marvin [25]) are shown. n.d. = not determined. Entry 2 was measured by potentiometric titrations according to [31] using a GLpK<sub>a</sub> from Sirius Analytical Instruments Ltd.

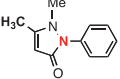
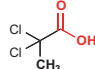
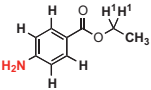
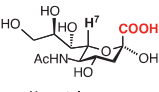
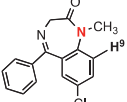
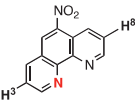

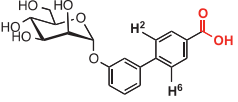
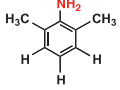
Entry	Compound name and structure (ionizable centers in red; reporter protons in bold)	Conc. [mM]	Ionizable group	$pK_a$ determined by $^1\text{H}$ chemical shifts (reporter proton)	$pK_a$ by UV spectroscopy	$pK_a$ by EPD [22]	In silico $pK_a$	
							Epik [24]	Marvin [25]
<i>Compounds with a single <math>pK_a</math></i>								
1	 phenazone	0.1	$\oplus\text{-NPh}$	0.91 (CH <sub>3</sub> )	n.d.	1.44	2.53	0.37
2	 2,2-dichloropropionic acid	0.1	—COOH	1.05 (CH <sub>3</sub> )	–	1.87	1.25	2.63
3	 benzocaine	0.1	$\oplus\text{-NH}_3$	2.18 ( <i>o</i> -H) 2.17 ( <i>m</i> -H) 2.16 (H <sup>1</sup> ) 2.17 (CH <sub>3</sub> )	n.d.	2.39	2.03	2.78
4	 N-acetyl-neuraminic acid	1	—COOH	2.45 (H <sup>7</sup> )	n.d.	2.60	2.85	2.72
5	 diazepam	0.1	$\oplus\text{-NCH}_3$	2.98 (H <sup>9</sup> )	n.d.	3.35	5.10	2.92
6	 5-nitro-1,10-phenanthroline	0.1	$\oplus\text{-N=H}$	3.21 (H <sup>3,8</sup> )	3.66	3.57 [32]	3.88	2.11
7	 acetyl salicylic acid	0.1	—COOH	3.20 ( <i>o</i> -H)	n.d.	3.50	4.57	3.41
8	 3'-( $\alpha$ -D-mannopyranosyloxy)-biphenyl-4-carboxylate	0.1	—COOH	3.56 (H <sup>2,6</sup> )	3.64	–	4.21	4.06
9	 2,6-dimethylaniline	0.1	$\oplus\text{-NH}_3$	3.60 ( <i>m</i> -H) 3.65 ( <i>p</i> -H) 3.60 (CH <sub>3</sub> )	4.14	–	3.53	4.31

Table 1 (Continued)

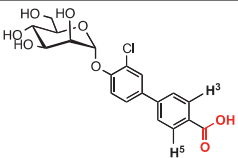
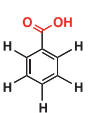
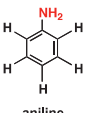
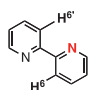
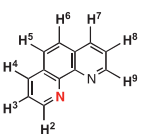
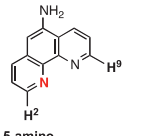
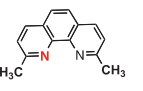
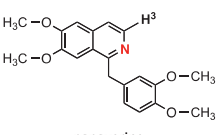
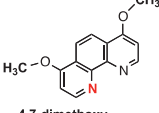
Entry	Compound name and structure (ionizable centers in red; reporter protons in bold)	Conc. [mM]	Ionizable group	pK <sub>a</sub> determined by <sup>1</sup> H chemical shifts (reporter proton)	pK <sub>a</sub> by UV spectroscopy	pK <sub>a</sub> by EPD [22]	In silico pK <sub>a</sub>	
							Epik [24]	Marvin [25]
10	 <b>3'-chloro-4'-(<math>\alpha</math>-D-mannopyranosyloxy)-biphenyl-4-carboxylate</b>	0.1	—COOH	4.05 (H <sup>3,5</sup> )	3.62	–	4.29	4.07
11	 <b>benzoic acid</b>	0.1	—COOH	3.97 ( <i>o</i> -H) 3.96 ( <i>m</i> -H) 3.96 ( <i>p</i> -H)	n.d.	3.98	4.20	4.08
12	 <b>aniline</b>	0.1	$\oplus$ -NH <sub>3</sub>	4.30 ( <i>o</i> -H) 4.32 ( <i>m</i> -H) 4.30 ( <i>p</i> -H)	n.d.	4.60 [33]	4.10	4.64
13	 <b>2,2'-bipyridine</b>	0.1	$\oplus$ -N <sup>+</sup> H=	4.50 (H <sup>6,6'</sup> )	4.54	4.44 [34]	4.50	3.30
14	 <b>1,10-phenanthroline</b>	0.1	$\oplus$ -N <sup>+</sup> H=	4.65 (H <sup>2,9</sup> ) 4.68 (H <sup>3,8</sup> ) 4.69 (H <sup>4,7</sup> ) 4.69 (H <sup>5,6</sup> )	5.00	4.80 [35]	4.92	3.00
15	 <b>5-amino-1,10-phenanthroline</b>	0.1	$\oplus$ -N <sup>+</sup> H=	5.33 (H <sup>2,9</sup> )	5.57	5.78 [32]	5.08	3.46
16	 <b>neocuproine</b>	0.1	$\oplus$ -N <sup>+</sup> H=	5.61 (CH <sub>3</sub> )	5.74	6.15 [35]	5.41	3.65
17	 <b>papaverine</b>	1	$\oplus$ -N <sup>+</sup> H=	6.14 (H <sup>3</sup> )	n.d.	6.39	6.67	6.03
18	 <b>4,7-dimethoxy-1,10-phenanthroline</b>	0.1	$\oplus$ -N <sup>+</sup> H=	6.38 (CH <sub>3</sub> )	6.69	–	5.60	4.26

Table 1 (Continued)

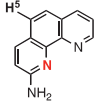
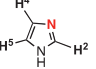
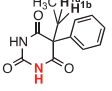
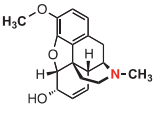
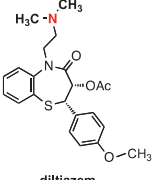
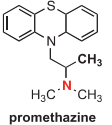
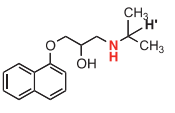
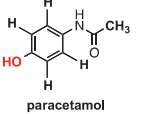
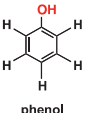
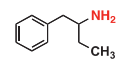
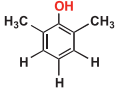
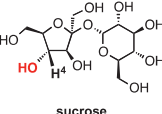
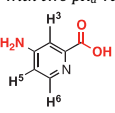
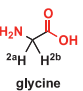
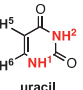

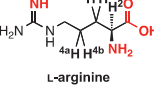

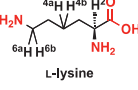
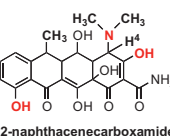
Entry	Compound name and structure (ionizable centers in red; reporter protons in bold)	Conc. [mM]	Ionizable group	pK <sub>a</sub> determined by <sup>1</sup> H chemical shifts (reporter proton)	pK <sub>a</sub> by UV spectroscopy	pK <sub>a</sub> by EPD [22]	In silico pK <sub>a</sub>	
							Epik [24]	Marvin [25]
19	 2-amino- 1,10-phenanthroline	0.1	$\text{-}\overset{\oplus}{\text{N}}\text{H}=\text{}$	6.40 (H <sup>5</sup> )	6.73	–	5.52	4.33
20	 imidazol	0.1	$\text{-}\overset{\oplus}{\text{N}}\text{H}=\text{}$	6.96 (H <sup>2</sup> ) 6.96 (H <sup>4,5</sup> )	n.d.	6.95 [36]	6.67	6.97
21	 phenobarbital	1	—NH	7.23 (H <sup>1</sup> )	n.d.	7.49	6.64	8.14
22	 codeine	1	$\text{-}\overset{\oplus}{\text{N}}\text{HCH}_3$	8.14 (N-CH <sub>3</sub> ) 8.11 (O-CH <sub>3</sub> )	n.d.	8.22	9.42	9.19
23	 diltiazem	1	$\text{-}\overset{\oplus}{\text{N}}(\text{CH}_3)_2$	7.79 (CH <sub>3</sub> )	n.d.	8.02	9.16	8.18
24	 promethazine	0.1	$\text{-}\overset{\oplus}{\text{N}}(\text{CH}_3)_2$	9.12 (CH <sub>3</sub> )	n.d.	9.00	8.75	9.14
25	 propranolol	0.1	$\text{-}\overset{\oplus}{\text{N}}\text{H}_2$	9.31 (H')	n.d.	9.53	9.09	9.67
26	 paracetamol	10	—OH	9.80 (o-H) 9.80 (m-H) 9.79 (CH <sub>3</sub> )	n.d.	9.63	10.05	9.46
27	 phenol	0.1	—OH	9.92 (o-H) 9.92 (m-H) 9.91 (p-H)	n.d.	10.01	9.92	10.02
28	 4-phenylbutylamine	0.5	$\text{-}\overset{\oplus}{\text{N}}\text{H}_3$	10.43 (CH <sub>3</sub> )	n.d.	10.50	9.94	10.04

Table 1 (Continued)

Entry	Compound name and structure (ionizable centers in red; reporter protons in bold)	Conc. [mM]	Ionizable group	$pK_a$ determined by $^1H$ chemical shifts (reporter proton)	$pK_a$ by UV spectroscopy	$pK_a$ by EPD [22]	In silico $pK_a$		
							Epik [24]	Marvin [25]	
29	 2,6-dimethylphenol	0.1	—OH	10.61 ( <i>m</i> -H) 10.62 ( <i>p</i> -H) 11.18 (CH <sub>3</sub> )	10.29	—	10.31	10.73	
30	 sucrose	0.5	—OH	12.82 (H <sup>4</sup> )	n.d.	12.60	13.08	13.84	
Compounds with two $pK_a$ values									
31	 4-aminopyridine -2-carboxylic acid	0.1	—COOH $\oplus$ —NH <sub>3</sub>	0.99 (H <sup>3</sup> ) 0.93 (H <sup>5</sup> ) 0.98 (H <sup>6</sup> ) 9.52 (H <sup>3</sup> ) 9.53 (H <sup>5</sup> ) 9.63 (H <sup>6</sup> )	n.d.	—	0.78	2.25	
32	 glycine	5	—COOH $\oplus$ —NH <sub>3</sub>	2.92 (H <sup>2</sup> ) 9.65 (H <sup>2</sup> )	n.d.	2.34 [37] 9.60 [37]	2.48	2.31 9.24	
33	 uracil	0.5	—NH <sup>1</sup> —NH <sup>2</sup>	9.34 (H <sup>5</sup> ) 9.31 (H <sup>6</sup> ) 13.76 (H <sup>5</sup> ) 13.50 (H <sup>6</sup> )	n.d.	9.21 13.28	9.10	9.77 13.79	
34	 serotonin	0.5	$\oplus$ —NH <sub>3</sub> —OH	10.00 (H <sup>9</sup> ) 10.04 (H <sup>8</sup> ) 10.77 (H <sup>2</sup> ) 10.99 (H <sup>4</sup> ) 10.90 (H <sup>6</sup> ) 10.91 (H <sup>7</sup> )	n.d.	9.97 10.91	9.73	9.31 10.00	
Compounds with three $pK_a$ values									
35	 L-arginine	10	—COOH $\oplus$ —NH <sub>3</sub> $\oplus$ =NH <sub>2</sub>	1.63 (H <sup>4</sup> ) 1.31 (H <sup>3</sup> ) 1.54 (H <sup>2</sup> ) 8.86 (H <sup>2</sup> ) 9.34 (H <sup>4</sup> ) 8.90 (H <sup>3</sup> ) 12.08 (H <sup>3</sup> ) 12.24 (H <sup>4</sup> )	n.d.	2.17 [37] 9.04 [37] 12.48 [37]	2.12	2.41 9.12 12.41	
36	 L-cysteine	10	—COOH —SH $\oplus$ —NH <sub>3</sub>	1.54 (H <sup>2</sup> ) 8.59 (H <sup>2</sup> ) 10.64 (H <sup>2</sup> )	n.d. n.d.	1.71 [37] 8.33 [37] 10.78 [37]	1.75	2.35 9.05 10.17	
37	 L-lysine	10	—COOH $\oplus$ —NH <sub>3</sub> $\oplus$ —NH <sub>3</sub>	1.56 (H <sup>2</sup> ) 1.61 (H <sup>4</sup> ) 9.03 (H <sup>2</sup> ) 9.14 (H <sup>4</sup> ) 10.31 (H <sup>4</sup> ) 10.53 (H <sup>6</sup> )	n.d.	2.18 [37] 8.95 [37] 10.53 [37]	2.12	2.74 9.44 10.29	
38	 2-naphthacene-carboxamide	0.1	—OH Ph—OH $\oplus$ —N(CH <sub>3</sub> ) <sub>2</sub> H	2.65 (H <sup>4</sup> ) 8.40 (CH <sub>3</sub> ) 8.79 (N—CH <sub>3</sub> )	3.13 7.40 9.35	— — —	4.85 6.71	4.24 7.83 9.00	

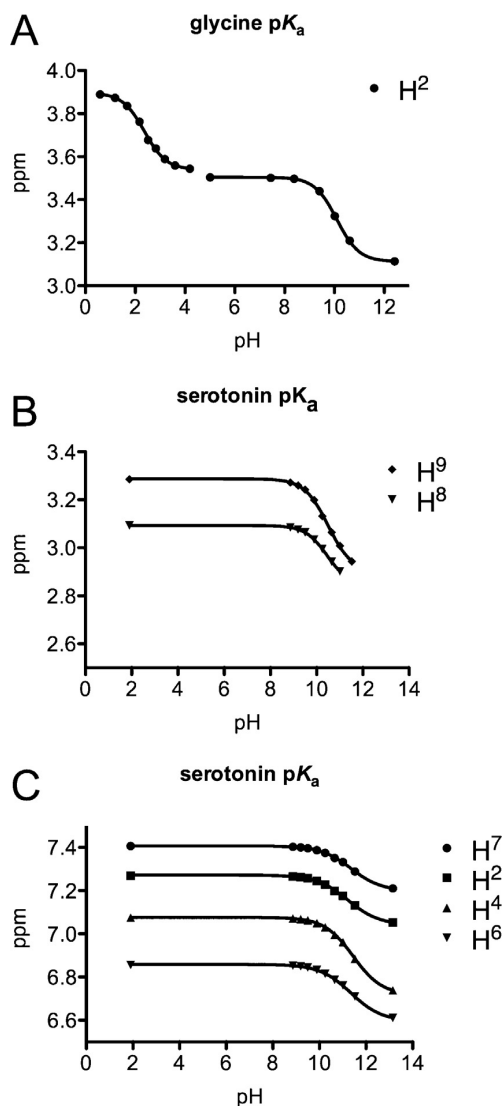


Fig. 3. Chemical shifts plotted against pH. The pK<sub>a</sub> can be deduced from the inflection point of the sigmoidal curves for (A) glycine and (B,C) serotonin.

and 2,6-dimethylphenol (entry 29), equal pK<sub>a</sub> values are obtained independent of the distance of the reporter proton to the ionizable center. Glycine is an example where the pK<sub>a</sub> values of two different ionizable centers can be determined with one reporter proton (Table 1, entry 32 and Fig. 3A). Moreover, the applicability to compounds with more than two ionizable centers is demonstrated in entries 35–38. However, not every chemical shift of the <sup>1</sup>H NMR spectra can be used for the analysis because the resonance of the internal standard (e.g. DMSO or dioxane) or of H<sub>2</sub>O may overlap with resonances of reporter protons.

#### 4. Conclusions

For the determination of pK<sub>a</sub> values by <sup>1</sup>H NMR, several features need to be considered. First, especially in cases where only a rough estimate of pK<sub>a</sub> values (±1.00) rather than high-accuracy data is required, the methodology is highly valuable because compound requisition in the microgram range and recording times of only a

few minutes per pH value are required. However, even in cases where high-accuracy data are requested, compound requisition could be kept low by applying small volume NMR tubes (volume of 200 μL) and/or increasing recording times. Second, compounds can be recovered because the method is non-destructive. Third, pK<sub>a</sub> determination in D<sub>2</sub>O is feasible when a correction factor is applied [28]. Fourth, an additional strength of this approach is that it allows the correlation of pK<sub>a</sub> values with the various protonation sites. Fifth, in cases where the chemical shifts of protons adjacent to the ionizable centers are not resolved, NMR spectroscopy with other nuclei, including <sup>13</sup>C, <sup>15</sup>N or <sup>19</sup>F, or 2D-methods, such as HSQC, could be applied. Finally, with the use of different solvents (e.g., CD<sub>3</sub>OD, CD<sub>3</sub>CN), solubility could be improved, allowing the determination of pK<sub>a</sub> values in sparingly soluble compounds.

In conclusion, <sup>1</sup>H NMR spectroscopy allows a fast, sensitive and reliable determination of pK<sub>a</sub> values over a broad pH-range, and can be used for compounds with more than one ionizable center. Furthermore, it is applicable to compounds with low solubility, and only microgram amounts of an analyte are required. Finally, the results from pK<sub>a</sub> determination by <sup>1</sup>H NMR correlate well with data obtained with the commonly used potentiometric and UV-spectroscopic methods.

#### Acknowledgements

The authors gratefully acknowledge the financial support by the Swiss National Science Foundation (Grant No. 200020120628). The authors express their gratitude to Dr. Rachel Hevey, Institute of Molecular Pharmacy, University of Basel for critical revision of the manuscript.

#### References

- [1] D. Horter, J.B. Dressman, Influence of physicochemical properties on dissolution of drugs in the gastrointestinal tract, *Adv. Drug Deliv. Rev.* 46 (2001) 75–87.
- [2] K. Box, C. Bevan, J. Comer, A. Hill, R. Allen, D. Reynolds, High-throughput measurement of pK<sub>a</sub> values in a mixed-buffer linear pH gradient system, *Anal. Chem.* 75 (2003) 883–892.
- [3] A. Avdeef, pH-metric log P. II: Refinement of partition coefficients and ionization constants of multiprotic substances, *J. Pharm. Sci.* 82 (1993) 183–190.
- [4] Y. Ishihama, M. Nakamura, T. Miwa, T. Kajima, N. Asakawa, A rapid method for pK<sub>a</sub> determination of drugs using pressure-assisted capillary electrophoresis with photodiode array detection in drug discovery, *J. Pharm. Sci.* 91 (2002) 933–942.
- [5] A.C. Lee, G.M. Crippen, Predicting pK<sub>a</sub>, *J. Chem. Inf. Model.* 49 (2009) 2013–2033.
- [6] D. Farcasiu, A. Ghenciu, Determination of acidity functions and acid strengths by C-13 NMR, *Prog. Nucl. Magn. Reson. Spectrosc.* 29 (1996) 129–168.
- [7] J.W. Paschal, D.E. Dorman, Determination of pK<sub>a</sub> values using <sup>15</sup>N- and <sup>13</sup>C-nuclear magnetic resonance spectroscopy – a case of apramycin, *Org. Magn. Res.* 11 (1978) 632–634.
- [8] J.A. Tossell, Boric acid, carbonic acid, and N-containing oxyacids in aqueous solution: ab initio studies of structure, pK<sub>a</sub>, NMR shifts, and isotopic fractionations, *Geochim. Cosmochim. Acta* 69 (2005) 5647–5658.
- [9] M.C. Malet-Martino, J. Bernadou, R. Martino, J.P. Armand, <sup>19</sup>F NMR spectrometry evidence for bile acid conjugates of α-fluoro-β-alanine as the main biliary metabolites of antineoplastic fluoropyrimidines in humans, *Drug Metab. Dispos.* 16 (1988) 78–84.
- [10] K.K. Millis, M.E. Colvin, E.M. Shulman-Roskes, S.M. Ludeman, O.M. Colvin, M.P. Gamcsik, Comparison of the protonation of isophosphoramidate mustard and phosphoramidate mustard, *J. Med. Chem.* 38 (1995) 2166–2175.
- [11] S. Berger, S. Braun, 200 and More NMR Experiments: A Practical Course, Wiley-VCH, Weinheim, 2004, pp. 290–292.
- [12] D.P. Cistola, D.M. Small, J.A. Hamilton, Ionization behavior of aqueous short-chain carboxylic acids – a <sup>13</sup>C-NMR study, *J. Lipid Res.* 23 (1982) 795–799.
- [13] M. Delfini, A.L. Segre, F. Conti, R. Barbucci, V. Barone, P. Ferruti, On the mechanism of protonation of triamines, *J. Chem. Soc. Perkin Trans. 2* (1980) 900–903.
- [14] M.J. Zhang, H.J. Vogel, Determination of the side-chain pK<sub>a</sub> values of the lysine-residues of calmodulin, *J. Biol. Chem.* 268 (1993) 22420–22428.
- [15] A.T. Clark, K. Smith, R. Mhandiram, S.P. Edmondson, J.W. Shriver, Carboxyl pK<sub>a</sub> values, ion pairs, hydrogen bonding, and the pH-dependence of folding of the hyperthermophile proteins Sac7d and Sso7d, *J. Mol. Biol.* 372 (2007) 992–1008.
- [16] E. Spink, S. Cosgrove, L. Rogers, C. Hewage, J.P.G. Malthouse, C-13 and H-1 NMR studies of ionizations and hydrogen bonding in chymotrypsin-glyoxal inhibitor complexes, *J. Biol. Chem.* 282 (2007) 7852–7861.
- [17] C.S. Handloser, M.R. Chakrabarty, M.W. Mosher, Experimental determination of pK<sub>a</sub> values by use of NMR chemical shifts, *J. Chem. Educ.* 50 (1973) 510–511.

- [18] A.D. Gift, S.M. Stewart, P.K. Bokashanga, Experimental determination of  $pK_a$  values by use of NMR chemical shifts, revisited, *J. Chem. Educ.* 89 (2012) 1458–1460.
- [19] J. Ollig, G. Hägele, NMR-controlled titrations of phosphorus-containing acids and bases, *Comp. Chem.* 19 (1995) 287–294.
- [20] D.L. Rabenstein, T.L. Sayer, Determination of microscopic acid dissociation-constants by nuclear magnetic resonance spectrometry, *Anal. Chem.* 48 (1976) 1141–1145.
- [21] J. Quijada, G. Lopez, R. Versace, L. Ramirez, M.L. Tasayco, On the NMR analysis of  $pK_a$  values in the unfolded state of proteins by extrapolation to zero denaturant, *Biophys. Chem.* 129 (2007) 242–250.
- [22] A. Avdeef, *Absorption and Drug Development: Solubility, Permeability, and Charge State*, Wiley-Interscience, Hoboken, NJ, 2003.
- [23] F. Milletti, L. Storch, L. Goracci, S. Bendels, B. Wagner, M. Kansy, G. Cruciani, Extending  $pK_a$  prediction accuracy: high-throughput  $pK_a$  measurements to understand  $pK_a$  modulation of new chemical series, *Eur. J. Med. Chem.* 45 (2010) 4270–4279.
- [24] J.C. Shelley, A. Chollet, L.L. Frye, J.R. Greenwood, M.R. Timlin, M. Uchimaya, Epik: a software program for  $pK_a$  prediction and protonation state generation for drug-like molecules, *J. Comput. Aided Mol. Des.* 21 (2007) 681–691.
- [25] Marvin 5.6.0.2, ChemAxon, 2011, <http://www.chemaxon.com/marvin/help/calculations/pKa.html> (23.11.13).
- [26] T. Klein, D. Abgottspon, M. Wittwer, S. Rabbani, J. Herold, X. Jiang, S. Kleeb, C. Lüthi, M. Scharenberg, J. Bezençon, E. Gubler, L. Pang, M. Smiesko, B. Cutting, O. Schwardt, B. Ernst, FimH antagonists for the oral treatment of urinary tract infections: from design and synthesis to in vitro and in vivo evaluation, *J. Med. Chem.* 53 (2010) 8627–8641.
- [27] H.E. Gottlieb, V. Kotlyar, A. Nudelman, NMR chemical shifts of common laboratory solvents as trace impurities, *J. Org. Chem.* 62 (1997) 7512–7515.
- [28] A. Krezel, W. Bal, A formula for correlating  $pK_a$  values determined in  $D_2O$  and  $H_2O$ , *J. Inorg. Biochem.* 98 (2004) 161–166.
- [29] K. Sarmini, E. Kenndler, Ionization constants of weak acids and bases in organic solvents, *J. Biochem. Biophys. Methods* 38 (1999) 123–137.
- [30] A. Avdeef, K.J. Box, J.E.A. Comer, M. Gilges, M. Hadley, C. Hibbert, W. Patterson, K.Y. Tam, pH-metric log P. 11:  $pK_a$  determination of water-insoluble drugs in organic solvent-water mixtures, *J. Pharm. Biomed. Anal.* 20 (1999) 631–641.
- [31] J. Olsen, P. Seiler, B. Wagner, H. Fischer, T. Tschopp, U. Obst Sander, D.W. Banner, M. Kansy, K. Müller, F. Diederich, A fluorine scan of the phenylammonium needle of tricyclic thrombin inhibitors: effects of fluorine substitution on  $pK_a$  and binding affinity and evidence for intermolecular C–F...CN interactions, *Org. Biomol. Chem.* 2 (2004) 1339–1352.
- [32] T. Ramirez-Silva, M. Gomez-Hernandez, D.L. Pacheco-Hernandez, A. Rojas-Hernandez, L. Galicia, Spectroscopy study of 5-amino-1,10-phenanthroline, *Spectrochim. Acta A* 60 (2004) 781–789.
- [33] Y. Altun, Study of solvent composition effects on the protonation equilibria of various anilines by multiple linear regression and factor analysis applied to the correlation between protonation constants and solvatochromic parameters in ethanol–water mixed solvents, *J. Solution Chem.* 33 (2004) 479–497.
- [34] M. Yasuda, K. Sone, K. Yamasaki, Stability of zinc and cadmium complexes with some methyl derivatives of 1,10-phenanthroline and 2,2'-bipyridine, *J. Phys. Chem.* 60 (1956) 1667–1668.
- [35] W.W. Brandt, D.K. Gullstrom, Studies on some ferrous complexes of substituted 1,10-phenanthrolines, *J. Am. Chem. Soc.* 74 (1952) 3532–3535.
- [36] T.C. Bruice, G.L. Schmir, Imidazole catalysis. 2. The reaction of substituted imidazoles with phenyl acetates in aqueous solution, *J. Am. Chem. Soc.* 80 (1958) 148–156.
- [37] R.M.C. Dawson, D.C. Elliott, W.H. Elliott, K.M. Jones, *Data for Biochemical Research*, Clarendon Press, Oxford, 1959.

Journal of Pharmaceutical and Biomedical Analysis, 93 (2014), J. Bezençon, M. B. Wittwer, B. Cutting, M. Smiesko, B. Wagner, M. Kansy, B. Ernst,  $pK_a$  Determination by  $^1H$ -NMR Spectroscopy - An Old Methodology Revisited, 147-155, Copyright (2014), with permission from Elsevier.

### **3.2. Preformulation Studies**

The preformulation studies were performed in collaboration with the master student Stefania Cigardi. The results obtained by the methods described below are presented in chapter 4.3.1 (page 123).

#### **Solubility Studies**

Kinetic and thermodynamic solubility were measured as described in former publication of our group.<sup>2-4</sup> Solvents used in the assay were modified by adding different concentration of solubilizers (Tween 80, Solutol HS, Cremophor EL, HP $\beta$ CD, DMSO, PEG400, and PG).

#### **Permeability Studies**

Caco-2 permeability studies were performed as described in former publication of our group.<sup>2-5</sup> Transport medium DMEM was adapted by adding solubilizers (Solutol HS, Tween 80).





### 3.3. Carrier-Mediated Transport Studies

These assays were performed in collaboration with Prof. Henriette Meyer zu Schwabedissen, Department of Pharmaceutical Sciences, University of Basel. The transport experiments and the radiolabeled (tritium-labeled) measurements were performed in the laboratory of Biopharmacy, whereas the LC-MS measurements and analysis of the results were done in our laboratory. The results of these transport studies are presented in chapter 4.2.1 (page 87).

#### Cell Culture

Wild-type Madin-Darby canine kidney II (MDCKII) and HeLa cells were cultivated in tissue culture flasks (BD Bioscience, Franklin Lakes, NJ, USA) with DMEM containing FCS (10%) and GlutaMAX (1%). Media of OATP2B1-MDCK-II, OATP1B3-MDCK-II, and OCT2-MDCK-II cells are additionally supplemented with hygromycin (200 µg/ml), G418 (600 µg/ml), and blasticidin (5 µg/ml), respectively. The cells were kept at 37°C in a humidified environment containing 5% CO<sub>2</sub> and the medium was changed every second day. When 90% confluence was reached, the cells were split with trypsin and distributed to new tissue culture flasks. Forty-eight hours prior to transport experiment MDCK-II cells were seeded in 24 well plates at a density of 50'000 - 70'000 cells/well. After 24h cultivation the cells were stimulated with sodium butyrate (2 mM) in the respective culture medium supplemented with the selecting agent. In case of adenoviral overexpression as used for OAT1 HeLa cells were infected with the OAT1-adenovirus or lacZ (50 pfu/cell) 48 h prior to the experiment and after 24 h incubation the media was changed and the cells were stimulated with sodium-butyrate (2 mM).

#### Transport Studies

Transport studies were performed at 37°C with incubation buffer containing 140 mM NaCl, 5 mM KCl, 1.2 mM MgSO<sub>4</sub>, 1 mM KH<sub>2</sub>PO<sub>4</sub>, 1.5 mM CaCl<sub>2</sub>, 5 mM glucose, and 12.5 mM HEPES (pH 7.3). For the transport studies at different pH (5.5, 6.0, 6.5, and 7.4), Krebs-henseleit buffer containing 118 mM NaCl, 25 mM NaHCO<sub>3</sub>, 1.2 mM KH<sub>2</sub>PO<sub>4</sub>, 2.5 mM CaCl<sub>2</sub>, 1.2 mM MgSO<sub>4</sub>, 11 mM glucose, and 4.7 mM KCl was used.

**Radiolabeled Uptake Studies.** Overexpression of a single drug transporter was confirmed as follows: The MDCK-II or HeLa cells with the corresponding overexpressed transporter (see Table 3.2) were seeded in 24-well plates (BD falcon, Franklin Lakes, NJ, USA), and cultured to confluence. 24 hours before the experiment was conducted, cells were incubated with 2 mM sodium butyrate. Directly before the experiment was conducted the cells were washed once with PBS (37°C), incubated with

the tritium-labeled substrate of the corresponding transporter (at 100'000 DPMI) for 5 or 10 minutes, washed 3 times with ice-cold (4°C) PBS, and lysed with 0.2% SDS containing 5 mM EDTA. An aliquot of the cell lysate was dissolved in 2 ml scintillation cocktail (Rotiszint) and intracellular accumulation of radioactivity was measured using a scintillation counter (type 1409, LKBWallac, Turku, Finland). MDCKII-Wild-type cells or HeLa cells, without the addition of the OAT1-adenovirus were used as a negative control.

**Table 3.2.** Cell lines, substrates, inhibitors, special treatments, and incubation times of the analyzed transporters (OATP2B1, OATP1B3, OCT2, and OAT1). <sup>†</sup>tritium-labeled. \*before experiment. pfu = plaque forming units

Transporter	Cell line	Substrate	Inhibitor	Special treatment	Incubation time
OATP2B1 <sup>19</sup>	MDCKII	E <sub>1</sub> S <sup>+</sup> , E <sub>1</sub> S	Atorvastatin	24 h* 2 mM sodium butyrat	10 min
OATP1B3	MDCKII	E <sub>2</sub> G <sup>+</sup>	Rifampicin	24 h* 2 mM sodium butyrat	10 min
OCT2	MDCKII	MPP <sup>+</sup>	Testosterone	24 h* 2 mM sodium butyrat	5 min
OAT1	HeLa	PAH <sup>+</sup>	Probenecid	48 h* 50 pfu virus/cell 24 h* 2 mM sodium butyrat	5 min

**Inhibition Studies.** Cells were treated the same way as described in the radiolabeled uptake studies. In addition, FimH antagonists were added during the incubation step of 5 or 10 min at final concentration of 10 to 100 µM (DMSO < 1%). A known inhibitor of the tritium-labeled substrate (see Table 3.2) was added in parallel to the FimH antagonists as a positive control. DMSO was used as blank and negative control. For IC<sub>50</sub> determination, series dilutions of FimH antagonists were added during the incubation step of 5 or 10 min, respectively. The cellular uptake of the radiolabeled substrate was determined as described previously. In all data analysis where inhibition is calculated, DMSO is considered as 100%.

**Uptake Studies of Unlabeled Compounds.** The uptake of the unlabeled known substrate (E<sub>1</sub>S) and the unlabeled FimH antagonists was determined by liquid chromatography mass spectrometry (LC-MS). Cells were treated as described in the radiolabeled uptake studies. After the incubation step of 5 to 10 min of the unlabeled compounds at final concentration of 10 to 40 µM and after the washing step with ice-cold PBS (4°C), samples were treated with one part lysis buffer and with two parts of

icecold MeOH solution. Samples were transferred to a 96 well plate and subsequently centrifuged (3700 rpm, 4°C, 10 min) and the supernatants were used for LC-MS analysis. Calibration curve with the same matrix was used for quantification of the samples.

**Statistical Analysis.** Experiments were performed with sample triplicates at least two to three times ( $n = 2-3$ ), and the results are expressed as % of DMSO control and show the mean with the corresponding standard deviation. Graphs and calculations were in general prepared by use of Microsoft Excel or GraphPad Prism® software 5.0f (GraphPad Software, Inc., La Jolla, CA). The half maximal inhibition concentration ( $IC_{50}$ ) values were calculated by nonlinear regression from a sigmoidal dose-response curve by use of Prism®. The Michaelis Menten constant ( $K_m$ ) and maximum transport velocity ( $V_{max}$ ) values were also calculated by nonlinear regression by Prism® by use of the following equation:  $Y = (V_{ma} \times X)/(K_m + X)$ , where Y is transport velocity per time and X is substrate concentration. Statistical differences among groups were evaluated by one-way ANOVA (between multiple groups) with Bonferroni's multiple comparison test (Prism 5.0f). When  $p < 0.05$ , statistical significance was considered to be achieved.

**Protein Determination.** The total cellular protein content was determined using Pierce BCA Protein Assay Kit according to manufacturer's specifications.



### 3.4. Cell Toxicity Studies

The cell toxicity studies were performed in collaboration with the master student Kaja Maier, with the Ph.D. student Simon Kleeb and with the internship student Noemi Cowan. The results obtained by the methods described below are presented in chapter 4.1 (page 76).

#### Cell Culture

The HepG2 cells were cultivated in tissue culture flasks (BD Biosciences, Franklin Lakes, NJ, USA) with DMEM high glucose medium containing FBS (10%), L-glutamine (2 mM), penicillin (100 U/ml) and streptomycin (100 µg/ml), and NEAA (1%). The cells were kept at 37°C in humidified air containing 5% CO<sub>2</sub>, and the medium was changed every second day. When 70-90% confluence was reached, the cells were split with trypsin in a 1:10 ratio and distributed to new tissue culture flasks. The cell number was determined using a Countess® Automated Cell Counter (Invitrogen, Carlsbad, CA, USA).

#### The MTT-Assay<sup>20</sup>

Cells were seeded at a density of  $2 \times 10^4$  cells/well to a 96-well tissue culture plate (BD Biosciences, Franklin Lakes, NJ, USA) with 100 µl/well. The plate was then incubated (37°C, 5% CO<sub>2</sub>) for 24 hours to let the cells adhere and grow.

Then, series of dilutions of terfenadine (positive control) and three test compounds (FimH antagonists) were prepared in DMSO. DMSO was used as control. After removal of the media from the 96-well plate, 100 µl of each compound concentration was applied in triplicates to the 96-well plate and incubated for 24 hours.

Afterwards, a 5 mg/ml MTT stock solution in PBS was diluted 1:10 in supplemented DMEM. After removing the compound solutions from the 96-well plate, 100 µl of the MTT solution was added to each well and the plate was incubated for two hours. Following MTT removal from the plate, 20 µl of a 3% SDS solution and 100 µl of a 0.04 N HCl-isopropanol solution were added to lyse the cells and dissolve the intracellular formazan crystals. For this purpose, the plate was put onto a Heidolph Titramax 1000 plate shaker (Heidolph Instruments GmbH & Co. KG, Schwabach, Germany) for 2.5 hours (600 rpm, 25°C). Finally, the optical density (OD) was measured with a UV-spectrometer (Spectra MAX 190, Molecular Devices, Sunnyvale, CA, USA) at 550 nm and the OD at 620 nm was subtracted to reduce the impact of interfering overlapping wavelengths.

**Statistical Analysis.** All experiments were performed in triplicates and results are represented by viabilities in % of the DMSO control with the corresponding standard deviation.

### 3.5. References

1. Kola, I.; Landis, J. Can the pharmaceutical industry reduce attrition rates? *Nat. Rev. Drug Discov.* **2004**, *3*, 711-5.
2. Klein, T.; Abgottspon, D.; Wittwer, M.; Rabbani, S.; Herold, J.; Jiang, X.; Kleeb, S.; Luethi, C.; Scharenberg, M.; Bezencon, J.; Gubler, E.; Pang, L.; Smiesko, M.; Cutting, B.; Schwardt, O.; Ernst, B. FimH Antagonists for the Oral Treatment of Urinary Tract Infections: From Design and Synthesis to *In Vitro* and *In Vivo* Evaluation. *J. Med. Chem.* **2010**, *53*, 8627-8641.
3. Pang, L.; Kleeb, S.; Lemme, K.; Rabbani, S.; Scharenberg, M.; Zalewski, A.; Schadler, F.; Schwardt, O.; Ernst, B. FimH antagonists: structure-activity and structure-property relationships for biphenyl alpha-D-mannopyranosides. *ChemMedChem* **2012**, *7*, 1404-22.
4. Kleeb, S.; Pang, L.; Mayer, K.; Eris, D.; Sigl, A.; Preston, R. C.; Zihlmann, P.; Sharpe, T.; Jakob, R. P.; Abgottspon, D.; Hutter, A. S.; Scharenberg, M.; Jiang, X.; Navarra, G.; Rabbani, S.; Smiesko, M.; Ludin, N.; Bezencon, J.; Schwardt, O.; Maier, T.; Ernst, B. FimH Antagonists: Bioisosteres To Improve the *In Vitro* and *In Vivo* PK/PD Profile. *J. Med. Chem.* **2015**, *58*, 2221-39.
5. Kleeb, S.; Jiang, X.; Frei, P.; Sigl, A.; Bezencon, J.; Bamberger, K.; Schwardt, O.; Ernst, B. FimH Antagonists: Phosphate Prodrugs Improve Oral Bioavailability. *J. Med. Chem.* **2016**, *59*, 3163-3182.
6. Bezencon, J.; Wittwer, M. B.; Cutting, B.; Smiesko, M.; Wagner, B.; Kansy, M.; Ernst, B. pKa determination by (1)H NMR spectroscopy - an old methodology revisited. *J. Pharm. Biomed. Anal.* **2014**, *93*, 147-55.
7. Dearden, J. C.; Bresnen, G. M. The Measurement of Partition-Coefficients. *Quant. Structure-Activity Relationships* **1988**, *7*, 133-144.
8. Waring, M. J. Lipophilicity in drug discovery. *Expert Opin. Drug Discov.* **2010**, *5*, 235-48.
9. Dressman, J. B.; Thelen, K.; Jantratid, E. Towards quantitative prediction of oral drug absorption. *Clin. Pharmacokinet.* **2008**, *47*, 655-67.
10. Jantratid, E.; Janssen, N.; Reppas, C.; Dressman, J. B. Dissolution media simulating conditions in the proximal human gastrointestinal tract: an update. *Pharm. Res.* **2008**, *25*, 1663-76.
11. Alsenz, J.; Kansy, M. High throughput solubility measurement in drug discovery and development. *Adv. Drug Deliv. Rev.* **2007**, *59*, 546-67.
12. Li, P.; Zhao, L. Developing early formulations: practice and perspective. *Int. J. Pharm.* **2007**, *341*, 1-19.
13. Kansy, M.; Senner, F.; Gubernator, K. Physicochemical high throughput screening: Parallel artificial membrane permeation assay in the description of passive absorption processes. *J. Med. Chem.* **1998**, *41*, 1007-1010.
14. Hubatsch, I.; Ragnarsson, E. G. E.; Artursson, P. Determination of drug permeability and prediction of drug absorption in Caco-2 monolayers. *Nat. Prot.* **2007**, *2*, 2111-2119.
15. Artursson, P.; Karlsson, J. Correlation between oral drug absorption in humans and apparent drug permeability coefficients in human intestinal epithelial (Caco-2) cells. *Biochem. Biophys. Res. Commun.* **1991**, *175*, 880-5.
16. Li, A. P.; Lu, C.; Brent, J. A.; Pham, C.; Fackett, A.; Ruegg, C. E.; Silber, P. M. Cryopreserved human hepatocytes: characterization of drug-metabolizing enzyme activities and applications in higher throughput screening assays for hepatotoxicity, metabolic stability, and drug-drug interaction potential. *Chem. Biol. Interact.* **1999**, *121*, 17-35.
17. Li, A. P. Screening for human ADME/Tox drug properties in drug discovery. *Drug Discov. Today* **2001**, *6*, 357-366.
18. Wan, H.; Rehngren, M. High-throughput screening of protein binding by equilibrium dialysis combined with liquid chromatography and mass spectrometry. *J. Chromatogr. A.* **2006**, *1102*, 125-34.
19. Grube, M.; Kock, K.; Oswald, S.; Draber, K.; Meissner, K.; Eckel, L.; Bohm, M.; Felix, S. B.; Vogelgesang, S.; Jedlitschky, G.; Siegmund, W.; Warzok, R.; Kroemer, H. K. Organic anion transporting polypeptide 2B1 is a high-affinity transporter for atorvastatin and is expressed in the human heart. *Clin. Pharmacol. Ther.* **2006**, *80*, 607-20.
20. Hamid, R.; Rotshteyn, Y.; Rabadi, L.; Parikh, R.; Bullock, P. Comparison of alamar blue and MTT assays for high through-put screening. *Toxicol. in Vitro* **2004**, *18*, 703-710.

---

## 4 Results and Discussion: FimH Antagonists

---

In this chapter, the physicochemical and pharmacokinetic properties of selected classes of FimH antagonists determined by published *in vitro* assays are summarized. The first subchapter will illustrate trends, classification systems, and to what extent FimH antagonists can be orally available, as well as potential modifications to improve the latter property. In the second through fourth subchapters, strategies to improve permeability and solubility are discussed and stability in gastrointestinal fluids is analyzed.

Parts of the data illustrated in this thesis are the result of former master students work (Kaja Maier, Stefania Cigardi, Karen Bamberger, Florentina Schädler, Noemi Cowan, Marcel Lindegger, and Philipp Dätwyler). The results for carrier-mediated transporters resulted from a collaboration with Prof. Dr. H. Meyer zu Schwabedissen (Group of Biopharmacy, Department of Pharmaceutical Sciences, University of Basel). FimH antagonists mentioned in this chapter were synthesized in-house by Bea Wagner, Dr. Oliver Schwardt, Dr. Tobias Klein, Dr. Xiaohua Jiang, Dr. Katharina Mayer, Dr. Lijuan Pang, Dr. Wojciech Schönemann, Margrit Hartmann, Philip Dätwyler, Priska Frei, Marcel Lindegger, Sophie Boschung, Hülya Süyün, Martina Haug, and Janno Herold.

At the beginning of the subchapter 4.1 - 4.4, unpublished results are presented. The subchapters 4.2 and 4.3 include publications. My specific contribution is mentioned at the beginning of each publication.

### 4.1 Trends to Predict Potential Oral Bioavailability of FimH Antagonists

Trends in *in vitro* pharmacokinetic properties are a useful tool for selecting specific compound classes, and to avoid attrition in a late pre-clinical stage.<sup>1</sup> To achieve oral availability as well as a therapeutic concentration in the bladder over an extended period of time, a number of key issues have to be fulfilled.

- Stability of the antagonist against various gastrointestinal conditions (pH, enzymatic activity) is required.
- Sufficient solubility is a prerequisite for successful absorption.
- To reach circulation, the intestinal mucosa has to be permeated.
- In case of a prodrug approach, hepatic first pass metabolism is requested.
- To reach the therapeutic target in the bladder, renal excretion of the active principle is required.

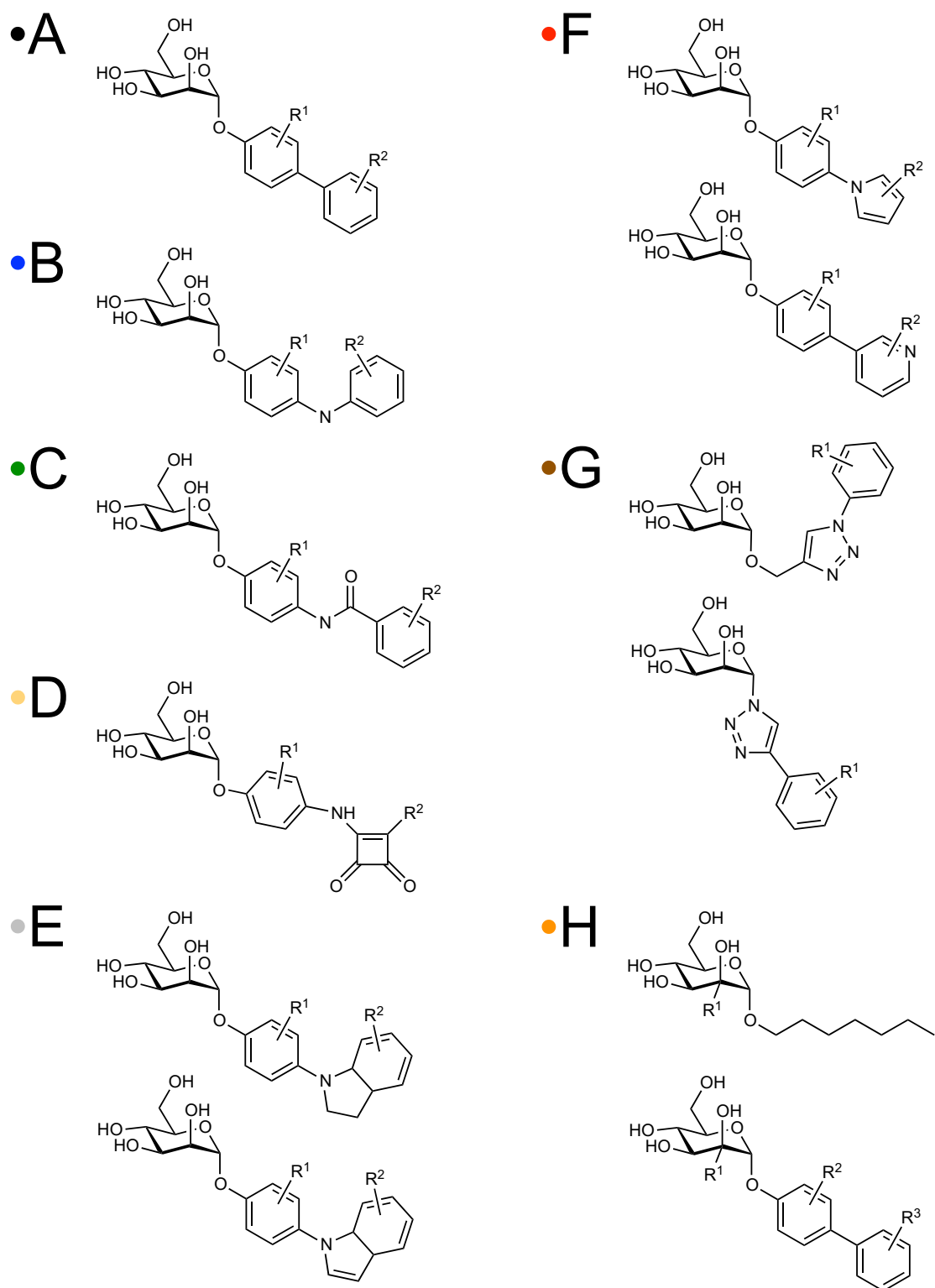
Carbohydrates have pharmacokinetic drawbacks, as they are too polar to permeate through the intestinal membrane when dosed orally.<sup>2</sup> Lipophilicity ( $\log P$ ) is a structural property with influence on both physicochemical (stability, solubility, and permeability) and biochemical properties (metabolic stability and plasma protein binding).<sup>3-5</sup> For this reason, mannosidic FimH antagonists with various aglycones as biphenyl,<sup>6-8</sup> phenylaminophenyl, benzamidylphenyl, phenylsquaramide, indolinyphenyl and indolyphenyl,<sup>9</sup> pyrrolyphenyl and pyridinyphenyl<sup>10</sup>, and phenyltriazolymethyl and phenyltriazolyl<sup>11</sup> were synthesized (Figure 4.1, A-G). In a second series, *n*-heptyl  $\alpha$ -D-mannosides and biphenyl  $\alpha$ -D-mannosides were branched at C-2 (Figure 4.1, H). In order to evaluate and compare the pharmacokinetic trends for these classes of FimH antagonists, the structural, physicochemical, and biochemical properties were determined within our PADMET (**p**hysicochemical properties, **a**bsorption, **d**istribution, **m**etabolism, **e**limination, **t**oxicity) platform.

#### The Influence of Lipophilicity on Other Physicochemical and Biochemical Properties

Figure 4.2 illustrates the correlation of  $\log D_{7.4}$  and passive transcellular permeability, as measured with the PAMPA assay<sup>12</sup>, for different classes of FimH antagonists. Compounds with  $\log D_{7.4} < 1$  show mainly low passive permeation, whereas compounds with  $\log D_{7.4} > 1$  exhibit a high when the  $\log P_e > -5.7$  cm/s or a low probability for  $\log P_e < -6.3$ .<sup>13</sup>

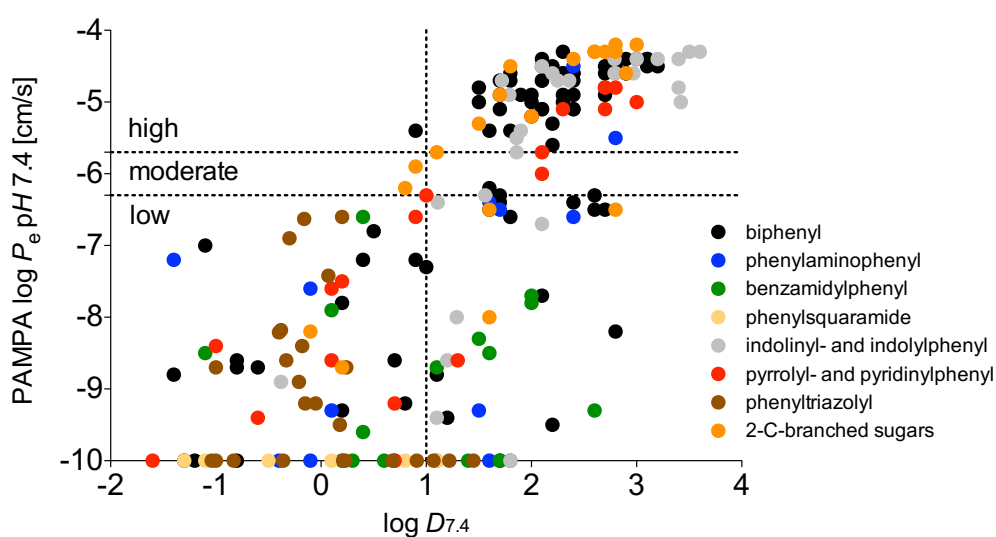
FimH antagonists containing phenylsquaramide (yellow) or phenyltriazolymethyl and phenyltriazolyl (brown) are not sufficiently lipophilic to be permeable, whereas 2-C-branched sugars (orange), biphenyl<sup>6-8</sup> (black), indolinyphenyl and indolyphenyl<sup>9</sup> (grey) or pyrrolyphenyl and pyridinyphenyl





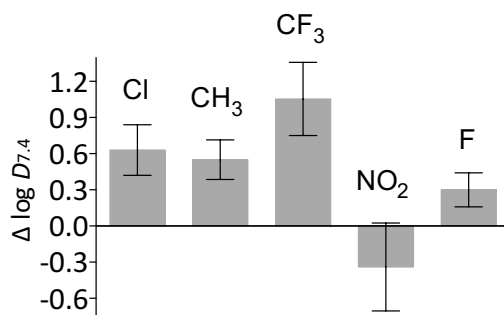
**Figure 4.1.** Classes of FimH antagonists: A) biphenyl<sup>6-8</sup> (black), B) phenylaminophenyl (blue), C) benzamidylphenyl (green), D) phenylsquaramides (yellow), E) indolinyphenyl and indolylphenyl<sup>9</sup> (grey), F) pyrrolylphenyl and pyridinylphenyl<sup>10</sup> (red), G) phenyltriazolylmethyl and phenyltriazolyl<sup>11</sup> (brown), H) 2-C-branched sugars (orange).

(red) exhibit a good correlation with  $r^2$ -values of 0.60, 0.52, 0.54, and 0.74, respectively (coefficient of determination). The family of phenylaminophenyl (blue) and the benzamidylphenyl (green) mannosides contains both lipophilic and hydrophilic compounds, and only a few of the lipophilic phenylaminophenyl are passively permeable. Lipophilicity has an impact on the partition between water and membrane, but does not allow predicting passive permeability.<sup>14</sup> Therefore, for predicting potential passive permeability both lipophilicity and effective permeability ( $\log P_e$  measured with the PAMPA)<sup>12</sup> results are necessary. Similar conclusions have been drawn for drug classes other than carbohydrates.<sup>3-5</sup> However, for compounds with  $\log D_{7.4} < 1$  or  $\log P_e < -6.3$  cm/s, ester prodrugs or transporter-targeting approaches should be evaluated.



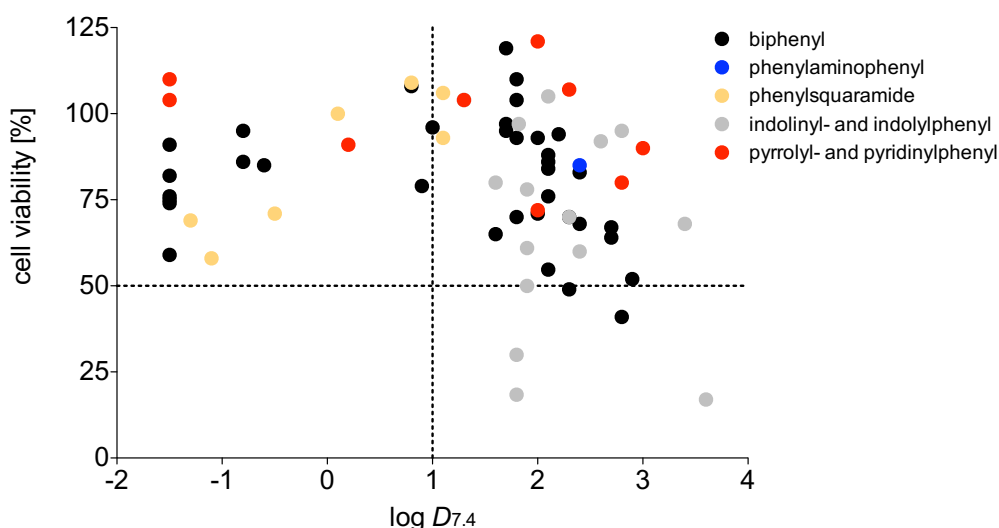
**Figure 4.2.** Plot of  $\log D_{7.4}$  versus PAMPA  $\log P_e$  (cm/s; pH 7.4) for different classes of FimH antagonists. Data represent the mean only. Standard deviations for PAMPA  $\log P_e$  values are  $\leq 2.0$  cm/s with the median of 0.1 cm/s and for  $\log D_{7.4}$  values  $\leq 0.2$  units with the median of 0.1 units ( $\log D_{7.4}$ , sextuplets; PAMPA  $\log P_e$ , quadruplets). Classes of FimH antagonists are shown in black (biphenyl<sup>6-8</sup>), blue (phenylaminophenyl), green (benzamidylphenyl), yellow (phenylsquaramide), grey (indolinyphenyl and indolyphenyl<sup>9</sup>), red (pyrrolylphenyl and pyridinyphenyl<sup>10</sup>), brown (phenyltriazolylmethyl and phenyltriazolyl<sup>11</sup>), and orange (2-C-branched sugars). Dashed lines on the y-axis indicate the threshold between low, moderate, and high effective permeability ( $-5.7$  cm/s < moderate  $\log P_e > -6.3$  cm/s).<sup>13</sup>

Substituents  $R^1$  or  $R^2$  of the aromatic ring system in the aglycone in the different classes of FimH antagonists A, C, E, and G (Figure 4.2) impact the  $\log D_{7.4}$  values (Figure 4.3). Whereas a chloro- (Cl), methyl- ( $\text{CH}_3$ ), trifluoromethyl- ( $\text{CF}_3$ ), or fluoro-substituent increases lipophilicity by  $0.6 \pm 0.2$ ,  $0.56 \pm 0.2$ ,  $1.1 \pm 0.3$ ,  $0.3 \pm 0.1$  units, respectively, a nitro- ( $\text{NO}_2$ ) group reduces lipophilicity ( $\Delta \log D_{7.4} = -0.3 \pm 0.3$ ).

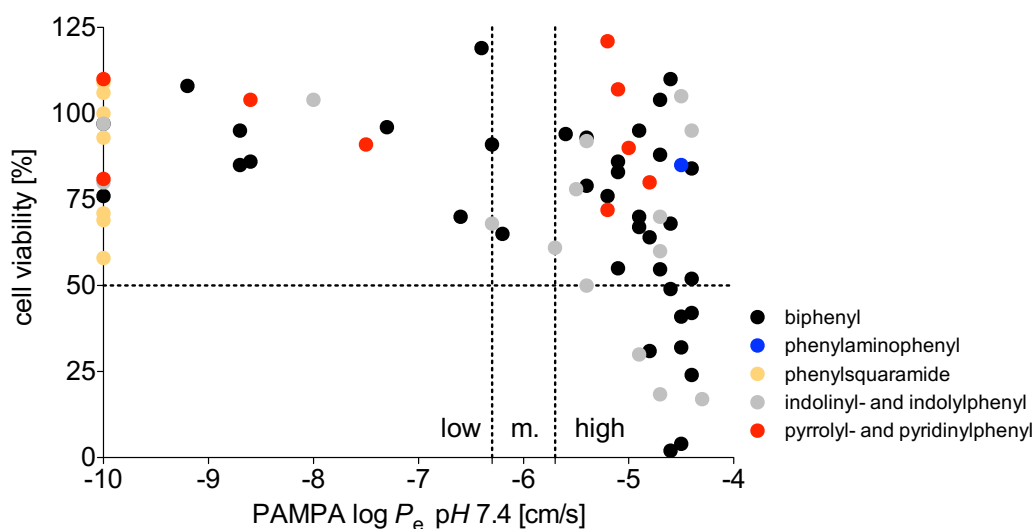


**Figure 4.3.** The impact on lipophilicity ( $\log D_{7.4}$ ) of aromatic substituents (Cl, CH<sub>3</sub>, CF<sub>3</sub>, NO<sub>2</sub>, and F) on the aglycone moiety of FimH antagonists including the classes: biphenyl, benzamidylphenyl, indolinyphenyl and indolyphenyl, and phenyltriazolymethyl and phenyltriazolyl. Data represent the mean with the corresponding standard deviation (Cl, n = 14; CH<sub>3</sub>, n = 6; CF<sub>3</sub>, n = 5; NO<sub>2</sub>, n = 5; F, n = 2).

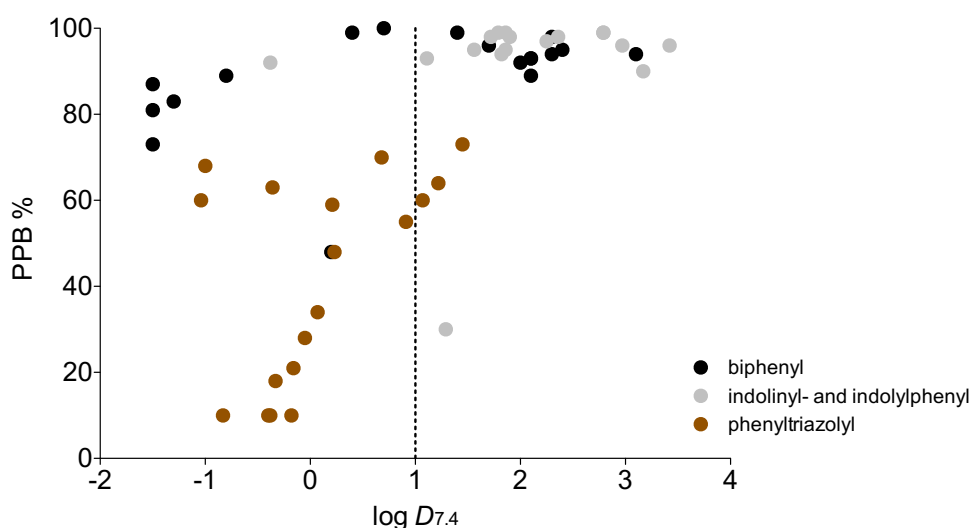
In addition,  $\log D_{7.4} > 1$  indicates a higher risk of cell toxicity (Figure 4.4) due to better permeability into cells (Figure 4.5). Cell toxicity influences cell-based assays and should be evaluated in order to exclude biased results. Lipophilicity also influences plasma protein binding (PPB). As can be seen in Figure 4.6, PPB is between 80 -100% (with four exceptions) where  $\log D_{7.4}$  is  $> 1$ . Clinical relevance of changes in PPB are low,<sup>15</sup> therefore no threshold can be made.



**Figure 4.4.** Plot of  $\log D_{7.4}$  versus cell viability (%) at a concentration of 100  $\mu\text{M}$  as determined with the 3-[4,5-dimethylthiazol-2-yl]-2,5-diphenyltetrazolium bromide (MTT) assay. Data represent the mean only. Standard deviations for  $\log D_{7.4}$  values are  $\leq 0.2$  units with the median of 0.1 units and for cell viability data  $\leq 26\%$  with the median of 5% ( $\log D_{7.4}$ , sextuplets; cell viability %, triplicates). Classes of FimH antagonists are shown in black (biphenyl<sup>6-8</sup>), blue (phenylaminophenyl), yellow (phenylsquaramides), grey (indolinyphenyl and indolyphenyl<sup>9</sup>), and red (pyrrolylphenyl and pyridinyphenyl<sup>10</sup>).



**Figure 4.5.** Plot of PAMPA  $\log P_e$  versus cell viability (%) at a concentration of 100  $\mu\text{M}$  as determined with the MTT assay. Data represent the mean only. Standard deviations for cell viability data are  $\leq 26\%$  with the median of 5% and for PAMPA  $\log P_e$  data  $\leq 2.0$  cm/s with the median of 0.1 units (cell viability %, triplicates; PAMPA  $\log P_e$  cm/s, quadruplets). Classes of FimH antagonists are shown in black (biphenyl<sup>6-8</sup>), blue (phenylaminophenyl), yellow (phenylsquaramides), grey (indolinyphenyl and indolyphenyl<sup>9</sup>), and red (pyrrolylphenyl and pyridinyphenyl<sup>10</sup>). Dashed lines on the x-axis show the threshold between low, moderate (m.), and high effective permeability ( $-5.7$  cm/s < moderate  $\log P_e$  >  $-6.3$  cm/s).<sup>13</sup>

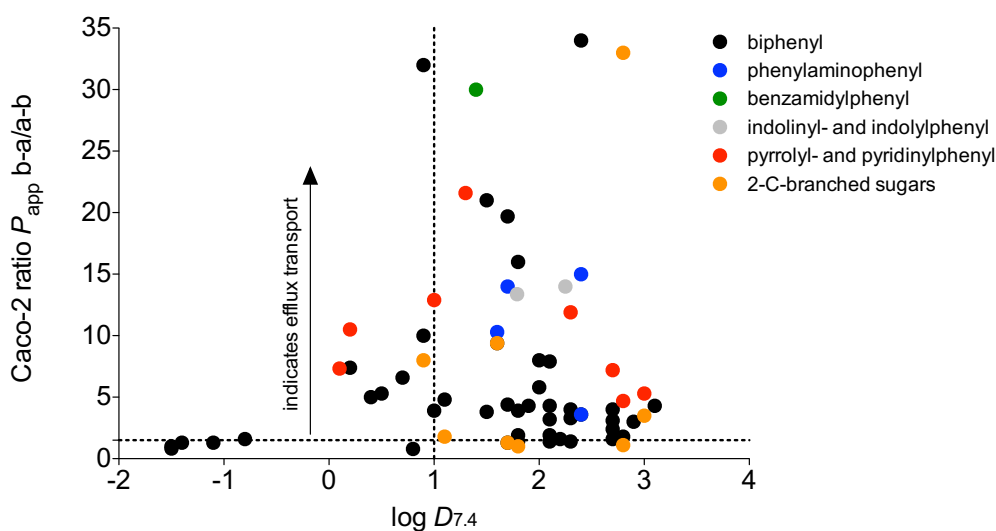


**Figure 4.6.** Plot of  $\log D_{7.4}$  versus plasma protein binding (PPB %). Data represent the mean only. Standard deviations for  $\log D_{7.4}$  values are  $\leq 0.2$  units with the median of 0.1 units and for PPB  $\leq 9\%$  with the median of 1% ( $\log D_{7.4}$ , sextuplets; PPB %, triplicates). Classes of FimH antagonists are shown in black (biphenyl<sup>6-8</sup>), grey (indolinyphenyl and indolyphenyl<sup>9</sup>), and brown (phenyltriazolylmethyl and phenyltriazolyl<sup>10</sup>).

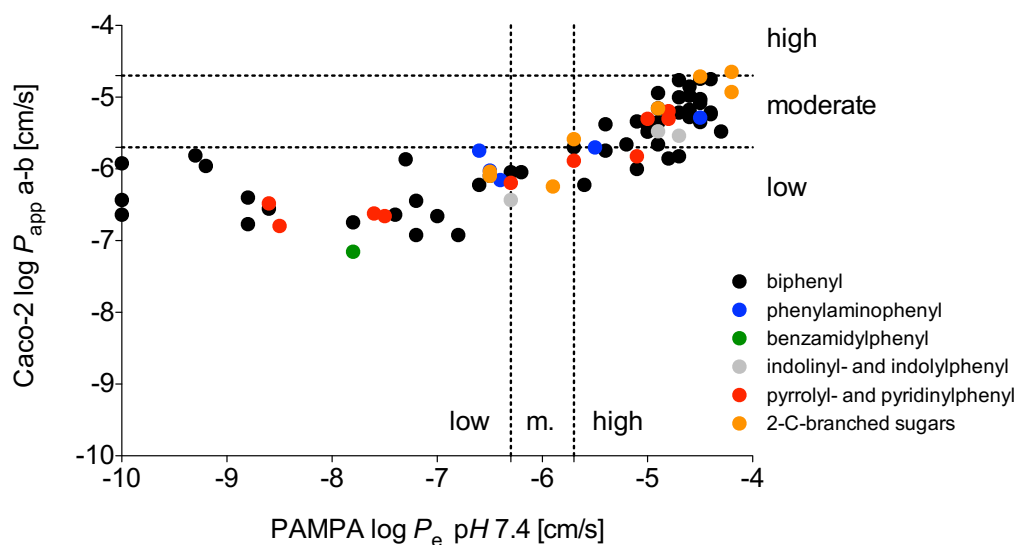
### Permeability measured in Caco-2 Versus Permeability measured in PAMPA

Caco-2 permeability studies are primarily performed with compounds showing moderate to high effective permeability ( $\log P_e > -6.3$  cm/s). Ratios of Caco-2  $P_{app}$  a-b/b-a  $> 1.5 - 2$  are an indication of efflux transport.<sup>16</sup> According to Figure 4.7 efflux transport was neither present for compounds with  $\log D_{7.4} < 0$ , nor for some of the lipophilic compounds. For lipophilic compounds indicating a possible efflux transport, further testing by saturation or inhibition of the transporter was performed.

Furthermore, it could be illustrated that for compounds with moderate and some with high permeability according to the PAMPA assay, only low Caco-2 permeability ( $\log P_{app}$  a-b  $< -5.7$  cm/s) was obtained. This could be due to their efflux transport, which decreases Caco-2  $P_{app}$  a-b. Overall, Caco-2 permeability data ( $\log P_{app}$  a-b) as compared with the effective permeability data ( $\log P_e$  determined with the PAMPA) showed a good correlation with an  $r^2$ -value of 0.61 (Figure 4.8).



**Figure 4.7.** Plot of  $\log D_{7.4}$  versus Caco-2 b-a/a-b ratio. Data represent the mean only. Standard deviations for  $\log D_{7.4}$  values are  $\leq 0.2$  units with the median of 0.1 units. Caco-2 ratios were calculated with the mean of  $P_{app}$  a-b and b-a ( $\log D_{7.4}$ , sextuplets; Caco-2  $P_{app}$  a-b and b-a, triplicates). Ratios  $> 1.5 - 2$  indicate an efflux transport.<sup>16</sup> Classes of FimH antagonists are shown in black (biphenyl<sup>6-8</sup>), blue (phenylaminophenyl), green (benzamidylphenyl), yellow (phenylsquaramides), grey (indolinyphenyl and indolyphenyl<sup>9</sup>), red (pyrrolylphenyl and pyridinylphenyl<sup>10</sup>), and orange (2-C-branched sugars).



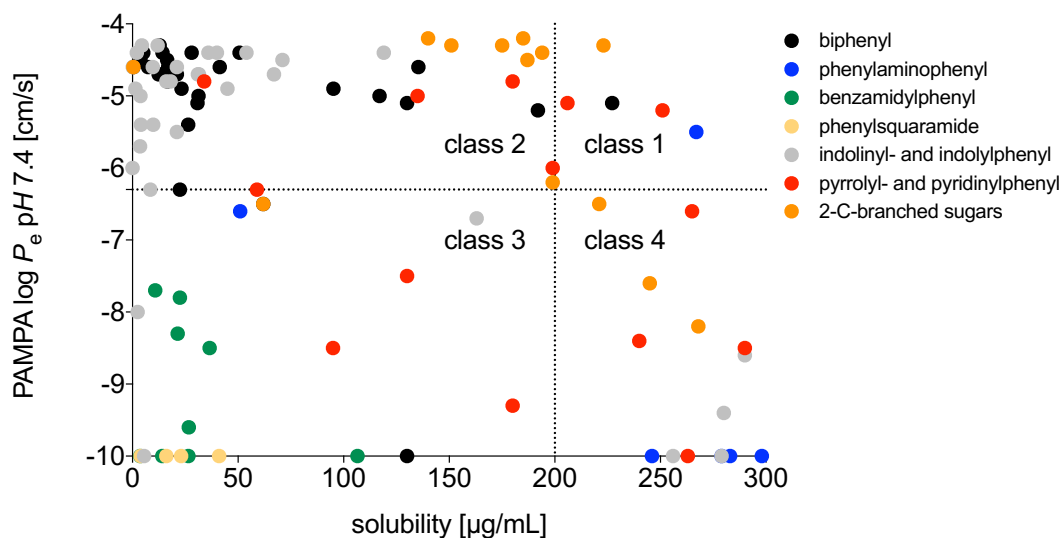
**Figure 4.8.** Plots of Caco-2 permeability  $\log P_{app}$  a-b (cm/s) versus PAMPA  $\log P_e$  (cm/s; pH 7.4). Data represent the mean only. Standard deviations for PAMPA  $\log P_e$  values are  $\leq 2.0$  cm/s with the median of 0.1 cm/s and for Caco-2  $P_{app} \leq 2.4 \times 10^{-6}$  cm/s with the median of  $0.32 \times 10^{-6}$  cm/s (Caco-2  $P_{app}$  a-b cm/s, triplicates; PAMPA  $\log P_e$  cm/s, quadruplets). Classes of FimH antagonists are shown in black (biphenyl<sup>6-8</sup>), blue (phenylaminophenyl), green (benzamidylphenyl), grey (indolinylnphenyl and indolyphenyl<sup>9</sup>), red (pyrrolylphenyl and pyridinylnphenyl<sup>10</sup>), and orange (2-C-branched sugars). Dashed lines on the x-axis show the threshold between low, moderate (m.), and high effective permeability ( $-5.7$  cm/s < moderate  $\log P_e$  >  $-6.3$  cm/s).<sup>13</sup>

### Effective Permeability Versus Solubility

Solubility and permeability are predictive for oral absorption. However, they are often negatively correlated to each other. As can be seen in Figure 4.9 improved  $\log P_e$  of biphenyl,<sup>6-8</sup> indolinylnphenyl and indolyphenyl,<sup>9</sup> or 2-C-branched sugars leads to a decrease in solubility. In general, compounds can be classified into four classes of the biopharmaceutical classification system (BCS): class 1 (high solubility, high permeability), class 2 (low solubility, high permeability), class 3 (high solubility, low permeability), and class 4 (low solubility, low permeability).<sup>17</sup> The threshold for effective permeability and solubility was set as described in Ref.<sup>13,18</sup> With class 1 compounds high oral bioavailability can be expected. To improve solubility and permeability ester prodrugs, phosphate prodrugs, and bioisosteres were synthesized and will be discussed in the next subchapters.

Since solubility can influence other *in vitro* screens, it should be determined early in the drug discovery process.<sup>19-21</sup> Kinetic solubility determination is fast and requires only small amount of a compound and is therefore the method of choice early in drug discovery. A solubility of  $\leq 50$   $\mu\text{g/mL}$  is required to exclude biased results. This threshold results from the concentrations required for other assays of the PADMET platform. In some cases, where solubility is lower than 50  $\mu\text{g/mL}$ , the

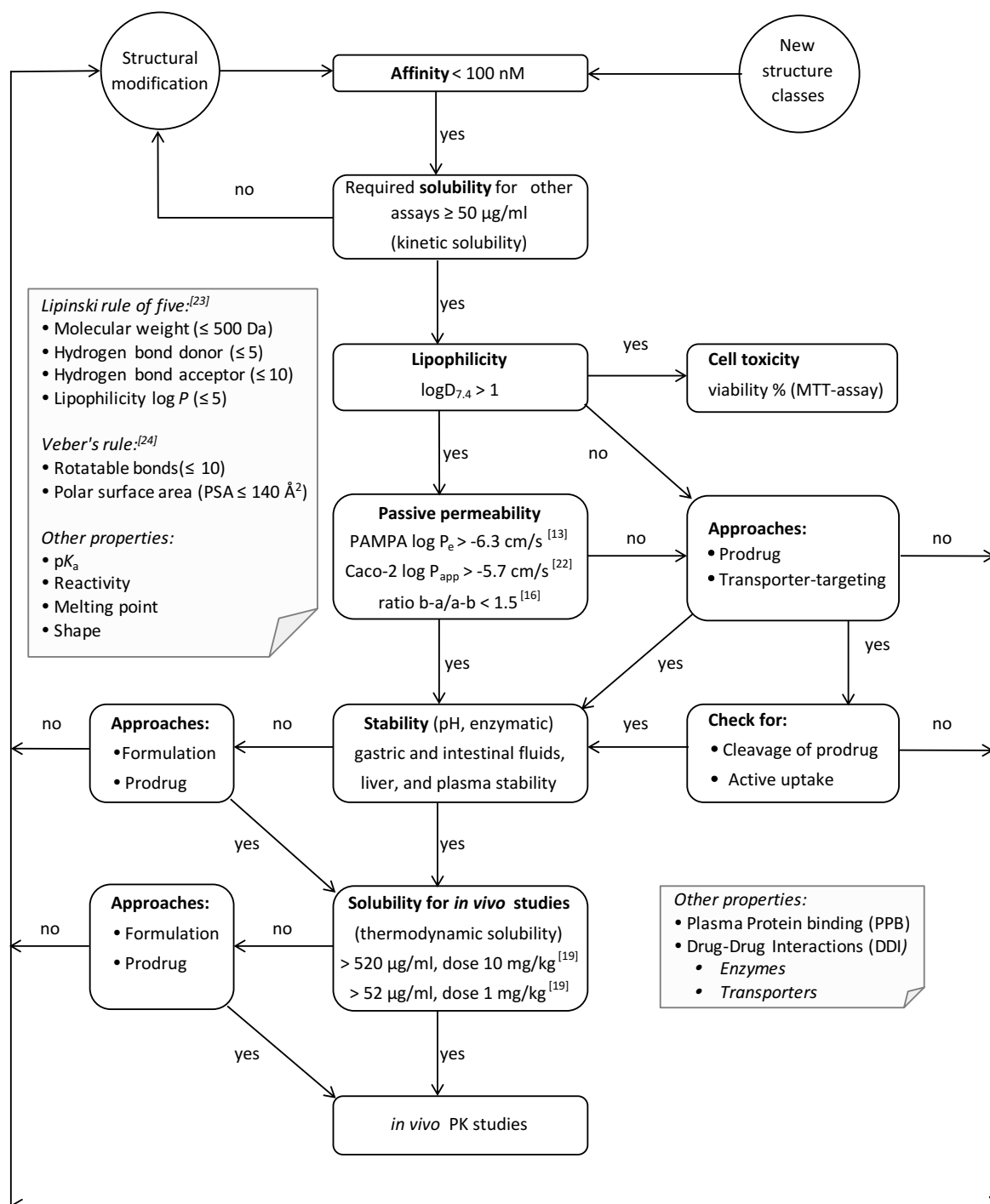
assay concentrations can be modified to a certain extent but need to be evaluated individually. Finally, the detection limit of the applied analytical devices (UV or LC-MS) have to be considered as well.



**Figure 4.9.** Plots of kinetic solubility ( $\mu\text{g/mL}$ ) versus PAMPA  $\log P_e$  ( $\text{cm/s}$ ;  $\text{pH } 7.4$ ). Data represent the mean only. Standard deviations for solubility are  $\leq 50 \mu\text{g/ml}$  with the median of  $3 \mu\text{g/ml}$  and for PAMPA  $\log P_e$  values  $\leq 2.0 \text{ cm/s}$  with the median of  $0.1 \text{ cm/s}$  (solubility, triplicates; PAMPA  $\log P_e$   $\text{cm/s}$ , quadruplets). Classes of FimH antagonists are shown in black (biphenyl<sup>6-8</sup>), blue (phenylaminophenyl), green (benzamidylphenyl), yellow (phenylsquaramides), grey (indolinylphenyl and indolylphenyl<sup>9</sup>), red (pyrrolylphenyl and pyridinylphenyl<sup>10</sup>), and orange (2-C-branched sugars). Dashed line on the y-axis indicates the threshold for low to moderate effective permeability ( $\log P_e > -6.3 \text{ cm/s}$ )<sup>12</sup> and the dashed line on the x-axis indicates the threshold for solubility defined by the biopharmaceutical classification system (BCS).<sup>17,18</sup>

In conclusion, the discussed trends and published thresholds were used to establish a decision tree for the prediction of potential oral bioavailability of a FimH antagonist (Figure 4.10). Based on the nanomolar affinities of a FimH antagonists, a minimum solubility of at least  $50 \mu\text{g/mL}$  is required before other assays are performed and to exclude biased results. Concerning lipophilicity, compounds with a  $\log D_{7.4} > 1$  are more likely to show passive permeability, whereas compounds with a  $\log D_{7.4} < 1$  should be screened for possible prodrug application or active uptake by transporters (for details refer to chapter 4.2, page 87). For the determination of passive permeability, PAMPA and Caco-2 assays were performed and the thresholds were set as described in Ref.<sup>13,15,21</sup> Furthermore, stability in gastrointestinal fluids is a prerequisite for permeability through the enterocytes (for details refer to chapter 4.4, page 217). Finally, the minimal required solubility for *in vivo* studies was calculated (dose vs. maximal volume for treatment), and prodrug approaches

(e.g. phosphate prodrugs), or solvent modification (e.g. preformulations) were applied for compounds with insufficient solubility (for details refer to chapter 4.3, page 123).



**Figure 4.10.** Decision tree to predict potential oral bioavailability of FimH antagonists.



## References

1. Kola, I.; Landis, J. Can the pharmaceutical industry reduce attrition rates? *Nat. Rev. Drug Discov.* **2004**, *3*, 711-5.
2. Ernst, B.; Magnani, J. L. From carbohydrate leads to glycomimetic drugs. *Nat. Rev. Drug Discov.* **2009**, *8*, 661-77.
3. Johnson, T. W.; Dress, K. R.; Edwards, M. Using the Golden Triangle to optimize clearance and oral absorption. *Bioorg. Med. Chem. Lett.* **2009**, *19*, 5560-4.
4. van de Waterbeemd, H.; Smith, D. A.; Beaumont, K.; Walker, D. K. Property-based design: Optimization of drug absorption and pharmacokinetics. *J. Med. Chem.* **2001**, *44*, 1313-1333.
5. Waring, M. J. Lipophilicity in drug discovery. *Expert Opin. Drug Discov.* **2010**, *5*, 235-48.
6. Klein, T.; Abgottspon, D.; Wittwer, M.; Rabbani, S.; Herold, J.; Jiang, X.; Kleeb, S.; Luethi, C.; Scharenberg, M.; Bezencon, J.; Gubler, E.; Pang, L.; Smiesko, M.; Cutting, B.; Schwaradt, O.; Ernst, B. FimH Antagonists for the Oral Treatment of Urinary Tract Infections: From Design and Synthesis to *in Vitro* and *in Vivo* Evaluation. *J. Med. Chem.* **2010**, *53*, 8627-8641.
7. Pang, L.; Kleeb, S.; Lemme, K.; Rabbani, S.; Scharenberg, M.; Zalewski, A.; Schadler, F.; Schwaradt, O.; Ernst, B. FimH antagonists: structure-activity and structure-property relationships for biphenyl alpha-D-mannopyranosides. *ChemMedChem* **2012**, *7*, 1404-22.
8. Kleeb, S.; Pang, L.; Mayer, K.; Eris, D.; Sigl, A.; Preston, R. C.; Zihlmann, P.; Sharpe, T.; Jakob, R. P.; Abgottspon, D.; Hutter, A. S.; Scharenberg, M.; Jiang, X.; Navarra, G.; Rabbani, S.; Smiesko, M.; Ludin, N.; Bezencon, J.; Schwaradt, O.; Maier, T.; Ernst, B. FimH Antagonists: Bioisosteres To Improve the *in Vitro* and *in Vivo* PK/PD Profile. *J. Med. Chem.* **2015**, *58*, 2221-39.
9. Jiang, X.; Abgottspon, D.; Kleeb, S.; Rabbani, S.; Scharenberg, M.; Wittwer, M.; Haug, M.; Schwaradt, O.; Ernst, B. Antiadhesion therapy for urinary tract infections--a balanced PK/PD profile proved to be key for success. *J. Med. Chem.* **2012**, *55*, 4700-13.
10. Pang, L.; Bezencon, J.; Kleeb, S.; Rabbani, S.; Sigl, A.; Smiesko, M.; Sager, C.P.; Eris, D.; Schwaradt, O.; Ernst, B. FimH Antagonists – Solubility vs. Permeability. *Carbohydrate Chemistry*, **2017**, *42*, 248-273.
11. Schwaradt, O.; Rabbani, S.; Hartmann, M.; Abgottspon, D.; Wittwer, M.; Kleeb, S.; Zalewski, A.; Smiesko, M.; Cutting, B.; Ernst, B. Design, synthesis and biological evaluation of mannosyl triazoles as FimH antagonists. *Bioorganic & Med. Chem.* **2011**, *19*, 6454-6473.
12. Kansy, M.; Senner, F.; Gubernator, K. Physicochemical high throughput screening: Parallel artificial membrane permeation assay in the description of passive absorption processes. *J. Med. Chem.* **1998**, *41*, 1007-1010.
13. Avdeef, A.; Bendels, S.; Di, L.; Faller, B.; Kansy, M.; Sugano, K.; Yamauchi, Y. PAMPA - Critical factors for better predictions of absorption. *J. Pharma. Sci.* **2007**, *96*, 2893-2909.
14. Guimaraes, C. R.; Mathiowetz, A. M.; Shalaeva, M.; Goetz, G.; Liras, S. Use of 3D properties to characterize beyond rule-of-5 property space for passive permeation. *J. Chem. Inf. Model* **2012**, *52*, 882-90.
15. Benet, L. Z.; Hoener, B. A. Changes in plasma protein binding have little clinical relevance. *Clin. Pharmacol. Ther.* **2002**, *71*, 115-21.
16. Hubatsch, I.; Ragnarsson, E. G. E.; Artursson, P. Determination of drug permeability and prediction of drug absorption in Caco-2 monolayers. *Nat. Protoc.* **2007**, *2*, 2111-2119.
17. Amidon, G. L.; Lennernäs, H.; Shah, V. P.; Crison, J. R. A theoretical basis for a biopharmaceutic drug classification: the correlation of *in vitro* drug product dissolution and *in vivo* bioavailability. *Pharm. Res.* **1995**, *12*, 413-420.
18. Benet, L. Z. The role of BCS (biopharmaceutics classification system) and BDDCS (biopharmaceutics drug disposition classification system) in drug development. *J. Pharm. Sci.* **2013**, *102*, 34-42.
19. Lipinski, C. A. Drug-like properties and the causes of poor solubility and poor permeability. *J. Pharmacol. Toxicol. Methods* **2000**, *44*, 235-249.
20. Di, L.; Kerns, E. H. Biological assay challenges from compound solubility: strategies for bioassay optimization. *Drug Discov. Today* **2006**, *11*, 446-51.
21. Di, L.; Fish, P. V.; Mano, T. Bridging solubility between drug discovery and development. *Drug Discov. Today* **2012**, *17*, 486-495.

22. Hou, T.; Wang, J.; Zhang, W.; Xu, X. ADME evaluation in drug discovery. 7. Prediction of oral absorption by correlation and classification. *J. Chem. Inf. Model* **2007**, *47*, 208-18.
23. Lipinski, C. A.; Lombardo, F.; Dominy, B. W.; Feeney, P. J. Experimental and computational approaches to estimate solubility and permeability in drug discovery and development settings. *Adv. Drug Deliv. Rev.* **1997**, *23*, 3-25.
24. Veber, D. F.; Johnson, S. R.; Cheng, H. Y.; Smith, B. R.; Ward, K. W.; Kopple, K. D. Molecular properties that influence the oral bioavailability of drug candidates. *J. Med. Chem.* **2002**, *45*, 2615-23.

## 4.2 Improved Permeability of FimH Antagonists

This chapter will focus on the study of active transport mechanisms and on structural modifications to gain actively translocated or more lipophilic compounds, which passively permeate the membranes (e.g. ester prodrug, Paper 2, page 107) to improve oral drug delivery.

The results of the carrier-mediated transporter studies were obtained in collaboration with the group of Prof. Dr. Henriette Meyer zu Schwabedissen, Janine Hussner, Dr. Katja Stangier, and Isabell Seibert (Group of Biopharmacy, Department of Pharmaceutical Sciences, University of Basel). FimH antagonists were synthesized in-house by W. Schönemann, Dr. X. Jiang, Dr. L. Pang, Dr. K. Mayer, P. Frei and Dr. O. Schwardt (Group of Molecular Pharmacy, Department of Pharmaceutical Sciences, University of Basel).

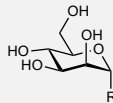
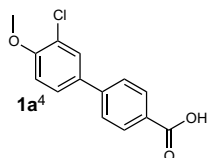
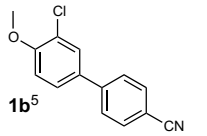
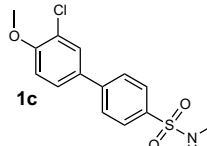
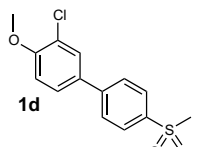
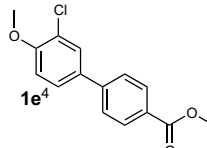
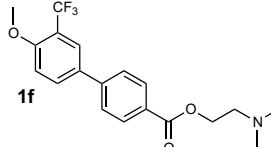
### 4.2.1 Carrier-Mediated Transport Studies with FimH Antagonists

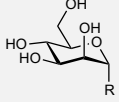
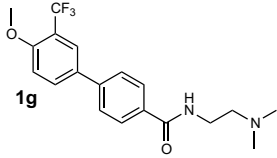
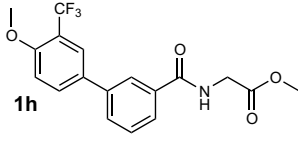
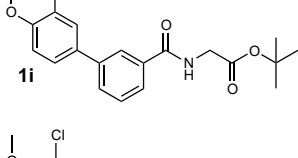
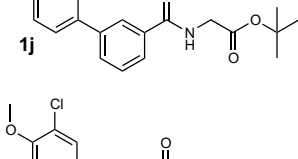
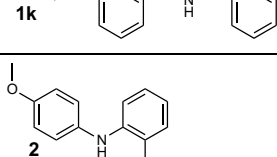
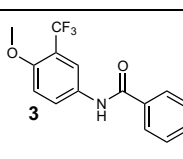
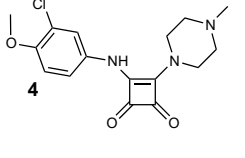
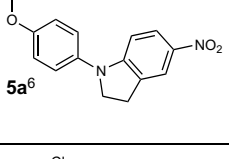
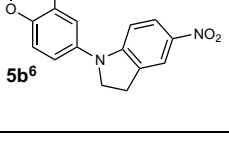

Since oral administration is the most convenient and common way of drug application, we are aiming for orally available FimH antagonists. Permeability through the enterocyte of the small intestines depending on passive/active uptake mechanisms is essential for oral drug delivery. For the FimH antagonists, renal elimination is further required to reach their target FimH at the tip of the bacterial pili, located in the bladder. Our aim is to identify antagonists, which first overcome the intestinal membrane to reach circulation and secondly are renally excreted such that high concentrations in the bladder over an extended period of time can be achieved and multiple dosing can be avoided. Since membrane transporters in the body, e.g. peptide transporter 1 (PEPT1; SLC15A1) or organic anion transporting polypeptide 2B1 (OATP2B1; SLCO2B1) can translocate drugs through membranes and therefore improve drug delivery,<sup>1,2</sup> the active transport mechanisms were analyzed by *in vitro* studies for the FimH antagonists. Interaction with drug transporters is not only of interest for drug delivery, but also for drug-drug interactions, which can have clinical effects as was shown in the case of digoxin and quinidine interacting with the efflux transporter P-gp.<sup>3</sup>

In this study, different mannosidic FimH antagonists with various aglycones and with various physicochemical properties (Table 4.1) were analyzed, that are biphenyl ( $\rightarrow$ **1a**,<sup>4</sup> **1b**,<sup>5</sup> **1c**, **1d**, **1e**,<sup>4</sup> and **1f** - **1k**), phenylaminophenyl ( $\rightarrow$ **2**), benzamidylphenyl ( $\rightarrow$ **3**), phenylsquaramide ( $\rightarrow$ **4**), indolylphenyl ( $\rightarrow$ **5a**,<sup>6</sup> **5b**,<sup>6</sup> **5c**, and **5d**), indolylphenyl ( $\rightarrow$ **6a**<sup>6</sup> and **6b**<sup>6</sup>), pyrrolylphenyl ( $\rightarrow$ **7**<sup>7</sup>) and pyridinephenyls ( $\rightarrow$ **8**<sup>7</sup> and **9**<sup>6</sup>), heptyl ( $\rightarrow$ **10**), phenyltriazolylmethyl ( $\rightarrow$ **11**<sup>8</sup>) phenyltriazolyl ( $\rightarrow$ **12**<sup>8</sup>), and guanidylphenyl mannosides ( $\rightarrow$ **13** and **14**). In a first screening, interaction of these FimH antagonists with the ubiquitously expressed uptake transporter OATP2B1, which is highly expressed in enterocytes and facilitates intestinal uptake of substrate drugs was evaluated.<sup>9,10</sup> In a second step,

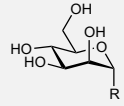
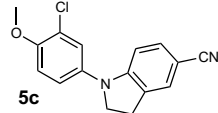
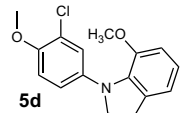
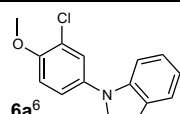
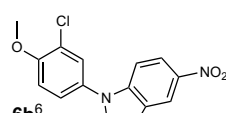
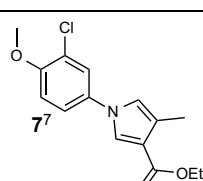
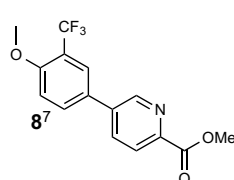
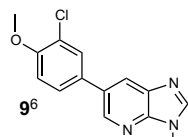
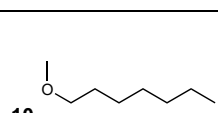
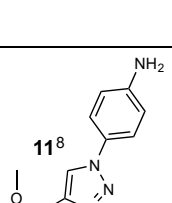
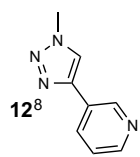
interaction of FimH antagonists with the OATP1B3 (SLCO1B3) transporter, present in the liver was considered to gain more structure property relationship (SPR) information regarding OATP transporters. Finally, the interaction of FimH antagonists with the organic cation transporter 2 (OCT2; SLC22A2) and the organic anion transporter 1 (OAT1; SLC22A6) involved in secretion of renal excretion will be evaluated.<sup>11</sup>

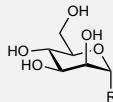
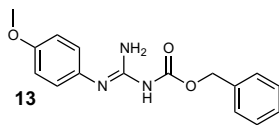
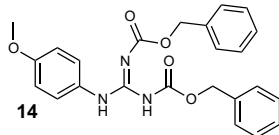
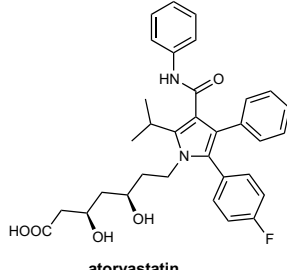
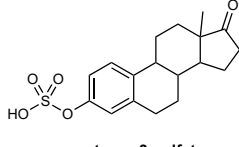
**Table 4.1.** Physiochemical ( $\log D_{7.4}$ , solubility and permeability) properties and cytotoxicity of various classes of FimH antagonists: biphenyl (**1a**<sup>4</sup>, **1b**<sup>5</sup>, **1c**, **1d**, **1e**<sup>4</sup>, **1f**, **1g**, **1h**, **1i**, **1j**, **1k**), phenylaminophenyl (**2**), benzamidylphenyl (**3**), phenylsquaramide (**4**), indolylphenyl (**5a**<sup>6</sup>, **5b**, **5c**<sup>6</sup>, **5d**), indolylphenyl (**6a**<sup>6</sup>, **6b**<sup>6</sup>), pyrrolyl- and pyridinephenyl (**7**, **8**, **9**<sup>6</sup>), heptyl (**10**), phenyltriazolymethyl, and phenyltriazolyl (**11**<sup>8</sup>, **12**<sup>8</sup>), guanidylphenyl (**13**, **14**) and the two control compounds for OATP2B1 transporter: atorvastatin (a known inhibitor and substrate) and estrone-3-sulfate ( $E_1S$ , a known substrate).<sup>19</sup> n.d. = not determined

 Compounds	$\log D_{7.4}$ <sup>a</sup>	Solubility <sup>b</sup> [ $\mu\text{g/mL}$ ] / pH	PAMPA $\log P_e$ [cm/s]	Cytotoxicity <sup>d</sup> MTT assay [% viability at 100 $\mu\text{M}$ ]
	-0.8	> 3000 / 6.5	-10	97 $\pm$ 5
	2.1 $\pm$ 0.0	192 $\pm$ 5 / 7.4	-5.2 $\pm$ 0.0 / 7.4	76 $\pm$ 5
	0.7 $\pm$ 0.1	> 250 / 7.4	-8.6 $\pm$ 0.2 / 7.4	n.d.
	1.0 $\pm$ 0.1	> 300 / 7.4	-7.3 $\pm$ 0.0 / 7.4	96 $\pm$ 4
	2.3	16.9 / 7.4	-4.6	49 $\pm$ 2
	1.7 $\pm$ 0.0	296 $\pm$ 8 / 7.4	-6.4 $\pm$ 0.0 / 7.4	119 $\pm$ 3

 <b>Compounds</b>	$\log D_{7.4}^a$	Solubility <sup>b</sup> [ $\mu\text{g/mL}$ ] / pH	PAMPA <sup>c</sup> $\log P_e$ [cm/s]	Cytotoxicity <sup>d</sup> MTT assay [% viability at 100 $\mu\text{M}$ ]
 <b>1g</b>	$0.7 \pm 0.0$	$333 \pm 3$ / 7.4	-10 / 7.4	n.d.
 <b>1h</b>	$1.7 \pm 0.1$	>360 / 7.4	-10 / 7.4	n.d.
 <b>1i</b>	$2.8 \pm 0.0$	$224 \pm 6$ / 7.4	$-8.2 \pm 2.1$ / 7.4	n.d.
 <b>1j</b>	$2.4 \pm 0.1$	$300 \pm 8$ / 7.4	$-6.4 \pm 0.1$ / 7.4	n.d.
 <b>1k</b>	$1.8 \pm 0.1$	$192 \pm 20$ / 7.4	-10 / 7.4	n.d.
 <b>2</b>	< -1.5	> 150 / 7.4	$-7.6 \pm 1.6$ / 7.4	n.d.
 <b>3</b>	$-1.1 \pm 0.2$	> 350 / 7.4	n.d.	n.d.
 <b>4</b>	$-1.3 \pm 0.1$	> 150 / 7.4	-10	$69 \pm 3$
 <b>5a<sup>6</sup></b>	1.9	24 / 6.5	-5.5	$78 \pm 0$
 <b>5b<sup>6</sup></b>	1.9	3.6 / 6.5	-5.7	$61 \pm 6$

#### 4 Results and Discussion: FimH Antagonists

 <b>Compounds</b>	<b>log D<sub>7.4</sub><sup>a</sup></b>	<b>Solubility<sup>b</sup></b> [μg/mL] / pH	<b>PAMPA<sup>c</sup></b> <b>log P<sub>e</sub></b> [cm/s]	<b>Cytotoxicity<sup>d</sup></b> <b>MTT assay</b> [% viability at 100 μM]
 <b>5c</b>	2.6 ± 0.1	9.8 ± 0.3 / 7.4	-5.4 ± 0.1 / 7.4	92 ± 4
 <b>5d</b>	2.2 ± 0.0	> 300 / 7.4	-4.6 ± 0.0 / 7.4	n.d.
 <b>6a<sup>6</sup></b>	1.8	31.5 / 6.5	-4.7	18 ± 10
 <b>6b<sup>6</sup></b>	1.8	1.4 / 6.5	-4.9	30 ± 19
 <b>77</b>	2.8 ± 0.1	> 180 / 7.4	-4.8 ± 0.1 / 7.4	80 ± 11
 <b>87</b>	1.3 ± 0.1	> 200 / 7.4	-8.6 ± 1.7 / 7.4	n.d.
 <b>96</b>	1.3	2.4 / 6.4	-8.0	104 ± 8
 <b>10</b>	1.65	> 3000 / 6.5	-4.9	95 ± 10
 <b>118</b>	0.2	> 2000 / 6.5	-6.6	n.d.
 <b>128</b>	-1.04	1378 / 5.30	-10	n.d.

 <b>Compounds</b>	<b>log <math>D_{7.4}</math><sup>a</sup></b>	<b>Solubility<sup>b</sup></b> [ $\mu\text{g}/\text{mL}$ ] / pH	<b>PAMPA<sup>c</sup></b> <b>log <math>P_e</math></b> [cm/s]	<b>Cytotoxicity<sup>d</sup></b> <b>MTT assay</b> [% viability at 100 $\mu\text{M}$ ]
 <b>13</b>	n.d.	> 400 / 7.4	$-10 \pm 0.0 / 7.4$	n.d.
 <b>14</b>	n.d.	$9.5 \pm 0.3 / 7.4$	$-5.0 \pm 0.1 / 7.4$	n.d.
<b>Control Compounds</b>				
 <b>atorvastatin</b>	n.d.	n.d.	$-5.4 \pm 0.0 / 7.4$	n.d.
 <b>estrone 3-sulfate</b>	n.d.	n.d.	$-6.7 \pm 0.1 / 7.4$	n.d.

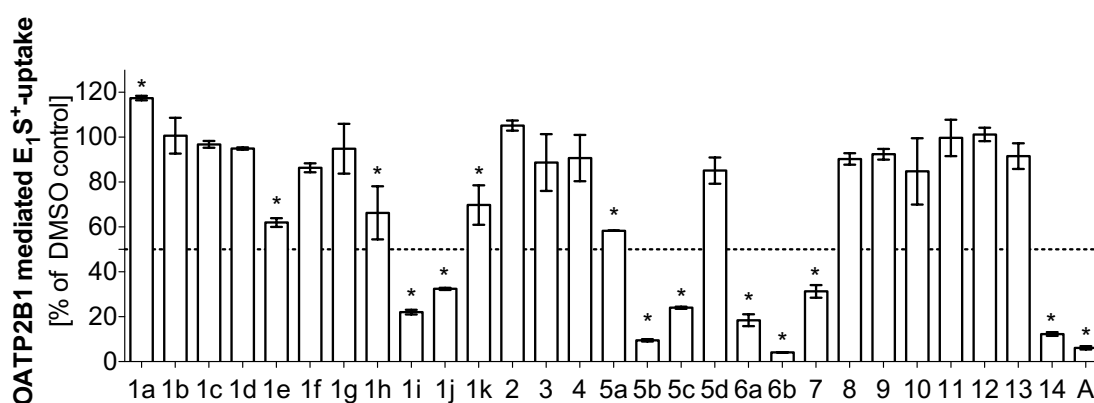
a) Partition coefficients ( $\log D_{7.4}$ ) were measured by a miniaturised shake-flask procedure at pH 7.4; values represent the mean with the corresponding standard deviation (sixtuplicates);<sup>12</sup> b) Thermodynamic solubility was determined at  $\text{pH} \leq 6.5$ ; Kinetic solubility at  $\text{pH} 7.4$ ; values represent the mean with the standard deviation (triplicates);<sup>13</sup> c)  $P_e$  = effective permeability: passive permeability through an artificial membrane was determined by the parallel artificial membrane permeability assay (PAMPA) at  $\text{pH} 7.4$ ; values represent the mean with the standard deviation (quadruplicates);<sup>14</sup> d) Cell toxicity was determined with HepG2 cells in a MTT assay; values represent the mean with the standard deviation (triplicates).<sup>15</sup>

### Interactions of FimH Antagonists with the Drug Transporter OATP2B1

To date, only a few data on the SPR of OATP2B1 are available.<sup>16,17</sup> A previous study showed that unlabeled estrone 3-sulfate ( $E_1S$ ) is actively transported into overexpressed MDCKII-OATP2B1 cells and is therefore classified as substrate of the transporter OATP2B1.<sup>18</sup> Therefore, inhibition of tritium labeled estrone-3-sulfate ( $E_1S^+$ ) uptake into MDCKII-OATP2B1 overexpressing cells by different classes of FimH antagonists was first analyzed. Then, the direct uptake of the FimH antagonists into MDCKII-OATP2B1 cells was addressed.

**OATP2B1 Inhibition Studies**

In a primary analysis, OATP2B1-overexpressing MDCKII cells were incubated with  $E_1S^+$  in presence of DMSO (negative control), various FimH antagonists, or the known inhibitor atorvastatin (positive control). After 10 min of incubation cells were washed with ice-cold PBS and radioactivity was determined. Eight of the 28 tested FimH antagonists exhibited potent inhibition with a reduction of the OATP2B1-mediated  $E_1S^+$  uptake to less than 50% compared to the negative control (100%, Figure 4.11). These eight FimH antagonists are the biphenyl mannosides **1i** and **1j**, the indolinyphenyl mannosides **5b** and **5c**, the indolylphenyl mannosides **6a** and **6b**, the pyrrolylphenyl mannoside **7**, and the guanidinyphenyl mannoside **14**.



**Figure 4.11.** Inhibition of OATP2B1-mediated  $E_1S^+$  uptake by FimH antagonists (**1a-1k**, **2 - 4**, **5a - 5d**, **6a**, **6b**, **7 - 14**) and by the known inhibitor atorvastatin (A) after incubation for 10 min. Compounds were applied at a concentration of 10  $\mu$ M. Data represent % of DMSO control and shows the mean with the corresponding standard deviation ( $n = 3$ ). Asterisk (\*) indicates significant difference to the DMSO control value ( $p < 0.05$ ).

In a second analysis, the half maximal inhibitory concentration ( $IC_{50}$ ) values of the eight potential inhibitors of the OATP2B1-mediated  $E_1S^+$  uptake was determined by applying series dilutions of these compounds during the incubation step. Their  $IC_{50}$ -values ranged from 0.19 to 4.72  $\mu$ M (Figure 4.13) and are comparable to the  $IC_{50}$ -value of atorvastatin (0.15  $\mu$ M, Figure 4.12).

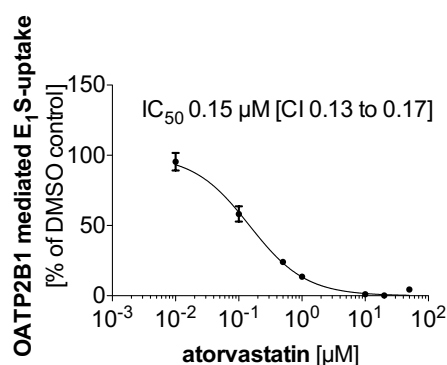
Small structural differences within various compound classes, e.i. biphenyl, indolinyphenyl, indolynphenyl, pyrrolylphenyl, and guanidinyphenyl showed to influence inhibition of the OATP2B1-mediated  $E_1S^+$  uptake.

*Biphenyl mannosides.* Compounds with substituents on the outer aromatic ring of the aglycone like the methyl ester ( $\rightarrow$ **1e**) and amides ( $\rightarrow$ **1h - 1k**) exhibit a greater impact on the OATP2B1-mediated

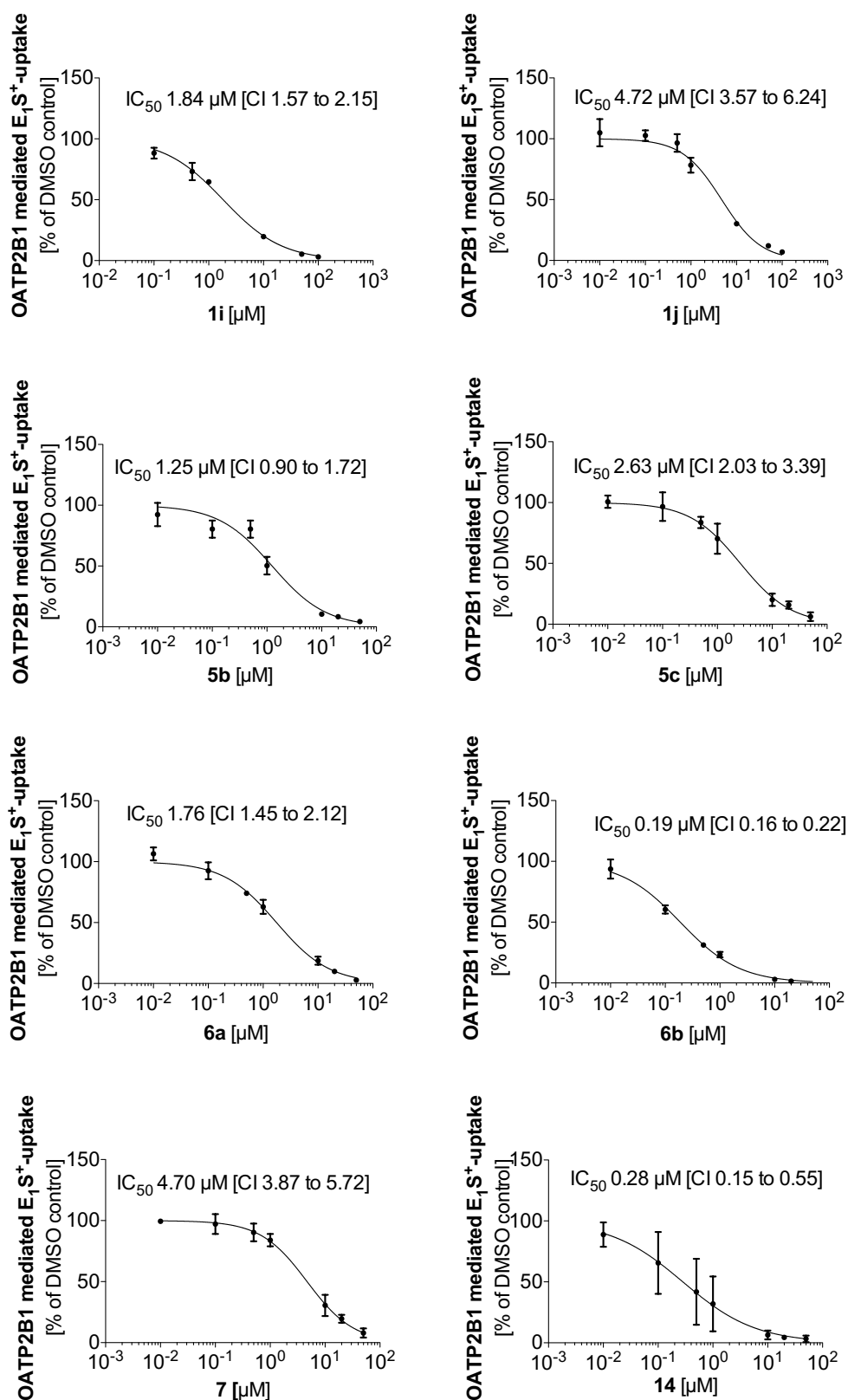


$E_1S^+$  uptake (< 80%) than compounds with other substituents at this position, i.e. the free carboxylic acid, the cyanide, the sulfonamide, and the sulfone ( $\rightarrow$ **1a** - **1d**, respectively, > 80%), the N,N-dimethylaminoethyl ester ( $\rightarrow$ **1f**, > 80%) or the N,N-dimethylaminoethyl amide ( $\rightarrow$ **1g**, > 80%). Furthermore, the compound **1i** with a glycine *tert*-butylester showed higher inhibition of the OATP2B1-mediated  $E_1S^+$  uptake (< 50%) than the analog with a glycine methylester ( $\rightarrow$ **1h**, > 50%). Compound **1i** with an *ortho*-trifluoromethyl moiety on the aromatic ring adjacent to the anomeric oxygen ( $\rightarrow$ **1i**) decreased the OATP2B1-mediated  $E_1S^+$  uptake by a factor of 1.5 compared to compound **1j** with a chloro substituent. These findings are comparable with their determined  $IC_{50}$  values ( $IC_{50}$  **1i** = 1.84 and  $IC_{50}$  **1j** = 4.72, Figure 4.13).

*Indoliny- and indolyphenyl mannosides.* In contrast to compound **5a**, which reduced the OATP2B1-mediated  $E_1S^+$  uptake to 60%, compound **5b** with a chloro substituent in the *ortho*-position of the aromatic ring adjacent to the anomeric oxygen decreased the uptake to less than 20%. In addition, increased inhibition could be observed for the indolinyphenyl mannoside with a nitro-substituent on the outer aromatic ring ( $\rightarrow$ **5b** and **6b**) with an OATP2B1-mediated  $E_1S^+$  uptake of less than 10%. These results are consistent with the  $IC_{50}$  value of **6b** ( $IC_{50}$  = 0.19  $\mu$ M, Figure 4.13) compared to the compound lacking the nitro-substituent ( $\rightarrow$ **6a**,  $IC_{50}$  = 1.76  $\mu$ M, Figure 4.13).



**Figure 4.12.**  $IC_{50}$  concentration of atorvastatin on OATP2B1-mediated  $E_1S^+$  uptake. Data represent % of DMSO control the mean with the standard deviation (triplicates).



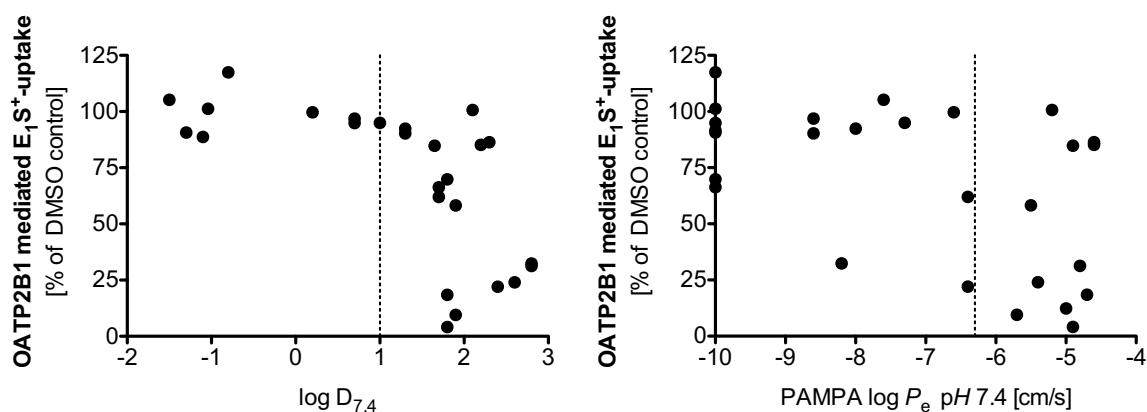
**Figure 4.13.**  $IC_{50}$  concentration of the eight analyzed FimH antagonists (**1i**, **1j**, **5b**, **5c**, **6a**, **6b**, **7**, and **14**) on OATP2B1-mediated  $E_1S^+$  uptake. Data represent % of DMSO control and the mean with the standard deviation (triplicates).

Replacing the nitro-substituent ( $\rightarrow$ **5b**) by a cyano group ( $\rightarrow$ **5c**) reduced inhibition of the OATP2B1-mediated  $E_1S^+$  uptake by a factor of 2.5. Furthermore,  $IC_{50}$  values of these two compounds revealed similar results ( $IC_{50}$  **5b** = 1.25  $\mu$ M and  $IC_{50}$  **5c** = 2.63  $\mu$ M). With a methoxy substituent in the *ortho*-position of the terminal aromatic ring ( $\rightarrow$ **5d**) no significant inhibition ( $E_1S^+$  uptake > 80%) could be observed.

*Pyrrolylphenyl and guanidinylphenyl mannosides.* Pyrrolylphenyl with an ester at the 3-position of the pyrrole moiety ( $\rightarrow$ **7**) and the guanidinylphenyl with two benzylcarbamates ( $\rightarrow$ **14**) showed significant inhibition of the OATP2B1-mediated  $E_1S^+$  uptake (< 50%, Figure 4.11;  $IC_{50}$  **7** = 4.70  $\mu$ M and  $IC_{50}$  **14** = 0.28  $\mu$ M, Figure 4.13). More FimH antagonists within these two compound classes should be screened to demonstrate the effect of small structural changes at the aglycones.

These results illustrate that introducing different substituents (i.e. esters, amides, carboxylate, or bioisosteres) on the outer aromatic ring of the aglycone or on the aromatic ring adjacent to the anomeric oxygen (chloro or trifluoromethyl) influence the inhibition of the OATP2B1-mediated  $E_1S^+$  uptake. However, more information is needed to determine SPR for the OATP2B1 transporter and therefore more FimH antagonists have to be screened for their inhibitory potential of the  $E_1S^+$  MDCKII-OATP2B1 mediated uptake.

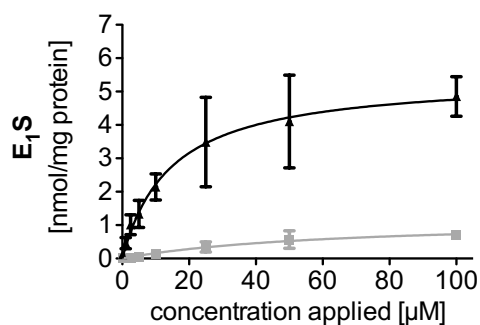
Opposing these inhibition data of the FimH antagonists to their physicochemical properties ( $\log D_{7.4}$  and  $\log P_e$ ) (Table 4.1), trends can be observed. Compounds with a  $\log D_{7.4} > 1$  and with moderate or high effective permeability ( $\log P_e < -6.3$  cm/s) can show an inhibitory effect on the OATP2B1-mediated  $E_1S^+$  uptake (Figure 4.14). These results lead to the assumption that the inhibitory binding site at the OATP2B1 transporter for the FimH antagonists could be allosteric and be located inside the membrane or the cell. For this purpose, direct uptake of the FimH antagonists into MDCKII-OATP2B1 cells were performed.



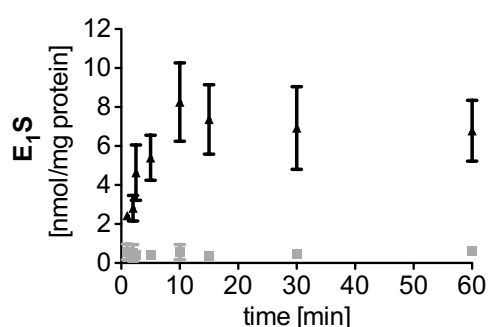
**Figure 4.14.** OATP2B1-mediated  $E_1S^+$  uptake vs.  $\log D_{7.4}$  and PAMPA  $\log P_e$  of the various FimH antagonists. Data are shown as mean only. Data of the MDCKII-OATP2B1-mediated  $E_1S^+$  uptake represent % of DMSO control and their standard deviations for OATP2B1-mediated  $E_1S^+$  uptake values are  $\leq 14.8\%$  with the median of 2.3%. Standard deviations for  $\log D_{7.4}$  values are  $\leq 0.2$  units with the median of 0.1 units and for  $\log P_e$  values  $\leq 2.1$  cm/s with the median of 0.1 cm/s.

#### ***OATP2B1 Uptake Studies***

OATP2B1-mediated uptake experiments with the identified FimH antagonist inhibitors **1i**, **1j**, **5b**, **5c**, **6a**, **6b**, **7**, and **14** were performed to consider the possibility of them being a substrate of the OATP2B1 transporter and sharing the same binding site as  $E_1S$ .<sup>19,20</sup> Atorvastatin, an example of being both, an inhibitor and substrate of the OATP2B1 transporter was included in these uptake studies.<sup>18</sup> In addition, unlabeled  $E_1S$  was used as a positive control for uptake into the MDCKII-OATP2B1 cells (determination of the intracellular concentrations by LC-MS). To demonstrate the expression of OATP2B1 in the transfected MDCKII cells, kinetics ( $K_m = 4.0 \mu\text{M}$ ) and time dependent uptake of the OATP2B1-substrate  $E_1S$  was analyzed in MDCKII OATP2B1 transfected and MDCKII Wild-type cells (Figure 4.15 and 4.16). Because MDCKII-Wild-type cells have a low expression of transporter proteins, they should always be used as a negative control to measure the background signal and to indicate the effective uptake of compounds with the investigated transporter when subtracting the MDCKII-Wild-type results from the OATP2B1 results.

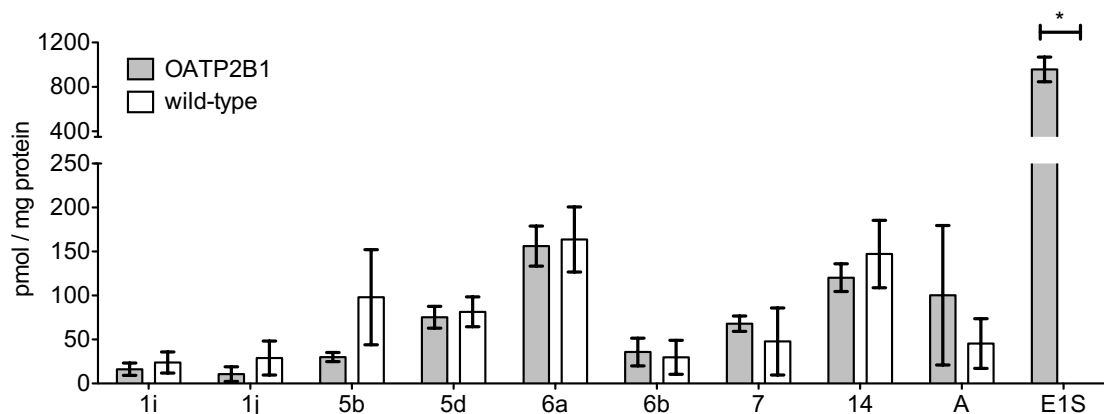


**Figure 4.15.** Concentration dependent uptake of  $\text{E}_1\text{S}$  in MDCKII-OATP2B1 (black,  $K_m = 4.0 \mu\text{M}$ ) compared to the uptake in MDCKII-Wild-type cells (grey). Cells were incubated with various concentrations of  $\text{E}_1\text{S}$  for 10 minutes. Values are indicated as mean with the standard deviation ( $n = 3$ ).



**Figure 4.16.** Time dependent uptake of  $\text{E}_1\text{S}$  in MDCKII-OATP2B1 (black) compared to the uptake in MDCKII-Wild-type cells (grey). Cells were incubated with  $50 \mu\text{M}$  of  $\text{E}_1\text{S}$  for various time points (1, 2, 2.5, 5, 10, 15, 30, and 60 minutes). Values are indicated as mean with the standard deviation ( $n = 3$ ).

In contrast to previous findings about atorvastatin we observed no significant uptake of atorvastatin into MDCKII-OATP2B1 cells.<sup>18,21,22</sup> Compared to atorvastatin (Figure 4.17), nine times higher concentrations and a greater difference between uptake into MDCKII-Wild-type cells and the uptake into MDCKII-OATP2B1 were achieved for  $\text{E}_1\text{S}$ . Assuming that passive diffusion depending on the compounds lipophilicity contributes to the uptake studies results effective permeability was determined for  $\text{E}_1\text{S}$  and atorvastatin (Table 4.1). Whereas atorvastatin is more lipophilic and therefore permeates passively through the membranes with a  $\log P_e$  of  $-5.4 \text{ cm/s}$  (Table 4.1),  $\text{E}_1\text{S}$  is rather hydrophilic and shows low passive permeation into the cells ( $\log P_e > -6.3 \text{ cm/s}$ , Table 4.1). This could explain the larger uptake differences between MDCKII-Wild-type and MDCKII-OATP2B1 cells for  $\text{E}_1\text{S}$  compared to atorvastatin.



**Figure 4.17.** Uptake of FimH antagonists (**1i**, **1j**, **5b**, **5d**, **6a**, **6b**, **7**, **14**) and the known substrate atorvastatin (A) and E<sub>1</sub>S into MDCKII-Wild-type (white) and MDCKII-OATP2B1 (grey) cells after incubation of 10 min. Compounds were applied at a concentration of 10  $\mu$ M. Values indicates mean with the standard deviation (triplicates). Asterisk (\*) indicates significant difference to the DMSO control value ( $p < 0.05$ ).

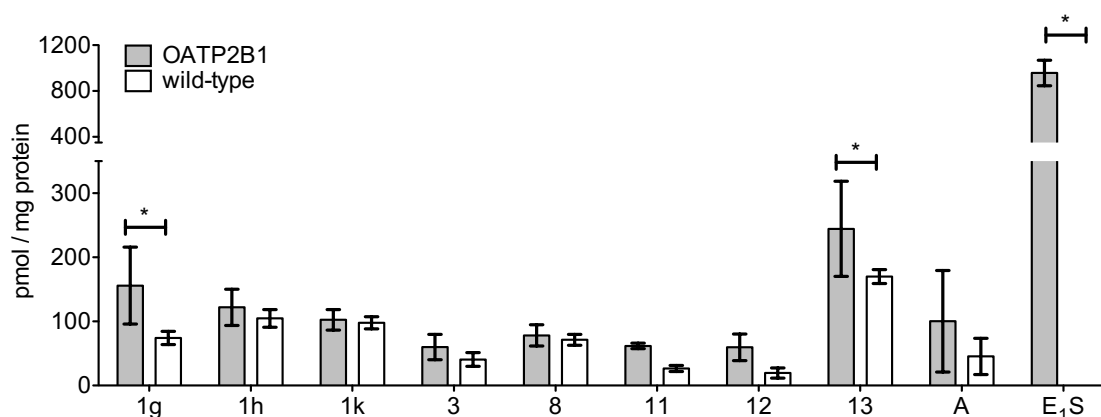
Nevertheless, none of the FimH antagonists could be identified as a substrate showing a significant difference between the results in the MDCKII-OATP2B1 cells and in the MDCKII-Wild-type control experiments. The two biphenyl mannosides **1i** and **1j** with low effective permeability ( $\log P_e < -6.3$  cm/s, Table 4.1) and the mannosides with moderate to high effective permeability, which are the indolinyphenyl **5b** and **5d**, the indolylphenyl **6a** and **6b**, the pyrrolyphenyl (**7**), and the guanidinyphenyl (**14**) showed no uptake into the MDCKII-OATP2B1 cells (Figure 4.17).

The issue to get reliable results when passive permeability is involved has been discussed previously by Krajcsi.<sup>23</sup> Analyzing efflux transporter in a monolayer will not work for compounds with low passive permeation, because the compound has to be in the cell or membrane in order to interact with the efflux transporter. Similarly, it may be assumed for uptake transporter, for which compounds with high permeability can hamper the uptake with the transporter, because the substrates can not interact with the transporters.<sup>20,23</sup>

Furthermore, multiple binding sites for substrates have to be taken into account.<sup>24</sup> A compound can inhibit the uptake of a substrate that shares its binding site, but no inhibition will be measured for a substrate with a distinct binding site, except there is an allosteric binding site.

Therefore, FimH antagonists having no influence on the MDCKII-OATP2B1-mediated E<sub>1</sub>S<sup>+</sup> uptake in the primary analysis (Figure 4.12) were included in the uptake study. One of the biphenyl mannosides ( $\rightarrow$ **1g**) and one of the guanidinyphenyl mannosides ( $\rightarrow$ **13**) with low effective permeability ( $\log P_e > -6.3$  cm/s) exhibited a significant uptake into the MDCKII-OATP2B1

overexpressed cells compared to wild-type cells (Figure 4.18). An explanation for this lacking of inhibition of these compounds (**1g** and **13**) but present uptake could be the existence of multiple binding sites for the OATP2B1 transporter. Low- and high- affinity sites were reported for the OATP2B1 transporter and it was shown that a high  $E_1S$  concentration (50  $\mu M$ ) target the low affinity and low  $E_1S$  concentration (0.005  $\mu M$ ) the high affinity site.<sup>24</sup> Therefore, further studies on low- and high- affinity sites with the FimH antagonists are necessary.



**Figure 4.18.** Uptake of FimH antagonists (**1g**, **1h**, **1k**, **3**, **8**, **11**, **12**, **13**), atorvastatin (A), and  $E_1S$  into MDCKII-OATP2B1 (grey) MDCKII-Wild-type (white) and after incubation for 10 min. Values indicates mean with the standard deviation ( $n = 2$ ). Asterisk (\*) indicates significant difference to the DMSO control value ( $p < 0.05$ ).

Another assumption for this issue that no OATP2B1 uptake can be observed with the known substrate atorvastatin or the FimH antagonists could be that the lipophilic compounds bind to intracellular components and are not available for detection with the LC-MS and therefore would bias the results of the uptake. For this purpose, further studies on the sample preparation will be performed and MDCKII-OATP2B1 vesicle will be prepared to investigate the influence of compound binding to intracellular components and its influence on the LC-MS detection.

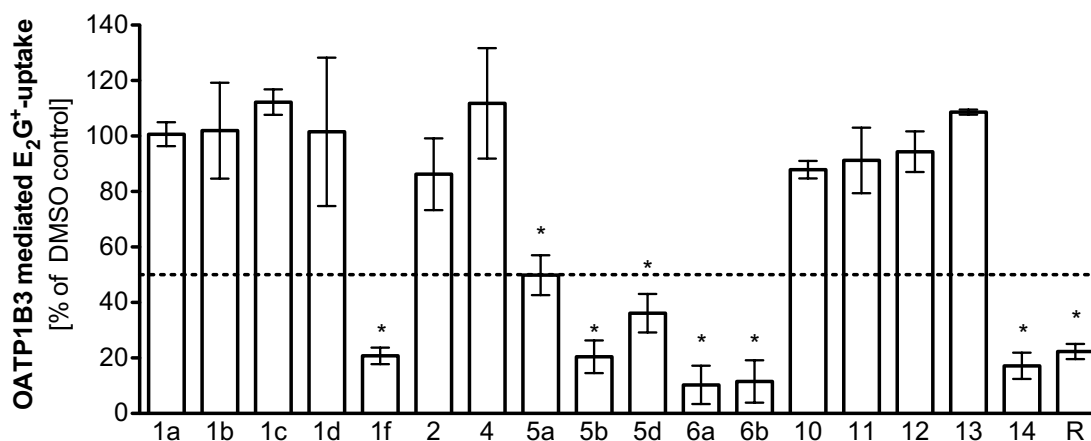
### Interactions of FimH Antagonists with the Drug Transporter OATP1B3

To obtain more information about SPR of OATP transporters, MDCKII-OATP1B3-mediated radiolabeled estradiol 17 $\beta$ -D-glucuronide [3H] ( $E_2G^+$ , known substrate of OATP1B3<sup>25</sup>) inhibition studies were performed with selected members of the FimH antagonists' family and compared to the results of OATP2B1.

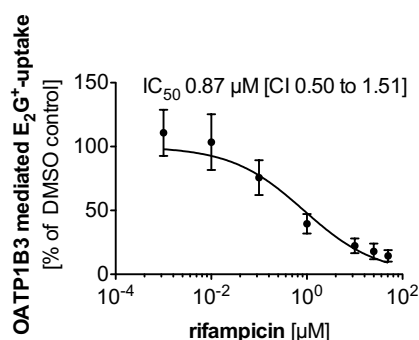
#### OATP1B3 Inhibition Studies

The biphenyl ester prodrug **1f**, the indolinyphenyl mannosides **5a**, **5b**, and **5d**, indolyphenyl mannosides **6a**, and **6b**, and the guanidinyphenyl mannoside **14** inhibit the OATP1B3-mediated  $E_2G^+$

uptake (< 50%, Figure 4.19). In addition, Rifampicin (known inhibitor) was used as a positive control and inhibited the uptake of  $E_2G^+$  with an  $IC_{50}$  value of 0.87  $\mu M$  (Figure 4.20).



**Figure 4.19.** Inhibition of OATP1B2-mediated  $E_2G^+$  uptake by FimH antagonists (**1a -1d**, **1f**, **2**, **4**, **5a**, **5b**, **5d**, **6a**, **6b**, **10 - 14**) and by the known inhibitor rifampicin (R) after incubation for 10 min. Compounds were applied at a concentration of 100  $\mu M$ . Data represent % of DMSO control and shows the mean with the standard deviation ( $n = 3$ ). Asterisk (\*) indicates significant difference to the DMSO control value ( $p < 0.05$ ).



**Figure 4.20.**  $IC_{50}$  concentration of rifampicin on OATP1B3-mediated  $E_2G^+$  uptake. Data represent mean with the standard deviation ( $n = 2$ ).

Comparing these interactions with the OATP2B1 transporter, similarities can be observed. Whereas interactions of the indoliny- and indolylphenyl mannosides **5b**, **5c**, **6a**, **6b** and the guanidinyphenyl mannoside **14** with both, OATP2B1 and OATP1B3 could be observed, compound **1f** and **5d** selectively interacts with the OATP1B3 transporter. To gain more information about the SPR of the OATP transporters the FimH antagonists **1e**, **1g - 1k**, **3**, **5a**, and **7 - 9**, which were only screened with OATP2B1, should be tested for OATP1B3 inhibition as well. Furthermore, due to cell toxicity (< 50% at 100  $\mu M$ ) and solubility (< 50  $\mu g/ml$ ) issues (Table 4.1), some of the compounds (**1f**, **5a**, **5b**, **5d**, **6a**, **6b**, **9**, and **14**) should be applied at lower concentration than 100  $\mu M$ .

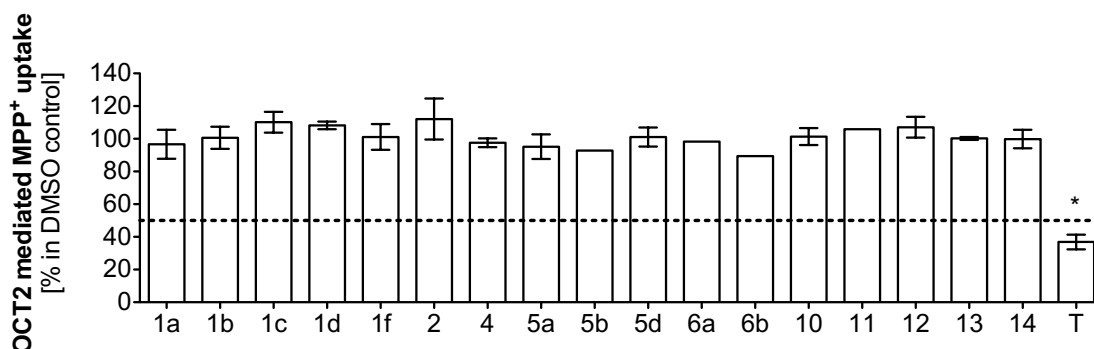


### Interactions of FimH Antagonists with the Drug Transporters OAT1 and OCT2

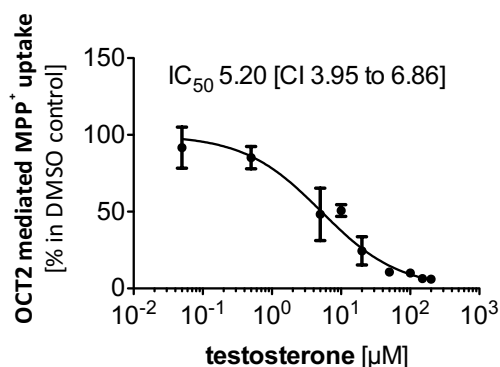
Renal elimination is required for the FimH antagonists to reach the target in the bladder. However, too fast clearance leads to a fast increase of the urine levels and a rapid decrease beyond the antiadhesive concentrations, requiring frequent dosing to maintain the therapeutic effect. Therefore, after glomerular filtration of the unbound compound only slow secretion of the drug is desired to avoid too fast clearance. Inhibition studies with MDCKII-OCT2-mediated radiolabeled methyl-4-phenyl-pyridinium acetate [3-H] (MPP<sup>+</sup>, known substrate of OCT2<sup>24</sup>) uptake and HeLa-OAT1-mediated radiolabeled [glycyl-2-3H]-4-aminohippuric acid (PAH<sup>+</sup>, known substrate of OAT1<sup>24</sup>) uptake were performed to exclude the interaction of the antagonists with the transporters involved in secretion.

#### OCT2 Inhibition Studies

None of the tested FimH antagonists inhibits the MDCKII-OCT2-mediated MPP<sup>+</sup> uptake (Figure 4.21). Testosterone, a known inhibitor was used as a positive control exhibiting an IC<sub>50</sub> of 5.2 μM (Figure 4.22).



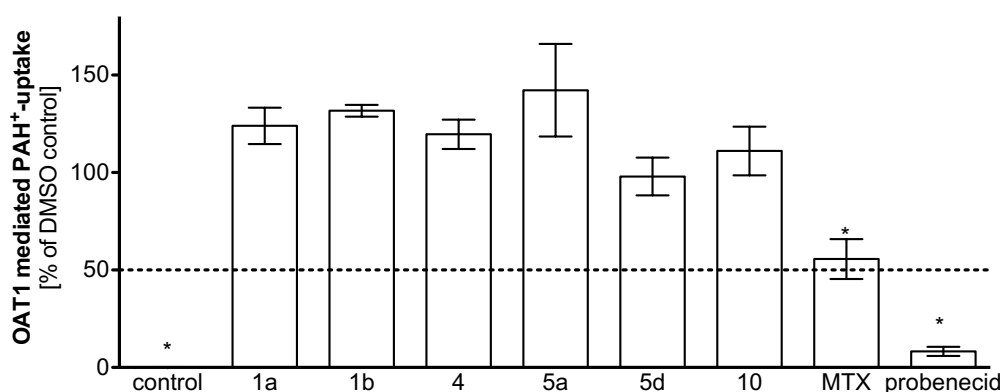
**Figure 4.21.** Inhibition of OCT2-mediated MPP<sup>+</sup> uptake by FimH antagonists (**1a -1d, 1f, 2, 4, 5a, 5b, 5d, 6a, 6b, 10 - 14**) and by the known inhibitor testosterone (T) after incubation for 5 min. Compounds were applied at a concentration of 100 μM. Data represent % of DMSO control and shows the mean with its corresponding standard deviation (n = 3). Asterisk (\*) indicates significant difference to the DMSO control value (p < 0.05).



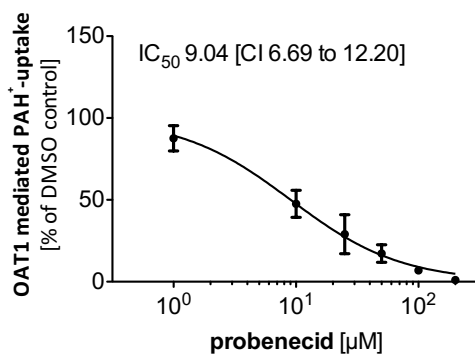
**Figure 4.22.** IC<sub>50</sub> concentration of testosterone on OCT2-mediated MPP<sup>+</sup> uptake. Data represent mean with the standard deviation (n = 2).

### OAT1 Inhibition Studies

HeLa cells were infected with an OAT1 adenovirus before transport experiments were performed. None of the tested FimH antagonists inhibits the HeLa-OAT1-mediated PAH<sup>+</sup> uptake (Figure 4.23). As a negative control HeLa cells without adenovirus were used and showed 0% uptake of the PAH<sup>+</sup>. Furthermore, the known inhibitor probenecid and the known substrate methotrexate (MTX) were included in the test series and exhibited an inhibition of the OAT1-mediated PAH<sup>+</sup> uptake < 60% and an IC<sub>50</sub> value of 9.04 µM was determined for probenecid (Figure 4.24).



**Figure 4.23.** Inhibition of OAT1-mediated PAH<sup>+</sup> uptake by FimH antagonists (**1a**, **1b**, **4**, **5a**, **5d**, and **10**), by the known inhibitor probenecid, and the known substrate methotrexate (MTX) after incubation for 5 min. Cells were infected with OAT1 adenovirus and cells without virus were used as control. Compounds were applied at a concentration of 100 µM. Data represent % of DMSO control and show the mean with the standard deviation (n = 3). Asterisk (\*) indicates significant difference to the DMSO control value (p < 0.05).



**Figure 4.24.**  $\text{IC}_{50}$  concentration of probenecid on OAT1-mediated PAH<sup>+</sup> uptake. Data represent the mean with the standard deviation ( $n = 2$ ).

In a further study, additional FimH antagonists should be screened and multiple binding sites should be analyzed for the OCT2 and OAT1 transporter to exclude interactions with FimH antagonists.

## Conclusion

In conclusion, interactions with the OATP2B1 transporter were exhibited with eight FimH antagonists [biphenyl ( $\rightarrow$ **1i** and **1j**), indolinyphenyl ( $\rightarrow$ **5a** and **5d**), indolyphenyl ( $\rightarrow$ **6a** and **6b**), pyrrolylphenyl ( $\rightarrow$ **7**), and guanidinyphenyl ( $\rightarrow$ **14**)  $\alpha$ -D-mannosides]. Small structural differences within a compound class could be observed. Whereas substitution with a chloro or trifluoromethyl at the aromatic ring adjacent to the anomeric oxygen of biphenyl and indolinyphenyl increases inhibition of the OATP2B1-mediated  $\text{E}_1\text{S}^+$  uptake, substitution at the outer aromatic ring with carboxylic acid ( $\rightarrow$ **1a**), cyanide, sulfonamide, sulfone ( $\rightarrow$ **1b** - **1d**), N,N-dimethylaminoethyl ester or the N,N-dimethylaminoethyl amide ( $\rightarrow$ **1f** and **1g**, respectively) did not show any inhibition. However, only for the biphenyl **1g** and the guanidinyphenyl mannoside **13**, without any inhibitory effect, OATP2B1-mediated uptake could be observed. For this reason, further studies analyzing multiple binding sites on the OATP2B1 transporter and  $\text{IC}_{50}$  of **1g** and **13** have to be determined for the low and high affinity-binding site of the transporter to prove the interactions with the OATP2B1 transporter. Furthermore, MDCKII-OATP2B1 vesicle will be prepared to investigate the influence of compound binding to intracellular components and its influence on the LC-MS detection.

Furthermore, interactions similar to the one of FimH antagonists with OATP2B1 could be observed for the OATP1B3 transporter. The biphenyl mannoside **1f** as one exception, which contained a N,N-dimethylaminoethyl ester substitution at the outer aromatic ring of the biphenyl and with a low inhibition of the OATP2B1-mediated  $\text{E}_1\text{S}^+$  uptake (>80%), showed an increased inhibition of the OATP1B3-mediated  $\text{E}_2\text{G}^+$  uptake (< 50%).

No interactions with the OCT2 and OAT1 transporter involved in the renal secretion were observed. For all transporters, further investigation regarding multiple binding sites,  $IC_{50}$  studies, and direct uptake studies of FimH antagonists are necessary.

#### **Outlook**

Once the drug has reached the cytosol of an enterocyte, it can be transported by transporters located at the basolateral side (e.g. MRP) into the blood or transported back into the intestine with efflux transporters (e.g. P-gp) localized at the apical site. Therefore, further investigation with the efflux transporter MRP and P-gp are of interest to show the limitation of oral availability of substrate drugs. Another transporter, which should be targeted to improve permeability and oral absorption, is the uptake transporter PEPT1 in the intestine. Therefore, PEPT1 will be analyzed for facilitating the intestinal membrane permeability of modified FimH antagonists. Furthermore, drug-drug interactions are of interest, not only with drug transporter, but also with metabolic enzymes as cytochrome P450.

## References

1. Rubio-Aliaga, I.; Daniel, H. Mammalian peptide transporters as targets for drug delivery. *Trends Pharmacol. Sci.* **2002**, *23*, 434-440.
2. Tamai, I. Oral drug delivery utilizing intestinal OATP transporters. *Adv. Drug Deliv. Rev.* **2012**, *64*, 508-514.
3. Fromm, M. F.; Kim, R. B.; Stein, C. M.; Wilkinson, G. R.; Roden, D. M. Inhibition of P-glycoprotein-mediated drug transport: A unifying mechanism to explain the interaction between digoxin and quinidine [seecomments]. *Circulation* **1999**, *99*, 552-557.
4. Klein, T.; Abgottspon, D.; Wittwer, M.; Rabbani, S.; Herold, J.; Jiang, X.; Kleeb, S.; Luethi, C.; Scharenberg, M.; Bezencon, J.; Gubler, E.; Pang, L.; Smiesko, M.; Cutting, B.; Schwardt, O.; Ernst, B. FimH Antagonists for the Oral Treatment of Urinary Tract Infections: From Design and Synthesis to *in Vitro* and *in Vivo* Evaluation. *J. Med. Chem.* **2010**, *53*, 8627-8641.
5. Kleeb, S.; Pang, L.; Mayer, K.; Eris, D.; Sigl, A.; Preston, R. C.; Zihlmann, P.; Sharpe, T.; Jakob, R. P.; Abgottspon, D.; Hutter, A. S.; Scharenberg, M.; Jiang, X.; Navarra, G.; Rabbani, S.; Smiesko, M.; Ludin, N.; Bezencon, J.; Schwardt, O.; Maier, T.; Ernst, B. FimH Antagonists: Bioisosteres To Improve the *in Vitro* and *in Vivo* PK/PD Profile. *J. Med. Chem.* **2015**, *58*, 2221-2139.
6. Jiang, X.; Abgottspon, D.; Kleeb, S.; Rabbani, S.; Scharenberg, M.; Wittwer, M.; Haug, M.; Schwardt, O.; Ernst, B. Antiadhesion therapy for urinary tract infections--a balanced PK/PD profile proved to be key for success. *J. Med. Chem.* **2012**, *55*, 4700-4713.
7. Pang, L.; Bezençon, J.; Kleeb, S.; Rabbani, S.; Sigl, A.; Smiesko, M.; Sager, C.P.; Eris, D.; Schwardt, O.; Ernst, B. FimH Antagonists – Solubility vs. Permeability. *Carbohydrate Chemistry*, **2017**, *42*, 248-273.
8. Schwardt, O.; Rabbani, S.; Hartmann, M.; Abgottspon, D.; Wittwer, M.; Kleeb, S.; Zalewski, A.; Smiesko, M.; Cutting, B.; Ernst, B. Design, synthesis and biological evaluation of mannosyl triazoles as FimH antagonists. *Bioorganic & Med. Chem.* **2011**, *19*, 6454-6473.
9. Nishimura, M.; Naito, S. Tissue-specific mRNA expression profiles of human ATP-binding cassette and solute carrier transporter superfamilies. *Drug Metab. Pharmacokinet.* **2005**, *20*, 452-477.
10. Kobayashi, D.; Nozawa, T.; Imai, K.; Nezu, J.; Tsuji, A.; Tamai, I. Involvement of human organic anion transporting polypeptide OATP-B (SLC21A9) in pH-dependent transport across intestinal apical membrane. *J. Pharmacol. Exp. Ther.* **2003**, *306*, 703-708.
11. Feng, B.; LaPerle, J. L.; Chang, G.; Varma, M. V. S. Renal clearance in drug discovery and development: molecular descriptors, drug transporters and disease state. *Expert Opinion on Drug Metab. & Toxicol.* **2010**, *6*, 939-952.
12. Waring, M. J. Lipophilicity in drug discovery. *Expert Opin. Drug Discov.* **2010**, *5*, 235-248.
13. Alsenz, J.; Kansy, M. High throughput solubility measurement in drug discovery and development. *Adv. Drug Deliv. Rev.* **2007**, *59*, 546-567.
14. Kansy, M.; Senner, F.; Gubernator, K. Physicochemical high throughput screening: Parallel artificial membrane permeation assay in the description of passive absorption processes. *J. Med. Chem.* **1998**, *41*, 1007-1010.
15. Hamid, R.; Rotshteyn, Y.; Rabadi, L.; Parikh, R.; Bullock, P. Comparison of alamar blue and MTT assays for high through-put screening. *Toxicol. in Vitro* **2004**, *18*, 703-710.
16. Stieger, B.; Hagenbuch, B. Organic anion-transporting polypeptides. *Curr. Top. Membr.* **2014**, *73*, 205-232.
17. Varma, M. V.; Ambler, C. M.; Ullah, M.; Rotter, C. J.; Sun, H.; Litchfield, J.; Fenner, K. S.; El-Kattan, A. F. Targeting intestinal transporters for optimizing oral drug absorption. *Curr. Drug Metab.* **2010**, *11*, 730-742.
18. Grube, M.; Kock, K.; Oswald, S.; Draber, K.; Meissner, K.; Eckel, L.; Bohm, M.; Felix, S. B.; Vogelgesang, S.; Jedlitschky, G.; Siegmund, W.; Warzok, R.; Kroemer, H. K. Organic anion transporting polypeptide 2B1 is a high-affinity transporter for atorvastatin and is expressed in the human heart. *Clin. Pharmacol. Ther.* **2006**, *80*, 607-620.
19. Matsson, P.; Pedersen, J. M.; Norinder, U.; Bergstrom, C. A.; Artursson, P. Identification of novel specific and general inhibitors of the three major human ATP-binding cassette transporters P-gp, BCRP and MRP2 among registered drugs. *Pharm. Res.* **2009**, *26*, 1816-1831.

20. Sugano, K.; Kansy, M.; Artursson, P.; Avdeef, A.; Bendels, S.; Di, L.; Ecker, G. F.; Faller, B.; Fischer, H.; Gerebtzoff, G.; Lennernaes, H.; Senner, F. Coexistence of passive and carrier-mediated processes in drug transport. *Nat. Rev. Drug Discov.* **2010**, *9*, 597-614.
21. Varma, M. V.; Rotter, C. J.; Chupka, J.; Whalen, K. M.; Duignan, D. B.; Feng, B.; Litchfield, J.; Goosen, T. C.; El-Kattan, A. F. pH-sensitive interaction of HMG-CoA reductase inhibitors (statins) with organic anion transporting polypeptide 2B1. *Mol. Pharm.* **2011**, *8*, 1303-1313.
22. Sai, Y.; Kaneko, Y.; Ito, S.; Mitsuoka, K.; Kato, Y.; Tamai, I.; Artursson, P.; Tsuji, A. Predominant contribution of organic anion transporting polypeptide OATP-B (OATP2B1) to apical uptake of estrone-3-sulfate by human intestinal Caco-2 cells. *Drug Metab. Dispos.* **2006**, *34*, 1423-1431.
23. Krajcsi, P. Drug-transporter interaction testing in drug discovery and development. *World J. Pharmacol.* **2013**, 35-46.
24. Shirasaka, Y.; Mori, T.; Shichiri, M.; Nakanishi, T.; Tamai, I. Functional pleiotropy of organic anion transporting polypeptide OATP2B1 due to multiple binding sites. *Drug Metab. Pharmacokinet.* **2012**, *27*, 360-364.
25. Giacomini, K. M.; Huang, S.-M.; Tweedie, D. J.; Benet, L. Z.; Brouwer, K. L. R.; Chu, X.; Dahlin, A.; Evers, R.; Fischer, V.; Hillgren, K. M.; Hoffmaster, K. A.; Ishikawa, T.; Keppler, D.; Kim, R. B.; Lee, C. A.; Niemi, M.; Polli, J. W.; Sugiyama, Y.; Swaan, P. W.; Ware, J. A.; Wright, S. H.; Yee, S. W.; Zamek-Gliszczynski, M. J.; Zhang, L.; International, T. Membrane transporters in drug development. *Nat. Rev. Drug Discov.* **2010**, *9*, 215-236.

#### 4.2.2 Paper 2 - Prodrug Approach

##### **FimH Antagonists for the Oral Treatment of Urinary Tract Infections: From Design and Synthesis to *in Vitro* and *in Vivo* Evaluation**

This publication describes the identification of biphenyl  $\alpha$ -D-mannopyranosides as potent FimH antagonists to inhibit the bacteria/host cell interaction. Experimental determination of physicochemical and pharmacokinetic properties of these FimH antagonists was performed. Furthermore, an ester prodrug approach is introduced as an appealing strategy for achieving good permeability.

##### **Contribution to the project:**

Jacqueline Bezençon performed some of the  $\log D$  and  $\log P_e$  results during her master thesis under the supervision of Dr. Matthias Wittwer.

The paper was published in the peer-reviewed *Journal of Medicinal Chemistry* in 2010:

T. Klein,\* D. Abgottspon,\* M. Wittwer,\* S. Rabbani,\* J. Herold,\* X. Jiang, S. Kleeb, C. Lüthi, M. Scharenberg, **J. Bezençon**, E. Gubler, L. Pang, M. Smiesko, B. Cutting, O. Schwaradt, B. Ernst, FimH antagonists for the oral treatment of urinary tract infections: from design and synthesis to *in vitro* and *in vivo* evaluation. *J. Med. Chem.* **2010**, *53*, 8627-8641.

\*contributed equally.

**FimH Antagonists for the Oral Treatment of Urinary Tract Infections: From Design and Synthesis to in Vitro and in Vivo Evaluation**Tobias Klein,<sup>†</sup> Daniela Abgottspon,<sup>†</sup> Matthias Wittwer,<sup>†</sup> Said Rabbani,<sup>†</sup> Janno Herold,<sup>†</sup> Xiaohua Jiang, Simon Kleeb, Christine Lüthi, Meike Scharenberg, Jacqueline Bezençon, Erich Gubler, Lijuan Pang, Martin Smiesko, Brian Cutting, Oliver Schwaradt, and Beat Ernst\**Institute of Molecular Pharmacy, Pharmazentrum, University of Basel, Klingelbergstrasse 50, CH-4056 Basel, Switzerland.*<sup>†</sup>These authors contributed equally to the project

Received August 4, 2010

Urinary tract infection (UTI) by uropathogenic *Escherichia coli* (UPEC) is one of the most common infections, particularly affecting women. The interaction of FimH, a lectin located at the tip of bacterial pili, with high mannose structures is critical for the ability of UPEC to colonize and invade the bladder epithelium. We describe the synthesis and the in vitro/in vivo evaluation of  $\alpha$ -D-mannosides with the ability to block the bacteria/host cell interaction. According to the pharmacokinetic properties, a prodrug approach for their evaluation in the UTI mouse model was explored. As a result, an orally available, low molecular weight FimH antagonist was identified with the potential to reduce the colony forming units (CFU) in the urine by 2 orders of magnitude and in the bladder by 4 orders of magnitude. With FimH antagonist **16b**, the great potential for the effective treatment of urinary tract infections with a new class of orally available anti-infectives could be demonstrated.

**Introduction**

Urinary tract infection (UTI<sup>(4)</sup>) is one of the most common infections, affecting millions of people each year. Particularly affected are women, who have a 40–50% risk to experience at least one symptomatic UTI episode at some time during their life. In addition, more than half of them experience a relapse of the infection within 6 months.<sup>1,2</sup>

Although UTIs rarely cause severe diseases such as pyelonephritis or urosepsis, they are associated with high incidence rate and consume considerable healthcare resources.<sup>3</sup> Uropathogenic *Escherichia coli* (UPEC) are the primary cause of UTIs, accounting for 70–95% of the reported cases. Symptomatic UTIs require antimicrobial treatment, often resulting in the emergence of resistant microbial flora. As a consequence, treatment of consecutive infections becomes increasingly difficult because the number of antibiotics is limited and the resistance of *E. coli* is increasing, especially in patients with diabetes, urinary tract anomaly, paraplegia, and those with permanent urinary catheter. Therefore, a new approach for the prevention and treatment of UTI with inexpensive, orally

applicable therapeutics with a low potential for resistance would have a great impact on patient care, public health care, and medical expenses.

UPEC strains express a number of well-studied virulence factors used for a successful colonization of their host.<sup>3–5</sup> One important virulence factor is located on type 1 pili, allowing UPEC to adhere and invade host cells within the urinary tract. It enables UPEC to attach to oligomannosides, which are part of the glycoprotein uroplakin Ia on the urinary bladder mucosa. This initial step prevents the rapid clearance of *E. coli* from the urinary tract by the bulk flow of urine and at the same time enables the invasion of the host cells.<sup>3,6</sup>

Type 1 pili are the most prevalent fimbriae encoded by UPEC, consisting of the four subunits FimA, FimF, FimG, and FimH, the latter located at the tip of the pili.<sup>7</sup> As a part of the FimH subunit, a carbohydrate-recognizing domain (CRD) is responsible for bacterial interactions with the host cells within the urinary tract.<sup>6</sup> The crystal structure of the FimH-CRD was solved<sup>8</sup> and its complexes with *n*-butyl  $\alpha$ -D-mannopyranoside<sup>9</sup> and Man $\alpha$ (1–3)[Man $\alpha$ (1–6)]Man<sup>10</sup> recently became available.

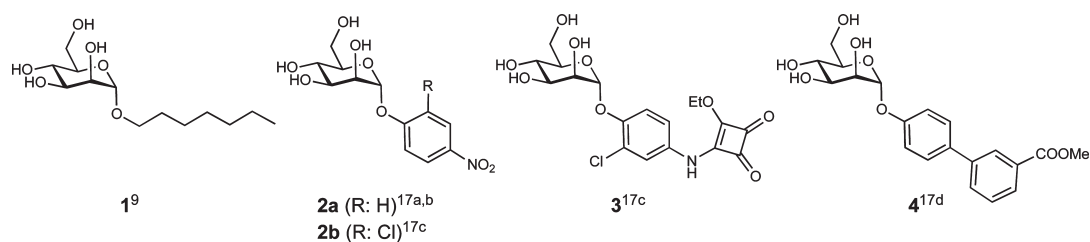
Previous studies showed that vaccination with FimH adhesion inhibits colonization and subsequent *E. coli* infection of the urothelium in humans.<sup>11,12</sup> In addition, adherence and invasion of host cells by *E. coli* can also be prevented by  $\alpha$ -D-mannopyranosides, which are potent antagonists of interactions mediated by type 1 pili.<sup>13</sup> Whereas  $\alpha$ -D-mannopyranosides efficiently prevent adhesion of *E. coli* to human urothelium, they are not exhibiting a selection pressure to induce antimicrobial resistance. Furthermore, environmental contamination is less problematic compared to antibiotics.<sup>14</sup>

More than two decades ago, Sharon and co-workers have investigated various mannosides and oligomannosides as

\*To whom correspondence should be addressed. Phone: +41 61 267 1551. Fax: +41 61 267 1552. E-mail: beat.ernst@unibas.ch.

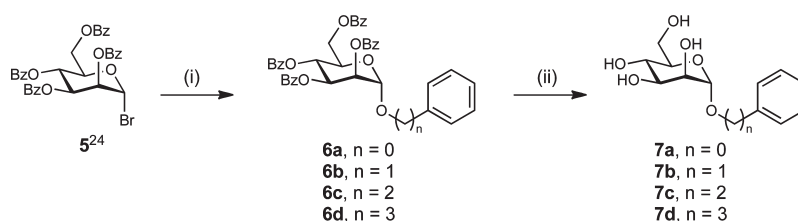
<sup>a</sup> Abbreviations: AUC, area under the curve; Caco-2 cells, Caucasian colon adenocarcinoma cells; CFU, colony forming units; CRD, carbohydrate recognition domain; DC-SIGN, dendritic cell-specific intercellular adhesion molecule-3-grabbing nonintegrin; CES, carboxylesterase; IC<sub>50</sub>, half maximal inhibitory concentration; iv, intravenous; D, distribution coefficient; GPE, guinea pig erythrocytes; LC-MS, liquid chromatography–mass spectrometry; MBP, mannose-binding protein; PAMPA, parallel artificial membrane permeation assay;  $P_{app}$ , apparent permeability;  $P_e$ , effective permeation; po, peroral; PPB, plasma protein binding; PSA, polar surface area; S, solubility; SAR, structure–activity relationship; sGF, simulated gastric fluid; sIF, simulated intestinal fluid; TEER, transepithelial resistance; UPEC, uropathogenic *E. coli*; UTI, urinary tract infection.





**Figure 1.** Known alkyl (**1**) and aryl (**2–4**)  $\alpha$ -D-mannosides exhibiting nanomolar affinities.

**Scheme 1.** Phenyl  $\alpha$ -D-Mannosides **7a–7d** with Spacers of Different Lengths between the Carbohydrate Moiety and the Phenyl Substituent<sup>a</sup>



<sup>a</sup> (i)  $\text{Ph}(\text{CH}_2)_n\text{OH}$ ,  $\text{Hg}(\text{CN})_2$ ,  $\text{HgBr}_2$ , DCM, 2 h to 7 d, rt, 57–99%; (ii) NaOMe, MeOH, 6–16 h, rt, 48–91%.

potential antagonists for type I fimbriae-mediated bacterial adhesion.<sup>15</sup> However, for these mannosides, only weak interactions in the milli- to micromolar range were observed. In contrast, numerous reports on glycoconjugate dendrimers with nanomolar affinities have been published.<sup>16</sup> However, on the basis of their large molecular weight and high polarity, they are predicted to exhibit only poor intestinal absorption and are therefore not amenable for oral dosing. Recently, some isolated reports on high affinity monovalent FimH antagonists were published<sup>17</sup> and, in one case, a systematic structure–activity relationship (SAR) profile was established.<sup>17d</sup> In summary,<sup>8,9,15–19</sup> long chain alkyl and aryl mannosides (selected examples are presented in Figure 1) displayed the highest affinity, likely due to hydrophobic interactions with two tyrosines and one isoleucine forming the entrance to the binding site, the so-called “tyrosine gate”.<sup>18</sup> Because binding affinities were obtained from diverse assay formats,<sup>9,17c,20</sup> a direct comparison of the affinities is difficult. On the basis of various crystal structures of methyl<sup>8</sup> and *n*-butyl  $\alpha$ -D-mannoside<sup>18</sup> as well as oligomannose-3<sup>9</sup> bound to FimH, Han et al. recently presented a rationale for the design of arylmannosides with increased affinities.<sup>17d</sup>

To date, a few reports on the *in vivo* potential of methyl  $\alpha$ -D-mannoside<sup>10,21,22</sup> and *n*-heptyl  $\alpha$ -D-mannoside (**1**)<sup>10</sup> are available. In all cases, the FimH antagonists were directly instilled into the bladder concomitantly with uropathogenic *E. coli* (UPEC). In this communication, we present for the first time nanomolar FimH antagonists exhibiting appropriate pharmacokinetic properties for *iv* and oral treatment of urinary tract infections.

## Results and Discussion

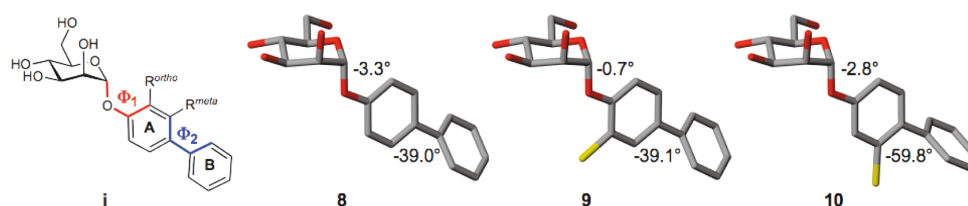
**Identification of Lead Mannoside.** In most of the reported FimH antagonists, aromatic aglycones have been applied.<sup>17</sup> However, only limited information on the optimal spacer length between the mannose moiety and the aromatic substituent is available. Generally, the aromatic moiety is directly fused to the anomeric oxygen.<sup>17a–d</sup> Extended spacers containing one<sup>17b,d</sup> or two<sup>17c</sup> methylene moieties were also reported,

however, the corresponding antagonists are not really comparable to each other because different assay formats were used for their evaluation. For the identification of the optimal spacer length, we therefore synthesized mannosides **7a–d** (Scheme 1). In a competitive binding assay,<sup>23</sup> mannoside **7a** showed a slightly higher affinity (Table 1, entry 2) compared with **7b–7d** (see Table 1, entries 3–5), confirming recent data for **7a** and **7b**.<sup>17d</sup>

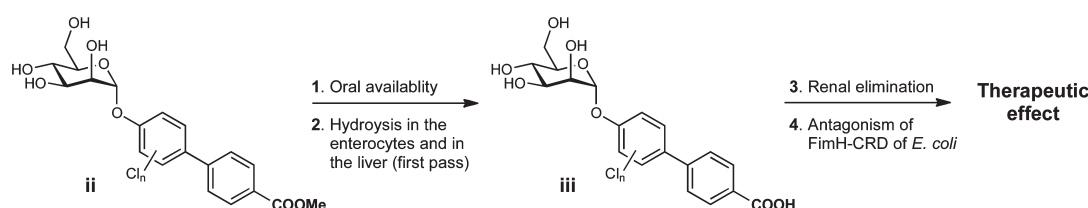
From the crystal structure of *n*-butyl  $\alpha$ -D-mannoside bound to FimH,<sup>18</sup> it becomes obvious that the hydrophobic rim formed by Tyr48, Tyr137, and Ile52 is not reached by an anomeric phenyl group. An extension by a second aromatic ring, i.e. a biphenyl  $\alpha$ -D-mannoside, however, should be compatible for  $\pi$ - $\pi$  stacking. Indeed, some recently published representatives of this compound class show excellent affinities.<sup>17d</sup>

To achieve an optimal fit with the hydrophobic binding site of FimH, the conformation of the biphenyl aglycone in **1** was modified by different substitution patterns on ring A (Figure 2). Because electron poor aromatic rings substantially improve the binding affinities of FimH antagonists (a 10-fold improvement is reported for **2B** vs **2A**<sup>17c</sup>), chloro substituents on ring A were used for the spatial exploration of the binding site. With substituents in *ortho*-position, only a minor change of the dihedral angle  $\Phi_1$  is observed ( $-3.3^\circ$  to  $-0.7^\circ$ ). However, by an increased rotational barrier, the conformational flexibility is limited. The dihedral angle  $\Phi_2$  between the conjugated aromatic rings results from an interplay between  $\pi$ -conjugation and steric effects.<sup>24,25</sup> By migrating the substituent to the *meta*-position, the torsion angle  $\Phi_2$  is substantially influenced. Whereas unsubstituted biphenyls show a global twisted minimum at a torsion angle  $\Phi_2$  of approximately  $39^\circ$ ,<sup>26</sup> substituents in the *meta*-position favor an increase of  $\Phi_2$  to  $60^\circ$ . Details of the conformational analyses are summarized in the Supporting Information.

**Design Strategy for Intestinal Absorption and Renal Elimination.** Besides high affinity, drug-like pharmacokinetic properties are a prerequisite for a successful *in vivo* application. In the present case, orally available FimH antagonists



**Figure 2.** Conformational changes of the biphenyl aglycone by chloro substitutions in *ortho*- and *meta*-position of ring A.



**Figure 3.** FimH antagonists with the pharmacodynamic and pharmacokinetic properties required for a therapeutic application. (1) For the prediction of oral availability, the PAMPA<sup>30</sup> and the Caco-2 cell assay<sup>31</sup> are applied. (2) The hydrolysis of ester **ii** to carboxylate **iii** is evaluated by mouse liver microsomes. (3) Renal excretion is estimated based on a positive correlation with polar descriptors (polar surface area, H-bond donors, H-bond acceptors, rotatable bonds).<sup>32</sup> (4) The potential of FimH antagonists is assessed with a target-based assay<sup>23</sup> and a function-based cellular assay.<sup>33</sup> For the evaluation of the therapeutic effect, a urinary tract infection mouse model (UTI mouse model in C3H/HeN mice) is applied.

that, once in circulation, are metabolically stable and undergo fast renal elimination, are required. This pharmacokinetic profile results from various serial and/or simultaneous processes that include dissolution, intestinal absorption, plasma protein binding, metabolic clearance, body distribution as well as renal and other clearance mechanisms. Because intestinal absorption and renal elimination are related to opposed properties, i.e. lipophilicity for intestinal absorption and hydrophilicity for renal elimination, a prodrug approach<sup>27</sup> was envisaged (Figure 3). Ester **ii** is expected to undergo intestinal absorption<sup>28</sup> and, later on, efficient hydrolysis to carboxylate **iii** by esterases<sup>29</sup> present in enterocytes lining the small intestine and in the liver.

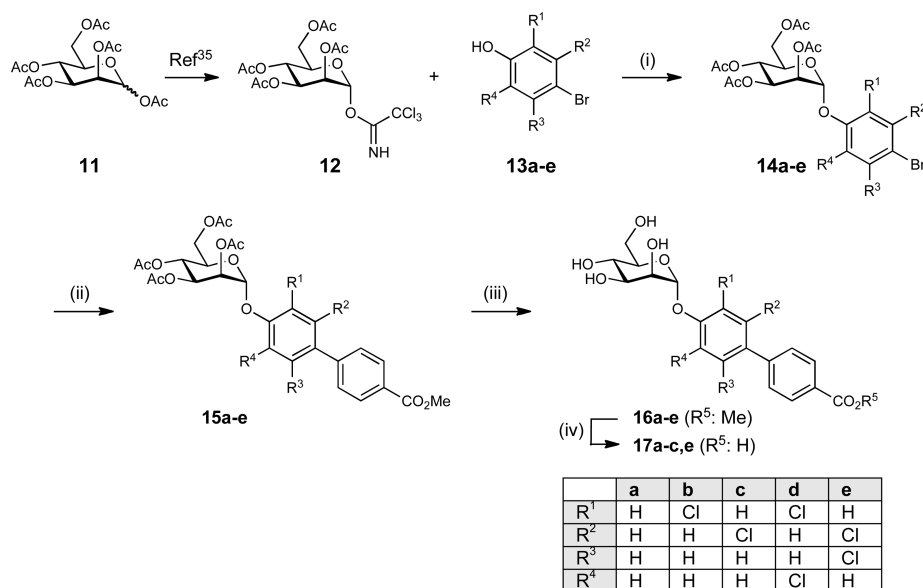
For renal clearance, the net result of glomerular filtration, active tubular secretion, and reabsorption, carboxylate **iii** should exhibit low lipophilicity ( $\log D_{7.4}$ ) and favorable polar descriptor values (polar surface area (PSA), H-bond capacity and rotatable bonds).<sup>32</sup> By contrast, lipophilic compounds are efficiently reabsorbed (as the passive reabsorption process occurs throughout the length of the nephron, whereas the secretion predominantly occurs at the proximal tubule). The estimated negative  $\log D_{7.4}$  for antagonists of type **iii** is expected to fulfill these specifications for an efficient renal elimination and a low reabsorption. Finally, once arrived at the site of action in the bladder, the antagonist binds to the carbohydrate recognition domain (CRD) located on the bacterial pili, thus interfering with the adhesion of *E. coli* to oligosaccharide structures on urothelial cells.<sup>34</sup> To identify antagonists with the pharmacokinetic properties required for oral absorption and fast renal elimination, it was planned to determine PK parameters such as  $\log D_{7.4}$ ,  $pK_a$ , solubility, plasma protein binding, metabolic stability, and oral availability using the parallel artificial membrane permeation assay (PAMPA)<sup>30</sup> and the Caco-2 cell assay.<sup>31</sup>

**Synthesis of FimH Antagonists.** The aglycone in the  $\alpha$ -1-position of D-mannose plays a ternary role, i.e. it mediates the lipophilic contact with the hydrophobic tyrosine gate, contains the elements required for intestinal absorption and, after metabolic cleavage of the prodrug, for a fast renal elimination.

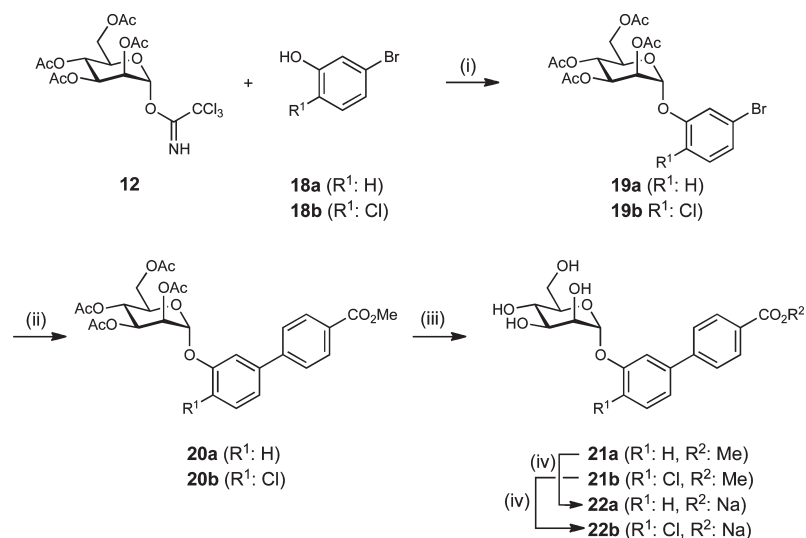
The syntheses of the *para*-substituted biphenyls **16a–e** and **17a–c,e** are outlined in Scheme 2. Lewis acid promoted glycosylation of the halogenated phenols **13a–e** with trichloroacetimidate **12**<sup>35</sup> yielded the phenyl  $\alpha$ -D-mannosides **14a–e**. In a palladium-catalyzed Suzuki coupling with 4-methoxycarbonylphenylboronic acid, the biphenyls **15a–e** were obtained. For the deprotection of the mannose moiety, Zemplén conditions were applied ( $\rightarrow$  **16a–e**). Finally, the methyl esters were saponified, yielding the sodium salts **17a–c,e**.

In a similar approach, two *meta*-substituted biphenyls in their ester form ( $\rightarrow$  **21a,b**) and as free acids ( $\rightarrow$  **22a,b**) were obtained (see Scheme 3).

**Binding Affinities and Activities.** For the biological in vitro evaluation of the FimH antagonists, two assay formats have been developed. For an initial characterization, a cell-free competitive binding assay<sup>23</sup> and, later on, a cell-based aggregation assay,<sup>33</sup> were applied. Whereas in the cell-free competitive binding assay only the CRD of the pili was used, the complete pili are present in the cell-based assay format. Furthermore, both formats are competitive assays, i.e. the analyzed antagonists compete with mannosides for the binding site. In the cell-free competitive binding assay, the competitors are polymer-bound trimannosides, whereas in the aggregation assay, the antagonist competes with more potent oligo- and polysaccharide chains present on the surface of erythrocytes.<sup>36</sup> Therefore, lower  $IC_{50}$  values are expected for the cell-free competitive binding assay. In addition, switching from the cell-free target-based assay to the function-based assay generally leads to a reduction of potency by several orders of magnitude. The interaction is further complicated by the existence of a high- and a low-affinity state of the CRD of FimH. Aprikian et al. experimentally demonstrated that in full-length fimbriae the pilin domain stabilizes the CRD domain in the low-affinity state, whereas the CRD domain alone adopts the high-affinity state.<sup>37</sup> It was recently shown that the pilin domain allosterically causes a twist in the  $\beta$ -sandwich fold of the CRD domain, resulting in a loosening of the binding pocket.<sup>38</sup> On

Scheme 2<sup>a</sup>

<sup>a</sup> (i) TMSOTf, toluene, rt, 5 h (42–77%); (ii) 4-methoxycarbonylphenylboronic acid, Cs<sub>2</sub>CO<sub>3</sub>, Pd(PPh<sub>3</sub>)<sub>4</sub>, dioxane, 120°C, 8 h (28–85%); (iii) NaOMe, MeOH, rt, 4–24 h (22–86%); (iv) NaOMe, MeOH, rt, then NaOH/H<sub>2</sub>O, rt, 16–24 h (63–94%).

Scheme 3<sup>a</sup>

<sup>a</sup> (i) TMSOTf, toluene, rt, 5 h (67–70%); (ii) 4-methoxycarbonylphenylboronic acid, Cs<sub>2</sub>CO<sub>3</sub>, Pd(PPh<sub>3</sub>)<sub>4</sub>, dioxane, 120°C, 8 h or Pd<sub>2</sub>(dba)<sub>3</sub>, S-Phos, dioxane, 80°C, overnight (46–56%); (iii) NaOMe, MeOH, rt, 24 h (52–67%); (iv) NaOMe, MeOH, rt, then NaOH/H<sub>2</sub>O, rt, 24 h (75–95%).

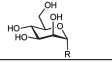
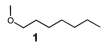
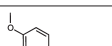
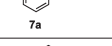
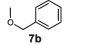
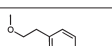
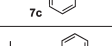
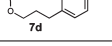
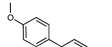
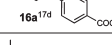
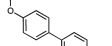
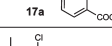
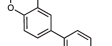
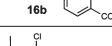
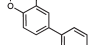
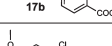
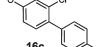
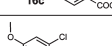
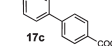
the basis of these findings, we expect a loss of affinity of our antagonists toward full-length fimbriae, when compared to the CRD domain alone.

**Cell-Free Competitive Binding Assay.** The cell-free inhibition assay is based on the interaction of a biotinylated polyacrylamide glycopolymer with the FimH-CRD as previously reported.<sup>23</sup> A recombinant protein consisting of the carbohydrate recognition domain of FimH linked with a thrombin cleavage site to a 6His-tag (FimH-CRD-Th-6His) was expressed in *E. coli* strain HM125 and purified by affinity chromatography. The IC<sub>50</sub> values of the test compounds were determined in microtiter plates coated with

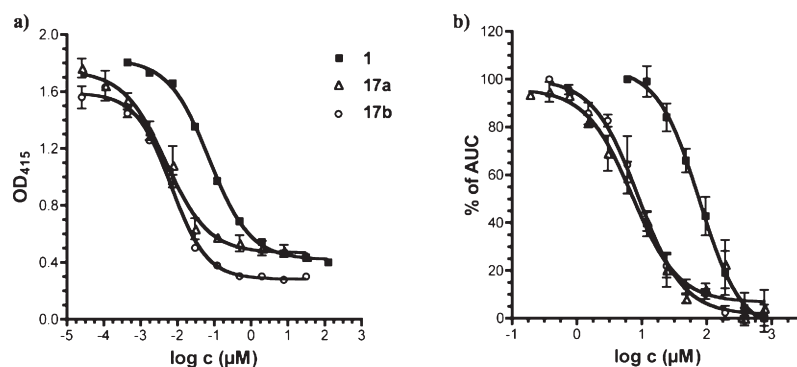
FimH-CRD-Th-6His. Complexation of the biotinylated glycopolymer with streptavidin coupled to horseradish peroxidase allowed the quantification of the binding properties of FimH antagonists (Figure 4a). To ensure comparability with different antagonists, the reference compound *n*-heptyl α-D-mannopyranoside (**1**)<sup>33</sup> was tested in parallel in each individual microtiter plate. The affinities are reported relative to *n*-heptyl α-D-mannopyranoside (**1**) as rIC<sub>50</sub> in Table 1.

The most active representatives from the ester group are **16a** (Table 1, entry 6) and **16b** (entry 8) with affinities in the low nanomolar range, which is an approximately 10-fold improvement compared to reference compound **1**. The

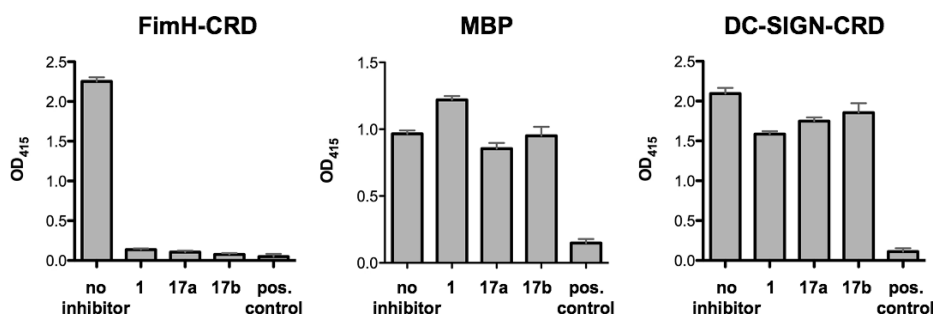
Table 1. Pharmacodynamic and Pharmacokinetic Parameters of FimH Antagonists<sup>a,b</sup>

		IC <sub>50</sub> binding assay [nM]	rIC <sub>50</sub>	IC <sub>50</sub> Aggrego- metry assay [μM]	PAMPA log P <sub>e</sub> [log(10 <sup>6</sup> cm/s)/ %Mm]	Caco-2 P <sub>app</sub> [10 <sup>5</sup> cm/s]	log D <sub>7.4</sub>	pK <sub>a</sub>	log S [μg/mL]/ pH	PPB [%]
1		73±7.9	1.0	77.14±8.7	-4.89/21	nd	1.65	-	>3000	81
2		150±11.5	1.9	nd	nd/nd	nd	nd	-	>3000	nd
3		364±16.8	4.6	nd	nd/nd	nd	nd	-	nd	nd
4		210±11.2	2.6	nd	nd/nd	nd	nd	-	nd	nd
5		253±13.4	3.2	nd	nd/nd	nd	nd	-	nd	nd
6		10.4±1.2	0.14	42±7	-4.7/<20%	4.23	2.14	-	33.8/6.51	93
7		17.1±2.2	0.15	45±8	np	nd	<-1.5	3.88	>3000/6.61	73
8		4.8±1.2	0.06	9±2.7	-4.6/41.00	2.05	2.32	-	11.9/6.53	94
9		6.7±2.1	0.09	10±2.3	np/3.5	nd	-0.77	3.98	>3000/6.50	89
10		22.0±8.4	0.30	41 <sup>b</sup>	-4.72/67.6	nd	2.42	-	11.5/6.50	95
11		27.6±3.9	0.38	17 <sup>b</sup>	np	nd	-1.33	3.95	>3000/6.50	83
12		16.0±0.8	0.22	14 <sup>b</sup>	-4.29/54.3	3.32	2.31	-	4.6/6.53	98
13		15.3±0.4	0.07	nd	-4.40/70.2	5.81	3.10	-	22.7/6.53	94
14		23.9±2.2	0.19	nd	nd/nd	nd	nd	nd	nd	nd
15		20.0±4.3	0.27	33 <sup>b</sup>	-5.01/60.7	4.88	2.02	-	37.6/6.52	92
16		38.7±5.2	0.53	45 <sup>b</sup>	np/9.7	nd	<-1.5	3.60	>3000/6.50	81
17		11.8±0.1	0.16	31 <sup>b</sup>	-4.69/51.7	1.63	1.70	-	24.3/6.54	96
18		29.2±0.7	0.40	nd	np/hr	0.55	<-1.5	3.41	>3000/6.5	87

<sup>a</sup> Single determination; P<sub>e</sub>, effective permeation; P<sub>app</sub>, apparent permeability; np, no permeation; nr, no retention; nd, not determined. <sup>b</sup> The IC<sub>50</sub>s were determined with the cell-free competitive binding assay.<sup>23</sup> The rIC<sub>50</sub> of each substance was calculated by dividing the IC<sub>50</sub> of the compound of interest by the IC<sub>50</sub> of the reference compound **1** (entry 1). This leads to rIC<sub>50</sub> values below 1.00 for derivatives binding better than **1** and rIC<sub>50</sub> values above 1.00 for compounds with a lower affinity than **1**. The aggregation of *E. coli* and GPE were determined in the aggregometry assay.<sup>33</sup> Passive permeation through an artificial membrane and retention therein was determined by PAMPA (parallel artificial membrane permeation assay).<sup>30</sup> The permeation through cell monolayers was assessed by a Caco-2 assay.<sup>31</sup> Distribution coefficients (log D values) were measured by a miniaturized shake flask procedure.<sup>44</sup> pK<sub>a</sub> values were determined by NMR spectroscopy.<sup>45</sup> Plasma protein binding (PPB) was assessed by a miniaturized equilibrium dialysis protocol.<sup>46</sup> Thermodynamic solubility (S) was measured by an equilibrium shake flask approach.<sup>47</sup>



**Figure 4.** Affinities were determined in two different competitive assay formats. (a) a cell-free competitive binding assay<sup>23</sup> and (b) a cell-based aggregometry assay.<sup>33</sup> For antagonists **17a**, **17b**, and the reference compound **1**, IC<sub>50</sub> values in the nM and μM range, respectively, were obtained. The 1000-fold difference between the two assay formats is due to the different competitors used as well as the different affinity states present in FimH, i.e. the high-affinity state present in the CRD used in the cell-free competitive binding assay and the low-affinity state present in the pili of *E. coli* used in the aggregometry assay.



**Figure 5.** Competitive binding assay using FimH-CRD-Th-6His, DC-SIGN-CRD-IgG-Fc,<sup>43</sup> and MBP to evaluate the selectivity of compounds **1**, **17a**, and **17b**. Inhibitory capacities of the compounds were tested at a concentration of 1 mM. As positive control, D-mannose at a concentration of 50 mM was used.

corresponding carboxylic acids **17a** (entry 7) and **17b** (entry 9) exhibited a small reduction in affinity but are still 5-fold more active than reference compound **1**. All the remaining antagonists listed in Table 1 are slightly less active. For the in vivo examination, antagonists **17a** and **17b** were therefore foreseen for iv application and the prodrug **16b** for oral application.

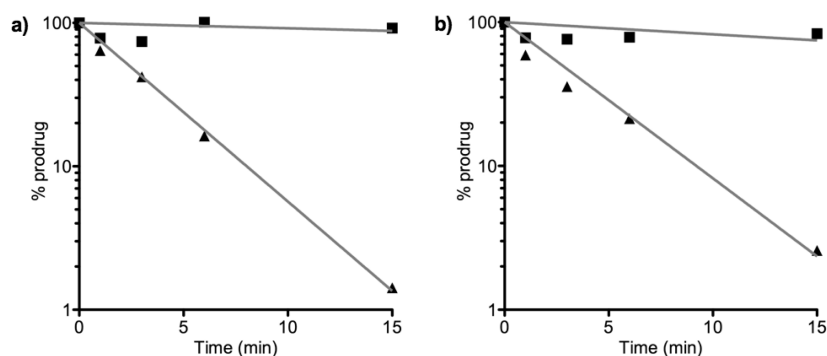
Target selectivity is a further important issue. Mammalian mannose receptors are part of various biological processes, e.g. in cell–cell adhesion (DC-SIGN, dendritic cell-specific intercellular adhesion molecule-3-grabbing nonintegrin),<sup>39</sup> in the regulation of serum glycoprotein homeostasis (mannose receptor)<sup>40</sup> or in the innate and adaptive immune system by recognizing molecular patterns on pathogens (e.g., mannose-binding protein, mannose receptor, DC-SIGN).<sup>39,41,42</sup> Non-specific interactions to the various mannose receptors by FimH inhibitors would have a profound impact on these processes. We therefore determined the affinity of reference compound **1** and the two antagonists **17a** and **17b** for two additional mannose binding proteins, DC-SIGN,<sup>39,43</sup> and MBP (mannose-binding protein)<sup>42</sup> (Figure 5). In both cases, affinities above 1 mM, i.e. a decrease of more than 5 orders of magnitude, was detected.

**Aggregometry Assay.** The potential of the biphenyl mannosides to disaggregate *E. coli* from guinea pig erythrocytes (GPE) was determined by a function-based aggregometry assay.<sup>33</sup> Antagonists were measured in triplicates, and the corresponding IC<sub>50</sub> values were calculated by plotting the

area under the curve (AUC) of disaggregation against the concentration of the antagonists. *n*-Heptyl α-D-mannopyranoside (**1**) was used again as reference compound and exhibits an IC<sub>50</sub> of 77.14 ± 8.7 μM. Antagonists **17a** and **17b** showed IC<sub>50</sub> values of 45 ± 8 μM and 10 ± 2.3 μM, respectively (Figure 4b). In general, the activities obtained from the aggregometry assay are approximately 1000-fold lower than the affinities determined in the target-based competitive assay (discussion see above).

**In Vitro Pharmacokinetic Characterization of FimH Antagonists.** For an application in the UTI mouse model, iv or po available FimH antagonists are required that, once absorbed to circulation, are metabolically stable and undergo fast renal elimination. Sufficient bioavailability requires a combination of high solubility and permeability to maximize absorption and low hepatic clearance to minimize first pass extraction. Furthermore, for efficient renal elimination, active and/or passive membrane permeability and low reabsorption in the renal tubuli is required. From the series of FimH antagonists with nanomolar in vitro activities (see Table 1), representatives with appropriate pharmacokinetic properties were selected for in vivo experiments based on the parameters shown below.

**Oral Absorption and Renal Excretion.** For the evaluation of oral absorption and renal excretion of the esters **16** and **21** as well as the acids **17** and **22** physicochemical parameters such as pK<sub>a</sub> values, lipophilicity (distribution coefficients, log *D*<sub>7.4</sub>), solubility, and permeability were determined



**Figure 6.** Incubation of (a) **16a** and (b) **16b** with pooled mouse liver microsomes (0.25 mg of protein/mL), in absence (▲) and in presence (■) of the specific carboxylesterase inhibitor bis(4-nitrophenyl) phosphate (BNPP).

(Table 1). Not surprisingly, the acids **17** and **22** showed log  $D_{7.4}$  values in the range of  $-1$  to  $-2$  and  $pK_a$  values of approximately 4. While these parameters are beneficial for renal excretion,<sup>32</sup> oral absorption by passive diffusion seems unlikely. Indeed, when the permeation through an artificial membrane (PAMPA<sup>30</sup>) was studied, neither significant permeation (log  $P_e$ ,  $P_e$ : effective permeation) nor membrane retention could be detected. Whereas for a successful oral absorption log  $P_e$  should be above  $-5.7$  and/or the membrane retention above 80%,<sup>48</sup> the corresponding values for the carboxylic acids **17** and **22** are far from being in this range (see Table 1, e.g. entries 7 and 9). However, log  $D_{7.4}$  values and PAMPA results were markedly improved for the esters **16** and **21** (Table 1, e.g. entries 6 and 8), suggesting that these FimH antagonists are orally absorbed. This assumption was fully confirmed in a cell-based permeation assay with Caco-2 cells.<sup>31</sup> For renal excretion, Varma et al.<sup>31</sup> correlated low lipophilicity and the presence of a charged state at physiological pH positively with enhanced elimination. On the basis of log  $D_{7.4}$  and  $pK_a$  summarized in Table 1, the carboxylates **17** and **22** fulfill these requirements. Overall, these results support the prodrug approach: (i) oral application of the esters **16** and **21** and (ii) renal elimination of the corresponding acids **17** and **22**.

**Solubility.** A major problem of the antagonists **16** and **21** is their insufficient solubility, ranging from 4.6 to 37.6  $\mu\text{g/mL}$ . Even though the solubility issue can be addressed by appropriate formulations, further structural modifications to improve solubility are necessary. Opposite to the esters, the corresponding carboxylates **17** and **22** showed excellent solubility ( $> 3$  mg/mL). This enables their iv application in physiological solutions (PBS) in the UTI model without further needs to develop suitable formulations (see below).

**Stability in Simulated Gastrointestinal Fluids.** To exclude degradation in the gastrointestinal tract prior to absorption, the stability of **1**, **16b**, and **17b** in simulated gastric fluid (sGF) and simulated intestinal fluid (sIF) was determined. All three antagonists proved to be sufficiently stable with more than 80% of the initial concentrations found after two hours.

**Metabolic Stability.** Because the prodrug approach is only applicable when the esters **16a** and **16b** are rapidly metabolically cleaved into the corresponding acids, their propensity to enzymatic hydrolysis by carboxylesterase (CES) was studied. Mammalian CESs are localized in the endoplasmatic reticulum of the liver and most other organs.<sup>29</sup> Because of the excellent affinity of the corresponding acids **17a** and

**17b** to FimH, we concentrated our metabolic studies on the ester prodrugs **16a** and **16b**, which were incubated with pooled male mouse liver microsomes to study the hydrolysis and the release of the metabolites. Preliminary experiments involving low substrate concentrations (2  $\mu\text{M}$ ) and a concentration of the microsomal protein of 0.25 mg/mL showed a fast degradation of the ester prodrugs (Figure 6). Addition of the specific CES inhibitor bis(4-nitrophenyl) phosphate (BNPP) prevented ester degradation, suggesting that the metabolic transformation can be attributed to CESs.<sup>49</sup>

On the basis of these *in vitro* results, we also expect fast hydrolysis of the esters *in vivo* at the first liver passage. Current studies are focusing on the kinetic parameters of the enzymatic ester cleavage.

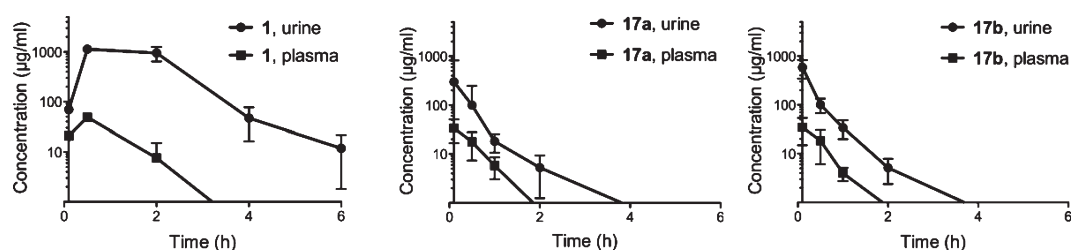
To reach the minimal therapeutic concentration in the bladder (approximately 1  $\mu\text{g/mL}$ , as estimated from a cell-based infection assay<sup>50</sup>), the FimH antagonists **17a** and **17b** should be efficiently renally eliminated and not further metabolically processed. Therefore, the metabolic fate of the free carboxylic acids **17a** and **17b** was examined. A common method to predict a compound's propensity to phase I metabolism is its incubation with liver microsomes in presence of NADPH.<sup>51</sup> Under these conditions, *in vitro* incubations of the free carboxylic acids **17a** and **17b** with pooled male mouse liver microsomes (0.5 mg microsomal protein/mL) did not show significant compound depletion over a period of 30 min, suggesting a high stability against cytochrome P450 mediated metabolism *in vivo*. However, phase II metabolic pathways such as glucuronidation remain to be studied in details.

**Plasma Protein Binding (PPB).** Compared to the corresponding esters **16** and **21**, the antagonists **17** and **22** exhibit 5–20% lower plasma protein binding, typically in the range of 73–89%. This rather low PPB beneficially influences renal excretion because, in line with the free drug hypothesis,<sup>52</sup> molecules bound to plasma proteins evade metabolism and excretion. However, for a concluding statement, the kinetics of PPB, i.e. association and dissociation rate constants, have to be determined because PPB alone is not necessarily predictive for distribution, metabolism, and clearance.<sup>53,54</sup>

**In Vivo Pharmacokinetics and Treatment Studies.** The two mannose derivatives methyl  $\alpha$ -D-mannoside and *n*-heptyl  $\alpha$ -D-mannoside (**1**) were previously tested in the UTI mouse model.<sup>10,21,22</sup> In all three studies, the FimH antagonists were first preincubated with the bacterial suspension, followed by transurethral inoculation. To efficiently reduce infection,



Antagonist	Compartment	$C_{\max}$ ( $\mu\text{g/mL}$ )	$\text{AUC}_{0-24}$ ( $\mu\text{g} \times \text{h/mL}$ )	PPB
<b>1</b>	plasma	$35 \pm 14.1$	$34.3 \pm 33.3$	81%
	urine	$951.4 \pm 249.6$	$2469.3 \pm 636.4$	
<b>17a</b>	plasma	$34.4 \pm 11.8$	$19.3 \pm 6.2$	73%
	urine	$509.6 \pm 427.5$	$139.9 \pm 118.8$	
<b>17b</b>	plasma	$39.4 \pm 15.7$	$20.8 \pm 7.3$	89%
	urine	$588.4 \pm 218.2$	$209.6 \pm 72.3$	



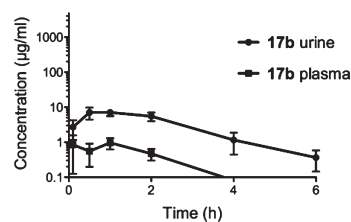
**Figure 7.** Determination of antagonist concentration in urine and plasma after a single iv application of 50 mg/kg. The data (table and graphs) show time-dependent urine and plasma concentrations of **1**, **17a**, and **17b**.

large amounts of methyl  $\alpha$ -D-mannoside had to be applied (up to 1 M).<sup>21</sup> For *n*-heptyl  $\alpha$ -D-mannoside (**1**), an approximately one  $\log_{10}$  unit reduction of bacterial counts in the bladder was reached with lower, but still millimolar, concentration.<sup>10</sup> In the previously presented studies, the FimH antagonists were exclusively instilled into the bladder, which is obviously not suitable for a therapeutic application. The aim of our project was therefore the identification of FimH antagonists suitable for iv or preferably po applications. Before infection studies in a mouse disease model could be performed, the in vivo pharmacokinetic parameters ( $C_{\max}$ , AUC) had to be determined to ensure the antagonists availability in the target organ (bladder).

**Pharmacokinetics of a Single iv Application in C3H/HeN Mice.** Plasma and urine concentrations of the FimH antagonists **1**, **17a**, and **17b** after iv application were determined. With a single dose of 50 mg/kg, the control compound **1** exhibited availability in the bladder over a period of 6 h after administration ( $n = 4$ ), whereas at similar doses, **17a** and **17b** showed lower urine concentrations over a reduced time period (max 2 h) ( $n = 6$ ). In Figure 7, the pharmacokinetic parameters are summarized. Overall, for all three compounds, higher availability of the antagonists in the urine was observed compared to the plasma. Because plasma protein binding is of comparable scale for the three compounds (see Table 1 and Figure 7), it similarly influences urine concentrations.

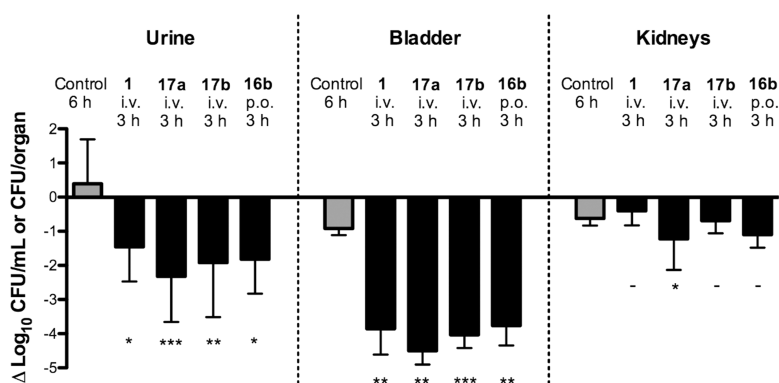
**Pharmacokinetics of a Single po Application in C3H/HeN Mice.** Aiming for an orally available FimH antagonist, the prodrug **16b** and its metabolite **17b** were tested. Because of the in vitro pharmacokinetic properties of **17b** (Table 1, entry 9), its low oral bioavailability after the administration of a single po dose (50 mg/kg) was not surprising. For the determination of the availability of a similar dose of **16b** at the target organ (bladder), plasma and urine concentrations were determined over a period of 24 h ( $n = 6$ ) (Figure 8). Because **16b** was designed as a prodrug expected to be rapidly

Antagonist applied	Antagonist detected	Compartment	$\text{AUC}_{0-24 \text{ p.o.}}$ ( $\mu\text{g} \times \text{h/mL}$ )
<b>17b</b>	<b>17b</b>	Plasma	n.d.
	<b>17b</b>	Urine	$2.7 \pm 3.2$
<b>16b</b>	<b>16b</b>	Plasma	$1.02 \pm 0.32$
		Urine	$1.89 \pm 0.37$
	<b>17b</b>	Plasma	$2.1 \pm 0.61$
		Urine	$21.69 \pm 3.88$



**Figure 8.** Determination of antagonist concentration in urine and plasma after a single po application of 50 mg/kg of antagonists **16b** and **17b**. The data (table and graph) show their time-dependent urine and plasma concentrations. When **17b** was orally applied, its plasma concentration was below the detection level, and only a small portion was present in the urine. However, after the application of the prodrug **16b**, metabolite **17b** was predominantly detected due to fast metabolic hydrolysis of **16b**. However, minor amounts of **16b** are still traceable in plasma as well as urine; nd, not detectable.

hydrolyzed, plasma and urine samples were analyzed not only for **16b** but also for its metabolite **17b**. **16b** was present only in minor concentrations in both plasma and urine. However, although the AUC of metabolite **17b** in urine is reduced by 90% compared to the iv application, its minimal therapeutic concentration can be maintained over a period of 2 to 3 h.



**Figure 9.** Treatment efficacy of the reference compound (**1**) and three FimH antagonists (**17a**, **17b**, **16b**) at a dosage of 50 mg/kg in the UTI mouse model after 3 h of infection, compared to a 6 h infection study ( $n = 6$ ). **1**, **17a**, and **17b** were applied iv into the tail vein, whereas **16b** was applied orally. As baseline (reference), the mean counts of the 3 h infection were subtracted from the results of the tested antagonists and the 6 h control group.  $P$  values were calculated by comparing the treatment groups with the 3 h control group. (\*)  $P < 0.05$ , (\*\*)  $P < 0.01$ , (\*\*\*)  $P < 0.001$ , (-) not significant (determined by Mann–Whitney test).

**UTI Mouse Model: Treatment Study.** Before treatment studies were started, the optimal infection profile was established. A 3 h infection exhibited the highest infection level in the C3H/HeN mouse strain. At longer infection times, e.g. 6 h, the control group showed indeed higher bacterial counts in the urine, however, the bladder and kidney counts already decreased due to self-clearance of the infection in the UTI mouse model.<sup>55</sup> For the in vivo UTI treatment studies (Figure 9), antagonists **1**, **17a**, **17b**, and **16b** were applied followed by infection with UPEC (UTI89). For each antagonist, a group of six animals was used. The animals were sacrificed 3 h after inoculation and urine and homogenized organs (bladder, kidneys) were examined for bacterial counts. The mean value in the untreated reference group ( $n = 6$ ) showed  $1.8 \times 10^6$  CFU/mL in the urine,  $1.4 \times 10^8$  CFU in the bladder and  $9.7 \times 10^6$  CFU in the kidneys. The bar diagram in Figure 9 summarizes the bacterial counts after iv (**1**, **17a**, and **17b**) and po (**16b**) treatment. The baseline represents the values obtained for the control group after 3 h and was used as reference for CFU reductions. **1** showed the lowest inhibition of growth in the urine with  $1.5 \log_{10}$  CFU reduction and an approximately  $4 \log_{10}$  reduction of bacterial counts in the bladder. After iv application of **17a**, a substantial decrease in the bacterial count was obtained ( $> 2 \log_{10}$  CFU reduction in the urine and  $4.5 \log_{10}$  reduction in the bladder). A slightly lower reduction was observed when **17b** was applied iv (a decrease of  $2 \log_{10}$  CFU in the urine and  $4 \log_{10}$  for bladder counts). Interestingly, almost the same reduction of the bacterial count was detected with orally applied **16b**.

In general, urine samples showed higher bacterial counts compared to the bladder. This could be due to the difficulties during urine sampling. We observed that infected C3H/HeN mice void considerably less urine (5–50  $\mu$ L) compared to healthy mice (50–100  $\mu$ L). As a consequence, the lower urine volume leads to a higher concentration of bacteria in the collected urine and therefore to higher bacterial counts compared to the bladder.

In all treated animals, bacterial counts were only marginally reduced in the kidneys. This lower response to the treatment with FimH antagonists is probably due to different bacterial adhesion mechanisms in bladder and kidney. Whereas in the bladder adhesion is mediated by type I pili (via the CRD of FimH), P pili-dependent interactions are crucial for the adhesion in the kidneys.<sup>6</sup>

## Summary and Conclusions

With the objective to develop an oral treatment of urinary tract infections, we have synthesized a series of potent small molecular weight FimH antagonists. Starting from the known antagonist phenyl  $\alpha$ -D-mannopyranoside (**7a**), two equally potent classes of biphenyl  $\alpha$ -D-mannopyranoside, those with an ester function (**16** and **21**) and those with a carboxylate (**17** and **22**) on the terminal aromatic ring, were synthesized. According to their pharmacokinetic properties, the acids **17** and **22** were not expected to be orally absorbed, a prediction that was also confirmed by an in vivo PK study. Therefore, a prodrug approach was envisaged. On the basis of permeation assays (PAMPA and Caco-2), the esters **16** and **22** were expected to exhibit oral availability. Moreover, metabolic studies with mouse liver microsomes proposed fast in vivo hydrolysis of orally applied **16b** to the corresponding carboxylate **17b**. In vivo PK studies in mice finally confirmed the in vitro prediction of a fast renal elimination of **17b** to the target organ, the bladder. When orally applied **16b** was tested in the UTI mouse model, it reduced the colony forming units (CFU) in the urine by 2 orders of magnitude and in the bladder by 4 orders of magnitude. As a result, a low molecular weight FimH antagonist suitable for the oral treatment of urinary tract infections was identified.

However, a number of parameters remain to be improved. Because the solubilities of the esters **16** and **22** are in the low  $\mu$ g/mL range, an iv application was impossible and the suspension in DMSO/1% Tween 80 used for oral dosing is not optimal. In addition, due to fast renal elimination, the minimal therapeutic concentration of **17b** in the bladder could only be maintained for 2–3 h. Because high plasma protein binding was observed, an unfavorable kinetic of dissociation of the active principle from plasma proteins followed by fast renal elimination might be the reason for these findings. An improvement of the corresponding pharmacokinetic parameters should positively influence the duration of action. Furthermore, a detailed analysis of the metabolic pathway of **16b** and its metabolite **17b** will elucidate their overall metabolic fate. Finally, a detailed PK/PD profile in the mouse model will elucidate the full potential of FimH antagonists for the therapy of urinary tract infections (UTI).

## Experimental Section

**General Methods.** NMR spectra were recorded on a Bruker Avance DMX-500 (500 MHz) spectrometer. Assignment of  $^1\text{H}$



and  $^{13}\text{C}$  NMR spectra was achieved using 2D methods (COSY, HSQC, TOCSY). Chemical shifts are expressed in ppm using residual  $\text{CHCl}_3$ ,  $\text{CHD}_2\text{OD}$ , and  $\text{H}_2\text{O}$  as references. Optical rotations were measured using Perkin-Elmer polarimeter 341. Electron spray ionization mass spectra (ESI-MS) were obtained on a Waters micromass ZQ. HRMS analysis were carried out using a Bruker Daltonics micrOTOF spectrometer equipped with a TOF hexapole detector. Microanalyses were performed at the Department of Chemistry, University of Basel, Switzerland. Microwave-assisted reactions were carried out with a CEM Discover and Explorer. Reactions were monitored by TLC using glass plates coated with silica gel 60 F<sub>254</sub> (Merck) and visualized by using UV light and/or by heating to 140 °C for 5 min with a molybdate solution (a 0.02 M solution of ammonium cerium sulfate dihydrate and ammonium molybdate tetrahydrate in aqueous 10%  $\text{H}_2\text{SO}_4$ ). Column chromatography was performed on a CombiFlash Companion (Teledyne-ISCO, Inc.) using RediSep normal phase disposable flash columns (silica gel). Reversed-phase chromatography was performed on LiChroprepRP-18 (Merck, 40–63  $\mu\text{m}$ ). Commercially available reagents were purchased from Fluka, Aldrich, Merck, AKSci, ASDI, or Alfa Aesar. Methanol (MeOH) was dried by refluxing with sodium methoxide and distilled immediately before use. Toluene was dried by filtration over  $\text{Al}_2\text{O}_3$  (Fluka, type 5016 A basic). Dioxane was dried by distillation from sodium/benzophenone.

**4-Bromophenyl 2,3,4,6-Tetra-O-acetyl- $\alpha$ -D-mannopyranoside (14a).** To a stirred solution of **12** (1.17 g, 3.00 mmol) and 4-bromophenol (**13a**, 623 mg, 3.60 mmol) in toluene (12 mL), TMSOTf (65  $\mu\text{L}$ , 0.36 mmol) was added dropwise under argon. The mixture was stirred at rt for 5 h and then diluted with toluene (15 mL) and washed with satd aq  $\text{NaHCO}_3$ . The organic layer was separated, and the aqueous layer was extracted three times with toluene. The combined organic layers were dried over  $\text{Na}_2\text{SO}_4$  and concentrated in vacuo. The residue was purified by flash chromatography on silica (petroleum ether/EtOAc, 19:1 to 1.5:1) to yield **14a** (1.17 g, 74%) as a white solid.

$^1\text{H}$  NMR (500 MHz,  $\text{CDCl}_3$ ):  $\delta$  2.06 (s, 9H, 3  $\text{COCH}_3$ ), 2.19 (s, 3H,  $\text{COCH}_3$ ), 4.06 (m, 2H, H-5, H-6a), 4.27 (dd,  $J = 5.6, 12.4$  Hz, 1H, H-6b), 5.36 (t,  $J = 10.2$  Hz, 1H, H-4), 5.43 (dd,  $J = 1.8, 3.5$  Hz, 1H, H-2), 5.48 (d,  $J = 1.7$  Hz, 1H, H-1), 5.53 (dd,  $J = 3.5, 10.1$  Hz, 1H, H-3), 6.98, 7.41 (AA', BB' of AA'BB',  $J = 9.0$  Hz, 4H,  $\text{C}_6\text{H}_4$ ).  $^{13}\text{C}$  NMR (125 MHz,  $\text{CDCl}_3$ ):  $\delta$  20.71, 20.73, 20.74, 20.9 (4  $\text{COCH}_3$ ), 62.1 (C-6), 65.9 (C-4), 68.8 (C-3), 69.2 (C-2), 69.3 (C-5), 95.9 (C-1), 115.6, 118.3, 132.6, 154.7 (6C,  $\text{C}_6\text{H}_4$ ), 170.0 (4C, 4 CO).

**4-Bromo-2-chlorophenyl 2,3,4,6-tetra-O-acetyl- $\alpha$ -D-mannopyranoside (14b).** According to the procedure described for **14a**, compound **12** (2.38 g, 4.84 mmol) and 4-bromo-2-chlorophenol (**13b**, 1.20 g, 5.80 mmol) were treated with TMSOTf (107 mg, 0.484 mmol) to yield **14b** (1.54 g, 59%) as a white solid.

$[\alpha]_D^{25} +60.6$  (c 0.40,  $\text{CHCl}_3$ ).  $^1\text{H}$  NMR (500 MHz,  $\text{CDCl}_3$ ):  $\delta$  2.02, 2.04, 2.18 (3s, 12H, 4  $\text{COCH}_3$ ), 4.05 (dd,  $J = 2.3, 12.2$  Hz, 1H, H-6a), 4.10 (ddd,  $J = 2.7, 5.3, 9.6$  Hz, 1H, H-5), 4.24 (dd,  $J = 5.4, 12.2$  Hz, 1H, H-6b), 5.35 (t,  $J = 10.1$  Hz, 1H, H-4), 5.48 (m, 2H, H-1, H-2), 5.56 (dd,  $J = 3.2, 10.1$  Hz, 1H, H-3), 7.03 (d,  $J = 8.8$  Hz, 1H,  $\text{C}_6\text{H}_3$ ), 7.30 (dd,  $J = 2.4, 8.8$  Hz, 1H,  $\text{C}_6\text{H}_3$ ), 7.53 (d,  $J = 2.4$  Hz, 1H,  $\text{C}_6\text{H}_3$ ).  $^{13}\text{C}$  NMR (125 MHz,  $\text{CDCl}_3$ ):  $\delta$  20.9, 21.1 (4C, 4  $\text{COCH}_3$ ), 62.3 (C-6), 65.9 (C-4), 68.9 (C-3), 69.4 (C-2), 70.1 (C-5), 96.9 (C-1), 115.9, 118.4, 125.7, 130.8, 133.3, 150.6 ( $\text{C}_6\text{H}_3$ ), 169.9, 170.0, 170.1, 170.7 (4 CO). ESI-MS calcd for  $\text{C}_{20}\text{H}_{22}\text{BrClNaO}_{10} [\text{M} + \text{Na}]^+$  559.0; found 559.0; Anal. Calcd for  $\text{C}_{20}\text{H}_{22}\text{BrClO}_{10}$ : C 44.67, H 4.12. Found: C 45.08, H 4.14.

**Methyl 4'-(2,3,4,6-Tetra-O-acetyl- $\alpha$ -D-mannopyranosyloxy)-biphenyl-4-carboxylate (15a).** A Schlenk tube was charged with **14a** (503 mg, 1.00 mmol), 4-methoxycarbonylphenylboronic acid (224 mg, 1.24 mmol), S-Phos (20.5 mg, 0.05 mmol), cesium carbonate (1.17 g, 3.6 mmol),  $\text{Pd}_2(\text{dba})_3$  (10.4 mg, 0.01 mmol), and a stirring bar. The tube was closed with a rubber septum and was evacuated and flushed with argon. This procedure was

repeated once, and then freshly degassed dioxane (5 mL) was added under a stream of argon. The reaction tube was quickly sealed and the contents were stirred at 80 °C overnight. The reaction mixture was cooled to rt, diluted with EtOAc (10 mL), washed with satd aq  $\text{NaHCO}_3$  (5 mL) and brine (5 mL), and dried over  $\text{Na}_2\text{SO}_4$ . The solvents were removed in vacuo, and the residue was purified by flash chromatography on silica (petroleum ether/EtOAc, 3:1 to 3:2) to give **15a** (474 mg, 85%) as a white solid.

$[\alpha]_D^{25} +80.8$  (c 1.00,  $\text{CHCl}_3$ ).  $^1\text{H}$  NMR (500 MHz,  $\text{CDCl}_3$ ):  $\delta$  2.02, 2.03, 2.04, 2.19 (4s, 12H,  $\text{COCH}_3$ ), 3.91 (s, 3H,  $\text{OCH}_3$ ), 4.08 (m, 2H, H-6a, H-5), 4.27 (dd,  $J = 5.2, 12.2$  Hz, 1H, H-6b), 5.37 (t,  $J = 10.1$  Hz, 1H, H-4), 5.45 (dd,  $J = 1.8, 3.4$  Hz, 1H, H-2), 5.56 (m, 2H, H-1, H-3), 7.16 (AA' of AA'BB',  $J = 8.7$  Hz, 2H,  $\text{C}_6\text{H}_4$ ), 7.57 (m, 4H,  $\text{C}_6\text{H}_4$ ), 8.07 (BB' of AA'BB',  $J = 8.4$  Hz, 2H,  $\text{C}_6\text{H}_4$ ).  $^{13}\text{C}$  NMR (125 MHz,  $\text{CDCl}_3$ ):  $\delta$  20.74, 20.75, 20.77, 21.0 (4  $\text{COCH}_3$ ), 52.2 ( $\text{OCH}_3$ ), 62.1 (C-6), 65.9 (C-4), 68.9 (C-3), 69.3, 69.4 (C-2, C-5), 95.8 (C-1), 116.9, 126.7, 128.5, 128.7, 130.2, 134.8, 144.8, 155.7 (12C, 2  $\text{C}_6\text{H}_4$ ), 167.0, 169.8, 170.0, 170.1, 170.6 (5 CO). ESI-MS calcd for  $\text{C}_{28}\text{H}_{30}\text{NaO}_{12} [\text{M} + \text{Na}]^+$  581.2; found 581.0.

**Methyl 4'-(2,3,4,6-Tetra-O-acetyl- $\alpha$ -D-mannopyranosyloxy)-3'-chlorobiphenyl-4-carboxylate (15b).** A microwave tube was charged with bromide **14b** (720 mg, 1.34 mmol), 4-methoxycarbonylphenylboronic acid (289 mg, 1.61 mmol), cesium carbonate (1.31 g, 4.02 mmol), and  $\text{Pd}(\text{PPh}_3)_4$  (77.4 mg, 0.067 mmol). The tube was sealed with a Teflon septum, evacuated through a needle, and flushed with argon. Degassed dioxane (1.5 mL) was added and the closed tube was degassed in an ultrasonic bath for 15 min, flushed again with argon for 20 min, and exposed to microwave irradiation at 120 °C for 500 min. The solvent was evaporated in vacuo. The residue was dissolved in DCM (10 mL), washed with brine (2  $\times$  10 mL), dried over  $\text{Na}_2\text{SO}_4$ , and concentrated in vacuo. The residue was purified by flash chromatography on silica (petroleum ether/EtOAc, 5:1 to 0.5:1) to yield **15b** (333 mg, 42%) as a white foam.

$[\alpha]_D^{25} +66.3$  (c 1.06,  $\text{CHCl}_3$ ).  $^1\text{H}$  NMR (500 MHz,  $\text{CDCl}_3$ ):  $\delta$  2.03, 2.06, 2.20 (3s, 12H,  $\text{COCH}_3$ ), 3.92 (s, 3H,  $\text{OCH}_3$ ), 4.08 (dd,  $J = 2.4, 12.3$  Hz, 1H, H-6a), 4.17 (m, 1H, H-5), 4.28 (dd,  $J = 5.4, 12.3$  Hz, 1H, H-6b), 5.39 (t,  $J = 10.6$  Hz, 1H, H-4), 5.54 (dd,  $J = 1.9, 3.4$  Hz, 1H, H-2), 5.59 (d,  $J = 1.8$  Hz, 1H, H-1), 5.62 (dd,  $J = 3.5, 10.1$  Hz, 1H, H-3), 7.24 (s, 1H,  $\text{C}_6\text{H}_3$ ), 7.44 (dd,  $J = 2.2, 8.5$  Hz, 1H,  $\text{C}_6\text{H}_3$ ), 7.57 (AA' of AA'BB',  $J = 8.5$  Hz, 2H,  $\text{C}_6\text{H}_4$ ), 7.65 (d,  $J = 2.2$  Hz, 1H,  $\text{C}_6\text{H}_3$ ), 8.08 (BB' of AA'BB',  $J = 8.5$  Hz, 2H,  $\text{C}_6\text{H}_4$ ).  $^{13}\text{C}$  NMR (125 MHz,  $\text{CDCl}_3$ ):  $\delta$  20.9, 21.0, 21.1 (4C, 4  $\text{COCH}_3$ ), 52.5 ( $\text{OCH}_3$ ), 62.3 (C-6), 66.0 (C-4), 69.0 (C-3), 69.5 (C-2), 70.0 (C-5), 96.8 (C-1), 117.4, 126.7, 126.9, 129.5, 130.5, 136.4, 143.6, 151.3 (12C,  $\text{C}_6\text{H}_3$ ,  $\text{C}_6\text{H}_4$ ), 167.0, 169.9, 170.0, 170.2, 170.7 (5 CO). ESI-MS calcd for  $\text{C}_{28}\text{H}_{29}\text{ClNaO}_{12} [\text{M} + \text{Na}]^+$  615.1; found 615.2. Anal. Calcd for  $\text{C}_{28}\text{H}_{29}\text{ClO}_{12}$ : C 56.71, H 4.93. Found: C 56.79, H 4.92.

**Methyl 4'-( $\alpha$ -D-Mannopyranosyloxy)-biphenyl-4-carboxylate (16a).**  $^{17}\text{d}$  To a solution of **15a** (170 mg, 0.304 mmol) in MeOH (3 mL) was added freshly prepared 1 M NaOMe in MeOH (100  $\mu\text{L}$ ) under argon. The mixture was stirred at rt until the reaction was complete (monitored by TLC), then neutralized with Amberlyst-15 ( $\text{H}^+$ ) ion-exchange resin, filtered, and concentrated in vacuo. The residue was purified by reversed-phase chromatography (RP-18,  $\text{H}_2\text{O}/\text{MeOH}$ , 1:0–1:1) to give **16a** (90 mg, 76%) as white solid.

$[\alpha]_D^{25} +82.8$  (c 0.2, MeOH).  $^1\text{H}$  NMR (500 MHz,  $\text{CD}_3\text{OD}$ ):  $\delta$  3.62 (m, 1H, H-5), 3.72 (m, 3H, H-4, H-6a, H-6b), 3.92 (m, 4H, H-3,  $\text{OCH}_3$ ), 4.03 (s, 1H, H-2), 5.55 (s, 1H, H-1), 7.24 (AA' of AA'BB',  $J = 8.0$  Hz, 2H,  $\text{C}_6\text{H}_4$ ), 7.64 (AA' of AA'BB',  $J = 7.5$  Hz, 2H,  $\text{C}_6\text{H}_4$ ), 7.71 (BB' of AA'BB',  $J = 8.0$  Hz, 2H,  $\text{C}_6\text{H}_4$ ), 8.07 (BB' of AA'BB',  $J = 7.5$  Hz, 2H,  $\text{C}_6\text{H}_4$ ).  $^{13}\text{C}$  NMR (125 MHz,  $\text{CD}_3\text{OD}$ ):  $\delta$  52.6 ( $\text{OCH}_3$ ), 62.7 (C-6), 68.3 (C-4), 72.0 (C-2), 72.4 (C-3), 75.5 (C-5), 100.1 (C-1), 118.2, 127.7, 131.1, 135.1, 146.6, 158.2, 160.3 (12C, 2  $\text{C}_6\text{H}_4$ ), 166.1 (CO). HR-MS calcd for  $\text{C}_{20}\text{H}_{22}\text{NaO}_8 [\text{M} + \text{Na}]^+$  413.1212; found 413.1218.

**Methyl 3'-Chloro-4'-( $\alpha$ -D-mannopyranosyloxy)-biphenyl-4-carboxylate (16b).** According to the procedure described for **16a**, compound **16b** was prepared from **15b** (764 mg, 1.29 mmol). Yield: 69 mg, 12%.

$[\alpha]_D^{25} +97.4$  (*c* 1.01, MeOH).  $^1\text{H NMR}$  (500 MHz,  $\text{CD}_3\text{OD}$ ):  $\delta$  3.64 (m, 1H, H-5), 3.72 (m, 1H, H-6a), 3.78 (m, 2H, H-4, H-6b), 3.91 (s, 3H,  $\text{OCH}_3$ ), 4.00 (dd,  $J = 3.4, 9.5$  Hz, 1H, H-3), 4.11 (dd,  $J = 1.8, 3.1$  Hz, 1H, H-2), 5.60 (d,  $J = 1.1$  Hz, 1H, H-1), 7.46 (d,  $J = 8.6$  Hz, 1H,  $\text{C}_6\text{H}_3$ ), 7.58 (dd,  $J = 2.2, 8.6$  Hz, 1H,  $\text{C}_6\text{H}_3$ ), 7.69 (AA' of AA'BB',  $J = 8.4$  Hz, 2H,  $\text{C}_6\text{H}_4$ ), 7.72 (d,  $J = 2.2$  Hz, 1H,  $\text{C}_6\text{H}_3$ ), 8.08 (BB' of AA'BB',  $J = 8.4$  Hz, 2H,  $\text{C}_6\text{H}_4$ ).  $^{13}\text{C NMR}$  (125 MHz,  $\text{CD}_3\text{OD}$ ):  $\delta$  52.7 ( $\text{OCH}_3$ ), 62.8 (C-6), 68.3 (C-4), 71.9 (C-2), 72.5 (C-3), 76.2 (C-5), 100.8 (C-1), 118.7, 125.58, 127.8, 127.9, 129.9, 130.3, 131.3, 136.4, 145.3, 153.5 (12C,  $\text{C}_6\text{H}_3$ ,  $\text{C}_6\text{H}_4$ ), 168.4 (CO). HR-MS calcd for  $\text{C}_{20}\text{H}_{21}\text{ClNaO}_8$  [ $\text{M} + \text{Na}$ ] $^+$  447.0823; found 447.082.

**Sodium 4'-( $\alpha$ -D-Mannopyranosyloxy)-biphenyl-4-carboxylate (17a).** To a solution of **15a** (228 mg, 0.408 mmol) in MeOH (6.0 mL) was added 1 M NaOMe in MeOH (60  $\mu\text{L}$ ) at rt. The reaction mixture was stirred at rt for 4 h, and then NaOH (82 mg) in water (6 mL) was added and stirring was continued at rt overnight. The reaction mixture was concentrated in vacuo, and the residue was purified by reversed-phase chromatography (RP-18,  $\text{H}_2\text{O}/\text{MeOH}$ , 1:0–1:1) to afford **17a** (96 mg, 63%) as a white solid.

$[\alpha]_D^{25} +103$  (*c* 0.10, MeOH).  $^1\text{H NMR}$  (500 MHz,  $\text{CD}_3\text{OD}$ ):  $\delta$  3.60 (m, 1H, H-5), 3.72 (m, 3H, H-6a, H-6b, H-4), 3.89 (dd,  $J = 3.4, 9.5$  Hz, 1H, H-3), 4.00 (dd,  $J = 1.8, 3.3$  Hz, 1H, H-2), 5.51 (s, 1H, H-1), 7.19, 7.60 (AA', BB' of AA'BB',  $J = 8.7$  Hz, 4H,  $\text{C}_6\text{H}_4$ ), 8.01 (d,  $J = 8.2$  Hz, 2H,  $\text{C}_6\text{H}_3$ ), 8.46 (s, 2H,  $\text{C}_6\text{H}_4$ ).  $^{13}\text{C NMR}$  (125 MHz,  $\text{CD}_3\text{OD}$ ):  $\delta$  63.2 (C-6), 68.9 (C-4), 72.6 (C-2), 73.0 (C-3), 76.1 (C-5), 100.7 (C-1), 118.7, 128.0, 129.9, 131.8 (12C, 2  $\text{C}_6\text{H}_4$ ). HR-MS calcd for  $\text{C}_{19}\text{H}_{20}\text{NaO}_8$  [ $\text{M} + \text{H}$ ] $^+$  399.1056; found 399.1052.

**Sodium 3'-Chloro-4'-( $\alpha$ -D-mannopyranosyloxy)-biphenyl-4-carboxylate (17b).** To a solution of **15b** (380 mg, 0.641 mmol) in MeOH (10 mL) was added 1 M NaOMe in MeOH (300  $\mu\text{L}$ ). After stirring at rt for 24 h, 0.5 M aq NaOH (18 mL) was added and stirring continued for another 24 h. The solution was concentrated in vacuo and the residue was purified by reversed-phase chromatography (RP-18,  $\text{H}_2\text{O}/\text{MeOH}$ , 1:0–1:1) to yield **17b** (222 mg, 80%) as a white solid.

$[\alpha]_D^{25} +61.6$  (*c* 1.00,  $\text{H}_2\text{O}$ ).  $^1\text{H NMR}$  (500 MHz,  $\text{D}_2\text{O}$ ):  $\delta$  3.66 (m, 1H, H-5), 3.73 (m, 2H, H-6a, H-6b), 3.79 (t,  $J = 9.8$  Hz, 1H, H-4), 4.07 (dd,  $J = 3.4, 9.8$  Hz, 1H, H-3), 4.14 (d,  $J = 1.4$  Hz, 1H, H-2), 5.47 (bs, 1H, H-1), 7.04 (d,  $J = 8.6$  Hz, 1H,  $\text{C}_6\text{H}_3$ ), 7.24 (d,  $J = 8.6$  Hz, 1H,  $\text{C}_6\text{H}_3$ ), 7.37 (AA' of AA'BB',  $J = 8.1$  Hz, 2H,  $\text{C}_6\text{H}_4$ ), 7.41 (bs, 1H,  $\text{C}_6\text{H}_3$ ), 7.86 (BB' of AA'BB',  $J = 8.1$  Hz, 2H,  $\text{C}_6\text{H}_4$ ).  $^{13}\text{C NMR}$  (125 MHz,  $\text{D}_2\text{O}$ ):  $\delta$  60.6 (C-6), 66.5 (C-4), 69.0 (C-2), 70.5 (C-3), 73.9 (C-5), 98.6 (C-1), 117.5, 123.9, 126.2, 126.4, 128.4, 129.6, 135.2, 135.3, 141.0, 150.4 (12C,  $\text{C}_6\text{H}_3$ ,  $\text{C}_6\text{H}_4$ ), 175.0 (CO). HR-MS calcd for  $\text{C}_{19}\text{H}_{18}\text{ClNaO}_8$  [ $\text{M} + \text{H}$ ] $^+$  433.0666; found 433.0670.

**Competitive Binding Assay.** A recombinant protein consisting of the CRD of FimH linked with a thrombin cleavage site to a 6His-tag (FimH-CRD-Th-6His) was expressed in *E. coli* strain HM125 and purified by affinity chromatography.<sup>23</sup> To determine the affinity of the various FimH antagonists, a competitive binding assay described previously<sup>23</sup> was applied. Microtiter plates (F96 MaxiSorp, Nunc) were coated with 100  $\mu\text{L}$ /well of a 10  $\mu\text{g}/\text{mL}$  solution of FimH-CRD-Th-6His in 20 mM HEPES, 150 mM NaCl, and 1 mM  $\text{CaCl}_2$ , pH 7.4 (assay buffer) overnight at 4  $^\circ\text{C}$ . The coating solution was discarded and the wells were blocked with 150  $\mu\text{L}$ /well of 3% BSA in assay buffer for 2 h at 4  $^\circ\text{C}$ . After three washing steps with assay buffer (150  $\mu\text{L}$ /well), a 4-fold serial dilution of the test compound (50  $\mu\text{L}$ /well) in assay buffer containing 5% DMSO and streptavidin-peroxidase coupled Man- $\alpha$ (1-3)-[Man- $\alpha$ (1-6)]-Man- $\beta$ (1-4)-GlcNAc- $\beta$ (1-4)-GlcNAc $\beta$  polyacrylamide (TM-PAA) polymer (50  $\mu\text{L}$ /well of a 0.5  $\mu\text{g}/\text{mL}$  solution) were added. On each individual microtiter plate, *n*-heptyl  $\alpha$ -D-mannopyranoside (**1**) was tested in parallel.

The plates were incubated for 3 h at 25  $^\circ\text{C}$  and 350 rpm and then carefully washed four times with 150  $\mu\text{L}$ /well assay buffer. After the addition of 100  $\mu\text{L}$ /well of 2,2'-azino-di-(3-ethylbenzthiazoline-6-sulfonic acid) (ABTS)-substrate, the colorimetric reaction was allowed to develop for 4 min and then stopped by the addition of 2% aqueous oxalic acid before the optical density (OD) was measured at 415 nm on a microplate-reader (Spectramax 190, Molecular Devices, California, USA). The  $\text{IC}_{50}$  values of the compounds tested in duplicates were calculated with prism software (GraphPad Software, Inc., La Jolla, California, USA). The  $\text{IC}_{50}$  defines the molar concentration of the test compound that reduces the maximal specific binding of TM-PAA polymer to FimH-CRD by 50%. The relative  $\text{IC}_{50}$  ( $\text{rIC}_{50}$ ) is the ratio of the  $\text{IC}_{50}$  of the test compound to the  $\text{IC}_{50}$  of *n*-heptyl  $\alpha$ -D-mannopyranoside (**1**).

**Selectivity for FimH vs Mannose-Binding Protein and DC-SIGN.** Recombinant FimH-CRD-Th-6His (10  $\mu\text{g}/\text{mL}$ ), DC-SIGN-CRD-Fc-IgG<sup>39</sup> (2.5  $\mu\text{g}/\text{mL}$ ), and mannose-binding protein<sup>42</sup> (MBP, 10  $\mu\text{g}/\text{mL}$ , R&D Systems, Minneapolis, MN) were each diluted in assay buffer (20 mM HEPES, pH 7.4, 150 mM NaCl, and 10 mM  $\text{CaCl}_2$ ) and were coated on microtiter plates (F96 MaxiSorp, Nunc) with 100  $\mu\text{L}$ /well overnight at 4  $^\circ\text{C}$ . The further steps were performed as described above.

**Aggregometry Assay.** The aggregometry assay was carried out as previously described.<sup>33</sup> In short, the percentage of aggregation of *E. coli* UTI89 with guinea pig erythrocytes (GPE) was quantitatively determined by measuring the optical density at 740 nm and 37  $^\circ\text{C}$  under stirring at 1000 rpm using an APACT 4004 aggregometer (Endotell AG, Allschwil, Switzerland). Bacteria were cultivated as described below (see in vivo models). GPE were separated from guinea pig blood (Charles River Laboratories, Sulzfeld, Germany) using Histopaque (density of 1.077 g/mL at 24  $^\circ\text{C}$ , Sigma-Aldrich, Buchs, Switzerland). Prior to the measurements, the cell densities of *E. coli* and GPE were adjusted to an  $\text{OD}_{600}$  of 4, corresponding to  $1.9 \times 10^8$  CFU/mL and  $2.2 \times 10^6$  cells/mL, respectively. For the calibration of the instrument, the aggregation of protein-poor plasma (PPP) using PBS alone was set as 100% and the aggregation of protein-rich plasma (PRP) using GPE as 0%. After calibration, measurements were performed with 250  $\mu\text{L}$  of GPE and 50  $\mu\text{L}$  of bacterial suspension and the aggregation monitored over 600 s. After the aggregation phase of 600 s, 25  $\mu\text{L}$  of antagonist in PBS was added to each cuvette and disaggregation was monitored for 1400 s. UTI89  $\Delta\text{fimA-H}$  was used as negative control.

**Determination of the Pharmacokinetic Parameters. Materials.** Dimethyl sulfoxide (DMSO), 1-octanol, pepsin, pancreatin, reduced nicotinamide adenine dinucleotide phosphate (NADPH), Dulbecco's Modified Eagle's Medium (DMEM) high glucose, and bis(4-nitrophenyl) phosphate (BNPP) were purchased from Sigma-Aldrich (Sigma-Aldrich, St. Louis MO, USA). PAMPA System Solution, GIT-0 Lipid Solution, and Acceptor Sink Buffer were ordered from pIon (pIon, Woburn MA, USA). L-Glutamine-200 mM (100 $\times$ ) solution, MEM nonessential amino acid (MEM-NEAA) solution, fetal bovine serum (FBS), and DMEM without sodium pyruvate and phenol red were bought from Invitrogen (Invitrogen, Carlsbad CA, USA). Human plasma was bought from Biopredic (Biopredic, Rennes, France) and acetonitrile (MeCN) from Acros (Acros Organics, Geel, Belgium). Pooled male mouse liver microsomes were purchased from BD Bioscience (BD Bioscience, Woburn, MA, USA). Magnesium chloride was bought from Fluka (Fluka Chemie GmbH, Buchs, Switzerland). Tris(hydroxymethyl)-aminomethane (TRIS) was obtained from AppliChem (AppliChem, Darmstadt, Germany). The Caco-2 cells were kindly provided by Prof G. Imanidis, FHNW, Muttentz, and originated from the American Type Culture Collection (Rockville, MD, USA).

**log  $D_{7.4}$  Determination.** The in silico prediction tool ALOGPS 2.1<sup>36</sup> was used to estimate the log *P* values of the compounds. Depending on these values, the compounds were classified into three categories: hydrophilic compounds (log *P*

**Table 2**

compound type	log <i>P</i>	ratios (1-octanol:buffer)
hydrophilic	<0	30:140, 40:130
moderately lipophilic	0–1	70:110, 110:70
lipophilic	>1	3:180, 4:180

below zero), moderately lipophilic compounds (log *P* between zero and one) and lipophilic compounds (log *P* above one). For each category, two different ratios (volume of 1-octanol to volume of buffer) were defined as experimental parameters (Table 2):

Equal amounts of phosphate buffer (0.1 M, pH 7.4) and 1-octanol were mixed and shaken vigorously for 5 min to saturate the phases. The mixture was left until separation of the two phases occurred, and the buffer was retrieved. Stock solutions of the test compounds were diluted with buffer to a concentration of 1 μM. For each compound, six determinations, i.e., three determinations per 1-octanol:buffer ratio, were performed in different wells of a 96-well plate. The respective volumes of buffer containing analyte (1 μM) were pipetted to the wells and covered by saturated 1-octanol according to the chosen volume ratio. The plate was sealed with aluminum foil, shaken (1350 rpm, 25 °C, 2 h) on a Heidolph Titramax 1000 plate-shaker (Heidolph Instruments GmbH & Co. KG, Schwabach, Germany) and centrifuged (2000 rpm, 25 °C, 5 min, 5804 R Eppendorf centrifuge, Hamburg, Germany). The aqueous phase was transferred to a 96-well plate for analysis by liquid chromatography–mass spectrometry (LC-MS).

log *D*<sub>7.4</sub> was calculated from the 1-octanol:buffer ratio (*o:b*), the initial concentration of the analyte in buffer (1 μM), and the concentration of the analyte in buffer (*c*<sub>B</sub>) with equilibration:

$$\log D_{7.4} = \log \left( \frac{1 \mu\text{M} - c_B}{c_B} \times \frac{1}{o:b} \right)$$

The average of the three log *D*<sub>7.4</sub> values per 1-octanol:buffer ratio was calculated. If the two mean values obtained for a compound did not differ by more than 0.1 unit, the results were accepted.

**Parallel Artificial Membrane Permeation Assay (PAMPA).** log *P*<sub>e</sub> was determined in a 96-well format with the PAMPA<sup>30</sup> permeation assay. For each compound, measurements were performed at three pH values (5.0, 6.2, 7.4) in quadruplicates. For this purpose, 12 wells of a deep well plate, i.e., four wells per pH value, were filled with 650 μL of System Solution. Samples (150 μL) were withdrawn from each well to determine the blank spectra by UV-spectroscopy (SpectraMax 190, Molecular Devices, Silicon Valley CAa, USA). Then, analyte dissolved in DMSO was added to the remaining System Solution to yield 50 μM solutions. To exclude precipitation, the optical density was measured at 650 nm, with 0.01 being the threshold value. Solutions exceeding this threshold were filtrated. Afterward, samples (150 μL) were withdrawn to determine the reference spectra. A further 200 μL were transferred to each well of the donor plate of the PAMPA sandwich (pIon, Woburn MA, USA, P/N 110 163). The filter membranes at the bottom of the acceptor plate were impregnated with 5 μL of GIT-0 Lipid Solution and 200 μL of Acceptor Sink Buffer were filled into each acceptor well. The sandwich was assembled, placed in the GutBox, and left undisturbed for 16 h. Then, it was disassembled and samples (150 μL) were transferred from each donor and acceptor well to UV-plates. Quantification was performed by both UV-spectroscopy and LC-MS. log *P*<sub>e</sub> values were calculated with the aid of the PAMPA Explorer Software (pIon, version 3.5).

**Colorectal Adenocarcinoma Cells (Caco-2 Cells) Permeation Assay.** The cells were cultivated in tissue culture flasks (BD Biosciences, Franklin Lakes NJ, USA) with DMEM high glucose medium, containing 1% L-glutamine solution, 1% MEM-NEAA solution, and 10% FBS. The cells were kept at

37 °C in humidified air containing 8% CO<sub>2</sub>, and the medium was changed every second to third day. When approximately 90% confluence was reached, the cells were split in a 1:10 ratio and distributed to new tissue culture flasks. At passage numbers between 60 and 65, they were seeded at a density of 5.33 × 10<sup>5</sup> cells per well to Transwell 6-well plates (Corning Inc., Corning NY, USA) with 2.5 mL of culture medium in the basolateral compartment and 1.5 mL (days 1–10) or 1.8 mL (from day 10 on) in the basolateral compartment. The medium was renewed on alternate days. Experiments were performed between days 19 and 21 postseeding. DMEM without sodium pyruvate and phenol red was used as transport medium for experiments. Previous to the experiment, the integrity of the Caco-2 monolayers was evaluated by measuring the transepithelial resistance (TEER) in transport medium (37 °C) with an Endohm tissue resistance instrument (World Precision Instruments Inc., Sarasota, FL, USA). Only wells with TEER values higher than 300 Ωcm<sup>2</sup> were used. Experiments were performed in triplicates. Transport medium (10 μL) from the apical compartments of three wells were replaced by the same volume of compound stock solutions (10 mM). The Transwell plate was then shaken (250 rpm) in the incubator. Samples (100 μL) were withdrawn after 5, 15, 30, 60, and 120 min from the basolateral compartment and concentrations were analyzed by HPLC. Apparent permeability coefficients (*P*<sub>app</sub>) were calculated according to the following equation

$$P_{\text{app}} = \frac{dQ}{dt} \times \frac{1}{A \times c_0}$$

where *dQ/dt* is the permeability rate, *A* the surface area of the monolayer, and *c*<sub>0</sub> the initial concentration in the donor compartment.<sup>31</sup> After the experiment, TEER values were assessed again for every well and results from wells with values below 300 Ωcm<sup>2</sup> were discarded.

**p*K*<sub>a</sub> Values.** The p*K*<sub>a</sub> values were determined as described elsewhere.<sup>45</sup> Briefly, the pH of a sample solution was gradually changed and the chemical shift of protons adjacent to ionizable centers was monitored by <sup>1</sup>H nuclear magnetic resonance (NMR) spectroscopy. The shift was plotted against the pH of the respective sample, and the p*K*<sub>a</sub> was read out from the inflection point of the resulting sigmoidal curve.

**Plasma Protein Binding (PPB).** The dialysis membranes (HTDialysis LCC, Gales Ferry, CT, USA; MWCO 12–14 K) were prepared according to company instructions. The human plasma was centrifuged (5800 rpm, 25 °C, 10 min), the pH of the centrifugate (without floating plasma lipids) was adjusted to 7.5, and analyte was added to yield 10 μM solutions. Equal volumes (150 μL) of phosphate buffer (0.1 M, pH 7.5) and analyte-containing plasma were transferred to the separated compartments of the assembled 96-well high throughput dialysis block (HTDialysis LCC, Gales Ferry, CT, USA). Measurements were performed in triplicates. The plate was covered with a sealing film and incubated (5 h, 37 °C). Buffer and plasma compartment were processed separately. From the buffer compartments, 90 μL were withdrawn and 10 μL of blank plasma were added. From the plasma compartments, 10 μL were withdrawn and 90 μL of blank buffer were added. After protein precipitation with 300 μL ice-cooled MeCN, the solutions were mixed, centrifuged (3600 rpm, 4 °C, 11 min), and 50 μL of the supernatant were retrieved. Analyte concentrations were determined by LC-MS. The fraction bound (*f*<sub>b</sub>) was calculated as follows:

$$f_b = 1 - \frac{c_b}{c_p}$$

where *c*<sub>b</sub> is the concentration in the buffer and *c*<sub>p</sub> the concentration in the plasma compartment. Values were accepted if the recovery of analyte was between 80 and 120%.

**Thermodynamic Solubility.** Microanalysis tubes (Labo-Tech J. Stofer LTS AG, Muttens, Switzerland) were charged with



1 mg of solid substance and 250  $\mu$ L of phosphate buffer (50 mM, pH 6.5). The samples were briefly shaken by hand and then sonicated for 15 min and vigorously shaken (600 rpm, 25 °C, 2 h) on a Eppendorf Thermomixer Comfort. Afterward, the samples were left undisturbed for 24 h. After measuring the pH, the saturated solutions were filtered through a filtration plate (MultiScreen HTS, Millipore, Billerica MA, USA) by centrifugation (1500 rpm, 25 °C, 3 min). Prior to concentration determination by LC-MS, the filtrates were diluted (1:1, 1:10 and 1:100 or, if the results were outside of the calibration range, 1:1000 and 1:10000). The calibration was based on six values ranging from 0.1 to 10  $\mu$ g/mL.

**Stability in Simulated Gastrointestinal Fluids.** Simulated gastric fluid (sGF) and simulated intestinal fluid (sIF) were prepared according to the United States Pharmacopeia (USP 28). sGF contained sodium chloride (200 mg), pepsin (320 mg), and 37% aq HCl (0.7 mL) in bidistilled water (100 mL). sIF consisted of monopotassium phosphate (680 mg), 0.2 M NaOH (7.7 mL), and pancreatin (1 g) in bidistilled water (100 mL). sIF was adjusted to pH 6 by adding 0.2 M NaOH. sGF and sIF were preheated (37 °C), and the compounds were added to yield 10  $\mu$ M solutions. Incubations were performed on a Eppendorf Thermomixer Comfort (500 rpm, 37 °C). Before starting the experiment ( $t = 0$  min) and after an incubation time of 15, 30, 60, and 120 min, samples (20  $\mu$ L) were withdrawn, precipitated with ice-cooled MeCN, and centrifuged (3600 rpm, 4 °C, 10 min). The concentrations of analyte in the supernatant were analyzed by LC-MS. Stability was expressed as percentage remaining compound relative to the initial concentration.

**In Vitro Metabolism: Ester Hydrolysis.** Incubations were performed in a 96-well format on a Eppendorf Thermomixer Comfort. Each compound was incubated with a reaction mixture (270  $\mu$ L) consisting of pooled male mouse liver microsomes in the presence of TRIS buffer (0.1 M, pH 7.4) and MgCl<sub>2</sub> (2 mM). After preheating (37 °C, 500 rpm, 10 min), the incubation was initiated by adding 30  $\mu$ L of compound solution (20  $\mu$ M) in TRIS buffer. The final concentration of the compounds was 2  $\mu$ M, and the microsomal concentration was 0.25 mg/mL. At the beginning of the experiment ( $t = 0$  min) and after an incubation time of 1, 3, 6, and 15 min, samples (50  $\mu$ L) were transferred to 150  $\mu$ L of ice-cooled MeCN, centrifuged (3600 rpm, 4 °C, 10 min), and 80  $\mu$ L of supernatant were transferred to a 96-well plate for LC-MS analysis. Metabolic degradation was assessed as percentage remaining compound versus incubation time. Control experiments were performed in parallel by preincubating the microsomes with the specific carboxylesterase inhibitor BNPP (1 mM) for 5 min before addition of the antagonists.

**In Vitro Metabolism: Cytochrome P450-Mediated Metabolism.** Incubations consisted of pooled male mouse liver microsomes (0.5 mg microsomal protein/mL), compounds (2  $\mu$ M), MgCl<sub>2</sub> (2 mM), and NADPH (1 mM) in a total volume of 300  $\mu$ L TRIS buffer (0.1 M, pH 7.4) and were performed in a 96-well plate on a Thermomixer Comfort. Compounds and microsomes were preincubated (37 °C, 700 rpm, 10 min) before NADPH was added. Samples (50  $\mu$ L) at  $t = 0$  min and after an incubation time of 5, 10, 20, and 30 min were quenched with 150  $\mu$ L of ice-cooled acetonitrile, centrifuged (3600 rpm, 4 °C, 10 min), and 80  $\mu$ L of each supernatant were transferred to a 96-well plate for LC-MS analysis. Control experiments without NADPH were performed in parallel.

**LC-MS Measurements.** Analyses were performed using a 1100/1200 series HPLC system coupled to a 6410 triple quadrupole mass detector (Agilent Technologies, Inc., Santa Clara, CA, USA) equipped with electrospray ionization. The system was controlled with the Agilent MassHunter Workstation Data Acquisition software (version B.01.04). The column used was an Atlantis T3 C18 column (2.1 mm  $\times$  50 mm) with a 3  $\mu$ m particle size (Waters Corp., Milford, MA, USA). The mobile phase consisted of two eluents: solvent A (H<sub>2</sub>O, containing 0.1%

formic acid, v/v) and solvent B (acetonitrile, containing 0.1% formic acid, v/v), both delivered at 0.6 mL/min. The gradient was ramped from 95% A/5% B to 5% A/95% B over 1 min, and then held at 5% A/95% B for 0.1 min. The system was then brought back to 95% A/5% B, resulting in a total duration of 4 min. MS parameters such as fragmentor voltage, collision energy, polarity were optimized individually for each drug, and the molecular ion was followed for each compound in the multiple reaction monitoring mode. The concentrations of the analytes were quantified by the Agilent Mass Hunter Quantitative Analysis software (version B.01.04).

**In Vivo Pharmacokinetic and Disease Model. Bacteria.** The clinical *E. coli* isolate UTI89<sup>55</sup> (UTI89wt) were kindly provided by the group of Prof. Urs Jenal, Biocenter, University of Basel. Microorganisms were stored at -70 °C and before experiment incubated for 24 h under static conditions at 37 °C in 10 mL of Luria-Bertani broth (Becton, Dickinson and Company, Le Pont de Claix, France) using 50 mL tubes. Prior to each experiment, the microorganisms were washed twice and resuspended in phosphate buffered saline (PBS, Hospital Pharmacy at the University Hospital Basel, Switzerland). Bacterial concentrations were determined by plating serial 1:10 dilutions on blood agar, followed by colony counting with 20–200 colonies after overnight incubation at 37 °C.

**Animals.** Female C3H/HeN mice weighing between 19 and 25 g were obtained from Charles River (Sulzfeld, Germany) and were housed four to a cage. Mice were kept under specific-pathogen-free conditions in the Animal House of the Department of Biomedicine, University Hospital Basel, and animal experimentation guidelines according to the regulations of Swiss veterinary law were followed. After seven days of acclimatization, 9- to 10-week old mice were used for the PK and infection studies. During the studies, animals were allowed free access to chow and water. Three days before infection studies and during infection, 5% D-(+)-glucose (AppliChem, Baden-Dättwil, Switzerland) was added to the drinking water to increase the number of bacterial counts in the urine and kidneys.<sup>57</sup>

**Pharmacokinetic Studies.** Single-dose pharmacokinetic studies were performed by iv and po application of the FimH antagonists at a concentration of 50 mg/kg followed by urine and plasma sampling. For iv application, the antagonists (**1**, **17a**, **17b**) were diluted in 100  $\mu$ L of PBS and injected into the tail vein. For po application, antagonist **1** was diluted in 200  $\mu$ L of PBS and antagonists **17b** and **16b** were first dissolved in DMSO (20 $\times$ ) and then slowly diluted to the final concentration (1 $\times$ ) in 1% Tween-80/PBS to obtain a suspension. Antagonists were applied iv by injection into the tail vein and po using a gavage followed by blood and urine sampling (10  $\mu$ L) after 6 min, 30 min, 1 h, 2 h, 4 h, 6 h, 8 h, and 24 h. Before analysis, proteins in blood and urine samples were precipitated using methanol (Acros Organics, Basel, Switzerland) and centrifuged for 11 min at 13000 rpm. The supernatant was transferred into a 96-well plate (0.5 mL, polypropylene, Agilent Technologies, Basel, Switzerland) and analyzed by LC-MS as described above.

**UTI Mouse Model.** Mice were infected as previously described.<sup>57</sup> In brief, before infection, all remaining urine was depleted from the bladder by gentle pressure on the abdomen. Mice were anesthetized with 2.5 vol% isoflurane/oxygen mixture (Attane, Minrad Inc., Buffalo, NY, USA) and placed on their back. Anesthetized mice were inoculated transurethrally with the bacterial suspension by use of a 2 cm polyethylene catheter (Intramedic polyethylene tubing, inner diameter 0.28 mm, outer diameter 0.61 mm, Beckton Dickinson, Allschwil, Switzerland), which was placed on a syringe (Hamilton Gastight Syringe 50  $\mu$ L, removable 30G needle, BGB Analytik AG, Boeckten, Switzerland). The catheter was gently inserted through the urethra until it reached the top of the bladder, followed by slow injection of 50  $\mu$ L of bacterial suspension at a concentration of approximately 10<sup>9</sup> to 10<sup>10</sup> CFU/mL.

**Antagonist Treatment Studies.** FimH antagonists were applied iv in 100  $\mu$ L of PBS into the tail vein or po as a suspension by the help

of a gavage, 10 min (**17a**, **17b**, **16b**) or 1 h before infection (**1**). Three h after the onset of infection, urine was collected by gentle pressure on the abdomen and then the mouse was sacrificed with CO<sub>2</sub>. Organs were removed aseptically and homogenized in 1 mL of PBS by using a tissue lyser (Retsch, Haan, Germany). Serial dilutions of urine, bladder, and kidneys were plated on Levine Eosin Methylene Blue Agar plates (Beckton Dickinson, Le Pont de Claix, France). CFU counts were determined after overnight incubation at 37 °C and expressed as CFU/mL for the urine and CFU/bladder and CFU/2 kidneys for the organs.

**Acknowledgment.** We thank Professor Rudi Glockshuber (ETH Zürich, Switzerland) for gratefully providing the plasmid pNT-FimH used for the cloning of the FimH CRD and *E. coli* strain HM 125. We thank Dr. Manfred Kansy and Dr. Christoph Funk, F. Hoffmann-La Roche AG, Basel, Switzerland, for supporting us with their expertise when we established the PADMET platform, and to Prof. Angelo Vedani, University of Basel, Switzerland, for fruitful discussions on conformational issues. We further appreciate the support by Prof. Dr. med. Radek Skoda, Department of Biomedicine, University Hospital Basel, Switzerland, for giving us access to the animal facility and Prof. Niels Frimodt-Møller, Statens Serum Institut, Copenhagen, Denmark for the introduction to the in vivo model. We thank Prof G. Imanidis, FHNW, Muttenz, Switzerland, for providing the Caco-2 cells, and Dr. M. Schneider, Department of Pharmaceutical Sciences, University of Basel, Switzerland, for his help during the assay build-up. We are grateful to Prof. Urs Jenal, Biocenter of the University of Basel, Switzerland, for the clinical *E. coli* isolate UTI89 and the FimH knock out strain UTI89Δ*fimA-H*. Finally, we thank the Swiss National Science Foundation (project K-32K1-120904) for their financial support.

**Supporting Information Available:** <sup>1</sup>H NMR spectra and HPLC traces for the target compounds **16a–e**, **17a–c,e**, **21a,b**, and **22a,b** and experimental and spectroscopic details for compounds **6a–d**, **7a–d**, **14c–e**, **15c–e**, **16c–e**, **17c,e**, **19a,b**, **20a,b**, and **21a,b**. This material is available free of charge via the Internet at <http://pubs.acs.org>.

## References

- Fihn, S. D. Clinical practice. Acute uncomplicated urinary tract infection in women. *N. Engl. J. Med.* **2003**, *349*, 259–266.
- Hooton, T. M. Recurrent urinary tract infection in women. *Int. J. Antimicrob. Agents* **2001**, *17*, 259–268.
- Wiles, T. J.; Kulescu, R. R.; Mulvey, M. A. Origins and virulence mechanisms of uropathogenic *Escherichia coli*. *Exp. Mol. Pathol.* **2008**, *85*, 11–19.
- Gouin, S. G.; Wellens, A.; Bouckaert, J.; Kovensky, J. Synthetic Multimeric Heptyl Mannosides as Potent Antiadhesives of Uropathogenic *Escherichia coli*. *ChemMedChem* **2009**, *4*, 749–755.
- Rosen, D. A.; Hung, C. S.; Kline, K. A.; Hultgren, S. J. Streptozocin-induced diabetic mouse model of urinary tract infection. *Infect. Immun.* **2008**, *76*, 4290–4298.
- Mulvey, M. A. Adhesion and entry of uropathogenic *Escherichia coli*. *Cell Microbiol.* **2002**, *4*, 257–271.
- Capitani, G.; Eidam, O.; Glockshuber, R.; Grutter, M. G. Structural and functional insights into the assembly of type 1 pili from *Escherichia coli*. *Microbes Infect.* **2006**, *8*, 2284–2290.
- Choudhury, D.; Thompson, A.; Stojanoff, V.; Langermann, S.; Pinkner, J.; Hultgren, S. J.; Knight, S. D. X-ray structure of the FimC–FimH chaperone–adhesin complex from uropathogenic *Escherichia coli*. *Science* **1999**, *285*, 1061–1066.
- Bouckaert, J.; Berglund, J.; Schembri, M.; Genst, E. D.; Cools, L.; Wuhler, M.; Hung, C. S.; Pinkner, J.; Slättergard, R.; Zavialov, A.; Choudhury, D.; Langermann, S.; Hultgren, S. J.; Wyns, L.; Klemm, P.; Oscarson, S.; Knight, S. D.; Greve, H. D. Receptor binding studies disclose a novel class of high-affinity inhibitors of the *Escherichia coli* FimH adhesin. *Mol. Microbiol.* **2005**, *55*, 441–455.
- Wellens, A.; Garofalo, C.; Nguyen, H.; Van Gerven, N.; Slättergard, R.; Hernalsteens, J.-P.; Wyns, L.; Oscarson, S.; De Greve, H.; Hultgren, S.; Bouckaert, J. Intervening with urinary tract infections using anti-adhesives based on the crystal structure of the FimH–oligomannose-3 complex. *PLoS ONE* **2008**, *3*, 4–13.
- Langermann, S.; Mollby, R.; Burlein, J. E.; Palaszynski, S. R.; Auguste, C. G.; DeFusco, A.; Strouse, R.; Schenerman, M. A.; Hultgren, S. J.; Pinkner, J. S.; Winberg, J.; Guldevall, L.; Soderhall, M.; Ishikawa, K.; Normark, S.; Koenig, S. Vaccination with FimH adhesin protects cynomolgus monkeys from colonization and infection by uropathogenic *Escherichia coli*. *J. Infect. Dis.* **2000**, *181*, 774–778.
- Langermann, S.; Palaszynski, S.; Barnhart, M.; Auguste, G.; Pinkner, J. S.; Burlein, J.; Barren, P.; Koenig, S.; Leath, S.; Jones, C. H.; Hultgren, S. J. Prevention of mucosal *Escherichia coli* infection by FimH-adhesin-based systemic vaccination. *Science* **1997**, *276*, 607–611.
- Bouckaert, J.; Mackenzie, J.; de Paz, J. L.; Chipwaza, B.; Choudhury, D.; Zavialov, A.; Mannerstedt, K.; Anderson, J.; Pierard, D.; Wyns, L.; Seeburger, P. H.; Oscarson, S.; De Greve, H.; Knight, S. D. The affinity of the FimH fimbrial adhesin is receptor-driven and quasi-independent of *Escherichia coli* pathotypes. *Mol. Microbiol.* **2006**, *61*, 1556–1568.
- Sharon, N. Carbohydrates as future anti-adhesion drugs for infectious diseases. *Biochim. Biophys. Acta* **2006**, *1760*, 527–537.
- (a) Firon, N.; Ofek, I.; Sharon, N. Interaction of mannose-containing oligosaccharides with the fimbrial lectin of *Escherichia coli*. *Biochem. Biophys. Res. Commun.* **1982**, *105*, 1426–1432. (b) Firon, N.; Ofek, I.; Sharon, N. Carbohydrate specificity of the surface lectins of *Escherichia coli*, *Klebsiella pneumoniae* and *Salmonella typhimurium*. *Carbohydr. Res.* **1983**, *120*, 235–249. (c) Sharon, N. Bacterial lectins, cell–cell recognition and infectious disease. *FEBS Lett.* **1987**, *217*, 145–157.
- (a) Neeser, J.-R.; Koellreutter, B.; Wuersch, P. Oligomannoside-type glycopeptides inhibiting adhesion of *Escherichia coli* strains mediated by type 1 pili: preparation of potent inhibitors from plant glycoproteins. *Infect. Immun.* **1986**, *52*, 428–436. (b) Lindhorst, T. K. Artificial multivalent sugar ligands to understand and manipulate carbohydrate–protein interactions. *Top. Curr. Chem.* **2002**, *218*, 201–235 (review); (c) Patel, A.; Lindhorst, T. K. A modular approach for the synthesis of oligosaccharide mimetics. *Carbohydr. Res.* **2006**, *341*, 1657–1668. (d) Nagahori, N.; Lee, R. T.; Nishimura, S.-L.; Pagé, S.; Roy, R.; Lee, Y. C. Inhibition of adhesion of type 1 fimbriated *Escherichia coli* to highly mannoseylated ligands. *ChemBioChem* **2002**, *3*, 836–844. (e) Appeldoorn, C. C. M.; Joosten, J. A. F.; Maate, F. A.; Dobrindt, U.; Hacker, J.; Liskamp, R. M. J.; Khan, A. S.; Pieters, R. J. Novel multivalent mannose compounds and their inhibition of the adhesion of type 1 fimbriated uropathogenic *E. coli*. *Tetrahedron Asymmetry* **2005**, *16*, 361–372. (f) Touaibia, M.; Wellens, A.; Shiao, T. C.; Wang, Q.; Sirois, S.; Bouckaert, J.; Roy, R. Mannosylated G(0) dendrimers with nanomolar affinities to *Escherichia coli* FimH. *ChemMedChem* **2007**, *2*, 1190–1201.
- (a) Firon, N.; Ashkenazi, S.; Mirelman, D.; Ofek, I.; Sharon, N. Aromatic alpha-glycosides of mannose are powerful inhibitors of the adherence of type 1 fimbriated *Escherichia coli* to yeast and intestinal epithelial cells. *Infect. Immun.* **1987**, *55*, 472–476. (b) Lindhorst, T. K.; Kötter, S.; Kubisch, J.; Krallmann-Wenzel, U.; Ehlers, S.; Kren, V. Effect of p-substitution of aryl α-D-mannosides on inhibiting mannose-sensitive adhesion of *Escherichia coli*—synthesis and testing. *Eur. J. Org. Chem.* **1998**, 1669–1674. (c) Sperling, O.; Fuchs, A.; Lindhorst, T. K. Evaluation of the carbohydrate recognition domain of the bacterial adhesin FimH: design, synthesis and binding properties of mannoside ligands. *Org. Biomol. Chem.* **2006**, *4*, 3913–3922. (d) Han, Z.; Pinker, J. S.; Ford, B.; Obermann, R.; Nolan, W.; Wildman, S. A.; Hobbs, D.; Ellenberger, T.; Cusumano, C. K.; Hultgren, S. J.; Janetka, J. W. Structure-Based Drug Design and Optimization of Mannoside Bacterial FimH Antagonists. *J. Med. Chem.* **2010**, *53*, 4779–4792. (e) Berglund, J.; Bouckaert, J.; De Greve, H.; Knight, S. Anti-adhesive compounds to prevent and treat bacterial infections. International Patent Application PCT/US 2005/089733, 2005.
- Hung, C. S.; Bouckaert, J.; Hung, D.; Pinkner, J.; Widberg, C.; DeFusco, A.; Auguste, C. G.; Strouse, R.; Langermann, S.; Waksman, G.; Hultgren, S. J. Structural basis of tropism of *Escherichia coli* to the bladder during urinary tract infection. *Mol. Microbiol.* **2002**, *44*, 903–918.
- Ernst, B.; Magnani, J. L. From carbohydrate leads to glycomimetic drugs. *Nature Rev. Drug Discovery* **2009**, *8*, 661–677.
- (a) Lindhorst, T. K.; Kieburg, C.; Krallmann-Wenzel, U. Inhibition of the type 1 fimbriae-mediated adhesion of *Escherichia coli* to erythrocytes by multiantennary α-mannosyl clusters: the effect of multivalency. *Glycoconjugate J.* **1998**, *15*, 605–613. (b) Dubber, M.; Sperling, O.; Lindhorst, T. K. Oligomannoside mimetics by glycosylation of 'octopus glycosides' and their investigation as inhibitors of type 1

- fimbriae-mediated adhesion of *Escherichia coli*. *Org. Biomol. Chem.* **2006**, *4*, 3901–3912. (c) Touaibia, M.; Wellens, A.; Shiao, T. C.; Wang, Q.; Sirois, S.; Bouckaert, J.; Roy, R. Mannosylated G0 dendrimers with nanomolar affinities to *Escherichia coli* FimH. *ChemMedChem* **2007**, *2*, 1190–1201.
- (21) Aronson, M.; Medalia, O.; Schori, L.; Mirelman, D.; Sharon, N.; Ofek, I. Prevention of colonization of the urinary tract of mice with *Escherichia coli* by blocking of bacterial adherence with methyl  $\alpha$ -D-mannopyranoside. *J. Infect. Dis.* **1979**, *139*, 329–332.
- (22) Swanborg Eden, C.; Freter, R.; Hagberg, L.; Hull, R.; Leffer, H.; Schoolnik, G. Inhibition of experimental ascending urinary tract infection by an epithelial cell-surface receptor analog. *Nature* **1982**, *298*, 560–562.
- (23) Rabbani, S.; Jiang, X.; Schwardt, O.; Ernst, B. Expression of the carbohydrate recognition domain of FimH and development of a competitive binding assay. *Anal. Biochem.* **2010**, *407*, 188–195.
- (24) Ness, R. K.; Fletcher, H. G.; Hudson, C. S. Reaction of 2,3,4,6-tetrabenzoyl- $\alpha$ -D-glucopyranosyl bromide and 2,3,4,6-tetrabenzoyl- $\alpha$ -D-mannopyranosyl bromide with methanol. Certain benzoylated derivatives of D-glucose and D-mannose. *J. Am. Chem. Soc.* **1950**, *72*, 2200–2205.
- (25) Sancho-Garcia, J. C.; Cornil, J. Anchoring the Torsional Potential of Biphenyl at the ab Initio Level: The Role of Basis Set versus Correlation Effects. *J. Chem. Theory Comput.* **2005**, *1*, 581–589.
- (26) Eaton, V. J.; Steele, D. Dihedral angle of biphenyl in solution and the molecular force field. *J. Chem. Soc., Faraday Trans. 2* **1973**, 1601–1608.
- (27) Albert, A. Chemical aspects of selective toxicity. *Nature* **1958**, *182*, 421–422.
- (28) Winiwarter, S.; Bonham, N. M.; Ax, F.; Hallberg, A.; Lennernäs, H.; Karlén, A. Correlation of Human Jejunal Permeability (in Vivo) of Drugs with Experimentally and Theoretically Derived Parameters. A Multivariate Data Analysis Approach. *J. Med. Chem.* **1998**, *41*, 4939–4949.
- (29) Taketani, M.; Shii, M.; Ohura, K.; Ninomiya, S.; Imai, T. Carboxylesterase in the liver and small intestine of experimental animals and human. *Life Sci.* **2007**, *81*, 924–932.
- (30) Kansy, M.; Senner, F.; Gubernator, K. Physicochemical High Throughput Screening: Parallel Artificial Membrane Permeation Assay in the Description of Passive Absorption Processes. *J. Med. Chem.* **1998**, *41*, 1007–1010.
- (31) Artursson, P.; Karlsson, J. Correlation between oral drug absorption in humans and apparent drug permeability coefficients in human intestinal epithelial (Caco-2) cells. *Biochem. Biophys. Res. Com.* **1991**, *175*, 880–885.
- (32) Varma, M. V. S.; Feng, B.; Obach, R. S.; Troutman, M. D.; Chupka, J.; Miller, H. R.; El-Kattan, A. Physicochemical Determinants of Human Renal Clearance. *J. Med. Chem.* **2009**, *52*, 4844–4852.
- (33) Abgottspon, D.; Rölli, G.; Hosch, L.; Steinhuber, A.; Jiang, X.; Schwardt, O.; Cutting, B.; Smiesko, M.; Jenal, U.; Ernst, B.; Trampuz, A. Development of an Aggregation Assay to Screen FimH Antagonists. *J. Microbiol. Methods* **2010**, *82*, 249–255.
- (34) Zhou, G.; Mo, W.-J.; Sebbel, P.; Min, G.; Neubert, T. A.; Glockshuber, R.; Wu, X.-R.; Sun, T.-T.; Kong, X.-P. Uroplakin Ia is the urothelial receptor for uropathogenic *Escherichia coli*: evidence from in vitro FimH binding. *J. Cell Sci.* **2001**, *114*, 4095–4103.
- (35) (a) Kartha, K. P. R.; Field, R. A. Iodine: a versatile reagent in carbohydrate chemistry. IV. Per-O-acetylation, regioselective acylation and acetyolysis. *Tetrahedron* **1997**, *53*, 11753–11766. (b) Chittaboina, S.; Hodges, B.; Wang, Q. A facile route for the regioselective deacetylation of peracetylated carbohydrates at anomeric position. *Lett. Org. Chem.* **2006**, *3*, 35–38. (c) Mori, M.; Ito, Y.; Ogawa, T. Total synthesis of the mollu-series glycosyl ceramides  $\alpha$ -D-Manp-(1 $\rightarrow$ 3)- $\beta$ -D-Manp-(1 $\rightarrow$ 4)- $\beta$ -D-Glcp-(1 $\rightarrow$ 1)-Cer and  $\alpha$ -D-Manp-(1 $\rightarrow$ 3)-[ $\beta$ -D-Xylp-(1 $\rightarrow$ 2)]- $\beta$ -D-Manp-(1 $\rightarrow$ 4)- $\beta$ -D-Glcp-(1 $\rightarrow$ 1)-Cer. *Carbohydr. Res.* **1990**, *195*, 199–224. (d) Egusa, K.; Kusumoto, S.; Fukase, K. Solid-phase synthesis of a phytoalexin elicitor pentasaccharide using a 4-azido-3-chlorobenzyl group as the key for temporary protection and catch-and-release purification. *Eur. J. Org. Chem.* **2003**, 3435–3445.
- (36) Giampapa, C. S.; Abraham, S. N.; Chiang, T. M.; Beachey, E. H. Isolation and characterization of a receptor for type 1 fimbriae of *Escherichia coli* from guinea pig erythrocytes. *J. Biol. Chem.* **1988**, *263*, 5362–5367.
- (37) Aprikian, P.; Tchesnokova, V.; Kidd, B.; Yakovenko, O.; Yarov-Yarovoy, V.; Trinchina, E.; Vogel, V.; Thomas, W.; Sokurenko, E. Interdomain interaction in the FimH adhesin of *Escherichia coli* regulates the affinity to mannose. *J. Biol. Chem.* **2007**, *282*, 23437–23446.
- (38) Trong, I. L.; Aprikian, P.; Kidd, B. A.; Forero-Shelton, M.; Tchesnokova, V.; Rajagopal, P.; Rodriguez, V.; Interlandi, G.; Klevit, R.; Vogel, V.; Stenkamp, R. E.; Sokurenko, E. V.; Thomas, W. E. Structural basis for mechanical force regulation of the adhesin FimH via finger trap-like beta sheet twisting. *Cell* **2010**, *141*, 645–655.
- (39) Khoo, U. S.; Chan, K. Y. K.; Chan, V. S. F.; Lin, C. L. S. DC-SIGN and L-SIGN: the SIGNs for infection. *J. Mol. Med.* **2008**, *86*, 861–874.
- (40) Lee, S. J.; Evers, S.; Roeder, D.; Parlow, A. F.; Risteli, J.; Risteli, L.; Lee, Y. C.; Feizi, T.; Langen, H.; Nussenzweig, M. C. Mannose receptor-mediated regulation of serum glycoprotein homeostasis. *Science* **2002**, *295*, 1898–1901.
- (41) East, L.; Isacke, C. M. The mannose receptor family. *Biochim. Biophys. Acta* **2002**, *1572*, 364–386.
- (42) Dommett, R. M.; Klein, N.; Turner, M. W. Mannose-binding lectin in innate immunity: past, present and future. *Tissue Antigens* **2006**, *68*, 193–209.
- (43) Scharenberg, M. Expression and purification of DC-SIGN-CRD-Fc-IgG. Unpublished results.
- (44) Dearden, J. C.; Bresnen, J. G. M. The measurement of partition coefficients. *QSAR Comb. Sci.* **1988**, *7*, 133–144.
- (45) Wittwer, M.; Bezençon, J.; Cutting, B.; Wagner, B.; Kansy, M.; Ernst, B. pK<sub>a</sub> determination by <sup>1</sup>H-NMR spectroscopy—an old methodology revisited. Unpublished results.
- (46) Banker, M. J.; Clark, T. H.; Williams, J. A. Development and validation of a 96-well equilibrium dialysis apparatus for measuring plasma protein binding. *J. Pharm. Sci.* **2003**, *92*, 967–974.
- (47) Kerns, E. H. High throughput physicochemical profiling for drug discovery. *J. Pharm. Sci.* **2001**, *90*, 1838–1858.
- (48) Avdeef, A.; Bendels, S.; Di, L.; Fallor, B.; Kansy, M.; Sugano, K.; Yamauchi, Y. Parallel artificial membrane permeability assay (PAMPA)-critical factors for better predictions of absorption. *J. Pharm. Sci.* **2007**, *96*, 2893–2909.
- (49) Brandt, E.; Heymann, E.; Mentlein, R. Selective inhibition of rat liver carboxylesterases by various organophosphorus diesters in vivo and in vitro. *Biochem. Pharmacol.* **1980**, *29*, 1927–1931.
- (50) Scharenberg, M.; Abgottspon, D. Personal communication.
- (51) Obach, R. S. Prediction of human clearance of twenty-nine drugs from hepatic microsomal intrinsic clearance data: an examination of in vitro half-life approach and nonspecific binding to microsomes. *Drug Metab. Dispos.* **1999**, *27*, 1350–1359.
- (52) Trainor, G. L. The importance of plasma protein binding in drug discovery. *Expert Opin. Drug Discovery* **2007**, *2*, 51–64.
- (53) Weisiger, R. A. Dissociation from albumin: a potentially rate-limiting step in the clearance of substances by the liver. *Proc. Natl. Acad. Sci. U.S.A.* **1985**, *82*, 1563–1567.
- (54) Urien, S.; Tillement, J.-P.; Barre, J. The significance of plasma protein binding in drug research. In *Pharmacokinetic Optimization in Drug Research: Biological, Physicochemical, and Computational Strategies*; Wiley-VCH: Weinheim, Germany, 2001; pp 189–197.
- (55) Mulvey, M. A.; Schilling, J. D.; Hultgren, S. J. Establishment of a persistent *Escherichia coli* reservoir during the acute phase of a bladder infection. *Infect. Immun.* **2001**, *69*, 4572–4579.
- (56) (a) VCCLAB, Virtual Computational Chemistry Laboratory; <http://www.vcclab.org>, 2005; (b) Tetko, I. V.; Gasteiger, J.; Todeschini, R.; Mauri, A.; Livingstone, D.; Ertl, P.; Palyulin, V. A.; Radchenko, E. V.; Zefirov, N. S.; Makarenko, A. S.; Tanchuk, V. Y.; Prokopenko, V. V. Virtual computational chemistry laboratory—design and description. *J. Comput.-Aided Mol. Des.* **2005**, *19*, 453–463.
- (57) Kern, M. B.; Frimodt-Møller, N.; Espersen, F. Effects of Sulfamethazole and Amdinocillin against *Escherichia coli* Strains (with Various Susceptibilities) in an Ascending Urinary Tract Infection Model. *Antimicrob. Agents Chemother.* **2003**, *47*, 1002–1009.

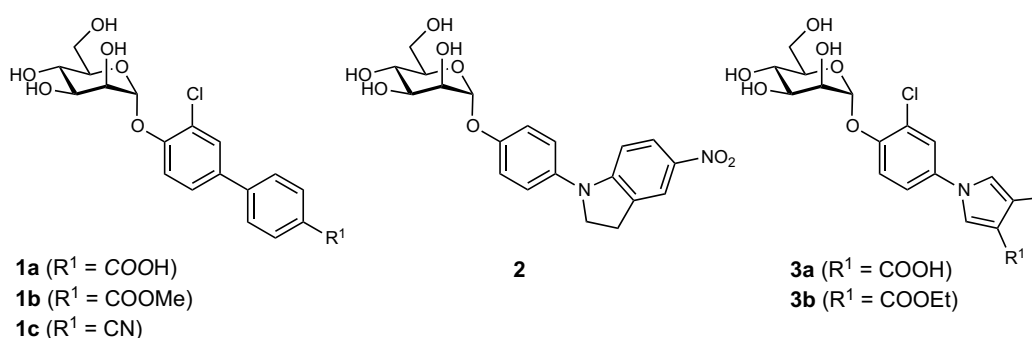
### 4.3 Improved Solubility of FimH Antagonists

In this chapter, the influence of structural modifications and the choice of solvent on the solubility of FimH antagonists are summarized. Three publications on this topic are attached (chapter 4.3.2 to 4.3.4). The data for the solvent modification studies originate in parts from the master thesis of Stefania Cigardi supervised by Jacqueline Bezençon.

#### 4.3.1 Approaches to Improve Solubility of FimH Antagonists

The required minimal solubility of a compound depends on the route of administration. For an intravenously applied drug, a liquid solution is required, because the injection of a precipitate can lead to embolism,<sup>1,2</sup> whereas a suspension is tolerated for an oral application. In this thesis, only the oral application of FimH antagonists is discussed. As proposed by Lipinski<sup>3</sup> and Curatolo<sup>4</sup>, the required minimal solubility for an orally administered drug is defined by its permeability and its dose. Our aim was to apply an oral dose of 10 mg/kg.<sup>5</sup> Therefore, assuming moderate permeability, a minimal solubility of 520 µg/ml is required (cf. chapter 2.1.2, Figure 2.3, page 32). Effective permeability ( $P_e$ ) was measured and classified with the parallel artificial membrane permeability assay (PAMPA)<sup>6</sup> and apparent permeability ( $P_{app}$ ) with the Caco-2 cell model, where a  $\log P_e$  between -5.7 to -6.3 cm/s and  $P_{app}$  a-b between 2 and 20 x 10<sup>-6</sup> cm/s was considered as moderate.<sup>7</sup>

Figure 4.25 presents the structures and Table 4.2 summarizes the binding affinities, and the physicochemical and pharmacokinetic properties of the analyzed FimH antagonists.



**Figure 4.25.** Structures of FimH antagonists **1a - 1c**,<sup>5,8</sup> **2**,<sup>9</sup> and **3a**, **3b**<sup>10</sup> analyzed for improved solubility.



**Table 4.2.** Binding affinity ( $IC_{50}$ ,  $K_D$ ), and physicochemical ( $\log D_{7.4}$ , solubility, effective and apparent permeability) and biochemical (metabolic stability) properties of FimH antagonists **1a** - **1c**,<sup>5,8</sup> **2**,<sup>9</sup> and **3a**, **3b**<sup>10</sup>.

Cpd.	$IC_{50}$ <sup>[a]</sup> [nM]	$K_D$ <sup>[b]</sup> [nM]	$\log D_{7.4}$ <sup>[c]</sup>	Solubility <sup>[d]</sup> [ $\mu\text{g/mL}$ ] /pH	PAMPA $\log P_e$ <sup>[e]</sup> [cm/s]	Caco-2 $P_{app}$ <sup>[f]</sup> [ $10^{-6}$ cm/s]		RML stability <sup>[g]</sup> $t_{1/2}$ [min]
						a→b	b→a	
<b>1a</b> <sup>8</sup>	6.7	n.d.	-0.77	> 3000 / 6.5	-10	$0.23 \pm 0.03$	$0.38 \pm 0.04$	-
<b>1b</b> <sup>8</sup>	4.8	n.d.	2.32	11.9 / 6.5	-4.6	$5.3 \pm 0.6$	$17.5 \pm 1.3$	2.1
<b>1c</b> <sup>5</sup>	10.1	< 1	$2.1 \pm 0.0$	$192 \pm 5 / 7.4$	$-5.2 \pm 0.0$	$2.2 \pm 0.4$	$22.1 \pm 1.5$	-
<b>2</b> <sup>9</sup>	20	n.d.	1.9	24 / 6.5	-5.5	$2.9 \pm 0.6$	$39.3 \pm 5.8$	-
<b>3a</b> <sup>10</sup>	25	-	$-0.5 \pm 0.1$	> 330 / 7.4	-10	n.d.	n.d.	-
<b>3b</b> <sup>10</sup>	-	7.5	2.8	> 180	-4.8	$6.4 \pm 0.7$	$30 \pm 2.9$	> 120

[a]  $IC_{50}$  values were determined in a cell-free competitive binding assay;<sup>11</sup> [b] Affinities ( $K_D$ ) of FimH antagonists to FimH-CRD-Th-His6 were determined in a competitive fluorescence polarization assay;<sup>5</sup> [c] Octanol-water partition coefficients ( $\log D_{7.4}$ ) were determined at pH 7.4 by a miniaturized shake-flask procedure;<sup>12</sup> [d] **1a**, **1b**, and **2**: Thermodynamic solubility, **1c** and **3a**, **3b**: Kinetic solubility;<sup>13</sup> [e]  $P_e$  = effective permeability: passive permeation through an artificial membrane was determined by the parallel artificial membrane permeability assay (PAMPA) at pH 7.4;<sup>6,14</sup> [f]  $P_{app}$  = apparent permeability: permeation through a Caco-2 cell monolayer was assessed in the absorptive (a→b) and secretory (b→a) directions in triplicate;<sup>15,16</sup> [g] Microsomal stability of the ester prodrugs **1b** and **3b** was determined with pooled rat liver microsomes (0.125 mg/mL) at pH 7.4 and 37°C in triplicates.<sup>17</sup>

Sufficient solubility (> 3000  $\mu\text{g/mL}$ ) was reported for the biphenyl  $\alpha$ -D-mannopyranoside **1a** substituted with a carboxylic acid on the outer aromatic ring of the aglycone. Because of the low passive membrane permeability ( $\log P_e = -10$  cm/s) an ester prodrug approach was studied (→**1b**, Paper 2, page 107). Cleavage by carboxylesterase (CE) released the active principle **1a** within minutes.<sup>8</sup> However, the ester prodrug **1b** exhibited insufficient solubility (11.9  $\mu\text{g/mL}$ ). Similar results were observed for the indolinyphenyl  $\alpha$ -D-mannopyranoside **2** with good permeability but low solubility (24  $\mu\text{g/mL}$ ).

Therefore, approaches to improve solubility were studied. Replacement of the carboxylate on the outer aromatic ring of the biphenyl  $\alpha$ -D-mannopyranoside (→**1a**) with bioisosteres (e.g. →**1c**, solubility 192  $\mu\text{M}$ , Paper 3, page 133) and the replacement of the outer ring of the biphenyl aglycone with a heteroaromatic ring (e.g. →**3a**, solubility > 330  $\mu\text{g/mL}$ , Paper 5, page 189) improved solubility as compared to the ester prodrug (→**1b**, solubility 11.9  $\mu\text{g/mL}$ ). Low passive permeability of compound **3a** ( $\log P_e = -10$  cm/s) was enhanced with an ester prodrug approach (→**3b**,  $\log P_e = -4.8$  cm/s, solubility > 180  $\mu\text{g/mL}$ ). The cleavage of the ester prodrug **3b** was measured to be very slow

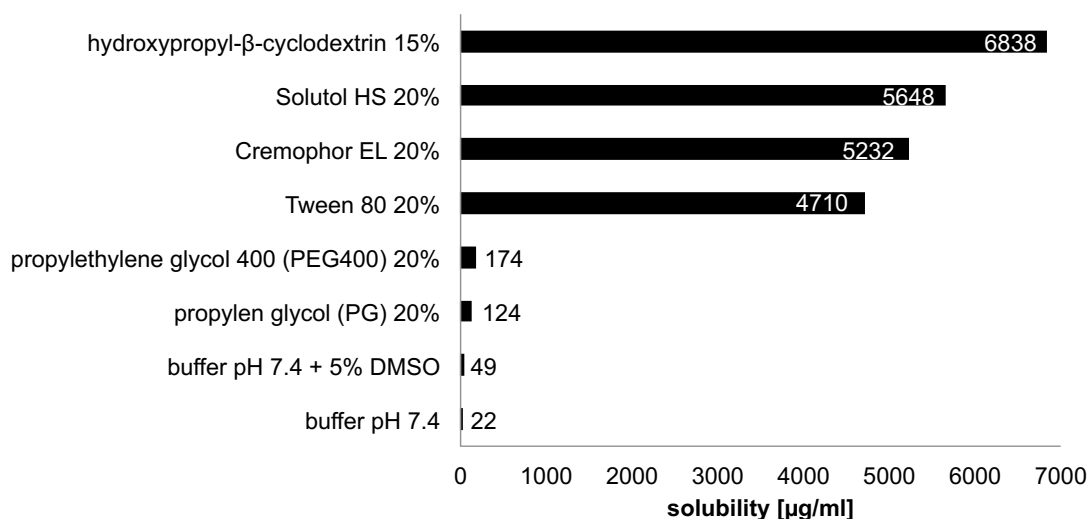


( $t_{1/2} > 120$  min). Since already the prodrug **3b** exhibits nanomolar affinity ( $K_D = 7.5$  nM), immediate hydrolysis after reaching systemic circulation is not necessary at all.

In addition, because of the high lipophilicity prodrug **3b** ( $\log D_{7.4} = 2.8$ ) has a higher reabsorption potential compared to the more polar active principle **3a** ( $\log D_{7.4}$  of -0.5). A rapid decrease below the antiadhesive concentration in the bladder as a consequence of a too fast renal excretion, can therefore be avoided.

Although moderate permeability and improved solubility could be obtained by structural modifications, solubility was still insufficient for an oral dose of 10 mg/kg ( $< 520$   $\mu\text{g/mL}$ ). Therefore, a phosphate prodrug approach (cf. Paper 4, page 153) was explored. In addition, solvent modifications were applied in order to avoid changes in pharmacodynamics induced by structural modifications,<sup>18</sup> as discussed in the next section.

The influence of various solubilizers as co-solvent, surfactants, and complexing agents was explored with antagonist **2** (solubility 24  $\mu\text{g/mL}$ ). By adding 5% DMSO (v/v), solubility could be improved by a factor of 2, with 20% (w/w) of other co-solvents such as propylene glycol (PG) and polyethylene glycol 400 (PEG400), by a factor of 5 and 7, respectively, and by the addition of 20% (w/w) of the surfactants Tween 80, Cremophor EL, and Solutol HS, and 15% (w/w) of the complexing agents hydroxypropyl- $\beta$ -cyclodextrin (HP $\beta$ CD) by more than a factor of 200 (Figure 4.26).



**Figure 4.26.** Thermodynamic solubility of **2** in different solvents; from bottom to top: phosphate buffer at pH 7.4, phosphate buffer at pH 7.4 with 5% (v/v) DMSO, 20% (w/w) propylene glycol (PG), 20% (w/w) polyethylene glycol 400 (PEG400), 20% (w/w) Tween 80, 20% (w/w) Cremophor EL, 20% (w/w) Solutol, and 15% (w/w) hydroxypropyl- $\beta$ -cyclodextrin (HP $\beta$ CD). Data represent a single measurement.

The use of solubilizers of up to 20% could be toxic to cells.<sup>19,20</sup> For this purpose, lower solubilizer concentrations were applied ( $\leq 1\%$ ). However, by adding high concentrations of co-solvents (DMSO, PG, and PEG400), only insufficient solubility ( $< 175 \mu\text{g/mL}$ ) of compound **2** could be achieved. Therefore, further studies were only performed with the surfactants Tween 80, Cremophor EL, and Solutol HS, and the complexing agent HP $\beta$ CD.

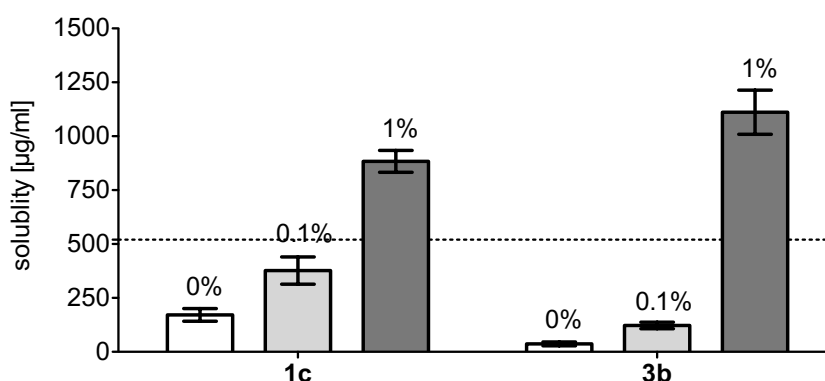
Similarly, as for high co-solvents concentration (5% - 20%), solubility of compound **2** could be improved by a factor of 2 to 8 by adding surfactants and complexing agents at very low concentrations (0.01%, 0.1%, and 1%, Table 4.3). Solubility higher than 209  $\mu\text{g/mL}$  with 1% of solubilizers (Tween 80, Cremophor EL, Solutol HS, and HP $\beta$ CD) means, that the total amount of compound **2** is dissolved, however the solution not saturated. In a next step, the assay should be run with higher concentrations to reach the equilibrium of dissolved and precipitated compound.

**Table 4.3.** Solubility of compound **2** in different solvents: buffer pH 7.4 and with the addition of the surfactants Tween 80, Cremophor EL, and Solutol HS, and the complexing agent hydroxypropyl- $\beta$ -cyclodextrin (HP $\beta$ CD) at different concentration (0.001% - 1%, w/w).

Solvent		Solubility <sup>a</sup> [ $\mu\text{g/mL}$ ]
buffer pH 7.4	-	24 / pH 6.5
Tween 80	1%	$> 209 \pm 0$
	0.1%	$68 \pm 3$
	0.01%	$33 \pm 4$
	0.001%	$30 \pm 1$
Cremophor EL	1%	$> 209 \pm 0$
	0.1%	$51 \pm 8$
	0.01%	$31 \pm 1$
	0.001%	$31 \pm 2$
Solutol HS	1%	$> 209 \pm 0$
	0.1%	$59 \pm 1$
	0.01%	$36 \pm 1$
	0.001%	$30 \pm 1$
hydroxypropyl- $\beta$ -cyclodextrin (HP $\beta$ CD)	1%	$> 209 \pm 0$
	0.1%	$112 \pm 7$
	0.05%	$73 \pm 5$
	0.01%	$35 \pm 5$

a) Kinetic aqueous solubility was measured in a 96-well format using the  $\mu\text{SOL}$  Explorer solubility analyzer. Data represent the mean with the standard deviation (triplicates). A final compound concentration of 0.5 mM was used in the assay.

However, because in absence of solubilizer compounds **1c** and **3b** have higher solubility ( $> 180 \mu\text{g/mL}$ ) than compound **2** ( $24 \mu\text{g/mL}$ ) and leading to higher concentrations in the bladder, thermodynamic solubility determinations were performed with these FimH antagonists (Table 4.2). Thermodynamic solubility of  $> 520 \mu\text{g/mL}$  was achieved for both compounds **1c** and **3b** with the addition of 1% Tween 80 (Figure 4.27).



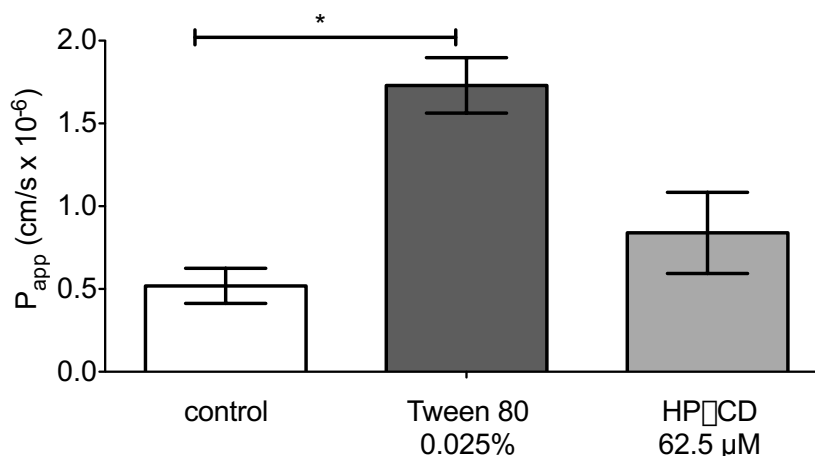
**Figure 4.27.** Thermodynamic solubility of compounds **1c** and **3** with the addition of Tween 80 at different percentages (0%, 0.1%, and 1%, w/w). Data represent the mean with the corresponding standard deviation (triplicates). Dashed line represents the required solubility of  $520 \mu\text{g/mL}$  for a dose of  $10 \text{ mg/kg}$ .<sup>3</sup>

Nevertheless, higher solubility of compound **1c** and **3b** ( $192 \mu\text{g/mL}$  and  $> 180 \mu\text{g/mL}$ , respectively, Table 4.2) with 1% of DMSO was reached with the kinetic solubility determination method compared to solubility in PBS buffer measured with the thermodynamic determination method ( $171 \mu\text{g/mL}$ ,  $37 \mu\text{g/mL}$ , respectively, Figure 4.27). This may be a consequence of the addition of the solubilizer DMSO, which preferentially helps the lipophilic compound **1c** and **3b** ( $\log D_{7,4} = 2.1$  and  $2.8$ , respectively) to dissolve in the aqueous buffer. Furthermore, overestimation of the solubility with oversaturation has to be taken into account when working with the kinetic solubility method.<sup>21,22</sup>

#### Influence of Solubilizers on Permeability

Surfactants (e.g. Tween 80, Cremophor EL, Solutol HS) and complexing agents (e.g. HP $\beta$ CD) can influence the permeability of a compound. Whereas surfactants can inhibit efflux transporters and increase permeability, complexing agents can form complexes with the drug and decrease permeability.<sup>23-25</sup> Efflux transport (ratio  $b-a/a-b$   $P_{\text{app}} > 1.5$ ) was observed for compound **1c**, **2**, and **3b** in the Caco-2 assay (Table 4.2). Addition of Tween 80 to the solvent leading to the inhibition of efflux transporters improves Caco-2  $P_{\text{app}}$  permeability of **1c** significantly (compared to the control without solubilizer) (Figure 4.28). Due to the cell toxicity potential of Tween 80 (Table 4.4), a very low

surfactant concentration of 0.025% was used in the Caco-2 cell assay. In contrast to Tween 80, no significant change in the Caco-2 permeability of compound **1c** could be demonstrated with the addition of HP $\beta$ CD.



**Figure 4.28.** Caco-2 permeability  $P_{app}$  a-b in cm/s of **1c** without any solubilizer (control, white), with the use of surfactant Tween 80 (0.025%, w/w) (dark grey), and with the use of the complexing agent HP $\beta$ CD with a molar ratio of 1:1 (62.5  $\mu$ M) (grey). Data represent mean with the corresponding standard deviation (triplicates). Initial compound concentration was 62.5  $\mu$ M. Asterisk (\*) indicates significant difference ( $p < 0.05$ ).

**Table 4.4.** Measured cell toxicity of Tween 80 (0.025% and 0.1%, w/w) and of hydroxypropyl- $\beta$ -cyclodextrin (HP $\beta$ CD) (0.01 and 1 mM).

Compound		Cell toxicity (% viability) <sup>a</sup>
Hydroxypropyl- $\beta$ -cyclodextrin (HP $\beta$ CD)	0.01 mM	92 $\pm$ 9
	1 mM	95 $\pm$ 1
Tween 80	0.025%	95 $\pm$ 5
	0.1%	53 $\pm$ 6

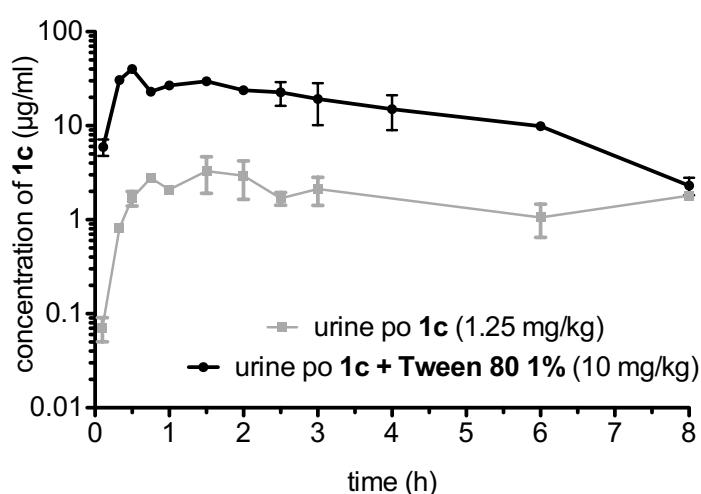
a) Cell toxicity was determined with HepG2 cells in a MTT assay; values represent the mean with the standard deviation (triplicates).<sup>26</sup>

### ***In Vivo* Pharmacokinetic Profiles**

Finally, compound **1c** was applied *in vivo* with PBS containing 1% Tween 80 and 5% DMSO and the urine levels were compared with PBS only. The dose applied with Tween 80 was eight times higher (10 mg/kg) than without Tween 80 (1.25 mg/kg), due to solubility issues of compound **1c**. When **1c** was applied with and without Tween 80,  $C_{max}$  was reached within 1 hour. However, the urine concentrations of **1c** when applied with Tween 80 were about fourteen times higher than those

reached without Tween 80 (Figure 4.29). This non-linear increase of urine concentrations illustrates the influence of Tween 80 on the efflux transporters in the intestine.

In a last step, *in vivo* infection studies of compound **1c** were performed obtaining a 100-fold (oral dose 1.25 mg/kg) and a 1000-fold (oral dose 10 mg/kg) bacterial load reduction 3 h after injection compared to the control group (cf. Paper 3, Figure 7, page 143).<sup>5</sup> For compound **3**, *in vivo* pharmacokinetics studies were performed illustrating a prolonged absorption over a time period of 3 h (cf. Paper 5, Figure 5, page 209).<sup>10</sup>



**Figure 4.29.** Urine concentration vs. time profile of **1c** applied with (black, 10 mg/kg) and without (grey, 1.25 mg/kg) preformulation (PBS containing 1% Tween 80 and 5% DMSO) upon oral administration in a mouse. Experiments and results by Anja Sigl (Department of Pharmaceutical Sciences, University of Basel).

### Summary and Conclusion

In summary, we improved oral bioavailability of the well-permeable and high-affinity FimH antagonists **1c** and **3** by enhancing their solubility above the requested level for a dose of 10 mg/kg (> 520 µg/mL) by adding the surfactant Tween 80. In addition, Tween 80 inhibited efflux transporters and increased permeability  $P_{app}$  a-b of **1c** in the Caco-2 cells thereby further enhancing the bioavailability as could be illustrated in the *in vivo* model. Importantly, every compound reacts differently by the addition of surfactants or complexing agents and should be analyzed individually before performing *in vivo* studies. Even though the solubility issue can be addressed by appropriate preformulation, further structural modifications of FimH antagonists to improve solubility have to be considered.

## References

1. Hedrich, H. J.; Bullock, G. R. *The laboratory mouse*. Elsevier Academic Press: Amsterdam ; Boston, 2004; p xvi, 600 p.
2. Woodard, G. *Methods of Animals Experimentation*. Academic Press: New York, 1965; Vol. 1.
3. Lipinski, C. A. Drug-like properties and the causes of poor solubility and poor permeability. *J. Pharmacol. Toxicol. Methods* **2000**, *44*, 235-249.
4. Curatolo, W. Physical chemical properties of oral drug candidates in the discovery and exploratory development settings. *Pharm. Sci. & Technol. Today* **1998**, *1*, 387-393.
5. Kleeb, S.; Pang, L.; Mayer, K.; Eris, D.; Sigl, A.; Preston, R. C.; Zihlmann, P.; Sharpe, T.; Jakob, R. P.; Abgottspon, D.; Hutter, A. S.; Scharenberg, M.; Jiang, X.; Navarra, G.; Rabbani, S.; Smiesko, M.; Ludin, N.; Bezencon, J.; Schwaradt, O.; Maier, T.; Ernst, B. FimH Antagonists: Bioisosteres To Improve the *in Vitro* and *in Vivo* PK/PD Profile. *J. Med. Chem.* **2015**, *58*, 2221-39.
6. Kansy, M.; Senner, F.; Gubernator, K. Physicochemical high throughput screening: Parallel artificial membrane permeation assay in the description of passive absorption processes. *J. Med. Chem.* **1998**, *41*, 1007-1010.
7. Hou, T.; Wang, J.; Zhang, W.; Xu, X. ADME evaluation in drug discovery. 7. Prediction of oral absorption by correlation and classification. *J. Chem. Inf. Model* **2007**, *47*, 208-18.
8. Klein, T.; Abgottspon, D.; Wittwer, M.; Rabbani, S.; Herold, J.; Jiang, X.; Kleeb, S.; Luethi, C.; Scharenberg, M.; Bezencon, J.; Gubler, E.; Pang, L.; Smiesko, M.; Cutting, B.; Schwaradt, O.; Ernst, B. FimH Antagonists for the Oral Treatment of Urinary Tract Infections: From Design and Synthesis to *in Vitro* and *in Vivo* Evaluation. *J. Med. Chem.* **2010**, *53*, 8627-8641.
9. Jiang, X.; Abgottspon, D.; Kleeb, S.; Rabbani, S.; Scharenberg, M.; Wittwer, M.; Haug, M.; Schwaradt, O.; Ernst, B. Antiadhesion therapy for urinary tract infections--a balanced PK/PD profile proved to be key for success. *J. Med. Chem.* **2012**, *55*, 4700-13.
10. Pang, L.; Bezençon, J.; Kleeb, S.; Rabbani, S.; Sigl, A.; Smiesko, M.; Sager, C.P.; Eris, D.; Schwaradt, O.; Ernst, B. FimH Antagonists – Solubility vs. Permeability. *Carbohydrate Chemistry*, **2017**, *42*, 248-273.
11. Rabbani, S.; Jiang, X.; Schwaradt, O.; Ernst, B. Expression of the carbohydrate recognition domain of FimH and development of a competitive binding assay. *Anal. Biochem.* **2010**, *407*, 188-195.
12. Waring, M. J. Lipophilicity in drug discovery. *Expert Opin. Drug Discov.* **2010**, *5*, 235-48.
13. Alsenz, J.; Kansy, M. High throughput solubility measurement in drug discovery and development. *Adv. Drug Deliv. Rev.* **2007**, *59*, 546-67.
14. Avdeef, A.; Bendels, S.; Di, L.; Faller, B.; Kansy, M.; Sugano, K.; Yamauchi, Y. PAMPA - Critical factors for better predictions of absorption. *J. Pharm. Sci.* **2007**, *96*, 2893-2909.
15. Hubatsch, I.; Ragnarsson, E. G. E.; Artursson, P. Determination of drug permeability and prediction of drug absorption in Caco-2 monolayers. *Nat. Protoc.* **2007**, *2*, 2111-2119.
16. Artursson, P.; Karlsson, J. Correlation between oral drug absorption in humans and apparent drug permeability coefficients in human intestinal epithelial (Caco-2) cells. *Biochem. Biophys. Res. Commun.* **1991**, *175*, 880-5.
17. Imai, T. Human carboxylesterase isozymes: catalytic properties and rational drug design. *Drug metab. and pharmacokinet.* **2006**, *21*, 173-185.
18. Kerns, E., H.; Di, L. *Drug-like Properties: Concepts, Structure Design and Methods, from ADME to Toxicity Optimization*. 1st ed.; Elsevier: London, 2008; p 526.
19. Ward, P. D.; Tippin, T. K.; Thakker, D. R. Enhancing paracellular permeability by modulating epithelial tight junctions. *Pharm. Sci. Technol. Today* **2000**, *3*, 346-358.
20. Majumdar, S.; Mitra, A. K. Chemical modification and formulation approaches to elevated drug transport across cell membranes. *Expert Opin. Drug Deliv.* **2006**, *3*, 511-27.
21. Bergstrom, C. A.; Holm, R.; Jorgensen, S. A.; Andersson, S. B.; Artursson, P.; Beato, S.; Borde, A.; Box, K.; Brewster, M.; Dressman, J.; Feng, K. I.; Halbert, G.; Kostewicz, E.; McAllister, M.; Muenster, U.; Thinnes, J.; Taylor, R.; Mullertz, A. Early pharmaceutical profiling to predict oral drug absorption: Current status and unmet needs. *Eur. J. Pharm. Sci.* **2013**, *57*, 173-199.

22. Saal, C.; Petereit, A. C. Optimizing solubility: kinetic versus thermodynamic solubility temptations and risks. *Eur. J. Pharm. Sci.* **2012**, *47*, 589-95.
23. Dahan, A.; Miller, J. M.; Hoffman, A.; Amidon, G. E.; Amidon, G. L. The solubility-permeability interplay in using cyclodextrins as pharmaceutical solubilizers: mechanistic modeling and application to progesterone. *J. Pharm. Sci.* **2010**, *99*, 2739-49.
24. Yamagata, T.; Kusuhara, H.; Morishita, M.; Takayama, K.; Benameur, H.; Sugiyama, Y. Improvement of the oral drug absorption of topotecan through the inhibition of intestinal xenobiotic efflux transporter, breast cancer resistance protein, by excipients. *Drug Metab. Dispos.* **2007**, *35*, 1142-8.
25. Nerurkar, M. M.; Burton, P. S.; Borchardt, R. T. The use of surfactants to enhance the permeability of peptides through Caco-2 cells by inhibition of an apically polarized efflux system. *Pharm. Res.* **1996**, *13*, 528-34.
26. Hamid, R.; Rotshteyn, Y.; Rabadi, L.; Parikh, R.; Bullock, P. Comparison of alamar blue and MTT assays for high through-put screening. *Toxicol. in Vitro* **2004**, *18*, 703-710.





### 4.3.2 Paper 3 - Structural and Solvent Modifications:

#### FimH Antagonists - Bioisosteres to Improve the PK/PD Profile

This publication explores various bioisosteres of the para-carboxylate moiety on the terminal ring of the biphenyl mannoside and assesses their binding affinity to the FimH-CRD. A competitive fluorescence polarization assay and isothermal titration calorimetry were implemented. Evaluation of physicochemical properties predictive for oral bioavailability and antagonist elimination complete the PK/PD profile. Furthermore, higher doses could be applied in the *in vivo* disease studies with the help of the surfactant Tween 80.

#### Contribution to the project:

Jacqueline Bezençon conducted all experiments regarding the preformulation of compound **10j** enabling higher dose application in the *in vivo* studies (see unpublished data at the beginning of chapter 4.3, page 123). She was further responsible for the revision of the pharmacokinetic part of the manuscript.

The paper was published in the peer-reviewed *Journal of Medicinal Chemistry* in 2015:

S. Kleeb,\* L. Pang,\* K. Mayer,\* D. Eris,\* A. Sigl,\* R. C. Preston, P. Zhilmann, T. Sharpe, R. P. Jakob, D. Abgottspon, A. S. Hutter, M. Scharenberg, X. Jiang, G. Navarra, S. Rabbani, M. Smiesko, N. Lüdin, **J. Bezençon**, O. Schwardt, T. Maier, B. Ernst, FimH Antagonists: Bioisosteres To Improve the *in Vitro* and *in Vivo* PK/PD Profile. *J. Med. Chem.* **2015**, *58*, 2221-2239.

\*contributed equally.

## FimH Antagonists: Bioisosteres To Improve the in Vitro and in Vivo PK/PD Profile

Simon Kleeb,<sup>†,||</sup> Lijuan Pang,<sup>†,||</sup> Katharina Mayer,<sup>†,||</sup> Deniz Eris,<sup>†,||</sup> Anja Sigl,<sup>†,||</sup> Roland C. Preston,<sup>†</sup> Pascal Zihlmann,<sup>†</sup> Timothy Sharpe,<sup>§</sup> Roman P. Jakob,<sup>‡</sup> Daniela Abgottspon,<sup>†</sup> Aline S. Hutter,<sup>†</sup> Meike Scharenberg,<sup>†</sup> Xiaohua Jiang,<sup>†</sup> Giulio Navarra,<sup>†</sup> Said Rabbani,<sup>†</sup> Martin Smiesko,<sup>†</sup> Nathalie Lüdin,<sup>†</sup> Jacqueline Bezençon,<sup>†</sup> Oliver Schwaradt,<sup>†</sup> Timm Maier,<sup>‡</sup> and Beat Ernst<sup>\*,†</sup>

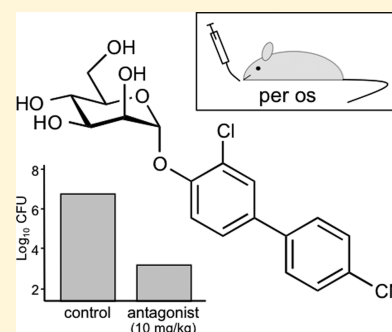
<sup>†</sup>Institute of Molecular Pharmacy, Pharmacenter, University of Basel, Klingelbergstrasse 50, CH-4056 Basel, Switzerland

<sup>‡</sup>Structural Biology, Biocenter, University of Basel, Klingelbergstrasse 70, CH-4056 Basel, Switzerland

<sup>§</sup>Biophysical Facility, Biocenter, University of Basel, Klingelbergstrasse 70, CH-4056 Basel, Switzerland

**S** Supporting Information

**ABSTRACT:** Urinary tract infections (UTIs), predominantly caused by uropathogenic *Escherichia coli* (UPEC), belong to the most prevalent infectious diseases worldwide. The attachment of UPEC to host cells is mediated by FimH, a mannose-binding adhesin at the tip of bacterial type 1 pili. To date, UTIs are mainly treated with antibiotics, leading to the ubiquitous problem of increasing resistance against most of the currently available antimicrobials. Therefore, new treatment strategies are urgently needed. Here, we describe the development of an orally available FimH antagonist. Starting from the carboxylate substituted biphenyl  $\alpha$ -D-mannoside **9**, affinity and the relevant pharmacokinetic parameters (solubility, permeability, renal excretion) were substantially improved by a bioisosteric approach. With 3'-chloro-4'-( $\alpha$ -D-mannopyranosyloxy)biphenyl-4-carbonitrile (**10j**) a FimH antagonist with an optimal in vitro PK/PD profile was identified. Orally applied, **10j** was effective in a mouse model of UTI by reducing the bacterial load in the bladder by about 1000-fold.



## INTRODUCTION

Urinary tract infection (UTI) is one of the most frequent infectious diseases worldwide and affects millions of people every year.<sup>1</sup> In more than 70% of the reported cases, uropathogenic *Escherichia coli* (UPEC) is the causal pathogen.<sup>2</sup> Acute, uncomplicated lower urinary tract infection, commonly referred to as cystitis, requires an antibiotic treatment for symptom relief (i.e., reduction of dysuria, frequent and urgent urination, bacteriuria, pyuria) and for prevention of more devastating or even life threatening complications like pyelonephritis and urosepsis.<sup>3,4</sup> However, the repeated use of antibacterial chemotherapeutics provokes antimicrobial resistance leading to treatment failure.<sup>5</sup> Hence, a new approach for the prevention and treatment of UTI with orally applicable therapeutics is urgently needed.<sup>6</sup>

UPEC undergo a well-defined infection cycle within the host.<sup>7</sup> The key step in pathogenesis is bacterial adhesion to the epithelial cells in the lower urinary tract.<sup>8</sup> This interaction prevents UPEC from clearance by the bulk flow of urine and enables the bacteria to colonize the epithelial cells. The adhesion is mediated by the virulence factor FimH located at the tip of bacterial type 1 pili.<sup>9,10</sup> FimH consists of two immunoglobulin-like domains: the N-terminal lectin domain and (connected by a short linker) the C-terminal pilin domain.<sup>11</sup> The lectin domain encloses the carbohydrate recognition domain (CRD) that binds

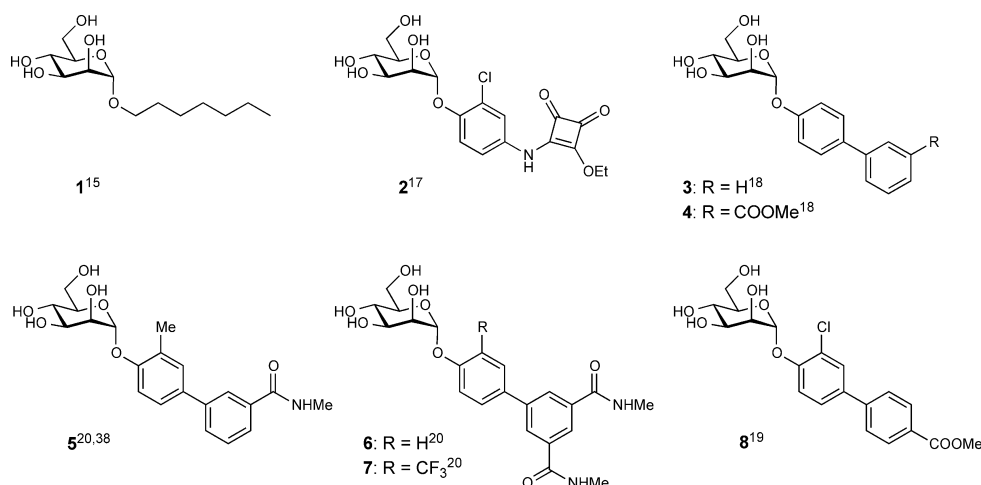
to the oligomannosides of the glycoprotein uroplakin Ia on the epithelial cell surface.<sup>12</sup> The pilin domain anchors the adhesin to the pilus and regulates the switch between two conformational states of the CRD with high and low affinity for mannoses, respectively.

More than 3 decades ago, Sharon and co-workers described various oligomannosides and aryl  $\alpha$ -D-mannosides as potential antagonists of the FimH-mediated bacterial adhesion.<sup>13,14</sup> However, only weak interactions in the milli- to micromolar range were observed. In recent years, several high-affinity monovalent mannose-based FimH antagonists with various aglycones like *n*-alkyl,<sup>15</sup> phenyl,<sup>16</sup> dioxycyclobutenyl-aminophenyl,<sup>17</sup> umbelliferyl,<sup>16</sup> biphenyl,<sup>18–22</sup> indol(in)-ylphenyl,<sup>23</sup> triazolyl,<sup>24</sup> and thiazolylamino<sup>25</sup> have been reported. In addition, different multivalent presentations of the mannose have been synthesized<sup>26–32</sup> and a heptavalent presentation of *n*-heptyl  $\alpha$ -D-mannoside (**1**) tethered to  $\beta$ -cyclodextrin proved to be highly effective when applied together with the UTI89 bacterial strain through a catheter into the bladder of C3H/HeN mice.<sup>32</sup> Importantly, adverse side effects resulting from nonselective binding of FimH antagonists (they are all  $\alpha$ -D-mannopyrano-

Received: October 3, 2014

Published: February 10, 2015





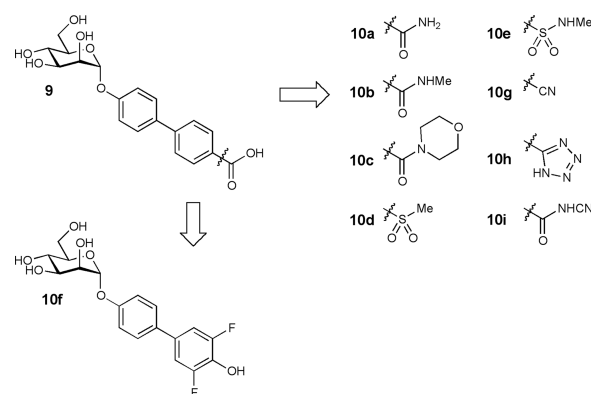
**Figure 1.** Monovalent FimH antagonists 1–4 acting as reference compounds and 5–8 which have been orally explored in in vivo disease models.

sides) to mannose receptors of the human host system have recently been ruled out.<sup>33</sup>

The high affinities of the monovalent  $\alpha$ -D-mannopyranosides are based on optimal interactions with the main structural features of the CRD:<sup>34–37</sup> first, the mannose binding pocket accommodating the mannose moiety by means of an extended hydrogen bond network and, second, the entrance to the binding site composed of three hydrophobic amino acids (Tyr48, Tyr137, and Ile52) and therefore referred to as “tyrosine gate” hosting aliphatic and aromatic aglycones. As an example, *n*-heptyl  $\alpha$ -D-mannopyranoside (**1**) exhibits nanomolar affinity due to hydrophobic contacts of the alkyl aglycone with the hydrophobic residues of the tyrosine gate.<sup>15</sup> Furthermore, aromatic aglycones, such as present in mannosides **2** and **3** (Figure 1), provide strong  $\pi$ - $\pi$  stacking interactions with the tyrosine gate. This interaction is further favored by the addition of an electron withdrawing substituent on the terminal ring of the biaryl portion ( $\rightarrow$ **4**).<sup>18,19</sup>

Recent in vivo PK studies in mice proved the high potential of the biphenyl  $\alpha$ -D-mannosides **5**–**8** for an oral treatment, although high doses ( $\geq 50$  mg/kg) were necessary to achieve the minimal concentrations required for the antiadhesive effect in the urinary bladder.<sup>19–21</sup> Moreover, the therapeutic effect could only be maintained for a few hours, i.e., 4 h for a po (per os) single-dose application of **7** (50 mg/kg), because of rapid elimination by glomerular filtration and low reabsorption from the primary urine in the renal tubules.<sup>20</sup>

To date, the physicochemical properties affecting the rate of renal excretion, i.e., lipophilicity and plasma protein binding (PPB), or metabolic liabilities promoting nonrenal elimination pathways have been barely investigated for FimH antagonists. The goal of the present study was to optimize the biphenyl  $\alpha$ -D-mannoside with respect to oral bioavailability and renal excretion. Starting from antagonist **9**<sup>19</sup> (Figure 2), we synthesized new biphenyl derivatives, characterized their affinity to the CRD, structurally investigated their binding mode, and determined physicochemical and pharmacokinetic parameters predictive for intestinal absorption and renal elimination. Furthermore, we determined in vivo PK (pharmacokinetics) of the most promising new antagonists in a mouse model. After oral administration, the compound with the best PK profile proved effective in reducing the bacterial loads upon bladder infection in a mouse model of UTI.



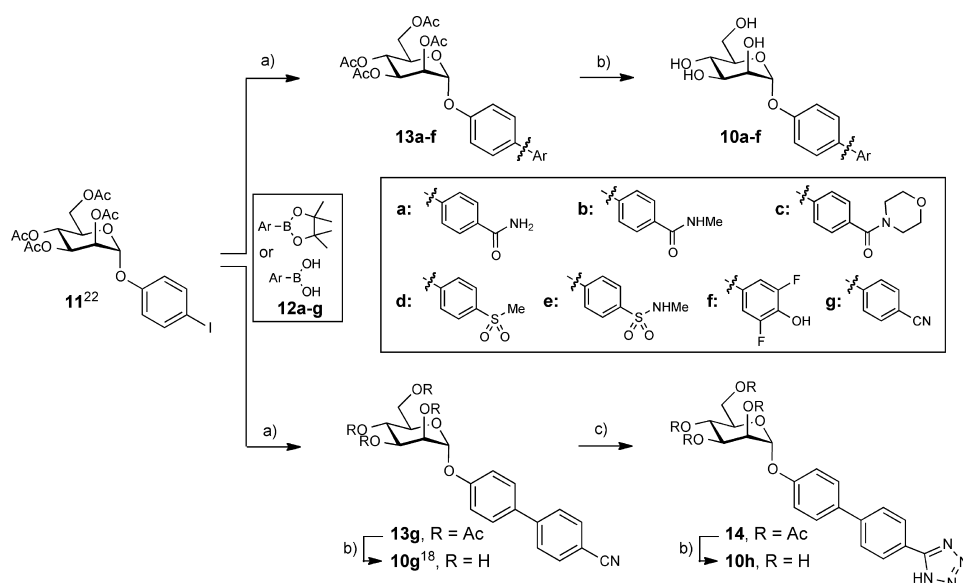
**Figure 2.** Bioisosteric replacement of the carboxylic acid substituent of biphenyl  $\alpha$ -D-mannopyranoside **9**.

## RESULTS AND DISCUSSION

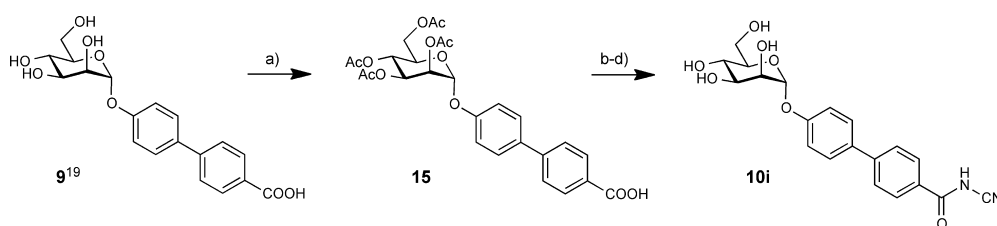
As previously reported, the carboxylate substituent present in the biphenyl mannoside **9** (its electron withdrawing potential being essential for an enhanced drug target interaction) strongly decreases the lipophilicity of the antagonist ( $\log D_{7,4} < -1.5$ <sup>19</sup>) in comparison to the *n*-heptyl ( $\rightarrow$ **1**,  $\log P = 1.7$ <sup>19</sup>) or the unsubstituted biphenyl aglycone ( $\rightarrow$ **3**,  $\log P = 2.1$ <sup>22</sup>). Since low lipophilicity is a major reason for low intestinal absorption and rapid renal excretion of the systemically available antagonist,<sup>19,23</sup> we aspired to improve oral bioavailability as well as renal excretion by replacing the carboxylate in **9** with various bioisosteric groups<sup>39</sup> (Figure 2).

**Synthesis.** Iodide **11** was prepared from peracetylated mannose and 4-iodophenol in the presence of  $\text{BF}_3 \cdot \text{Et}_2\text{O}$ .<sup>22</sup> In a palladium-catalyzed Miyaura–Suzuki coupling<sup>40</sup> with the boronic acid or boronate derivatives **12a–g**, the biphenyl derivatives **13a–g** were obtained in good to excellent yields. Final deprotection yielded the test compounds **10a–g**. When microwave-assisted reaction conditions<sup>41</sup> were utilized, the conversion of aryl nitrile **13g** to tetrazole **14** proceeded rapidly and with good yield. After deprotection of **14** using Zemplén conditions, the test compound **10h** was obtained (Scheme 1).

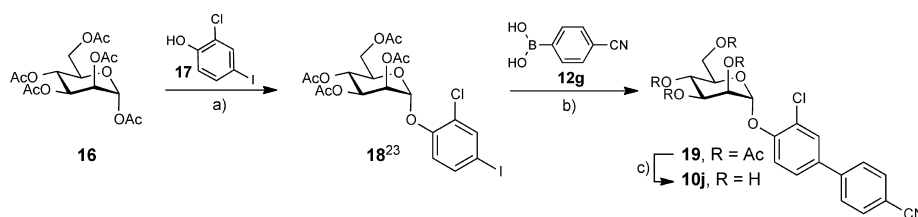
The cyanobenzamide derivative **10i** (Scheme 2) was obtained from **9** by peracetylation ( $\rightarrow$ **15**) followed by conversion of the

Scheme 1<sup>a</sup>

<sup>a</sup>(a) Pd(Cl<sub>2</sub>)dppf·CH<sub>2</sub>Cl<sub>2</sub>, K<sub>3</sub>PO<sub>4</sub>, DMF, 80 °C, 4 h (13a–g, 44–99%); (b) NaOMe, MeOH, rt, 4 h (10a–h, 29–86%); (c) TMSN<sub>3</sub>, Bu<sub>2</sub>Sn(O), DME, 150 °C, microwave, 10 min (81%).

Scheme 2<sup>a</sup>

<sup>a</sup>(a) (i) Ac<sub>2</sub>O, DMAP, pyridine, 0 °C to rt, overnight; (ii) sat. NaHCO<sub>3</sub> aq, DCM, rt, 2 h (15, 53%); (b) 1-chloro-*N,N,2*-trimethyl-1-propenylamine, toluene, 0 °C to rt, 2 h; (c) NaH, NH<sub>2</sub>CN, DMF, 0 °C to rt, overnight; (d) NaOMe, MeOH, rt, 4 h (10i, 21% for three steps).

Scheme 3<sup>a</sup>

<sup>a</sup>(a) BF<sub>3</sub>·Et<sub>2</sub>O, CH<sub>2</sub>Cl<sub>2</sub>, 40 °C (76%); (b) Pd(Cl<sub>2</sub>)dppf·CH<sub>2</sub>Cl<sub>2</sub>, K<sub>3</sub>PO<sub>4</sub>, DMF, 80 °C (75%); (c) NaOMe, MeOH, rt, 4 h (48%).

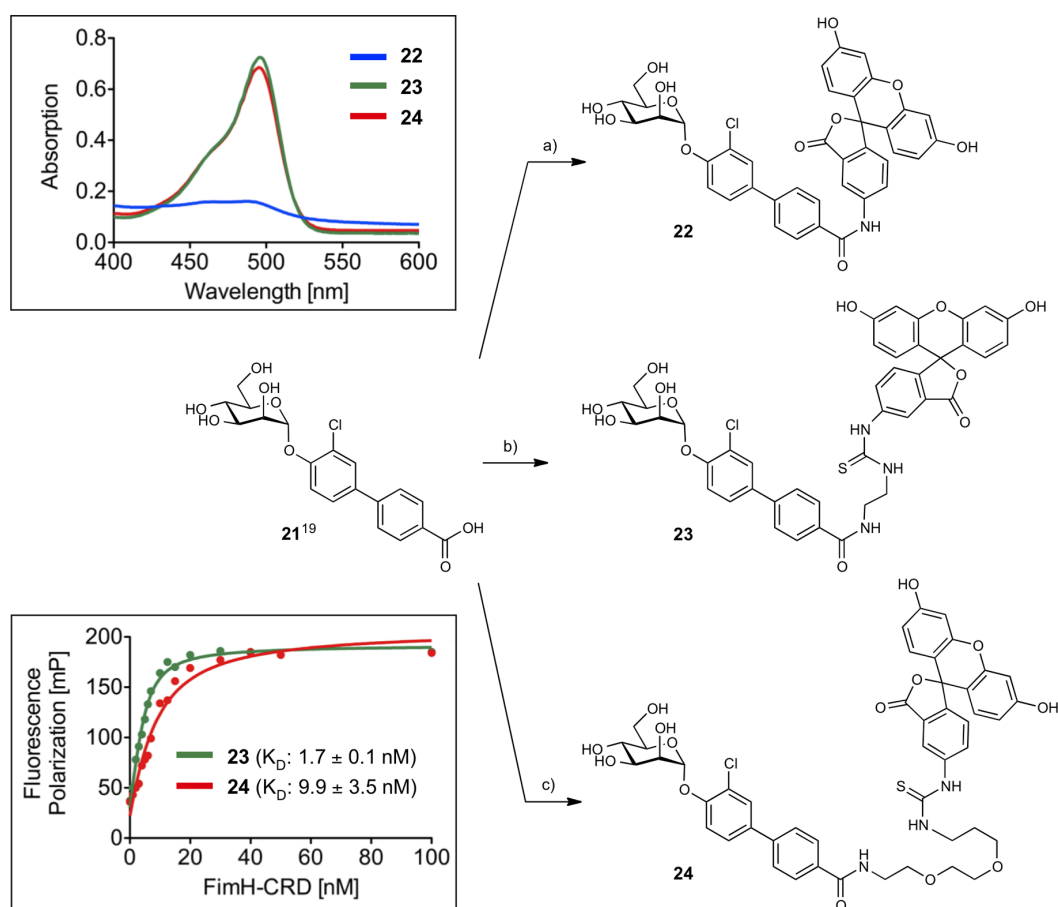
carboxylic acid into its acid chloride with 1-chloro-*N,N,2*-trimethyl-1-propenylamine.<sup>42</sup> Without isolation, the acid chloride was reacted with sodium hydrogen cyanamide in DMF followed by deacetylation under Zemplén conditions to yield the test compound 10i.

Finally, to further improve the pharmacokinetic properties of mannoside 10g<sup>18</sup> (see Table 3), a chloride substituent was introduced to the ortho-position of the aromatic ring adjacent to the anomeric oxygen. For its synthesis, peracetylated  $\alpha$ -D-mannose (16) was coupled with 2-chloro-4-iodophenol (17) using BF<sub>3</sub>·Et<sub>2</sub>O as promoter ( $\rightarrow$ 18, 76%). After the introduction

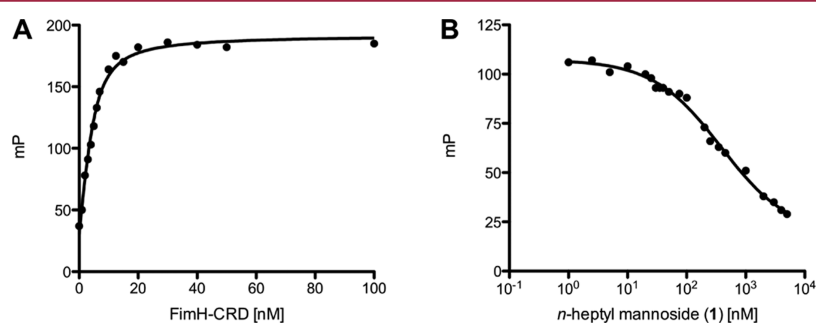
of the second aromatic ring by Miyaura–Suzuki coupling ( $\rightarrow$ 19, 75%), deprotection yielded mannoside 10j (Scheme 3).

**Binding Affinity.** The binding affinity of heptyl mannoside 1, the biphenyl mannosides 3, 9, 20,<sup>18</sup> and the bioisosteres 10a–j was determined in a competitive fluorescence polarization assay (FP assay) and with isothermal titration calorimetry (ITC). A protein construct consisting of the CRD with a C-terminal His-tag with a thrombin cleavage site (FimH-CRD-Th-His<sub>6</sub>) was used for all experiments.<sup>43</sup>

**Competitive Fluorescence Polarization Assay.** For the rapid evaluation of binding affinity, we established a competitive

Scheme 4<sup>a</sup>

<sup>a</sup>(a) 1-[(1-(Cyano-2-ethoxy-2-oxoethylideneaminoxy)dimethylaminomorpholinomethylene)]methanaminium hexafluorophosphate (COMU),  $\text{NEt}_3$ , fluoresceinamine, DMF, rt, 7 h (22, 19%); b) (i) DIC, NHS, *N*-Boc-ethylenediamine, DMF, rt, 12 h; (ii) TFA, DCM, rt, 10 min (68% over two steps), (iii) fluorescein isothiocyanate (FITC),  $\text{NEt}_3$ , DMF, rt, 3 h (23, 48%); c) (i) DIC, NHS, *N*-Boc-PEG2- $\text{NH}_2$ , DMF, rt, 14 h; (ii) TFA, DCM, rt, 30 min (62% over two steps); (iii) FITC, DMF, rt (24, 65%).



**Figure 3.** (A) Direct binding curve of the labeled competitor **23** obtained by adding a linear dilution of FimH-CRD (0–100 nM) and a constant concentration of competitor **23** (5 nM). The  $K_D$  was determined by fitting the experimental data to a single-site binding fit that accounts for ligand depletion. In three FP based direct binding experiments the  $K_D$  of competitor **23** was determined to be 1.7 nM. (B) Inhibition curve of *n*-heptyl mannoside (**1**) from the competitive FP assay. The  $\text{IC}_{50}$  value was determined by nonlinear least-squares fitting to a standard four-parameter equation. A modified Cheng–Prusoff equation<sup>45</sup> was used to calculate the corresponding  $K_D$  value ( $K_D = 28.3$  nM).

binding assay based on fluorescence polarization (FP). Similar formats have been applied before for the detection of carbohydrate–lectin interactions.<sup>18,44</sup> In this assay, the antagonist of interest displaces a fluorescently labeled competitor from

the binding site, thereby causing a reduction in fluorescence polarization.<sup>45</sup> To identify the optimal competitor, fluorescein isothiocyanate (FITC) was connected to the FimH ligand **21** by three linkers of different lengths ( $\rightarrow$ **22–24**, Scheme 4). For

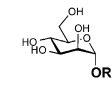
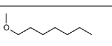
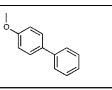
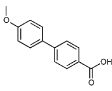
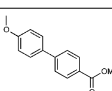
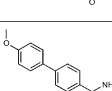
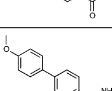
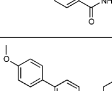
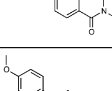
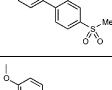
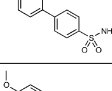
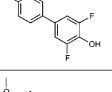
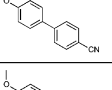
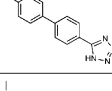
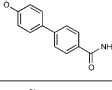
optimal sensitivity and signal-to-noise ratio, three main parameters need to be considered: (i) the affinity of the competitor should not be impaired by the fluorescent label; (ii) the conformational flexibility of the label upon binding of the competitor to the CRD should be low; (iii) the fluorescence properties of the label should not be affected by the connected ligand.<sup>46–48</sup> A change in fluorescence properties was observed for reporter ligand **22** in which the label was linked to the biphenyl aglycone by an amide bond. The absorption spectrum revealed a lack of the characteristic fluorescein absorption peak at 494 nm (Scheme 4), likely due to an extension of the conjugated system to the biphenyl moiety of the ligand. The elongated saturated spacer groups in competitors **23** and **24** ensured that the expected spectral properties of the dye were retained (Scheme 4).

For the determination of their binding affinity, fixed concentrations of the reporter ligands **23** and **24** were incubated for 24 h with a linear dilution of the FimH-CRD (0–100 nM). FP was measured using a plate reader, with polarized excitation at 485 nm and emission at 528 nm measured through appropriately oriented polarizers. Fitting the single-site binding function of Cooper<sup>49</sup> to the observed FP data resulted for compound **23** in a dissociation constant ( $K_D = 1.7$  nM, Figure 3A) similar to that of the unlabeled parent compound **21**,<sup>19</sup> whereas **24** showed a 5-fold lower affinity (9.9 nM) (Scheme 4). Therefore, the reporter ligand **23** fulfills all characteristics as an optimal competitor and was used for the FP assay.

For the test compounds **1**, **3**, **9**, **20**, and **10a–j**, a 24 h incubation time was applied before FP was measured because of the long residence time of FimH antagonists ( $t_{1/2} > 3.5$  h, Figure 3B<sup>50</sup>). The 24 h incubation period was empirically determined to be necessary to reach equilibrium between reporter ligand and compound of interest.  $IC_{50}$  values were obtained by nonlinear least-squares regression (standard four-parameter dose–response curve) and converted to  $K_D$  values using a modified Cheng–Prusoff equation.<sup>45</sup> This equation accounts for the ligand depletion effect in competitive titrations involving high-affinity interaction partners present in similar concentrations. Under these conditions, the free concentration of an interacting species cannot be assumed to equal the total concentration.

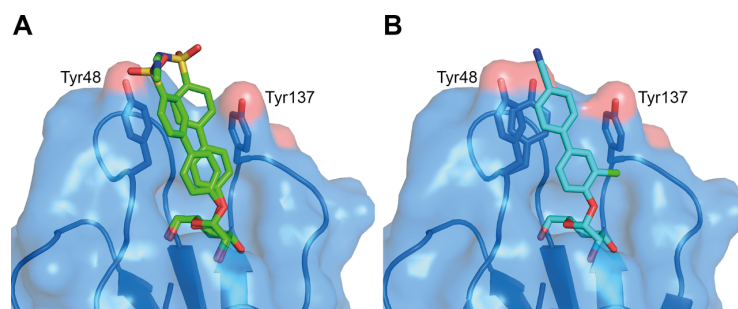
The  $K_D$  values determined for the test compounds **1**, **3**, **9**, **20**, and **10a–j** are summarized in Table 1. Against our expectations, the biphenyl mannosides **3** and **9** exhibit similar affinities (Table 1), despite the presence of an electron withdrawing carboxylate substituent in antagonist **9**. According to the crystal structure of FimH cocrystallized with the sulfonamide derivative **10e** (Figure 4A), the outer aromatic ring of the biphenyl aglycone forms  $\pi$ – $\pi$  interactions with the electron rich Tyr48, which is part of the tyrosine gate of FimH.<sup>15</sup> A reduction of electron density of the aglycone by the electron withdrawing carboxylate was expected to enforce these  $\pi$ – $\pi$  stacking interactions and lead to improved affinity. However, this beneficial effect might be compensated by an entropic penalty originating from the improved  $\pi$ – $\pi$  stacking to Tyr48 that might lead to the reduced flexibility of both protein and antagonist. Furthermore, a beneficial enthalpy effect might be partially compensated by an enthalpy penalty originating from the desolvation of the charged carboxylate in **9**<sup>51</sup> (see also Experimental Section). Although this substituent is solvent exposed, at least a partial desolvation may be necessary upon antagonist binding. To prove this assumption, we replaced the carboxylate by the corresponding methyl ester ( $\rightarrow$ **20**)<sup>18</sup> in order to reduce the desolvation penalty and, as predicted by the Hammett constant  $\sigma_p$ ,<sup>52</sup> to further improve the  $\pi$ – $\pi$  stacking.

**Table 1.** Affinities ( $K_D$ ) of FimH Antagonists to FimH-CRD-Th-His<sub>6</sub><sup>b</sup>

Entry	Compd		Affinity $K_D$ [nM]
1	<b>1</b>		28.3 ± 5.0
2	<b>3</b>		15.1 ± 2.2
3	<b>9</b>		17.9 ± 1.5
4	<b>20</b>		3.6 ± 0.9
5	<b>10a</b>		2.8 ± 0.3
6	<b>10b</b>		2.9 ± 0.5
7	<b>10c</b>		3.0 ± 0.1
8	<b>10d</b>		1.7 ± 0.2
9	<b>10e</b>		2.7 ± 0.4
10	<b>10f</b>		3.7 ± 0.2
11	<b>10g</b>		2.0 ± 0.6
12	<b>10h</b>		5.7 ± 0.1
13	<b>10i</b>		8.4 ± 0.3
14	<b>10j</b>		< 1 <sup>a)</sup>

<sup>a</sup>The  $K_D$  value of **10j** was approximated to be in the subnanomolar range. The  $IC_{50}$  value obtained in the competitive FP assay was equal to the lowest value that can be resolved by the assay, indicating stoichiometric titration of **10j** due to its high affinity. Consequently, its  $K_D$  must be below the  $K_D$  of competitor **23**. <sup>b</sup>Dissociation constants ( $K_D$ ) were determined in a competitive fluorescence polarization assay.





**Figure 4.** Ligand binding poses determined by X-ray cocrystallization with compounds **10e** resolved to 1.07 Å (A) and **10j** resolved to 1.10 Å (B). The electron density surrounding the aglycone of **10e** indicates flexibility of the aglycone and was modeled in two poses. Both compounds bind in a similar pose with a well-defined hydrogen network surrounding the mannose moiety and  $\pi$ - $\pi$  stacking interactions between the second aromatic ring and Tyr48 side chain (A). In contrast, in the FimH-CRD/**10j** structure the amino acid side chain of Y48 can be modeled in two distinct rotamers, suggesting flexibility also of the receptor (B).

Indeed, a 6-fold improvement in affinity was achieved. However, since the methyl ester undergoes rapid enzyme-mediated hydrolysis *in vivo*,<sup>19</sup> it will not be available at the place of action in the urinary bladder. The methyl ester was therefore replaced by metabolically stable bioisosteres<sup>39</sup> exhibiting comparable electron withdrawing properties<sup>52</sup> (Table 1, entries 5–13). The most potent derivatives **10d**, **10e**, and **10g** showed affinities in the low nanomolar range.

As previously reported,<sup>22</sup> a chloro substituent in the ortho-position of the aromatic ring adjacent to the anomeric oxygen is favorable for affinity and improves the physicochemical properties relevant for oral bioavailability. Indeed, the corresponding antagonist **10j** was the most potent compound tested in this study.

**Isothermal Titration Calorimetry (ITC).** To further confirm our hypothesis regarding  $\pi$ - $\pi$  stacking and desolvation, we performed ITC experiments with the reference compound **1**, the unsubstituted biphenyl mannoside **3**, the carboxylic acid **9**, and the bioisosteres **10b–e,g,j** (Table 2). ITC allows the simultaneous determination of the stoichiometry ( $N$ ), the change in enthalpy ( $\Delta H$ ) and the dissociation constant ( $K_D$ ) for ligand–protein binding.<sup>53,54</sup> The reliable determination of these three parameters requires well-defined sigmoidal titration curves characterized by the dimensionless Wiseman parameter  $c$  ( $c = Mt(0) K_D^{-1}$ , where  $Mt(0)$  is the initial macromolecule concentration).<sup>55</sup> To be sure that data can be fitted with confidence, the  $c$ -value should be between 1 and 1000 (ideally between 5 and 500),<sup>56</sup> which could be achieved for the antagonists **3** and **9**. For titrations involving low micromolar  $Mt(0)$  and interactions in the low nanomolar or picomolar range, as suggested for the bioisosteres **10b–j**,  $c$ -values above 1000 were expected. Since these conditions lead to steep titration curves that do not allow the determination of the curve slope representing  $1/K_D$ , we applied an alternative, competitive format referred to as displacement assay.<sup>57,58</sup> First, FimH-CRD-Th-His<sub>6</sub> was preincubated with the low affinity antagonist *n*-heptyl 2-deoxy- $\alpha$ -D-mannopyranoside (**25**, for synthesis see Supporting Information). The high-affinity bioisosteres of interest were titrated into the protein–ligand complex giving well-defined sigmoidal titration curves.

The resulting  $K_D$  values (Table 2) correspond well with the data obtained from the FP assay (Table 1). A comparison of the thermodynamic fingerprints of antagonists **3** and **9** reveals that the more favorable enthalpic contribution resulting from facilitated  $\pi$ - $\pi$  stacking leads to a net enthalpy gain ( $\Delta\Delta H =$

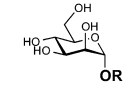
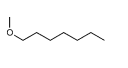
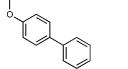
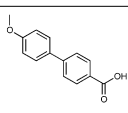
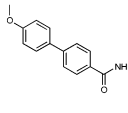
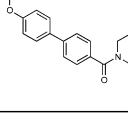
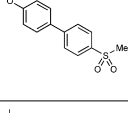
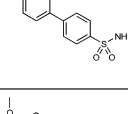
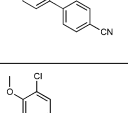
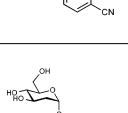
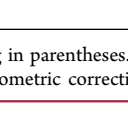
$-3.7$  kJ/mol). However, an even greater increase in enthalpy is likely countered by the enthalpy costs for desolvation of the electron withdrawing carboxylate.

The gain in enthalpy is in turn compensated by an unfavorable entropy ( $-T\Delta\Delta S = 3.2$  kJ/mol) as a result of the reduced flexibility of both the antagonist and the Tyr48 side chain caused by the improved interaction. This is not entirely outweighed by the beneficial entropy contribution related to the partial desolvation of the carboxylate and the related release of water into the bulk. Added together, the enthalpy and entropy contributions of antagonists **3** and **9** result in similar affinities ( $K_D$  of 17.7 and 15.0 nM, respectively).

In contrast, the replacement of the carboxylate group by various neutral bioisosteres (entries 4–7) reduces the enthalpy costs for desolvation (see calculated free energies of desolvation, Experimental Section) and therefore leads to a markedly improved enthalpy ( $\Delta\Delta H$  from  $-3.5$  to  $-5.8$  kJ/mol). As a result, an up to 5-fold improvement of the  $K_D$  values was achieved. Finally, with a cyano substituent (entries 8 and 9), the enthalpy term was further improved ( $\Delta\Delta H = -3.7$  kJ/mol) because of a reduced desolvation penalty and improved  $\pi$ - $\pi$  stacking interactions. However, this beneficial component is again partially compensated by a decrease in entropy. This can be attributed, first, to the loss of flexibility of the tightly bound ligand (Figure 4B) and, second, to the smaller surface area of the cyano substituent compared to amide, sulfonamide, and sulfone, which results in a smaller number of water molecules being released to bulk upon binding.

**X-ray Crystallography.** To determine the binding poses of the bioisosteres, we cocrystallized the compounds **10e** and **10j** with the FimH-CRD (Figure 4). Atomic resolution crystal structures were obtained at 1.07 Å (**10e**) and 1.10 Å (**10j**). As observed in previous mannoside cocrystal structures,<sup>15,18,36</sup> the mannose moiety forms an extensive hydrogen bond network to the well-defined binding site with all of its hydroxyl groups. The biphenyl aglycone is located between the tyrosine gate residues (Tyr48/Tyr137). The  $\pi$ - $\pi$  stacking of the second aromatic ring of the aglycone to the side chain of Tyr48 contributes most to the interaction energy of the aglycone moiety. Interactions to the Tyr137 side chain on the other hand are only limited. Whereas a previously published crystal structure of a biphenyl mannoside in complex with FimH-CRD suffers from crystal contacts of binding site residues (Tyr48 side chain to backbone oxygen of Val27) possibly causing the distortion of the binding site,<sup>18</sup> the binding sites of our structures are mostly solvent exposed. This

Table 2. Thermodynamic Parameters from ITC for Selected FimH Antagonists Binding to FimH-CRD-Th-His<sub>6</sub><sup>d</sup>

Entry	Compd		$K_D^{[a]}$ [nM]	$\Delta G$ [kJ/mol]	$\Delta H^{[a]}$ [kJ/mol]	$-T\Delta S$ [kJ/mol]	$n$	Type of measurement
1	<b>1</b> <sup>[b,c]</sup>		28.9 (25.8 – 32.3)	-43.0	-50.3 (-50.2 – -50.7)	7.3	1.00	direct
2	<b>3</b> <sup>[b]</sup>		17.7 (14.1 – 22.3)	-44.2	-45.0 (-44.5 – -45.6)	0.8	1.07	direct
3	<b>9</b>		15.0 (13.4 – 16.7)	-44.7	-48.7 (-48.4 – -49.0)	4.0	1.05	direct
4	<b>10b</b>		4.3 (3.2 – 5.6)	-47.8	-54.5 (-54.1 – -54.9)	6.7	1.02	competitive vs. <b>25</b>
5	<b>10c</b>		5.0 (3.8 – 6.6)	-47.4	-54.5 (-54.1 – -54.8)	7.1	0.97	competitive vs. <b>25</b>
6	<b>10d</b>		3.0 (2.1 – 4.2)	-48.7	-52.3 (-51.5 – -53.1)	3.6	0.99	competitive vs. <b>25</b>
7	<b>10e</b>		3.5 (2.9 – 4.3)	-48.2	-52.2 (-51.6 – -52.8)	3.9	1.06	competitive vs. <b>25</b>
8	<b>10g</b>		2.8 (2.3 – 3.3)	-48.8	-58.2 (-57.8 – -58.6)	9.4	1.00	competitive vs. <b>25</b>
9	<b>10j</b>		1.3 (1.1 – 1.6)	-50.7	-60.9 (-60.4 – -61.4)	10.1	1.01	competitive vs. <b>25</b>
10	<b>25</b>		9'386 (8'555 – 10'287)	-28.7	-19.5 (-19.1 – -20.0)	-9.1	1.00	direct

<sup>a</sup>95% confidence interval from fitting in parentheses. <sup>b</sup>Global fit including two direct titration measurements. <sup>c</sup>ITC data were previously published with an  $n$ -value of 0.82.<sup>37</sup> <sup>d</sup> $n$ , stoichiometric correction factor.

revealed the flexibility of the aglycone in the FimH-CRD/**10e** structure, since the electron density toward the solvent-exposed sulfonamide indicates that there is not one single orientation. Therefore, the aglycone was modeled in two distinct poses. In contrast, in the FimH-CRD/**10j** structure the amino acid side chain of Y48 can be modeled in two distinct rotamers, suggesting flexibility also of the receptor.

**Physicochemical Properties and in Vitro Pharmacokinetics.** Intestinal absorption and renal excretion are prerequisites for a successful oral treatment of UTI with FimH

antagonists. Furthermore, reabsorption of antagonist from the renal ultrafiltrate is desirable for maintaining the minimal antiadhesive concentration in the target organ, namely, the bladder, over an extended period of time. To estimate the influence of the bioisostere approach on oral bioavailability and the rate of renal excretion, we determined lipophilicity by means of the octanol–water distribution coefficient ( $\log D_{7.4}$ ),<sup>59</sup> aqueous solubility, and membrane permeability in the artificial membrane permeability assay (PAMPA)<sup>60</sup> and the colorectal adenocarcinoma (Caco-2) cell monolayer model.<sup>61</sup>



Table 3. Physicochemical and in Vitro Pharmacokinetic Parameters<sup>h</sup>

compd	pK <sub>a</sub> <sup>a</sup>	log D <sub>7.4</sub> <sup>b</sup>	solubility [μg/mL]/pH <sup>c</sup>	PAMPA log P <sub>e</sub> [cm/s]/pH <sup>d,e</sup>	Caco-2 P <sub>app</sub> [10 <sup>-6</sup> cm/s] <sup>e</sup>		PPB f <sub>b</sub> [%] <sup>f</sup>	metabolic stability t <sub>1/2</sub> [min] <sup>g</sup>
					a → b	b → a		
1		1.65	>3000	-4.89	7.0 ± 0.6	9.4 ± 0.2	81	13
3		2.1 ± 0.1	21 ± 1/7.4	-4.7 ± 0.1/7.4	10.0 ± 0.9	19.0 ± 1.2	93 ± 1	nd
20		2.14	33.8/6.51	-4.7	4.23	nd	93	1.0
9	3.88	<-1.5	>3000/6.61	no permeation	nd	nd	73	>60
10a		0.5 ± 0.1	12 ± 1/7.4	-6.8 ± 0.3/7.4	0.12 ± 0.01	0.61 ± 0.03	nd	nd
10b		0.8 ± 0.0	122 ± 13/7.4	-9.2 ± 1.4/7.4	1.10 ± 0.82	0.87 ± 0.15	nd	nd
10c		0.2 ± 0.1	>250/7.4	-7.8 ± 0.3/7.4	0.18 ± 0.07	1.30 ± 0.03	48 ± 2	>60
10d		0.4 ± 0.0	246 ± 17/7.4	-7.2 ± 0.0/7.4	0.36 ± 0.01	1.76 ± 0.12	99 ± 1	>60
10e		0.7 ± 0.1	>250/7.4	-8.6 ± 0.2/7.4	0.28 ± 0.23	1.82 ± 0.14	>99	>60
10f	6.5	1.1 ± 0.0	>150/3.0	-7.7 ± 0.8/5.0	0.40 ± 0.02	1.90 ± 0.17	nd	nd
			>150/7.4	-8.8 ± 0.1/7.4				
10g		1.4 ± 0.0	186 ± 4/7.6	-5.7 ± 0.0/7.4	2.0 ± 0.1	13.2 ± 2.1	99 ± 0	>60
10h	3.7	-1.4 ± 0.1	11 ± 0/3.0	-9.3 ± 1.4/5.0	0.17 ± 0.00	0.22 ± 0.01	nd	nd
			273 ± 2/7.4	-8.8 ± 1.4/7.4				
10i	2.5	-1.1 ± 0.1	>150/3.0	-6.8 ± 0.2/5.0	0.22 ± 0.14	0.29 ± 0.03	nd	nd
			>150/7.4	-7.0 ± 0.1/7.4				
10j		2.1 ± 0.0	192 ± 5/7.4	-5.2 ± 0.0/7.4	2.2 ± 0.4	22.1 ± 1.5	89 ± 1	>60

<sup>a</sup>pK<sub>a</sub> values were determined by NMR spectroscopy. <sup>b</sup>Octanol–water distribution coefficients (log D<sub>7.4</sub>) were determined by a miniaturized shake-flask procedure at pH 7.4. Values represent the mean ± SD of sextuplicate measurements.<sup>59</sup> <sup>c</sup>Kinetic solubility was measured in a 96-well format using the μSOL Explorer solubility analyzer at the indicated pH in triplicate. <sup>d</sup>P<sub>e</sub> = effective permeability. Passive permeation through an artificial membrane was determined by the parallel artificial membrane permeation assay (PAMPA). Values represent the mean ± SD of quadruplicate measurements performed at the indicated pH.<sup>60</sup> <sup>e</sup>P<sub>app</sub> = apparent permeability. Permeation through a Caco-2 cell monolayer was assessed in the absorptive (a → b) and secretory (b → a) directions in triplicate.<sup>61</sup> <sup>f</sup>Plasma protein binding (PPB) was determined by equilibrium dialysis in triplicate.<sup>62</sup> <sup>g</sup>Metabolic stability was determined by incubating the compounds (2 μM) with pooled rat liver microsomes (RLM, 0.5 mg/mL) in the presence of NADPH (1 mM, compounds 1, 9, 10c–e,g,j) or without NADPH (compound 20).<sup>63</sup> <sup>h</sup>nd = not determined.

**Oral Bioavailability.** Oral bioavailability of a compound relies on solubility, permeation through the membranes lining the intestine, and stability against first pass metabolism.<sup>64,65</sup> As discussed by Lipinski<sup>66</sup> and Curatolo,<sup>67</sup> dose and permeability define the minimum aqueous solubility required for oral administration. Thus, a dose of 1 mg/kg of a moderately permeable compound requires a solubility of at least 52 μg/mL. Whereas sufficient aqueous solubility (>3000 μg/mL) was reported for *n*-heptyl α-mannopyranoside (1),<sup>19</sup> the unsubstituted biphenyl α-D-mannopyranoside 3 and the antagonists bearing a methylcarboxylate, carboxamide, or tetrazole substituent (compounds 20, 10a, and 10h) were found to be scarcely soluble.<sup>22</sup> As proposed by Ishikawa,<sup>68</sup> a possible reason is the apolar and planar aglycone. By contrast, the polar carboxylic acid moiety present in antagonist 9 or the substituents in the bioisosteres 10b–j enhance solubility to 122–273 μg/mL, a level sufficient for in vivo PK studies. For in vivo disease studies, however, dosages of up to 10 mg/kg were foreseen (see below), requiring a solubility of 520 μg/mL.<sup>66,67</sup> For this reason, surfactant Tween 80 (1%) had to be added.

Furthermore, permeability data derived from PAMPA<sup>69</sup> and the Caco-2 model<sup>70</sup> suggest moderate to high permeation of the moderately lipophilic antagonists 1, 3, and 20 (log D<sub>7.4</sub> > 1.6) through the intestinal membranes. The bioisosteres 10a–f,h,i, although slightly more permeable than the strongly hydrophilic carboxylic acid derivative 9, show only low values of permeability compared to *n*-heptyl α-D-mannopyranoside (1) or the unsubstituted biphenyl mannoside 3. However, the *p*-cyanobiphenyl derivatives 10g and 10j display elevated log D<sub>7.4</sub> and effective permeability (log P<sub>e</sub>) in the range for successful intestinal absorption. Regarding both sufficient aqueous solubility and elevated membrane permeability, the *p*-cyano substituted bioisosteres 10g and 10j are thus the most promising

candidates for oral absorption. Moreover, combining the bioisosteric replacement with the addition of a chloro substituent in the ortho-position of the aromatic ring adjacent to the anomeric oxygen (→10j)<sup>22</sup> resulted in the most advantageous physicochemical profile for oral bioavailability.

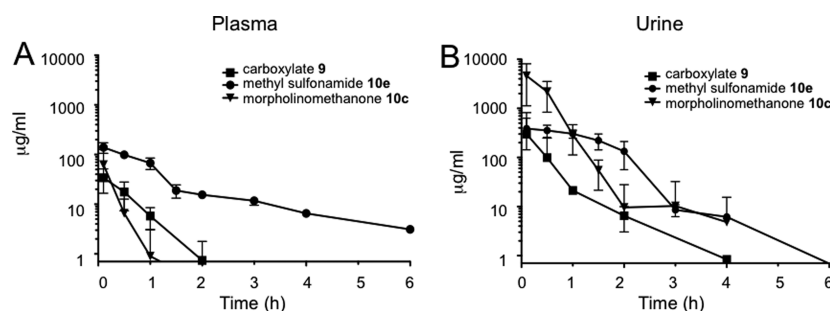
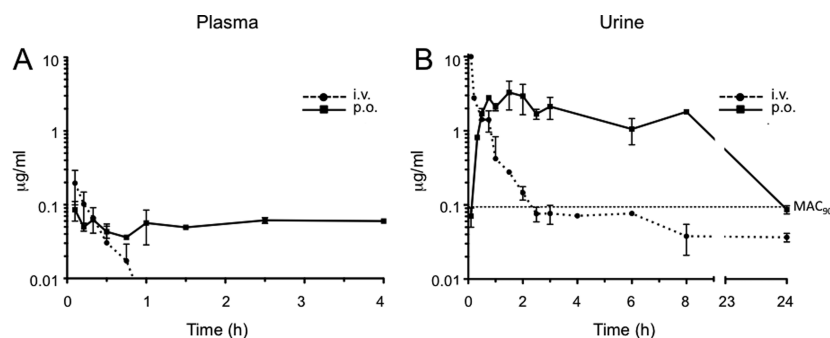
**Renal Excretion.** The rate of renal excretion depends on the rate of glomerular filtration and the propensity to tubular secretion and reabsorption of an antagonist.<sup>71</sup> Only the fraction that is not bound to plasma proteins is expected to enter the glomerular filtrate.<sup>72</sup> Plasma protein binding (PPB) data indicating the fraction bound (f<sub>b</sub>) are listed in Table 2.<sup>62</sup> The biphenyls 9 and 10c were identified as moderate binders to plasma proteins (f<sub>b</sub> ≤ 65%), which suggests a low impact of PPB on antagonist filtration. The f<sub>b</sub> values of the antagonists 1, 3, 20, and 10j were between 80% and 93%, whereas the bioisosteres 10d,e,g showed particularly high protein binding (f<sub>b</sub> ≥ 99%) implying slow compound entry into the primary urine. However, the kinetic aspects of PPB, that is, association and dissociation rate constants, remain to be determined to quantify precisely the influence of PPB on filtration.<sup>73</sup>

Furthermore, log D<sub>7.4</sub> was identified as key determinant of tubular reabsorption.<sup>74–76</sup> Accordingly, lipophilic compounds are predominantly reabsorbed from the renal filtrate. Given that renal clearance is the major route of elimination, this will result in a slow but steady excretion into the bladder. In contrast, hydrophilic compounds are poorly reabsorbed and thus quickly renally eliminated, which leads to high initial compound levels in the urine but narrows the time range where the minimal antiadhesive concentration is maintained. Consequently, low log D<sub>7.4</sub> as shown for the antagonists 9, 10h, and 10i implies low tubular reabsorption and rapid elimination of the filtered molecules by the urine. Otherwise, log D<sub>7.4</sub> between 0.2 and 0.7, such as determined for the bioisosteres 10a–e, suggests

**Table 4.** Pharmacokinetic Parameters Determined after a Single iv Application of Compounds 9, 10c, 10e, and 10j in Female C3H/HeN Mice<sup>a</sup>

compd	plasma							urine, $C_{max}$ ( $\mu\text{g/mL}$ )
	$C_0$ ( $\mu\text{g/mL}$ )	dose (mg/kg)	$V_z$ (mL)	$t_{1/2}$ (h)	$AUC_{0-inf}$ ( $\mu\text{g}\cdot\text{h/mL}$ )	$CL_{tot}$ (mL/h)		
9	40	50	25.2	0.33	23.5	53.1	300	
10c	109.7	50	28.3	0.4	25.3	49.4	4611	
10e	151.6	50	19.5	1.9	175.1	7.1	387	
10j	0.36	0.625	52.8	0.17	0.07	218	10	

<sup>a</sup>Values were calculated using PKSolver.<sup>78</sup>  $C_0$ , initial concentration;  $V_z$ , volume of distribution in terminal phase; AUC, area under the curve;  $CL_{tot}$ , total clearance;  $C_{max}$ , maximal concentration.

**Figure 5.** Antagonist concentrations in (A) plasma and (B) urine after a single iv application of 9, 10c, and 10e (50 mg/kg).**Figure 6.** Antagonist concentrations in (A) plasma and (B) urine after a single iv and po application of compound 10j (iv, 0.625 mg/kg; po, 1.25 mg/kg). MAC<sub>90</sub> is the minimal antiadhesive concentration to inhibit 90% adhesion (0.094  $\mu\text{g/mL}$ ).

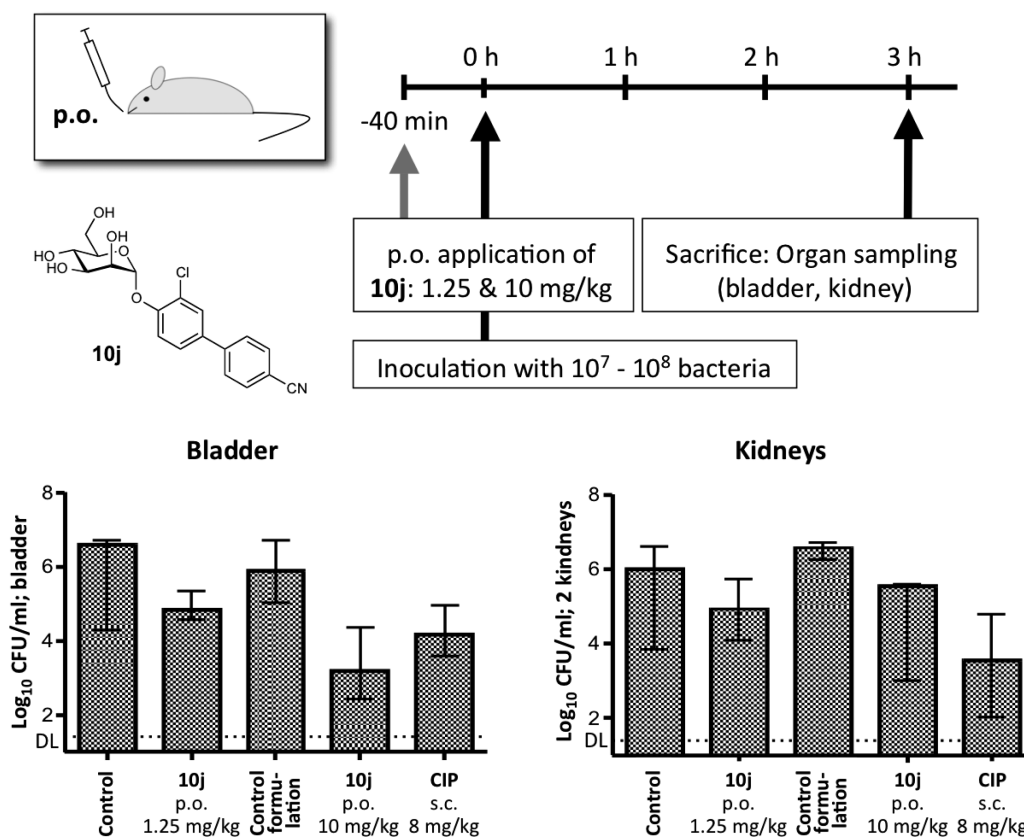
increasing propensity to tubular reuptake, whereas  $\log D_{7,4} > 1$  as shown for heptyl mannoside 1 and the biphenyl mannosides 3, 20, 10g, 10f, and 10j is optimal for tubular reabsorption from the glomerular filtrate and thus for slow renal clearance.

**Metabolic Stability.** Increasing lipophilicity is usually paralleled by increasing susceptibility to metabolism.<sup>77</sup> Liabilities toward metabolic clearance pathways that prevent the intact antagonist from reaching the target in the bladder were therefore of interest. To assess their propensity to cytochrome P450 (CYP450) mediated metabolism, heptyl mannoside 1, the carboxylic acid derivative 9, and the bioisosteres 10c–e, g, j were incubated with rat liver microsomes (RLM, 0.5 mg/mL) in the presence of the cofactor  $\beta$ -nicotinamide adenine dinucleotide phosphate (NADPH).<sup>63</sup> To confirm the high propensity of the methyl ester present in antagonist 20 to carboxylesterase (CES) mediated hydrolysis, this antagonist was incubated with RLM only. The profiles of unchanged compound versus time revealed high susceptibility of heptyl mannoside 1 to CYP450-mediated metabolism ( $t_{1/2} = 13$  min) and rapid hydrolysis of the ester 20 by the hepatic CES ( $t_{1/2} = 1.0$  min). Otherwise, the bioisosteres 10c–e, g, j were stable against enzyme-mediated bioconversion

( $t_{1/2} > 60$  min), suggesting lower propensity to metabolic, nonrenal elimination pathways.

Considering PPB, lipophilicity, and metabolic stability data, we therefore expected (i) a steady release of compounds 10d, e, g, j into the bladder because of high PPB decelerating glomerular filtration (10d, e, g) and/or high  $\log D_{7,4}$  supporting tubular reabsorption (10g, j), (ii) a fast excretion of antagonists 9 and 10c via the urine due to low PPB and low  $\log D_{7,4}$ , and (iii) a rapid clearance of heptyl mannoside 1 from the body by renal and metabolic pathways. Compounds featuring high propensity to renal excretion as major route of elimination (10c, 10e and 10j) were selected for in vivo PK studies in a mouse model.

**Pharmacokinetic Studies in C3H/HeN Mice.** This first part of our study explored the predicted effects of lipophilicity, PPB, and metabolic stability on antagonist disposition and elimination upon a single dose iv application (50 mg/kg) of compounds 10c and 10e. The PK parameters of these applications and those of the previously published carboxylate 9 are summarized in Table 4. The table also contains the results of the iv administration of compound 10j (0.625 mg/kg).



**Figure 7.** Preventive efficacy of **10j** in the UTI mouse model 3 h after infection. The bars depict the median bacterial load with the interquartile range in the different study groups. Shown are the results of the control group (PBS), control group formulation (5% DMSO in PBS containing 1% Tween 80), and the intervention groups with the preventive applications of either 1.25 or 10 mg/kg **10j** po or 8 mg/kg CIP sc (representing the murine dose equivalent to a human standard dose).<sup>81</sup> DL, detection limit. CFU, colony forming units.

In contrast to the fast plasma clearance of antagonists **9** and **10c** (Figure 5A), the methylsulfonamide bioisostere **10e** attained higher initial concentration in plasma ( $C_0$ ) and lower total clearance ( $CL_{tot}$ ). Therefore, it could be detected until 6 h after application, resulting in markedly higher plasma AUC. The observed high  $C_0$  of compound **10e** may be attributed to a small volume of distribution ( $V_z$ ) resulting from the high PPB ( $f_b \geq 99\%$ ).<sup>72</sup> In urine (Figure 5B), the carboxylic acid **9** and the morpholinomethanone **10c** displayed high levels immediately following administration and a rapid concentration decrease within the first 2 h, reflecting the rapid elimination from plasma. Fast renal excretion as major route of elimination can be rationalized by the physicochemical properties of the antagonists **9** and **10c**, that is, moderate PPB and  $\log D_{7.4}$ , as well as high metabolic stability. Otherwise, the methylsulfonamide bioisostere **10e** showed sustained compound levels in urine over a period of 2 h and subsequent slow decrease until 6 h after administration. This sustained renal excretion is a result of the interplay of the antagonist's elevated PPB and  $\log D_{7.4}$ .

In a second study, the *p*-cyano bioisostere **10j**, characterized by a high oral absorption potential, was administered as a single dose iv (0.625 mg/kg) and po (1.25 mg/kg). The plasma concentration curve upon iv dosing displays a steep decline within the first hour after application, while the po curve shows a prolonged period where absorption and elimination are in equilibrium (Figure 6A). The urine concentration profiles

(Figure 6B) parallel the plasma curves obtained by the two modes of application; i.e., high plasma clearance upon iv bolus injection led to high initial antagonist levels in urine and a rapid concentration decline. By contrast, sustained plasma concentrations upon po administration resulted in prolonged urine levels.

As a result, urine concentrations exceed the minimum level required for the antiadhesive effect as estimated from the *in vitro* cell infection model<sup>79</sup> (minimal antiadhesion concentration,<sup>23</sup>  $MAC_{90} = 0.094 \mu\text{g/mL}$ ) for more than 8 h upon oral single-dose administration (Figure 6B).

**Infection Study in C3H/HeN Mice.** In a preventive study, six mice were inoculated with UTI89 following an oral application of **10j** (1.25 mg/kg) 40 min prior to infection. Three hours after inoculation, the animals were sacrificed and bladder and kidneys were removed. Organs were homogenized and analyzed for bacterial counts. The effect of the FimH antagonist was compared to a 8 mg/kg dose of ciprofloxacin (CIP), applied subcutaneously (sc) 10 min before infection. CIP is used as standard antibiotic therapy in humans for the treatment of UTI.<sup>80</sup> In mice, the dose of 8 mg/kg sc was shown to mimic the standard human dose regarding peak levels and the  $AUC_{24}$  in serum.<sup>81</sup> The median reductions in bacterial counts in mice treated with **10j** and CIP compared to the control group 3 h after infection are displayed in Figure 7.

The median value in the untreated control group showed bacterial counts of  $6.6 \log_{10}$  colony forming units (CFU) in the bladder and  $6 \log_{10}$  CFU in the kidneys. After oral application of 1.25 mg/kg **10j**, bacterial loads in the bladder decreased by 1.78  $\log_{10}$  CFU and 1.07  $\log_{10}$  CFU in the kidneys. The lower reduction in the kidneys is most likely due to the differing adhesion mechanisms between bladder and kidneys (type 1 pili vs P-pili), which is not targeted by **10j**.<sup>82</sup> With CIP (8 mg/kg sc) a substantial reduction in both bladder and kidneys (median reductions of 2.44  $\log_{10}$  and 2.47  $\log_{10}$ , respectively) was observed. Despite the low oral dose of **10j** (1.25 mg/kg), the approximately 100-fold reduction of CFU in the bladder promised an even higher effect upon dose increase to 10 mg/kg. Since the solubility of **10j** for this increased dose is too low (192  $\mu\text{g/mL}$ ), we used 5% DMSO and surfactant Tween 80 (1%) as solubilizer. To effectively compare the effect of a higher dose of **10j**, a control group receiving the formulation only (5% DMSO in PBS containing 1% Tween 80, termed control group formulation) was tested in parallel. When 10 mg/kg **10j** was applied, bacterial loads in the bladder decreased by 2.68  $\log_{10}$  CFU/mL compared to the control group formulation, clearly exceeding the effect of CIP with a reduction of 2.44  $\log_{10}$  CFU/mL. However, only a moderate reduction of 1.04  $\log_{10}$  CFU was achieved in the kidneys.

## SUMMARY AND CONCLUSION

Recently, numerous monovalent alkyl and aryl  $\alpha$ -D-mannopyranosides have been described as potent FimH antagonists. However, most of them suffer from insufficient pharmacokinetic properties, i.e., modest bioavailability and short duration of the therapeutic effect in the bladder, their site of action. As a consequence, high doses at short intervals are required to achieve antiadhesive effects over an extended period of time. Therefore, the goal of the present study was an appropriate optimization of the pharmacokinetic profile of biphenyl  $\alpha$ -D-mannopyranosides while keeping their high affinity to the CRD of FimH. The starting point was the biphenylcarboxylate **9** where the critical carboxylate was replaced by bioisosteres.<sup>39,83</sup>

With a series of bioisosteres, a 3- to 5-fold improvement of affinity was achieved compared to **9**. Although binding necessitates only partial desolvation of the carboxylate and its bioisosteric replacements, a reduction of the enthalpy penalty for desolvation<sup>51</sup> was identified as the source of the improved affinity exhibited by the bioisosteres. Thermodynamic evaluation of antagonists **10b–e** revealed almost identical enthalpy contribution to binding. However, for antagonists with the *p*-cyano substituent (**10g** and **10j**) an enhancement of up to  $-8.7$  kJ/mol was observed, indicating a reduced desolvation penalty and an improved stacking as derived from the crystal structure of **10j** cocrystallized with the CRD of FimH (Figure 4B). On the other hand, higher affinity originating from a reduction of conformational flexibility of ligand and protein resulted in a concomitant entropy penalty of up to 6.5 kJ/mol.

In addition to the improved pharmacodynamics, the relevant pharmacokinetic parameters (solubility, permeability, renal excretion) were substantially improved. With 3'-chloro-4'-( $\alpha$ -D-mannopyranosyloxy)biphenyl-4-carbonitrile (**10j**), a FimH antagonist with an optimal in vitro PK/PD profile was identified. The *p*-cyano substituent conferred lipophilicity and high binding to plasma proteins, which slowed the rate of renal excretion. Despite higher lipophilicity, antagonist **10j** was insensitive to CYP450-mediated metabolism and therefore predominantly eliminated via the renal pathway. In vivo experiments confirmed

the excellent PK profile of **10j** with steady renal excretion for more than 8 h after oral application (1.25 mg/kg), suggesting a long-lasting antiadhesive effect. Finally, the preventive oral application of **10j** (10 mg/kg) reduced the bacterial load in the bladder by almost 1000-fold 3 h after infection. Although the first 3 h of the infection do not represent the complete infection cycle, they represent the time span of bacteria adhering and invading urothelial cells.<sup>84,85</sup> Nevertheless, the effect of FimH antagonist **10j** within a longer infection time and at higher dosing will be the subject of future investigations.

## EXPERIMENTAL SECTION

**Synthesis.** The synthesis of compounds **10a–d**, **10f**, **10g**, **10i**, **13a–d**, **13f**, **13g**, **15**, **18**, and **25**, including compound characterization data, can be found in the Supporting Information.

**General Methods.** NMR spectra were recorded on a Bruker Avance DMX-500 (500.1 MHz) spectrometer. Assignment of <sup>1</sup>H and <sup>13</sup>C NMR spectra was achieved using 2D methods (COSY, HSQC, HMBC). Chemical shifts are expressed in ppm using residual CHCl<sub>3</sub>, CHD<sub>2</sub>OD, or H<sub>2</sub>O as references. Optical rotations were measured using PerkinElmer polarimeter 341. Electron spray ionization mass spectra were obtained on a Waters micromass ZQ. The LC/HRMS analyses were carried out using a Agilent 1100 LC equipped with a photodiode array detector and a Micromass QTOF I equipped with a 4 GHz digital time converter. Microwave-assisted reactions were carried out with a CEM Discover and Explorer. Reactions were monitored by TLC using glass plates coated with silica gel 60 F<sub>254</sub> (Merck) and visualized by using UV light and/or by charring with a molybdate solution (a 0.02 M solution of ammonium cerium sulfate dihydrate and ammonium molybdate tetrahydrate in aqueous 10% H<sub>2</sub>SO<sub>4</sub>). MPLC separations were carried out on a CombiFlash Companion or Rf (Teledyne Isco) equipped with RediSep normal-phase or RP-18 reversed-phase flash columns. LC-MS separations were done on a Waters system equipped with sample manager 2767, pump 2525, PDA 2525, and Micromass ZQ. All compounds used for biological assays are at least of 95% purity based on HPLC analytical results. Commercially available reagents were purchased from Fluka, Aldrich, Alfa Aesar, or abcr GmbH & Co. KG (Germany). Solvents were purchased from Sigma-Aldrich or Acros and were dried prior to use where indicated. Methanol (MeOH) was dried by refluxing with sodium methoxide and distilled immediately before use. Dimethoxyethane (DME) was dried by filtration over Al<sub>2</sub>O<sub>3</sub> (Fluka, type 5016 A basic).

**4'-(2,3,4,6-Tetra-O-acetyl- $\alpha$ -D-mannopyranosyloxy)-N-methylbiphenyl-4-sulfonamide (13e).** A Schlenk tube was charged with aryl iodide **11**<sup>22</sup> (116 mg, 0.21 mmol), 4-(*N*-methylsulfamoyl)phenylboronic acid (**12e**, 50 mg, 0.23 mmol), Pd(dppf)Cl<sub>2</sub>·CH<sub>2</sub>Cl<sub>2</sub> (5 mg, 0.006 mmol), K<sub>3</sub>PO<sub>4</sub> (67 mg, 0.32 mmol), and a stirring bar. The tube was closed with a rubber septum and was evacuated and flushed with argon. This procedure was repeated once, and then anhydrous DMF (1 mL) was added under a stream of argon. The mixture was degassed in an ultrasonic bath and flushed with argon for 5 min and then stirred at 80 °C overnight. The reaction mixture was cooled to rt, diluted with EtOAc (50 mL), and washed with water (50 mL) and brine (50 mL). The organic layer was dried over Na<sub>2</sub>SO<sub>4</sub> and concentrated in vacuo. The residue was purified by MPLC on silica gel (petroleum ether/EtOAc) to afford **13e** (105 mg, 84%) as a white solid. [ $\alpha$ ]<sub>D</sub><sup>20</sup> +56.4 (c 0.50, MeOH). <sup>1</sup>H NMR (500 MHz, CDCl<sub>3</sub>):  $\delta$  = 7.92–7.90 (m, 2H, Ar–H), 7.70–7.68 (m, 2H, Ar–H), 7.57–7.55 (m, 2H, Ar–H), 7.21–7.19 (m, 2H, Ar–H), 5.60–5.57 (m, 2H, H-1, H-3), 5.48 (dd, *J* = 1.8, 3.4 Hz, 1H, H-2), 5.40 (t, *J* = 10.0 Hz, 1H, H-4), 4.38 (dd, *J* = 5.4, 10.8 Hz, 1H, NH), 4.30 (dd, *J* = 4.9, 12.3 Hz, 1H, H-6a), 4.13–4.08 (m, 2H, H-5, H-6b), 2.72 (d, *J* = 5.4 Hz, 3H, NCH<sub>3</sub>), 2.22, 2.07, 2.05, 2.04 (4 s, 12H, 4 COCH<sub>3</sub>). <sup>13</sup>C NMR (126 MHz, CDCl<sub>3</sub>):  $\delta$  = 170.55, 170.06, 170.03, 169.75 (4 CO), 155.97, 144.81, 137.16, 134.09, 128.62, 127.85, 127.39, 117.01 (Ar–C), 95.78 (C-1), 69.34 (C-5), 69.31 (C-2), 68.81 (C-3), 65.86 (C-4), 62.07 (C-6), 29.44 (NHCH<sub>3</sub>), 20.92, 20.74, 20.72 (4C, 4 COCH<sub>3</sub>). ESI-MS *m/z*, calcd for C<sub>27</sub>H<sub>31</sub>NNaO<sub>12</sub>S [M + Na]<sup>+</sup>: 616.1. Found: 616.1.



**4'-( $\alpha$ -D-Mannopyranosyloxy)-N-methylbiphenyl-4-sulfonamide (10e).** To a solution of 13e (40 mg, 0.07 mmol) in dry MeOH (5 mL) was added freshly prepared 1 M NaOMe/MeOH (0.1 equiv) under argon. The mixture was stirred at rt until the reaction was complete (monitored by TLC), then neutralized with Amberlyst-15 (H<sup>+</sup>) ion-exchange resin, filtered, and concentrated in vacuo. The residue was purified by MPLC on silica gel (DCM/MeOH, 10:1 to 7:1) to afford 10e (22 mg, 76%) as white solid.  $[\alpha]_D^{20} +105.7$  (c 0.30, MeOH). <sup>1</sup>H NMR (500 MHz, CD<sub>3</sub>OD):  $\delta$  = 7.90–7.88 (m, 2H, Ar–H), 7.80–7.79 (m, 2H, Ar–H), 7.66–7.64 (m, 2H, Ar–H), 7.26–7.25 (m, 2H, Ar–H), 5.58 (d, *J* = 1.7 Hz, 1H, H-1), 4.06 (dd, *J* = 1.8, 3.3 Hz, 1H, H-2), 3.96 (dd, *J* = 3.4, 9.5 Hz, 1H, H-3), 3.79–3.74 (m, 3H, H-4, H-6a, H-6b), 3.63 (ddd, *J* = 2.5, 5.2, 9.7 Hz, 1H, H-5), 2.57 (s, 3H, NHCH<sub>3</sub>). <sup>13</sup>C NMR (126 MHz, CD<sub>3</sub>OD):  $\delta$  = 158.34, 146.13, 138.67, 134.55, 129.53, 128.82, 128.21, 118.29 (Ar–C), 100.09 (C-1), 75.53 (C-5), 72.42 (C-3), 71.96 (C-2), 68.32 (C-4), 62.68 (C-6), 29.31 (NHCH<sub>3</sub>). HRMS *m/z*, calcd for C<sub>19</sub>H<sub>23</sub>NNaO<sub>8</sub>S [M + Na]<sup>+</sup>: 448.1037. Found: 448.1038.

**5-(4'-(2,3,4,6-Tetra-O-acetyl- $\alpha$ -D-mannopyranosyloxy)-biphenyl-4-yl)-1H-tetrazole (14).** A Schlenk tube was charged with 13g (30 mg, 0.06 mmol), trimethylsilyl azide (16  $\mu$ L, 0.12 mmol), dibutyltin oxide (2 mg, 0.006 mmol), DME (1 mL), and a stirring bar. The mixture was heated to 150 °C for 10 min by microwave irradiation. The reaction mixture was cooled to rt and then concentrated in vacuo. The residue was purified by MPLC on silica gel (DCM/MeOH, 9:1 to 8:1) to afford 14 (26 mg, 81%) as a colorless oil.  $[\alpha]_D^{20} +56.1$  (c 0.3, MeOH). <sup>1</sup>H NMR (500 MHz, CDCl<sub>3</sub>):  $\delta$  = 8.25–8.15 (m, 2H, Ar–H), 7.75–7.65 (m, 2H, Ar–H), 7.60–7.55 (m, 2H, Ar–H), 7.20–7.17 (m, 2H, Ar–H), 5.64–5.55 (m, 2H, H-1, H-3), 5.49 (dd, *J* = 1.7, 3.3 Hz, 1H, H-2), 5.40 (t, *J* = 10.1 Hz, 1H, H-4), 4.31 (dd, *J* = 5.3, 12.4 Hz, 1H, H-6a), 4.17–4.06 (m, 2H, H-5, H-6b), 2.22, 2.07, 2.06, 2.05 (4 s, 12H, 4 COCH<sub>3</sub>). <sup>13</sup>C NMR (126 MHz, CDCl<sub>3</sub>):  $\delta$  = 170.67, 170.14, 170.11, 169.81 (4 CO), 155.61, 128.36, 127.84, 127.49, 116.93 (Ar–C), 95.78 (C-1), 69.36 (C-5), 69.26 (C-2), 68.90 (C-3), 65.89 (C-4), 62.12 (C-6), 20.92, 20.76, 20.73 (4 COCH<sub>3</sub>). ESI-MS *m/z*, calcd for C<sub>27</sub>H<sub>28</sub>N<sub>4</sub>NaO<sub>10</sub> [M + Na]<sup>+</sup>: 591.2. Found: 591.1.

**5-(4'-( $\alpha$ -D-Mannopyranosyloxy)biphenyl-4-yl)-1H-tetrazole (10h).** Prepared according to the procedure described for 10e from 14 (26 mg, 0.03 mmol). Yield: 18 mg (quant) as a white solid.  $[\alpha]_D^{20} +112.1$  (c 0.1, MeOH/H<sub>2</sub>O, 2:1). <sup>1</sup>H NMR (500 MHz, CD<sub>3</sub>OD):  $\delta$  = 7.98–7.96 (m, 2H, Ar–H), 7.72–7.71 (m, 2H, Ar–H), 7.58–7.54 (m, 2H, Ar–H), 7.16–7.13 (m, 2H, Ar–H), 5.46 (d, *J* = 1.7 Hz, 1H, H-1), 3.94 (dd, *J* = 1.9, 3.5 Hz, 1H, H-2), 3.83 (dd, *J* = 3.4, 9.5 Hz, 1H, H-3), 3.68–3.61 (m, 3H, H-4, H-6a, H-6b), 3.52 (ddd, *J* = 2.5, 5.4, 9.7 Hz, 1H, H-5). <sup>13</sup>C NMR (126 MHz, CD<sub>3</sub>OD):  $\delta$  = 158.19, 145.07, 134.97, 129.29, 128.74, 128.55, 118.26 (Ar–C), 100.13 (C-1), 75.52 (C-5), 72.42 (C-3), 71.98 (C-2), 68.33 (C-4), 62.69 (C-6). HRMS *m/z*, calcd for C<sub>19</sub>H<sub>21</sub>N<sub>4</sub>O<sub>6</sub> [M + H]<sup>+</sup>: 401.1456. Found: 401.1450.

**4'-(2,3,4,6-Tetra-O-acetyl- $\alpha$ -D-mannopyranosyloxy)-3'-chlorobiphenyl-4-carbonitrile (19).** Prepared according to the procedure described for 13e from aryl iodide 18<sup>23</sup> (79 mg, 0.135 mmol), 12g (22 mg, 0.15 mmol), Pd(dppf)Cl<sub>2</sub>·CH<sub>2</sub>Cl<sub>2</sub> (3.3 mg, 4  $\mu$ mol), and K<sub>3</sub>PO<sub>4</sub> (57 mg, 0.27 mmol). Yield: 57 mg (75%) as a white solid.  $[\alpha]_D^{20} +77.7$  (c 0.5, CHCl<sub>3</sub>). <sup>1</sup>H NMR (500 MHz, CDCl<sub>3</sub>):  $\delta$  = 7.72 (d, *J* = 8.3 Hz, 2H, Ar–H), 7.63 (m, 3H, Ar–H), 7.43 (dd, *J* = 2.2, 8.6 Hz, 1H, Ar–H), 7.27 (d, *J* = 8.6 Hz, 1H, Ar–H), 5.64–5.59 (m, 2H, H-1, H-2), 5.54 (dd, *J* = 1.9, 3.2 Hz, 1H, H-3), 5.41 (t, *J* = 10.1 Hz, 1H, H-4), 4.28 (dd, *J* = 5.2, 12.3 Hz, 1H, H-6a), 4.17 (ddd, *J* = 2.1, 5.1, 10.0 Hz, 1H, H-5), 4.10 (dd, *J* = 2.2, 12.3 Hz, 1H, H-6b), 2.21 (s, 3H, COCH<sub>3</sub>), 2.12–2.00 (m, 9H, 3 COCH<sub>3</sub>). <sup>13</sup>C NMR (126 MHz, CDCl<sub>3</sub>):  $\delta$  = 170.54, 170.08, 169.90, 169.84, (4C, CO) 151.67, 143.61, 135.29, 132.87, 129.41, 127.53, 126.60, 125.20, 118.79, 117.36, 111.47 (Ar–C, CN), 96.72 (C-1), 70.00 (C-5), 69.39 (C-3), 68.82 (C-2), 65.86 (C-4), 62.16 (C-6), 20.98, 20.81, 20.79, 20.78 (4 COCH<sub>3</sub>). ESI-MS *m/z*, calcd for C<sub>27</sub>H<sub>26</sub>ClNNaO<sub>10</sub> [M + Na]<sup>+</sup>: 582.1. Found: 582.1.

**3'-Chloro-4'-( $\alpha$ -D-mannopyranosyloxy)biphenyl-4-carbonitrile (10j).** Prepared according to the procedure described for 10e from 19 (36 mg, 0.06 mmol). Yield: 12 mg (48%) as a white solid.  $[\alpha]_D^{20} +109.4$  (c 0.23, MeOH). <sup>1</sup>H NMR (500 MHz, CD<sub>3</sub>OD):  $\delta$  = 7.80–7.72 (m, 5H, Ar–H), 7.59 (dd, *J* = 2.2, 8.6 Hz, 1H, Ar–H), 7.48 (d, *J* = 8.7 Hz, 1H, Ar–H), 5.62 (d, *J* = 1.4 Hz, 1H, H-1), 4.12 (dd, *J* = 1.8, 3.3 Hz, 1H,

H-2), 4.00 (dd, *J* = 3.4, 9.5 Hz, 1H, H-3), 3.83–3.68 (m, 3H, H-4, H-6a, H-6b), 3.63 (ddd, *J* = 2.3, 5.4, 9.6 Hz, 1H, H-5). <sup>13</sup>C NMR (126 MHz, CD<sub>3</sub>OD):  $\delta$  = 153.65, 145.15, 135.42, 133.86, 129.82, 128.53, 127.87, 125.47, 119.70, 118.59 (Ar–C), 111.97 (CN), 100.66 (C-1), 76.05 (C-5), 72.39 (C-3), 71.80 (C-2), 68.20 (C-4), 62.65 (C-6). IR (KBr),  $\nu$  = 3400 (OH), 2227 (C $\equiv$ N), 1606, 1487 (Ar–C=C) cm<sup>-1</sup>. HRMS *m/z*, calcd for C<sub>19</sub>H<sub>18</sub>ClNNaO<sub>6</sub> [M + Na]<sup>+</sup>: 414.0715. Found: 414.0721.

**3'-Chloro-N-(3',6'-dihydroxy-3-oxo-3H-spiro-[isobenzofuran-1,9'-xanthen]-5-yl)-4'-( $\alpha$ -D-mannopyranosyloxy)biphenyl-4-carboxamide (22).** Compound 21 (10.0 mg, 0.024 mmol), fluoresceinamine isomer I (12.7 mg, 0.037 mmol), and COMU (20.9 mg, 0.049 mmol) were dissolved in dry DMF (1 mL). Then NEt<sub>3</sub> (10  $\mu$ L, 0.073 mmol) was added and the mixture was stirred at rt for 7 h. 1 N HCl in DMF was added until acid reaction on pH paper and the mixture was concentrated. The residue was dissolved in DCM/MeOH (3:1) and loaded onto a silica gel column. The complex mixture of compounds was only partially resolved. The fractions containing the product were collected, concentrated, and purified by preparative HPLC (gradient H<sub>2</sub>O/MeCN, +0.2% HCO<sub>2</sub>H) to afford compound 22 (5 mg, 19%).  $[\alpha]_D^{20} +21.1$  (c 0.10, MeOH). <sup>1</sup>H NMR (500 MHz, CD<sub>3</sub>OD):  $\delta$  = 8.26 (d, *J* = 8.4 Hz, 2H, Ar–H), 7.88–7.74 (m, 3H, Ar–H), 7.66 (dd, *J* = 2.2, 8.6 Hz, 1H, Ar–H), 7.51 (d, *J* = 8.7 Hz, 1H, Ar–H), 7.29 (dd, *J* = 1.9, 5.3 Hz, 2H, Ar–H), 7.19 (dd, *J* = 2.1, 8.3 Hz, 1H, Ar–H), 7.08–6.99 (m, 2H, Ar–H), 6.95 (d, *J* = 8.7 Hz, 1H, Ar–H), 6.72 (dd, *J* = 5.5, 10.6 Hz, 2H, Ar–H), 6.61 (dd, *J* = 2.3, 8.7 Hz, 1H, Ar–H), 5.65 (s, 1H, H-1), 4.15 (dd, *J* = 1.8, 3.2 Hz, H-2), 4.03 (dd, *J* = 3.4, 9.5 Hz, H-3), 3.87–3.72 (m, 3H, H-4, H-6a, H-6b), 3.65 (m, 1H, H-5). <sup>13</sup>C NMR (126 MHz, CD<sub>3</sub>OD):  $\delta$  = 137.50, 136.01, 131.90, 130.24, 130.20, 129.87, 129.24, 128.03, 127.91, 125.79, 125.46, 124.73, 118.99, 118.76, 118.65 (Ar–C), 100.73 (C-1), 76.06 (C-5), 72.42 (C-3), 71.85 (C-2), 68.24 (C-4), 62.69 (C-2). ESI-MS *m/z*, calcd for C<sub>39</sub>H<sub>31</sub>ClNO<sub>12</sub> [M + H]<sup>+</sup>: 740.2. Found: 740.2.

**3'-Chloro-N-(2-(3-(3',6'-dihydroxy-3-oxo-3H-spiro-[isobenzofuran-1,9'-xanthen]-5-yl)thioureido)ethyl)-4'-( $\alpha$ -D-mannopyranosyloxy)biphenyl-4-carboxamide (23).** To a stirred solution of compound 21 (25 mg, 0.061 mmol) in dry DMF (1 mL), NHS (21 mg, 0.183 mmol) was added, followed by DIC (9.2 mg, 0.073 mmol). The mixture was stirred at rt for 2 h. Then *N*-Boc-ethylendiamine (10.7 mg, 0.067 mmol) was added and the reaction was stirred for 10 h. It was then cooled down to 0 °C, diluted with water, and concentrated. Chromatography on silica gel (DCM/MeOH) yielded 23 mg (0.042 mmol, 68%) of *tert*-butyl (3'-chloro-4'-( $\alpha$ -D-mannopyranosyloxy)biphenyl-4-yl-carboxamido)ethylcarbamate. This product was dissolved in DCM (3 mL), and TFA (1 mL) was added. The solid dissolved during addition of TFA. After 10 min the reaction was complete. The mixture was evaporated, and excess TFA was removed in high vacuum. The intermediate *N*-(2-aminoethyl)-3'-chloro-4'-( $\alpha$ -D-mannopyranosyloxy)biphenyl-4-carboxamide TFA salt (23 mg, 0.042 mmol, quant) was used directly in the next step. It was dissolved in dry DMF (0.5 mL), and NEt<sub>3</sub> (12.8 mg, 0.127 mmol) was added. The mixture was cooled to 0 °C. Then FITC (14.8 mg, 0.038 mmol) was added and the mixture was stirred for 3 h in the dark. The mixture was then coevaporated with water, taken up in MeOH/10% aq acetic acid and evaporated. Chromatography on silica gel (DCM/MeOH) yielded compound 23, contaminated with triethylammonium acetate. The compound was then redissolved in MeOH, and 0.5 N HCl in MeOH was added. The mixture was evaporated and chromatographed on silica gel to yield pure 23 (15 mg, 47%).  $[\alpha]_D^{20} +12.1$  (c 0.30, MeOH). <sup>1</sup>H NMR (500 MHz, CD<sub>3</sub>OD):  $\delta$  = 8.12 (s, 1H), 7.92 (d, *J* = 8.3 Hz, 2H, Ar–H), 7.70 (dd, *J* = 5.0, 13.1 Hz, 2H, Ar–H), 7.64 (d, *J* = 8.3 Hz, 2H, Ar–H), 7.54 (dd, *J* = 2.2, 8.6 Hz, 1H, Ar–H), 7.46 (d, *J* = 8.7 Hz, 1H, Ar–H), 7.09 (d, *J* = 8.2 Hz, 1H, Ar–H), 6.74 (s, 2H), 6.69 (d, *J* = 1.4 Hz, 2H, Ar–H), 6.55 (d, *J* = 8.4 Hz, 2H, Ar–H), 5.63 (d, *J* = 1.3 Hz, H-1), 4.15 (dd, *J* = 1.8, 3.1 Hz, H-2), 4.03 (dd, *J* = 3.4, 9.5 Hz, H-3), 3.94 (s, 2H, CH<sub>2</sub>), 3.86–3.64 (m, 6H, H-4, H-5, H-6, CH<sub>2</sub>). <sup>13</sup>C NMR (126 MHz, CD<sub>3</sub>OD):  $\delta$  = 153.21, 143.84, 136.41, 129.66, 129.18, 127.76, 127.70, 125.37, 118.64, 103.62 (Ar–C), 100.75 (C-1), 76.00 (C-5), 72.41 (C-3), 71.86 (C-2), 68.24 (C-4), 62.69 (C-6), 40.76 (CH<sub>2</sub>). ESI-MS *m/z*, calcd for C<sub>42</sub>H<sub>37</sub>ClN<sub>3</sub>O<sub>12</sub>S [M + H]<sup>+</sup>: 842.2. Found: 842.2.

**3'-Chloro-N-(2-(2-(2-(3-(3',6'-dihydroxy-3-oxo-3H-spiro[isobenzofuran-1,9'-xanthene]-5-yl)thioureido)ethoxy)ethoxy)ethyl)-4'-( $\alpha$ -D-mannopyranosyloxy)biphenyl-4-carboxamide (24).** Compound 21 (280 mg, 0.68 mmol) was dissolved in dry DMF (5 mL) under argon. Then NHS (235 mg, 2.04 mmol) was added, followed by DIC (0.12 mL, 0.78 mmol) and the mixture was stirred at rt for 4 h. Then Boc-PEG2-NH<sub>2</sub> (186 mg, 0.75 mmol) was added, and the mixture was stirred at rt under argon for 10 h. It was then slowly diluted with water and concentrated. The residue was purified by chromatography on silica gel (DCM/MeOH) to give *tert*-butyl (2-(2-(2-(3'-chloro-4'-( $\alpha$ -D-mannopyranosyloxy)biphenyl-4-ylcarboxamido)ethoxy)ethoxy)ethyl)-carbamate (300 mg, 0.468 mmol, 69%). Then the carbamate was suspended in DCM (3 mL), and TFA (1 mL) was added dropwise at rt. After 30 min, the solvents were evaporated and the crude mixture was dissolved in CHCl<sub>3</sub>/MeOH (6:4, +0.5% conc NH<sub>4</sub>OH) and transferred to a silica gel column, eluting with the same solvent mixture, to yield N-(2-(2-(2-aminoethoxy)ethoxy)ethyl)-3'-chloro-4'-( $\alpha$ -D-mannopyranosyloxy)biphenyl-4-carboxamide (228 mg, 90%). A fraction of the amine (10 mg, 0.018 mmol) was dissolved in dry DMF (0.5 mL) and cooled to 0 °C. FITC (6.5 mg, 0.017 mmol) was added, and the mixture was stirred for 1 h. The mixture was concentrated and the residue was purified by chromatography on silica (DCM/MeOH) to yield 24 (10 mg, 65%). <sup>1</sup>H NMR (500 MHz, CD<sub>3</sub>OD):  $\delta$  = 8.21 (d, *J* = 1.4 Hz, 1H, Ar-H), 7.88 (d, *J* = 8.3 Hz, 2H, Ar-H), 7.68 (d, *J* = 2.2 Hz, 2H, Ar-H), 7.63 (d, *J* = 8.3 Hz, 2H, Ar-H), 7.53 (dd, *J* = 2.2, 8.6 Hz, 1H, Ar-H), 7.43 (d, *J* = 8.7 Hz, 1H, Ar-H), 7.09 (d, *J* = 8.2 Hz, 1H, Ar-H), 6.68 (d, *J* = 2.3 Hz, 2H, Ar-H), 6.65 (dd, *J* = 2.6, 8.6 Hz, 2H, Ar-H), 6.53 (dd, *J* = 1.6, 8.7 Hz, 2H, Ar-H), 5.61 (d, *J* = 1.3 Hz, 1H, H-1), 4.14 (dd, *J* = 1.8, 3.2, Hz, 1H, H-2), 4.03 (dd, *J* = 3.4, 9.5 Hz, 1H, H-3), 3.93–3.53 (m, 16H), 3.37 (s, 2H, NCH<sub>2</sub>), 1.30 (s, 2H, CH<sub>2</sub>). <sup>13</sup>C NMR (126 MHz, CD<sub>3</sub>OD):  $\delta$  = 170.01 (CO), 153.17, 143.72, 136.37, 134.37, 130.39, 129.69, 129.04, 127.78, 127.73, 125.35, 118.60, 103.60 (Ar-C), 100.72 (C-1), 75.97 (C-5), 72.41 (C-3), 71.86, 71.40, 70.59 (5C, C-2, OCH<sub>2</sub>), 68.23 (C-4), 62.64 (C-6), 49.88, 45.49, 40.97 (CH<sub>2</sub>). ESI-MS *m/z*, calcd for C<sub>46</sub>H<sub>44</sub>ClN<sub>3</sub>O<sub>14</sub>S [M + H]<sup>+</sup>: 930.2. Found: 930.4.

**Competitive Fluorescence Polarization Assay.** *Expression and Purification of CRD of FimH.* A recombinant protein consisting of the CRD of FimH linked to a 6His-tag via a thrombin cleavage site (FimH-CRD-Th-His<sub>6</sub>) was expressed in *E. coli* strain HM125 and purified by affinity chromatography as previously described.<sup>43</sup>

*K<sub>D</sub> Determination of FITC-Labeled Ligands.* The functionalized ligands (23, 24) were prepared as a 10 mM stock solution in pure DMSO (Sigma-Aldrich, Buchs, Switzerland). All further dilutions of compounds and FimH-CRD-Th-His<sub>6</sub> protein were prepared in assay buffer (20 mM HEPES, 150 mM NaCl, 50  $\mu$ g/mL BSA, pH 7.4). BSA was added to the assay buffer to prevent nonspecific binding of protein to the plastic surface. Binding isotherms for the fluorescent ligands were obtained in direct binding studies by adding a constant concentration of ligand (final concentration 5 nM) and a linear dilution of protein (final concentration 0–100 nM) to a final volume of 200  $\mu$ L in 96-well, black, flat bottom NBS plates (Corning Inc., Corning, NY, USA). After incubation of the plate for 24 h at rt with gentle shaking, the fluorescence polarization was measured with the Synergy H1 hybrid multimode microplate reader (BioTek Instruments Inc., Winooski, VT, USA) with polarized excitation at 485 nm and emission measured at 528 nm through polarizing filters parallel and perpendicularly oriented to the incident polarized light. *K<sub>D</sub>* values were determined by plotting the FP readout as a function of the protein concentration and applying the following single-site binding equation (eq 1) that accounts for ligand depletion:

$$S_{\text{obs}} = S_{\text{F}} + (S_{\text{B}} - S_{\text{F}}) \times \left( \frac{C_{\text{P}} + C_{\text{L}} + K_{\text{D}} - \sqrt{(C_{\text{P}} + C_{\text{L}} + K_{\text{D}})^2 - 4C_{\text{P}}C_{\text{L}}}}{2C_{\text{L}}} \right) \quad (1)$$

where *S<sub>obs</sub>* is the observed signal from the ligand, *S<sub>F</sub>* is the signal from free ligand, *S<sub>B</sub>* is the signal from bound ligand, *C<sub>P</sub>* is the total concentration of protein, and *C<sub>L</sub>* is the total concentration of ligand.<sup>49</sup>

*K<sub>D</sub> Determination of FimH Antagonists.* The fluorescently labeled ligand 23 was used for the competitive fluorescence polarization assay. A linear dilution of nonlabeled FimH antagonist with final concentrations ranging from 0 to 10  $\mu$ M was titrated into 96-well, black, flat-bottom NBS plates (Corning Inc.) to a final volume of 200  $\mu$ L containing a constant concentration of protein (final concentration 25 nM) and FITC-labeled ligand which was fixed at a higher concentration in competitive binding assays than in direct binding experiments to obtain higher fluorescence intensities (final concentration 20 nM). Prior to measuring the fluorescence polarization, the plates were incubated on a shaker for 24 h at rt until the reaction reached equilibrium. The IC<sub>50</sub> value was determined with Prism (GraphPad Software Inc., La Jolla, CA, USA) by applying a standard four-parameter IC<sub>50</sub> function. The obtained IC<sub>50</sub> values were converted into their corresponding *K<sub>D</sub>* values using the derivation of the Cheng–Prusoff equation.<sup>45</sup> This variation of the Cheng–Prusoff equation is applied to competition assays with tight-binding inhibitors and includes terms to correct for ligand depletion effects. However, the *K<sub>D</sub>* for antagonists having a higher affinity toward FimH than the labeled ligand could not be accurately determined.<sup>45</sup>

**Isothermal Titration Calorimetry (ITC).** All ITC experiments were performed with the FimH-CRD-Th-His<sub>6</sub> protein using a VP-ITC instrument from MicroCal, Inc. (Malvern Instruments, Worcestershire, U.K.) with a sample cell volume of 1.4523 mL. The measurements were performed with 0–5% DMSO at 25 °C, a stirring speed of 307 rpm, and 10  $\mu$ cal s<sup>-1</sup> reference power. The protein samples were dialyzed in assay buffer prior to all experiments. Because of the high protein consumption of ITC, only the experiments for the reference compounds (1, 3, and 25) were measured in duplicates. Compounds 1, 3, 9, and 25 were measured in a direct fashion by titration of ligand (100–2,000  $\mu$ M) into protein (8.6–55  $\mu$ M) with injections of 3–8  $\mu$ L at intervals of 10 min to ensure nonoverlapping peaks. The quantity *c* = Mt(0)*K<sub>D</sub>*<sup>-1</sup>, where Mt(0) is the initial macromolecule concentration, is of importance in titration microcalorimetry. The *c*-values of the direct titrations were below 1000 and thus within the reliable range. For the compounds 10b–e, 10g, and 10j additional competitive ITC experiments were performed because of their high affinity resulting in *c*-values above 1000 for direct titrations. These ligands (600  $\mu$ M) were titrated into protein (30  $\mu$ M), which was preincubated with compound 25 (300  $\mu$ M) resulting in sigmoidal titration curves. Because of slow reaction kinetics, titration intervals of 20 min were used.

Baseline correction and peak integration were performed using the Origin 7 software (OriginLab, Northampton, MA, USA). An initial 2  $\mu$ L injection was excluded from data analysis. Baseline subtraction and curve-fitting with the three variables *N* (concentration correction factor), *K<sub>D</sub>* (dissociation constant), and  $\Delta H^\circ$  (change in enthalpy) were performed with the SEDPHAT software, version 10.40 (National Institutes of Health).<sup>86</sup> A global fitting analysis was performed for the competition titration (10b–e, 10g, or 10j competing for the protein binding site with compound 25) and the direct titration of the competitor (compound 25 binding to protein) to fit for *K<sub>D</sub>*,  $\Delta H^\circ$  and *N* were fitted from direct titrations of 10b–e, 10g, or 10j into protein. For the compounds 3, 9, and 25 binding to protein all variables could be determined from a global analysis of the direct titration.

The thermodynamic parameters were calculated with the following equation (eq 2):

$$\Delta G^\circ = \Delta H^\circ - T\Delta S^\circ = RT \ln K_{\text{D}} = -RT \ln K_{\text{A}} \quad (2)$$

where  $\Delta G^\circ$ ,  $\Delta H^\circ$ , and  $\Delta S^\circ$  are the changes in free energy, enthalpy, and entropy of binding, respectively, *T* is the absolute temperature, and *R* is the universal gas constant (8.314 J mol<sup>-1</sup> K<sup>-1</sup>). The 95% confidence intervals of the measurements were calculated for the two variables *K<sub>D</sub>* and  $\Delta H^\circ$  with the one-dimensional error surface projection within the SEDPHAT software.

**Calculation of the Free Energy of Desolvation.** The three-dimensional representation for each of the aglycons (4-methoxybiphenyl scaffold, Figure 8) was built in the Maestro<sup>87</sup> modeling environment, and the global minimum conformation was identified by performing 500 iterations of the mixed torsional/low-mode conformational sampling in combination with the OPLS-2005 force-field and the implicit solvent model (water) as implemented in the MacroModel

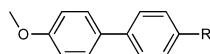


Figure 8. 4-Methoxybiphenyl scaffold of aglycons.

9.9.<sup>88</sup> The global minimum structures were used as input for the AMSOL 7.1 program<sup>89</sup> to obtain the free energy of desolvation  $\Delta G_{\text{des}}$  (Table 5) with the SM5.4A solvation model<sup>90</sup> and the AM1<sup>91</sup> level of theory (used keywords “AM1 SM5.4A SOLVNT=WATER TRUES”).

Table 5. Aqueous Free Energy of Desolvation

R	$\Delta G_{\text{des}}$ [kJ/mol]
neutral	
H	15.6
CONHCH <sub>3</sub>	39.9
COOCH <sub>3</sub>	23.0
SO <sub>2</sub> NHCH <sub>3</sub>	65.5
SO <sub>2</sub> CH <sub>3</sub>	56.4
4-morpholineamide	45.3
CN	22.0
deprotonated	
COO <sup>-</sup>	298.2
SO <sub>2</sub> -N <sup>-</sup> -Me	342.0

**Determination of the MAC<sub>90</sub> by Flow Cytometry.** The MAC<sub>90</sub> was determined in principle as in the previously published flow cytometry assay<sup>79</sup> but with some modifications. The human epithelial bladder carcinoma cell line 5637 (DSMZ, Braunschweig, Germany) was grown in RPMI 1640 medium, supplemented with 10% fetal calf serum (FCS), 100 U/mL penicillin, and 100  $\mu$ g/mL streptomycin at 37 °C, 5% CO<sub>2</sub>. All solutions were purchased from Invitrogen (Basel, Switzerland). The cells were subcultured 1:6 twice per week [using trypsin/EDTA (Sigma-Aldrich) for the detachment]. Two days before infection,  $1.8 \times 10^5$  cells were seeded in each well of a 24-well plate in RPMI 1640 containing 10% FCS without antibiotics. The cell density was approximately  $(3-5) \times 10^5$  cells/well at the assay day.

For infection, the GFP-expressing clinical *E. coli* isolate UTI89<sup>92</sup> (UTI89 wt) and the GFP-expressing FimA-H knockout strain UTI89  $\Delta$ fimA-H were used (strains were provided by Prof. Urs Jenal, Biocenter, University of Basel, Switzerland).<sup>79</sup> Bacteria were cultivated at 37 °C in 10 mL Luria–Bertani (LB) broth (Becton, Dickinson and Company) overnight, harvested by centrifugation (3800 rpm, 10 min), and washed three times in phosphate buffered saline (PBS, Sigma-Aldrich), and a bacterial solution of OD<sub>600</sub> of 0.75 in RPMI + 10% FCS was prepared. For the determination of the MAC<sub>90</sub> value, the IC<sub>90</sub>, linear dilutions of the FimH antagonist were prepared in 5% DMSO and PBS. Bacteria and antagonists were preincubated for 10 min at 37 °C, before cells were infected with either only 200  $\mu$ L of bacterial solution of UTI89 or UTI89  $\Delta$ fimA-H (positive and negative controls), or 225  $\mu$ L of the preincubated bacteria–antagonist mixture. Infection lasted for 1.5 h. During this time infected cells were incubated at 37 °C. Then, cells were washed with PBS and detached from wells by the addition of 150  $\mu$ L of trypsin and incubation at 37 °C for 10 min, before flushing from wells PBS containing 2% FCS and transferred to tubes. To dilute the trypsin, cells were centrifuged at 13 000 rpm, 1 min, 600  $\mu$ L of the supernatant was discarded, and the pellet was resuspended in the remaining 300  $\mu$ L of PBS containing 2% FCS. Samples were stored on ice until measurement. Before analysis with the flow cytometer (Becton Dickinson, FACSCanto II), the samples were gently mixed and filtered using a 35  $\mu$ m nylon mesh (Corning Life Sciences) to prevent cellular aggregation. Cells were gated with linear scaling for side scatter (SSC) and forward scatter (FSC) and GFP intensity of live cells was evaluated. IC<sub>90</sub> values were determined by plotting the concentration of the antagonist in a logarithmic mode versus the mean fluorescence intensity (MFI) of living cells and by fitting a dose–response curve (variable slope, four parameters) with the Prism software (GraphPad Prism).

**X-ray Analysis of the Antagonists 10e and 10j Cocrystallized with FimH-CRD.** *FimH-CRD/10e Cocrystallization.* Initial FimH-CRD (18 mg/mL in 20 mM HEPES, pH 7.4) crystals were obtained in complex with 4-(5-nitroindolin-1-yl)phenyl  $\alpha$ -D-mannopyranoside (5 mM).<sup>23</sup> Crystals were grown in sitting-drop vapor diffusion at 20 °C with 200 nL of protein–antagonist mixture together with 200 nL of precipitant solution in well D3 (0.2 M sodium phosphate monobasic monohydrate, 20% w/v PEG 3,350) of the PEG/Ion HT screen (Hampton Research, CA, USA). Cubic crystals appeared within 1 week, which served as cross-seeding crystals. A solution of FimH-CRD (20 mg/mL) and 10e (5 mM) was mixed with 0.2 M sodium phosphate monobasic monohydrate, 20% w/v PEG 400 with 0.5  $\mu$ L of each solution. Streak-seeding was performed after 1 day of incubation. Cubic FimH-CRD/10e crystals formed within 24 h. Crystals were flash cooled to 100 K with perfluoropolyether cryo oil (Hampton Research, CA, USA) as cryoprotectant. Data were collected with synchrotron radiation ( $\lambda = 0.999\ 99\ \text{\AA}$ ) at the PXIII beamline, Swiss Light Source, Switzerland.

*FimH-CRD/10j Cocrystallization.* Cocrystals were initially grown in sitting-drop vapor diffusion at 20 °C with 0.5  $\mu$ L of a mixture of FimH-CRD (20 mg/mL) and 10j (5 mM) together with 0.5  $\mu$ L of 0.1 M HEPES, pH 7.5, 2 M ammonium sulfate. Platelike crystals formed within 2 weeks and were used as seeds for subsequent crystallization. Diffraction quality crystals were grown by streak-seeding in 0.5  $\mu$ L of FimH-CRD (10 mg/mL) with 10j (2.5 mM) and 0.5  $\mu$ L of 0.1 M HEPES, pH 7.5, 1.25 M ammonium sulfate. The drops were covered with perfluoropolyether cryo oil prior to flash cooling to 100 K. Data were collected with synchrotron radiation ( $\lambda = 1.000\ 03\ \text{\AA}$ ) at the PXIII beamline, Swiss Light Source, Switzerland.

*Structure Determination and Refinement.* Data were indexed and integrated with the XDS package<sup>93</sup> for the FimH-CRD/10e cocrystal structure, and with mosflm<sup>94</sup> for the FimH-CRD/10j cocrystal structure (Table 6). Scaling was performed with XDS and SCALA included in the CCP4 suite, respectively.<sup>95</sup> Structures were solved by molecular

Table 6. Data Collection and Refinement Statistics for FimH-CRD/10e and FimH-CRD/10j Cocrystals

	FimH-CRD/10e	FimH-CRD/10j
PDB code	4CSS	4CST
space group	$P2_12_12_1$	$P2_12_12_1$
no. of molecules in the asymmetric unit	1	1
Cell Dimensions		
<i>a</i> , <i>b</i> , <i>c</i> (Å)	48.38, 56.23, 61.59	48.84, 55.89, 61.00
$\alpha$ , $\beta$ , $\gamma$ (deg)	90, 90, 90	90, 90, 90
Data Collection		
beamline	Swiss Light Source PXIII	Swiss Light Source PXIII
resolution range (Å) <sup>a</sup>	30.0–1.07 (1.13–1.07)	23.5–1.10 (1.12–1.10)
unique observations <sup>a</sup>	72000 (9354)	66470 (2500)
average multiplicity <sup>a</sup>	10.9 (3.7)	5.4 (2.4)
completeness (%)	96.1 (78.0)	97.2 (76.5)
$R_{\text{merge}}$ <sup>a</sup>	0.056 (0.57)	0.051 (0.305)
mean $I/\sigma(I)$ <sup>a</sup>	21.5 (2.22)	15.5 (2.9)
Refinement		
resolution range (Å)	15.7–1.07	23.5–1.10
$R$ , $R_{\text{free}}$	11.2, 13.2	11.4, 13.0
rms deviation from ideal bond length (Å)	0.010	0.010
rms deviation from ideal bond angle (deg)	1.170	1.420

<sup>a</sup>Values in parentheses are for highest-resolution shell.



replacement with PHASER<sup>96</sup> using the FimH-CRD-butyl  $\alpha$ -D-mannopyranoside complex (PDB code 1UWF) as search model. The structures were iteratively built using the COOT software<sup>97</sup> and refined with the PHENIX software.<sup>98</sup> Geometric restraints for **10e** and **10j** were generated with PRODRG.<sup>99</sup> The models were validated using molprobit.<sup>100</sup> Residues 113–115 were not modeled in the **10e** structure because of disorder. Furthermore, the ligand was modeled in two possible conformations. For both ligands, electron density is reduced on the second aromatic ring because of flexibility of the ligand.

**Physicochemical and in Vitro Pharmacokinetic Studies.**  
**Materials.** Dimethyl sulfoxide (DMSO), 1-propanol, 1-octanol, Dulbecco's modified Eagle medium (DMEM)—high glucose, L-glutamine solution, penicillin–streptomycin solution, Dulbecco's phosphate buffered saline (DPBS), trypsin–EDTA solution, magnesium chloride hexahydrate, and reduced nicotinamide adenine dinucleotide phosphate (NADPH) were purchased from Sigma-Aldrich. MEM nonessential amino acid (MEM-NEAA) solution, fetal bovine serum (FBS), and DMEM without sodium pyruvate and phenol red were bought from Invitrogen (Carlsbad, CA, USA). PRISMA HT universal buffer, GIT-0 Lipid Solution, and Acceptor Sink Buffer were ordered from pIon (Woburn, MA, USA). Human plasma was bought from Biopredic (Rennes, France), and acetonitrile (MeCN) and methanol (MeOH) were from Acros Organics (Geel, Belgium). Pooled male rat liver microsomes were purchased from BD Bioscience (Franklin Lakes, NJ, USA). Tris(hydroxymethyl)aminomethane (TRIS) was obtained from AppliChem (Darmstadt, Germany). The Caco-2 cells were kindly provided by Prof. G. Imanidis, FHNW, Muttentz, and originated from the American Type Culture Collection (Rockville, MD, USA).

$pK_a$ . The  $pK_a$  values were determined as described elsewhere.<sup>101</sup> In brief, the pH of a sample solution was gradually changed and the chemical shift of protons adjacent to ionizable centers was monitored by <sup>1</sup>H nuclear magnetic resonance (NMR) spectroscopy. The shift was plotted against the pH of the respective sample, and the  $pK_a$  was read out from the inflection point of the resulting sigmoidal curve.

$\log D_{7.4}$ . The *in silico* prediction tool ALOGPS<sup>102</sup> was used to estimate  $\log P$  values of the compounds. Depending on these values, the compounds were classified into three categories: hydrophilic compounds ( $\log P$  below zero), moderately lipophilic compounds ( $\log P$  between zero and one), and lipophilic compounds ( $\log P$  above one). For each category, two different ratios (volume of 1-octanol to volume of buffer) were defined as experimental parameters (Table 7).

**Table 7. Compound Classification Based on Estimated  $\log P$  Values**

compd type	$\log P$	ratio (1-octanol/buffer)
hydrophilic	<0	30:140, 40:130
moderately lipophilic	0–1	70:110, 110:70
lipophilic	>1	3:180, 4:180

Equal amounts of phosphate buffer (0.1 M, pH 7.4) and 1-octanol were mixed and shaken vigorously for 5 min to saturate the phases. The mixture was left until separation of the two phases occurred, and the buffer was retrieved. Stock solutions of the test compounds were diluted with buffer to a concentration of 1  $\mu$ M. For each compound, six determinations, that is, three determinations per 1-octanol/buffer ratio, were performed in different wells of a 96-well plate. The respective volumes of buffer containing analyte (1  $\mu$ M) were pipetted to the wells and covered by saturated 1-octanol according to the chosen volume ratio. The plate was sealed with aluminum foil, shaken (1350 rpm, 25 °C, 2 h) on a Heidolph Titramax 1000 plate-shaker (Heidolph Instruments GmbH & Co. KG, Schwabach, Germany), and centrifuged (2000 rpm, 25 °C, 5 min, 5804 R Eppendorf centrifuge, Hamburg, Germany). The aqueous phase was transferred to a 96-well plate for analysis by LC–MS.

The  $\log D_{7.4}$  coefficient was calculated from the 1-octanol/buffer ratio ( $o/b$ ), the initial concentration of the analyte in buffer (1  $\mu$ M), and the concentration of the analyte in buffer ( $c_B$ ) with eq 3:

$$\log D_{7.4} = \log \left( \frac{1 \mu\text{M} - c_B}{c_B} \frac{1}{o/b} \right) \quad (3)$$

**Aqueous Solubility.** Solubility was determined in a 96-well format using the  $\mu$ SOL Explorer solubility analyzer (pIon, version 3.4.0.5). For each compound, measurements were performed at pH 3.0 and 7.4 in triplicate. For this purpose, six wells of a deep well plate, that is, three wells per pH value, were filled with 300  $\mu$ L of PRISMA HT universal buffer, adjusted to pH 3.0 or 7.4 by adding the requested amount of NaOH (0.5 M). Aliquots (3  $\mu$ L) of a compound stock solution (10–50 mM in DMSO) were added and thoroughly mixed. The final sample concentration was 0.1–0.5 mM, and the residual DMSO concentration was 1.0% (v/v) in the buffer solutions. After 15 h, the solutions were filtered (0.2  $\mu$ m 96-well filter plates) using a vacuum to collect manifold (Whatman Ltd., Maidstone, U.K.) to remove the precipitates. Equal amounts of filtrate and 1-propanol were mixed and transferred to a 96-well plate for UV/vis detection (190–500 nm, SpectraMax 190). The amount of material dissolved was calculated by comparison with UV/vis spectra obtained from reference samples, which were prepared by dissolving compound stock solution in a 1:1 mixture of buffer and 1-propanol (final concentrations 0.017–0.083 mM).

**Parallel Artificial Membrane Permeation Assay (PAMPA).** Effective permeability ( $\log P_e$ ) was determined in a 96-well format with the PAMPA.<sup>60</sup> For each compound, measurements were performed at pH 5.0 and 7.4 in quadruplicates. Eight wells of a deep well plate, that is, four wells per pH value, were filled with 650  $\mu$ L of PRISMA HT universal buffer adjusted to pH 5.0 or 7.4 by adding the requested amount of NaOH (0.5 M). Samples (150  $\mu$ L) were withdrawn from each well to determine the blank spectra by UV/vis spectroscopy (190–500 nm, SpectraMax 190). Then analyte dissolved in DMSO was added to the remaining buffer to yield 50  $\mu$ M solutions. To exclude precipitation, the optical density was measured at 650 nm, with 0.01 being the threshold value. Solutions exceeding this threshold were filtered. Afterward, samples (150  $\mu$ L) were withdrawn to determine the reference spectra. Further 200  $\mu$ L was transferred to each well of the donor plate of the PAMPA sandwich (pIon, P/N 110163). The filter membranes at the bottom of the acceptor plate were infused with 5  $\mu$ L of GIT-0 lipid solution, and 200  $\mu$ L of Acceptor Sink Buffer was filled into each acceptor well. The sandwich was assembled, placed in the GutBox, and left undisturbed for 16 h. Then it was disassembled and samples (150  $\mu$ L) were transferred from each donor and acceptor well to UV plates for determination of the UV/vis spectra. Effective permeability ( $\log P_e$ ) was calculated from the compound flux deduced from the spectra, the filter area, and the initial sample concentration in the donor well with the aid of the PAMPA Explorer software (pIon, version 3.5).

**Colorectal Adenocarcinoma (Caco-2) Cell Permeation Assay.** Caco-2 cells were cultivated in tissue culture flasks (BD Biosciences) with DMEM high glucose medium, containing L-glutamine (2 mM), nonessential amino acids (0.1 mM), penicillin (100 U/mL), streptomycin (100  $\mu$ g/mL), and fetal bovine serum (10%). The cells were kept at 37 °C in humidified air containing 5% CO<sub>2</sub>, and the medium was changed every second day. When approximately 90% confluence was reached, the cells were split in a 1:10 ratio and distributed to new tissue culture flasks. At passage numbers between 60 and 65, they were seeded at a density of  $5.3 \times 10^5$  cells per well to Transwell six-well plates (Corning Inc.) with 2.5 mL of culture medium in the basolateral and 1.8 mL in the apical compartment. The medium was renewed on alternate days. Permeation experiments were performed between days 19 and 21 after seeding. Prior to the experiment, the integrity of the Caco-2 monolayers was evaluated by measuring the transepithelial electrical resistance (TEER) with an Endohm tissue resistance instrument (World Precision Instruments Inc., Sarasota, FL, USA). Only wells with TEER values higher than 250  $\Omega$  cm<sup>2</sup> were used. Experiments were performed in the apical-to-basolateral (absorptive) and basolateral-to-apical (secretory) directions in triplicate. Transport medium (DMEM without sodium pyruvate and phenol red) was withdrawn from the donor compartments of three wells and replaced by the same volume of compound stock solution (10 mM in DMSO) to reach an initial sample concentration of 62.5  $\mu$ M. The Transwell plate was then shaken (600 rpm, 37 °C) on a Heidolph



Titramax 1000 plate-shaker. Samples (40  $\mu\text{L}$ ) were withdrawn from the donor and acceptor compartments 30 min after initiation of the experiment, and the compound concentrations were determined by LC–MS (see below). Apparent permeability ( $P_{\text{app}}$ ) was calculated according to eq 4:

$$P_{\text{app}} = \frac{dQ}{dt} \frac{1}{Ac_0} \quad (4)$$

where  $dQ/dt$  is the compound flux ( $\text{mol s}^{-1}$ ),  $A$  is the surface area of the monolayer ( $\text{cm}^2$ ), and  $c_0$  is the initial concentration in the donor compartment ( $\text{mol cm}^{-3}$ ).<sup>60</sup> After the experiment, TEER values were assessed again for each well and results from wells with values below 250  $\Omega \text{ cm}^2$  were discarded.

**Plasma Protein Binding (PPB).** PPB was determined in a 96-well format using a high throughput dialysis block (HTD96b; HTDialysis LCC, Gales Ferry, CT, USA). For each compound, measurements were performed in triplicate. Dialysis membranes (MWCO 12–14 K; HTDialysis LCC) were hydrated according to the instructions of the manufacturer and placed into the dialysis block. Human plasma was centrifuged (5800 rpm, 5  $^{\circ}\text{C}$ , 10 min), the pH of the supernatant (without floating plasma lipids) was adjusted to 7.4 by adding the requested amount of HCl (4 M), and analyte was added to yield a final concentration of 10  $\mu\text{M}$ . Equal volumes (150  $\mu\text{L}$ ) of plasma containing the analyte or TRIS–HCl buffer (0.1 M, pH 7.4) were transferred to the compartments separated by the dialysis membrane. The block was covered with a sealing film and left undisturbed (5 h, 37  $^{\circ}\text{C}$ ). Afterward, samples (90  $\mu\text{L}$ ) were withdrawn from the buffer compartments and diluted with plasma (10  $\mu\text{L}$ ). From the plasma compartments, samples (10  $\mu\text{L}$ ) were withdrawn and diluted with TRIS–HCl buffer (90  $\mu\text{L}$ ). The solutions were further diluted with ice-cooled MeCN (300  $\mu\text{L}$ ) to precipitate the proteins and centrifuged (3600 rpm, 4  $^{\circ}\text{C}$ , 10 min). The supernatants (50  $\mu\text{L}$ ) were retrieved, and the analyte concentrations were determined by LC–MS (see below). The fraction bound ( $f_b$ ) was calculated as follows (eq 5):

$$f_b = 1 - \frac{c_b}{c_p} \quad (5)$$

where  $c_b$  is the concentration of the analyte withdrawn from the buffer compartment before dilution and  $c_p$  is the concentration in the plasma compartment. The values were accepted if the recovery of analyte was between 80% and 120% of the initial amount.

**Cytochrome P450 Mediated Metabolism.** Incubations consisted of pooled male rat liver microsomes (0.5 mg microsomal protein/mL), test compound (2  $\mu\text{M}$ ),  $\text{MgCl}_2$  (2 mM), and NADPH (1 mM) in a total volume of 300  $\mu\text{L}$  TRIS–HCl buffer (0.1 M, pH 7.4) and were performed in a 96-well plate on a Thermomixer Comfort (Eppendorf). Compounds and microsomes were preincubated (37  $^{\circ}\text{C}$ , 700 rpm, 10 min) before NADPH was added. Samples (50  $\mu\text{L}$ ) at  $t = 0$  min and after an incubation time of 5, 10, 20, and 30 min were quenched with 150  $\mu\text{L}$  of ice-cooled MeOH, centrifuged (3600 rpm, 4  $^{\circ}\text{C}$ , 10 min), and 80  $\mu\text{L}$  of supernatant was transferred to a 96-well plate for LC–MS analysis (see below). The metabolic half-life ( $t_{1/2}$ ) was calculated from the slope of the linear regression from the log percentage remaining compound versus incubation time relationship. Control experiments without NADPH were performed in parallel.

**LC–MS Measurements.** Analyses were performed using an 1100/1200 series HPLC system coupled to a 6410 triple quadrupole mass detector (Agilent Technologies, Inc., Santa Clara, CA, USA) equipped with electrospray ionization. The system was controlled with the Agilent MassHunter Workstation Data Acquisition software (version B.01.04). The column used was an Atlantis T3 C18 column (2.1 mm  $\times$  50 mm) with a 3  $\mu\text{m}$  particle size (Waters Corp., Milford, MA, USA). The mobile phase consisted of eluent A ( $\text{H}_2\text{O}$  containing 0.1% formic acid (for 10a–f, h, i), or 10 mM ammonium acetate, pH 5.0 in 95:5,  $\text{H}_2\text{O}/\text{MeCN}$  (for 10g, j)) and eluent B (MeCN containing 0.1% formic acid). The flow rate was maintained at 0.6 mL/min. The gradient was ramped from 95% A/5% B to 5% A/95% B over 1 min and then held at 5% A/95% B for 0.1 min. The system was then brought back to 95% A/5% B, resulting in a total duration of 4 min. MS parameters such as fragmentor voltage,

collision energy, polarity were optimized individually for each analyte, and the molecular ion was followed for each compound in the multiple reaction monitoring mode. The concentrations of the analytes were quantified by the Agilent Mass Hunter Quantitative Analysis software (version B.01.04).

**In Vivo Studies. Animals.** Female C3H/HeN mice weighing between 19 and 25 g were obtained from Charles River Laboratories (Sulzfeld, Germany) or Harlan (Venray, The Netherlands) and were housed three or four per cage. The mice were kept under specific pathogen-free conditions in the Animal House of the Department of Biomedicine, University Hospital of Basel, and animal experimentation guidelines according to the regulations of the Swiss veterinary law were followed. After 7 days of acclimatization, 9- to 10-week-old mice were used for the studies. Animals had free access to chow and water at any time and were kept in a 12 h/12 h light/dark cycle. For administration volumes and sampling the good practice guidelines were followed.<sup>103</sup>

**Pharmacokinetic Studies.** The single-dose studies for the first experiment set were performed by intravenous application of FimH antagonists at a dosage of 50 mg/kg body weight, followed by plasma and urine sampling. Antagonists were diluted in PBS (Sigma-Aldrich) for injection into the tail vein. Blood and urine samples (10  $\mu\text{L}$ ) were taken at 6 and 30 min and at 1, 2, 4, 6, and 8 h after injection. For the PK studies with 10j, the antagonist was dissolved in PBS with 5% DMSO (Sigma-Aldrich) and injected into the tail vein (0.625 mg/kg) or given orally (1.25 mg/kg) using a gavage (syringes from BD Micro Fine, U-100 Insuline, 30 G with BD Microlance 3, 25 G needles, Becton Dickinson and Soft-Ject, 1 mL syringes from Henke Suss Wolf; gavage from Fine Science Tools). Blood and urine were sampled (10  $\mu\text{L}$ ) after 7, 13, 20, 30, 45 min and after 1, 1.5, 2, 2.5, 3, 4, 6, 8, and 24 h. Both blood and urine samples were directly diluted after sampling with MeOH (Acros Organics) to precipitate the proteins and centrifuged for 11 min at 13 000 rpm. The supernatants were transferred to a 96-well plate (Agilent Technologies, 0.5 mL, polypropylene), and the analyte concentrations were determined by LC–MS (see above).

**Infection Study.** For all infection studies, the drinking water of the mice was replaced by water containing 5% glucose (monohydrate from AppliChem, BioChemica), 3 days before the start of the experiment. 10j was dosed at 1.25 mg/kg (in 5% DMSO and PBS) and 10 mg/kg (in 5% DMSO in PBS containing 1% Tween 80, all purchased from Sigma-Aldrich) and applied orally via gavage to six and four mice, respectively, as described in the section Pharmacokinetic Studies, 40 min prior to infection. Ciprofloxacin (Ciproxin solution, 2 mg/mL, Bayer) was dosed with 8 mg/kg, which would correspond to a human dose of 500 mg,<sup>81</sup> subcutaneously 10 min prior to infection with UT189 to 4 mice. The values for the control group (PBS, po) resulted from the infection of 11 mice. Four mice were orally treated with the formulation vehicle for 10j (5% DMSO in PBS containing 1% Tween 80) and termed controls formulation. Before infection, remaining urine in the bladder was expelled by gentle pressure on the abdomen. Mice were anesthetized in 2.5 vol % isoflurane/oxygen mixture (Attane, Minrad Inc., USA) and placed on their back. Infection was performed transurethrally using a polyethylene catheter (Intramedic polyethylene tubing, inner diameter 0.28 mm, outer diameter 0.61 mm, Becton Dickinson), on a syringe (Hamilton Gastight Syringe 50  $\mu\text{L}$ , removable 30G needle, BGB Analytik AG, Switzerland). After gentle insertion of the catheter into the bladder, 50  $\mu\text{L}$  of bacterial suspension of UT189 ( $5.5 \times 10^9$  to  $2.25 \times 10^{10}$  CFU/mL) was slowly injected. This corresponded to approximately  $10^7$ – $10^8$  CFU per mouse. Mice were killed by  $\text{CO}_2$  3 h after inoculation, and bladder and kidneys were aseptically removed. Organs were homogenized in 1 mL of PBS using a tissue lyser (Retsch, Germany). Serial dilutions of bladder and kidneys were plated on Levine Eosin Methylene Blue Agar plates (Becton Dickinson), and CFUs were counted after overnight incubation at 37  $^{\circ}\text{C}$ .

## ■ ASSOCIATED CONTENT

### Supporting Information

HPLC data and chromatograms of target compounds and  $^1\text{H}$  NMR spectra of the synthetic compounds. This material is available free of charge via the Internet at <http://pubs.acs.org>.

## AUTHOR INFORMATION

### Corresponding Author

\*Phone: +41 61 267 15 51. Fax: +41 61 267 15 52. E-mail: beat.ernst@unibas.ch.

### Author Contributions

<sup>†</sup>S.K., L.P., K.M., D.E., and A.S. contributed equally to the project.

### Notes

The authors declare no competing financial interest.

## ACKNOWLEDGMENTS

The authors thank Prof. Dr. med. Radek Skoda, Department of Biomedicine, University Hospital Basel, Switzerland, for giving us access to the animal facility. The financial support by the Swiss National Science Foundation (SNF Interdisciplinary Grant K-32K1-120904) is gratefully acknowledged.

## ABBREVIATIONS USED

$\Delta H$ , change in enthalpy;  $\Delta S$ , change in entropy; AUC, area under the curve; BSA, bovine serum albumin;  $C_{max}$ , maximal concentration; Caco-2, colorectal adenocarcinoma; CFU, colony forming unit;  $CL_{tot}$ , total clearance; CRD, carbohydrate recognition domain;  $C_0$ , initial concentration; DL, detection limit; FITC, fluorescein isothiocyanate; FP, fluorescence polarization; ITC, isothermal titration calorimetry; iv, intravenous;  $K_D$ , dissociation constant;  $MAC_{90}$ , minimal antiadhesion concentration to inhibit 90% adhesion; PAMPA, parallel artificial membrane permeation assay;  $P_{app}$ , apparent permeability; PD, pharmacodynamics;  $P_e$ , effective permeability; PK, pharmacokinetics; po, per os; sc, subcutaneous; UPEC, uropathogenic *Escherichia coli*; UTI, urinary tract infection;  $V_d$ , volume of distribution in terminal phase

## REFERENCES

- (1) Foxman, B.; Barlow, R.; D'Arcy, H.; Gillespie, B.; Sobel, J. D. Urinary tract infection: self-reported incidence and associated costs. *Ann. Epidemiol.* **2000**, *10*, 509–515.
- (2) Ronald, A. The etiology of urinary tract infection: traditional and emerging pathogens. *Am. J. Med.* **2002**, *113* (Suppl. 1A), 14S–19S.
- (3) Fihn, S. D. Acute uncomplicated urinary tract infection in women. *N. Engl. J. Med.* **2003**, *349*, 259–266.
- (4) Hooton, T. M.; Besser, R.; Foxman, B.; Fritsche, T. R.; Nicolle, L. E. Acute uncomplicated cystitis in an era of increasing antibiotic resistance: a proposed approach to empirical therapy. *Clin. Infect. Dis.* **2004**, *39*, 75–80.
- (5) Sanchez, G. V.; Master, R. N.; Karlowsky, J. A.; Bordon, J. M. In vitro antimicrobial resistance of urinary *Escherichia coli* isolates among U.S. outpatients from 2000 to 2010. *Antimicrob. Agents Chemother.* **2012**, *56*, 2181–2183.
- (6) Clatworthy, A. E.; Pierson, E.; Hung, D. T. Targeting virulence: a new paradigm for antimicrobial therapy. *Nat. Chem. Biol.* **2007**, *3*, 541–548.
- (7) Mulvey, M. A.; Schilling, J. D.; Martinez, J. J.; Hultgren, S. J. Bad bugs and beleaguered bladders: interplay between uropathogenic *Escherichia coli* and innate host defenses. *Proc. Natl. Acad. Sci. U.S.A.* **2000**, *97*, 8829–8835.
- (8) Schilling, J. D.; Mulvey, M. A.; Hultgren, S. J. Structure and function of *Escherichia coli* type 1 pili: new insight into the pathogenesis of urinary tract infections. *J. Infect. Dis.* **2001**, *183* (Suppl. 1), S36–S40.
- (9) Wiles, T. J.; Kulesus, R. R.; Mulvey, M. A. Origins and virulence mechanisms of uropathogenic *Escherichia coli*. *Exp. Mol. Pathol.* **2008**, *85*, 11–19.
- (10) Capitani, G.; Eidam, O.; Glockshuber, R.; Grütter, M. G. Structural and functional insights into the assembly of type 1 pili from *Escherichia coli*. *Microbes Infect.* **2006**, *8*, 2284–2290.
- (11) Le Trong, I.; Aprikian, P.; Kidd, B. A.; Forero-Shelton, M.; Tchesnokova, V.; Rajagopal, P.; Rodriguez, V.; Interlandi, G.; Klevit, R.; Vogel, V.; Stenkamp, R. E.; Sokurenko, E. V.; Thomas, W. E. Structural basis for mechanical force regulation of the adhesin FimH via finger trap-like  $\beta$  sheet twisting. *Cell* **2010**, *141*, 645–655.
- (12) Sharon, N. Carbohydrates as future anti-adhesion drugs for infectious diseases. *Biochim. Biophys. Acta* **2006**, *1760*, 527–537.
- (13) Firon, N.; Itzhak, O.; Sharon, N. Interaction of mannose-containing oligosaccharides with the fimbrial lectin of *Escherichia coli*. *Biochem. Biophys. Res. Commun.* **1982**, *105*, 1426–1432.
- (14) Firon, N.; Ofek, I.; Sharon, N. Carbohydrate specificity of the surface lectins of *Escherichia coli*, *Klebsiella pneumoniae*, and *Salmonella typhimurium*. *Carbohydr. Res.* **1983**, *120*, 235–249.
- (15) Bouckaert, J.; Berglund, J.; Schembri, M.; De Genst, E.; Cools, L.; Wührer, M.; Hung, C.-S.; Pinkner, J.; Slättegård, R.; Zavialov, A.; Choudhury, D.; Langermann, S.; Hultgren, S. J.; Wyns, L.; Klemm, P.; Oscarson, S.; Knight, S. D.; De Greve, H. Receptor binding studies disclose a novel class of high-affinity inhibitors of the *Escherichia coli* FimH adhesin. *Mol. Microbiol.* **2005**, *55*, 441–455.
- (16) Firon, N.; Ashkenazi, S.; Mirelman, D.; Ofek, I.; Sharon, N. Aromatic alpha-glycosides of mannose are powerful inhibitors of the adherence of type 1 fimbriated *Escherichia coli* to yeast and intestinal epithelial cells. *Infect. Immun.* **1987**, *55*, 472–476.
- (17) Sperling, O.; Fuchs, A.; Lindhorst, T. K. Evaluation of the carbohydrate recognition domain of the bacterial adhesin FimH. Design, synthesis and binding properties of mannoside ligands. *Org. Biomol. Chem.* **2006**, *4*, 3913–3922.
- (18) Han, Z.; Pinkner, J. S.; Ford, B.; Obermann, R.; Nolan, W.; Wildman, S. A.; Hobbs, D.; Ellenberger, T.; Cusumano, C. K.; Hultgren, S. J.; Janetka, J. W. Structure-based drug design and optimization of mannoside bacterial FimH antagonists. *J. Med. Chem.* **2010**, *53*, 4779–4792.
- (19) Klein, T.; Abgottspon, D.; Wittwer, M.; Rabbani, S.; Herold, J.; Jiang, X.; Kleeb, S.; Lüthi, C.; Scharenberg, M.; Bezençon, J.; Gubler, E.; Pang, L.; Smiesko, M.; Cutting, B.; Schwardt, O.; Ernst, B. FimH antagonists for the oral treatment of urinary tract infections: from design and synthesis to in vitro and in vivo evaluation. *J. Med. Chem.* **2010**, *53*, 8627–8641.
- (20) Cusumano, C. K.; Pinkner, J. S.; Han, Z.; Greene, S. E.; Ford, B. A.; Crowley, J. R.; Henderson, J. P.; Janetka, J. W.; Hultgren, S. J. Treatment and prevention of urinary tract infection with orally active FimH inhibitors. *Sci. Transl. Med.* **2011**, *3*, 109ra115.
- (21) Han, Z.; Pinkner, J. S.; Ford, B.; Chorem, E.; Crowley, J. M.; Cusumano, C. K.; Campbell, S.; Henderson, J. P.; Hultgren, S. J.; Janetka, J. W. Lead optimization studies on FimH antagonists: discovery of potent and orally bioavailable ortho-substituted biphenyl mannosides. *J. Med. Chem.* **2012**, *55*, 3945–3959.
- (22) Pang, L.; Kleeb, S.; Lemme, K.; Rabbani, S.; Scharenberg, M.; Zalewski, A.; Schädler, F.; Schwardt, O.; Ernst, B. FimH antagonists: structure–activity and structure–property relationships for biphenyl  $\alpha$ -D-mannopyranosides. *ChemMedChem* **2012**, *7*, 1404–1422.
- (23) Jiang, X.; Abgottspon, D.; Kleeb, S.; Rabbani, S.; Scharenberg, M.; Wittwer, M.; Haug, M.; Schwardt, O.; Ernst, B. Anti-adhesion therapy for urinary tract infections—a balanced PK/PD profile proved to be key for success. *J. Med. Chem.* **2012**, *55*, 4700–4713.
- (24) Schwardt, O.; Rabbani, S.; Hartmann, M.; Abgottspon, D.; Wittwer, M.; Kleeb, S.; Zalewski, A.; Smiesko, M.; Cutting, B.; Ernst, B. Design, synthesis and biological evaluation of mannosyl triazoles as FimH antagonists. *Bioorg. Med. Chem.* **2011**, *19*, 6454–6473.
- (25) Brument, S.; Sivignon, A.; Dumych, T. I.; Moreau, N.; Roos, G.; Guérardel, Y.; Chalopin, T.; Deniaud, D.; Bilyy, R. O.; Darfeuille-Michaud, A.; Bouckaert, J.; Gouin, S. G. Thiazolylaminomannosides as potent antiadhesives of type 1 piliated *Escherichia coli* isolated from Crohn's disease patients. *J. Med. Chem.* **2013**, *56*, 5395–5406.
- (26) Lindhorst, T. K.; Kieburg, C.; Krallmann-Wenzel, U. Inhibition of the type 1 fimbriae-mediated adhesion of *Escherichia coli* to erythrocytes by multiantennary D-mannosyl clusters: the effect of multivalency. *Glycoconjugate J.* **1998**, *15*, 605–613.

- (27) Nagahori, N.; Lee, R. T.; Nishimura, S.-L.; Pagé, S.; Roy, R.; Lee, Y. C. Inhibition of adhesion of type 1 fimbriated *Escherichia coli* to highly mannosylated ligands. *ChemBioChem* **2002**, *3*, 836–844.
- (28) Appeldoorn, C. C. M.; Joosten, J. A. F.; Maate, F. A.; Dobrindt, U.; Hacker, J.; Liskamp, R. M. J.; Khan, A. S.; Pieters, R. J. Novel multivalent mannose compounds and their inhibition of the adhesion of type 1 fimbriated uropathogenic *E. coli*. *Tetrahedron: Asymmetry* **2005**, *16*, 361–372.
- (29) Patel, A.; Lindhorst, T. K. A modular approach for the synthesis of oligosaccharide mimetics. *Carbohydr. Res.* **2006**, *341*, 1657–1668.
- (30) Touaibia, M.; Wellens, A.; Shiao, T. C.; Wang, Q.; Sirois, S.; Bouckaert, J.; Roy, R. Mannosylated G(0) dendrimers with nanomolar affinities to *Escherichia coli* FimH. *ChemMedChem* **2007**, *2*, 1190–1201.
- (31) Durka, M.; Buffet, K.; Iehl, J.; Holler, M.; Nierengarten, J.-F.; Taganna, J.; Bouckaert, J.; Vincent, S. P. The functional valency of dodecamannosylated fullerenes with *Escherichia coli* FimH—towards novel bacterial antiadhesives. *Chem. Commun.* **2011**, *47*, 1321–1323.
- (32) Bouckaert, J.; Li, Z.; Xavier, C.; Almant, M.; Cavelliers, V.; Lahoutte, T.; Weeks, S. D.; Kovensky, J.; Gouin, S. G. Heptyl  $\alpha$ -D-mannosides grafted on a  $\beta$ -cyclodextrin core to interfere with *Escherichia coli* adhesion: an in vivo multivalent effect. *Chem.—Eur. J.* **2013**, *19*, 7847–7855.
- (33) Scharenberg, M.; Schwardt, O.; Rabbani, S.; Ernst, B. Target selectivity of FimH antagonists. *J. Med. Chem.* **2012**, *55*, 9810–9816.
- (34) Choudhury, D.; Thompson, A.; Stojanoff, V.; Langermann, S.; Pinkner, J.; Hultgren, S. J.; Knight, S. D. X-ray structure of the FimC-FimH chaperone-adhesin complex from uropathogenic *Escherichia coli*. *Science* **1999**, *285*, 1061–1066.
- (35) Hung, C.-S.; Bouckaert, J.; Hung, D.; Pinkner, J.; Widberg, C.; DeFusco, A.; Auguste, C. G.; Strouse, R.; Langermann, S.; Waksman, G.; Hultgren, S. J. Structural basis of tropism of *Escherichia coli* to the bladder drug in urinary tract infection. *Mol. Microbiol.* **2002**, *44*, 903–915.
- (36) Wellens, A.; Garofalo, C.; Nguyen, H.; Van Gerven, N.; Slättegård, R.; Henalsteens, J.-P.; Wyns, L.; Oscarson, S.; De Greve, H.; Hultgren, S. J.; Bouckaert, J. Intervening with urinary tract infections using anti-adhesives based on the crystal structure of the FimH-oligomannose-3 complex. *PLoS One* **2008**, *3*, e2040.
- (37) Wellens, A.; Lahmann, M.; Touaibia, M.; Vaucher, J.; Oscarson, S.; Roy, R.; Remaut, H.; Bouckaert, J. The tyrosine gate as a potential entropic lever in the receptor-binding site of the bacterial adhesin FimH. *Biochemistry* **2012**, *51*, 4790–4799.
- (38) Totsika, M.; Kostakioti, M.; Hannan, T. J.; Upton, M.; Beatson, S. A.; Janetka, J. W.; Hultgren, S. J.; Schembri, M. A. A FimH inhibitor prevents acute bladder infection and treats chronic cystitis caused by multidrug-resistant uropathogenic *Escherichia coli* ST131. *J. Infect. Dis.* **2013**, *208*, 921–928.
- (39) Meanwell, M. A. Synopsis of some recent tactical application of bioisosteres in drug design. *J. Med. Chem.* **2011**, *54*, 2529–2591.
- (40) Prieto, M.; Zurita, E.; Rosa, E.; Luño, L.; Lloyd-Williams, P.; Giralt, E. Arylboronic acids and arylpinacolboronate esters in Suzuki coupling reactions involving indoles. Partner role swapping and heterocycle protection. *J. Org. Chem.* **2004**, *69*, 6812–6820.
- (41) Schulz, M. J.; Coats, S. J.; Hlasta, D. J. Microwave-assisted preparation of aryltetrazoleboronate esters. *Org. Lett.* **2004**, *6*, 3265–3268.
- (42) Devos, A.; Remion, J.; Frisque-Hesbain, A. M.; Colens, A.; Ghosez, L. Synthesis of acyl halides under very mild conditions. *J. Chem. Soc., Chem. Commun.* **1979**, 1180–1181.
- (43) Rabbani, S.; Jiang, X.; Schwardt, O.; Ernst, B. Expression of the carbohydrate recognition domain of FimH and development of a competitive binding assay. *Anal. Biochem.* **2010**, *407*, 188–195.
- (44) Waetherman, R. V.; Kiessling, L. L. Fluorescence anisotropy assay reveals affinities of C- and O-glycosides for concanavalin A. *J. Org. Chem.* **1996**, *61*, 534–538.
- (45) Cer, R. Z.; Mudunuri, U.; Stephens, R.; Lebeda, F. J. IC50-to-Ki: a web-based tool for converting IC50 to Ki values for inhibitors of enzyme activity and ligand binding. *Nucleic Acids Res.* **2009**, *37*, W441–W445.
- (46) Lynch, B. A.; Loiacono, K. A.; Tiong, C. L.; Adams, S. E.; MacNeil, I. A. A fluorescence polarization based Src-SH2 binding assay. *Anal. Biochem.* **1997**, *247*, 77–82.
- (47) Wu, P.; Brasseur, M.; Schindler, U. A high-throughput STAT binding assay using fluorescence polarization. *Anal. Biochem.* **1997**, *249*, 29–36.
- (48) Huang, X. Fluorescence polarization competition assay: the range of resolvable inhibitor potency is limited by the affinity of the fluorescent ligand. *J. Biomol. Screening* **2003**, *8*, 34–38.
- (49) Cooper, A. *Biophysical Chemistry*, 2nd ed.; RSC Publishing: Cambridge, U.K., 2011; pp 122–123.
- (50) Scharenberg, M.; Jiang, X.; Pang, L.; Navarra, G.; Rabbani, S.; Binder, F.; Schwardt, O.; Ernst, B. Kinetic properties of carbohydrate-lectin interactions: FimH antagonists. *ChemMedChem* **2014**, *9*, 78–83.
- (51) Cabani, S.; Gianni, P.; Mollica, V.; Lepori, L. Group contribution to the thermodynamic properties of non-ionic solutes in dilute aqueous solution. *J. Solution Chem.* **1981**, *10*, 563–595.
- (52) Hansch, C.; Leo, A.; Taft, R. W. A survey of Hammett substituent constants and resonance and field parameters. *Chem. Rev.* **1991**, *91*, 165–195.
- (53) Chen, A.; Wadso, I. Simultaneous determination of delta G, delta H and delta S by an automatic microcalorimetric titration technique: application to protein ligand binding. *J. Biochem Biophys Methods* **1982**, *6*, 307–316.
- (54) Freire, E.; Mayorga, O. L.; Straume, M. Isothermal titration calorimetry. *Anal. Chem.* **1990**, *62*, 950A–959A.
- (55) Wiseman, T.; Williston, S.; Brandts, J. F.; Lin, L.-N. Rapid measurement of binding constants and heats of binding using a new titration calorimeter. *Anal. Biochem.* **1989**, *179*, 131–137.
- (56) Turnbull, W. B.; Daranas, A. H. On the value of c: can low affinity systems be studied by isothermal titration calorimetry? *J. Am. Chem. Soc.* **2003**, *125*, 14859–14866.
- (57) Sigurskjold, B. W. Exact analysis of competition ligand binding by displacement isothermal titration calorimetry. *Anal. Biochem.* **2000**, *277*, 260–266.
- (58) Velazquez-Campoy, A.; Freire, E. Isothermal titration calorimetry to determine association constants for high-affinity ligands. *Nat. Protoc.* **2006**, *1*, 186–191.
- (59) Dearden, J. C.; Bresnen, G. M. The measurement of partition coefficients. *QSAR Comb. Sci.* **1988**, *7*, 133–144.
- (60) Kansy, M.; Senner, F.; Gubernator, K. Physicochemical high throughput screening: parallel artificial membrane permeation assay in the description of passive absorption processes. *J. Med. Chem.* **1998**, *41*, 1007–1010.
- (61) Hubatsch, I.; Ragnarsson, E. G. E.; Artursson, P. Determination of drug permeability and prediction of drug absorption in Caco-2 monolayers. *Nat. Protoc.* **2007**, *2*, 2111–2119.
- (62) Banker, M. J.; Clark, T. H.; Williams, J. A. Development and validation of a 96-well equilibrium dialysis apparatus for measuring plasma protein binding. *J. Pharm. Sci.* **2003**, *92*, 967–974.
- (63) Obach, R. S. Prediction of human clearance of twenty-nine drugs from hepatic microsomal intrinsic clearance data: an examination of in vitro half-life approach and nonspecific binding to microsomes. *Drug Metab. Dispos.* **1999**, *27*, 1350–1359.
- (64) Chaturvedi, P. R.; Decker, C. J.; Odinecs, A. Prediction of pharmacokinetic properties using experimental approaches during early drug discovery. *Curr. Opin. Chem. Biol.* **2001**, *5*, 452–463.
- (65) Di, L.; Kerns, E. H. Profiling drug-like properties in discovery research. *Curr. Opin. Chem. Biol.* **2003**, *7*, 402–408.
- (66) Lipinski, C. A. Drug-like properties and the causes of poor solubility and poor permeability. *J. Pharmacol. Toxicol. Methods* **2000**, *44*, 235–249.
- (67) Curatolo, W. Physical chemical properties of oral drug candidates in the discovery and exploratory development settings. *Pharm. Sci. Technol. Today* **1998**, *1*, 387–393.
- (68) Ishikawa, M.; Hashimoto, Y. Improvement in aqueous solubility in small molecule drug discovery programs by disruption of molecular planarity and symmetry. *J. Med. Chem.* **2011**, *54*, 1539–1554.



- (69) Avdeef, A.; Bendels, S.; Di, L.; Faller, B.; Kansy, M.; Sugano, K.; Yamauchi, Y. PAMPA – critical factors for better predictions of absorption. *J. Pharm. Sci.* **2007**, *96*, 2893–2909.
- (70) Artursson, P.; Karlsson, J. Correlation between oral drug absorption in humans and apparent drug permeability coefficients in human intestinal epithelial (Caco-2) cells. *Biochem. Biophys. Res. Commun.* **1991**, *175*, 880–885.
- (71) Feng, B.; LaPerle, J. L.; Chang, G.; Varma, M. V. S. Renal clearance in drug discovery and development: molecular descriptors, drug transporters and disease state. *Expert Opin. Drug. Metab. Toxicol.* **2010**, *6*, 939–952.
- (72) Schmidt, S.; Gonzalez, D.; Derendorf, H. Significance of protein binding in pharmacokinetics and pharmacodynamics. *J. Pharm. Sci.* **2010**, *99*, 1107–1122.
- (73) Weisiger, R. A. Dissociation from albumin: A potentially rate-limiting step in the clearance of substances by the liver. *Proc. Natl. Acad. Sci. U.S.A.* **1985**, *82*, 1563–1567.
- (74) Smith, D. A.; Jones, B. C.; Walker, D. K. Design of drugs involving the concepts and theories of drug metabolism and pharmacokinetics. *Med. Res. Rev.* **1996**, *16*, 243–266.
- (75) Van de Waterbeemd, H.; Smith, D. A.; Beaumont, K.; Walker, D. K. Property-based design: optimization of drug absorption and pharmacokinetics. *J. Med. Chem.* **2001**, *44*, 1313–1333.
- (76) Varma, M. V. S.; Feng, B.; Obach, R. S.; Troutman, M. D.; Chupka, J.; Miller, H. R.; El-Kattan, A. Physicochemical determinants of human renal clearance. *J. Med. Chem.* **2009**, *52*, 4844–4852.
- (77) Waring, M. J. Lipophilicity in drug discovery. *Expert Opin. Drug Discovery* **2010**, *5*, 235–248.
- (78) Zhang, Y.; Huo, M.; Solver, P. K. An add-in program for pharmacokinetic and pharmacodynamic data analysis in Microsoft Excel. *Comput. Methods Programs Biomed.* **2010**, *99*, 306–314.
- (79) Scharenberg, M.; Abgottspon, D.; Cicek, E.; Jiang, X.; Schwardt, O.; Rabbani, S.; Ernst, B. Cytometry-based assay for screening FimH antagonists. *Assay Drug Dev. Technol.* **2011**, *9*, 455–464.
- (80) Hooton, T. M. Fluoroquinolones and resistance in the treatment of uncomplicated urinary tract infection. *Int. J. Antimicrob. Agents* **2003**, *22*, 65–72.
- (81) Jakobsen, L.; Cattoir, V.; Jensen, K. S.; Hammerum, A. M.; Nordmann, P.; Frimodt-Møller, N. Impact of low-level fluoroquinolone resistance genes *qnrA1*, *qnrB19*, and *qnrS1* on ciprofloxacin treatment of isogenic *Escherichia coli* strains in a murine urinary tract infection model. *J. Antimicrob. Chemother.* **2012**, *67*, 2438–2444.
- (82) Mulvey, M. A. Adhesion and entry of uropathogenic *Escherichia coli*. *Cell. Microbiol.* **2002**, *4*, 257–271.
- (83) Ballatore, C.; Huryn, D. M.; Smith, A. B. Carboxylic acid (bio)isosteres in drug design. *ChemMedChem* **2013**, *8*, 385–395.
- (84) Justice, S. S.; Hung, C.; Theriot, J. A.; Fletcher, D. A.; Anderson, G. G.; Footer, M. J.; Hultgren, S. J. Differentiation and developmental pathways of uropathogenic *Escherichia coli* in urinary tract pathogenesis. *Proc. Natl. Acad. Sci. U.S.A.* **2004**, *101*, 1333–1338.
- (85) Mulvey, M. A.; Schilling, J. D.; Hultgren, S. J. Establishment of a persistent *Escherichia coli* reservoir during the acute phase of a bladder infection. *Infect. Immun.* **2001**, *69*, 4572–9.
- (86) Houtman, J. C.; Brown, P. C.; Bowden, B.; Yamaguchi, H.; Appella, E.; Samelson, L. E.; Schuck, P. Studying multisite binary and ternary protein interactions by global analysis of isothermal titration calorimetry data in SEDPHAT: application to adaptor protein complexes in cell signaling. *Protein Sci.* **2007**, *16*, 30–42.
- (87) *Maestro*, version 9.3; Schrödinger, LLC: New York, NY, 2012.
- (88) *MacroModel*, version 9.9; Schrödinger, LLC: New York, NY, 2012.
- (89) Hawkins, G. D.; Giesen, D. J.; Lynch, G. C.; Chambers, C. C.; Rossi, L.; Storer, J. W.; Li, J.; Thompson, J. D.; Winget, P.; Lynch, B. J.; Rinaldi, D.; Liotard, D. A.; Cramer, C. J.; Truhlar, D. G. *AMSOL*, version 7.1; University of Minnesota: Minneapolis, MN, 2003; based in part on the following: Liotard, D. A.; Healy, E. F.; Ruiz, J. M.; Dewar, M. J. S. *AMPAC*, version 2.1; Semichem, Inc.: Shawnee, KS.
- (90) Chambers, C. C.; Hawkins, G. D.; Cramer, C. J.; Truhlar, D. G. Model for aqueous solvation based on class IV atomic charges and first solvation shell effects. *J. Phys. Chem.* **1996**, *100*, 16385–16398.
- (91) Dewar, M. J. S.; Zoebisch, E. G.; Healy, E. F.; Stewart, J. J. P. AM1: a new general purpose quantum mechanical molecular model. *J. Am. Chem. Soc.* **1993**, *115*, 5348–5348 [Erratum to *J. Am. Chem. Soc.* **1985**, *107*, 3902–3909].
- (92) Mulvey, M. A.; Schilling, J. D.; Hultgren, S. J. Establishment of a persistent *Escherichia coli* reservoir during the acute phase of a bladder infection. *Infect. Immun.* **2001**, *69*, 4572–4579.
- (93) Kabsch, W. Automatic processing of rotation diffraction data from crystals of initially unknown symmetry and cell constants. *J. Appl. Crystallogr.* **1993**, *26*, 795–800.
- (94) Leslie, A. G. W. The integration of macromolecular diffraction data. *Acta Crystallogr. D* **2006**, *62*, 48–57.
- (95) Winn, M. D.; Ballard, C. C.; Cowtan, K. D.; Dodson, E. J.; Emsley, P.; Evans, P. R.; Keegan, R. M.; Krissinel, E. B.; Leslie, A. G. W.; McCoy, A.; McNicholas, S. J.; Murshudov, G. N.; Pannu, N. S.; Potterton, E. A.; Powell, H. R.; Read, R. J.; Vagin, A.; Wilson, K. S. Overview of the CCP4 suite and current developments. *Acta Crystallogr. D* **2011**, *67*, 235–242.
- (96) McCoy, A. J. Solving structures of protein complexes by molecular replacement with Phaser. *Acta Crystallogr. D* **2007**, *63*, 32–41.
- (97) Emsley, P.; Cowtan, K. Coot: model-building tools for molecular graphics. *Acta Crystallogr. D* **2004**, *60*, 2126–2132.
- (98) Adams, P. D.; Grosse-Kunstleve, R. W.; Hung, L.-W.; Ioerger, T. R.; McCoy, A. J.; Moriarty, N. W.; Read, R. J.; Sacchettini, J. C.; Sauter, N. K.; Terwilliger, T. C. PHENIX: building new software for automated crystallographic structure determination. *Acta Crystallogr., Sect. D: Biol. Crystallogr.* **2002**, *58*, 1948–1954.
- (99) van Aalten, D. M. F.; Bywater, R.; Findlay, J. B. C.; Hendlich, M.; Hooft, R. W. W.; Vriend, G. PRODRG, a program for generating molecular topologies and unique molecular descriptors from coordinates of small molecules. *J. Comput.-Aided Mol. Des.* **1996**, *10*, 255–262.
- (100) Chen, V. B.; Arendall, W. B.; Headd, J. J.; Keedy, D. A.; Immormino, R. M.; Kapral, G. J.; Murray, L. W.; Richardson, J. S.; Richardson, D. C. MolProbity: all-atom structure validation for macromolecular crystallography. *Acta Crystallogr. D* **2010**, *66*, 12–21.
- (101) Bezençon, J.; Wittwer, M. B.; Cutting, B.; Smiesko, M.; Wagner, B.; Kansy, M.; Ernst, B.  $pK_a$  determination by  $^1\text{H}$  NMR spectroscopy—an old methodology revisited. *J. Pharm. Biomed. Anal.* **2014**, *93*, 147–155.
- (102) (a) VCCLAB, Virtual Computational Chemistry Laboratory, 2005. <http://www.vcclab.org> (accessed August 14, 2012). (b) Tetko, I. V.; Gasteiger, J.; Todeschini, R.; Mauri, A.; Livingstone, D.; Ertl, P.; Palyulin, V. A.; Radchenko, E. V.; Zefirov, N. S.; Makarenko, A. S.; Tanchuk, V. Y.; Prokopenko, V. V. Virtual computational chemistry laboratory—design and description. *J. Comput.-Aided Mol. Des.* **2005**, *19*, 453–463.
- (103) Diehl, K.-H.; Hull, R. A. Good practice guide to the administration of substances and removal of blood, including routes and volumes. *J. Appl. Toxicol.* **2001**, *21*, 15–23.

### 4.3.3 Paper 4 - Structural Modifications:

#### FimH Antagonists: Phosphate Prodrugs Improve Oral Bioavailability

The low aqueous solubility of the biphenyl and indolinyphenyl mannosides could be improved by a phosphate ester prodrug approach. A Caco-2 cell model is implemented to characterize the enzyme-mediated cleavage of the phosphate moiety and the subsequent permeation of the pharmacologically active parent compound through a confluent cell monolayer. *In vivo* pharmacokinetic studies completed the phosphate ester prodrug approach.

#### Contribution to the project:

Jacqueline Bezençon performed the assays regarding the phosphatase-mediated release of the parent compound as well as the *in vitro* absorption studies in collaboration with Simon Kleeb. In addition, she prepared the biorelevant media and measured stability of the phosphate ester prodrugs in collaboration with the master student Karen Bamberger. Furthermore, she interpreted the resulting data and revisited the manuscript except for the synthesis section. She designed the Graphical Abstract.

The paper was published in the peer-reviewed *Journal of Medicinal Chemistry* in 2016:

S. Kleeb,\* X. Jiang,\* P. Frei,\* A. Sigl,\* **J. Bezençon**, K. Bamberger, O. Schwardt, B. Ernst, FimH Antagonists: Phosphate Prodrugs Improve Oral Bioavailability. *J. Med. Chem.* **2016**, Mar. 18 [Epub ahead of print]

\*contributed equally.

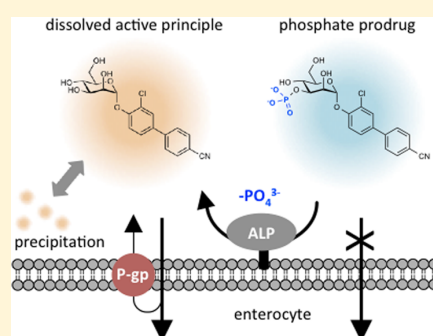
## FimH Antagonists: Phosphate Prodrugs Improve Oral Bioavailability

Simon Kleeb, Xiaohua Jiang, Priska Frei, Anja Sigl, Jacqueline Bezençon, Karen Bamberger, Oliver Schwardt, and Beat Ernst\*

Institute of Molecular Pharmacy, Pharmacenter, University of Basel, Klingelbergstrasse 50, 4056 Basel, Switzerland

## S Supporting Information

**ABSTRACT:** The widespread occurrence of urinary tract infections has resulted in frequent antibiotic treatment, contributing to the emergence of antimicrobial resistance. Alternative approaches are therefore required. In the initial step of colonization, FimH, a lectin located at the tip of bacterial type 1 pili, interacts with mannosylated glycoproteins on the urothelial mucosa. This initial pathogen/host interaction is efficiently antagonized by biaryl  $\alpha$ -D-mannopyranosides. However, their poor physicochemical properties, primarily resulting from low aqueous solubility, limit their suitability as oral treatment option. Herein, we report the syntheses and pharmacokinetic evaluation of phosphate prodrugs, which show an improved aqueous solubility of up to 140-fold. In a Caco-2 cell model, supersaturated solutions of the active principle were generated through hydrolysis of the phosphate esters by brush border-associated enzymes, leading to a high concentration gradient across the cell monolayer. As a result, the in vivo application of phosphate prodrugs led to a substantially increased  $C_{max}$  and prolonged availability of FimH antagonists in urine.



## INTRODUCTION

Urinary tract infections (UTIs) are the most frequent cause of bacteriosis in humans, affecting millions of people worldwide.<sup>1</sup> They remain one of the most common indications for prescribing antibiotics to alleviate symptoms (dysuria, frequent and urgent urination, bacteriuria, and pyuria) and to prevent complications (pyelonephritis and urosepsis).<sup>2</sup> However, the frequent and repeated use of antibiotics can induce antimicrobial resistance; therefore, alternative prevention and treatment strategies are urgently needed.<sup>3</sup>

Uropathogenic *Escherichia coli* (UPEC) strains are the causative agent of more than 70% of all UTI episodes.<sup>4,5</sup> The initial step in pathogenesis involves bacterial adherence to the bladder cell surface, preventing UPEC from being cleared by the bulk flow of urine and enabling the bacteria to colonize the urothelial cells.<sup>6</sup> Among the different adhesins expressed on the bacterial surface, mannose-binding type 1 pili are the most prevalent. They consist of a helical rod containing 500–3000 copies of the structural subunit FimA as well as one copy of the FimF, FimG, and FimH subunits.<sup>7</sup> The FimH subunit is expressed at the distal tip of each pilus and exhibits the carbohydrate recognition domain (CRD), which interacts with the mannosylated glycoprotein uroplakin 1a on the mucosal surface of the bladder.<sup>8</sup>

More than three decades ago, Sharon and co-workers described various oligomannosides and aryl  $\alpha$ -D-mannosides as potential antagonists of FimH-mediated bacterial adhesion.<sup>9,10</sup> This led to subsequent reports on several monovalent mannose-based FimH antagonists containing various aglycones, such as *n*-alkyl,<sup>11</sup> phenyl,<sup>12</sup> dioxycyclobutenylaminophenyl,<sup>13</sup> umbelliferyl,<sup>14</sup> biphenyl,<sup>14–19</sup> indol(in)ylphenyl,<sup>20</sup> triazolyl,<sup>21</sup> or

thiazolylamino.<sup>22</sup> In addition, different multivalent presentations of mannose derivatives have been explored.<sup>23–29</sup> Most importantly, it was recently shown that these  $\alpha$ -D-mannopyranosides did not elicit adverse side effects caused by the nonselective binding of FimH antagonists to various mammalian mannose receptors.<sup>30</sup>

In vivo studies in a mouse disease model confirmed the therapeutic potential of biaryl mannosides for an oral treatment of UTI.<sup>15–17,19</sup> However, because only low oral bioavailability could be achieved, basic determinants such as aqueous solubility and membrane permeability should be further optimized.<sup>31</sup> One possible solution is offered by a phosphate prodrug approach, which is applied either when the active principle exhibits high membrane permeability but suffers from low aqueous solubility<sup>32</sup> or when the therapeutic dose exceeds the maximum amount of drug that can be dissolved into intestinal fluids.<sup>33</sup> In a phosphate prodrug approach, the active principle is rapidly released by endogenous phosphatases, such as alkaline phosphatase, an enzyme particularly abundant on the brush border of enterocytes.<sup>34</sup>

The application of this prodrug principle has led to various marketed drugs, such as prednisolone phosphate (1),<sup>35</sup> the antiretroviral drug fosamprenavir (2),<sup>34,36</sup> or the chemotherapeutic drug fludarabine phosphate (Figure 1).<sup>37</sup>

The goal of the present study was to optimize the physicochemical profile of the biaryl mannosides 3–5 by phosphorylation, enhancing aqueous solubility and, consequently, the oral availability.

Received: December 11, 2015

Published: March 9, 2016

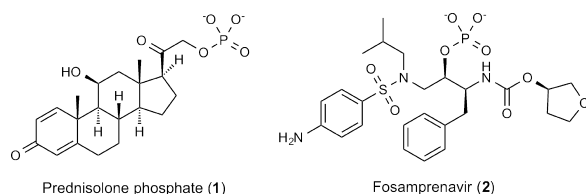


Figure 1. Phosphate prodrugs of marketed drugs.

## RESULTS AND DISCUSSION

Although exhibiting nanomolar affinity and high permeability, one drawback of FimH antagonists 3–5<sup>14,18–20</sup> is their low aqueous solubility, resulting in limited oral bioavailability. They are therefore perfect candidates for a phosphate prodrug approach. Table 1 summarizes their previously reported binding affinities ( $IC_{50}$ )<sup>14,18–20</sup> as well as their physicochemical properties (solubility, lipophilicity, and permeability).

For identifying the optimal position of the phosphate promoiety on the mannoside core of FimH antagonists 3–5, a series of phosphate esters was synthesized (Figure 2) and their solubility determined. In the prodrugs 6a–d and 7a–d, the phosphate ester bond was directly linked to the various hydroxyl groups of the mannose moiety. Alternatively, an acetal linker was used in prodrugs 6e and 8 to increase the distance between the enzymatic cleavage site and thereby enhance accessibility of the phosphate ester and subsequently the dephosphorylation rate. When prodrugs 6e and 8 are dephosphorylated, the intermediate hemiacetal is expected to collapse, spontaneously releasing the active principle 3 or 5 accompanied by formaldehyde.<sup>45</sup>

**Synthesis of Phosphates 6a–d.** 2-Phosphate 6a of biphenyl  $\alpha$ -D-mannopyranoside (3) was synthesized according to the procedure depicted in Scheme 1. Starting from 3,<sup>14,18</sup> a benzylidene acetal ( $\rightarrow$ 9) was formed to protect the 4- and 6-

OH of the mannose moiety. The 3-position was subsequently protected by a regioselective dibutyltin oxide-mediated benzylation ( $\rightarrow$ 10) and then phosphorylation using dibenzyl *N,N*-diisopropyl-phosphoramidite in the presence of 1,2,4-triazole, followed by oxidation with *tert*-butylhydroperoxide, afforded the protected intermediate 11. Global deprotection via catalytic hydrogenation yielded 2-phosphate 6a.

For the synthesis of 3-phosphate 6b, the 3-position of 3 was regioselectively benzylated ( $\rightarrow$ 12), followed by perbenzylation to give 13 (Scheme 2). Cleavage of the benzyl group by hydrogenation ( $\rightarrow$ 14) and subsequent phosphorylation afforded an inseparable 3:2-mixture of the protected 3- and 2-phosphates 15 and 16 due to partial migration of the 2-benzoyl moiety. Upon deprotection via catalytic hydrogenation, pure 3-phosphate 6b could be isolated.

For the synthesis of 4-phosphate 6c, 9 was benzyloated ( $\rightarrow$ 17). Reductive opening of the benzylidene acetal with  $Me_3N \cdot BH_3$  and  $AlCl_3$  afforded precursor 18 (Scheme 3). Phosphorylation ( $\rightarrow$ 19) and subsequent deprotection yielded 4-phosphate 6c.

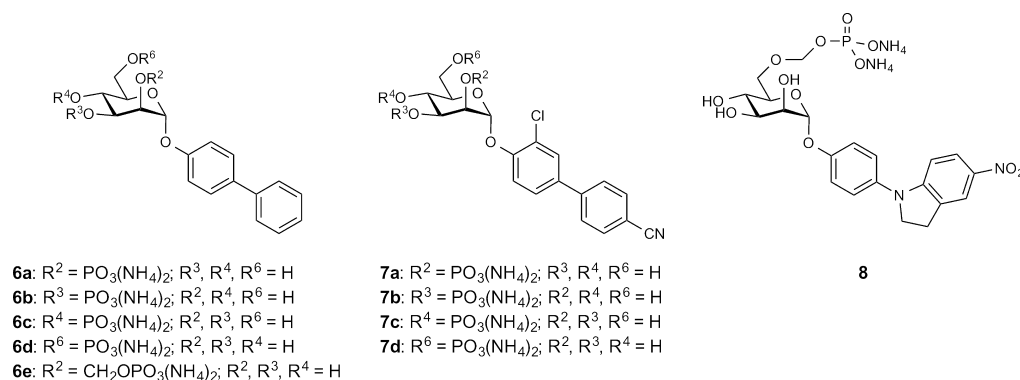
For the synthesis of 6-phosphate 6d, mannoside 3 was tritylated in the 6-position, followed by perbenzylation ( $\rightarrow$ 20) and removal of the trityl group (Scheme 4). Then, intermediate 21 was phosphorylated ( $\rightarrow$ 22) and final global deprotection gave 6-phosphate 6d.

**Synthesis of Phosphates 7a–d.** Because of the labile chloro- and cyano-substituents present in biphenyl  $\alpha$ -D-mannopyranoside 4,<sup>19</sup> the 2-phosphate 7a was obtained via a modified strategy (Scheme 5), omitting a potentially intractable hydrogenation step. Therefore, after protecting the 4- and 6-OH of 4 with a benzylidene acetal ( $\rightarrow$ 23), the 3-OH of the mannose moiety was selectively benzyloated to afford 24.<sup>46</sup> Phosphorylation of the 2-OH group with bis[2-(trimethylsilyl)ethyl] *N,N*-diisopropylphosphoramidite in the presence of 1,2,4-triazole, and subsequent oxidation with *tert*-butylhydro-

Table 1. Binding Affinities and Physicochemical Properties of the Biaryl  $\alpha$ -D-Mannopyranosides 3–5<sup>f</sup>

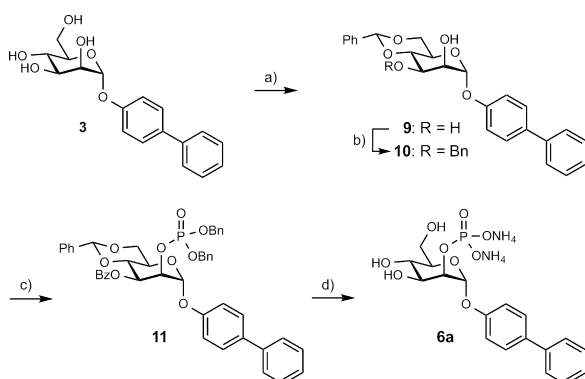
Cpd		$IC_{50}$ <sup>[a]</sup> [nM]	Solubility <sup>[b]</sup> [ $\mu$ g/mL]	$\log P$ <sup>[c]</sup>	PAMPA $\log P_e$ <sup>[d]</sup> [cm/s]	Caco-2 $P_{app}$ <sup>[e]</sup> [ $10^{-6}$ cm/s]	
						a $\rightarrow$ b	b $\rightarrow$ a
3 <sup>14,18</sup>		84.9	21	2.1	-4.7	10.0 $\pm$ 0.9	19.0 $\pm$ 1.2
4 <sup>19</sup>		10.1	192	2.1	-5.2	2.2 $\pm$ 0.4	22.1 $\pm$ 1.5
5 <sup>20</sup>		20	24	1.9	-5.5	2.9 $\pm$ 0.6	39.3 $\pm$ 5.8

<sup>a</sup> $IC_{50}$  values were determined in a cell-free competitive binding assay.<sup>38</sup> <sup>b</sup>Thermodynamic solubility for compounds 5; kinetic solubility for compound 3 and 4.<sup>39</sup> <sup>c</sup>Octanol–water partition coefficients ( $\log P$ ) were determined by a miniaturized shake-flask procedure.<sup>40</sup> <sup>d</sup> $P_e$  = effective permeability: passive permeation through an artificial membrane was determined by the parallel artificial membrane permeability assay (PAMPA).<sup>41,42</sup> <sup>e</sup> $P_{app}$  = apparent permeability: permeation through a Caco-2 cell monolayer was assessed in the absorptive (a  $\rightarrow$  b) and secretory (b  $\rightarrow$  a) directions in triplicate.<sup>43,44</sup> <sup>f</sup> $IC_{50}$  values, aqueous solubility,  $\log P$ , PAMPA, and Caco-2 cell data were adopted from refs 18–20. The  $IC_{50}$  of antagonist 4 and Caco-2  $P_{app}$  values of antagonist 5 were obtained according to the procedure described in ref 18.



**Figure 2.** Phosphate monoesters **6a–e** of biphenyl  $\alpha$ -D-mannopyranoside **3**, **7a–d** of substituted biphenyl  $\alpha$ -D-mannopyranoside **4** and **8** from indolinyphenyl  $\alpha$ -D-mannopyranoside **5**.

### Scheme 1<sup>a</sup>



<sup>a</sup>(a) PhCH(OMe)<sub>2</sub>, *p*-TsOH, DMF, 50 °C, overnight (70%); (b) (i) Bu<sub>2</sub>SnO, toluene, 135 °C, 3 h, (ii) BnBr, toluene, 115 °C, overnight (80%); (c) dibenzyl *N,N*-diisopropylphosphoramidite, 1,2,4-triazole, MeCN, 0 °C to rt, overnight; then 70% aq *tert*-BuOOH, rt, 1 h (62%); (d) (i) H<sub>2</sub> (4 bar), Pd(OH)<sub>2</sub>/C, EtOAc, cat. HOAc, overnight, (ii) 25% aq NH<sub>3</sub>/MeOH (4:1), rt, overnight (45%).

peroxide, yielded intermediate **25**. After cleavage of the (trimethylsilyl)ethyl esters with TFA ( $\rightarrow$ **26**) and subsequent ester hydrolysis upon treatment with NH<sub>3</sub>/MeOH, 2-phosphate **7a** was obtained.

Regioselective 3-allylation of **4** ( $\rightarrow$ **27**) followed by benzylation of the 2-, 4-, and 6-OH gave **28** (Scheme 6). Subsequent cleavage of the allyl group with PdCl<sub>2</sub> ( $\rightarrow$ **29**) and phosphorylation afforded intermediate **30** and final deprotection 3-phosphate **7b**.

4-Phosphate **7c** was synthesized in three steps via regioselective dibutyltin oxide-mediated acetylation of **4** in the 2-, 3-, and 6-position<sup>47</sup> ( $\rightarrow$ **31**), phosphorylation of the 4-OH ( $\rightarrow$ **32**), and subsequent cleavage of all protecting groups (Scheme 7).

For the synthesis of 6-phosphate **7d**, a similar protection strategy as for **6d** was used (Scheme 8). The parent compound **4** was tritylated in the 6-position ( $\rightarrow$ **33**), followed by perbenzylation ( $\rightarrow$ **34**) and removal of the trityl group. Phosphorylation of intermediate **35** ( $\rightarrow$ **36**) and final global deprotection afforded 6-phosphate **7d**.

**Synthesis of Acetal-Linked Phosphates 6e and 8.** Synthesis of the acetal-linked phosphate **6e** of biphenyl  $\alpha$ -D-

mannopyranoside (**3**) was achieved by first introducing a 6-*O*-(thiomethyl)methyl group on intermediate **21** with DMSO-acetic anhydride under acidic conditions ( $\rightarrow$ **37**, Scheme 9). Subsequent treatment with phosphoric acid and *N*-iodosuccinimide gave phosphate **38**. Finally, debenzoylation with NH<sub>3</sub>/MeOH provided the target compound **6e**.

The acetal-linked phosphate **8** was prepared analogously from indolinyphenyl  $\alpha$ -D-mannopyranoside **5**<sup>20</sup> (Scheme 10). Selective TBS-protection of the 6-OH, followed by perbenzylation ( $\rightarrow$ **39**), and cleavage of the silyl ether yielded precursor **40**. After the introduction of a 6-*O*-(thiomethyl)-methyl group with DMSO-acetic anhydride ( $\rightarrow$ **41**), treatment with phosphoric acid and *N*-iodosuccinimide ( $\rightarrow$ **42**) and debenzoylation, test compound **8** was obtained.

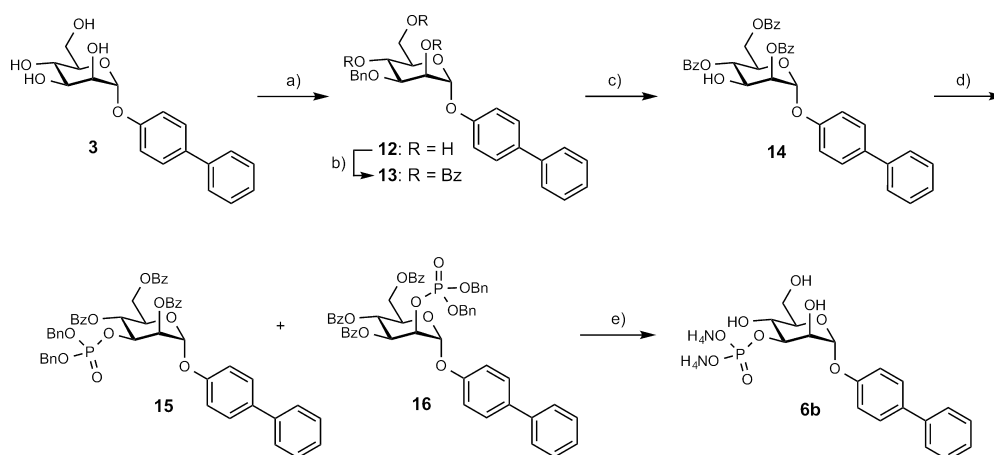
**Solubility.** The thermodynamic solubility of the phosphate prodrugs was determined in phosphate buffer (50 mM, pH 6.5). The expected improvement of aqueous solubility, which exceeds those of the active principles **3–5** by several orders of magnitude (Table 2), could be confirmed.

**ALP-Mediated Hydrolysis.** ALP-mediated hydrolysis of the various phosphate esters was studied in Caco-2 cells, which express phosphatase on the apical brush border surface of the confluent cell monolayer.<sup>48</sup> The experimental half-life (*t*<sub>1/2</sub>) was calculated from the concentration of remaining prodrug vs incubation time (Table 2).

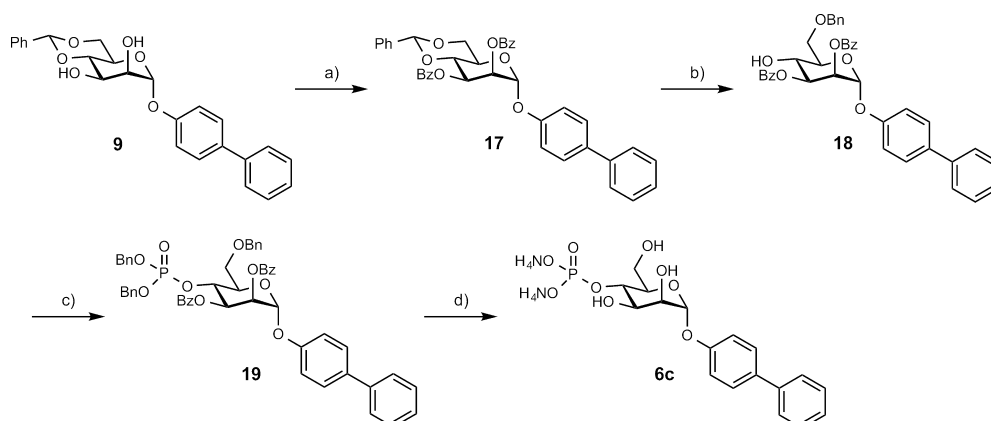
Depending on the position of the promoiety, the prodrugs showed varying propensity to dephosphorylation (Figure 3). The 2- and 3-phosphate esters (**6a**, **6b**, **7a**, and **7b**) were rapidly hydrolyzed (*t*<sub>1/2</sub> < 15 min), whereas the 4- and 6-phosphate esters (**6c**, **6d**, **7c**, and **7d**) showed prolonged half-lives (*t*<sub>1/2</sub> > 40 min). Improved stability of the latter likely results from reduced access to the ester bonds at C4 and C6 because of steric hindrance.<sup>45,49,50</sup> Therefore, with the introduction of a linker ( $\rightarrow$ **6e**, **8**), accessibility can be improved and the susceptibility to ALP-mediated cleavage was markedly increased (*t*<sub>1/2</sub> = 8.7 and 11 min, respectively).

Owing to their high propensity to ALP-mediated hydrolysis, the phosphate esters **6a**, **6b**, **7a**, **7b**, and **8** were almost entirely converted to parent drug within 60 min (Figure 3). For example, Figure 4 depicts the concentration of prodrug **7b** 60 min after application to either the apical or the basolateral side of the Caco-2 system. When applied to the apical chamber, the prodrug was almost quantitatively hydrolyzed. However, when applied to the basal chamber, the prodrug remained the prominent species detected, due to the lack of ALP on the basal



Scheme 2<sup>a</sup>

<sup>a</sup>(a) (i)  $\text{Bu}_2\text{SnO}$ , MeOH, reflux, 5 h, (ii) BnBr, toluene, 115 °C, overnight (36%); (b) BzCl, cat. DMAP, pyr, rt, overnight (99%); (c)  $\text{H}_2$  (4 bar),  $\text{Pd}(\text{OH})_2/\text{C}$ , dioxane/EtOAc, cat. AcOH, rt, overnight (73%); (d) dibenzyl *N,N*-diisopropylphosphoramidite (90%), 1,2,4-triazole, MeCN, 0 °C to rt, overnight, then 70% aq *tert*-BuOOH, rt, 1 h (80%, 3:2 mixture of 2- and 3-phosphate derivatives); (e) (i)  $\text{H}_2$  (1 bar),  $\text{Pd}(\text{OH})_2/\text{C}$ , EtOAc, 5 h, (ii) 25% aq  $\text{NH}_3/\text{MeOH}$  (4:1), rt, overnight (7%).

Scheme 3<sup>a</sup>

<sup>a</sup>(a) BzCl, cat. DMAP, pyr, rt, overnight (60%); (b)  $\text{Me}_3\text{N}\cdot\text{BH}_3$ ,  $\text{AlCl}_3$ , THF/ $\text{H}_2\text{O}$ , rt, 1 h (67%); (c) dibenzyl *N,N*-diisopropylphosphoramidite (90%), 1,2,4-triazole, MeCN, 0 °C to rt, overnight, then 70% aq *tert*-BuOOH, 1 h (53%); (d)  $\text{H}_2$ ,  $\text{Pd}(\text{OH})_2/\text{C}$ , EtOH/EtOAc, 5 h, quant; (e) 25% aq  $\text{NH}_3/\text{MeOH}$  (4:1), rt, overnight (56%).

Caco-2 cell membrane.<sup>48</sup> In addition, irrespective of dosing on the apical or basal side, the prodrug could not be detected in the receiver compartment, which corroborates the poor membrane permeability of the polar phosphate ester (Figure 4).

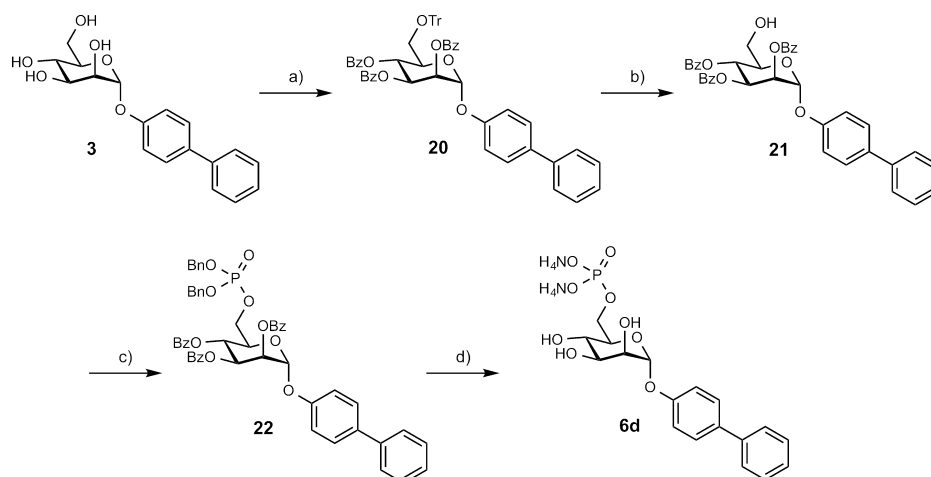
**Stability in Biorelevant Media.** Because chemical stability at various pH conditions and stability for degradation by digestive enzymes (simulated gastric and intestinal fluids,<sup>51,52</sup> for composition, see Table S1 in Supporting Information) turned out to be high (>80% after 2 h; Figure 5), the phosphate prodrugs **7a**, **7c**, and **7d** appear optimally suited to mitigate the solubility problem.

**Oral Bioavailability.** For oral administration of a phosphate prodrug several absorption rate-limiting factors need to be considered. In addition to unsuitably slow ALP-mediated hydrolysis of the phosphate prodrug, low solubility,

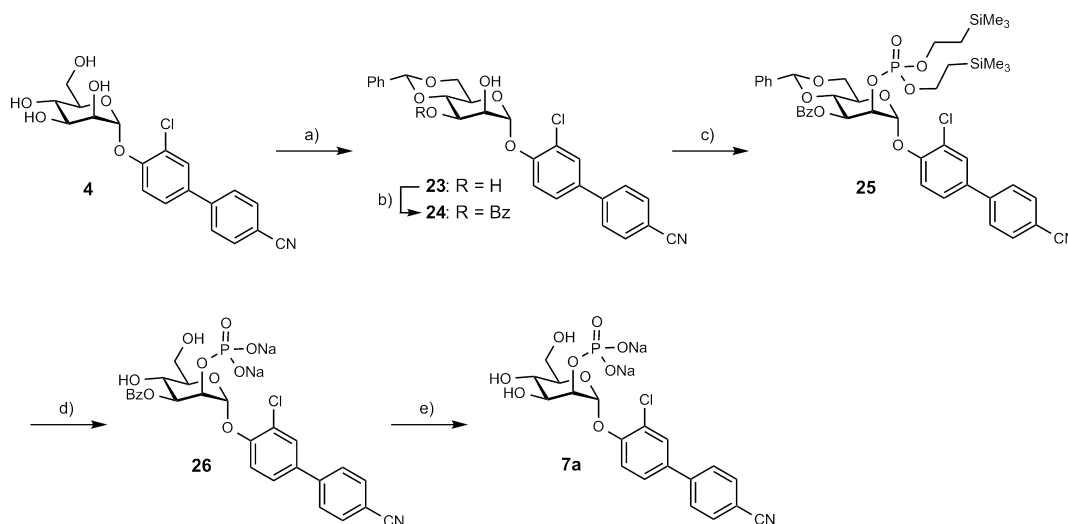
poor permeability, and efflux of the active principle can also limit oral absorption.

**In Vitro Pharmacokinetic Evaluation.** To further examine the benefits associated with improved solubility obtained upon phosphorylation of the active principle, the most labile phosphate prodrugs, **6e**, **7b**, and **8** ( $t_{1/2} \leq 12$  min, Table 2), were applied to the apical chambers of the Caco-2 system, and the accumulation of active principles **3**, **4**, and **5** on the basal side of the cell monolayer was monitored (Figure 6a–c). Applying either the active principle or the respective prodrug at equal concentrations (62.5  $\mu\text{M}$ ) to the apical chamber resulted in similar basolateral concentrations of the active principle, i.e., the hydrolysis is not the rate limiting step. When higher apical doses of the phosphate prodrugs were applied, the basolateral concentrations were markedly increased (Figure 6a–c).

Once a prodrug has been hydrolyzed in vivo, physicochemical properties of the active principle (i.e., solubility and

Scheme 4<sup>a</sup>

<sup>a</sup>(a) (i) TrCl, cat. DMAP, pyr, 80 °C, overnight, (ii) BzCl, 50 °C, overnight (88%); (b) FeCl<sub>3</sub>/H<sub>2</sub>O, DCM, rt, 5 h (62%); (c) dibenzyl *N,N*-diisopropylphosphoramidite (90%), 1,2,4-triazole, MeCN, 0 °C to rt, overnight, then 70% aq *tert*-BuOOH, rt, 1 h (66%); (d) (i) H<sub>2</sub>, Pd(OH)<sub>2</sub>/C, EtOH/EtOAc, overnight, (ii) 25% aq NH<sub>3</sub>/MeOH (4:1), rt, overnight (55%).

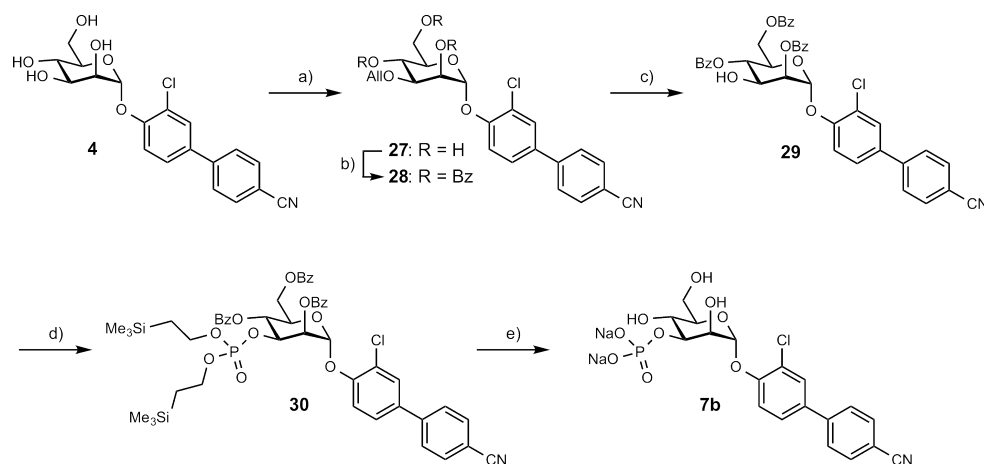
Scheme 5<sup>a</sup>

<sup>a</sup>(a) PhCH(OMe)<sub>2</sub>, *p*-TsOH, rt, 17 h (22%); (b) BzCl, DCM/pyr, 0 °C to rt, 3 h (60%); (c) bis[2-(trimethylsilyl)ethyl] *N,N*-diisopropylphosphoramidite, 1,2,4-triazole, MeCN, 0 °C to rt, 16 h, then 70% aq *tert*-BuOOH, rt, 1 h (55%); (d) TFA/DCM (1:4), rt, 2 h (61%); (e) 25% aq NH<sub>3</sub>/MeOH (4:1), rt, 16 h (71%).

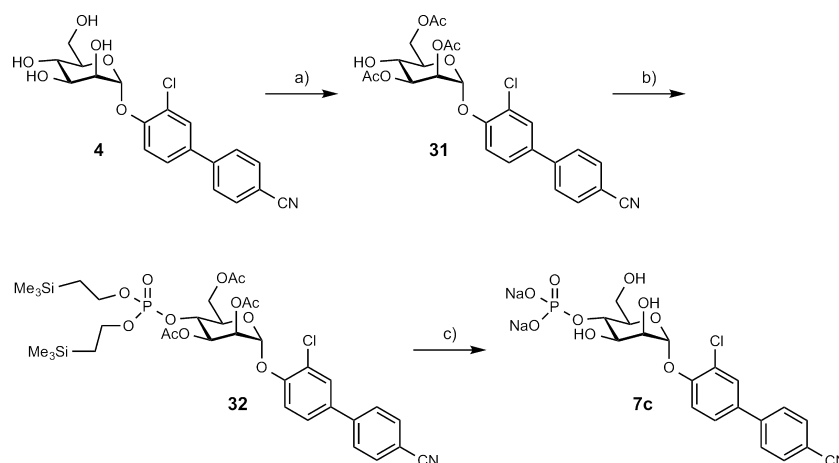
permeability) became the rate-limiting steps for absorption. When after rapid hydrolysis ( $t_{1/2} < 15$  min, Table 2) the active principle precipitated due to low solubility, the available amount for absorption was reduced. Although the active principles 3 and 5 show similar solubilities (Table 1), different basolateral concentrations were observed (Figure 6a,c). In contrast, the basolateral concentrations of compound 3 were similar or higher compared to those of compound 4 (Figure 6a,b) even though compound 4 has an 8-fold higher solubility (Table 1). On the basis of permeability data derived from PAMPA,<sup>39</sup> high passive permeability was predicted for all three antagonists ( $\log P_e < -5.7$  cm/s, Table 1).<sup>42</sup> However, for the antagonists 4 and 5, efflux ratios ( $b-a/a-b$ )  $> 2$  (Table 1) in bidirectional Caco-2 experiments were observed, indicating the

involvement of an efflux transporter (e.g., P-gp).<sup>44</sup> Because of the high apical concentrations reached from fast ALP-mediated hydrolysis of prodrugs 7b and 8, saturation of the transporter mediated efflux occurred, leading to increased basolateral concentrations of 4 and 5 (Figure 6b,c). In contrast, 3 exhibited an efflux ratio  $< 2$  (Table 1), i.e., the basolateral concentration rose proportionally to the amount of applied prodrug and did not display saturation kinetics (Figure 6a).<sup>53</sup>

**In Vivo Pharmacokinetic Studies.** In the mouse PK model, an increased intestinal uptake was anticipated for the prodrug 7c due to its increased solubility and slower hydrolysis rate. The prodrugs 7b, 7c, and 8 were administered per os at a dose of 10 mg/kg but could not be detected in plasma or urine samples. The oral bioavailability of active principle 4 upon administering

Scheme 6<sup>a</sup>

<sup>a</sup>(a) (i)  $\text{Bu}_2\text{SnO}$ , toluene, 80 °C, 6 h, (ii) AllBr,  $\text{Bu}_4\text{NI}$ , toluene, 80 °C, 20 h (55%); (b) BzCl, cat. DMAP, pyr, rt, overnight (87%); (c)  $\text{PdCl}_2$ , MeOH, 40 °C, 5 h (84%); (d) (i) bis[2-(trimethylsilyl)ethyl] *N,N*-diisopropylphosphoramidite, 1,2,4-triazole, MeCN, 0 °C to rt, 15 h, then 70% aq *tert*-BuOOH, rt, 2 h (32%); (e) (i) TFA/DCM (1:4), rt, 1.5 h, (ii) 25% aq  $\text{NH}_3/\text{MeOH}$  (4:1), rt, overnight (45%).

Scheme 7<sup>a</sup>

<sup>a</sup>(a) (i)  $\text{Bu}_2\text{SnO}$ , MeOH, 70 °C, 2 h, (ii)  $\text{Ac}_2\text{O}$ , MeCN, rt, 16 h (21%); (b) (i) bis[2-(trimethylsilyl)ethyl] *N,N*-diisopropylphosphoramidite, 1,2,4-triazole, MeCN, 0 °C to rt, 15 h, then 70% aq *tert*-BuOOH, rt, 2 h (62%); (c) (i) TFA/DCM (1:4), rt, 2 h; (ii) 25% aq  $\text{NH}_3/\text{MeOH}$  (4:1), rt, 2 h (98%).

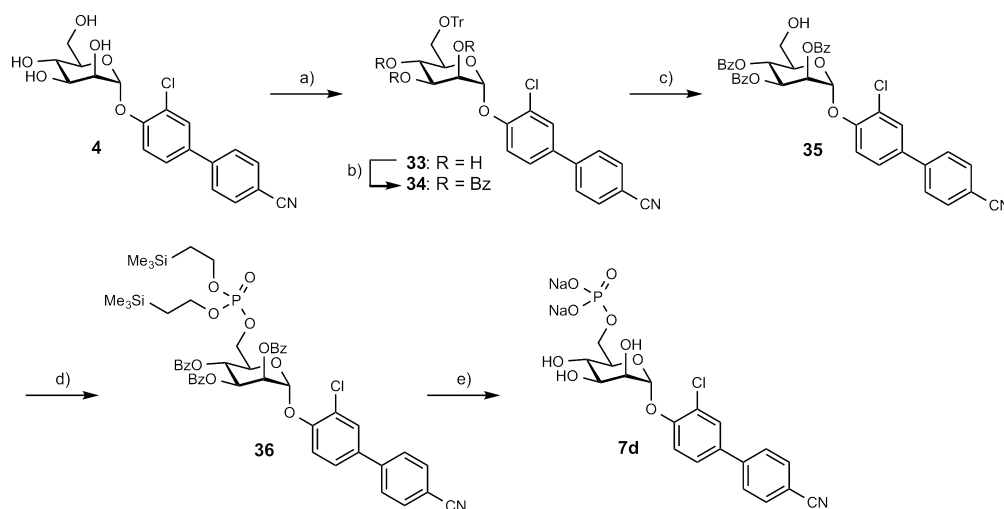
prodrug **7b** and **7c** and of active principle **5** upon administration of prodrug **8** are illustrated in Figure 7. Table 3 summarizes the pharmacokinetic parameters ( $C_{\text{max}}$ ,  $T_{\text{max}}$  and urine  $\text{AUC}_{0-24}$ ) of the different po applications.

Given the almost identical propensity to ALP-mediated hydrolysis of **7b** and **8**, the different urine profiles must be related to physicochemical properties of their active principles **4** and **5**. Indeed, antagonist **5**, besides having an 8-times lower solubility and therefore a higher propensity to precipitate after release in the small intestines, also permeates biological membranes less easily (shown in the PAMPA results, Table 1). In fact, urine  $\text{AUC}_{0-24}$  and  $C_{\text{max}}$  of **5** were similar to the pharmacokinetic parameters of **4** when applied at a dose of 1.25 mg/kg (Table 3).

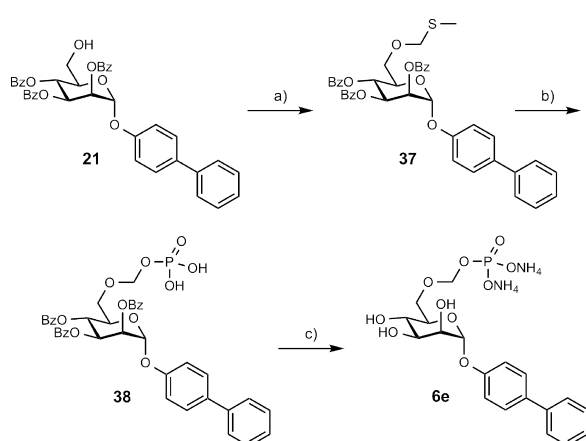
Because prodrugs **7b** and **8** are rapidly hydrolyzed in vitro, we also assessed the impact of slower ALP-mediated bioactivation and availability of the related active principle in

urine. For this purpose, we administered prodrug **7c** (in vitro  $t_{1/2}$  of 43 min, Table 2) at a dose of 10 mg/kg (Figure 7). After applying **7c**, compound **4** reached  $C_{\text{max}}$  (57  $\mu\text{g}/\text{mL}$ , Table 3) after only 26 min, as compared to 40.7  $\mu\text{g}/\text{mL}$  at 54 min for **7b**; it then remained at elevated levels for the next 3 h. Within the observation period of 3–24 h postadministration, urine levels of the two prodrugs dropped steadily. However, at 6 h, the concentration of active principle **4** originating from prodrug **7c** was approximately three times higher than the one reached with **7b**, resulting in a 2-fold increased urine  $\text{AUC}_{0-24}$  of **7c**.

The lower concentration of active principle **4** upon po application of **7b** as compared to **7c** can be rationalized by several pharmacokinetic effects. First, the fast dephosphorylation of **7b** leads to a local accumulation of **4** at the brush border in the small intestine. Because of insufficient solubility, the active principle **4** could suffer from precipitation. Because of the slower cleavage of the promoity in prodrug **7c**, the

Scheme 8<sup>a</sup>

<sup>a</sup>(a) TrCl, cat. DMAP, pyr, 80 °C, 16 h (80%); (b) BzCl, cat. DMAP, pyr, rt, 6 h (79%); (c) FeCl<sub>3</sub>, H<sub>2</sub>O, rt, 5 h (85%); (d) (i) bis-[2-(trimethylsilyl)ethyl] *N,N*-diisopropylphosphoramidite, 1,2,4-triazole, MeCN, 0 °C to rt, 15 h, then 70% aq *tert*-BuOOH, rt, 1.5h (59%); (e) (i) TFA/DCM (1:4), rt, 2 h, (ii) 25% aq NH<sub>3</sub>/MeOH (4:1), rt, overnight (68%).

Scheme 9<sup>a</sup>

<sup>a</sup>(a) DMSO, Ac<sub>2</sub>O/AcOH, rt, overnight (35%); (b) H<sub>3</sub>PO<sub>4</sub>, NIS, THF, 0 °C to rt, 1 h (58%); (c) 25% aq NH<sub>3</sub>/MeOH (4:1), rt, overnight (50%).

solubility limit of **4** takes longer to reach, enabling an improved absorption of the active principle. Moreover, although high concentrations of **4** saturate P-gp, its efflux activity still contributes to accumulated concentrations of **4** and consequently to precipitation and intestinal elimination. A slower prodrug hydrolysis apparently optimizes the timely interplay between parent drug uptake and P-gp-mediated efflux, leading to higher net absorption and urine concentrations.

Next, we addressed the question of whether increased solubility indeed leads to higher availability of active principle in the urine. Therefore, urine concentration profiles upon po application of 1.25 mg/kg (based on maximal solubility) or 7.7 mg/kg of **4** (applied as a suspension corresponding to 10 mg/kg of prodrug) were determined (Figure 7).

Oral application of the suspension of **4** resulted in a urine AUC<sub>0–24</sub> of 106.8 μg × h/mL (*C*<sub>max</sub> of 23.6 μg/mL, Table 3) as

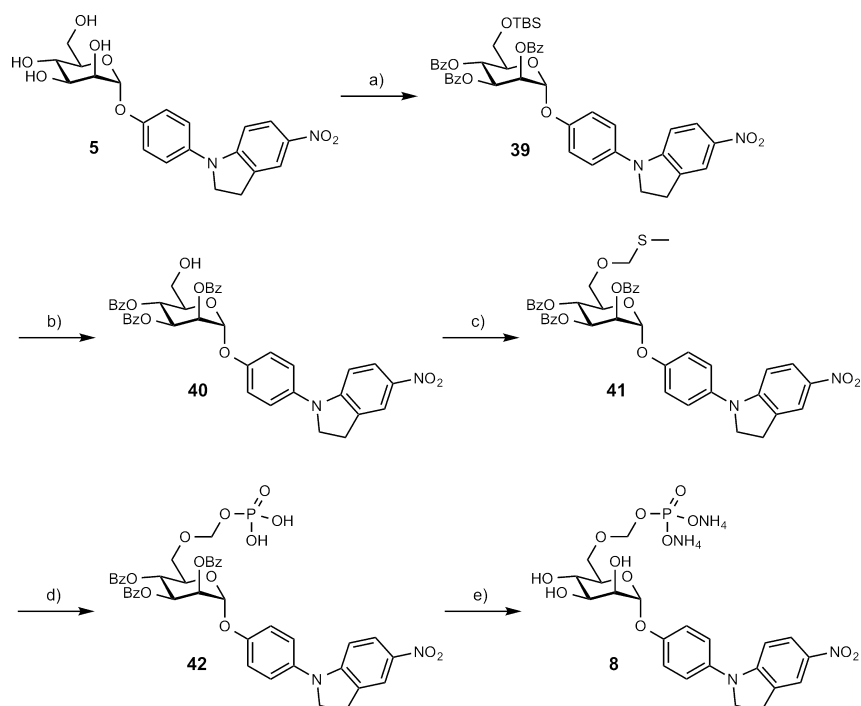
compared to a urine AUC<sub>0–24</sub> of 226.4 μg × h/mL (*C*<sub>max</sub> of 57 μg/mL, Table 3), achieved with the corresponding prodrug **7c**, demonstrating the beneficial effect of increased solubility on intestinal uptake. In addition, the application of **4** at two doses (1.25 and 7.7 mg/kg; 6.16 times greater) resulted in parallel curves with a similar *T*<sub>max</sub> and an approximate difference in urine AUC<sub>0–24</sub> of a factor of 5 and *C*<sub>max</sub> of a factor of 6 (Table 3). This is a useful observation for future dose-finding in patients.

## SUMMARY AND CONCLUSIONS

For the successful oral application of a phosphate prodrug of an active principle that displays moderate to high membrane permeability but insufficient solubility, several prerequisites need to be fulfilled. Obviously, the solubility of the prodrug should allow dissolving of the required dose (e.g., in our case 10 mg/kg). Second, because phosphate prodrugs are too polar to permeate the enterocyte layer, an efficient release of the active principle is required. Finally, slow enzymatic hydrolysis is preferred to avoid precipitation of the poorly soluble active principle.

We have demonstrated the advantages of the phosphate prodrug approach as applied to FimH antagonists with an insufficient solubility but high passive permeability. An increase in solubility of up to 140-fold could be reached upon phosphorylation of the active principle. Furthermore, either fast or slow hydrolysis was observed, depending on the position of the phosphate moiety on the mannose ring. When the phosphate ester bond was directly linked at the C2- or C3-position of mannose (→ **6a**, **6b**, **7a**, **7b**) or when an acetal linker at C6- was used (→ **6e** and **8**), enzymatic cleavage was fast (*t*<sub>1/2</sub> < 15 min). In contrast, a phosphate at the C4- or C6-position (→ **6c**, **6d**, **7c**, and **7d**) showed an enhanced enzymatic stability (*t*<sub>1/2</sub> > 40 min).

Interestingly, even when the rates of hydrolysis were similar, e.g., for prodrugs **7b** and **8**, different physicochemical properties (solubility and permeability) of their active principles influenced the *in vivo* PK properties. For antagonist **5**, which

Scheme 10<sup>a</sup>

<sup>a</sup>(a) (i) TBSCl, cat. DMAP, pyr, rt, overnight, (ii) BzCl, rt, 2 h, (quant); (b) 1 M H<sub>2</sub>SO<sub>4</sub>/MeOH, rt, 1.5 h (73%); (c) DMSO/Ac<sub>2</sub>O/HOAc, rt, overnight (74%); (d) H<sub>3</sub>PO<sub>4</sub>/NIS/THF, 0 °C to rt, 1 h (67%); (e) 25% aq NH<sub>3</sub>/MeOH/DCM, rt, overnight (41%).

**Table 2. Aqueous Solubility and Caco-2 Phosphatase-Mediated Hydrolysis ( $t_{1/2}$ ) of Prodrugs 6a–e, 7a–d, 8, and Their Active Principles 3–5, Respectively**

compd	solubility [ $\mu\text{g/mL}$ ]	$t_{1/2}$ [min]
3, active principle <sup>14,18</sup>	21	
6a	>3000	12
6b	>3000	13
6c	2703	>60
6d	>3000	>60
6e	>3000	8.7
4, active principle <sup>19</sup>	192	
7a	>3000	13
7b	>3000	12
7c	>3000	43
7d	>3000	48
5, active principle <sup>20</sup>	24	
8	>3000	11

has an 8-fold lower solubility as compared to 4, the risk of precipitation from a supersaturated solution in the small intestines needs to be taken into account.

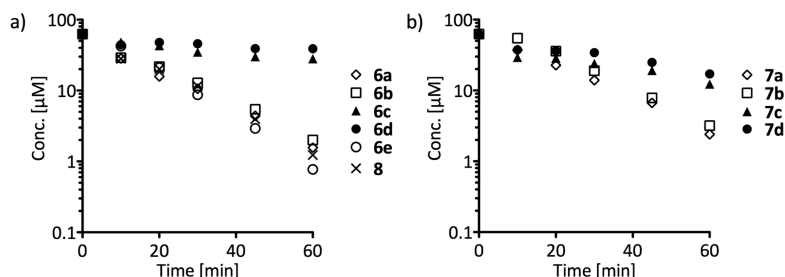
Furthermore, a high concentration gradient across the Caco-2 cell monolayer, as was reached with the more soluble phosphate prodrugs, promotes absorptive flux of the active principles 3, 4, and 5 and apparently saturates the efflux carrier activity of 4 and 5. This observation was confirmed in an *in vivo* PK study in mice, where urine AUC<sub>0–24</sub> of the active principle 4 could be doubled when prodrug 7c was applied instead of active principle 4. Moreover, *in vivo* administration of slowly hydrolyzed prodrug 7c ( $t_{1/2} < 40$  min) exhibited an increase in urine AUC<sub>0–24</sub> as compared to a phosphate prodrug with fast

enzymatic cleavage (7b,  $t_{1/2} < 15$  min). Slower conversion to the active principle prolonged intestinal uptake and renal excretion by improving the interplay between solubility, drug uptake, and saturation of P-gp mediated efflux.

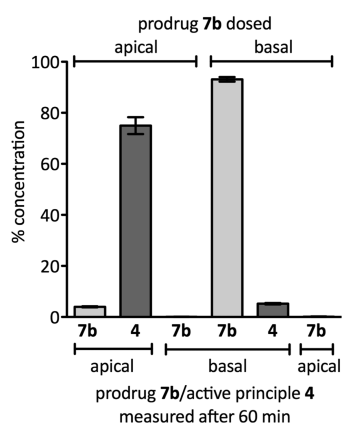
## EXPERIMENTAL SECTION

**Synthesis. General Methods.** NMR spectra were recorded on a Bruker Avance DMX-500 (500.1 MHz) spectrometer. Assignment of <sup>1</sup>H and <sup>13</sup>C NMR spectra was achieved using 2D methods (COSY, HSQC). Chemical shifts are expressed in ppm using residual CHCl<sub>3</sub> or MeOH as references. Optical rotations were measured with a PerkinElmer polarimeter 341. Electrospray ionization mass spectrometry (ESI-MS) data were obtained on a Waters Micromass ZQ instrument. Microwave-assisted reactions were carried out with a CEM Discover and Explorer. Reactions were monitored by TLC using glass plates coated with silica gel 60 F254 (Merck) and visualized by UV light and/or by charring with a molybdate solution (0.02 M solution of ammonium cerium sulfate dihydrate and ammonium molybdate tetrahydrate in aqueous 10% H<sub>2</sub>SO<sub>4</sub>). Medium pressure chromatography (MPLC) separations were carried out on a CombiFlash Companion or R<sub>f</sub> from Teledyne Isco equipped with RediSep normal-phase or RP-18 reversed-phase flash columns. Commercially available reagents were purchased from Fluka, Aldrich, or Alfa Aesar (Germany). Solvents were purchased from Sigma-Aldrich (Buchs, Switzerland) or Acros Organics (Geel, Belgium) and were dried prior to use where indicated. MeOH was dried by reflux with sodium methoxide and distilled and stored under argon atmosphere. Dichloromethane (DCM) and acetonitrile (MeCN) were dried by filtration over Al<sub>2</sub>O<sub>3</sub> (Fluka, type 5016 A basic) and stored over molecular sieves under argon. Molecular sieves (4 Å) were activated in vacuo at 300 °C for 0.5 h before use.

**Compound Purity.** Each test compound was purified by chromatography on silica (DCM/MeOH) or reversed-phase chromatography (RP-18, H<sub>2</sub>O/MeOH) prior to HPLC, HRMS, NMR, and



**Figure 3.** Decomposition of phosphomonoester prodrugs **6a–d** and **7a–d** and phosphonooxymethyl ether prodrugs **6e** and **8** in the apical compartment of the Caco-2 cell assay: (a) **6a–e**, **8**; (b) **7a–d**. Prodrugs dissolved in Dulbecco's Modified Eagle's Medium ( $62.5 \mu\text{M}$ ) were applied to the apical chamber and the concentrations of unchanged prodrug were monitored by LC-MS.



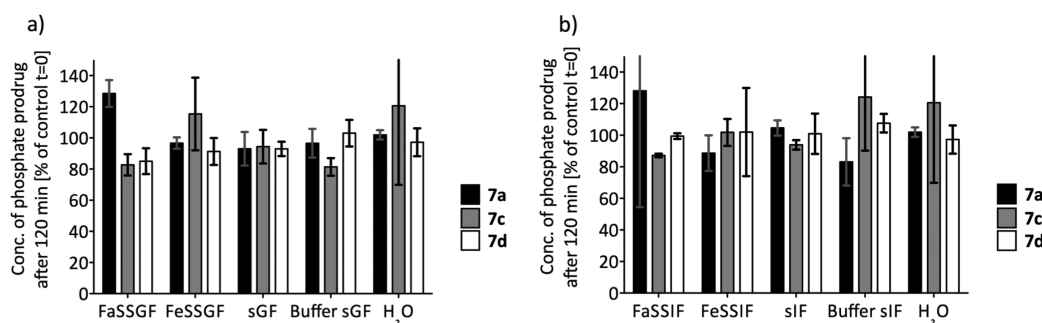
**Figure 4.** Conversion of prodrug **7b** to the active principle **4** in a Caco-2 cell monolayer model after 60 min of incubation. A prodrug solution ( $62.5 \mu\text{M}$ ) was applied either into the apical or basal chamber. Columns represent the percentage concentrations of prodrug and active principle 60 min after initiation of the experiment. Concentration of prodrug **7b** determined at time point  $t = 0$  min is defined as 100%.

activity testing. The purity of all test compounds was determined by NMR and HPLC [method A: Beckman Coulter Gold, consisting of pump 126, DAD 168 (190–410 nm) and autosampler 508; column, Waters Atlantis T3,  $3 \mu\text{m}$ ,  $2.1 \text{ mm} \times 100 \text{ mm}$ ; A,  $\text{H}_2\text{O} + 0.1\% \text{ TFA}$ ; B,  $\text{MeCN} + 0.1\% \text{ TFA}$ ; gradient, 5% B for 0.5 min, 5% B  $\rightarrow$  70% B over

19.5 min; flow rate, 0.5 mL/min. Method B: Agilent 1100/1200 with UV detection (190–410 nm); column, Waters Atlantis T3,  $3 \mu\text{m}$ ,  $2.1 \text{ mm} \times 100 \text{ mm}$ ; A,  $\text{H}_2\text{O} + 0.01\% \text{ TFA}$ ; B,  $\text{MeCN} + 0.01\% \text{ TFA}$ ; gradient, 5% B for 1 min, 5% B  $\rightarrow$  95% B over 19 min; flow rate, 0.5 mL/min. Detection: 254 nm.] to be  $\geq 95\%$  (for  $^1\text{H}$  NMR spectra and HPLC traces, see [Supporting Information](#)).

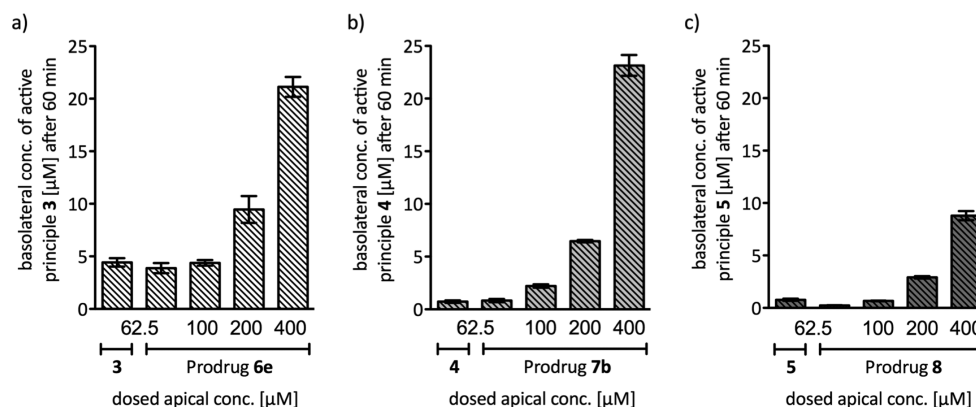
**General Procedure for Phosphorylation.** To an ice-cooled solution ( $0^\circ\text{C}$ ) of protected mannoside (1 equiv) and 1,2,4-triazole (4 equiv) in dry MeCN was added dibenzyl *N,N*-diisopropylphosphoramidite or bis[2-(trimethylsilyl)ethyl] *N,N*-diisopropylphosphoramidite (2 equiv), and the mixture was stirred for 30 min at  $0^\circ\text{C}$  and then overnight at rt. Then, 70% aq *tert*-butylhydroperoxide (4 equiv) was added and the solution was stirred for 1 h. The reaction was quenched with 1 M aq  $\text{Na}_2\text{S}_2\text{O}_3$  and 1 M aq  $\text{NaHCO}_3$ , and the mixture was extracted twice with DCM. The combined organic layers were dried over  $\text{Na}_2\text{SO}_4$ , filtered, and the solvents removed in vacuo. The residue was purified by MPLC on silica gel (petroleum ether/EtOAc) to yield the phosphorylated compounds.

**Biphenyl 2-O-Phosphoryl- $\alpha$ -D-mannopyranoside Diammonium Salt (6a).** Hydrogenolysis of compound **11** (100 mg, 0.129 mmol) was conducted in a Parr shaker with 10% Pd(OH) $_2$ /C (12 mg) and a catalytic amount of HOAc in EtOAc (6.0 mL) under hydrogen (4 bar) at rt overnight. Then, the reaction suspension was filtered through Celite and the filtrate was concentrated in vacuo. The residue was stirred in 25% aq  $\text{NH}_3$  (4 mL) and MeOH (1 mL) overnight. Then, the solvents were removed under reduced pressure, and the residue was purified by MPLC on silica (DCM/MeOH/ $\text{H}_2\text{O}$ , 6:4:0.6) to give **6a** (26.0 mg, 45%) as a white solid;  $[\alpha]_{\text{D}}^{20} + 66.7$  ( $c$  0.12,  $\text{H}_2\text{O}$ ).  $^1\text{H}$  NMR ( $\text{D}_2\text{O}$ , 500 MHz):  $\delta$  = 3.77–3.82 (m, 3H, H-5, H-6), 3.87 (t,  $J$  = 10.0 Hz, 1H, H-4), 4.14 (ddd,  $J$  = 2.0, 3.0, 10.0 Hz, 1H, H-3), 4.62 (ddd,  $J$  = 2.0, 3.0, 8.5 Hz, 1H, H-2), 5.89 (d,  $J$  = 1.5 Hz, 1H, H-1), 7.31

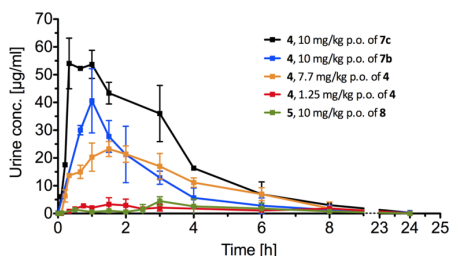


**Figure 5.** Stability of the phosphate prodrugs **7a** (black column), **7c** (gray column), and **7d** (white column) in biorelevant media. Percentage of the remaining compound concentration relative to the initial concentration ( $t = 0$  min) after 120 min of incubation in (a) simulated gastric fluids (FaSSGF, fasted-state simulated gastric fluid; FeSSGF, fed-state simulated gastric fluid; sGF, simulated gastric fluid; buffer sGF, prepared equally to sGF but without pepsin) and (b) simulated intestinal fluids (FaSSIF, fasted-state simulated intestinal fluid; FeSSIF, fed-state simulated intestinal fluid; sIF, simulated intestinal fluid; buffer sIF, prepared equally to sIF but without pancreatin) are shown. For composition see [Table S1](#) in Supporting Information.  $\text{H}_2\text{O}$  was used as a reference media. Data represent the mean (triplicates) with its corresponding standard deviation.





**Figure 6.** Accumulation of active principle (a) 3, (b) 4, and (c) 5 in the basal receiver chamber of a Caco-2 cell system 60 min after applying (a) active principle 3 or prodrug 6e, (b) active principle 4 or prodrug 7b, and (c) active principle 5 or prodrug 8 into the apical chamber. The active principles were dosed at a concentration of 62.5  $\mu\text{M}$ , which corresponds to approximately the aqueous solubilities of 3 and 5. The phosphate prodrugs were dosed at four different concentrations (62.5, 100, 200, and 400  $\mu\text{M}$ ).



**Figure 7.** Urine concentrations of active principle 4 in C3H/HeN mice upon po administration of 4 (1.25 and 7.7 mg/kg po) or the related phosphate prodrugs 7b, 7c (10 mg/kg po) and the urine concentration of the active principle 5 upon po administration of phosphate prodrug 8 (10 mg/kg po). Shown are mean values with standard deviations for groups of three (4, 1.25 mg/kg, 7b, 7c, and 8) or five (4, 7.7 mg/kg) mice.

(m, 2H, Ar-H), 7.44 (m, 1H, Ar-H), 7.55 (t,  $J = 7.5$  Hz, 2H, Ar-H), 7.71 (m, 4H, Ar-H).  $^{13}\text{C}$  NMR ( $\text{D}_2\text{O}$ , 126 MHz):  $\delta = 60.5$  (C-6), 66.6 (C-4), 70.1 (d,  $J = 5$  Hz, C-3), 73.5 (C-5), 73.6 (d,  $J = 5$  Hz, C-2), 97.0 (d,  $J = 3$  Hz, C-1), 117.2, 117.6, 126.7, 127.4, 128.0, 128.2, 129.1, 135.3, 140.0, 155.0 (12C, Ar-C). ESI-MS:  $m/z$ : calcd for  $\text{C}_{18}\text{H}_{20}\text{O}_9\text{P} [\text{M} - 2\text{NH}_4 + \text{H}]^-$ , 411.08; found, 411.06.

**Biphenyl 3-O-Phosphoryl- $\alpha$ -D-mannopyranoside Diammonium Salt (6b).** Hydrogenolysis of a 3:2-mixture of 15 and 16 (130 mg, 0.144 mmol) in EtOAc (6 mL) was conducted in the presence of 10%  $\text{Pd}(\text{OH})_2/\text{C}$  (15 mg) with a hydrogen balloon at rt for 5 h. Then, the reaction suspension was filtered through Celite and the filtrate was concentrated in vacuo. The residue was stirred in 25% aq  $\text{NH}_3$  (4 mL) and MeOH (1 mL) at rt overnight. The solvents were removed under reduced pressure, and the residue was purified by MPLC on silica gel

(DCM/MeOH/ $\text{H}_2\text{O}$ , 6:4:0.6) to provide 6b (4.5 mg, 7%, still containing some of the 2-phosphate impurity) as white solid;  $[\alpha]_{\text{D}}^{20} + 91.7$  (c 0.12,  $\text{D}_2\text{O}$ ).  $^1\text{H}$  NMR ( $\text{D}_2\text{O}$ , 500 MHz):  $\delta = 3.75\text{--}3.83$  (m, 3H, H-5, H-6), 3.92 (t,  $J = 9.5$  Hz, 1H, H-4), 4.39 (m, 1H, H-2), 4.55 (dt,  $J = 3.0, 9.0$  Hz, 1H, H-3), 5.72 (s, 1H, H-1), 7.32 (m, 2H, Ar-H), 7.45 (m, 1H, Ar-H), 7.54 (t,  $J = 7.5$  Hz, 2H, Ar-H), 7.71 (m, 4H, Ar-H).  $^{13}\text{C}$  NMR ( $\text{D}_2\text{O}$ , 126 MHz):  $\delta = 61.4$  (C-6), 66.9 (d,  $J = 3$  Hz, C-4), 70.0 (d,  $J = 3$  Hz, C-2), 74.0 (C-5), 75.0 (d,  $J = 5$  Hz, C-3), 98.5 (C-1), 118.1, 118.3, 127.31, 127.34, 128.0, 128.8, 129.8, 135.8, 140.6, 155.7 (12C, Ar-C). ESI-MS:  $m/z$ : calcd for  $\text{C}_{18}\text{H}_{20}\text{O}_9\text{P} [\text{M} - 2\text{NH}_4 + \text{H}]^-$ , 411.08; found, 411.12.

**Biphenyl 4-O-Phosphoryl- $\alpha$ -D-mannopyranoside Diammonium Salt (6c).** Hydrogenolysis of 19 (80 mg, 90  $\mu\text{mol}$ ) was done in EtOAc (4 mL) in the presence of 10%  $\text{Pd}(\text{OH})_2/\text{C}$  (12 mg) with hydrogen balloon at rt overnight. Then the reaction suspension was filtered through Celite, and the filtrate was concentrated in vacuo to provide the debenzylated intermediate. The crude intermediate (52 mg) was stirred in MeOH (1 mL) and 25% aq  $\text{NH}_3$  (4 mL) overnight. The solvent was removed under reduced pressure, and the residue was purified by MPLC on silica (DCM/MeOH/ $\text{H}_2\text{O}$ , 4:1:0.1) to yield 6c (18 mg, 56%) as a white solid;  $[\alpha]_{\text{D}}^{20} + 104.8$  (c 0.20,  $\text{H}_2\text{O}$ ).  $^1\text{H}$  NMR ( $\text{D}_2\text{O}$ , 500 MHz):  $\delta = 3.75\text{--}3.87$  (m, 3H, H-5, H-6), 4.24 (m, 3H, H-2, H-3, H-4), 5.70 (s, 1H, H-1), 7.30 (d,  $J = 8.5$  Hz, 2H, Ar-H), 7.43 (t,  $J = 7.5$  Hz, 1H, Ar-H), 7.54 (t,  $J = 8.0$  Hz, 2H, Ar-H), 7.70 (d,  $J = 8.0$  Hz, 4H, Ar-H).  $^{13}\text{C}$  NMR ( $\text{D}_2\text{O}$ , 126 MHz):  $\delta = 60.6$  (C-6), 69.6 (C-2), 69.7 (d,  $J = 5$  Hz, C-4), 70.7 (C-3), 72.6 (d,  $J = 7$  Hz, C-5), 97.9 (C-1), 117.6, 126.7, 127.4, 128.2, 129.1, 135.3, 140.0, 155.1 (12C, Ar-C). ESI-MS:  $m/z$ : calcd for  $\text{C}_{18}\text{H}_{20}\text{O}_9\text{P} [\text{M} - 2\text{NH}_4 + \text{H}]^-$ , 411.08; found, 411.11.

**Biphenyl 6-O-Phosphoryl- $\alpha$ -D-mannopyranoside Diammonium Salt (6d).** Hydrogenolysis of 22 (64.0 mg, 70.0  $\mu\text{mol}$ ) was done in EtOAc/EtOH (5 mL, 3:2) in the presence of 10%  $\text{Pd}(\text{OH})_2/\text{C}$  (7.5 mg) with hydrogen balloon at rt overnight. The reaction suspension

**Table 3. Pharmacokinetic Parameters ( $C_{\text{max}}$ ,  $T_{\text{max}}$ , and Urine  $\text{AUC}_{0\text{--}24}$ ) Determined after a Single po Application of Compounds 4, 7b, 7c, and 8, in Female C3H/HeN mice.<sup>44</sup>**

parameter	4	4	7b (prodrug of 4)	7c (prodrug of 4)	8 (prodrug of 5)
dose (mg/kg) po	1.25	7.7	10	10	10
$C_{\text{max}}$ ( $\mu\text{g}/\text{mL}$ )	$3.9 \pm 1.9$	$23.6 \pm 3.1$	$40.7 \pm 11.4$	$57.0 \pm 4.2$	$4.5 \pm 1.6$
$T_{\text{max}}$ (h)	$1.4 \pm 0.6$	$1.4 \pm 0.2$	$0.9 \pm 0.2$	$0.44 \pm 0.2$	$3.0 \pm 0.0$
urine $\text{AUC}_{0\text{--}24}$ ( $\mu\text{g} \times \text{h}/\text{mL}$ )	$21.5 \pm 5.2$	$106.8 \pm 18.0$	$103.9 \pm 7.7$	$226.4^* \pm 42.8$	$24.6 \pm 10.7$

<sup>a</sup>Values were calculated using PKsolver and are shown as mean with standard deviation.<sup>54</sup>  $C_{\text{max}}$ , maximal concentration;  $T_{\text{max}}$ , time were  $C_{\text{max}}$  is reached; AUC, area under the curve. <sup>\*</sup>Statistical differences at  $p < 0.001$  (Two-Way ANOVA, Prism; GraphPad Software, version 5.0f), compared to all other po applications.

was filtered through Celite, and the filtrate was concentrated in vacuo. The crude intermediate was stirred in MeOH (1 mL) and 25% aq NH<sub>3</sub> (4 mL) overnight. The solvents were removed under reduced pressure, and the residue was purified by MPLC on silica (DCM/MeOH/H<sub>2</sub>O, 4:1:0.1) to yield **6d** (16.0 mg, 55%) as a white solid;  $[\alpha]_D^{20} + 74.1$  (c 0.16, H<sub>2</sub>O). <sup>1</sup>H NMR (D<sub>2</sub>O, 500 MHz):  $\delta = 3.83$  (m, 1H, H-5), 3.89 (ddd,  $J = 1.9, 4.9, 12.0$  Hz, 1H, H-6a), 4.01 (t,  $J = 9.9$  Hz, 1H, H-4), 4.08 (m, 1H, H-6b), 4.11 (dd,  $J = 3.5, 10.0$  Hz, 1H, H-3), 4.21 (dd,  $J = 1.8, 3.4$  Hz, 1H, H-2), 5.69 (d,  $J = 1.4$  Hz, 1H, H-1), 7.28 (m, 2H, Ar-H), 7.49 (t,  $J = 7.4$  Hz, 1H, Ar-H), 7.54 (t,  $J = 7.7$  Hz, 2H, Ar-H), 7.70 (d,  $J = 8.7$  Hz, 4H, Ar-H). <sup>13</sup>C NMR (D<sub>2</sub>O, 126 MHz):  $\delta = 62.6$  ( $J = 4$  Hz, C-6), 65.8 (C-4), 70.0, 70.1 (C-2, C-3), 72.9 (d,  $J = 8$  Hz, C-5), 98.4 (C-1), 117.5, 127.4, 126.7, 128.3, 129.1, 135.3, 140.0, 155.1 (12C, Ar-C). ESI-MS:  $m/z$ : calcd for C<sub>15</sub>H<sub>20</sub>O<sub>9</sub>P [M - 2NH<sub>4</sub> + H]<sup>+</sup>, 411.08; found, 411.09.

**Biphenyl 6-O-(Phosphonooxymethyl)- $\alpha$ -D-mannopyranoside Diammonium Salt (6e).** Compound **38** (110 mg, 0.146 mmol) was stirred in MeOH (1 mL) and 25% aq NH<sub>3</sub> (4 mL) overnight. The solvents were removed under reduced pressure, and the residue was purified by MPLC on RP-18 (H<sub>2</sub>O/MeOH) to yield **6e** (32.3 mg, 50%) as a white solid;  $[\alpha]_D^{20} + 75.5$  (c 0.32, H<sub>2</sub>O). <sup>1</sup>H NMR (D<sub>2</sub>O, 500 MHz):  $\delta = 3.85$  (dd,  $J = 2.0, 11.5$  Hz, 1H, H-6a), 3.88 (m, 1H, H-5), 3.93 (t,  $J = 9.5$  Hz, 1H, H-4), 4.10 (dd,  $J = 3.5, 9.5$  Hz, 1H, H-3), 3.97 (dd,  $J = 4.0, 11.5$  Hz, 1H, H-6b), 4.22 (dd,  $J = 2.0, 3.5$  Hz, 1H, H-2), 4.94 (A of ABX,  $J = 5.5, 11.0$  Hz, 1H, CH<sub>2</sub>), 5.04 (B of ABX,  $J = 5.5, 8.5$  Hz, 1H, CH<sub>2</sub>), 5.69 (d, 1.5 Hz, 1H, H-1), 7.28 (m, 2H, Ar-H), 7.44 (m, 1H, Ar-H), 7.54 (m, 2H, Ar-H), 7.69–7.72 (m, 4H, Ar-H). <sup>13</sup>C NMR (D<sub>2</sub>O, 126 MHz):  $\delta = 66.1$  (C-4), 66.6 (C-6), 69.9 (C-2), 70.3 (C-3), 72.2 (C-5), 90.4 (d,  $J = 4$  Hz, CH<sub>2</sub>), 98.3 (C-1), 117.5, 126.7, 127.4, 128.3, 128.8, 129.1, 132.5, 135.4, 140.0, 155.0 (12C, Ar-C). ESI-MS:  $m/z$ : calcd for C<sub>19</sub>H<sub>22</sub>O<sub>10</sub>P [M - 2NH<sub>4</sub> + H]<sup>+</sup>, 441.10; found, 440.92.

**3'-Chloro-4'-(2-O-phosphoryl- $\alpha$ -D-mannopyranosyloxy)-biphenyl-4-carbonitrile Disodium Salt (7a).** Compound **26** (34.7 mg, 56.0  $\mu$ mol) was dissolved in MeOH (0.25 mL) and 25% aq NH<sub>3</sub> (1 mL). The mixture was stirred for 16 h at rt. The solvents were removed in vacuo, and the residue was dissolved in H<sub>2</sub>O (0.5 mL) containing a drop of 1 M aq NaOH and purified by MPLC on RP-18 (H<sub>2</sub>O/MeOH) to yield pure 2-phosphate **7a** (20.4 mg, 71%) as the sodium salt;  $[\alpha]_D^{20} + 17.9$  (c 0.78, H<sub>2</sub>O). <sup>1</sup>H NMR (500 MHz, D<sub>2</sub>O):  $\delta = 3.70$ –3.82 (m, 3H, H-5, H-6), 3.92 (t,  $J = 9.8$  Hz, 1H, H-4), 4.13 (dd,  $J = 3.0, 9.7$  Hz, 1H, H-3), 4.66 (dt,  $J = 2.4, 8.3$  Hz, 1H, H-2), 5.97 (d,  $J = 1.2$  Hz, 1H, H-1), 7.40 (d,  $J = 8.7$  Hz, 1H, Ar-H), 7.45–7.53 (m, 4H, Ar-H), 7.66 (d,  $J = 8.4$  Hz, 2H, Ar-H). <sup>13</sup>C NMR (126 MHz, D<sub>2</sub>O):  $\delta = 62.0$  (C-6), 68.6 (C-4), 72.3 (d,  $J = 3$  Hz, C-3), 73.8 (d,  $J = 4$  Hz, C-2), 99.2 (d,  $J = 5$  Hz, C-1), 111.0, 118.9, 121.2, 125.5, 128.2, 128.4, 130.1, 134.4, 135.4, 144.7, 152.5 (13C, 12 Ar-C, CN). IR (KBr):  $\nu = 3436$  (vs, OH), 2230 (w, CN) cm<sup>-1</sup>. ESI-MS:  $m/z$ : calcd for C<sub>19</sub>H<sub>18</sub>ClNO<sub>6</sub>P [M - 2Na + H]<sup>+</sup>, 470.04; found, 469.96.

**3'-Chloro-4'-(3-O-phosphoryl- $\alpha$ -D-mannopyranosyloxy)-biphenyl-4-carbonitrile Disodium Salt (7b).** A solution of **30** (89.1 mg, 90  $\mu$ mol) in dry DCM (2 mL) was treated with TFA (500  $\mu$ L) for 1.5 h at rt under argon. Then, the mixture was evaporated to dryness in vacuo to yield the benzoylated intermediate, which was dissolved in MeOH (1 mL) and 25% aq NH<sub>3</sub> (4 mL). The mixture was stirred at rt overnight. The solvents were removed in vacuo, and the residue was dissolved in H<sub>2</sub>O (1 mL) containing two drops of 1 M aq NaOH and purified by MPLC on RP-18 (H<sub>2</sub>O/MeOH, 95:5–4:1) to yield **7b** (20.7 mg, 45%);  $[\alpha]_D^{20} + 42.5$  (c 0.82, H<sub>2</sub>O). <sup>1</sup>H NMR (500 MHz, D<sub>2</sub>O):  $\delta = 3.74$  (dd,  $J = 5.8, 12.4$  Hz, 1H, H-6a), 3.77–3.83 (m, 2H, H-6b, H-5), 3.91 (t,  $J = 9.6$  Hz, 1H, H-4), 4.43 (dd,  $J = 1.8, 3.4$  Hz, 1H, H-2), 4.55 (dt,  $J = 3.4, 8.8$  Hz, 1H, H-3), 5.76 (d,  $J = 1.5$  Hz, 1H, H-1), 7.42 (d,  $J = 8.7$  Hz, 1H, Ar-H), 7.58 (dd,  $J = 2.3, 8.7$  Hz, 1H, Ar-H), 7.71 (d,  $J = 8.5$  Hz, 2H, Ar-H), 7.75 (d,  $J = 2.3$  Hz, 1H, Ar-H), 7.80 (d,  $J = 8.5$  Hz, 2H, Ar-H). <sup>13</sup>C NMR (126 MHz, D<sub>2</sub>O):  $\delta = 62.2$  (C-6), 68.3 (d,  $J = 3$  Hz, C-4), 70.9 (d,  $J = 4$  Hz, C-2), 74.9 (d,  $J = 5$  Hz, C-3), 75.3 (C-5), 99.8 (C-1), 111.1, 121.2, 125.7, 128.2, 128.6, 130.3, 134.4, 135.9, 144.9, 152.5 (13C, 12 Ar-C, CN). IR (KBr):  $\nu = 3436$  (vs, OH), 2230 (w, CN) cm<sup>-1</sup>. ESI-MS:  $m/z$ : calcd for C<sub>19</sub>H<sub>18</sub>ClNO<sub>6</sub>P [M - 2NH<sub>4</sub> + H]<sup>+</sup>, 470.04; found, 470.12.

**3'-Chloro-4'-(2,3,4-O-benzoyl-4-O-phosphoryl- $\alpha$ -D-mannopyranosyloxy)-biphenyl-4-carbonitrile Disodium Salt (7c).** Prepared according to the procedure described for **7b**. Compound **32** (37.3 mg, 27  $\mu$ mol) was subsequently treated with TFA (300  $\mu$ L) in DCM (1.2 mL) for 2 h, and then with MeOH (0.5 mL) and 25% aq NH<sub>3</sub> (2 mL) for 2 h. Purification by MPLC on RP-18 (H<sub>2</sub>O/MeOH, 95:5–4:1) yielded **7c** (23.6 mg, 98%);  $[\alpha]_D^{20} + 70.0$  (c 0.81, H<sub>2</sub>O). <sup>1</sup>H NMR (500 MHz, D<sub>2</sub>O):  $\delta = 3.64$ –3.71 (m, 2H, H-6a, H-5), 3.85 (dd,  $J = 4.1, 12.5$  Hz, 1H, H-6b), 4.17–4.28 (m, 3H, H-3, H-2, H-4), 5.56 (s, 1H, H-1), 7.11 (d,  $J = 1.9$  Hz, 1H, Ar-H), 7.16 (d,  $J = 8.7$  Hz, 1H, Ar-H), 7.19 (m, 3H, Ar-H), 7.41 (d,  $J = 8.3$  Hz, 2H, Ar-H). <sup>13</sup>C NMR (126 MHz, D<sub>2</sub>O):  $\delta = 60.7$  (C-6), 69.2 (d,  $J = 5$  Hz, C-4), 69.6, 70.9 (C-2, C-3), 73.3 (d,  $J = 7$  Hz, C-5), 98.6 (C-1), 109.5, 117.5, 124.1, 126.6, 128.2, 132.8, 134.0, 142.7, 151.4 (13C, 12 Ar-C, CN). IR (KBr):  $\nu = 3433$  (vs, OH), 2227 (w, CN) cm<sup>-1</sup>. ESI-MS:  $m/z$ : calcd for C<sub>19</sub>H<sub>18</sub>ClNO<sub>6</sub>P [M - 2Na + H]<sup>+</sup>, 470.04; found, 470.07.

**3'-Chloro-4'-(6-O-phosphoryl- $\alpha$ -D-mannopyranosyloxy)-biphenyl-4-carbonitrile Disodium Salt (7d).** Prepared according to the procedure described for **7b**. Compound **36** (50.8 mg, 90  $\mu$ mol) was subsequently treated with TFA (400  $\mu$ L) in DCM (1.6 mL) for 2 h and then with MeOH (0.5 mL) and 25% aq NH<sub>3</sub> (2 mL) overnight. Purification by MPLC on RP-18 (H<sub>2</sub>O/MeOH, 95:5–4:1) yielded **7d** (18.1 mg, 68%);  $[\alpha]_D^{20} + 40.3$  (c 0.58, H<sub>2</sub>O). <sup>1</sup>H NMR (500 MHz, D<sub>2</sub>O):  $\delta = 3.75$  (d,  $J = 9.6$  Hz, 1H, H-5), 3.81 (m, 1H, H-6a), 4.04–4.13 (m, 2H, H-4, H-6b), 4.15 (dd,  $J = 3.4, 10.1$  Hz, 1H, H-3), 4.25 (dd,  $J = 1.8, 3.3$  Hz, 1H, H-2), 5.66 (d,  $J = 1.4$  Hz, 1H, H-1), 7.23 (d,  $J = 8.7$  Hz, 1H, Ar-H), 7.33 (d,  $J = 2.3$  Hz, 1H, Ar-H), 7.35–7.41 (m, 3H, Ar-H), 7.55 (d,  $J = 8.4$  Hz, 2H, Ar-H). <sup>13</sup>C NMR (126 MHz, D<sub>2</sub>O):  $\delta = 62.8$  (d,  $J = 4$  Hz, C-6), 66.2 (C-4), 70.5, 70.6 (C-2, C-3), 74.2 (d,  $J = 7$  Hz, C-5), 99.3 (C-1), 110.0, 118.0, 120.3, 124.6, 127.3, 129.1, 133.4, 134.5, 143.6, 152.0 (13C, 12 Ar-C, CN). IR (KBr):  $\nu = 3436$  (vs, OH), 2225 (w, CN) cm<sup>-1</sup>. ESI-MS:  $m/z$ : calcd for C<sub>19</sub>H<sub>18</sub>ClNO<sub>6</sub>P [M - 2Na + H]<sup>+</sup>, 470.04; found, 470.02.

**4-(5-Nitroindolin-1-yl)phenyl 6-O-(phosphonooxy)-methyl  $\alpha$ -D-Mannopyranoside Diammonium Salt (8).** Compound **42** (278 mg, 0.337 mmol) was stirred in a mixture of MeOH (5 mL), DCM (4 mL), and 25% aq NH<sub>3</sub> (8 mL) overnight. The solvent was removed under reduced pressure, and the residue was purified by MPLC on RP-18 (H<sub>2</sub>O/MeOH) to give **8** (78 mg, 41%). <sup>1</sup>H NMR (D<sub>2</sub>O, 500 MHz):  $\delta = 3.21$  (t,  $J = 8.4$  Hz, 2H, CH<sub>2</sub>), 3.81 (dd,  $J = 1.8, 11.3$  Hz, 1H, H-6a), 3.86 (m, 1H, H-5), 3.91 (t,  $J = 9.7$  Hz, 2H, NCH<sub>2</sub>), 3.96 (dd,  $J = 4.2, 11.3$  Hz, 1H, H-6b), 4.04 (dd,  $J = 3.5, 9.6$  Hz, 1H, H-3), 4.14 (t,  $J = 8.8$  Hz, 2H, CH<sub>2</sub>), 4.16 (dd,  $J = 1.8, 3.4$  Hz, 1H, H-2), 4.89 (A of ABX,  $J = 5.6, 10.8$  Hz, 1H, CH<sub>2</sub>), 5.00 (B of ABX,  $J = 5.6, 8.1$  Hz, 1H, CH<sub>2</sub>), 5.60 (s, 1H, H-1), 6.86 (d,  $J = 8.9$  Hz, 1H, Ar-H), 7.22 (d,  $J = 8.9$  Hz, 2H, Ar-H), 7.39 (d,  $J = 8.8$  Hz, 2H, Ar-H), 8.01 (s, 1H, Ar-H), 8.05 (d,  $J = 9.3$  Hz, 1H, Ar-H). <sup>13</sup>C NMR (D<sub>2</sub>O, 126 MHz):  $\delta = 26.3$  (CH<sub>2</sub>), 53.6 (NCH<sub>2</sub>), 66.1, 66.3 (C-4, C-6), 69.9 (C-2), 70.2 (C-3), 72.3 (C-5), 90.1 (d,  $J = 4$  Hz, CH<sub>2</sub>), 98.7 (C-1), 105.6, 118.1, 121.2, 121.9, 122.0, 127.0, 132.5, 136.6, 137.5, 151.9, 154.6 (12C, 12 Ar-C). ESI-MS:  $m/z$ : calcd for C<sub>21</sub>H<sub>24</sub>N<sub>2</sub>O<sub>12</sub>P [M - 2NH<sub>4</sub> + H]<sup>+</sup>, 527.11; found, 527.18.

**Biphenyl 4,6-O-Benzylidene- $\alpha$ -D-mannopyranoside (9).** To a mixture of biphenyl  $\alpha$ -D-mannopyranoside (**1**)<sup>14,18</sup> (1.16 g, 3.51 mmol) and benzaldehyde dimethyl acetal (1.58 mL, 10.5 mmol) in dry MeCN/DMF (10 mL/1 mL) was added *p*-toluenesulfonic acid (40 mg). The reaction mixture was stirred at 80 °C overnight and then neutralized with satd aq NaHCO<sub>3</sub>. Then the mixture was diluted with DCM (20 mL) and washed with water (2  $\times$  10 mL) and brine (10 mL). The organic layer was dried over Na<sub>2</sub>SO<sub>4</sub> and concentrated. The residue was purified by MPLC on silica (DCM/MeOH, 20:1–9:1) to afford **9** (1.03 g, 70%) as a white solid;  $[\alpha]_D^{20} + 163.1$  (c 1.09, CHCl<sub>3</sub>/MeOH, 1:1). <sup>1</sup>H NMR (CDCl<sub>3</sub>, 500 MHz):  $\delta = 3.83$  (t,  $J = 10.0$  Hz, 1H, H-6a), 3.99 (td,  $J = 4.5, 9.5$  Hz, 1H, H-5), 4.04 (t,  $J = 9.5$  Hz, 1H, H-4), 4.22 (dd,  $J = 5.0, 10.0$  Hz, 1H, H-6b), 4.28 (m, 1H, H-2), 4.33 (dd,  $J = 3.5, 9.5$  Hz, 1H, H-3), 5.60 (s, 1H, PhCH), 5.66 (s, 1H, H-1), 7.13 (m, 2H, Ar-H), 7.31–7.50 (m, 8H, Ar-H), 7.55 (m, 4H, Ar-H). <sup>13</sup>C NMR (CDCl<sub>3</sub>, 126 MHz):  $\delta = 63.8$  (C-5), 68.6 (C-3), 68.7 (C-6), 70.9 (C-2), 78.7 (C-4), 98.1 (C-1), 102.3 (PhCH), 116.6, 126.3, 126.8, 127.0, 128.3, 128.4, 128.8, 129.0, 129.3, 129.7, 134.5, 135.7, 137.1,



140.5, 155.4 (18C, Ar-C). ESI-MS:  $m/z$ : calcd for  $C_{25}H_{24}NaO_6$  [ $M + Na$ ] $^+$ , 443.15; found, 443.12.

**Biphenyl 3-O-Benzyl-4,6-O-benzylidene- $\alpha$ -D-mannopyranoside (10).** A suspension of **9** (380 mg, 0.900 mmol) and dibutyltin oxide (247 mg, 0.990 mmol) in dry toluene (6 mL) was refluxed at 135 °C for 3 h. The mixture was concentrated to dryness, and tetrabutylammonium bromide (320 mg, 0.990 mmol) and benzyl bromide (0.13 mL, 1.08 mmol) in dry toluene (6 mL) were added. The reaction mixture was stirred at 115 °C overnight, the solvent was removed under reduced pressure, and the residue was purified by MPLC on silica (petroleum ether/EtOAc, 6:1–4:1) to give **10** (370 mg, 80%) as a white solid;  $[\alpha]_D^{20} + 139.6$  ( $c$  2.66,  $CHCl_3$ ).  $^1H$  NMR ( $CDCl_3$ , 500 MHz):  $\delta$  = 3.87 (t,  $J$  = 10.5 Hz, 1H, H-6a), 4.01 (td,  $J$  = 5.0, 10.0 Hz, 1H, H-5), 4.17 (dd,  $J$  = 3.0, 9.5 Hz, 1H, H-3), 4.20–4.26 (m, 2H, H-6b, H-4), 4.31 (dd,  $J$  = 1.5, 3.0 Hz, 1H, H-2), 4.82 (d,  $J$  = 12.0 Hz, 1H,  $OCH_2Ph$ ), 4.97 (d,  $J$  = 12.0 Hz, 1H,  $OCH_2Ph$ ), 5.66 (s, 1H, PhCH), 5.69 (d,  $J$  = 1.0 Hz, 1H, H-1), 7.13 (m, 2H, Ar-H), 7.37–7.46 (m, 10H, Ar-H), 7.51–7.58 (m, 7H, Ar-H).  $^{13}C$  NMR ( $CDCl_3$ , 126 MHz):  $\delta$  = 64.0 (C-5), 68.7 (C-6), 70.0 (C-2), 73.3 ( $OCH_2Ph$ ), 75.4 (C-3), 78.7 (C-4), 97.9 (C-1), 101.7 (PhCH), 116.7, 126.1, 126.8, 127.8, 127.0, 127.8, 128.0, 128.3, 128.5, 128.7, 128.8, 128.9, 129.0, 129.7, 134.5, 135.7, 137.4, 137.9, 140.5, 155.3 (24C, Ar-C). ESI-MS:  $m/z$ : calcd for  $C_{33}H_{30}NaO_6$  [ $M + Na$ ] $^+$ , 533.19; found, 533.17.

**Biphenyl 2-O-Dibenzylphosphoryl-3-O-benzyl-4,6-O-benzylidene- $\alpha$ -D-mannopyranoside (11).** According to the general procedure, compound **10** (194 mg, 0.250 mmol) was reacted with 1,2,4-triazole (69.5 mg, 1.00 mmol) and dibenzyl *N,N*-diisopropylphosphoramidite (90%, 187  $\mu$ L, 0.500 mmol) in MeCN (3.0 mL), followed by treatment with 70% aq *tert*-butylhydroperoxide (150  $\mu$ L) to yield **11** (120 mg, 62%) as a white solid;  $[\alpha]_D^{20} + 55.3$  ( $c$  0.38, DCM).  $^1H$  NMR ( $CDCl_3$ , 500 MHz):  $\delta$  = 3.81 (t,  $J$  = 10.5 Hz, 1H, H-6a), 3.99 (td,  $J$  = 5.0, 10.0 Hz, 1H, H-5), 4.11 (t,  $J$  = 10.0 Hz, 1H, H-4), 4.22 (m, 2H, H-3, H-6b), 4.85 (m, 2H,  $OCH_2Ph$ ), 5.30 (m, 1H, H-2), 5.08–5.12 (m, 4H,  $OCH_2Ph$ ), 5.62 (m, 2H, H-1, PhCH), 7.03 (m, 2H, Ar-H), 7.26–7.58 (m, 27H, Ar-H).  $^{13}C$  NMR ( $CDCl_3$ , 126 MHz):  $\delta$  = 64.6 (C-5), 68.5 (C-6), 69.5 (d,  $J$  = 6 Hz,  $OCH_2Ph$ ), 69.6 (d,  $J$  = 6 Hz,  $OCH_2Ph$ ), 72.8 ( $OCH_2Ph$ ), 73.9 (d,  $J$  = 5 Hz, C-3), 74.6 (d,  $J$  = 6 Hz, C-2), 78.2 (C-4), 97.2 (d,  $J$  = 3 Hz, C-1), 101.6 (PhCH), 116.8, 126.0, 126.8, 126.9, 127.0, 127.6, 127.7, 127.74, 127.85, 127.92, 128.19, 128.22, 128.3, 128.45, 128.52, 128.6, 128.7, 128.9, 135.66, 135.71, 135.76, 135.8, 135.9, 137.4, 137.5, 138.0, 140.5, 155.0 (36C, Ar-C). ESI-MS:  $m/z$ : calcd for  $C_{46}H_{44}O_9P$  [ $M + H$ ] $^+$ , 771.27; found, 771.37.

**Biphenyl 3-O-Benzyl- $\alpha$ -D-mannopyranoside (12).** Biphenyl  $\alpha$ -D-mannopyranoside (3, 665 mg, 2.00 mmol) and dibutyltin oxide (548 mg, 2.20 mmol) were dissolved in dry MeOH (10 mL). The mixture was refluxed for 5 h and then concentrated to dryness under reduced pressure. To a solution of the residue in dry toluene (10 mL) were added tetrabutylammonium bromide (709 mg, 2.20 mmol) and benzyl bromide (285  $\mu$ L, 2.40 mmol). The mixture was stirred at 115 °C overnight and then concentrated to dryness in vacuo. The residue was purified by chromatography on silica (petroleum ether/EtOAc, 4:1–1:3) to yield **12** (306 mg, 36%) as a white solid;  $[\alpha]_D^{20} + 99.8$  ( $c$  1.38,  $CHCl_3$ ).  $^1H$  NMR ( $CDCl_3$ , 500 MHz):  $\delta$  = 3.00 (s, 3H, 2,4,6-OH), 3.71 (m, 2H, H-5, H-6a), 3.81 (m, 1H, H-6b), 3.96 (dd,  $J$  = 3.0, 9.5 Hz, 1H, H-3), 4.17 (m, 2H, H-2, H-4), 4.70 (d,  $J$  = 11.5 Hz, 1H,  $OCH_2Ph$ ), 4.79 (d,  $J$  = 11.5 Hz, 1H,  $OCH_2Ph$ ), 5.65 (d,  $J$  = 1.5 Hz, 1H, H-1), 7.10 (m, 2H, Ar-H), 7.31–7.44 (m, 8H, Ar-H), 7.50–7.52 (m, 4H, Ar-H).  $^{13}C$  NMR ( $CDCl_3$ , 126 MHz):  $\delta$  = 61.5 (C-6), 65.5 (C-4), 67.9 (C-2), 72.3 ( $OCH_2Ph$ ), 72.8 (C-5), 79.4 (C-3), 97.7 (C-1), 116.6, 126.8, 126.9, 128.26, 128.29, 128.3, 128.7, 128.8, 135.6, 137.4, 140.5, 155.4 (18C, Ar-C). ESI-MS:  $m/z$ : calcd for  $C_{23}H_{26}NaO_6$  [ $M + Na$ ] $^+$ , 445.16; found, 445.14.

**Biphenyl 2,4,6-Tri-O-benzyl-3-O-benzyl- $\alpha$ -D-mannopyranoside (13).** To a solution of **12** (306 mg, 0.724 mmol) in pyridine (5 mL) were added benzoyl chloride (400  $\mu$ L, 3.43 mmol) and DMAP (5 mg). The reaction mixture was stirred at rt overnight then quenched with MeOH (0.5 mL) and concentrated under reduced pressure. The residue was purified by MPLC on silica (petroleum ether/EtOAc, 4:1–3:1) to yield **13** (499 mg, 99%) as a white solid;  $[\alpha]_D^{20} + 7.1$  ( $c$  1.52,  $CHCl_3$ ).  $^1H$  NMR ( $CDCl_3$ , 500 MHz):  $\delta$  = 4.40–4.46 (m, 3H,

H-6a, H-3, H-5), 4.62–4.65 (m, 2H,  $OCH_2Ph$ , H-6b), 4.79 (d,  $J$  = 12.4 Hz, 1H,  $OCH_2Ph$ ), 5.80 (d,  $J$  = 2.0 Hz, 1H, H-1), 5.91 (dd,  $J$  = 2.0, 3.0 Hz, 1H, H-2), 5.97 (t,  $J$  = 9.7 Hz, 1H, H-4), 7.12–7.23 (m, 7H, Ar-H), 7.34 (m, 3H, Ar-H), 7.42–7.54 (m, 11H, Ar-H), 7.61 (m, 2H, Ar-H), 8.03 (m, 4H, Ar-H), 8.16 (m, 2H, Ar-H).  $^{13}C$  NMR ( $CDCl_3$ , 126 MHz):  $\delta$  = 63.0 (C-6), 68.0 (C-4), 68.5 (C-5), 69.6 (C-2), 71.3 ( $OCH_2Ph$ ), 74.1 (C-3), 96.3 (C-1), 116.9, 126.8, 127.0, 127.7, 127.9, 128.2, 128.26, 128.28, 128.4, 128.5, 128.7, 129.3, 129.4, 129.7, 129.8, 129.9, 130.0, 132.9, 133.3, 133.4, 135.9, 137.3, 140.3, 155.2 (36C, Ar-C), 165.4, 165.7, 166.1 (3 CO). ESI-MS:  $m/z$ : calcd for  $C_{46}H_{38}NaO_9$  [ $M + Na$ ] $^+$ , 757.24; found, 757.29.

**Biphenyl 2,4,6-Tri-O-benzoyl- $\alpha$ -D-mannopyranoside (14).** Hydrogenolysis of **13** (499 mg, 0.679 mmol) was conducted in dioxane/EtOAc (6 mL, 5:1) in the presence of 10% Pd(OH) $_2$ /C (50 mg) and a catalytic amount of AcOH in a Parr shaker under hydrogen (4 bar) at rt overnight. The reaction suspension was filtered through Celite, and the filtrate was concentrated in vacuo. The residue was purified by MPLC on silica (petroleum ether/EtOAc, 9:1–4:1) to give **14** (314 mg, 73%) as colorless syrup;  $[\alpha]_D^{20} + 56.5$  ( $c$  1.02,  $CHCl_3$ ).  $^1H$  NMR ( $CDCl_3$ , 500 MHz):  $\delta$  = 2.58 (d,  $J$  = 8.0 Hz, 1H, 3-OH), 4.48 (m, 2H, H-5, H-6a), 4.64 (m, 2H, H-3, H-6b), 5.66 (dd,  $J$  = 2.0, 3.5 Hz, 1H, H-2), 5.77 (t,  $J$  = 9.5 Hz, 1H, H-4), 5.82 (d,  $J$  = 2.0 Hz, 1H, H-1), 7.31–7.35 (m, 3H, Ar-H), 7.22 (m, 2H, Ar-H), 7.42–7.53 (m, 11H, Ar-H), 7.61 (m, 2H, Ar-H), 7.97 (dd,  $J$  = 1.0, 8.0 Hz, 2H, Ar-H), 8.10 (m, 4H, Ar-H).  $^{13}C$  NMR ( $CDCl_3$ , 126 MHz):  $\delta$  = 63.0 (C-6), 69.0, 69.2 (C-5, C-3), 72.6 (C-2), 70.2 (C-4), 95.7 (C-1), 116.8, 126.8, 127.0, 128.3, 128.4, 128.6, 128.8, 129.1, 129.0, 129.7, 129.9, 130.0, 133.1, 133.69, 133.73, 136.0, 140.4, 155.2 (30C, Ar-C), 165.9, 166.1, 166.8 (3 CO). ESI-MS:  $m/z$ : calcd for  $C_{39}H_{32}NaO_9$  [ $M + Na$ ] $^+$ , 667.19; found, 667.29.

**Biphenyl 2,4,6-Tri-O-benzoyl-3-dibenzylphosphoryl- $\alpha$ -D-mannopyranoside (15).** According to the general procedure, compound **14** (211 mg, 0.335 mmol) was reacted with 1,2,4-triazole (92.5 mg, 1.34 mmol) and dibenzyl *N,N*-diisopropylphosphoramidite (90%, 250  $\mu$ L, 0.670 mmol) in MeCN (5 mL), followed by treatment with 70% aq *tert*-butylhydroperoxide (190  $\mu$ L, 1.34 mmol) to yield **15** and the 2-phosphoryl derivative **16** (245 mg, 80%) as an inseparable 3:2 mixture.

Analytical data for **15**:  $^1H$  NMR ( $CDCl_3$ , 500 MHz):  $\delta$  = 4.62 (m, 2H, H-5, H-6a), 4.76 (dd,  $J$  = 7.5, 12.0 Hz, 1H, H-6b), 4.85–5.11 (m, 4H,  $OCH_2Ph$ ), 5.55 (td,  $J$  = 3.5, 9.0 Hz, 1H, H-3), 5.81 (d,  $J$  = 1.5 Hz, 1H, H-1), 5.87 (dd,  $J$  = 1.9, 3.4 Hz, 1H, H-2), 6.04 (m, 1H, H-4), 6.92–8.11 (m, 34H, Ar-H).  $^{13}C$  NMR ( $CDCl_3$ , 126 MHz):  $\delta$  = 62.8 (C-5), 67.6 (d,  $J$  = 6 Hz, C-4), 69.5 (C-6), 69.8 (d,  $J$  = 5.6 Hz,  $CH_2Ph$ ), 71.0 (d,  $J$  = 2 Hz, C-2), 69.8 (d,  $J$  = 6 Hz,  $CH_2Ph$ ), 73.7 (d,  $J$  = 5 Hz, C-3), 95.7 (C-1), 116.8, 126.8, 127.6, 127.7, 127.9, 128.0, 128.20, 128.23, 128.27, 128.32, 128.4, 128.50, 128.54, 128.57, 128.62, 129.7, 129.9, 130.0, 133.0, 133.5, 133.6, 136.1, 140.3, 155.1 (42C, Ar-C), 165.3, 165.5, 166.0 (3 CO). ESI-MS:  $m/z$ : calcd for  $C_{53}H_{43}NaO_{12}P$  [ $M + Na$ ] $^+$ , 927.25; found, 927.23.

Analytical data for **16**:  $^1H$  NMR ( $CDCl_3$ , 500 MHz):  $\delta$  = 4.62 (m, 1H, H-6a), 4.51 (m, 1H, H-5), 4.42 (m, 1H, H-6b), 4.85–5.11 (m, 4H,  $OCH_2Ph$ ), 5.20 (m, 1H, H-2), 5.66 (d,  $J$  = 1.5 Hz, 1H, H-1), 5.95 (td,  $J$  = 2.7, 10.0 Hz, 1H, H-3), 6.04 (m, 1H, H-4), 6.92–8.11 (m, 34H, Ar-H). ESI-MS:  $m/z$ : calcd for  $C_{53}H_{45}NaO_{12}P$  [ $M + Na$ ] $^+$ , 927.25; found, 927.23.

**Biphenyl 2,3-Di-O-benzoyl-4,6-O-benzylidene- $\alpha$ -D-mannopyranoside (17).** To a solution of compound **9** in pyridine (5 mL) were added benzoyl chloride (0.33 mL, 2.84 mmol) and DMAP (5 mg). The mixture was stirred at rt overnight and then concentrated under reduced pressure. The residue was purified by MPLC on silica (petroleum ether/EtOAc, 6:1–4:1) to provide **17** (270 mg, 60%) as a white solid;  $[\alpha]_D^{20} + 21.8$  ( $c$  1.08,  $CHCl_3$ ).  $^1H$  NMR ( $CDCl_3$ , 500 MHz):  $\delta$  = 4.00 (t,  $J$  = 9.5 Hz, 1H, H-6a), 4.32–4.38 (m, 2H, H-6b, H-5), 4.48 (t,  $J$  = 9.5 Hz, 1H, H-4), 5.73 (s, 1H, PhCH), 5.82 (d,  $J$  = 1.5 Hz, 1H, H-1), 5.97 (dd,  $J$  = 1.5, 3.5 Hz, 1H, H-2), 6.10 (dd,  $J$  = 3.5, 10.5 Hz, 1H, H-3), 7.25 (m, 2H, Ar-H), 7.35–7.39 (m, 6H, Ar-H), 7.45–7.61 (m, 11H, Ar-H), 7.68 (t,  $J$  = 7.5 Hz, 1H, Ar-H), 7.99 (m, 2H, Ar-H), 8.17 (m, 2H, Ar-H).  $^{13}C$  NMR ( $CDCl_3$ , 126 MHz):  $\delta$  = 64.6 (C-5), 68.7 (C-6), 68.8 (C-3), 70.8 (C-2), 76.6 (C-4), 96.7 (C-1), 102.0 (PhCH), 116.8, 126.1, 126.9, 127.0, 128.2, 128.25, 128.3, 128.4,

128.6, 128.7, 129.0, 129.3, 129.6, 129.8, 129.9, 130.1, 133.1, 133.6, 136.0, 136.9, 140.5, 155.1 (30C, Ar-C), 165.36, 165.45 (2 CO). ESI-MS:  $m/z$ : calcd for  $C_{39}H_{32}NaO_8 [M + Na]^+$ , 651.20; found, 651.17.

**Biphenyl 2,3-Di-O-benzoyl-6-O-benzyl- $\alpha$ -D-mannopyranoside (18).** To a solution of **17** (270 mg, 0.429 mmol) in dry THF (4 mL) were added  $Me_3N \cdot BH_3$  (125 mg, 1.72 mmol) and  $AlCl_3$  (341 mg, 2.56 mmol). After 15 min,  $H_2O$  (15.5  $\mu$ L) was added and the reaction mixture was stirred at rt for 45 min. The reaction was quenched with 1 M aq HCl, diluted with DCM (20 mL), and washed with water (10 mL) and brine (10 mL). The combined organic layers were dried over  $Na_2SO_4$ . The solvent was removed under reduced pressure and the residue purified by MPLC on silica (petroleum ether/EtOAc, 6:1–3:1) to afford **18** (178 mg, 67%) as a white solid;  $[\alpha]_D^{20} + 10.8$  (c 1.21,  $CHCl_3$ ).  $^1H$  NMR ( $CDCl_3$ , 500 MHz):  $\delta$  = 3.85 (dd,  $J$  = 4.0, 11.0 Hz, 1H, H-6a), 3.97 (dd,  $J$  = 4.5, 11.0 Hz, 1H, H-6b), 4.14 (m, 1H, H-5), 4.53 (t,  $J$  = 10.0 Hz, 1H, H-4), 4.59 (d,  $J$  = 12.0 Hz, 1H,  $OCH_2Ph$ ), 4.70 (d,  $J$  = 12.0 Hz, 1H,  $OCH_2Ph$ ), 5.79 (d,  $J$  = 1.5 Hz, 1H, H-1), 5.81 (dd,  $J$  = 1.5, 3.0 Hz, 1H, H-2), 5.85 (dd,  $J$  = 3.5, 9.5 Hz, 1H, H-3), 7.24 (m, 2H, Ar-H), 7.33–7.39 (m, 7H, Ar-H), 7.42–7.48 (m, 5H, Ar-H), 7.54–7.57 (m, 5H, Ar-H), 7.62 (t,  $J$  = 7.5 Hz, 1H, Ar-H), 7.98 (m, 2H, Ar-H), 8.10 (m, 2H, Ar-H).  $^{13}C$  NMR ( $CDCl_3$ , 126 MHz):  $\delta$  = 67.4 (C-4), 69.8 (C-6), 70.3 (C-2), 72.0 (C-5), 72.6 (C-3), 73.7 ( $OCH_2Ph$ ), 96.0 (C-1), 116.8, 126.9, 127.0, 127.6, 127.7, 128.3, 128.4, 128.6, 128.7, 129.88, 129.92, 133.4, 133.5, 135.9, 137.9, 140.5, 155.4 (30C, Ar-C), 165.5, 166.7 (2 CO). ESI-MS:  $m/z$ : calcd for  $C_{39}H_{34}NaO_8 [M + Na]^+$ , 653.22; found, 653.25.

**Biphenyl 4-O-Dibenzylphosphoryl-2,3-di-O-benzoyl-6-O-benzyl- $\alpha$ -D-mannopyranoside (19).** According to the general procedure, compound **18** (160 mg, 0.253 mmol) was reacted with 1,2,4-triazole (70.0 mg, 1.01 mmol) and dibenzyl  $N,N$ -diisopropylphosphoramidite (90%, 190  $\mu$ L, 0.510 mmol) in MeCN (2 mL), followed by treatment with 70% aq *tert*-butylhydroperoxide (200  $\mu$ L) to yield **19** (120 mg, 53%) as a glassy solid;  $[\alpha]_D^{20} + 29.2$  (c 1.18,  $CHCl_3$ ).  $^1H$  NMR ( $CDCl_3$ , 500 MHz):  $\delta$  = 3.85 (dd,  $J$  = 1.5, 11.0 Hz, 1H, H-6a), 3.94 (dd,  $J$  = 4.0, 11.5 Hz, 1H, H-6b), 4.24 (m, 1H, H-5), 4.56 (s, 2H,  $OCH_2Ph$ ), 4.63 (dd,  $J$  = 8.5, 12.0 Hz, 1H,  $OCH_2Ph$ ), 4.74 (dd,  $J$  = 7.0, 12.0 Hz, 1H,  $OCH_2Ph$ ), 4.81 (dd,  $J$  = 8.5, 12.0 Hz, 1H,  $OCH_2Ph$ ), 4.88 (dd,  $J$  = 7.5, 12.0 Hz, 1H,  $OCH_2Ph$ ), 5.43 (q,  $J$  = 9.5 Hz, 1H, H-4), 5.79 (d,  $J$  = 2.0 Hz, 1H, H-1), 5.85 (dd,  $J$  = 2.0, 3.0 Hz, 1H, H-2), 6.04 (dd,  $J$  = 3.5, 10.0 Hz, 1H, H-3), 6.92 (m, 2H, Ar-H), 7.11–7.61 (m, 28H, Ar-H), 7.99 (dd,  $J$  = 1.0, 8.5 Hz, 2H, Ar-H), 8.04 (dd,  $J$  = 1.0, 8.0 Hz, 2H, Ar-H).  $^{13}C$  NMR ( $CDCl_3$ , 126 MHz):  $\delta$  = 68.4 (C-6), 69.2 (d,  $J$  = 5 Hz,  $OCH_2Ph$ ), 69.3 (d,  $J$  = 6 Hz,  $OCH_2Ph$ ), 70.3 (C-2), 70.5 (d,  $J$  = 2 Hz, C-3), 71.4 (d,  $J$  = 6 Hz, C-5), 71.6 (d,  $J$  = 6 Hz, C-4), 73.4 ( $OCH_2Ph$ ), 95.8 (C-1), 116.9, 126.9, 127.0, 127.39, 127.43, 127.45, 127.5, 127.7, 127.9, 128.2, 128.27, 128.32, 128.36, 128.40, 128.5, 128.6, 128.7, 129.4, 130.0, 133.2, 133.5, 135.3, 135.4, 135.5, 135.6, 136.0, 138.3, 140.5, 155.4 (42C, Ar-C), 165.4, 165.5 (2 CO). ESI-MS:  $m/z$ : calcd for  $C_{53}H_{47}NaO_{11}P [M + Na]^+$ , 913.28; found, 913.31.

**Biphenyl 2,3,4-Tri-O-benzoyl-6-O-trityl- $\alpha$ -D-mannopyranoside (20).** To a solution of **3** (414 mg, 1.24 mmol) in pyridine were added trityl chloride (417 mg, 1.49 mmol) and DMAP (10 mg). The mixture was stirred at 80 °C overnight and then cooled to rt. Then, benzoyl chloride (50  $\mu$ L, 4.92 mmol) was added and the mixture was stirred at 50 °C overnight. The mixture was diluted with DCM (50 mL) and washed with 0.1 M aq HCl (20 mL) and satd aq  $NaHCO_3$  (20 mL). The organic layer was dried over  $Na_2SO_4$ , filtered, and the solvent removed in vacuo. The residue was purified by MPLC on silica (petroleum ether/EtOAc, 6:1–4:1) to give **20** (1.35 g, 88%), which contained some perbenzoylated substance as impurity but was used in the next step without a second purification.

**Biphenyl 2,3,4-Tri-O-benzoyl- $\alpha$ -D-mannopyranoside (21).** To a solution of **20** (1.35 g, 1.52 mmol) in dry DCM were added anhydrous  $FeCl_3$  (493 mg, 3.04 mmol) and distilled water (3.28 mL, 18.2 mmol). The mixture was stirred at rt for 5 h. Then, the mixture was diluted with DCM (50 mL) and washed with water (30 mL). The organic layer was dried over  $Na_2SO_4$ , filtered, and the solvent removed in vacuo. The residue was purified by MPLC on silica (petroleum ether/EtOAc) to yield **21** (608 mg, 62%);  $[\alpha]_D^{20} -1.8$  (c 0.75, DCM).  $^1H$

NMR ( $CDCl_3$ , 500 MHz):  $\delta$  = 2.70 (dd,  $J$  = 6.0, 8.4 Hz, 1H, 6-OH), 3.76 (ddd,  $J$  = 3.3, 5.9, 13.0 Hz, 1H, H-6a), 3.85 (ddd,  $J$  = 2.0, 8.5, 12.8 Hz, 1H, H-6a), 4.21 (dt,  $J$  = 2.6, 10.1 Hz, 1H, H-5), 5.90 (d,  $J$  = 1.7 Hz, 1H, H-1), 5.91 (dd,  $J$  = 1.9, 3.3 Hz, 1H, H-2), 5.98 (t,  $J$  = 10.1 Hz, 1H, H-4), 6.25 (dd,  $J$  = 3.4, 10.1 Hz, 1H, H-3), 7.26–7.35 (m, 5H, Ar-H), 7.39–7.48 (m, 5H, Ar-H), 7.51–7.59 (m, 7H, Ar-H), 7.65 (m, 1H, Ar-H), 7.88 (m, 2H, Ar-H), 8.01 (m, 2H, Ar-H), 8.15 (m, 2H, Ar-H).  $^{13}C$  NMR ( $CDCl_3$ , 126 MHz):  $\delta$  = 61.2 (C-6), 67.1 (C-4), 69.5 (C-3), 70.5 (C-2), 71.8 (C-5), 96.1 (C-1), 116.8, 127.0, 127.1, 128.4, 128.5, 128.6, 128.8, 128.9, 129.1, 129.2, 129.8, 130.0, 130.1, 133.4, 133.8, 133.9, 136.2, 140.5, 155.4 (30C, Ar-C), 165.6, 165.7, 166.7 (3 CO). ESI-MS:  $m/z$ : calcd for  $C_{39}H_{32}NaO_9 [M + Na]^+$ , 667.19; found, 667.22.

**Biphenyl 6-O-Dibenzylphosphoryl-2,3,4-tri-O-benzoyl- $\alpha$ -D-mannopyranoside (22).** According to the general procedure, compound **21** (107 mg, 0.158 mmol) was reacted with 1,2,4-triazole (44.0 mg, 0.632 mmol) and dibenzyl  $N,N$ -diisopropylphosphoramidite (90%, 120  $\mu$ L, 0.316 mmol) in MeCN (2 mL), followed by treatment with 70% aq *tert*-butylhydroperoxide (86  $\mu$ L, 0.632 mmol) to yield **22** (94.4 mg, 66%) as a glassy solid;  $[\alpha]_D^{20} -0.7$  (c 0.28, DCM).  $^1H$  NMR ( $CDCl_3$ , 500 MHz):  $\delta$  = 4.27 (m, 2H, H-6), 4.46 (m, 1H, H-5), 4.93–5.02 (m, 4H,  $OCH_2Ph$ ), 5.80 (d,  $J$  = 1.7 Hz, 1H, H-1), 5.90 (dd,  $J$  = 2.0, 3.1 Hz, 1H, H-2), 6.07 (t,  $J$  = 10.0 Hz, 1H, H-4), 6.13 (dd,  $J$  = 3.3, 10.0 Hz, 1H, H-3), 7.19–7.63 (m, 18H, Ar-H), 7.89 (m, 2H, Ar-H), 7.98 (m, 2H, Ar-H), 8.15 (m, 2H, Ar-H).  $^{13}C$  NMR ( $CDCl_3$ , 126 MHz):  $\delta$  = 65.8 (d,  $J$  = 5 Hz, C-6), 66.4 (C-4), 69.4 (d,  $J$  = 4 Hz,  $OCH_2Ph$ ), 69.5 (d,  $J$  = 4 Hz,  $OCH_2Ph$ ), 69.9 (C-3), 70.3 (d,  $J$  = 8 Hz, C-5), 70.4 (C-2), 96.1 (C-1), 117.0, 127.0, 127.1, 127.8, 128.0, 128.4, 128.45, 128.46, 128.5, 128.6, 133.4, 133.7, 135.7, 135.8, 136.3, 140.4, 155.5 (42C, Ar-C), 165.4, 165.5, 165.6 (3 CO). ESI-MS:  $m/z$ : calcd for  $C_{53}H_{45}NaO_{12}P [M + Na]^+$ , 927.25; found, 927.23.

**4'-(4,6-O-Benzylidene- $\alpha$ -D-mannopyranosyloxy)-3'-chloro-biphenyl-4-carbonitrile (23).** To a solution of **4**<sup>19</sup> (500 mg, 1.28 mmol) in anhydrous DMF (20 mL) were added benzaldehyde dimethyl acetal (575  $\mu$ L, 3.83 mmol) and *p*-toluenesulfonic acid (20 mg). The mixture was stirred at 50 °C overnight. Then, the reaction mixture was neutralized with satd aq  $NaHCO_3$  (10 mL), diluted with DCM (30 mL), and washed with water ( $3 \times 10$  mL) and brine (10 mL). The organic layer was dried over  $Na_2SO_4$ , filtered, and the solvents removed in vacuo. The residue was purified by MPLC on silica (DCM/MeOH, 1:0–5:1, + 0.5%  $NEt_3$ ) to yield **23** (132 mg, 22%);  $[\alpha]_D^{20} + 62.3$  (c 0.59,  $CHCl_3/MeOH$ , 1:1).  $^1H$  NMR (500 MHz,  $CDCl_3$ ):  $\delta$  = 3.76 (t,  $J$  = 10.2 Hz, 1H, H-6a), 3.91 (td,  $J$  = 4.8, 9.8 Hz, 1H, H-5), 3.99 (t,  $J$  = 9.4 Hz, 1H, H-4), 4.14 (dd,  $J$  = 4.8, 10.3 Hz, 1H, H-6a), 4.28–4.33 (m, 2H, H-2, H-3), 5.53 (s, 1H, PhCH), 5.62 (s, 1H, H-1), 7.19 (m, 1H, Ar-H), 7.29–7.31 (m, 3H, Ar-H), 7.38 (m, 1H, Ar-H), 7.40–7.44 (m, 2H, Ar-H), 7.54–7.58 (m, 3H, Ar-H), 7.63–7.67 (m, 2H, Ar-H).  $^{13}C$  NMR (126 MHz,  $CDCl_3$ ):  $\delta$  = 64.2 (C-5), 68.5, 70.6 (3C, C-2, C-3, C-6), 78.4 (C-4), 98.7 (C-1), 102.4 (PhCH), 111.2, 116.8, 118.7, 124.6, 126.2, 126.6, 127.4, 128.4, 132.5, 143.7, 151.8 (19 C, 18 Ar-C, CN). ESI-MS:  $m/z$ : calcd for  $C_{33}H_{26}ClNNaO_7 [M + Na]^+$ , 502.90; found, 502.04.

**4'-(3-O-Benzoyl-4,6-O-benzylidene- $\alpha$ -D-mannopyranosyloxy)-3'-chloro-biphenyl-4-carbonitrile (24).** To a solution of **23** (131 mg, 0.275  $\mu$ mol) in DCM/pyridine (6 mL, 5:1) was added dropwise over 30 min a 0.1 M benzoyl chloride solution in dry DCM (2.8 mL, 0.280 mmol) at 0 °C under argon. The mixture was stirred another 30 min at 0 °C, then the ice-bath was removed and stirring continued for 2 h at rt. Then, the mixture was diluted with DCM (10 mL) and washed with 0.1 M aq HCl (5 mL) and satd aq  $NaHCO_3$  (10 mL). The organic layer was dried with  $Na_2SO_4$ , filtered, and concentrated. The residue was purified by MPLC on silica (petroleum ether/EtOAc, + 0.5%  $NEt_3$ ) to yield **24** (96.8 mg, 60%);  $[\alpha]_D^{20} + 113.8$  (c 1.02, DCM).  $^1H$  NMR (500 MHz,  $CDCl_3$ ):  $\delta$  = 3.91 (t,  $J$  = 10.2 Hz, 1H, H-6a), 4.17 (td,  $J$  = 4.9, 9.7 Hz, 1H, H-5), 4.24 (dd,  $J$  = 4.8, 10.2 Hz, 1H, H-6b), 4.45 (t,  $J$  = 9.9 Hz, 1H, H-4), 4.65 (dd,  $J$  = 1.6, 3.2 Hz, 1H, H-2), 5.64 (s, 1H, PhCH), 5.70 (d,  $J$  = 1.2 Hz, 1H, H-1), 7.25–7.34 (m, 4H, Ar-H), 7.37–7.47 (m, 5H, Ar-H), 7.51–7.60 (m, 4H, Ar-H), 7.51–7.60 (m, 2H, Ar-H), 8.06–8.11 (m, 2H, Ar-H).  $^{13}C$  NMR (126 MHz,  $CDCl_3$ ):  $\delta$  = 65.1 (C-5), 68.4 (C-6), 69.1 (C-2), 71.2 (C-3), 75.6 (C-

4), 99.1 (C-1), 101.8 (PhCH), 110.8, 116.9, 118.6, 124.8, 126.0, 126.3, 127.2, 128.1, 128.3, 132.6, 133.2, 136.9, 143.5, 151.6 (25C, 24 Ar-C, CN), 165.7 (CO). IR (KBr):  $\nu = 3437$  (vs, OH), 2227 (m, CN), 1721 (vs, C=O)  $\text{cm}^{-1}$ . ESI-MS:  $m/z$ : calcd for  $\text{C}_{33}\text{H}_{26}\text{ClNNaO}_7$  [ $\text{M} + \text{Na}$ ] $^+$ , 606.13; found, 606.11.

**4'-(3-O-Benzoyl-4,6-O-benzylidene-2-O-bis[2-(trimethylsilyl)ethoxy]phosphoryl- $\alpha$ -D-mannopyranosyloxy)-3'-chloro-biphenyl-4-carbonitrile (25).** According to the general procedure, compound 24 (96.8 mg, 0.166 mmol) was reacted with 1,2,4-triazole (45.8 mg, 0.663 mmol) and bis[2-(trimethylsilyl)ethyl]  $N,N$ -diisopropylphosphoramidite (136  $\mu\text{L}$ , 0.331 mmol) in MeCN (3.0 mL), followed by treatment with 70% aq *tert*-butylhydroperoxide (91  $\mu\text{L}$ , 0.663 mmol) to yield 25 (79.6 mg, 55%) as a 4:1-mixture of 2- and 3-phosphorylated isomers.  $^1\text{H}$  NMR (500 MHz,  $\text{CDCl}_3$ ):  $\delta = -0.09, -0.02$  (2s, 18H, 2 Si( $\text{CH}_3$ ) $_3$ ), 0.92–0.106 (m, 4H, 2 Si $\text{CH}_2$ ), 3.87 (td,  $J = 4.5, 10.1$  Hz, 1H, H-6a), 4.12 (m, 6H, H-5, H-6b, 2 O $\text{CH}_2$ ), 4.36 (t,  $J = 9.9$  Hz, 1H, H-4), 5.17 (ddd,  $J = 1.7, 3.1, 9.1$  Hz, 1H, H-2), 5.63 (s, 1H, PhCH), 5.81 (m, 1H, H-3), 5.84 (d,  $J = 1.5$  Hz, 1H, H-1), 7.22–7.33 (m, 4H, Ar-H), 7.37–7.45 (m, 4H, Ar-H), 7.46–7.56 (m, 2H, Ar-H), 7.57–7.64 (m, 3H, Ar-H), 7.66–7.71 (m, 2H, Ar-H), 8.08–8.14 (m, 2H, Ar-H).  $^{13}\text{C}$  NMR (126 MHz,  $\text{CDCl}_3$ ):  $\delta = -1.7, -1.6$  (6C, Si( $\text{CH}_3$ ) $_3$ ), 19.4 (d,  $J = 5$  Hz, 2C, 2 Si $\text{CH}_2$ ), 65.2 (C-5), 66.9 (t,  $J = 6$  Hz, 2C, 2 O $\text{CH}_2$ ), 68.4 (C-6), 69.1 (d,  $J = 5$  Hz, C-3), 73.2 (d,  $J = 5$  Hz, C-2), 75.4 (C-4), 97.8 (d,  $J = 2$  Hz, C-1), 101.9 (PhCH), 111.1, 117.1, 118.6, 125.0, 126.2, 126.4, 127.3, 128.2, 128.3, 128.6, 129.0, 129.7, 129.9, 130.0, 132.6, 133.2, 134.9, 136.8, 143.5, 151.5 (25C, 24 Ar-C, CN), 165.6 (CO). ESI-MS:  $m/z$ : calcd for  $\text{C}_{49}\text{H}_{67}\text{ClN}_2\text{O}_{10}\text{PSi}_2$  [ $\text{M} + \text{NET}_3 + \text{H}$ ] $^+$ , 965.38; found, 965.53.

**4'-(3-O-Benzoyl-2-O-phosphoryl- $\alpha$ -D-mannopyranosyloxy)-3'-chloro-biphenyl-4-carbonitrile Disodium Salt (26).** A solution of 25 (79.6 mg, 0.275 mmol) in dry DCM (1.5 mL) was treated with TFA (150  $\mu\text{L}$ ) for 1 h at rt under argon. Then, a drop of water was added and stirring continued for 30 min. The solvents were removed in vacuo, and the residue was dissolved in  $\text{H}_2\text{O}$  (1 mL) containing a drop of 1 M aq NaOH and purified by MPLC on RP-18 ( $\text{H}_2\text{O}/\text{MeOH}$ , 95:5–4:1) to yield 26 (34.7 mg, 61%) as a 4:1-mixture of 2- and 3-phosphate.  $^1\text{H}$  NMR (500 MHz,  $\text{CD}_3\text{OD}$ ):  $\delta = 3.78$ –3.90 (m, 3H, H-5, H-6), 4.20 (t,  $J = 9.9$  Hz, 1H, H-4), 5.01 (ddd,  $J = 2.0, 3.1, 9.4$  Hz, 1H, H-2), 5.60–5.65 (td,  $J = 2.6, 10.1$  Hz, 1H, H-3), 5.91 (d,  $J = 1.6$  Hz, 1H, H-1), 7.45–7.53 (m, 3H, Ar-H), 7.57–7.65 (m, 2H, Ar-H), 7.75–7.81 (m, 5H, Ar-H), 8.15–8.18 (m, 2H, Ar-H).  $^{13}\text{C}$  NMR (126 MHz,  $\text{CD}_3\text{OD}$ ):  $\delta = 62.2$  (C-6), 65.3 (C-4), 73.9 (dd,  $J = 5.8$  Hz, 2C, C-2, C-3), 76.3 (C-5), 98.8 (d,  $J = 2$  Hz, C-1), 112.0, 118.8, 119.7, 125.8, 127.9, 131.0, 133.9, 136.0, 145.0, 153.2 (19C, 18 Ar-C, CN), 167.8 (CO). ESI-MS:  $m/z$ : calcd for  $\text{C}_{26}\text{H}_{22}\text{ClNO}_{10}\text{P}$  [ $\text{M} - 2\text{Na} + \text{H}$ ] $^-$ , 574.07; found, 574.21.

**4'-(3-O-Allyl- $\alpha$ -D-mannopyranosyloxy)-3'-chloro-biphenyl-4-carbonitrile (27).** A suspension of 4 (90.1 mg, 0.230 mmol) and dibutyltin oxide (62.7 mg, 0.252 mmol) in toluene (4 mL) was stirred for 6 h at 80  $^\circ\text{C}$  under argon. Then, tetrabutylammonium iodide (78.1 mg, 0.242 mmol) and allyl bromide (23  $\mu\text{L}$ , 0.277 mmol) were added to the still turbid mixture and stirring was continued for another 20 h at 80  $^\circ\text{C}$ . Afterward, the solvent was removed in vacuo, and the residue was purified by MPLC on RP-18 ( $\text{H}_2\text{O}/\text{MeOH}$ ) to yield 27 (54.7 mg, 55%) as a colorless solid.  $^1\text{H}$  NMR (500 MHz,  $\text{CD}_3\text{OD}$ ):  $\delta = 3.65$  (d,  $J = 6.3$  Hz, 1H, H-5), 3.72 (dd,  $J = 5.3, 12.0$  Hz, 1H, H-6a), 3.78 (dd,  $J = 2.5, 12.0$  Hz, 1H, H-6b), 3.83–3.90 (m, 2H, H-3, H-4), 4.20–4.32 (m, 3H, H-2, allyl-H1a, allyl-H1b), 5.22 (dd,  $J = 1.7, 10.4$  Hz, 1H, allyl-H3a), 5.39 (dd,  $J = 1.7, 17.3$  Hz, 1H, allyl-H3b), 5.64 (d,  $J = 1.8$  Hz, 1H, H-1), 6.04 (ddd,  $J = 5.9, 10.4, 16.3$  Hz, 1H, allyl-H2), 7.48 (d,  $J = 8.7$  Hz, 1H, Ar-H), 7.60 (dd,  $J = 2.3, 8.6$  Hz, 1H, Ar-H), 7.75 (d,  $J = 2.3$  Hz, 1H, Ar-H), 7.76–7.80 (m, 4H, Ar-H).  $^{13}\text{C}$  NMR (126 MHz,  $\text{CD}_3\text{OD}$ ):  $\delta = 62.6$  (C-6), 67.1 (C-4), 68.6 (C-2), 72.1 (allyl-C1), 76.1 (C-5), 79.6 (C-3), 100.5 (C-1), 111.8, 117.9, 118.6, 119.8, 125.5, 127.9, 128.5, 129.8, 133.9, 135.5, 136.4, 145.1, 153.6 (15C, 12 Ar-C, CN, allyl-C2, allyl-C3). ESI-MS:  $m/z$ : calcd for  $\text{C}_{22}\text{H}_{22}\text{ClNNaO}_6$  [ $\text{M} + \text{Na}$ ] $^+$ , 454.10; found, 453.89.

**4'-(3-O-Allyl-2,4,6-tri-O-benzoyl- $\alpha$ -D-mannopyranosyloxy)-3'-chloro-biphenyl-4-carbonitrile (28).** To a solution of 27 (194 mg, 0.449 mmol) and DMAP (10 mg) in pyridine (5 mL) was added

benzoyl chloride (261  $\mu\text{L}$ , 2.25 mmol) under argon. The mixture was stirred at rt overnight. MeOH (1 mL) was added, and the mixture was stirred for 10 min. Then, the solvents were removed under reduced pressure and the residue was dissolved in DCM (20 mL) and washed with 1 M aq HCl (10 mL) and satd aq  $\text{NaHCO}_3$  (10 mL). The organic phase was dried ( $\text{Na}_2\text{SO}_4$ ) and concentrated. The residue was purified by MPLC on silica (petroleum ether/EtOAc) to yield 28 (292 mg, 87%) as a foam;  $[\alpha]_{\text{D}}^{20} + 44.1$  (c 1.46,  $\text{CHCl}_3$ ).  $^1\text{H}$  NMR (500 MHz,  $\text{CDCl}_3$ ):  $\delta = 4.13$  (m, 1H, allyl-H1a), 4.24 (dd,  $J = 5.4, 13.0$  Hz, 1H, allyl-H1b), 4.42–4.49 (m, 2H, H-5, H-6a), 4.52 (dd,  $J = 3.3, 9.8$  Hz, 1H, H-3), 5.16 (dd,  $J = 1.1, 10.3$  Hz, 1H, allyl-H3a), 5.29 (dd,  $J = 1.5, 17.2$  Hz, 1H, allyl-H3b), 5.79 (dd,  $J = 5.9, 10.4, 16.7$  Hz, 1H, allyl-H2), 5.87 (d,  $J = 1.8$  Hz, 1H, H-1), 5.91 (m, 1H, H-2), 5.98 (t,  $J = 9.8$  Hz, 1H, H-4), 7.30–7.39 (m, 4H, Ar-H), 7.41–7.45 (m, 2H, Ar-H), 7.46–7.53 (m, 2H, Ar-H), 7.57–7.63 (m, 3H, Ar-H), 7.68 (m, 1H, Ar-H), 7.70–7.74 (m, 2H, Ar-H), 8.00–8.05 (m, 2H, Ar-H), 8.10–8.17 (m, 4H, Ar-H).  $^{13}\text{C}$  NMR (126 MHz,  $\text{CDCl}_3$ ):  $\delta = 62.8$  (C-6), 67.8 (C-4), 68.8 (C-2), 70.2 (C-5), 71.1 (allyl-C1), 73.9 (C-3), 96.5 (C-1), 111.1, 116.9, 118.2, 118.6, 124.4, 127.2, 128.4, 129.9, 132.6, 132.9, 133.3, 133.8, 143.3, 151.6 (33C, 30 Ar-C, CN, allyl-C2, allyl-C3), 165.4, 165.7, 166.0 (3 CO). ESI-MS:  $m/z$ : calcd for  $\text{C}_{43}\text{H}_{34}\text{ClNNaO}_9$  [ $\text{M} + \text{Na}$ ] $^+$ , 766.18; found, 768.12.

**4'-(2,4,6-Tri-O-benzoyl- $\alpha$ -D-mannopyranosyloxy)-3'-chloro-biphenyl-4-carbonitrile (29).** A flask was charged with 28 (292 mg, 0.391 mmol), anhydrous  $\text{PdCl}_2$  (10.8 mg, 0.118 mmol), and a magnetic stirring bar. The flask was evacuated and flushed with argon. The procedure was repeated twice. Then, dry MeOH (4 mL) was added and the mixture was stirred at 40  $^\circ\text{C}$  for 5 h. The mixture was filtered and the filtrate concentrated in vacuo. The residue was purified by MPLC on silica (petroleum ether/EtOAc) to yield 29 (231 mg, 84%);  $[\alpha]_{\text{D}}^{20} + 55.0$  (c 1.01,  $\text{CHCl}_3$ ).  $^1\text{H}$  NMR (500 MHz,  $\text{CDCl}_3$ ):  $\delta = 4.35$ –4.41 (m, 2H, H-5, H-6a), 4.57 (m, 1H, H-6b), 4.66 (dd,  $J = 3.4, 9.9$  Hz, 1H, H-3), 5.65 (dd,  $J = 1.8, 3.4$  Hz, 1H, H-2), 5.73 (t,  $J = 9.8$  Hz, 1H, H-4), 5.81 (d,  $J = 1.7$  Hz, 1H, H-1), 7.18–7.27 (m, 4H, Ar-H), 7.34–7.45 (m, 5H, Ar-H), 7.49–7.59 (m, 5H, Ar-H), 7.62–7.67 (m, 2H, Ar-H), 7.87–7.92 (m, 2H, Ar-H), 8.00–8.05 (m, 4H, Ar-H).  $^{13}\text{C}$  NMR (126 MHz,  $\text{CDCl}_3$ ):  $\delta = 62.7$  (C-6), 68.8 (C-3), 69.8 (C-5), 69.9 (C-4), 72.3 (C-2), 96.1 (C-1), 111.2, 116.9, 118.7, 124.6, 127.3, 128.6, 128.9, 129.7, 132.7, 133.1, 133.8, 134.5, 151.5 (31C, 30 Ar-C, CN), 165.8, 165.9, 166.8 (3 CO). IR (KBr):  $\nu = 3446$  (m, OH), 2228 (m, CN), 1725 (vs, C=O)  $\text{cm}^{-1}$ . ESI-MS:  $m/z$ : calcd for  $\text{C}_{40}\text{H}_{30}\text{ClNNaO}_9$  [ $\text{M} + \text{Na}$ ] $^+$ , 726.15; found, 726.49.

**4'-(2,4,6-Tri-O-benzoyl-3-O-bis[2-(trimethylsilyl)ethoxy]phosphoryl- $\alpha$ -D-mannopyranosyloxy)-3'-chloro-biphenyl-4-carbonitrile (30).** According to the general procedure, compound 29 (198 mg, 0.281 mmol) was reacted with 1,2,4-triazole (77.8 mg, 1.13 mmol) and bis[2-(trimethylsilyl)ethyl]  $N,N$ -diisopropylphosphoramidite (232  $\mu\text{L}$ , 0.563 mmol) in MeCN (3 mL), followed by treatment with 70% aq *tert*-butylhydroperoxide (154  $\mu\text{L}$ , 1.13 mmol) to yield 30 (89.1 mg, 32%);  $[\alpha]_{\text{D}}^{20} + 35.9$  (c 0.99,  $\text{CHCl}_3$ ).  $^1\text{H}$  NMR (500 MHz,  $\text{CDCl}_3$ ):  $\delta = -0.10, 0.00$  (2s, 18H, 2 Si( $\text{CH}_3$ ) $_3$ ), 0.69–0.85 (m, 2H, Si $\text{CH}_2$ ), 1.01–1.09 (m, 2H, Si $\text{CH}_2$ ), 3.83–3.98 (m, 2H, O $\text{CH}_2$ ), 4.09–4.21 (m, 2H, O $\text{CH}_2$ ), 4.49–4.57 (m, 2H, H-5, H-6a), 4.67 (d,  $J = 10.1$  Hz, 1H, H-6b), 5.55 (ddd,  $J = 3.4, 9.5$  Hz, 1H, H-3), 5.92 (d,  $J = 1.6$  Hz, 1H, H-1), 5.99 (dd,  $J = 1.9, 3.3$  Hz, 1H, H-2), 6.12 (t,  $J = 9.8$  Hz, 1H, H-4), 7.34–7.40 (m, 4H, Ar-H), 7.48–7.58 (m, 5H, Ar-H), 7.63–7.73 (m, 5H, Ar-H), 7.76–7.80 (m, 2H, Ar-H), 8.03–8.06 (m, 2H, Ar-H), 8.17–8.20 (m, 2H, Ar-H), 8.21–8.25 (m, 2H, Ar-H).  $^{13}\text{C}$  NMR (126 MHz,  $\text{CDCl}_3$ ):  $\delta = -1.9, -1.8$  (6C, 2 Si( $\text{CH}_3$ ) $_3$ ), 19.0 (d,  $J = 6$  Hz, Si $\text{CH}_2$ ), 19.3 (d,  $J = 6$  Hz, Si $\text{CH}_2$ ), 62.5 (C-6), 66.5 (d,  $J = 1$  Hz, O $\text{CH}_2$ ), 66.6 (d,  $J = 1$  Hz, O $\text{CH}_2$ ), 67.3 (d,  $J = 5$  Hz, C-4), 70.0 (C-5), 70.8 (d,  $J = 2$  Hz, C-2), 72.6 (d,  $J = 5$  Hz, C-3), 96.4 (C-1), 111.2, 117.4, 118.6, 124.9, 128.2, 129.1, 129.1, 129.6, 130.1, 132.6, 132.9, 133.5, 133.7, 135.0 (31C, 30 Ar-C, CN), 165.32, 165.34, 165.8 (3 CO). ESI-MS:  $m/z$ : calcd for  $\text{C}_{50}\text{H}_{55}\text{ClNNaO}_{12}\text{PSi}_2$  [ $\text{M} + \text{Na}$ ] $^+$ , 1006.26; found, 1006.44.

**4'-(2,3,6-Tri-O-acetyl- $\alpha$ -D-mannopyranosyloxy)-3'-chloro-biphenyl-4-carbonitrile (31).** According to a described procedure,<sup>47</sup> a solution of 4 (100 mg, 0.255 mmol) and dibutyltin oxide (340 mg, 0.562 mmol) in dry MeOH (5 mL) was stirred under reflux for 2 h at



70 °C. Afterward, the solvent was removed in vacuo and the residue was dissolved in dry MeCN (5 mL) and cooled to 0 °C. Then, a solution of Ac<sub>2</sub>O (80 μL, 0.842 mmol) in dry MeCN (1 mL) was added dropwise at 0 °C. The mixture was stirred at rt for 16 h. The reaction was quenched with MeOH (1 mL), the solvents were removed in vacuo, and the residue was purified by MPLC on silica (petroleum ether/EtOAc) to yield **31** (27.0 mg, 21%);  $[\alpha]_{\text{D}}^{20} + 63.6$  (c 0.98, CHCl<sub>3</sub>). <sup>1</sup>H NMR (500 MHz, CDCl<sub>3</sub>): δ = 2.06, 2.11, 2.16 (3s, 9H, 3 COCH<sub>3</sub>), 3.94 (t, J = 9.8 Hz, 1H, H-4), 2.02 (ddd, J = 2.1, 4.6, 9.9 Hz, 1H, H-5), 4.27 (dd, J = 2.1, 12.3 Hz, 1H, H-6a), 4.50 (dd, J = 4.7, 12.3 Hz, 1H, H-6b), 5.47 (dd, J = 3.5, 9.7 Hz, 1H, H-3), 5.50 (dd, J = 1.8, 3.4 Hz, 1H, H-2), 5.58 (d, J = 1.6 Hz, 1H, H-1), 7.26 (m, 1H, Ar-H), 7.41 (dd, J = 2.3, 8.6 Hz, 1H, Ar-H), 7.59–7.62 (m, 3H, Ar-H), 7.68–7.72 (m, 2H, Ar-H). <sup>13</sup>C NMR (126 MHz, CDCl<sub>3</sub>): δ = 20.7, 20.8, 20.8 (3 COCH<sub>3</sub>), 62.8 (C-6), 65.5 (C-4), 69.4 (C-2), 71.1 (C-3), 72.2 (C-5), 96.7 (C-1), 111.2, 117.2, 118.7, 125.0, 126.4, 127.4, 129.2, 132.7, 134.9, 143.5, 151.6 (13C, 12 Ar-C, CN), 169.9, 170.8, 171.3 (3 CO). IR (KBr): ν = 3436 (vs, OH), 2229 (m, CN), 1756 (vs, C=O) cm<sup>-1</sup>. ESI-MS: m/z: calcd for C<sub>25</sub>H<sub>24</sub>ClNNaO<sub>9</sub> [M + Na]<sup>+</sup>, 540.10; found, 540.08.

**4'-(2,3,6-Tri-O-acetyl-4-O-bis[2-(trimethylsilyl)ethoxy]phosphoryl-α-D-mannopyranosyloxy)-3'-chloro-biphenyl-4-carbonitrile (32).** According to the general procedure, compound **31** (39.3 mg, 76 μmol) was reacted with 1,2,4-triazole (21.0 mg, 0.304 mmol) and bis[2-(trimethylsilyl)ethyl] N,N-diisopropylphosphoramidite (63 μL, 0.152 mmol) in MeCN (1 mL), followed by treatment with 70% aq tert-butylhydroperoxide (42 μL, 0.304 mmol) to yield **32** (37.3 mg, 62%);  $[\alpha]_{\text{D}}^{20} + 65.0$  (c 1.07, CHCl<sub>3</sub>). <sup>1</sup>H NMR (500 MHz, CDCl<sub>3</sub>): δ = 0.04, 0.05 (2s, 18H, 2 Si(CH<sub>3</sub>)<sub>3</sub>), 1.04–1.14 (m, 4H, 2 SiCH<sub>2</sub>), 2.04, 2.13, 2.20 (3s, 9H, 3 COCH<sub>3</sub>), 4.08–4.19 (m, 5H, H-5, 2 OCH<sub>2</sub>), 4.33 (dd, J = 5.2, 12.3 Hz, 1H, H-6a), 4.42 (dd, J = 2.0, 12.3 Hz, 1H, H-6b), 4.79 (q, J = 9.6 Hz, 1H, H-4), 5.51 (dd, J = 1.8, 3.5 Hz, 1H, H-2), 5.59 (d, J = 1.7 Hz, 1H, H-1), 5.68 (dd, J = 3.6, 9.7 Hz, 1H, H-3) 7.27 (m, 1H, Ar-H), 7.43 (dd, J = 2.3, 8.6 Hz, 1H, Ar-H), 7.60–7.65 (m, 3H, Ar-H), 7.70–7.74 (m, 2H, Ar-H). <sup>13</sup>C NMR (126 MHz, CDCl<sub>3</sub>): δ = -1.6, -1.5 (6C, 2 Si(CH<sub>3</sub>)<sub>3</sub>), 19.5, 19.6 (2 SiCH<sub>2</sub>), 20.7, 20.8, 20.9 (3 COCH<sub>3</sub>), 62.2 (C-6), 66.7 (d, J = 2 Hz, OCH<sub>2</sub>), 66.8 (d, J = 1 Hz, OCH<sub>2</sub>), 68.8 (d, J = 2 Hz, C-3), 69.5 (C-2), 70.4 (d, J = 6 Hz) and 70.5 (d, J = 5 Hz) (C-4, C-5), 96.4 (C-1), 111.3, 117.3, 118.6, 125.0, 126.4, 127.4, 129.2, 132.7, 135.1, 143.5, 151.6 (13C, 12 Ar-C, CN), 169.7, 169.9, 170.3 (3 CO). IR (KBr): ν = 2229 (m, CN), 1753 (vs, C=O) cm<sup>-1</sup>. ESI-MS: m/z: calcd for C<sub>35</sub>H<sub>49</sub>ClNNaO<sub>12</sub>PSi<sub>2</sub> [M + Na]<sup>+</sup>, 820.21; found, 820.14.

**3'-Chloro-4'-(6-O-trityl-α-D-mannopyranosyloxy)-biphenyl-4-carbonitrile (33).** To a solution of **4** (150 mg, 0.383 mmol) in pyridine were added trityl chloride (128 mg, 0.459 mmol) and DMAP (5 mg). The mixture was stirred at 80 °C for 16 h. Then, the solvent was removed in vacuo and the residue was purified by MPLC on silica (petroleum ether/EtOAc, + 0.5% NEt<sub>3</sub>) to yield **33** (189 mg, 80%). <sup>1</sup>H NMR (500 MHz, CD<sub>3</sub>OD): δ = 3.30 (dd, J = 7.5, 16.1 Hz, 1H, H-6a), 3.46 (d, J = 9.3 Hz, 1H, H-6b), 3.63 (t, J = 9.7 Hz, 1H, H-4), 3.88 (t, J = 9.0 Hz, 1H, H-5), 4.02 (dd, J = 3.3, 9.4 Hz, 1H, H-3), 4.20 (m, 1H, H-2), 5.75 (s, 1H, H-1), 7.03–7.16 (m, 10H, Ar-H), 7.26–7.35 (m, 6H, Ar-H), 7.55 (d, J = 8.3 Hz, 2H, Ar-H), 7.58–7.64 (m, 3H, Ar-H), 7.70 (d, J = 2.0 Hz, 2H, Ar-H). <sup>13</sup>C NMR (126 MHz, CD<sub>3</sub>OD): δ = 65.0 (C-6), 68.7 (C-4), 71.5 (C-2), 72.6 (C-3), 75.0 (C-5), 87.54 (CPh<sub>3</sub>), 99.9 (C-1), 111.7, 118.7, 119.7, 127.7, 127.8, 128.3, 129.7, 133.7, 134.9, 144.7, 145.3, 153.3 (31C, 30 Ar-C, CN). ESI-MS: m/z: calcd for C<sub>39</sub>H<sub>44</sub>ClNNaO<sub>9</sub> [M + Na]<sup>+</sup>, 656.18; found, 656.15.

**4'-(2,3,4-Tri-O-benzoyl-6-O-trityl-α-D-mannopyranosyloxy)-3'-chloro-biphenyl-4-carbonitrile (34).** Prepared according to the procedure described for **28** from **33** (189 mg, 0.299 mmol), benzoyl chloride (173 μL, 1.21 mmol), and DMAP (10 mg) to yield **34** (223 mg, 79%);  $[\alpha]_{\text{D}}^{20} + 8.1$  (c 1.10, CHCl<sub>3</sub>). <sup>1</sup>H NMR (500 MHz, CDCl<sub>3</sub>): δ = 3.42–3.50 (m, 2H, H-6), 4.39 (m, 1H, H-5), 6.05 (d, J = 1.5 Hz, 1H, H-1), 6.10 (dd, J = 1.9, 3.2 Hz, 1H, H-2), 6.15 (dd, J = 3.3, 10.1 Hz, 1H, H-3), 6.23 (t, J = 10.1 Hz, 1H, H-4), 7.10–7.19 (m, 9H, Ar-H), 7.28–7.39 (m, 4H, Ar-H), 7.41–7.60 (m, 12H, Ar-H), 7.63–7.71 (m, 3H, Ar-H), 7.81–7.85 (m, 2H, Ar-H), 7.93–7.98 (m, 2H, Ar-H), 8.23–8.28 (m, 2H, Ar-H). <sup>13</sup>C NMR (126 MHz, CDCl<sub>3</sub>): δ = 62.0

(C-6), 66.7 (C-4), 70.0 (C-3), 70.3 (C-2), 71.6 (C-5), 86.6 (CPh<sub>3</sub>), 96.4 (C-1), 111.0, 118.6, 124.8, 126.5, 126.8, 127.2, 127.6, 128.1, 128.2, 128.4, 128.6, 128.9, 128.97, 129.02, 129.55, 129.61, 129.8, 132.5, 133.1, 133.6, 134.6, 143.4, 143.5, 151.6 (49C, 48 Ar-C, CN), 165.0, 165.3, 165.4 (3 CO). IR (KBr): ν = 2227 (m, CN), 1731 (vs, C=O) cm<sup>-1</sup>. ESI-MS: m/z: calcd for C<sub>59</sub>H<sub>44</sub>ClNNaO<sub>9</sub> [M + Na]<sup>+</sup>, 968.26; found, 968.47.

**4'-(2,3,4-Tri-O-benzoyl-α-D-mannopyranosyloxy)-3'-chloro-biphenyl-4-carbonitrile (35).** Prepared according to the procedure described for **21** by reacting **34** (122 mg, 0.129 mmol) with FeCl<sub>3</sub> (41.8 mg, 0.258 mmol) and water (27.9 μL, 1.55 mmol) in DCM (10 mL) for 5 h to yield **35** (77.4 mg, 85%);  $[\alpha]_{\text{D}}^{20} + 6.2$  (c 1.02, CHCl<sub>3</sub>). <sup>1</sup>H NMR (500 MHz, CDCl<sub>3</sub>): δ = 3.80 (qd, J = 2.7, 13.1 Hz, 2H, H-6) 4.25 (d, J = 10.0 Hz, 1H, H-5), 5.95 (s, 1H, H-1), 5.96–6.03 (m, 2H, H-2, H-4), 6.29 (dd, J = 3.4, 10.2 Hz, 1H, H-3), 7.25–7.32 (m, 2H, Ar-H), 7.38–7.56 (m, 8H, Ar-H), 7.61–7.73 (m, 6H, Ar-H), 7.88 (d, J = 7.3 Hz, 2H, Ar-H), 8.01 (d, J = 7.3 Hz, 2H, Ar-H), 8.14 (d, J = 7.2 Hz, 2H, Ar-H). <sup>13</sup>C NMR (125 MHz, CDCl<sub>3</sub>): δ = 60.9 (C-6), 66.8 (C-4), 69.2 (C-3), 70.2 (C-2), 72.3 (C-5), 96.6 (C-1), 111.2, 117.0, 118.6, 124.9, 126.5, 127.3, 128.3, 128.4, 128.5, 128.7, 128.9, 129.2, 129.6, 129.90, 129.91, 132.7, 133.3, 133.7, 133.8, 134.9, 143.5, 151.6 (31C, 30 Ar-C, CN), 165.37, 165.43, 166.6 (3 CO). IR (KBr): ν = 3436 (vs, OH), 2228 (m, CN), 1731 (vs, C=O) cm<sup>-1</sup>. ESI-MS: m/z: calcd for C<sub>40</sub>H<sub>30</sub>ClNNaO<sub>9</sub> [M + Na]<sup>+</sup>, 726.15; found, 726.24.

**4'-(2,3,4-Tri-O-benzoyl-6-O-bis[2-(trimethylsilyl)ethoxy]phosphoryl-α-D-mannopyranosyloxy)-3'-chloro-biphenyl-4-carbonitrile (36).** According to the general procedure, compound **35** (61.3 mg, 87 μmol) was reacted with 1,2,4-triazole (24.1 mg, 0.348 mmol) and bis[2-(trimethylsilyl)ethyl] N,N-diisopropylphosphoramidite (72 μL, 0.174 mmol) in MeCN (2 mL), followed by treatment with 70% aq tert-butylhydroperoxide (48 μL, 0.348 mmol) to yield **36** (50.8 mg, 59%). <sup>1</sup>H NMR (500 MHz, CDCl<sub>3</sub>): δ = -0.07, -0.04 (2 s, 18H, 2 Si(CH<sub>3</sub>)<sub>3</sub>), 0.94–1.03 (m, 4H, 2 SiCH<sub>2</sub>), 4.03–4.15 (m, 4H, 2 OCH<sub>2</sub>), 4.26 (dd, J = 3.8, 5.6 Hz, 2H, H-6), 4.52 (m, 1H, H-5), 5.86 (d, J = 1.7 Hz, 1H, H-1), 5.97 (dd, J = 2.0, 3.2 Hz, 1H, H-2), 6.07 (t, J = 10.1 Hz, 1H, H-4), 6.15 (dd, J = 3.3, 10.1 Hz, 1H, H-3), 7.27–7.33 (m, 2H, Ar-H), 7.37–7.54 (m, 8H, Ar-H), 7.61–7.76 (m, 6H, Ar-H), 7.85–7.89 (m, 2H, Ar-H), 7.95–8.00 (m, 2H, Ar-H), 8.11–8.15 (m, 2H, Ar-H). <sup>13</sup>C NMR (126 MHz, CDCl<sub>3</sub>): δ = -1.65, -1.64 (6C, 2 Si(CH<sub>3</sub>)<sub>3</sub>), 19.4 (d, J = 6 Hz, SiCH<sub>2</sub>), 19.5 (d, J = 6 Hz, SiCH<sub>2</sub>), 65.3 (d, J = 5 Hz, C-6), 66.1 (C-4), 66.4 (d, J = 6 Hz, 2 OCH<sub>2</sub>), 69.5 (C-3), 70.1 (C-2), 70.8 (d, J = 8 Hz, C-5), 96.9 (C-1), 111.3, 117.7, 118.6, 125.1, 126.7, 127.4, 128.3, 128.4, 128.7, 128.8, 128.9, 129.0, 129.2, 129.7, 129.8, 130.0, 132.7, 133.3, 133.5, 133.7, 135.2, 143.5, 151.9 (31C, 30 Ar-C, CN), 165.2, 165.35, 165.39 (3 CO). ESI-MS: m/z: calcd for C<sub>50</sub>H<sub>55</sub>ClNNaO<sub>12</sub>PSi<sub>2</sub> [M + Na]<sup>+</sup>, 1006.26; found, 1006.52.

**Biphenyl 2,3,4-Tri-O-benzoyl-6-O-(methylthiomethyl)-α-D-mannopyranoside (37).** To a solution of compound **21** (469 mg, 0.726 mmol) in Ac<sub>2</sub>O (2.5 mL) and AcOH (0.25 mL) was added DMSO (2.5 mL). The mixture was stirred at rt for 24 h, then diluted with EtOAc (50 mL) and washed with satd aq NaHCO<sub>3</sub> (2 × 20 mL) and H<sub>2</sub>O (2 × 20 mL) and brine (20 mL). The organic layer was dried over Na<sub>2</sub>SO<sub>4</sub> and the solvents removed under diminished pressure. The residue was purified by MPLC on silica (petroleum ether/EtOAc, 9:1–6:1) to yield **37** (171 mg, 35%), which contained some impurities but was used in the next step without further purification.

**Biphenyl 2,3,4-Tri-O-benzoyl-6-O-(phosphonoxy)-methyl-α-D-mannopyranoside (38).** Compound **37** (170 mg, 0.250 mmol) was dissolved in a premixture of H<sub>3</sub>PO<sub>4</sub> (147 mg, 1.50 mmol) in THF (1.5 mL). Then, N-iodosuccinimide (84.0 mg, 0.375 mmol) was added and the mixture was stirred for 15 min at 0 °C and for 1 h at rt. The reaction was then quenched with 1 M aq Na<sub>2</sub>S<sub>2</sub>O<sub>3</sub>, diluted with DCM/MeOH (20 mL, 4:1), and washed with satd aq NaHCO<sub>3</sub> (10 mL). The organic layer was dried over Na<sub>2</sub>SO<sub>4</sub> and the solvents were removed in vacuo at <20 °C. The residue was purified by MPLC on silica (DCM/MeOH, 1:0–3.5:1) to yield **38** (110 mg, 58%). <sup>1</sup>H NMR (CD<sub>3</sub>OD, 500 MHz): δ = 3.90 (dd, J = 4.5, 11.6 Hz, 1H, H-6a), 4.01 (d, J = 10.2 Hz, 1H, H-6b), 4.47 (m, 1H, H-5), 5.06 (A of ABX, J = 5.5, 9.5 Hz, 1H, CH<sub>2</sub>), 5.16 (B of ABX, J = 5.5, 9.1 Hz, 1H, CH<sub>2</sub>), 5.89

(s, 1H, H-1), 5.92 (s, 1H, H-2), 6.05 (m, 2H, H-4, H-3), 7.26–7.68 (m, 18 H, Ar-H), 7.79 (d,  $J = 7.6$  Hz, 2H, Ar-H), 7.96 (d,  $J = 7.6$  Hz, 2H, Ar-H), 8.13 (d,  $J = 7.5$  Hz, 2H, Ar-H).  $^{13}\text{C}$  NMR ( $\text{CD}_3\text{OD}$ , 126 MHz):  $\delta = 68.2$  (C-4), 68.7 (C-6), 71.5 (C-2), 71.86 (C-5), 71.9 (C-3), 92.8 (d,  $J = 4$  Hz,  $\text{CH}_2$ ), 97.6 (C-1), 118.4, 127.7, 128.0, 129.3, 129.4, 129.6, 129.8, 129.9, 130.3, 130.4, 130.5, 130.6, 130.7, 130.9, 134.5, 134.6, 134.9, 137.4, 141.8, 156.8 (30C, Ar-C), 166.8, 167.0 (3C, 3 CO). ESI-MS:  $m/z$ : calcd for  $\text{C}_{40}\text{H}_{35}\text{NaO}_{13}\text{P}$  [ $\text{M} + \text{Na}$ ] $^+$ , 777.17; found, 777.13.

**4-(5-Nitroindolin-1-yl)phenyl-2,3,4-tri-O-benzoyl-6-O-(tert-butylsilyldimethyl)- $\alpha$ -D-mannopyranoside (39).** To a solution of **5** $^{20}$  (709 mg, 1.69 mmol) in pyridine were added *tert*-butyldimethylsilyl chloride (319 mg, 2.12 mmol) and DMAP (20.6 mg), and the mixture was stirred at rt overnight. Then, a solution of benzoyl chloride (0.98 mL, 8.45 mmol) in pyridine (2.0 mL) was added and the mixture was stirred at rt for 2 h. The mixture was diluted with DCM (30 mL) and subsequently washed with 0.1 M aq HCl (10 mL) and satd aq  $\text{NaHCO}_3$  (10 mL). The organic layer was dried over  $\text{Na}_2\text{SO}_4$ , filtered, and the solvent removed in vacuo. The residue was purified by MPLC on silica (petroleum ether/EtOAc, 9:1–7:3) to yield crude **39** (1.43 g, quant) as a yellow solid, which was used in the next step without further purification.  $^1\text{H}$  NMR ( $\text{CDCl}_3$ , 500 MHz):  $\delta = -0.01$  (s, 3H, Si( $\text{CH}_3$ ) $_2$ ), 0.00 (s, 3H, Si( $\text{CH}_3$ ) $_2$ ), 0.87 (s, 9H, C( $\text{CH}_3$ ) $_3$ ), 3.22 (t,  $J = 8.5$  Hz, 2H,  $\text{CH}_2$ ), 3.83 (dd,  $J = 2.3, 11.5$  Hz, 1H, H-6a), 3.88 (dd,  $J = 4.7, 11.5$  Hz, 1H, H-6b), 4.10 (t,  $J = 8.7$  Hz, 2H,  $\text{NCH}_2$ ), 4.43 (m, 1H, H-5), 5.77 (d,  $J = 1.8$  Hz, 1H, H-1), 5.87 (m, 1H, H-2), 6.03–6.15 (m, 2H, H-3, H-4), 6.77 (d,  $J = 8.9$  Hz, 1H, Ar-H), 7.22–7.31 (m, 6H, Ar-H), 7.38 (t,  $J = 7.8$  Hz, 2H, Ar-H), 7.41–7.55 (m, 5H, Ar-H), 7.60–7.67 (m, 1H, Ar-H), 7.88 (dd,  $J = 1.2, 8.3$  Hz, 2H, Ar-H), 7.94–8.01 (m, 3H, Ar-H), 8.03 (dd,  $J = 2.3, 8.9$  Hz, 1H, Ar-H), 8.14 (dd,  $J = 1.2, 8.3$  Hz, 1H, Ar-H).  $^{13}\text{C}$  NMR ( $\text{CDCl}_3$ , 126 MHz):  $\delta = -5.51, -5.50$  (Si( $\text{CH}_3$ ) $_2$ ), 25.8 (3C, C( $\text{CH}_3$ ) $_3$ ), 27.1 ( $\text{CH}_2$ ), 53.7 ( $\text{NCH}_2$ ), 62.1 (C-6), 66.6 (C-3), 70.3, 70.4 (C-2, C-4), 72.3 (C-5), 96.4 (C-1), 105.3, 118.0, 121.1, 122.0, 126.1, 128.3, 128.4, 128.43, 128.6, 129.1, 129.2, 129.3, 129.7, 129.8, 130.0, 131.0, 133.2, 133.3, 133.6, 136.8, 139.1, 152.8, 153.8 (30C, Ar-C), 165.3, 165.6, 165.7 (3 CO). ESI-MS:  $m/z$ : calcd for  $\text{C}_{47}\text{H}_{48}\text{N}_2\text{NaO}_{11}\text{Si}$  [ $\text{M} + \text{Na}$ ] $^+$ , 867.29; found, 867.25.

**4-(5-Nitroindolin-1-yl)phenyl-2,3,4-tri-O-benzoyl- $\alpha$ -D-mannopyranoside (40).** A solution of **39** (1.43 g, 1.69 mmol) in DCM/MeOH (16 mL, 1:1) was treated with 1 M  $\text{H}_2\text{SO}_4$  in MeOH (1.6 mL) for 1.5 h at rt. The reaction mixture was neutralized with  $\text{NET}_3$ , and the solvents were removed in vacuo. The residue was purified by MPLC on silica (petroleum ether/EtOAc, 3:1–3:2) to yield **40** (900 mg, 73%).  $^1\text{H}$  NMR ( $\text{CDCl}_3$ , 500 MHz):  $\delta = 3.22$  (t,  $J = 8.6$  Hz, 2H,  $\text{CH}_2$ ), 3.77 (dd,  $J = 3.3, 13.0$  Hz, 1H, H-6a), 3.84 (dd,  $J = 1.8, 13.0$  Hz, 1H, H-6b), 4.11 (t,  $J = 9.4$  Hz, 2H,  $\text{NCH}_2$ ), 4.20 (m, 1H, H-5), 5.83 (d,  $J = 1.6$  Hz, 1H, H-1), 5.88 (dd,  $J = 1.9, 3.3$  Hz, 1H, H-2), 5.96 (t,  $J = 10.1$  Hz, 1H, H-4), 6.22 (dd,  $J = 3.4, 10.2$  Hz, 1H, H-3), 6.78 (d,  $J = 8.9$  Hz, 1H, Ar-H), 7.21–7.34 (m, 6H, Ar-H), 7.37–7.43 (m, 3H, Ar-H), 7.45 (t,  $J = 7.4$  Hz, 1H, Ar-H), 7.50–7.57 (m, 3H, Ar-H), 7.65 (t,  $J = 7.5$  Hz, 1H, Ar-H), 7.84–7.89 (m, 2H, Ar-H), 7.97–8.02 (m, 3H, Ar-H), 8.04 (dd,  $J = 2.3, 8.9$  Hz, 1H, Ar-H), 8.12–8.16 (m, 2H, Ar-H).  $^{13}\text{C}$  NMR ( $\text{CDCl}_3$ , 126 MHz):  $\delta = 27.1$  ( $\text{CH}_2$ ), 53.7 ( $\text{NCH}_2$ ), 61.1 (C-6), 67.0 (C-4), 69.3 (C-3), 70.4 (C-2), 71.8 (C-5), 96.4 (C-1), 105.4, 117.6, 121.1, 122.0, 126.1, 127.0, 128.3, 128.4, 128.5, 128.6, 128.7, 129.0, 129.03, 129.5, 129.7, 129.9, 130.0, 131.1, 133.4, 133.77, 133.8, 137.0, 139.2, 152.5, 153.6 (30C, Ar-C), 165.5, 165.6, 166.6 (3 CO). ESI-MS:  $m/z$ : calcd for  $\text{C}_{41}\text{H}_{34}\text{N}_2\text{NaO}_{11}$  [ $\text{M} + \text{Na}$ ] $^+$ , 753.21; found, 753.33.

**4-(5-Nitroindolin-1-yl)phenyl-2,3,4-tri-O-benzoyl-6-O-(methylthio)methyl  $\alpha$ -D-mannopyranoside (41).** Degassed DMSO (2.5 mL) was added to a degassed mixture of **40** (200 mg, 0.273 mmol) in  $\text{Ac}_2\text{O}$  (1.65 mL) and HOAc (0.5 mL). The mixture was stirred at rt overnight, then diluted with EtOAc (20 mL) and subsequently washed with satd aq  $\text{NaHCO}_3$  ( $2 \times 10$  mL),  $\text{H}_2\text{O}$  ( $2 \times 10$  mL), and brine (10 mL). The organic layer was dried over  $\text{Na}_2\text{SO}_4$  and concentrated. The residue was purified by MPLC on silica (petroleum ether/EtOAc, 3:1–7:3) to yield **41** (160 mg, 74%).  $^1\text{H}$  NMR ( $\text{CDCl}_3$ , 500 MHz):  $\delta = 2.08$  (s, 3H,  $\text{CH}_3$ ), 3.23 (t,  $J = 8.6$  Hz, 2H,  $\text{CH}_2$ ), 3.72 (dd,  $J = 2.4, 11.1$  Hz, 1H, H-6a), 3.89 (dd,  $J = 4.5, 11.2$

Hz, 1H, H-6b), 4.12 (m, 2H,  $\text{NCH}_2$ ), 4.43 (m, 1H, H-5), 4.61, 4.72 (A, B of ABX,  $J = 11.6$  Hz, 2H,  $\text{CH}_2$ ), 5.79 (d,  $J = 1.6$  Hz, 1H, H-1), 5.86 (m, 1H, H-2), 6.03–6.11 (m, 2H, H-3, H-4), 6.78 (d,  $J = 8.9$  Hz, 1H, Ar-H), 7.22–7.33 (m, 7H, Ar-H), 7.36–7.42 (m, 2H, Ar-H), 7.46 (t,  $J = 7.4$  Hz, 1H, Ar-H), 7.48–7.56 (m, 3H, Ar-H), 7.64 (t,  $J = 7.5$  Hz, 1H, Ar-H), 7.85–7.91 (m, 2H, Ar-H), 7.96–8.01 (m, 3H, Ar-H), 8.04 (dd,  $J = 2.2, 8.8$  Hz, 1H, Ar-H), 8.10–8.17 (m, 2H, Ar-H).  $^{13}\text{C}$  NMR ( $\text{CDCl}_3$ , 126 MHz):  $\delta = 13.9$  ( $\text{CH}_3$ ), 27.1 ( $\text{CH}_2$ ), 53.7 ( $\text{NCH}_2$ ), 66.3 (C-6), 67.8 (C-4), 70.1 (C-3), 70.4 (C-2), 71.7 (C-5), 75.9 ( $\text{CH}_2$ ), 96.5 (C-1), 105.4, 117.9, 121.1, 122.0, 126.1, 128.4, 128.5, 128.7, 129.0, 129.2, 129.7, 129.8, 131.0, 131.1, 133.3, 133.4, 133.7, 139.0, 139.2, 152.7, 153.7 (30C, Ar-C), 165.5, 165.60, 165.62 (3 CO). ESI-MS:  $m/z$ : calcd for  $\text{C}_{43}\text{H}_{38}\text{N}_2\text{NaO}_{11}\text{S}$  [ $\text{M} + \text{Na}$ ] $^+$ , 813.21; found, 813.32.

**4-(5-Nitroindolin-1-yl)phenyl 2,3,4-tri-O-benzoyl-6-O-(phosphonoxy)methyl  $\alpha$ -D-manno-pyranoside (42).** Compound **41** (400 mg, 0.500 mmol) was dissolved in a mixture of  $\text{H}_3\text{PO}_4$  (366 mg, 3.73 mmol) in THF (5 mL). Then, *N*-iodosuccinimide (225 mg, 1.00 mmol) was added and the mixture was stirred for 15 min at 0  $^\circ\text{C}$  and for 1 h at rt. The reaction was quenched with 1 M aq  $\text{Na}_2\text{S}_2\text{O}_3$  and 28% aq ammonia (2 mL), then the volatiles were removed in vacuo at  $<30$   $^\circ\text{C}$ . The residue was purified by MPLC on silica (DCM/[MeOH/ $\text{H}_2\text{O}$  10:1], 1:0–3.5:1) to yield slightly impure **42** (278 mg, 67%), which was used in the next step without further purification.

#### Physicochemical and Pharmacokinetic Characterization.

**Materials.** Dimethyl sulfoxide (DMSO), hydrochloric acid  $\geq 37\%$  (HCl), pepsin (from porcine gastric mucosa,  $\geq 250$  units/mg solid), pancreatin (from porcine pancreas, 4 $\times$  USP specifications), acetic acid, sodium taurocholate hydrate, lecithin, sodium acetate trihydrate, maleic acid, glyceryl monooleate, sodium oleate, Dulbecco's Modified Eagle's Medium (DMEM)-high glucose, L-glutamine solution, penicillin–streptomycin solution, Dulbecco's Phosphate Buffered Saline (DPBS), and trypsin-EDTA solution were purchased from Sigma-Aldrich (St. Louis, MO, USA). MEM nonessential amino acid (MEM-NEAA) solution, fetal bovine serum (FBS), and DMEM without sodium pyruvate and phenol red were bought from Invitrogen (Carlsbad, CA, USA). Methanol (MeOH), acetonitrile (MeCN), and dichloromethane (DCM) were obtained from Acros Organics (Geel, Belgium). Monopotassium phosphate ( $\text{KH}_2\text{PO}_4$ ) and sodium hydroxide (NaOH) were bought from Merck (Merck KGaA, Darmstadt, Germany). Sodium chloride (NaCl) was purchased from Hanseler (Hanseler AG, AR, Switzerland). Long-life, heat-treated and homogenized milk (UHTmilk) containing 3.5% fat was bought from Coop (Coop Qualite & Prix, Switzerland). The Caco-2 cells were kindly provided by Prof. G. Imanidis, FHNW, Muttentz, and originated from the American Type Culture Collection (Rockville, MD, USA).

**Aqueous Solubility.** Microanalysis tubes (LaboTech J. Stofer LTS AG, Muttentz, Switzerland) were charged with 500  $\mu\text{g}$  of solid substance and 100  $\mu\text{L}$  of phosphate buffer (50 mM, pH 6.5). The tubes were briefly shaken by hand, sonicated for 15 min, and vigorously shaken (600 rpm, 25  $^\circ\text{C}$ , 2 h) on an Eppendorf Thermomixer Comfort (Eppendorf, Hamburg, Germany). Afterward, they were left undisturbed for 24 h. Then, the compound solutions were filtered (MultiScreen HTS 96-well filtration system, Millipore, Billerica, MA) by centrifugation (1500 rpm, 25  $^\circ\text{C}$ , 3 min). The filtrates were further diluted with buffer (1:1000 and 1:10000), and the concentrations were determined by LC-MS (see below).

**Colorectal Adenocarcinoma (Caco-2) Cell Permeation Assay and Hydrolysis Studies.** Caco-2 cells were cultivated in tissue culture flasks (BD Biosciences, Franklin Lakes, NJ, USA) with DMEM high glucose medium, containing L-glutamine (2 mM), nonessential amino acids (0.1 mM), penicillin (100 U/mL), streptomycin (100  $\mu\text{g}/\text{mL}$ ), and fetal bovine serum (10%). The cells were kept at 37  $^\circ\text{C}$  in humidified air containing 5%  $\text{CO}_2$ , and the medium was changed every second day. When approximately 90% confluence was reached, the cells were split in a 1:10 ratio and distributed to new tissue culture flasks. At passage numbers between 60 and 65, they were seeded at a density of  $5.3 \times 10^5$  cells per well to Transwell six-well plates (Corning Inc., Corning, NY, USA) with 2.5 mL of culture medium in the basolateral and 2.0 mL in the apical compartment. The medium was renewed on

alternate days. Enzymatic hydrolysis and permeation experiments were performed between days 19 and 21 post seeding. Prior to the experiment, the integrity of the Caco-2 monolayers was evaluated by measuring the transepithelial electrical resistance (TEER) with an Endohm tissue resistance instrument (World Precision Instruments Inc., Sarasota, FL, USA). Only wells with TEER values higher than 250  $\Omega$   $\text{cm}^2$  were used. After the experiment, TEER values were assessed again for each well, and results from wells with values below 250  $\Omega$   $\text{cm}^2$  were discarded.

Permeation experiments with the compounds 3–5 were performed in the apical-to-basolateral and basolateral-to-apical directions in triplicates. Transport medium (DMEM without sodium pyruvate and phenol red) was withdrawn from the donor compartments of three wells and replaced by the same volume of compound stock solution (10 mM in DMSO) to reach an initial sample concentration of 62.5  $\mu\text{M}$ . The Transwell plate was shaken (600 rpm, 37  $^\circ\text{C}$ ) on a Heidolph Titramax 1000 plate-shaker (Heidolph Instruments GmbH & Co. KG, Schwabach, Germany). Samples (40  $\mu\text{L}$ ) were withdrawn from the donor and acceptor compartments 30 min after initiation of the experiment, and the compound concentrations were determined by LC-MS. Apparent permeability ( $P_{\text{app}}$ ) was calculated according to eq 1:

$$P_{\text{app}} = \frac{dQ}{dt} \times \frac{1}{A \times c_0} \quad (1)$$

where  $dQ/dt$  is the compound flux ( $\text{mol s}^{-1}$ ),  $A$  the surface area of the monolayer ( $\text{cm}^2$ ), and  $c_0$  the initial concentration in the donor compartment ( $\text{mol cm}^{-3}$ ).<sup>19</sup>

Hydrolysis studies with the compounds 6a–e, 7a–d, and 8 were performed in triplicates. Transport medium was withdrawn from the apical compartments of three wells and replaced by the same volume of compound stock solution (10 mM in  $\text{H}_2\text{O}$ ) to reach an initial sample concentration of 62.5  $\mu\text{M}$ . The Transwell plate was shaken (600 rpm, 37  $^\circ\text{C}$ ) on a Heidolph Titramax 1000 plate-shaker. Samples (40  $\mu\text{L}$ ) were withdrawn from the apical compartment 10, 20, 30, 45, and 60 min after the initiation of the experiment and the concentrations of prodrug were determined by LC-MS. Metabolic half-life ( $t_{1/2}$ ) was calculated from the slope of the linear regression from the natural log remaining compound concentration versus incubation time relationship.

Studies of hydrolysis and subsequent permeation in the apical-to-basolateral and basolateral-to-apical directions were performed with compound 7b in triplicate. Transport medium was withdrawn from the apical or basal donor compartments of three wells and replaced by the same volume of compound stock solution (10 mM in  $\text{H}_2\text{O}$ ) to reach an initial sample concentration of 62.5  $\mu\text{M}$ . The Transwell plate was shaken (600 rpm, 37  $^\circ\text{C}$ ) on a Heidolph Titramax 1000 plate-shaker. Samples (40  $\mu\text{L}$ ) were withdrawn from the apical and basal compartments 60 min after the initiation of the experiment, and the concentrations of prodrug 7b and active principle 4 were determined by LC-MS.

Studies of hydrolysis and subsequent permeation in the apical-to-basolateral direction were performed with the compounds 6e, 7b, and 8 at different concentrations (100, 200, or 400  $\mu\text{M}$ ) in duplicate. Transport medium was withdrawn from the apical compartments of two wells and replaced by the same volume of compound stock solution (16, 32, or 64 mM in  $\text{H}_2\text{O}$ ) to reach initial sample concentrations of 100, 200, or 400  $\mu\text{M}$ . The Transwell plate was shaken (600 rpm, 37  $^\circ\text{C}$ ) on a Heidolph Titramax 1000 plate-shaker. Samples (40  $\mu\text{L}$ ) were withdrawn from the basal compartments 60 min after the initiation of the experiment and the concentrations of prodrug 6e, 7b, and 8 as well as active principle 3–5, respectively, were determined by LC-MS.

**Stability Studies in Biorelevant Media.** Biorelevant media were prepared according to United States Pharmacopeia (USP) specifications and Dressman et al.<sup>51,52</sup> as described below and are considered to be stable at ambient storage conditions for at least 72 h.<sup>55</sup> Table S1 (see Supporting Information) shows the composition of these

biorelevant media used to mimic gastric and intestinal conditions.<sup>51,52,55</sup>

**Simulated Gastric Fluid (sGF) and Simulated Intestinal Fluid (sIF).** sGF and sIF were prepared according to the United States Pharmacopeia (USP 28).<sup>51</sup> For the preparation of sGF, sodium chloride, and pepsin were mixed in bidistilled water and then the pH was adjusted to 1.2 by adding 37% aq HCl. For sIF, monopotassium phosphate and pancreatin were mixed in bidistilled water and then the pH was adjusted to 6.8 by adding 0.2 M NaOH. In parallel, two buffer solutions were prepared equally to sGF and sIF, without pepsin (buffer sGF) and pancreatin (buffer sIF), respectively.

**Fasted State Simulated Gastric Fluid (FaSSGF).** First, a NaCl solution was prepared and its pH was adjusted to 1.6 with 37% aq HCl. The solution was then transferred into a round-bottom flask, and sodium taurocholate hydrate was dissolved by continuous stirring. Then, a freshly prepared solution of lecithin in dichloromethane (DCM) (100 mg/mL) was added. The resulting emulsion was turbid. The DCM was then evaporated at 40  $^\circ\text{C}$ . For the first 15 min, the pressure was kept at 650 mbar. It was then decreased stepwise to a final pressure of 100 mbar and maintained for another 15 min. The product was a clear solution, having no perceptible smell of DCM. Next, pepsin was added under continuous stirring and, as a last step, the pH (1.6) and the volume of the solution were adjusted.

**Fed State Simulated Gastric Fluid (FeSSGF).** Sodium acetate trihydrate and NaCl were dissolved in bidistilled water. Acetic acid was added followed by a pH adjustment to 5.0 with 0.2 M NaOH. The resulting solution was mixed 1:1 with ultrahigh temperature milk.

**Fasted State Simulated Intestinal Fluid (FaSSIF).** Blank buffer was prepared using appropriate amounts of NaCl, sodium hydroxide, and maleic acid in bidistilled water, and the pH was then adjusted to 6.5 with 0.2 M NaOH. The solution was then transferred into a round-bottom flask and sodium taurocholate hydrate was added under continuous stirring. Afterward, a freshly prepared solution of lecithin in DCM (100 mg/mL) was added. The resulting emulsion was turbid. The DCM was then evaporated at 40  $^\circ\text{C}$  (same procedure as for the FaSSGF). As a last step, the volume and pH (6.5) of the solution were adjusted again.

**Fed State Simulated Intestinal Fluid (FeSSIF).** Blank buffer was prepared using appropriate amounts of NaCl, sodium hydroxide, and maleic acid in bidistilled water, and the pH was then adjusted to 5.8 with 0.2 M NaOH. The solution was transferred into a round-bottom flask, and sodium taurocholate hydrate was added under continuous stirring. Afterward, a freshly prepared solution of lecithin in dichloromethane (DCM) (100 mg/mL) was added. The resulting emulsion was turbid. The DCM was then evaporated at 40  $^\circ\text{C}$  (same procedure as for the FaSSGF). A freshly prepared solution of glyceryl monooleate in DCM (50 mg/mL) was added, and a second evaporation step was performed. Next, appropriate amounts of sodium oleate and pancreatin were added slowly under continuous stirring and, as a last step, the volume and pH (5.8) of the solution were adjusted again.

**Stability Assay.** All fluids were preheated at 37  $^\circ\text{C}$ . The compounds (7a, 7c, and 7d) were then added to yield 20  $\mu\text{M}$  solutions ( $t = 0$  min). Incubations were performed on a Heidolph 1000 incubator (500 rpm, 37  $^\circ\text{C}$ ). After an incubation time of 0, 10, 20, 30, 60, and 120 min, samples (30  $\mu\text{L}$ ) were withdrawn, precipitated with ice-cooled methanol (120  $\mu\text{L}$ ), put into the freezer ( $-20$   $^\circ\text{C}$ , 10 min), and then centrifuged (13200 rpm, 3 min). The supernatant was transferred into a 96-well plate. The concentration of analyte in the supernatant was analyzed by LC-MS.

**LC-MS Measurement.** Analyses were performed using an 1100/1200 series HPLC system coupled to a 6410 triple quadrupole mass detector (Agilent Technologies, Inc., Santa Clara, CA, USA) equipped with electrospray ionization. The system was controlled with the Agilent MassHunter workstation data acquisition software (version B.01.04). The column used was an Atlantis T3 C18 column (2.1 mm  $\times$  50 mm) with a 3  $\mu\text{m}$  particle size (Waters Corp., Milford, MA, USA). The mobile phase consisted of two eluents: eluent A ( $\text{H}_2\text{O}$ , containing 0.1% formic acid, v/v for compounds 5, 6a–e, 7c, 7d, and 8; ammonium acetate buffer, 10 mM, pH 5 for compounds 3 and 4;



formiate buffer, 10 mM, pH 3 for compounds **7a** and **7b**) and eluent B (MeCN, containing 0.1% formic acid, v/v), delivered at 0.6 mL/min. The gradient was ramped from 95% A/5% B to 5% A/95% B over 1 min and then held at 5% A/95% B for 0.1 min. The system was then brought back to 95% A/5% B, resulting in a total duration of 4 min. MS parameters such as fragmentor voltage, collision energy, polarity were optimized individually for each analyte, and the molecular ion was followed for each compound in the multiple reaction monitoring mode. The concentrations of the analytes were quantified by the Agilent Mass Hunter quantitative analysis software (version B.01.04).

**In Vivo Pharmacokinetics.** For the PK studies, eight-week-old female C3H/HeN mice (21–27 g) from Harlan (Venray, The Netherlands) were purchased. The mice were housed in groups of three to five per cage and kept under specific pathogen-free conditions in the Animal House of the Department of Biomedicine, University Hospital of Basel. For experimentation, all guidelines according to the Swiss veterinary law were followed. The animals were kept in a 12 h/12 h light/dark cycle and had chow and water ad libitum. After 1 week of acclimatization, the mice were used in groups of three (five for **4**, 7.7 mg/kg) for the pharmacokinetic studies. Compounds were diluted in PBS and applied using an oral gavage (1.25 and 7.7 mg/kg for **4**, and 10 mg/kg for **8** and **7b**, **7c**). Prodrug solutions consisted of prodrug (min. 94%) and active principle (max 6%). Blood and urine samples (10  $\mu$ L) were taken before the experiment (0 min) and at 6, 13, 20, 40 min, 1, 1.5, 2, 3, 4, 6, 8, and 24 h after administration. Directly after sampling, the samples were diluted in methanol (1:5) to precipitate proteins. After centrifugation (11 min, 13000 rpm), the supernatant was transferred to a 96-well plate and analyzed by LC-MS as described before. The samples at 0 min were used to define the detection limit in plasma and urine. Sampling and administration was performed following the guidelines in ref **56**.

## ■ ASSOCIATED CONTENT

### Supporting Information

The Supporting Information is available free of charge on the ACS Publications website at DOI: 10.1021/acs.jmedchem.5b01923.

Composition of biorelevant media, HPLC data, and chromatograms for target compounds, <sup>1</sup>H NMR spectra for target compounds (PDF)

## ■ AUTHOR INFORMATION

### Corresponding Author

\*Phone: +41 61 267 15 51. Fax: +41 61 267 15 52. E-mail: beat.ernst@unibas.ch.

### Author Contributions

S.K., X.J., and P.F. contributed equally to the project

### Notes

The authors declare no competing financial interest.

## ■ ACKNOWLEDGMENTS

We thank Prof. Dr. med. Radek Skoda, Department of Biomedicine, University Hospital Basel, Switzerland, for giving us access to the animal facility and Rachel Hevey for critical reading of the manuscript.

## ■ ABBREVIATIONS USED

ALP, alkaline phosphatase;  $C_{max}$ , maximum concentration; Caco-2 cells, colorectal adenocarcinoma cells; compd, compound; CRD, carbohydrate recognition domain; EtOAc, ethyl acetate; FimH, fimbrial adhesive protein H; FaSSGF, fasted state simulated gastric fluid; FeSSGF, fed state simulated gastric fluid; LC-MS, liquid chromatography–mass spectrometry; MeCN, acetonitrile; MPLC, medium pressure liquid chromatography; NIS, *N*-iodosuccinimide; *P*, octanol–water partition

coefficient;  $P_{app}$ , apparent permeability;  $P_e$ , effective permeability; PAMPA, parallel artificial membrane permeability assay; PK, pharmacokinetic;  $t_{1/2}$ , half-life;  $T_{max}$ , time when maximum concentration is observed; UPEC, uropathogenic *Escherichia coli*; UTI, urinary tract infection

## ■ REFERENCES

- (1) Fihn, S. D. Clinical practice. Acute uncomplicated urinary tract infection in women. *N. Engl. J. Med.* **2003**, *349*, 259–266.
- (2) Wiles, T. J.; Kulesus, R. R.; Mulvey, M. A. Origins and virulence mechanisms of uropathogenic *Escherichia coli*. *Exp. Mol. Pathol.* **2008**, *85*, 11–19.
- (3) Sanchez, G. V.; Master, R. N.; Karlowsky, J. A.; Bordon, J. M. In vitro antimicrobial resistance of urinary *Escherichia coli* isolates among U.S. outpatients from 2000 to 2010. *Antimicrob. Agents Chemother.* **2012**, *56*, 2181–2183.
- (4) Hooton, T. M.; Stamm, W. E. Diagnosis and treatment of uncomplicated urinary tract infection. *Infect. Dis. Clin. North Am.* **1997**, *11*, 551–581.
- (5) Swanborg, C.; Godaly, G. Bacterial virulence in urinary tract infection. *Infect. Dis. Clin. North Am.* **1997**, *11*, 513–529.
- (6) Schilling, J. D.; Mulvey, M. A.; Hultgren, S. J. Structure and function of *Escherichia coli* type 1 pili: new insight into the pathogenesis of urinary tract infections. *J. Infect. Dis.* **2001**, *183*, S36–S40.
- (7) Capitani, G.; Eidam, O.; Glockshuber, R.; Grütter, M. G. Structural and functional insights into the assembly of type 1 pili from *Escherichia coli*. *Microbes Infect.* **2006**, *8*, 2284–2290.
- (8) Sharon, N. Carbohydrates as future anti-adhesion drugs for infectious diseases. *Biochim. Biophys. Acta, Gen. Subj.* **2006**, *1760*, 527–537.
- (9) Firon, N.; Ofek, I.; Sharon, N. Interaction of mannose-containing oligosaccharides with the fimbrial lectin of *Escherichia coli*. *Biochem. Biophys. Res. Commun.* **1982**, *105*, 1426–1432.
- (10) Firon, N.; Ofek, I.; Sharon, N. Carbohydrate specificity of the surface lectins of *Escherichia coli*, *Klebsiella pneumoniae*, and *Salmonella typhimurium*. *Carbohydr. Res.* **1983**, *120*, 235–249.
- (11) Bouckaert, J.; Berglund, J.; Schembri, M.; De Genst, E.; Cools, L.; Wuhler, M.; Hung, C.-S.; Pinkner, J.; Slättegård, R.; Zavaliov, A.; Choudhury, D.; Langermann, S.; Hultgren, S. J.; Wyns, L.; Klemm, P.; Oscarson, S.; Knight, S. D.; De Greve, H. Receptor binding studies disclose a novel class of high-affinity inhibitors of the *Escherichia coli* FimH adhesin. *Mol. Microbiol.* **2005**, *55*, 441–455.
- (12) Firon, N.; Ashkenazi, S.; Mirelman, D.; Ofek, I.; Sharon, N. Aromatic alpha-glycosides of mannose are powerful inhibitors of the adherence of type 1 fimbriated *Escherichia coli* to yeast and intestinal epithelial cells. *Infect. Immun.* **1987**, *55*, 472–476.
- (13) Sperling, O.; Fuchs, A.; Lindhorst, T. K. Evaluation of the carbohydrate recognition domain of the bacterial adhesin FimH. Design, synthesis and binding properties of mannoside ligands. *Org. Biomol. Chem.* **2006**, *4*, 3913–3922.
- (14) Han, Z.; Pinkner, J. S.; Ford, B.; Obermann, R.; Nolan, W.; Wildman, S. A.; Hobbs, D.; Ellenberger, T.; Cusumano, C. K.; Hultgren, S. J.; Janetka, J. W. Structure-based drug design and optimization of mannoside bacterial FimH antagonists. *J. Med. Chem.* **2010**, *53*, 4779–4792.
- (15) Klein, T.; Abgottsporn, D.; Wittwer, M.; Rabbani, S.; Herold, J.; Jiang, X.; Kleeb, S.; Lüthi, C.; Scharenberg, M.; Bezençon, J.; Gubler, E.; Pang, L.; Smiesko, M.; Cutting, B.; Schwardt, O.; Ernst, B. FimH antagonists for the oral treatment of urinary tract infections: from design and synthesis to in vitro and in vivo evaluation. *J. Med. Chem.* **2010**, *53*, 8627–8641.
- (16) Cusumano, C. K.; Pinkner, J. S.; Han, Z.; Greene, S. E.; Ford, B. A.; Crowley, J. R.; Henderson, J. P.; Janetka, J. W.; Hultgren, S. J. Treatment and prevention of urinary tract infection with orally active FimH inhibitors. *Sci. Transl. Med.* **2011**, *3*, 109ra115.
- (17) Han, Z.; Pinkner, J. S.; Ford, B.; Choresell, E.; Crowley, J. M.; Cusumano, C. K.; Campbell, S.; Henderson, J. P.; Hultgren, S. J.

- Janetka, J. W. Lead optimization studies on FimH antagonists: discovery of potent and orally bioavailable *ortho*-substituted biphenyl mannosides. *J. Med. Chem.* **2012**, *55*, 3945–3959.
- (18) Pang, L.; Kleeb, S.; Lemme, K.; Rabbani, S.; Scharenberg, M.; Zalewski, A.; Schädler, F.; Schwardt, O.; Ernst, B. FimH antagonists: structure-activity and structure-property relationships for biphenyl  $\alpha$ -D-mannopyranosides. *ChemMedChem* **2012**, *7*, 1404–1422.
- (19) Kleeb, S.; Pang, L.; Mayer, K.; Eris, D.; Sigl, A.; Preston, R. C.; Zihlmann, P.; Abgottspon, D.; Hutter, A.; Scharenberg, M.; Jiang, X.; Navarra, G.; Rabbani, S.; Smiesko, M.; Lüdin, N.; Jakob, R. P.; Bezençon, J.; Schwardt, O.; Maier, T.; Sharpe, T.; Ernst, B. FimH antagonists: bioisosteres to improve the in vitro and in vivo PK/PD profile. *J. Med. Chem.* **2015**, *58*, 2221–2239.
- (20) Jiang, X.; Abgottspon, D.; Kleeb, S.; Rabbani, S.; Scharenberg, M.; Wittwer, M.; Haug, M.; Schwardt, O.; Ernst, B. Anti-adhesion therapy for urinary tract infections – a balanced PK/PD profile proved to be key for success. *J. Med. Chem.* **2012**, *55*, 4700–4713.
- (21) Schwardt, O.; Rabbani, S.; Hartmann, M.; Abgottspon, D.; Wittwer, M.; Kleeb, S.; Zalewski, A.; Smiesko, M.; Cutting, B.; Ernst, B. Design, synthesis and biological evaluation of mannosyl triazoles as FimH antagonists. *Bioorg. Med. Chem.* **2011**, *19*, 6454–6473.
- (22) Brument, S.; Sivignon, A.; Dumych, T. I.; Moreau, N.; Roos, G.; Guérardel, Y.; Chalopin, T.; Deniaud, D.; Bilyy, R. O.; Darfeuille-Michaud, A.; Bouckaert, J.; Gouin, S. G. Thiazolylaminomannosides as potent antiadhesives of type 1 piliated *Escherichia coli* isolated from Crohn's disease patients. *J. Med. Chem.* **2013**, *56*, 5395–5406.
- (23) Lindhorst, T. K.; Kieburg, C.; Krallmann-Wenzel, U. Inhibition of the type 1 fimbriae-mediated adhesion of *Escherichia coli* to erythrocytes by multiantennary D-mannosyl clusters: The effect of multivalency. *Glycoconjugate J.* **1998**, *15*, 605–613.
- (24) Nagahori, N.; Lee, R. T.; Nishimura, S.-L.; Pagé, S.; Roy, R.; Lee, Y. C. Inhibition of adhesion of type 1 fimbriated *Escherichia coli* to highly mannosylated ligands. *ChemBioChem* **2002**, *3*, 836–844.
- (25) Appeldoorn, C. C. M.; Joosten, J. A. F.; Ait el Maate, F. A.; Dobrindt, U.; Hacker, J.; Liskamp, R. M. J.; Khan, A. S.; Pieters, R. J. Novel multivalent mannose compounds and their inhibition of the adhesion of type 1 fimbriated uropathogenic *E. coli*. *Tetrahedron: Asymmetry* **2005**, *16*, 361–372.
- (26) Patel, A.; Lindhorst, T. K. A modular approach for the synthesis of oligosaccharide mimetics. *Carbohydr. Res.* **2006**, *341*, 1657–1668.
- (27) Touaibia, M.; Wellens, A.; Shiao, T. C.; Wang, Q.; Sirois, S.; Bouckaert, J.; Roy, R. Mannosylated M(0) dendrimers with nanomolar affinities to *Escherichia coli* FimH. *ChemMedChem* **2007**, *2*, 1190–1201.
- (28) Durka, M.; Buffet, K.; Iehl, J.; Holler, M.; Nierengarten, J.-F.; Taganna, J.; Bouckaert, J.; Vincent, S. P. The functional valency of dodecamannosylated fullerenes with *Escherichia coli* FimH - towards novel bacterial antiadhesives. *Chem. Commun.* **2011**, *47*, 1321–1323.
- (29) Bouckaert, J.; Li, Z.; Xavier, C.; Almant, M.; Cavelliers, V.; Lahoutte, T.; Weeks, S. D.; Kovensky, J.; Gouin, S. G. Heptyl  $\alpha$ -D-mannosides grafted on a  $\beta$ -cyclodextrin core to interfere with *Escherichia coli* adhesion: An in vivo multivalent effect. *Chem. - Eur. J.* **2013**, *19*, 7847–7855.
- (30) Scharenberg, M.; Schwardt, O.; Rabbani, S.; Ernst, B. Target selectivity of FimH antagonists. *J. Med. Chem.* **2012**, *55*, 9810–9816.
- (31) Van de Waterbeemd, H.; Smith, D. A.; Beaumont, K.; Walker, D. K. Property-based design: Optimization of drug absorption and pharmacokinetics. *J. Med. Chem.* **2001**, *44*, 1313–1333.
- (32) Amidon, G. L.; Lennernäs, H.; Shah, V. P.; Crison, J. R. A theoretical basis for a biopharmaceutical drug classification: the correlation of in vitro drug product dissolution and in vivo bioavailability. *Pharm. Res.* **1995**, *12*, 413–420.
- (33) Heimbach, T.; Oh, D.-M.; Li, L. Y.; Forsberg, M.; Savolainen, J.; Leppänen, J.; Matsunaga, Y.; Flynn, G.; Fleisher, D. Absorption rate limit considerations for oral phosphate prodrugs. *Pharm. Res.* **2003**, *20*, 848–856.
- (34) Stella, V. J.; Nti-Addae, K. W. Prodrug strategies to overcome poor water solubility. *Adv. Drug Delivery Rev.* **2007**, *59*, 677–694.
- (35) Stewart, B. H.; Amidon, G. L.; Brabec, R. K. Uptake of prodrugs by rat intestinal mucosal cells: mechanism and pharmaceutical implications. *J. Pharm. Sci.* **1986**, *75*, 940–945.
- (36) Wire, M. B.; Shelton, M. J.; Studenberg, S. Fosamprenavir: clinical pharmacokinetics and drug interactions of the amprenavir prodrug. *Clin. Pharmacokinet.* **2006**, *45*, 137–168.
- (37) Hersh, M. R.; Kuhn, J. G.; Phillips, J. L.; Clark, G.; Ludden, T. M.; Von Hoff, D. D. Pharmacokinetic study of fludarabine phosphate (NSC 312887). *Cancer Chemother. Pharmacol.* **1986**, *17*, 277–280.
- (38) Rabbani, S.; Jiang, X. H.; Schwardt, O.; Ernst, B. Expression of the carbohydrate recognition domain of FimH and development of a competitive binding assay. *Anal. Biochem.* **2010**, *407*, 188–195.
- (39) Alsenz, J.; Kansy, M. High throughput solubility measurement in drug discovery and development. *Adv. Drug Delivery Rev.* **2007**, *59*, 546–567.
- (40) Waring, M. J. Lipophilicity in drug discovery. *Expert Opin. Drug Discovery* **2010**, *5*, 235–248.
- (41) Kansy, M.; Senner, F.; Gubernator, K. Physicochemical high throughput screening: Parallel artificial membrane permeation assay in the description of passive absorption processes. *J. Med. Chem.* **1998**, *41*, 1007–1010.
- (42) Avdeef, A.; Bendels, S.; Di, L.; Faller, B.; Kansy, M.; Sugano, K.; Yamauchi, Y. PAMPA - Critical factors for better predictions of absorption. *J. Pharm. Sci.* **2007**, *96*, 2893–2909.
- (43) Artursson, P.; Karlsson, J. Correlation between oral drug absorption in humans and apparent drug permeability coefficients in human intestinal epithelial (Caco-2) cells. *Biochem. Biophys. Res. Commun.* **1991**, *175*, 880–885.
- (44) Hubatsch, I.; Ragnarsson, E. G. E.; Artursson, P. Determination of drug permeability and prediction of drug absorption in Caco-2 monolayers. *Nat. Protoc.* **2007**, *2*, 2111–2119.
- (45) DeGoeij, D. A.; Grampovnik, D. J.; Flosi, W. J.; Marsh, K. C.; Wang, X. C.; Klein, L. L.; McDaniel, K. F.; Liu, Y.; Long, M. A.; Kati, W. M.; Molla, A.; Kempf, D. J. Water-soluble prodrugs of the human immunodeficiency virus protease inhibitors lopinavir and ritonavir. *J. Med. Chem.* **2009**, *52*, 2964–2970.
- (46) Ma, Z.; Zhang, J.; Kong, F. Facile synthesis of arabinomannose penta- and decasaccharide fragments of the lipoarabinomannan of the equine pathogen, *Rhodococcus equi*. *Carbohydr. Res.* **2004**, *339*, 1761–1771.
- (47) Dong, H.; Pei, Z.; Byström, S.; Ramström, O. Reagent-Dependent Regioselective Control in Multiple Carbohydrate Esterifications. *J. Org. Chem.* **2007**, *72*, 1499–1502.
- (48) Yuan, H.; Li, N.; Lai, Y. Evaluation of in vitro models for screening phosphatase-mediated bioconversion of phosphate ester prodrugs. *Drug Metab. Dispos.* **2009**, *37*, 1443–1447.
- (49) Kearny, A. S.; Stella, V. J. The in vitro enzymic liabilities of chemically distinct phosphomonoester prodrugs. *Pharm. Res.* **1992**, *9*, 497–503.
- (50) Dhareshwar, S. S.; Stella, V. J. A novel prodrug strategy for beta-dicarbonyl carbon acids: syntheses and evaluation of the physicochemical characteristics of C-phosphoryloxymethyl (POM) and phosphoryloxymethyl (POMOM) prodrug derivatives. *J. Pharm. Sci.* **2010**, *99*, 2711–2723.
- (51) *The United States Pharmacopeia (USP 28)*; U. S. Pharmacopeia: Rockville, MD, 2004.
- (52) Dressman, J. B.; Thelen, K.; Jantravid, E. Towards quantitative prediction of oral drug absorption. *Clin. Pharmacokinet.* **2008**, *47*, 655–667.
- (53) Stephens, R. H.; O'Neill, C. A.; Warhurst, A.; Carlson, G. L.; Rowland, M.; Warhurst, G. Kinetic profiling of P-glycoprotein-mediated drug efflux in rat and human intestinal epithelia. *J. Pharmacol. Exp. Ther.* **2001**, *296*, 584–591.
- (54) Zhang, Y.; Huo, M.; Zhou, J.; Xie, S. PKSolver: An add-in program for pharmacokinetic and pharmacodynamic data analysis in Microsoft Excel. *Comput. Methods Programs Biomed.* **2010**, *99*, 306–314.



(55) Jantratid, E.; Janssen, N.; Reppas, C.; Dressman, J. B. Dissolution media simulating conditions in the proximal human gastrointestinal tract: an update. *Pharm. Res.* **2008**, *25*, 1663–1676.

(56) Diehl, K.-H.; Hull, R.; Morton, D.; Pfister, R.; Rabemampianina, Y.; Smith, D.; Vidal, J.-M.; Van de Vorstenbosch, C. A good practice guide to the administration of substances and removal of blood, including routes and volumes. *J. Appl. Toxicol.* **2001**, *21*, 15–23.



## Supporting Information

### **FimH Antagonists - Phosphate Prodrugs Improve Oral Bioavailability**

Simon Kleeb, Xiaohua Jiang, Priska Frei, Anja Sigl, Jacqueline Bezençon, Karen Bamberger, Oliver Schwardt, and Beat Ernst

Institute of Molecular Pharmacy, Pharmacenter, University of Basel, Klingelbergstrasse 50, 4056 Basel (Switzerland)

#### **Contents**

Composition of Biorelevant Media .....	S2
Purity of Target Compounds .....	S3
HPLC Traces of Target Compounds .....	S4
<sup>1</sup> H NMR Spectra of Target Compounds .....	S8
References .....	S13

**Composition of Biorelevant Media****Table S1.** Biorelevant media. Composition of the used simulated gastric and intestinal fluids (FaSSGF, FeSSGF, FaSSIF, FeSSIF, sGF, buffer sGF, sIF, and buffer sIF).

Components	FaSSGF <sup>a)</sup>	FeSSGF <sup>b)</sup>	FaSSIF <sup>c)</sup>	FeSSIF <sup>d)</sup>	sGF <sup>e)</sup>	buffer sGF <sup>f)</sup>	sIF <sup>g)</sup>	buffer sIF <sup>h)</sup>
Sodium taurocholate hydrate [mmol/L]	0.08		3	10				
Lecithin [mmol/L]	0.02		0.2	2				
Pepsin [mg/mL]	0.1				3.2			
Glycerol monooleate [mmol/L]				5				
Sodium oleate [mmol/L]				0.8				
Pancreatin [mg/mL]				2.5			2.5	
Acetic acid [mmol/L]		17.12						
Maleic acid [mmol/L]			19.12	55.02				
Sodium hydroxide [mmol/L]			34.8	81.65				
Sodium acetate trihydrate [mmol/L]		29.75						
Sodium chloride [mmol/L]	34.2	237.02	68.62	125.5	34.22	34.22		
Monopotassium phosphate [mmol/L]							49.97	49.97
NaOH 0.2 mmol/L		q.s.	q.s.	q.s.			q.s.	q.s.
HCl 37%	q.s.				q.s.	q.s.		
pH	1.6	5	6.5	5.8	1.2	1.2	6.8	6.8

a) FaSSGF: fasted-state simulated gastric fluid<sup>S1</sup>; b) FeSSGF: fed-state simulated gastric fluid; 1:1 mix with ultra-high temperature milk<sup>S1</sup>; c) FaSSIF: fasted-state simulated intestinal fluid, updated version<sup>S1</sup>; d) FeSSIF: fed-state simulated intestinal fluid, updated version<sup>S1</sup>; e) sGF: simulated gastric fluid<sup>S3</sup>; f) buffer sGF: prepared equally to sGF but without pepsin; g) sIF: simulated intestinal fluid<sup>S3</sup>; h) buffer sIF: prepared equally to sIF but without pancreatin

**Purity of Target Compounds****HPLC Analysis**

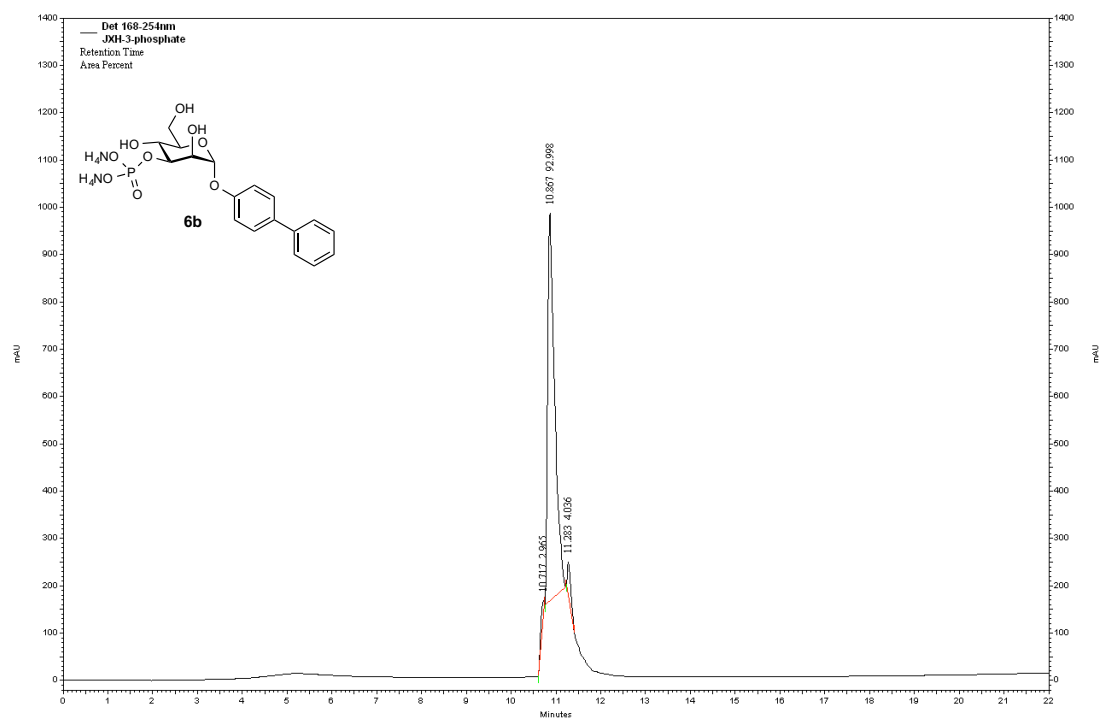
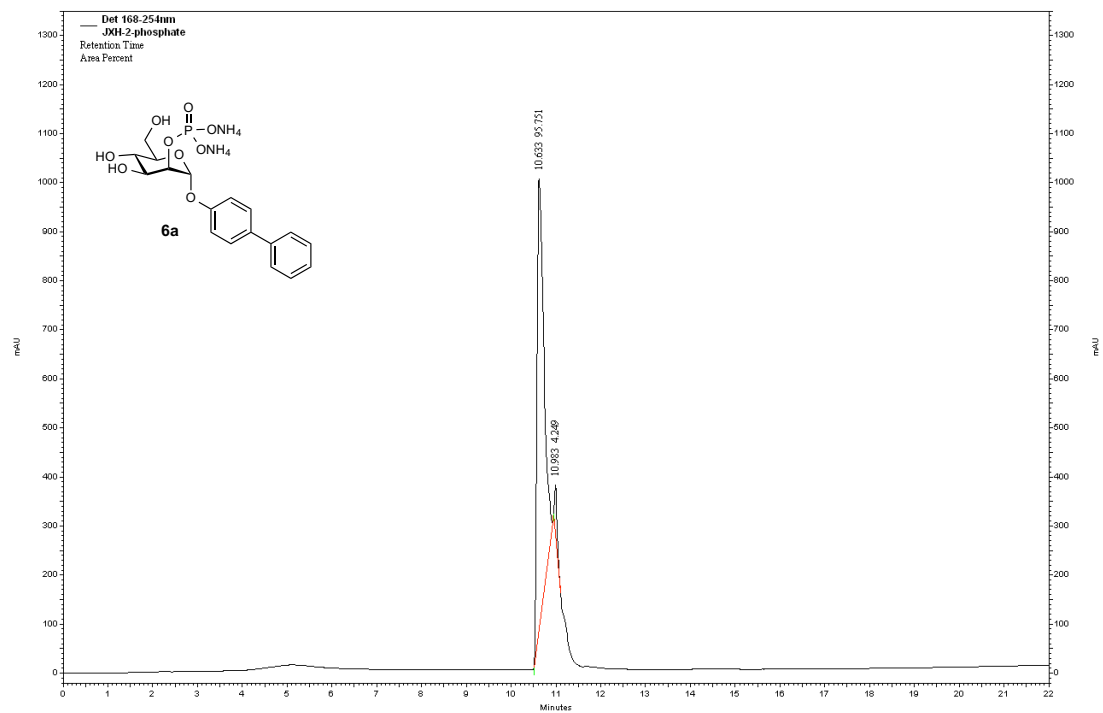
**Method A:** System: Beckman Coulter Gold, consisting of pump 126, DAD 168 (190-400 nm) and auto-sampler 508. Column: Waters Atlantis T3, 3  $\mu\text{m}$ , 2.1  $\times$  100 mm. A: Water + 0.1% TFA; B: MeCN + 0.1% TFA. Detection: 254 nm. Gradient: 5% B for 0.5 min, 5% B  $\rightarrow$  70% B over 19.5 min; flow rate: 0.5 mL/min.

**Method B:** System: Agilent 1100/1200 with UV detection (190-410 nm). Column: Waters Atlantis T3, 3  $\mu\text{m}$ , 2.1  $\times$  100 mm. A: Water + 0.01% TFA; B: MeCN + 0.01% TFA. Detection: 254 nm. Gradient: 5% B for 1 min, 5% B  $\rightarrow$  95% B over 19 min; flow rate: 0.5 mL/min.

Compound	Method	Retention time [min]	Purity [%] <sup>[a]</sup>
<b>6a</b>	A	10.633	> 99.5
<b>6b</b>	A	10.867	97.0
<b>6c</b>	A	11.533	> 99.5
<b>6d</b>	A	11.017	> 99.5
<b>6e</b>	A	11.133	97.0
<b>7a</b>	B	8.212	99.1
<b>7b</b>	B	8.157	97.4
<b>7c</b>	B	8.478	> 99.5
<b>7d</b>	B	8.904	99.5
<b>8</b>	A	11.667	> 99.5

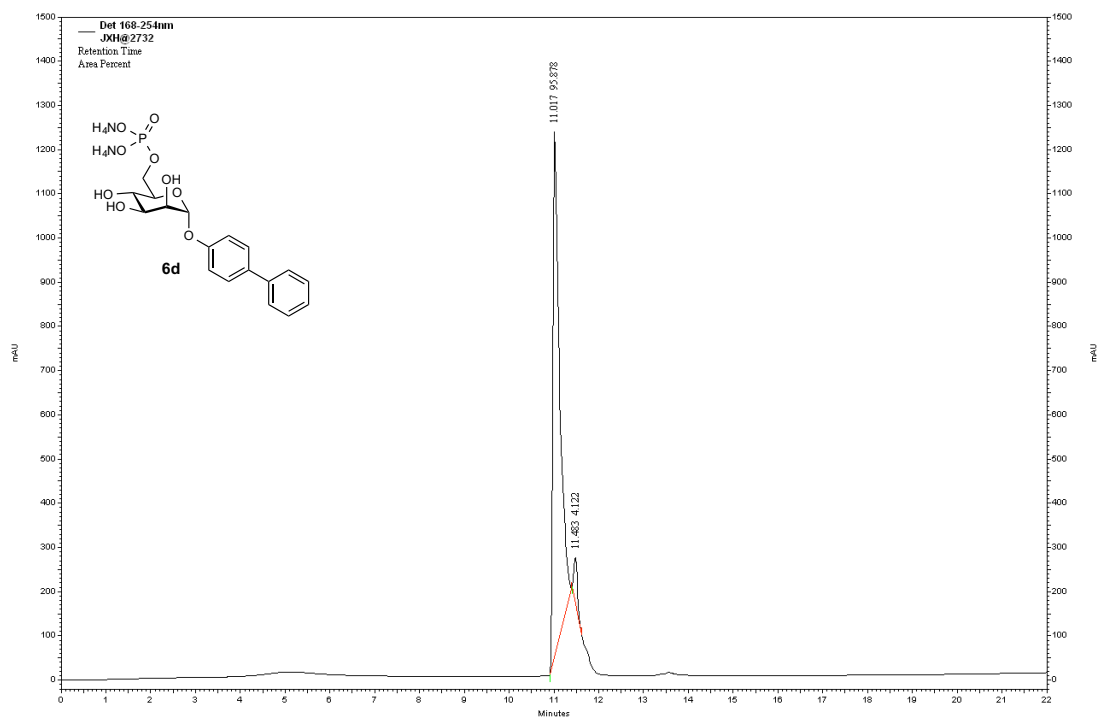
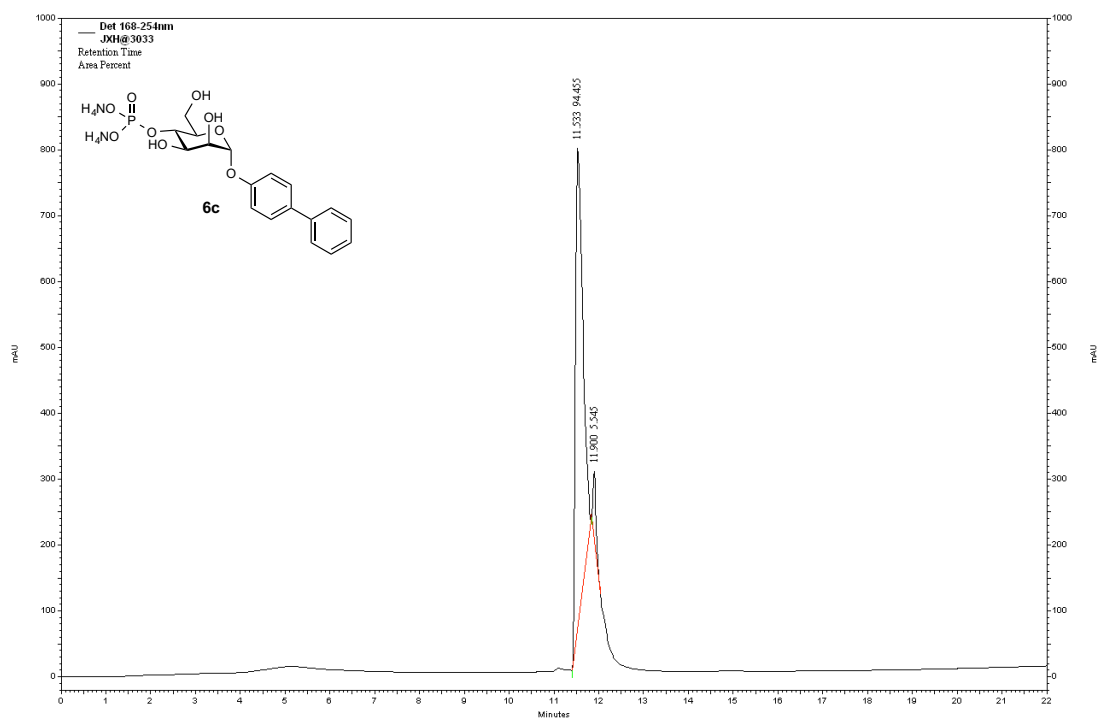
<sup>[a]</sup> In the case of diammonium salts (**6a-e** & **8**) double- or triple-peaks were observed due to protonation during HPLC.

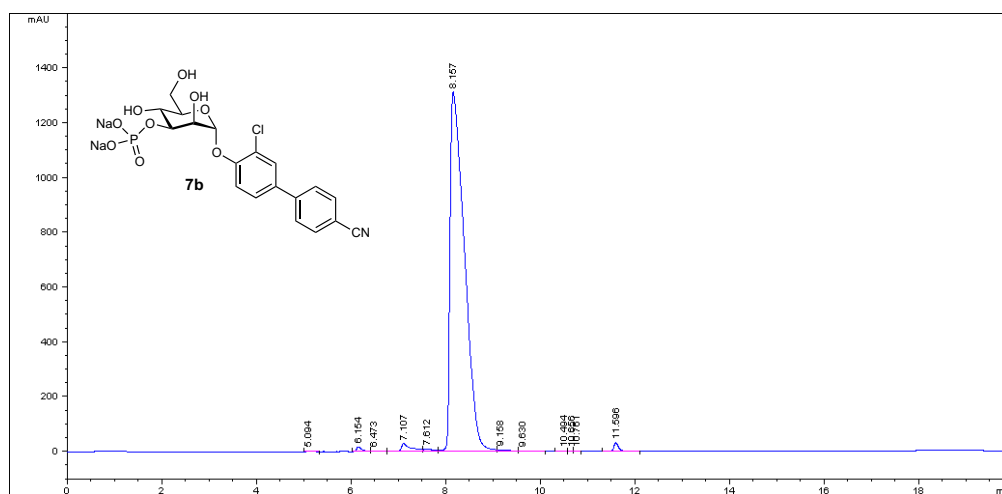
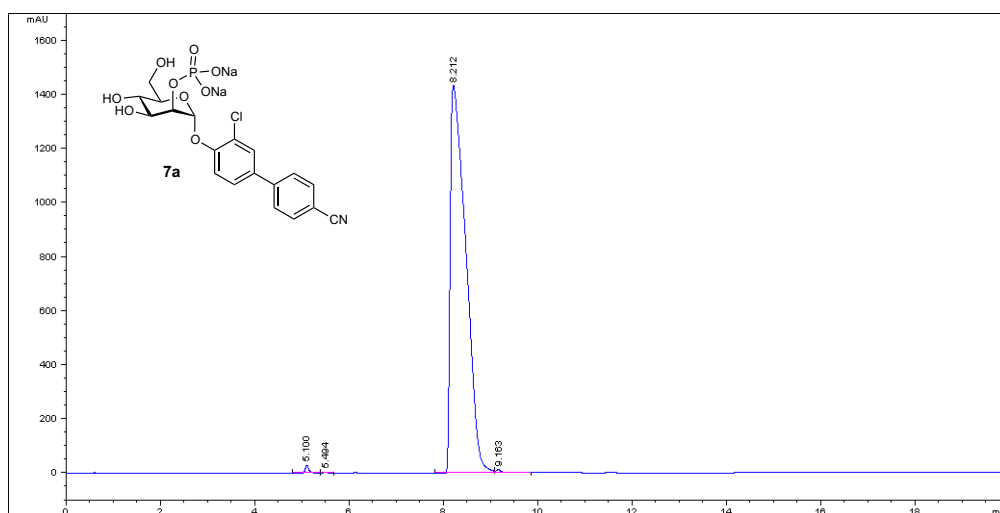
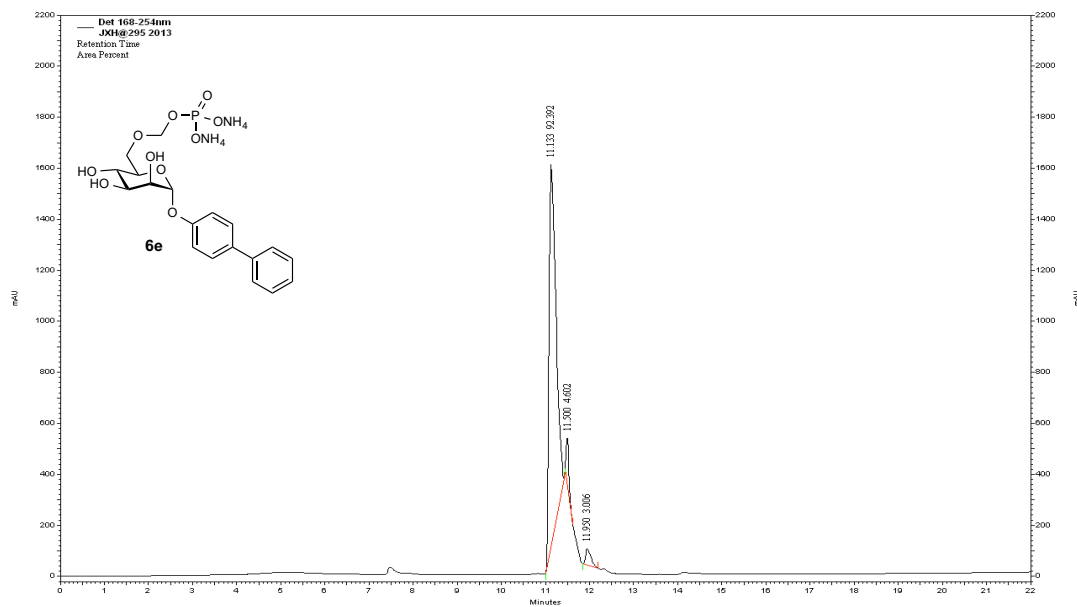
## HPLC Traces of Target Compounds



## Supporting Information

## FimH Antagonists - Phosphate Prodrugs Improve Oral Bioavailability

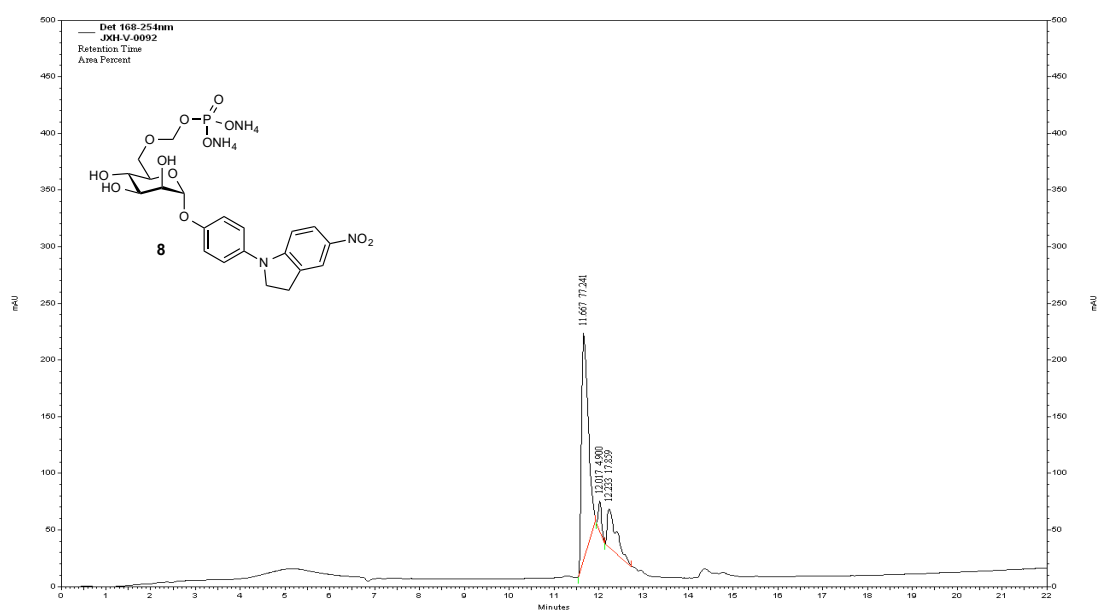
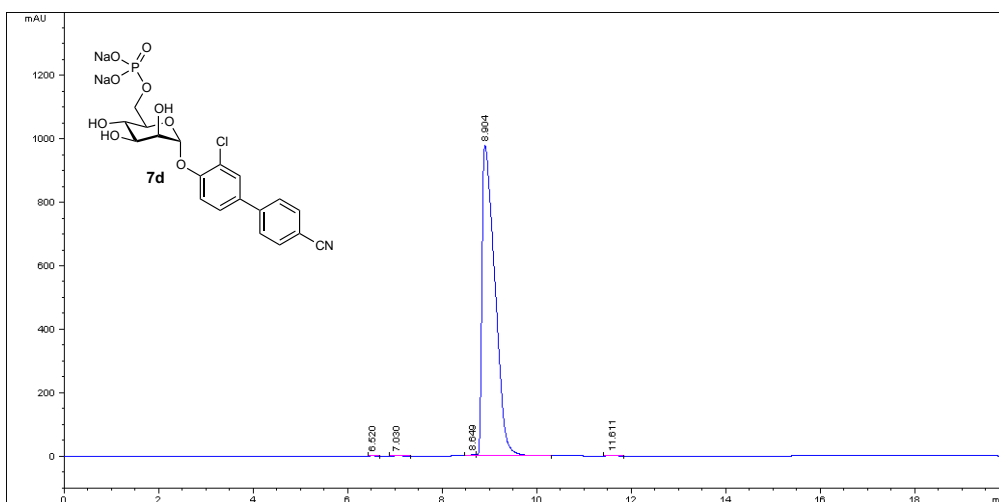
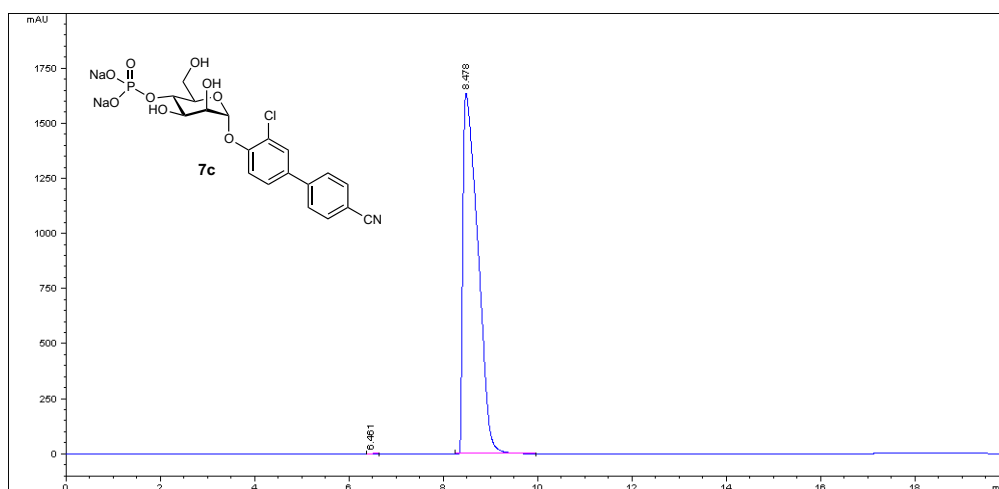


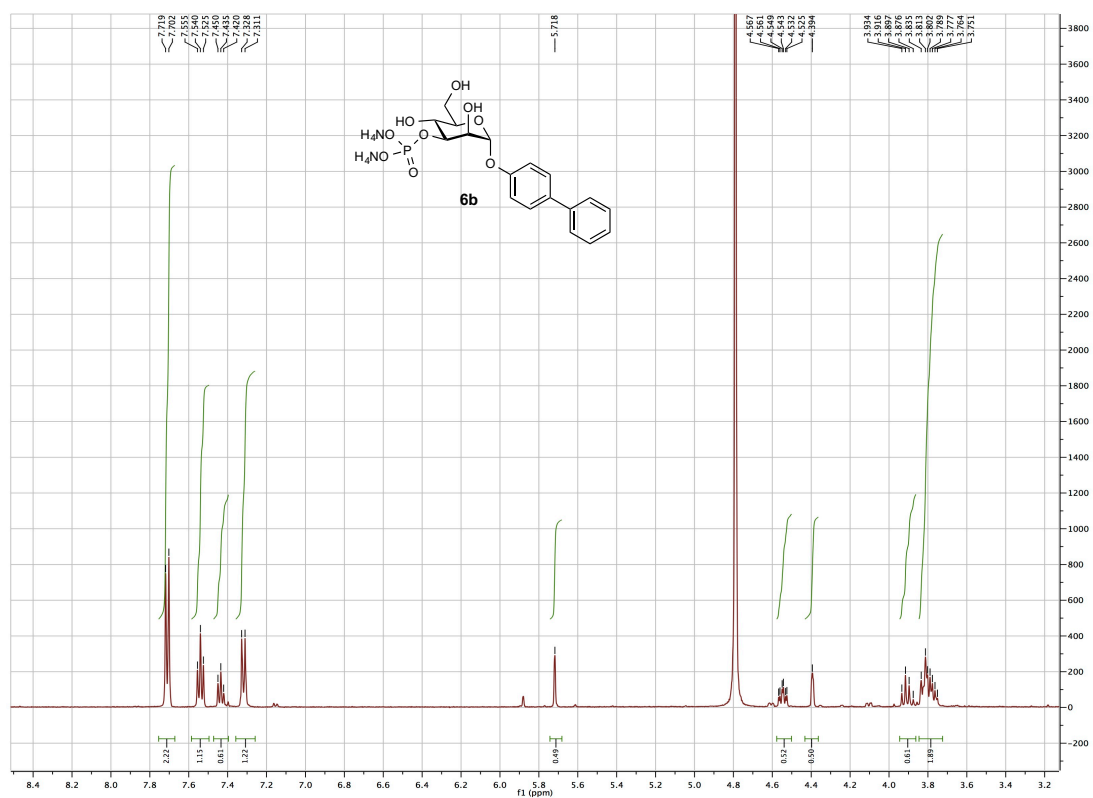
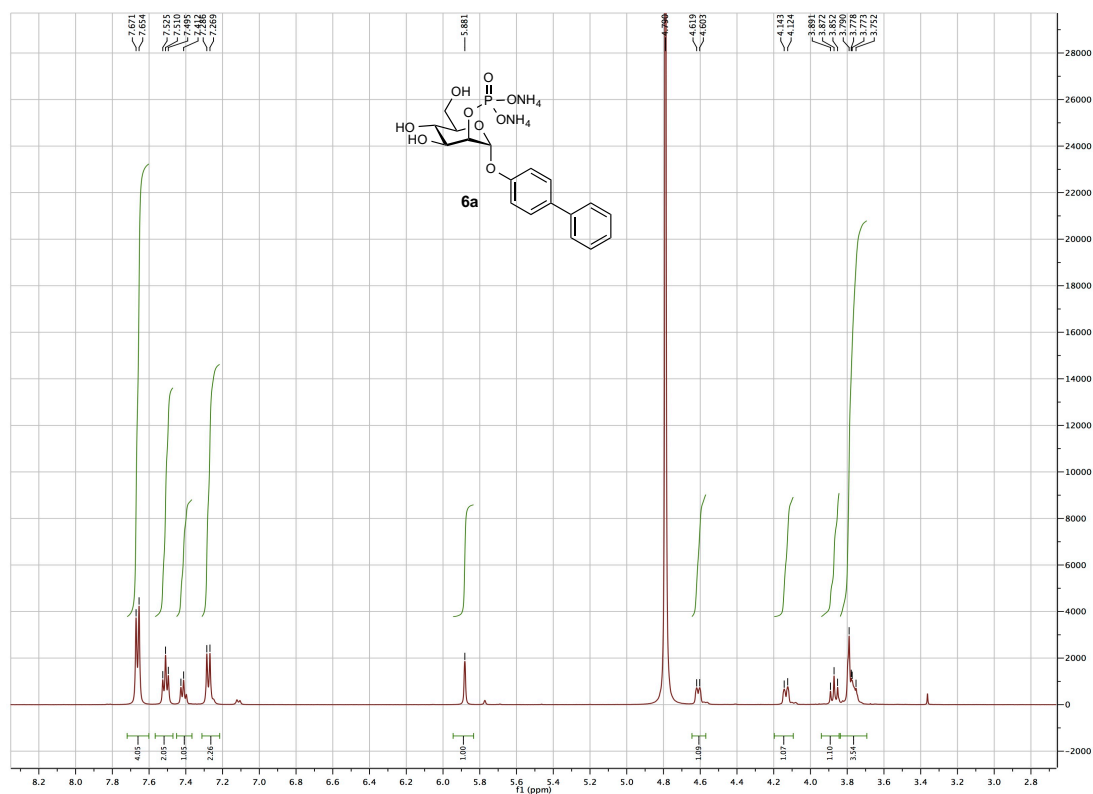




## Supporting Information

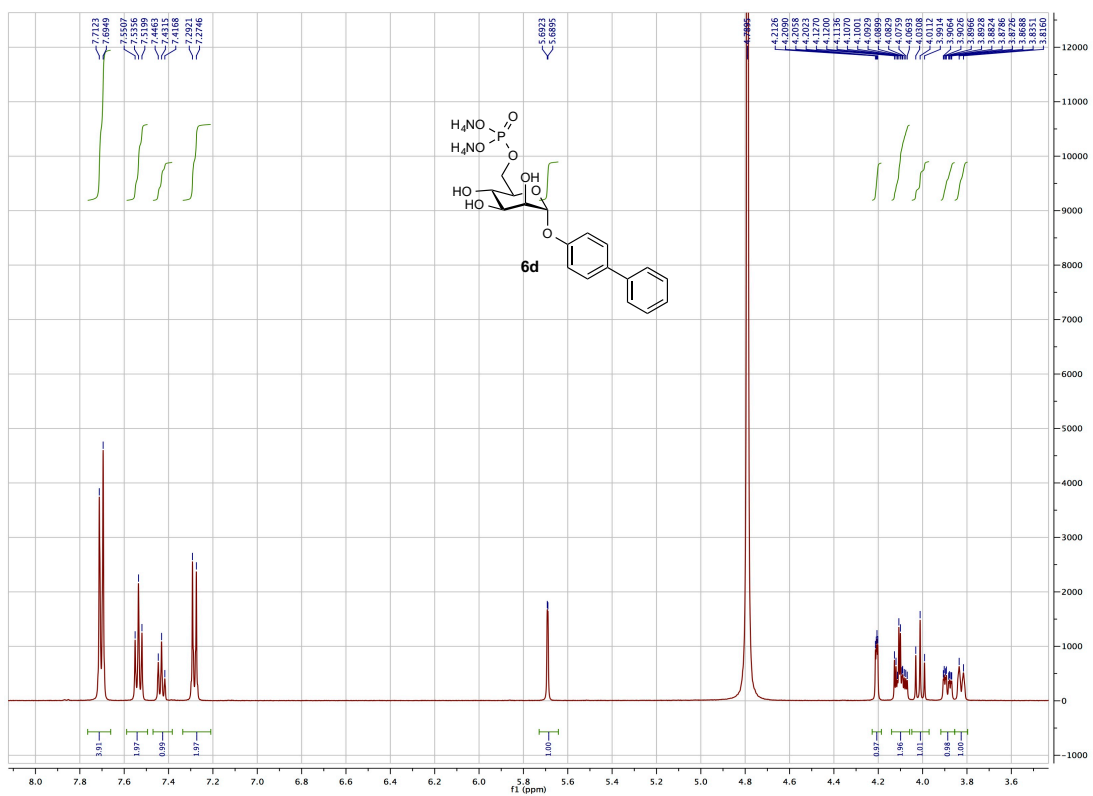
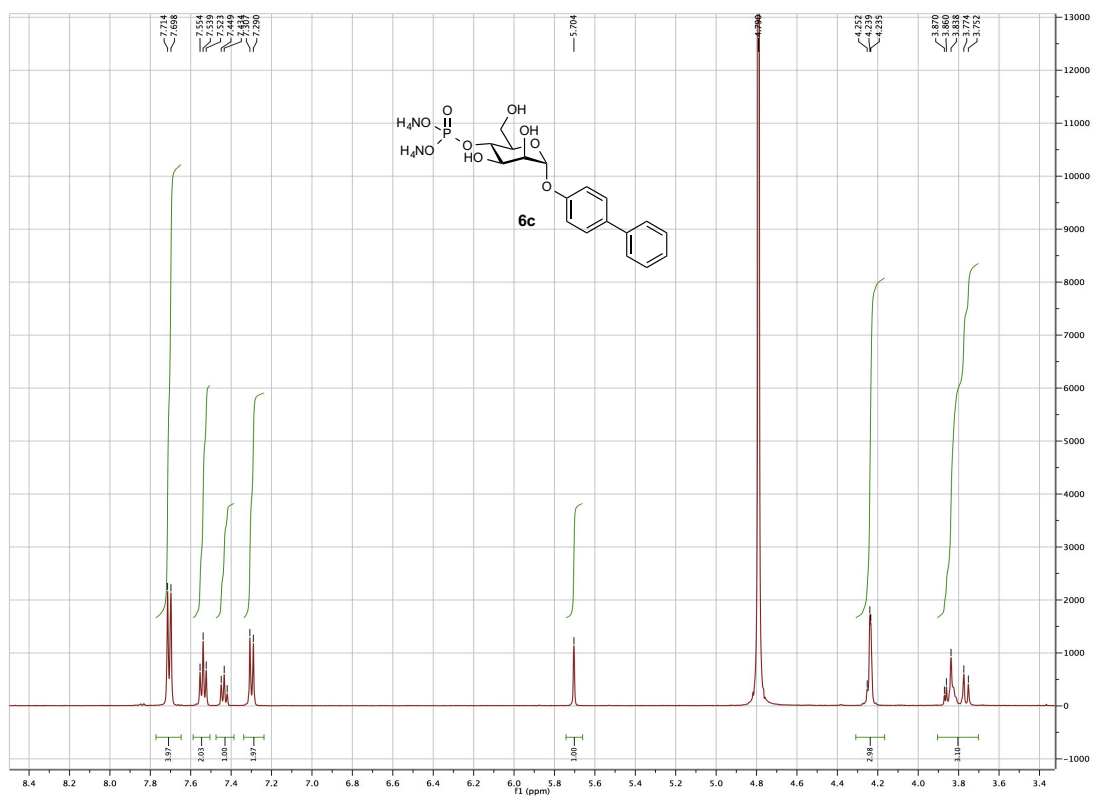
## FimH Antagonists - Phosphate Prodrugs Improve Oral Bioavailability



**<sup>1</sup>H NMR Spectra of Target Compounds**

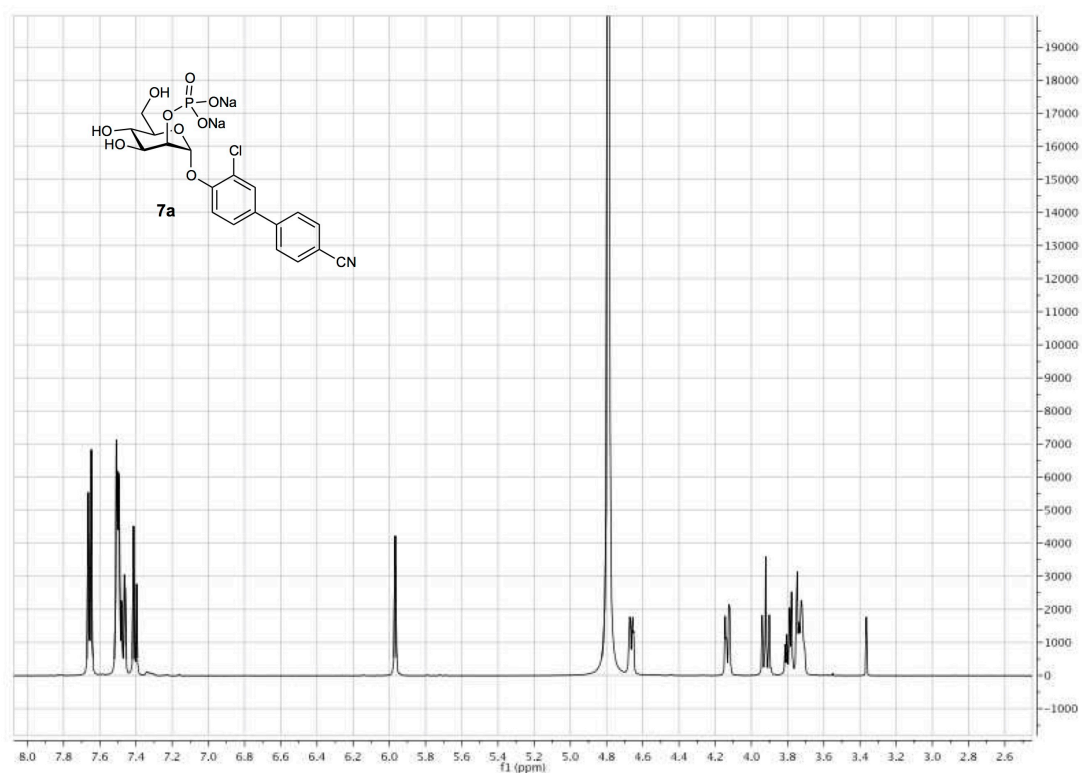
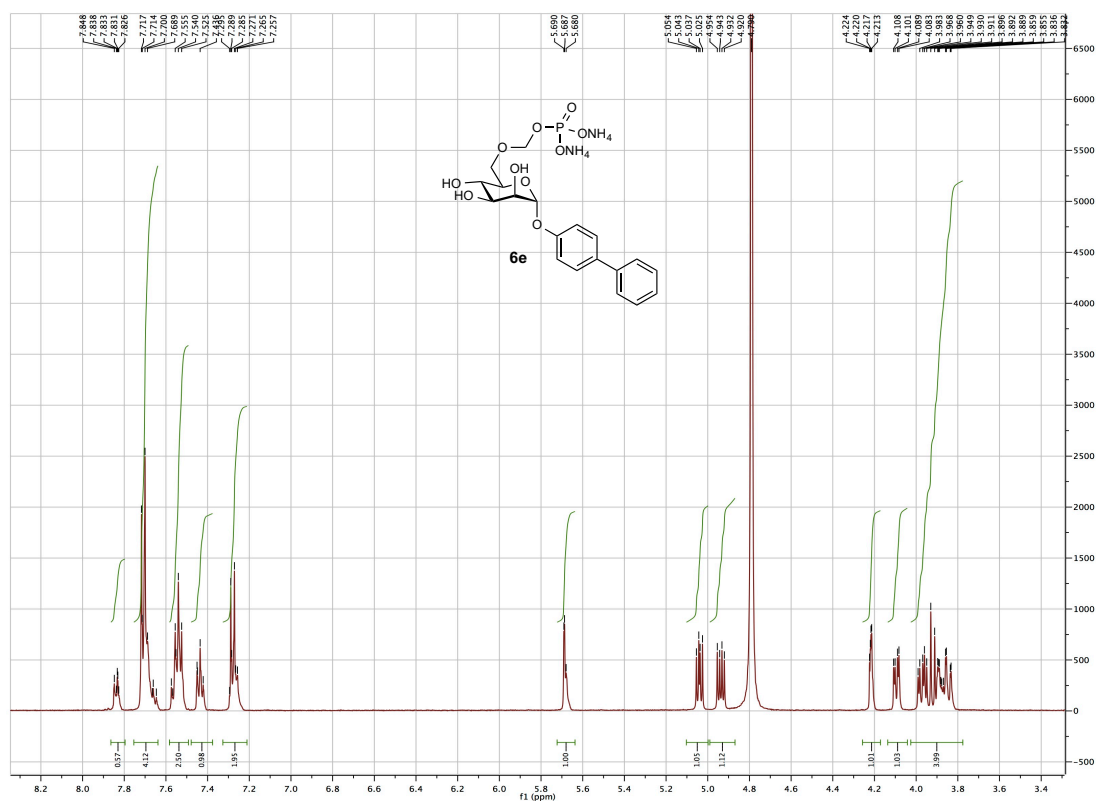
## Supporting Information

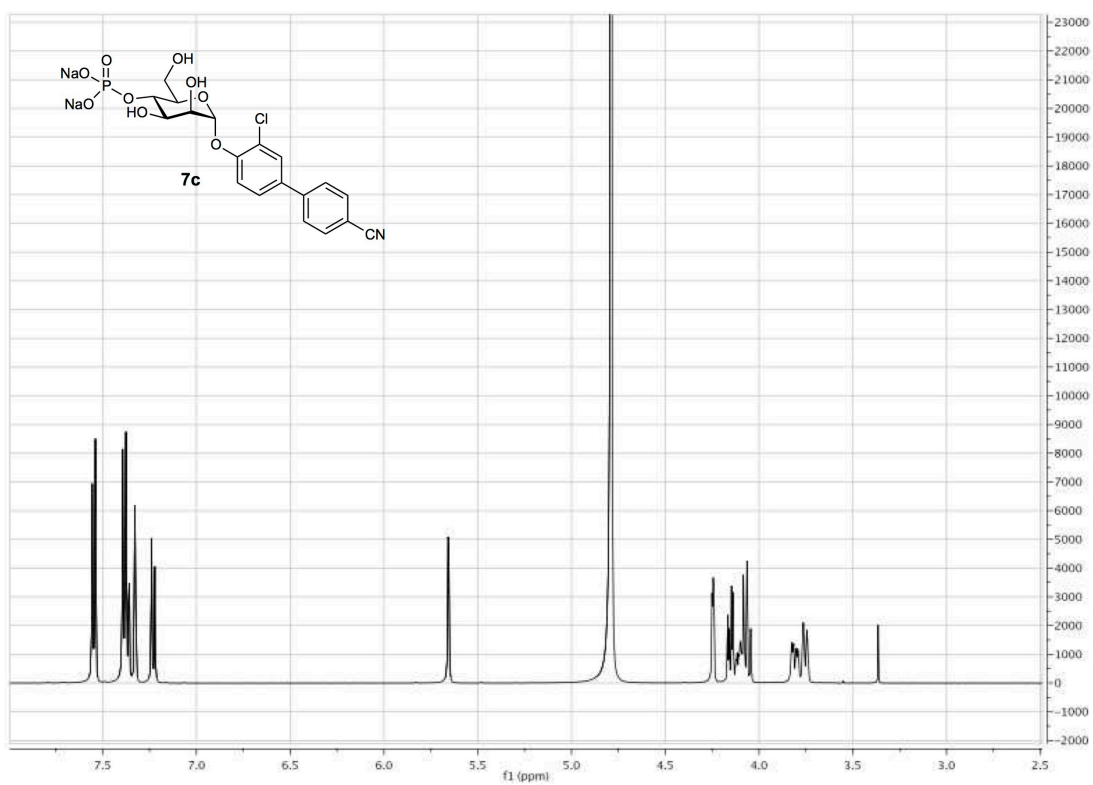
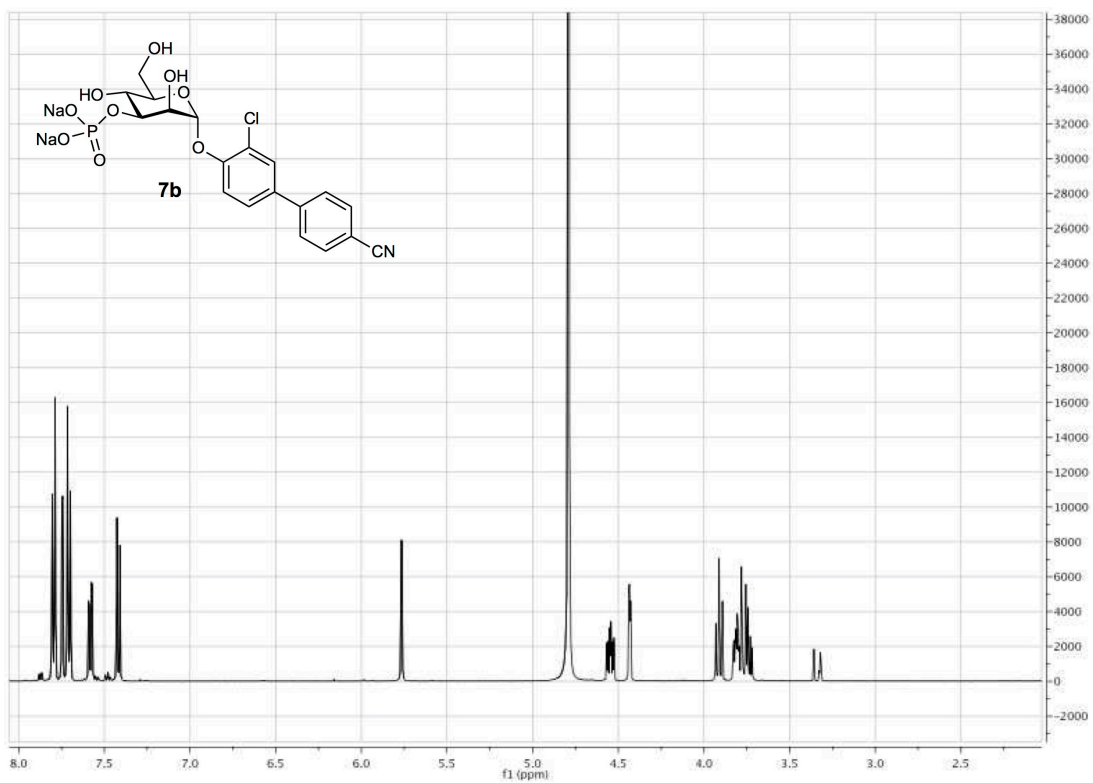
## FimH Antagonists - Phosphate Prodrugs Improve Oral Bioavailability

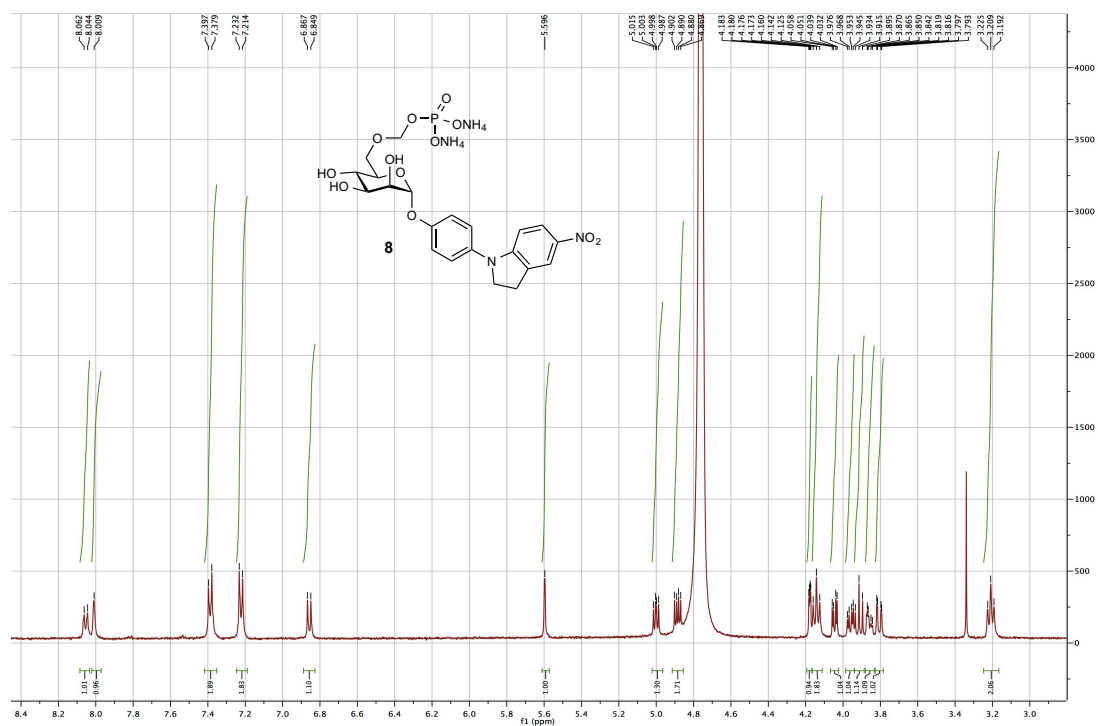
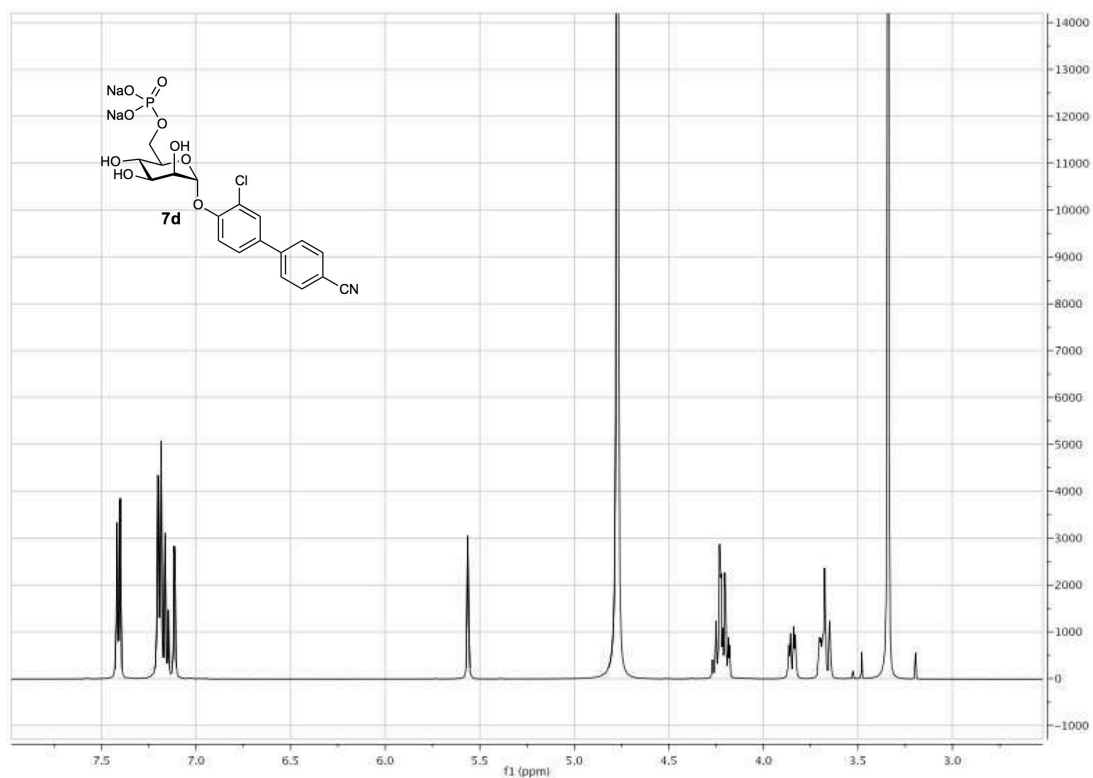


## Supporting Information

## FimH Antagonists - Phosphate Prodrugs Improve Oral Bioavailability







**References**

- (S1) Jantratid, E.; Janssen, N.; Reppas, C.; Dressman, J. B. Dissolution media simulating conditions in the proximal human gastrointestinal tract: an update. *Pharm. Res.* **2008**, *25*, 1663-1676.
- (S2) Dressman, J. B.; Thelen, K.; Jantratid, E. Towards quantitative prediction of oral drug absorption. *Clin. Pharmacokinet.* **2008**, *47*, 655-667.
- (S3) “The United States Pharmacopeia (USP 28)”. **2004**.





#### 4.3.4 Paper 5 - Structural and Solvent Modifications:

##### FimH Antagonists – Solubility vs. Permeability

This paper addresses the low aqueous solubility of the methyl ester prodrugs. Two major strategies were outlined; first, rearrangement of the substitution pattern of the biphenyl aglycone and second, introduction of aromatic heterocycles as terminal ring of the biaryl moiety. The influence of these modifications on binding affinity to the FimH-CRD and the physicochemical profiles of the antagonists were revealed in detail. *In vivo* pharmacokinetics and disease studies completed the study.

##### Contribution to the project:

Jacqueline Bezençon was responsible for the characterization of the physicochemical and *in vitro* pharmacokinetic properties of the diverse biaryl  $\alpha$ -D-mannopyranosides in collaboration with Simon Kleeb. Furthermore, she conducted all experiments regarding the preformulation of compound **41f** for higher dose application in the *in vivo* studies (see unpublished data at the beginning of chapter 4.3, page 123) and revisited the pharmacokinetic part.

The paper was published as a Book Chapter in *Carbohydrate Chemistry* 2017:

L. Pang,\* **J. Bezençon**,\* S. Kleeb,\* S. Rabbani, A. Sigl, M. Smiesko, C.P. Sager, D. Eris, O. Schwardt, B. Ernst, FimH Antagonists – Solubility vs. Permeability. *Carbohydrate Chemistry*, **2017**, *42*, 248-273.

\*contributed equally.

## FimH antagonists – solubility vs. permeability

Lijuan Pang,<sup>†</sup> Jacqueline Bezençon,<sup>†</sup> Simon Kleeb,<sup>†</sup> Said Rabbani, Anja Sigl, Martin Smiesko, Christoph P. Sager, Deniz Eris, Oliver Schwardt and Beat Ernst\*

DOI: 10.1039/9781782626657-00248

Urinary tract infections (UTIs) caused by uropathogenic *Escherichia coli* (UPEC) are among the most prevalent infections worldwide. Since frequent antibiotic treatment favors the emergence of antibiotic resistance, efficient non-antibiotic strategies are urgently needed. The first step of the pathogenesis of UTI is the bacterial adherence to urothelial host cells, a process mediated by the mannose-binding adhesin FimH located at the tip of bacterial pili. In a preliminary study, biphenyl  $\alpha$ -D-mannopyranosides with an electron-withdrawing carboxylate on the aglycone were identified as potent FimH antagonists. Although passive permeability could be established by masking the carboxylate as an ester, insufficient solubility and fast hydrolysis did not allow to maintain the therapeutic concentration in the bladder for the requested period of time. By modifying the substitution pattern, molecular planarity and symmetry of the biphenyl aglycone could be disrupted leading to improved solubility. In addition, when heteroatoms were introduced to the aglycone, antagonists with further improved solubility, metabolic stability as well as passive permeability were obtained. The best representative, the pyrrolylphenyl mannoside **42f** exhibited therapeutic urine concentration for up to 6 h and is therefore a promising oral candidate for UTI prevention and/or treatment.

### 1 Introduction

Urinary tract infections (UTIs) – also known as acute cystitis or bladder infections – are among the most prevalent infectious diseases worldwide. UTIs affect millions of people every year and account for significant morbidity and high medical costs.<sup>1</sup> Since symptomatic UTIs require antibiotic treatment and recurrent antibiotic exposure leads to the ubiquitous problem of antimicrobial resistance, efficient non-antibiotic prevention and treatment strategies are urgently needed.<sup>2</sup> More than 70% of UTIs are caused by uropathogenic *Escherichia coli* (UPEC).<sup>1a,3</sup> In the first step of the infection, UPEC adhere to urothelial cells, which prevents them from being cleared by micturition but also triggers the invasion into host cells.<sup>4</sup> This initial contact is mediated by the bacterial adhesin FimH located at the tip of type 1 pili.<sup>5</sup> FimH consists of an N-terminal lectin domain and a C-terminal pilin domain. The carbohydrate recognition domain (CRD) of the lectin domain specifically recognizes oligmannosides being part of the glycoprotein uroplakin Ia located on the urinary bladder mucosa, whereas the pilin domain regulates the switch between the various affinity states of the CRD.<sup>6</sup> Blocking the FimH-CRD with carbohydrates or mimetics thereof prevents

*Institute of Molecular Pharmacy, Pharmacenter, University of Basel, Klingelbergstr. 50, 4056 Basel, Switzerland. E-mail: beat.ernst@unibas.ch*

<sup>†</sup>These authors equally contributed to this work.

the bacterial adhesion as well as the subsequent infection. This approach is therefore regarded as a potential therapy for prevention and/or treatment of UTIs.<sup>7</sup>

Over the last three decades, mannosides and oligomannosides with various aglycones, such as *n*-alkyl,<sup>8d</sup> phenyl,<sup>8e</sup> dioxocyclobutenylamino-phenyl,<sup>8f</sup> umbelliferyl,<sup>8e</sup> biphenyl,<sup>8g-k</sup> indol(in)ylphenyl,<sup>8l</sup> triazolyl<sup>8m</sup> or thiazolylamino<sup>8n</sup> have been tested as potential antagonists for preventing type 1 pili-mediated bacterial adhesion.<sup>8</sup> In addition, different multi-valent presentations of mannose derivatives have been explored.<sup>9</sup>

In general, when a daily therapy is required, oral administration is the standard care. To achieve oral availability as well as a therapeutic concentration in the bladder over an extended period of time, successful oral absorption (*i.e.* solubility and permeability), metabolic stability, and slow and prolonged renal excretion (*i.e.* renal reabsorption) are required. As previously described,<sup>8h</sup> the carboxylic acid moiety in biphenyl  $\alpha$ -D-mannoside **1a** – its electron-withdrawing potential is essential for an enhanced  $\pi$ - $\pi$  stacking interaction – impairs the membrane permeability and, as a consequence, the potential for oral absorption. Therefore, the polar carboxylate was masked as ester ( $\rightarrow$ **1b**<sup>8h</sup>), exhibiting comparable electron withdrawing properties but improving passive permeability and renal reabsorption by increased lipophilicity. However, since the ester **1b** was characterized by low aqueous solubility (12  $\mu\text{g mL}^{-1}$ ) and fast metabolic cleavage ( $t_{1/2}$  = 2.1 min), the absorptive flux through the intestinal mucosa was limited and the renal excretion accelerated.<sup>10</sup> As a consequence, the therapeutic concentration in the bladder could not be maintained for a sufficient period of time.<sup>8h</sup> Therefore, emanating from antagonist **1b**, these pharmacokinetic drawbacks were addressed by structural modifications of the aglycone (Fig. 1).

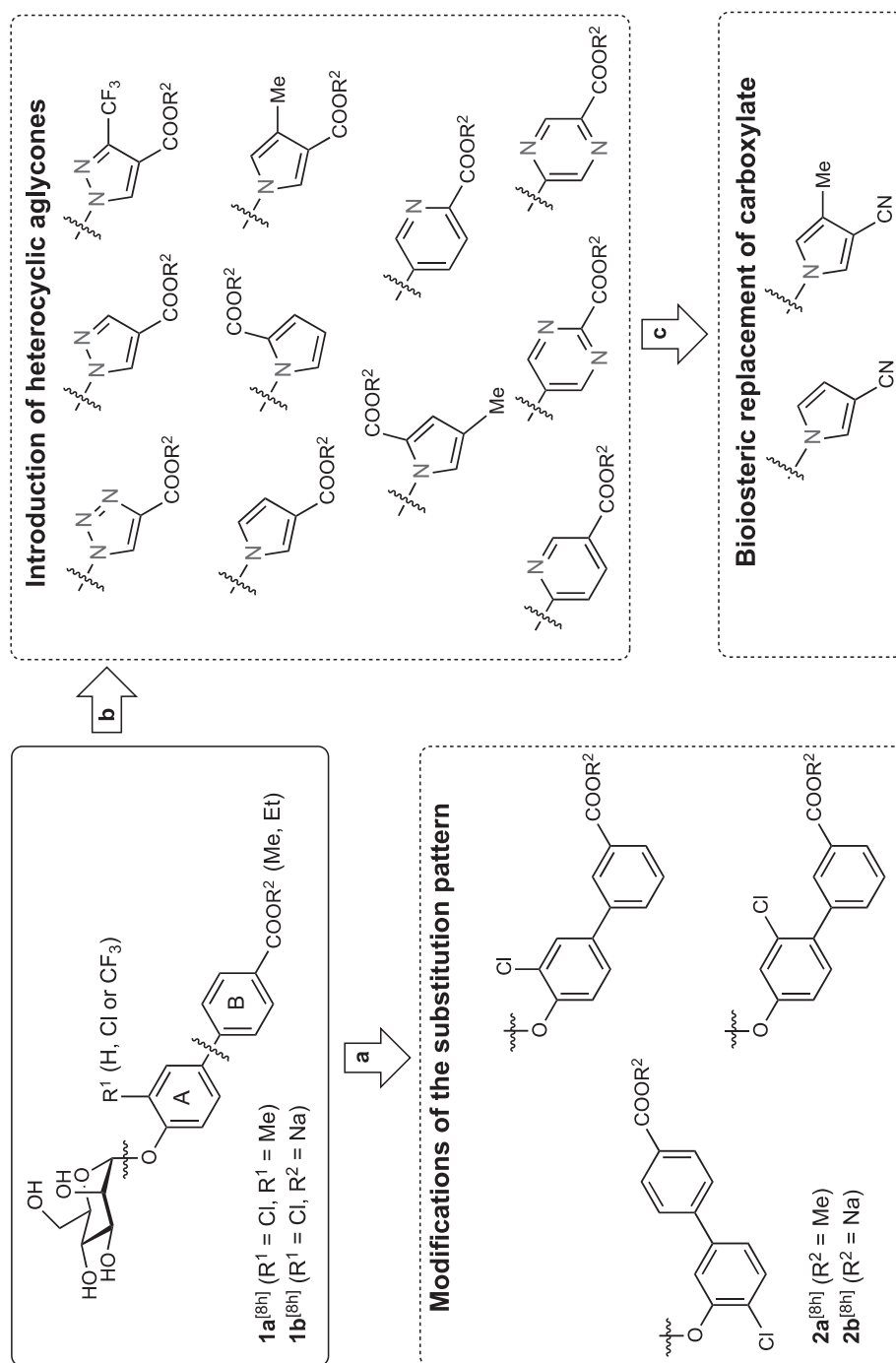
## 2 Results and discussion

To improve relevant pharmacokinetic parameters (*i.e.* oral absorption, metabolism and renal excretion of FimH antagonist **1b**), we focused on three approaches. First, the molecular planarity and symmetry of the biphenyl aglycone was disrupted by modifying the substitution pattern<sup>11</sup> (Fig. 1a). Second, the hydrophobicity was improved by heterocyclic biaryl aglycones (Fig. 1b). Finally, oral availability was improved by replacing the carboxylic acid by the bioisosteric cyano group (Fig. 1c).<sup>8o,11,12</sup>

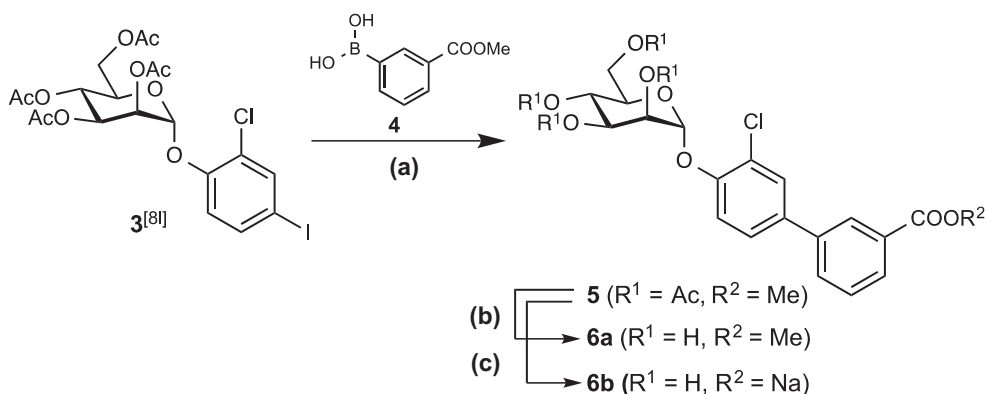
### 2.1 Synthesis of FimH antagonists

**Biphenyl mannosides** (Schemes 1 and 2). Compounds **1a,b**, and **2a,b** (Table 1) were synthesized as previously described.<sup>8h</sup> For the synthesis of **6a** and **6b**, iodide **3**<sup>8l</sup> was reacted with boronic acid **4** in a palladium-catalyzed Suzuki–Miyaura coupling to yield mannoside **5**. Subsequent deprotection afforded the test compounds **6a** and **6b** (Scheme 1).

Lewis acid-promoted glycosylation of phenol **8** with fluoride **7**<sup>13</sup> followed by a Suzuki–Miyaura coupling of bromide **9** with boronic acid **4** gave **10** (Scheme 2). Finally, deprotection yielded biphenyls **11a** and **11b**.



**Fig. 1** Variations of the aglycone of FimH antagonists **1a** and **1b** by (a) modifying the substitution pattern, (b) introducing heteroaryl aglycones and (c) replacing the carboxylate moiety with a bioisosteric cyano group. Ring A is adjacent to the anomeric center, whereas ring B is in the terminal position.

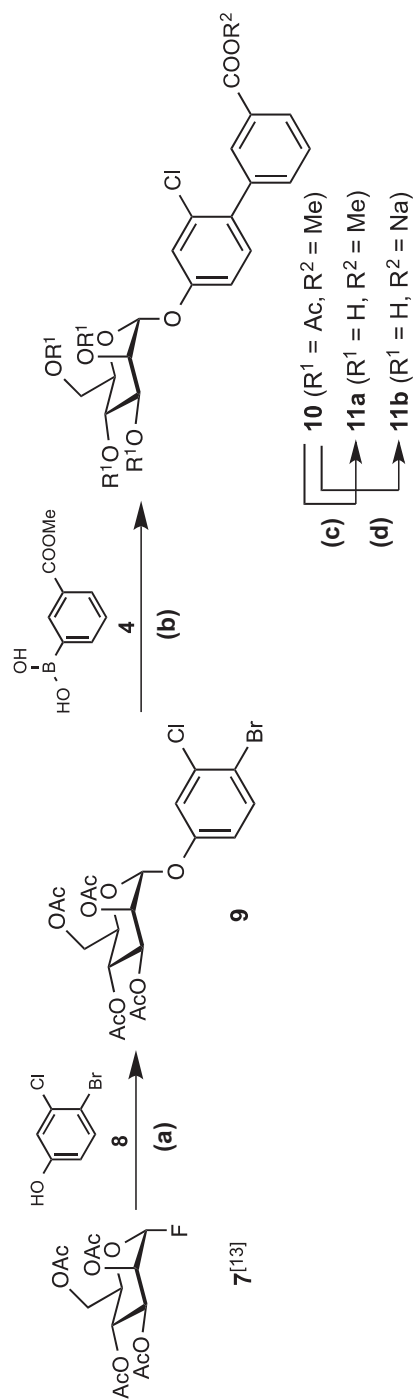


**Scheme 1** (a)  $\text{Pd}(\text{Cl}_2)\text{dppf} \cdot \text{CH}_2\text{Cl}_2$ ,  $\text{K}_3\text{PO}_4$ , DMF, 80 °C, overnight (70%); (b) NaOMe, MeOH, rt, 4 h (quant.); (c) 0.2 N aq. NaOH, MeOH, rt, overnight (50%).

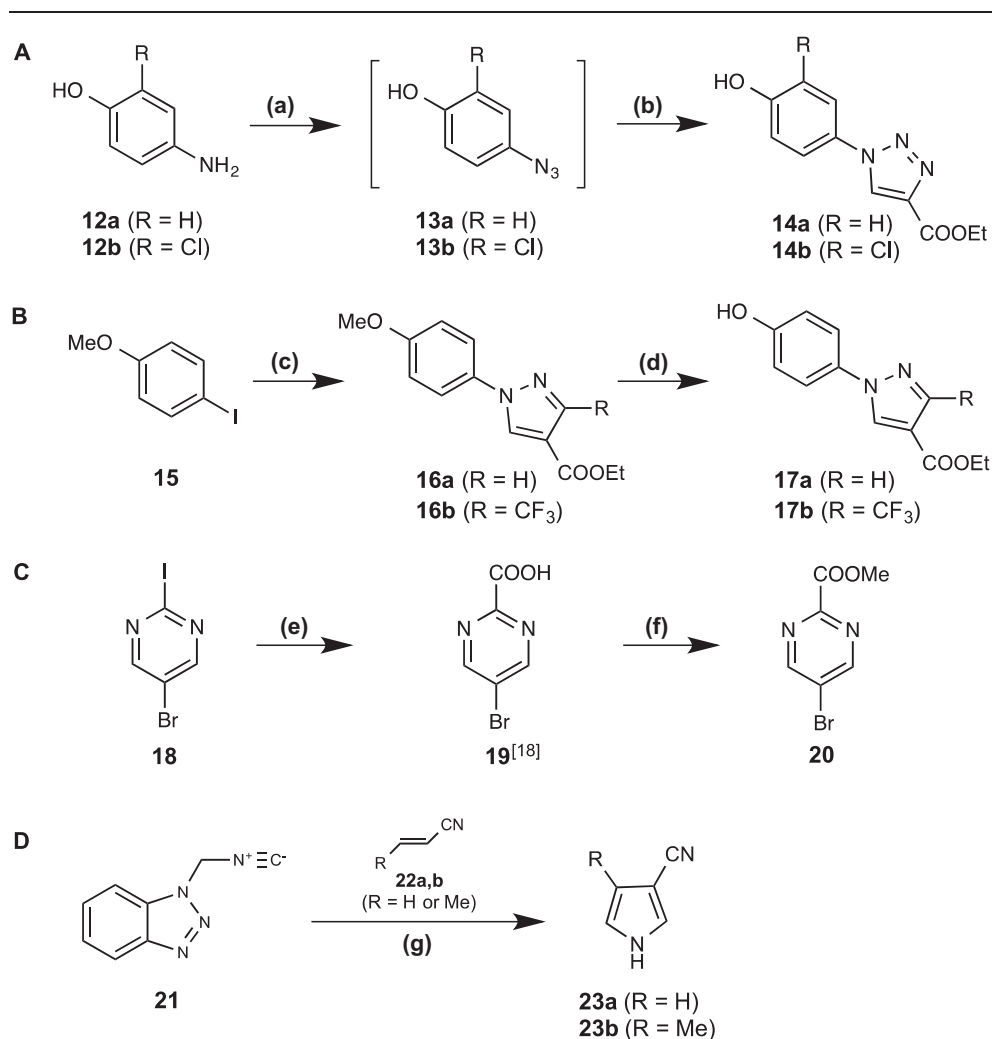
**Heteroaromatic building blocks** (Scheme 3). Starting with the commercial aminophenols **12a,b**, the azidophenols **13a,b** were obtained *via* a diazotransfer reaction using freshly prepared triflyl azide in pyridine and copper(II) sulfate as catalyst.<sup>14</sup> Because of low stability, **13a,b** were used without purification in a subsequent copper(I)-catalyzed Huisgen cycloaddition<sup>15</sup> with ethyl propiolate, yielding the triazolylphenols **14a,b** (Scheme 3A). By using an Ullmann-type copper-diamine-catalyzed *N*-arylation,<sup>16</sup> 1*H*-pyrazole-4-carboxylate was coupled with 4-iodoanisole (**15**) in *N*-methyl-2-pyrrolidone (NMP) to furnish **16a**. Because of the low reactivity of the ethyl 3-trifluoromethyl-1*H*-pyrazole-4-carboxylate, the coupling reaction was carried out under solvent-free conditions to yield **16b** in quantitative yield. Demethylation of **16** with  $\text{AlCl}_3$  gave the pyrazolylphenol derivatives **17**. Due to the instability of **17b** under  $\text{AlCl}_3/n\text{Bu}_4\text{NI}$  conditions, a solution of  $\text{AlCl}_3$  in 1-dodecanethiol was used to accelerate the reaction and to suppress byproduct formation (Scheme 3B).<sup>17</sup> The pyrimidinyl derivative **20** was prepared *via* a *n*BuLi-mediated carboxylation with  $\text{CO}_2$  followed by esterification (Scheme 3C).<sup>18</sup> To synthesize the cyano-substituted pyrroles **23a,b**, benzotriazol-1-ylmethyl isocyanide (**21**) was treated with the electron-deficient alkenes **22a,b** under basic heterocyclization conditions (Scheme 3D).<sup>19</sup>

**Triazolylphenyl and pyrazolylphenyl mannosides** (Scheme 4). Mannosylation of the phenols **14a,b** and **17a,b** (see Scheme 3A & B) with mannosyl fluoride **7**<sup>13</sup> and  $\text{BF}_3 \cdot \text{Et}_2\text{O}$  as promoter, yielded exclusively the  $\alpha$ -mannosides **24a,b** and **27a,b**. Deacetylation ( $\rightarrow$ **25a-c** and **28a,b**) followed by ester hydrolysis gave the test compounds **26a,b** and **29a,b**.

**Pyridinylphenyl, pyrazinylphenyl, and pyrimidinylphenyl mannosides** (Scheme 5). Mannosyl fluoride **7**<sup>13</sup> was treated with 4-iodophenol or 4-bromo-2-trifluoromethylphenol in the presence of  $\text{BF}_3 \cdot \text{Et}_2\text{O}$ . The resulting iodide **30**<sup>8k</sup> and bromide **36**<sup>8k</sup> were transformed into the boronic acid pinacol esters **31**<sup>8k</sup> and **37** under Miyaura-borylation conditions. In a palladium-catalyzed Miyaura–Suzuki coupling<sup>20</sup> of the heteroaryl halides **20** (see Scheme 3C) and **32a-c** (commercially available) with boronic acid ester **31**, heteroarylphenyl mannosides **33a-d** were obtained in good to excellent yields. Similarly, mannoside **38** was prepared by coupling of ester **37** and pyridinylchloride **32a**. Deacetylation under Zemplén



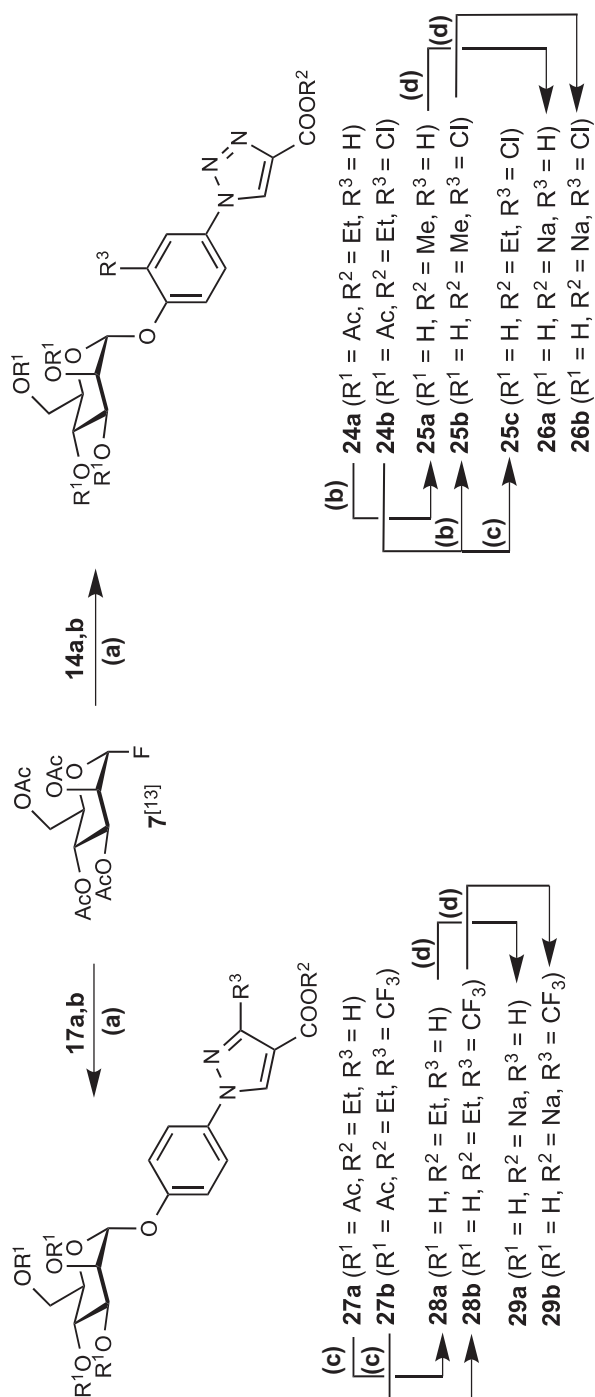
**Scheme 2** (a)  $\text{BF}_3 \cdot \text{Et}_2\text{O}$ , DCM, mol. sieves 4 Å, 0 °C to rt, overnight (90%); (b)  $\text{Pd}(\text{Cl}_2)\text{dppf} \cdot \text{CH}_2\text{Cl}_2$ ,  $\text{K}_3\text{PO}_4$ , DMF, 80 °C, overnight (76%); (c) NaOMe, MeOH, rt, 4 h (quant.); (d) 0.2 N aq. NaOH, MeOH, rt, overnight (61%).



**Scheme 3** (a) TfN<sub>3</sub>, CuSO<sub>4</sub>, triethylamine, pyridine, 0 °C to rt, 2 h; (b) ethyl propiolate, CuSO<sub>4</sub> · 5H<sub>2</sub>O, sodium ascorbate, tBuOH/H<sub>2</sub>O (1 : 1), rt, 30 min (yield for two steps: 77% for **14a**, 48% for **14b**); (c) ethyl 1*H*-pyrazole-4-carboxylate or ethyl 3-trifluoromethyl-1*H*-pyrazole-4-carboxylate, CuI, *trans*-*N,N'*-dimethyl-1,2-cyclohexanediamine, K<sub>2</sub>CO<sub>3</sub>, NMP as solvent for **16a** and solvent free for **16b**, 110 °C, 24 h (80% for **16a**, quant. for **16b**); (d) AlCl<sub>3</sub>, cat. *n*Bu<sub>4</sub>Nl, DCE (for **17a**), or AlCl<sub>3</sub> in 1-dodecanethiol (for **17b**), 0 °C to rt (60% for **17a**, 26% for **17b**); (e) i. *n*BuLi, hexane, toluene, -78 °C, 1 h; ii. CO<sub>2</sub> (g), -78 °C to rt, 7 h; (f) conc. H<sub>2</sub>SO<sub>4</sub> (0.8 equiv.), MeOH, reflux, overnight (37% for two steps); (g) nitrile **22a,b**, tBuOK, THF, 0 °C to reflux, 2 h (60% for **23a**, 54% for **23b**).

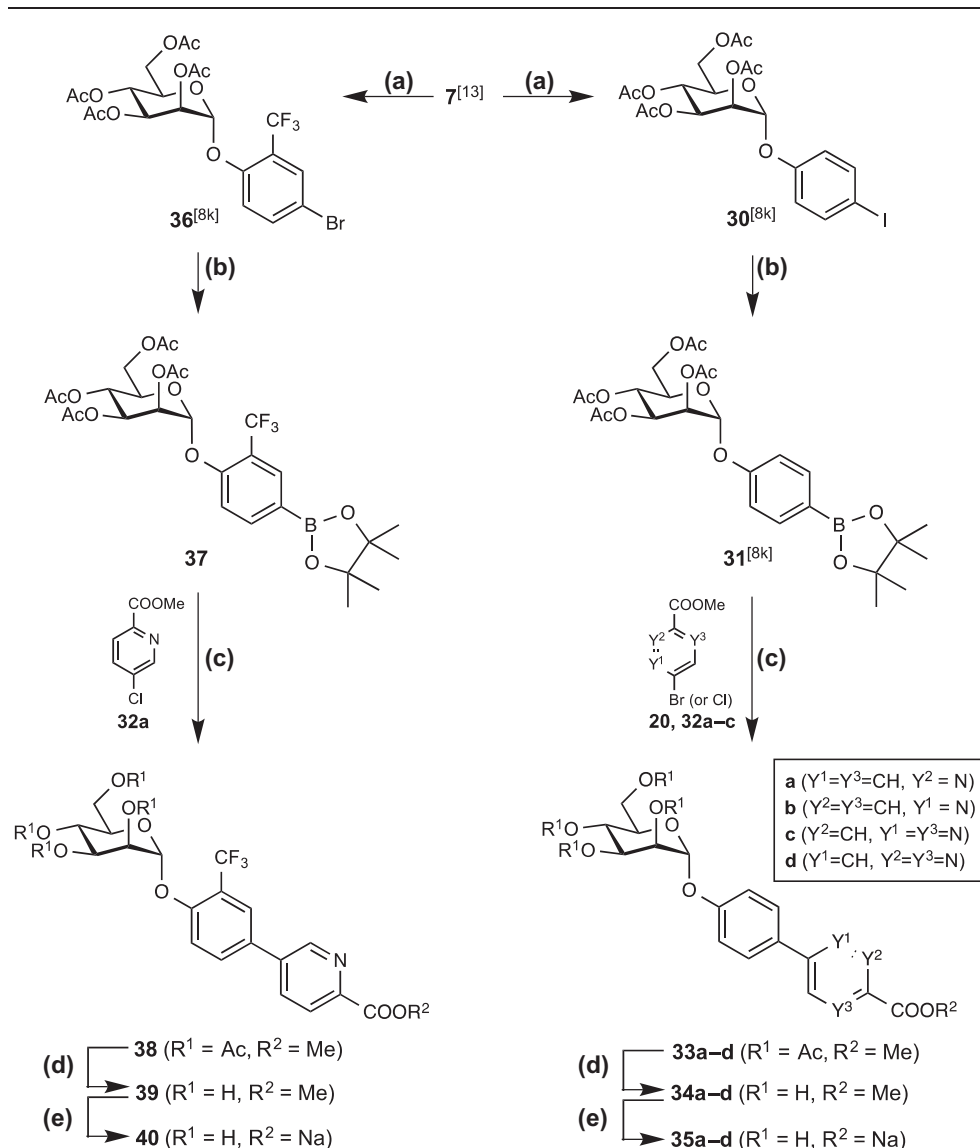
conditions (→ **34a–d**, **39**) followed by saponification of the methyl ester yielded the sodium salts **35a–d** and **40**.

**Pyrrolylphenyl mannosides** (Schemes 6 and 7). In a copper catalyzed *N*-arylation, pyrroles **23a,b** (see Scheme 3D) and **23c–f** (commercial) were coupled with mannoside **3**<sup>8l</sup> (*ortho*-Cl) to yield the pyrrolylphenyl mannosides **41a–f** (Scheme 6).<sup>17</sup> Under similar conditions, mannosides **30** (without *ortho*-substituent) and **36** (*ortho*-CF<sub>3</sub>) were coupled with pyrrole **23f** to yield **47** and **48** (Scheme 7). Because of partial deacetylation of the sugar moiety during *N*-arylation, the crude products were reacylated to facilitate purification. Deacetylation of the mannose moiety (→ **42a–f**, **49** and **50**) followed by saponification of the alkyl esters gave the test compounds **43–46**, **51** and **52**.



**Scheme 4** (a) BF<sub>3</sub>·Et<sub>2</sub>O, DCM, mol. sieves 4 Å, 0 °C to rt, overnight (79% for 24a, 76% for 24b, 98% for 27a, 64% for 27b); (b) NaOMe, MeOH, rt, 4 h (74% for 25a, 80% for 25b); (c) NaOEt, EtOH, rt, overnight (74% for 28a, 82% for 28b); (d) 0.2 N aq. NaOH, MeOH, rt, overnight (30% for 26a, 90% for 26b, 70% for 29a, 79% for 29b).

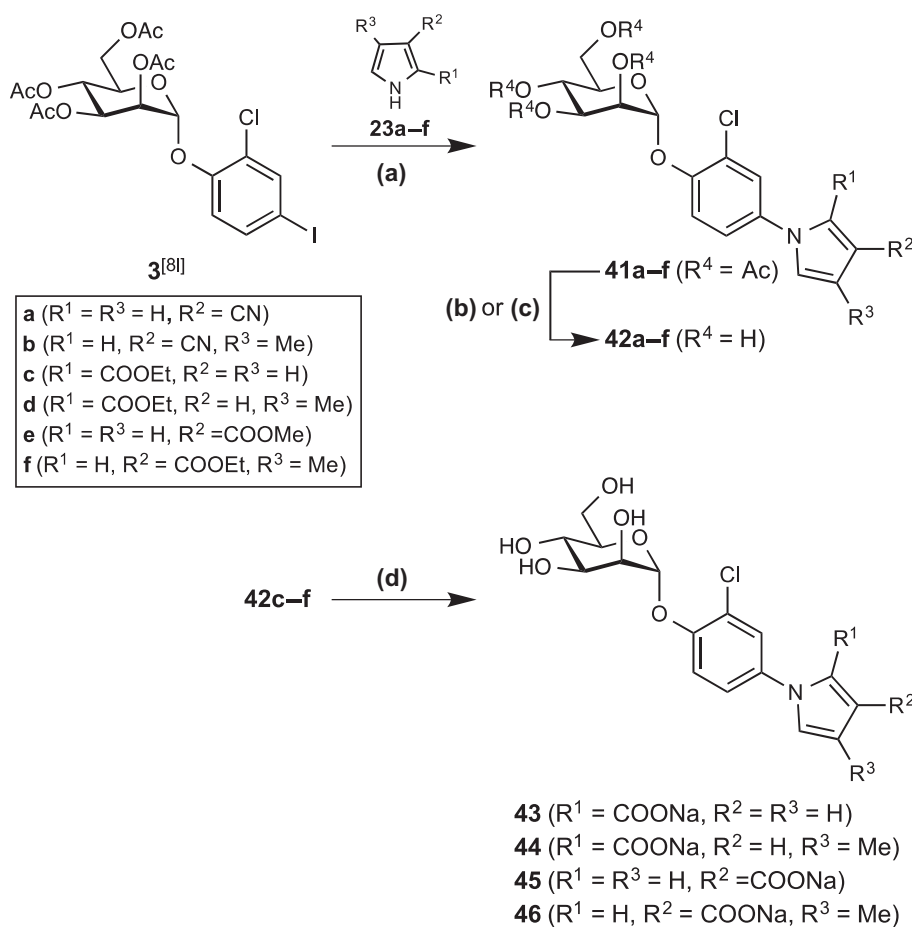




**Scheme 5** (a) 4-Iodophenol or 4-bromo-2-trifluoromethylphenol,  $BF_3 \cdot Et_2O$ , DCM, mol. sieves 4 Å, 0 °C to rt, overnight (70%<sup>Bk</sup> for **30**, 80%<sup>Bk</sup> for **36**); (b) bis(pinacolato)diborone,  $Pd(Cl_2)dppf \cdot CH_2Cl_2$ , KOAc, DMF, 85 °C, overnight (80% for **31**, 83% for **37**); (c)  $Pd(Cl_2)dppf \cdot CH_2Cl_2$ ,  $K_3PO_4$ , DMF, 85 °C, overnight (60% for **33a**, 80% for **33b**, 68% for **33c**, 40% for **33d**, 57% for **38**); (d) NaOMe, MeOH, rt, 4 h (36% for **34a**, 24% for **34b**, 36% for **34c**, 89% for **34d**, 60% for **39**); (e) 0.2 N aq. NaOH, MeOH, rt, overnight (32% for **35a**, 48% for **35b**, 44% for **35c**, 60% for **35d**, 90% for **40**).

## 2.2 Physicochemical properties and *in vitro* pharmacokinetics of FimH antagonists

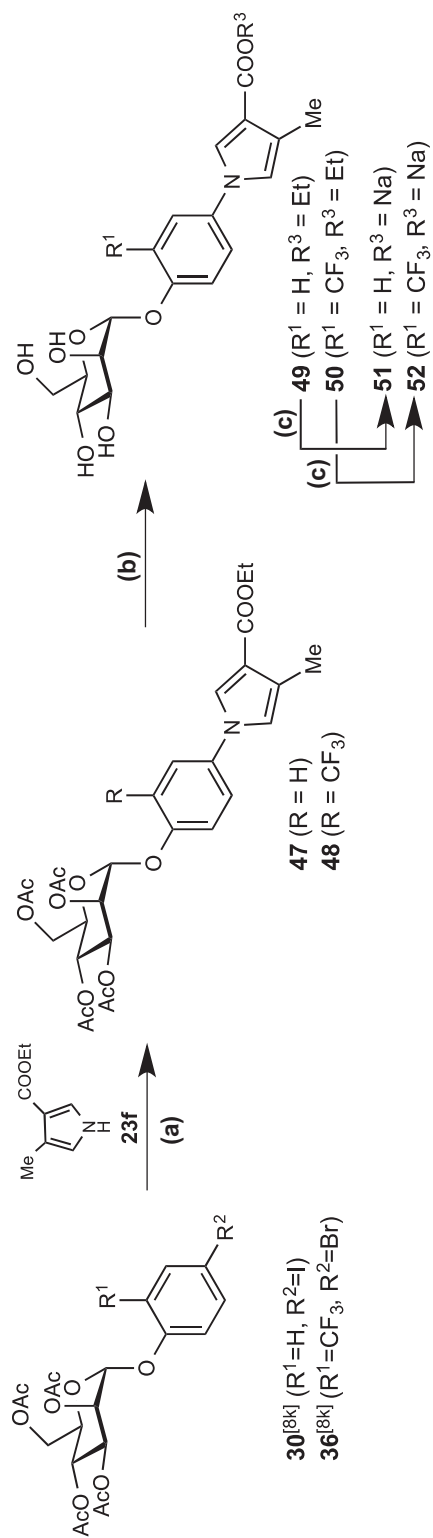
For the assessment of the potential for intestinal absorption, physicochemical properties, *i.e.* lipophilicity ( $\log D_{7.4}$ ), aqueous solubility, and permeability through an artificial membrane (PAMPA,  $\log P_e$ ) as well as a Caco-2 cell monolayer ( $P_{app}$ ) were determined (Table 1).<sup>21-24</sup> The following permeability thresholds for the effective permeability  $\log P_e$  (low permeability is expected for  $\log P_e < -6.3$   $cm\ s^{-1}$ ; moderate  $\leq -5.7$   $cm\ s^{-1}$ ; high  $> -5.7$   $cm\ s^{-1}$ )<sup>25</sup> and for apparent permeability  $P_{app}$  (low permeability is expected for  $P_{app} < 2 \times 10^{-6}$   $cm\ s^{-1}$ ; moderate  $\leq 20 \times 10^{-6}$   $cm\ s^{-1}$ ;



**Scheme 6** (a) i. CuI, ( $\pm$ )-*trans*-1,2-diaminocyclohexane,  $\text{K}_3\text{PO}_4$ , 1,4-dioxane,  $110^\circ\text{C}$ , overnight; ii.  $\text{Ac}_2\text{O}$ , DMAP, pyridine, rt, overnight (44% for **41a**, 92% for **41b**, 33% for **41c**, 64% for **41d**, 99% for **41e**, 77% for **41f**); (b) NaOMe, MeOH, rt, 4 h (65% for **42a**, 38% for **42b**, 83% for **42e**); (c) NaOEt, EtOH, rt, overnight (91% for **42c**, 61% for **42d**, 93% for **42f**); (d) NaOH, MeOH/ $\text{H}_2\text{O}$  (1 : 2), rt, 12–48 h (58% for **43**, 40% for **44**, 20% for **45**, 57% for **46**).

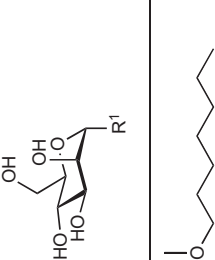
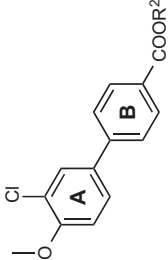
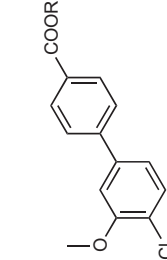
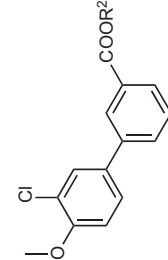
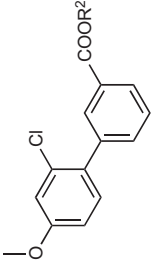


high  $> 20 \times 10^{-6} \text{ cm s}^{-1}$ )<sup>26</sup> were used to classify the antagonists. As expected, all metabolites, *i.e.* the free carboxylates showed no or low permeability ( $\log P_e < -6.3 \text{ cm s}^{-1}$ ) and are not further discussed in this section. Furthermore, the esters were incubated with rat liver microsomes (RLM) for estimating their susceptibility to carboxylesterase (CES)-mediated hydrolysis.<sup>27</sup> Table 1 indicates the metabolic half lives ( $t_{1/2}$ ) as determinants of the rate of bioconversion to the respective acid.

**Solubility of biphenyl mannosides.** As observed in our previous study,<sup>8h</sup> the biphenyl derivatives **1a** and **2a** (Table 1, entries 2 & 4) showed low aqueous solubility ( $\leq 24 \mu\text{g mL}^{-1}$ , Table 1), probably due to the symmetrical *para*-substitution leading to stacking effects. In order to disrupt this symmetry, the carboxylic acid moiety in **1a** was moved from the *para*- to the *meta*-position ( $\rightarrow$  **6a**, entry 6). Since the dihedral angle remained unaffected (Fig. 2; global minima values calculated with MacroModel, version 9.9<sup>30</sup>) only moderately improved aqueous solubility ( $41 \mu\text{g mL}^{-1}$ , Table 1) resulted. However, when the chloro substituent on ring A was shifted from the *ortho*- to the *meta*-position ( $\rightarrow$  **11a**, entry 8), the dihedral angle was enlarged from  $39.6^\circ$  in **6a** to  $60.3^\circ$  in **11a** (Fig. 2). The resulting



**Scheme 7** (a) i. CuI, ( $\pm$ )-*trans*-1,2-diaminocyclohexane,  $K_3PO_4$ , 1,4-dioxane,  $110^\circ C$ , overnight; ii.  $Ac_2O$ , DMAP, pyridine, rt, overnight (94% for **47**, 49% for **48**); (b) NaOEt, EtOH, rt, overnight (46% for **49**, 85% for **50**); (c) NaOH, MeOH/H<sub>2</sub>O (1:2), rt, 48 h (99% for **51**, 35% for **52**).

**Table 1** Physicochemical ( $\log D_{7.4}$ , solubility, PAMPA, and Caco-2), *in vitro* pharmacokinetic (microsomal stability) and pharmacodynamics ( $IC_{50}$ ) parameters of FimH antagonists; ring A is adjacent to the anomeric center, whereas ring B is in the terminal position.

Entry	Compound	Binding Assay <sup>a</sup>		$\log D_{7.4}^b$	Solubility <sup>c</sup> [ $\mu\text{g mL}^{-1}$ ]	PAMPA $\log P_e^d$ [ $\text{cm s}^{-1}$ ]	Caco-2 $P_{\text{app}}^e$ [ $10^{-6} \text{ cm s}^{-1}$ ]		Microsomal stability $t_{1/2}^f$ [min]
		$IC_{50}$ [nM]	$rIC_{50}$				a→b	b→a	
1	<b>53</b> <sup>8d</sup> 	54.9	1	1.7	>3000 <sup>g</sup>	-4.9	7.0 ± 0.6	9.4 ± 0.2	n.d. <sup>h</sup>
2	<b>1a</b> <sup>8h</sup> ( $R^2 = \text{Me}$ ) <b>1b</b> <sup>8h</sup> ( $R^2 = \text{Na}$ ) 	4.8	0.09	2.3	11.9 <sup>g</sup>	-4.6	5.3 ± 0.6	17.5 ± 1.3	2.1
3	<b>1b</b> <sup>8h</sup> ( $R^2 = \text{Na}$ ) 	6.7	0.12	-0.8	>3000 <sup>g</sup>	-10.0 ± 0.0	0.23 ± 0.03	0.38 ± 0.04	n.d. <sup>h</sup>
4	<b>2a</b> <sup>8h</sup> ( $R^2 = \text{Me}$ ) <b>2b</b> <sup>8h</sup> ( $R^2 = \text{Na}$ ) 	11.8	0.21	1.7 ± 0.1	24.3 <sup>g</sup>	-4.7	6.1 ± 1.2	21.1 ± 1.2	22
5	<b>2b</b> <sup>8h</sup> ( $R^2 = \text{Na}$ ) 	29	0.53	<-1.5	>3000 <sup>g</sup>	-10.0 ± 0.0	1.2 ± 0.4	1.2 ± 0.1	n.d. <sup>h</sup>
6	<b>6a</b> ( $R^2 = \text{Me}$ ) <b>6b</b> ( $R^2 = \text{Na}$ ) 	16.8	0.31	2.7 ± 0.1	41 ± 3	-4.6 ± 0.2	6.7 ± 0.4	20.7 ± 2.5	72
7	<b>6b</b> ( $R^2 = \text{Na}$ ) 	12	0.22	n.d. <sup>h</sup>	n.d. <sup>h</sup>	n.d. <sup>h</sup>	n.d. <sup>h</sup>	n.d. <sup>h</sup>	n.d. <sup>h</sup>
8	<b>11a</b> ( $R^2 = \text{Me}$ ) <b>11b</b> ( $R^2 = \text{Na}$ ) 	23.3	0.42	2.7 ± 0.1	134 ± 6	-4.5 ± 0.1	4.5 ± 0.3	10.8 ± 0.7	13
9	<b>11b</b> ( $R^2 = \text{Na}$ ) 	53	0.97	n.d. <sup>h</sup>	n.d. <sup>h</sup>	n.d. <sup>h</sup>	n.d. <sup>h</sup>	n.d. <sup>h</sup>	n.d. <sup>h</sup>

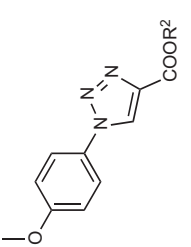
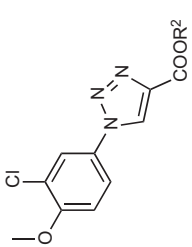
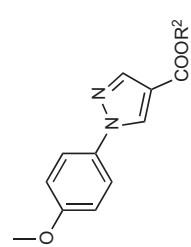
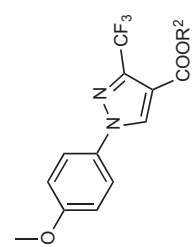
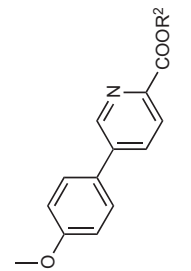
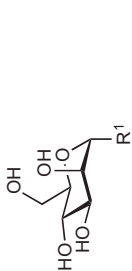
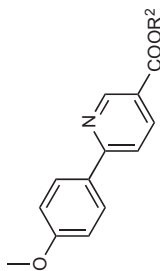
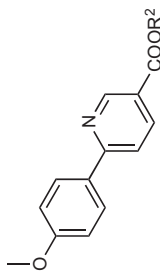
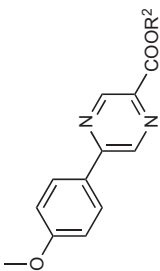
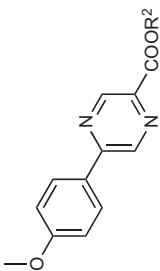
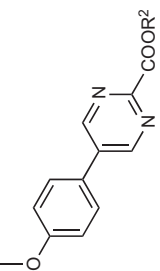
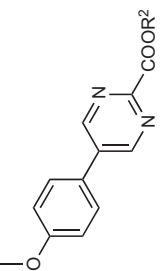
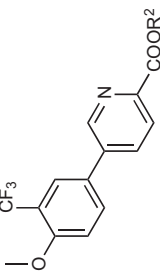
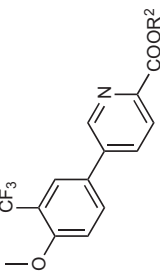
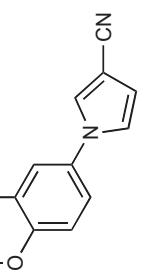
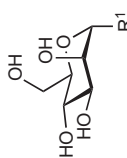
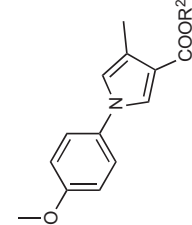
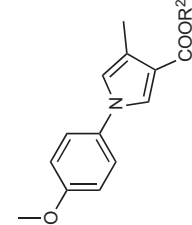
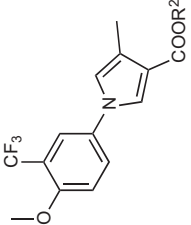
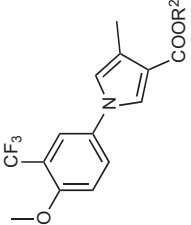
10	25a (R <sup>2</sup> = Me)		7.6	0.14	-0.6 ± 0.0	>180	-9.4 ± 0.3	n.d. <sup>h</sup>	n.d. <sup>h</sup>	38
11	26a (R <sup>2</sup> = Na)		16	0.29	n.d. <sup>h</sup>	>180	-10.0 ± 0.0	n.d. <sup>h</sup>	n.d. <sup>h</sup>	n.d. <sup>h</sup>
12	25b (R <sup>2</sup> = Me)		10.5	0.19	0.0 ± 0.0	>150	-9.1 ± 1.8	n.d. <sup>h</sup>	n.d. <sup>h</sup>	32
13	25c (R <sup>2</sup> = Et)		n.d. <sup>h</sup>	—	0.7 ± 0.0	>150	-10	n.d. <sup>h</sup>	n.d. <sup>h</sup>	42
14	26b (R <sup>2</sup> = Na)		21	0.38	< -1.5	>150	-6.7 ± 0.1	n.d. <sup>h</sup>	n.d. <sup>h</sup>	n.d. <sup>h</sup>
15	28a (R <sup>2</sup> = Et)		32.4	0.59	0.9 ± 0.0	>180	-6.6 ± 0.1	n.d. <sup>h</sup>	n.d. <sup>h</sup>	>120
16	29a (R <sup>2</sup> = Na)		111	2.02	n.d. <sup>h</sup>	>180	-10.0 ± 0.0	n.d. <sup>h</sup>	n.d. <sup>h</sup>	n.d. <sup>h</sup>
17	28b (R <sup>2</sup> = Et)		31.9	0.58	2.1 ± 0.0	>180	-5.7 ± 0.1	1.3 ± 0.1	12.4 ± 2.4	113
18	29b (R <sup>2</sup> = Na)		112	2.04	< -1.5	>180	-10.0 ± 0.0	n.d. <sup>h</sup>	n.d. <sup>h</sup>	n.d. <sup>h</sup>
19	34a (R <sup>2</sup> = Me)		n.d. <sup>h</sup>	—	0.2 ± 0.0	>130	-7.5 ± 0.2	0.22 ± 0.05	2.3 ± 0.1	10
20	35a (R <sup>2</sup> = Na)		16	0.29	n.d. <sup>h</sup>	>180	-8.6 ± 1.6	n.d. <sup>h</sup>	n.d. <sup>h</sup>	n.d. <sup>h</sup>

Table 1 (Continued)

Entry	Compound		Binding Assay <sup>a</sup>		logD <sub>7.4</sub> <sup>b</sup>	Solubility <sup>c</sup> [μg mL <sup>-1</sup> ]	PAMPA logP <sub>e</sub> <sup>d</sup> [cm s <sup>-1</sup> ]	Caco-2 P <sub>app</sub> <sup>e</sup> [10 <sup>-6</sup> cm s <sup>-1</sup> ]		Microsomal stability t <sub>1/2</sub> <sup>f</sup> [min]
			IC <sub>50</sub> [nM]	rC <sub>50</sub>				a→b	b→a	
21	34b (R <sup>2</sup> = Me)		28.6	0.52	1.0 ± 0.0	59 ± 6	-6.3 ± 0.0	0.64 ± 0.06	8.3 ± 0.4	11
22	35b (R <sup>2</sup> = Na)		46	0.84	< -1.5	> 180	-8.5 ± 1.8	n.d. <sup>h</sup>	n.d. <sup>h</sup>	n.d. <sup>h</sup>
23	34c (R <sup>2</sup> = Me)		33.1	0.60	0.1 ± 0.1	> 150	-7.6 ± 0.0	0.24 ± 0.01	1.8 ± 0.2	11
24	35c (R <sup>2</sup> = Na)		39	0.71	< -1.5	> 180	-8.6 ± 1.6	n.d. <sup>h</sup>	n.d. <sup>h</sup>	n.d. <sup>h</sup>
25	34d (R <sup>2</sup> = Me)		10.2	0.19	< -1.0	95 ± 6	-8.5 ± 0.1	0.16 ± 0.03	0.22 ± 0.05	24
26	35d (R <sup>2</sup> = Na)		35	0.64	n.d. <sup>h</sup>	n.d. <sup>h</sup>	-7.6 ± 1.6	n.d. <sup>h</sup>	n.d. <sup>h</sup>	n.d. <sup>h</sup>
27	39 (R <sup>2</sup> = Me)		9.3	0.17	1.3 ± 0.1	> 180	-8.6 ± 1.7	0.33 ± 0.04	7.2 ± 0.7	8.2
28	40 (R <sup>2</sup> = Na)		20	0.36	< -1.5	> 180	-9.3 ± 1.4	n.d. <sup>h</sup>	n.d. <sup>h</sup>	n.d. <sup>h</sup>
29	42a		29	0.53	1.5 ± 0.1	> 180	-8.8 ± 2.0	n.d. <sup>h</sup>	n.d. <sup>h</sup>	n.d. <sup>h</sup>

30	42b		25	0.46	2.0 ± 0.1	69 ± 20	-6.3 ± 0.1	n.d. <sup>h</sup>	n.d. <sup>h</sup>	n.d. <sup>h</sup>
31	42c (R <sup>2</sup> = Et)		60.7	1.11	2.0 ± 0.0	>180	-5.2 ± 0.0	n.d. <sup>h</sup>	n.d. <sup>h</sup>	>120
32	43 (R <sup>2</sup> = Na)		75	1.37	< -1.5	>180	-10.0 ± 0.0	n.d. <sup>h</sup>	n.d. <sup>h</sup>	n.d. <sup>h</sup>
33	42d (R <sup>2</sup> = Et)		42.3	0.77	2.7 ± 0.0	34 ± 4	-4.8 ± 0.1	5.0 ± 0.2	35.6 ± 1.0	84
34	44 (R <sup>2</sup> = Na)		23	0.42	0.7 ± 0.1	>180	-9.2 ± 1.7	n.d. <sup>h</sup>	n.d. <sup>h</sup>	n.d. <sup>h</sup>
35	42e (R <sup>2</sup> = Me)		18.5	0.34	2.1 ± 0.2	>180	-6.0 ± 0.1	n.d. <sup>h</sup>	n.d. <sup>h</sup>	>120
36	45 (R <sup>2</sup> = Na)		25	0.46	< -1.5	>180	-10.0 ± 0.0	n.d. <sup>h</sup>	n.d. <sup>h</sup>	n.d. <sup>h</sup>
37	42f (R <sup>2</sup> = Et)		15.2	0.28	2.8 ± 0.1	>180	-4.8 ± 0.1	6.4 ± 0.7	30.0 ± 2.9	>120
38	46 (R <sup>2</sup> = Na)		25	0.46	-0.5 ± 0.1	>180	-10.0 ± 0.0	n.d. <sup>h</sup>	n.d. <sup>h</sup>	n.d. <sup>h</sup>

Table 1 (Continued)

Entry	Compound		Binding Assay <sup>a</sup>		log <i>D</i> <sub>7.4</sub> <sup>b</sup>	Solubility <sup>c</sup> [μg mL <sup>-1</sup> ]	PAMPA log <i>P</i> <sub>e</sub> <sup>d</sup> [cm s <sup>-1</sup> ]	Caco-2		Microsomal stability <i>t</i> <sub>1/2</sub> <sup>f</sup> [min]
			IC <sub>50</sub> [nM]	rIC <sub>50</sub>				<i>P</i> <sub>app</sub> <sup>e</sup> [10 <sup>-6</sup> cm s <sup>-1</sup> ]	a→b	
39	49 (R <sup>2</sup> = Et)		64.8	1.18	2.3 ± 0.0	>180	-5.1 ± 0.1	1.5 ± 0.5	17.2 ± 0.6	>120
40	51 (R <sup>2</sup> = Na)		65	1.18	-1.0 ± 0.1	>180	-8.4 ± 1.8	n.d. <sup>h</sup>	n.d. <sup>h</sup>	n.d. <sup>h</sup>
41	50 (R <sup>2</sup> = Et)		36.9	0.67	3.0 ± 0.1	135 ± 6	-5.0 ± 0.2	5.0 ± 0.3	26.1 ± 1.5	>120
42	52 (R <sup>2</sup> = Na)		19	0.35	0.1 ± 0.2	>180	-8.6 ± 1.7	n.d. <sup>h</sup>	n.d. <sup>h</sup>	n.d. <sup>h</sup>

<sup>a</sup>The IC<sub>50</sub> values were determined with a cell-free competitive binding assay.<sup>28</sup> The rIC<sub>50</sub> values were calculated by dividing the IC<sub>50</sub> of the compound of interest by the IC<sub>50</sub> of reference compound 53. This leads to rIC<sub>50</sub> values below 1.0 for derivatives with higher affinity than reference 53 and rIC<sub>50</sub> above 1.0 for compounds with lower affinity than 53.

<sup>b</sup>Octanol-water distribution coefficients at pH 7.4 (log*D*<sub>7.4</sub>) were determined by a miniaturized shake flask procedure. The values are indicated as mean ± SD of sextuplicate determinations.<sup>21</sup>

<sup>c</sup>Kinetic solubility was measured in a 96-well format in triplicate at pH 7.4 using the μSOL Explorer solubility analyzer.<sup>22</sup>

<sup>d</sup>Permeation through an artificial membrane (log*P*<sub>e</sub>, effective permeability) was determined by PAMPA (parallel artificial membrane permeability assay) in quadruplicate at pH 7.4.<sup>23,25</sup>

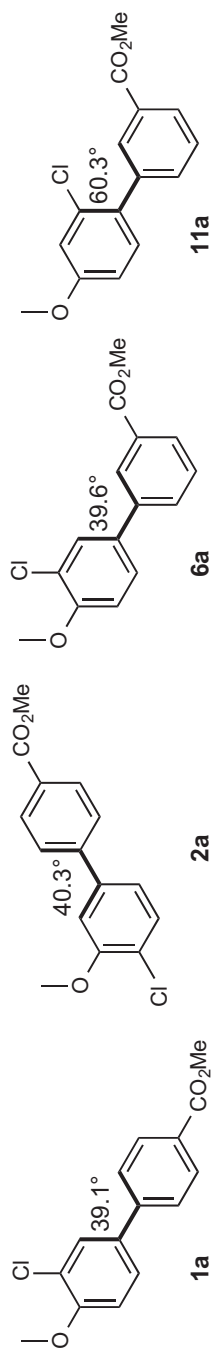
<sup>e</sup>Permeation through a Caco-2 cell monolayer (*P*<sub>app</sub>, apparent permeability) was assessed in the absorptive (a→b) and secretory (b→a) directions in triplicate.<sup>24,29</sup>

<sup>f</sup>Microsomal stability was determined in duplicate with pooled male rat liver microsomes (RLM, 0.125 mg mL<sup>-1</sup>) at pH 7.4 and 37 °C.<sup>27</sup>

<sup>g</sup>Thermodynamic solubility obtained according to the procedure described in ref. 8*h*.

<sup>h</sup>n.d., not determined.





**Fig. 2** Dihedral angles between the aromatic rings of biaryl aglycones of biaryl  $\alpha$ -D-mannopyranosides (**1a**, **2a**, **6a**, and **11a**). The global minima values were calculated with MacroModel (version 9.9).<sup>30</sup>

disruption of the molecular planarity enhanced aqueous solubility up to 3-fold (from 41 to 134  $\mu\text{g mL}^{-1}$ ).

**Permeability of biphenyl mannosides.** Due to their high lipophilicity ( $\log D_{7.4} \geq 1.7$ ), all biphenyl mannosides showed high effective ( $\log P_e > -5.7 \text{ cm s}^{-1}$ ) and moderate apparent ( $P_{\text{app}} > 2 \times 10^{-6} \text{ cm s}^{-1}$ ) permeability.

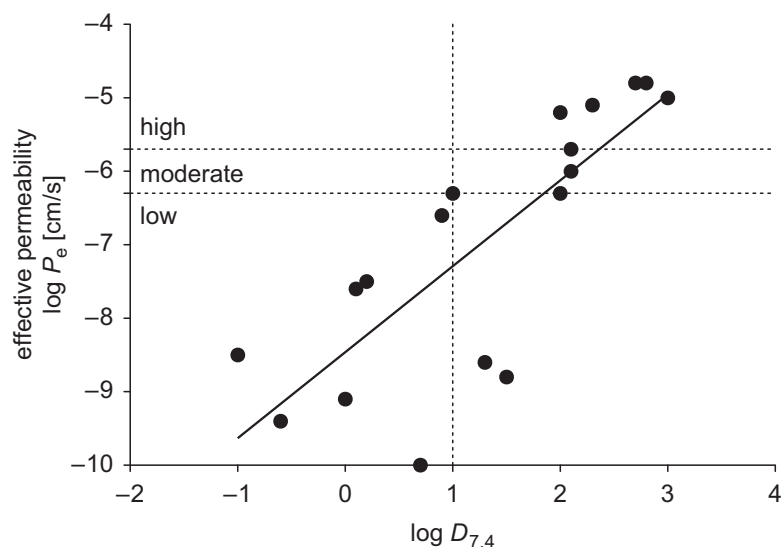
**Metabolic stability of biphenyl mannosides.** Incubation with rat liver microsomes (RLM) induced a fast degradation of prodrug **1a** ( $t_{1/2}$  2.1 min, Table 1, entry 2). The esters of the biphenyl mannosides **2a** ( $t_{1/2}$  22 min, entry 4), **6a** ( $t_{1/2}$  72 min, entry 6), and **11a** ( $t_{1/2}$  13 min, entry 8) were less susceptible to the carboxylesterase (CES)-mediated metabolic turnover. The differing rates of hydrolysis may result from the change in the molecular geometry and therefore in the accessibility of the ester by the serine hydrolase CES.<sup>31</sup> We therefore attributed the rate differences of the CES-mediated hydrolysis primarily to the differing geometry of the aglycones, which, in case of **1a**, obviously orients the ester bond within the active site in an optimal position.

Overall, despite elevated solubility (134  $\mu\text{g mL}^{-1}$ ) and high effective permeability ( $\log P_e -4.5 \text{ cm s}^{-1}$ ) of ester **11a**, fast metabolic ester hydrolysis ( $t_{1/2} < 15 \text{ min}$ ) reduces its therapeutic potential. Especially, the accelerated renal excretion of the polar metabolite (*i.e.* free carboxylate) impedes the maintenance of the therapeutic concentration in the bladder over an extended period of time.

**Solubility of heteroaryl mannosides.** In general, heterobiaryl mannosides (Table 1, entries 10–42) exhibited markedly higher aqueous solubility than the reference compound biphenyl  $\alpha$ -D-mannoside **1a** (12  $\mu\text{g mL}^{-1}$ ). Triazole ( $\rightarrow$ **25a–c**, entries 10, 12 & 13), pyrazole ( $\rightarrow$ **28a**, entry 15), and pyridine derivatives ( $\rightarrow$ **34a–d**, entries 19, 21, 23 & 25) exhibit higher solubility, due to increased polarity ( $\log D_{7.4} < 1$ ). For the pyrazolylphenyl ( $\rightarrow$ **28b**, entry 17), the pyridinylphenyl ( $\rightarrow$ **39**, entry 27), and the pyrrolylphenyl mannosides (entries 29–42) high solubility was determined despite high lipophilicity ( $\log D_{7.4} > 1$ ). As a trade-off, **42d** (entry 33) became the least soluble representative among all assessed heteroaryl mannosides (34  $\mu\text{g mL}^{-1}$ ).

**Permeability of heteroaryl mannosides.** As expected, the increase in polarity and solubility (*e.g.*  $\rightarrow$ **25a**,  $\log D_{7.4} -0.6$ , entry 10) leads to a reduced permeability ( $\log P_e -9.4 \text{ cm s}^{-1}$ ), *i.e.* poor oral absorption. Figure 3 illustrates the correlation between lipophilicity ( $\log D_{7.4}$ ) and the effective permeability ( $\log P_e$ ) of the heteroaryl mannoside esters and bioisosteres (entries 10–42). In general, heteroaryl mannosides with lipophilicity  $\log D_{7.4} > 1$  have moderate to high effective permeability.

To enhance lipophilicity two strategies were explored: First, an *ortho*-chloro substituent was introduced to ring A of the biaryl aglycone of **25a** ( $\rightarrow$ **25b**, entry 12) and, second, the methyl ester was replaced by an ethyl ester ( $\rightarrow$ **25c**, entry 13). However, both strategies did not or only marginally influence the  $\log P_e$  values and therewith the oral absorption potential. For the pyrazolylphenyl derivative **28a** (entry 15), although slightly more lipophilic than the triazolylphenyl **25c** (entry 13), low effective permeability ( $\log P_e -6.6 \text{ cm s}^{-1}$ ) was observed. By introducing a



**Fig. 3** Plot of  $\log D_{7.4}$  versus effective permeability  $\log P_e$  ( $\text{cm s}^{-1}$ ; pH 7.4) for heteroaryl mannoside esters (entries 10–28, 31–42) and bioisosteres (entries 29 & 30). Data represent the mean only (Goodness of fit, R square = 0.64). Dashed lines on the y-axis indicate the thresholds between low, moderate, and high effective permeability (low  $< -6.3 \text{ cm s}^{-1}$ , moderate  $\log P_e \leq -5.7 \text{ cm s}^{-1}$  < high).<sup>25</sup> Dashed line on the x-axis represent the thresholds for lipophilicity ( $\log D_{7.4} > 1$ ), where moderate effective permeability is reached.

trifluoromethyl substituent on the pyrazole moiety ( $\rightarrow$  **28b**, entry 17), both lipophilicity (permeability) and solubility were improved, presumably sufficient for a successful intestinal uptake. Whereas introducing an *ortho*-trifluoromethyl substituent to ring A of the biaryl aglycone ( $\rightarrow$  **39**, entry 27) exhibited despite increased lipophilicity only low effective permeability ( $\log P_e -8.6 \text{ cm s}^{-1}$ ). By contrast, the pyrrolylphenyl mannosides **42a–f**, **49** and **50** (Table 1) with  $\log D$  values of 1.5 to 3 and the  $\log P_e$  values of  $-6.3$  to  $-4.8 \text{ cm s}^{-1}$  suggest modest to high permeability. Starting from antagonist **42c** (entry 31), the introduction of a 4-methyl substituent ( $\rightarrow$  **42d**, entry 33) increased permeability, however, limited solubility to  $34 \mu\text{g mL}^{-1}$ . In the case of the pyrrolylphenyl derivative **42e** (entry 35), both solubility and permeability could be successively enhanced by introducing a methyl substituent in the 4-position of the pyrrole moiety ( $\rightarrow$  **49**, entry 39) and by modifying the *ortho*-substituent on ring A of the biaryl aglycone ( $\rightarrow$  **50**, entry 41 & **42f**, entry 37). Especially, for the antagonists **42f** and **50**, the effective permeability (PAMPA,  $\log P_e -4.8 \text{ cm s}^{-1}$  and  $-5.0 \text{ cm s}^{-1}$ , respectively) suggests a high oral absorption potential. Moreover, the absorptive flux (apical  $\rightarrow$  basal) through the Caco-2 cell monolayer was moderate ( $\log P_{\text{app}} > 2 \times 10^{-6} \text{ cm s}^{-1}$ ). Although the ratio  $P_{\text{app},b \rightarrow a}/P_{\text{app},a \rightarrow b} > 2$  implies efflux-carrier activity,<sup>29</sup> we expected high systemic *in vivo* availability of **42f** and **50**, notably because efflux transporters at human intestines are considered to be easily saturable when compounds are administered at elevated doses (*e.g.*  $> 100 \text{ mg}$ ).<sup>32</sup> As expected, the bioisosteric replacement of the carboxylic moiety by a cyano group ( $\rightarrow$  **42a,b**, entries 29 & 30) increased lipophilicity, but the PAMPA data still indicate

low permeability for both derivatives ( $\log P_e -8.8 \text{ cm s}^{-1}$  and  $-6.3 \text{ cm s}^{-1}$ , respectively).

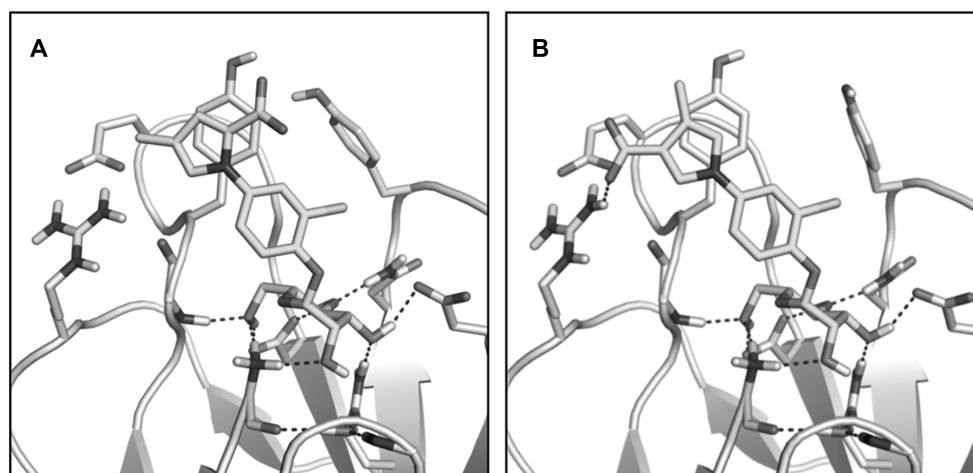
**Metabolic stability of heteroaryl mannosides.** All five-membered heteroaryl derivatives with ester functions (triazoles  $\rightarrow$  entries 10–14, pyrazoles  $\rightarrow$  entries 15–18, and pyrroles  $\rightarrow$  entries 29–42, Table 1) were found to be less susceptible to CES-mediated bioconversion ( $t_{1/2} > 30 \text{ min}$ ) than the parent biphenyl mannoside **1a**. Surprisingly, the pyrrolylphenyl esters **42e,f**, **49**, and **50** even proved to be metabolically stable and were only slowly hydrolyzed by carboxylesterases ( $t_{1/2} > 120 \text{ min}$ ). In contrast, derivatives with six-membered heterocyclic moieties (entries 19–28) were cleaved extremely fast ( $t_{1/2} < 15 \text{ min}$ ) with rates comparable to biphenyl mannoside **1a**.

### 2.3 *In vitro* binding affinities

Binding affinities were determined in a cell-free competitive binding assay (Table 1).<sup>28</sup> Surprisingly, affinities of the esters (biphenyls and heteroaryl mannosides) were slightly improved compared to the corresponding acids, probably due to reduced desolvation costs.

**Biphenyl mannosides.** A comparison of antagonist **1b** (entry 3) with its regioisomers **2b**, **6b**, and **11b** (entries 5, 7 & 9) indicates that changing the position of the carboxylic acid on the terminal ring B of the biphenyl aglycone as well as modifying the substitution pattern on ring A substantially reduced affinity. As previously reported, the *ortho*-chloro substituent present in the antagonists **1b** and **6b** provides additional van der Waals contacts leading to binding affinity in the low nanomolar range.<sup>8k</sup>

**Heteroaryl mannosides.** All heteroaryl mannosides (entries 10–42) were weaker binders than the biphenyl mannoside **1b**, however also showed  $\text{IC}_{50}$  values in the nanomolar range. *In silico* studies obtained with flexible docking (Glide software package<sup>33</sup>) to the FimH-CRD suggested a similar ‘out-docking mode’ (Fig. 4) for all heteroaryl mannosides (entries 10–42), establishing  $\pi$ - $\pi$ -stacking with Tyr48 of the tyrosine gate.<sup>8g</sup>



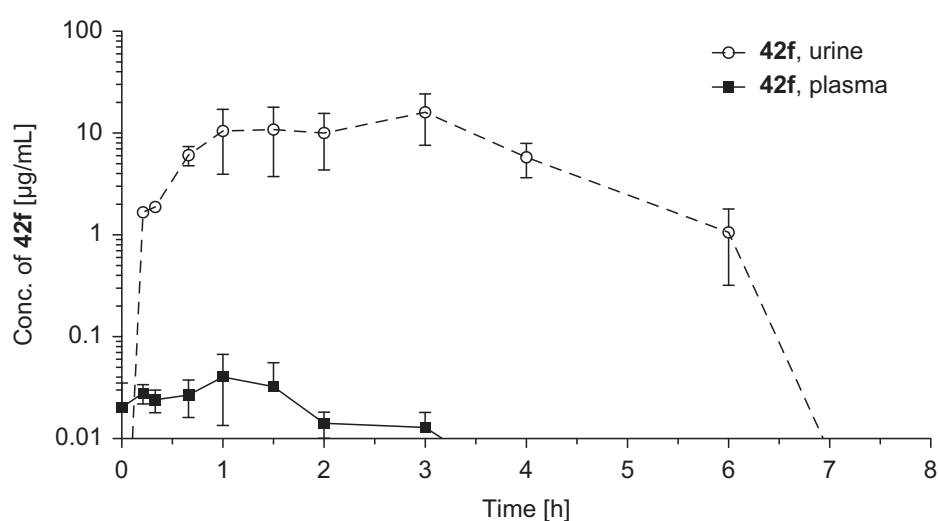
**Fig. 4** *In silico* docking studies obtained with flexible docking (Glide software package<sup>33</sup>) to the FimH-CRD (PDB ID: 4XO8); top-scored binding modes of (A) **44** (Table 1, entry 34) and (B) **46** (entry 38).

Therefore, it is quite surprising that the triazolylphenyl mannosides (entries 10–14) and the pyrrolylphenyl mannosides (entries 29–42) showed approximately five-fold higher affinity than the pyrazolylphenyl analogues (entries 15–18). Furthermore, the substitution pattern had also an influence on the binding affinity as observed for the various pyrrolylphenyl mannosides (entries 29–42). In agreement with previous observations,<sup>8i,k</sup> an *ortho*-chloro or an *ortho*-trifluoromethyl substituent on ring A improved affinity approximately 3-fold (**51**, entry 40 *vs.* **46**, entry 38 & **52**, entry 42). Furthermore, the position of the electron-withdrawing carboxylic acid substituent in ring B affected the binding affinity as well. In the 3-position ( $\rightarrow$ **45**, entry 36) a three-fold affinity increase compared to the 2-position ( $\rightarrow$ **43**, entry 32) was observed. With an additional 4-methyl group, affinity was improved by a factor of three (**43**, entry 32 *vs.* **44**, entry 34), presumably due to sterically favored  $\pi$ - $\pi$  stacking interactions between the heteroaromatic ring B and Tyr48 of the tyrosine gate.

#### 2.4 *In vivo* pharmacokinetic study

Antagonist **42f** (entry 37, Table 1) exhibiting the best *in vitro* PK/PD profile was selected for an *in vivo* pharmacokinetic study. Since its solubility is not sufficient for the planned dose of  $10 \text{ mg kg}^{-1}$ ,<sup>10a</sup> 5% DMSO and 1% surfactant Tween 80 were used as solubilizer. The concentration–time profiles in urine and plasma are shown in Fig. 5.

Plasma concentrations of **42f** were low, with a  $C_{\text{max}}$  of only  $0.04 \text{ } \mu\text{g mL}^{-1}$  between 40 min and 1.5 h and dropped below the detection limit 3 h post application. In contrast, antagonist **42f** rapidly accumulates in the urine with a  $C_{\text{max}}$  ranging from 10 to  $16 \text{ } \mu\text{g mL}^{-1}$  at 1 to 3 h post application. After a stable concentration plateau, which is slightly shifted in time compared to plasma peak levels, **42f** could not be detected in urine 7 h post application.



**Fig. 5** Urine (dashed line) and plasma (continuous line) concentrations over time of the pyrrolylphenyl mannoside **42f** after an application of a dose of  $10 \text{ mg kg}^{-1}$  (PBS containing 5% DMSO and 1% Tween 80). Shown are mean values with standard error of the mean for groups of three mice (C3H/HeN). The detection limit was at  $0.02 \text{ } \mu\text{g mL}^{-1}$ .

Accumulation in urine, resulting in a relatively constant plateau concentration over a time-period of about 3 h, can be related to several important interplaying mechanisms. Both, PAMPA<sup>23</sup> and transport through a Caco-2 cell monolayer predicted high ( $\log P_e -4.8 \text{ cm s}^{-1}$ ) to moderate ( $P_{\text{app,a-b}} 6.4 \times 10^{-6} \text{ cm s}^{-1}$ , Table 1) permeability for **42f**.<sup>25,26</sup> Although **42f** is a substrate of efflux transporters (Caco-2 cell experiment; b-a/a-b ratio  $> 2$ , Table 1),<sup>29</sup> the efflux transporters (*e.g.* P-gp) can be saturated by the applied high dose of  $10 \text{ mg kg}^{-1}$ .<sup>32,34</sup> Once in circulation, antagonist **42f** is filtered through the renal glomeruli in the kidneys. Based on its metabolic stability and a  $\log D_{7.4}$  value of 2.8, reabsorption from the filtrate in the proximal tubuli can be expected, leading to the observed delayed renal excretion.<sup>10b,34,35</sup> In summary, the observed PK profile of **42f** results from a good oral absorption (*i.e.* sufficient solubility and saturation of efflux transporter) with a delayed and prolonged elimination *via* the kidneys due to renal reabsorption.

### 3 Conclusions

Starting from ester **1a**, the present study aimed to optimize solubility and metabolic stability issues of biaryl mannosides in order to achieve high oral absorption of the ester and slow enzyme-mediated release of the polar metabolites.

First, our strategy to disrupt molecular planarity and symmetry of the biphenyl mannosides by modifying the substitution pattern, proved to be successful for improving solubility. Compared to antagonist **1a**, the ester **11a** showed a ten-fold improved solubility whereas membrane permeability remained high. However, since hepatic esterases rapidly convert ester **11a** to carboxylate **11b**, re-absorption from the tubuli is not possible leading to fast renal excretion. Furthermore, changing the positions of the substituents on the aglycone decreased affinity to the FimH-CRD, overriding the gain in the intestinal uptake potential (entries 4, 6 & 9).

In a second approach, the improvement of solubility and metabolic stability based on heterocyclic aglycones was studied. Thereby, triazole (**25a-c**, entries 10, 12 & 13), pyrazole (**28a,b**, entries 15 & 17), and six-membered heterocyclic moieties (**34a-d**, entries 19, 21, 23 & 25 and **39**, entry 27) proved highly beneficial to the aqueous solubility but in turn reduced lipophilicity and membrane permeability. Overall, only poor oral absorption could be observed. By contrast, the pyrrolylphenyl mannosides – optimized by the introduction of a chloro or trifluoromethyl substituent on ring A and a methyl group on the heterocycle (**42f** and **50**, entries 37 & 41) – exhibited sufficient permeability as well as aqueous solubility. Furthermore, incubations with rat liver microsomes, revealed low propensity to enzyme-mediated hydrolysis ( $t_{1/2} > 120 \text{ min}$ ), supporting slow elimination due to expected renal re-absorption of the metabolically stable esters.

In summary, our study exemplifies the benefits of two approaches: Rearrangement of the substitution pattern to improve aqueous solubility and introduction of heteroaromatic aglycones to improve aqueous solubility and metabolic stability. For the ester **42f**, an optimal balance of



pharmacodynamic, physicochemical and *in vitro* pharmacokinetic properties was realized. The measured high urine drug levels of **42f** (see Fig. 5) over an extended period of time considerably limit the dosing frequency and makes **42f** a promising candidate to be tested in a UTI disease model.

## Abbreviations

Caco-2 cells	colorectal adenocarcinoma cells
CES	carboxylesterase
$C_{\max}$	maximal concentration
CRD	carbohydrate recognition domain
$D$	octanol–water distribution coefficient
HPLC	high performance liquid chromatography
$IC_{50}$	half maximal inhibitory concentration
LC-MS	liquid chromatography mass spectrometry
PAMPA	parallel artificial membrane permeability assay
$P_{\text{app}}$	apparent permeability
$P_e$	effective permeability
RLM	rat liver microsomes
UPEC	uropathogenic <i>Escherichia coli</i>
UTI	urinary tract infection

## Acknowledgements

The authors thank Prof. Dr med. Radek Skoda, Department of Biomedicine, University Hospital Basel, Switzerland, for giving us access to the animal facility. The financial support by the Swiss National Science Foundation (CS: SNF grant 200020\_146202; DE: 31003A\_144183; SK: 200020\_129935) is gratefully acknowledged.

## References

- (a) T. M. Hooton and W. E. Stamm, Diagnosis and treatment of uncomplicated urinary tract infection, *Infect. Dis. Clin. North Am.*, 1997, **11**, 551–581; (b) T. J. Wiles, R. R. Kulesus and M. A. Mulvey, Origins and virulence mechanisms of uropathogenic *Escherichia coli*, *Exp. Mol. Pathol.*, 2008, **85**, 11–19; (c) S. D. Fihn, Acute uncomplicated urinary tract infection in women, *N. Engl. J. Med.*, 2003, **349**, 259–266.
- (a) J. D. Schilling and S. J. Hultgren, Recent advances into the pathogenesis of recurrent urinary tract infections: the bladder as a reservoir for uropathogenic *Escherichia coli*, *Int. J. Antimicrob. Agents*, 2002, **19**, 457–460; (b) M. Blango and M. Mulvey, Persistence of uropathogenic *Escherichia coli* in the face of multiple antibiotics, *Antimicrob. Agents Chemother.*, 2010, **54**, 1855–1863.
- C. Svanborg and G. Godaly, Bacterial virulence in urinary tract infection, *Infect. Dis. Clin. North Am.*, 1997, **11**, 513–529.
- (a) M. A. Mulvey, Adhesion and entry of uropathogenic *Escherichia coli*, *Cell. Microbiol.*, 2002, **4**, 257–271; (b) D. S. Eto, T. A. Jones, J. L. Sundsbak and M. A. Mulvey, Integrin-mediated host cell invasion by type 1-piliated uropathogenic *Escherichia coli*, *PLoS Pathog.*, 2007, **3**, e100.

- 5 G. Capitani, O. Eidam, R. Glockshuber and M. G. Grütter, Structural and functional insights into the assembly of type 1 pili from *Escherichia coli*, *Microbes Infect.*, 2006, **8**, 2284–2290.
- 6 (a) I. Le Trong, P. Aprikian, B. A. Kidd, M. Forero-Shelton, V. Tchesnokova, P. Rajagopal, V. Rodriguez, G. Interlandi, R. Klevit, V. Vogel, R. E. Stenkamp, E. V. Sokurenko and W. E. Thomas, Structural basis for mechanical force regulation of the adhesin FimH via finger trap-like  $\beta$  sheet twisting, *Cell*, 2010, **141**, 645–655; (b) M. M. Sauer, R. P. Jakob, J. Eras, S. Baday, D. Eris, G. Navarra, S. Bernèche, B. Ernst, T. Maier and R. Glockshuber, Catch-bond mechanism of the bacterial adhesin FimH, *Nat. Commun.*, 2016, **7**, 10738.
- 7 N. Sharon, Carbohydrates as future anti-adhesion drugs for infectious diseases, *Biochim. Biophys. Acta*, 2006, **1760**, 527–537.
- 8 (a) N. Firon, I. Ofek and N. Sharon, Interaction of mannose-containing oligosaccharides with the fimbrial lectin of *Escherichia coli*, *Biochem. Biophys. Res. Commun.*, 1982, **105**, 1426–1432; (b) N. Firon, I. Ofek and N. Sharon, Carbohydrate specificity of the surface lectins of *Escherichia coli*, *Klebsiella pneumoniae*, and *Salmonella typhimurium*, *Carbohydr. Res.*, 1983, **120**, 235–249; (c) N. Sharon, Bacterial lectins, cell-cell recognition and infectious disease, *FEBS Lett.*, 1987, **217**, 145–157; (d) J. Bouckaert, J. Berglund, M. Schembri, E. De Genst, L. Cools, M. Wuhler, C.-S. Hung, J. Pinkner, R. Slättegård, A. Zavialov, D. Choudhury, S. Langermann, S. J. Hultgren, L. Wyns, P. Klemm, S. Oscarson, S. D. Knight and H. De Greve, Receptor binding studies disclose a novel class of high-affinity inhibitors of the *Escherichia coli* FimH adhesin, *Mol. Microbiol.*, 2005, **55**, 441–455; (e) N. Firon, S. Ashkenazi, D. Mirelman, I. Ofek and N. Sharon, Aromatic alpha-glycosides of mannose are powerful inhibitors of the adherence of type 1 fimbriated *Escherichia coli* to yeast and intestinal epithelial cells, *Infect. Immun.*, 1987, **55**, 472–476; (f) O. Sperling, A. Fuchs and T. K. Lindhorst, Evaluation of the carbohydrate recognition domain of the bacterial adhesin FimH. Design, synthesis and binding properties of mannoside ligands, *Org. Biomol. Chem.*, 2006, **4**, 3913–3922; (g) Z. Han, J. S. Pinkner, B. Ford, R. Obermann, W. Nolan, S. A. Wildman, D. Hobbs, T. Ellenberger, C. K. Cusumano, S. J. Hultgren and J. W. Janetka, Structure-based drug design and optimization of mannoside bacterial FimH antagonists, *J. Med. Chem.*, 2010, **53**, 4779–4792; (h) T. Klein, D. Abgottspon, M. Wittwer, S. Rabbani, J. Herold, X. Jiang, S. Kleeb, C. Lüthi, M. Scharenberg, J. Bezençon, E. Gubler, L. Pang, M. Smiesko, B. Cutting, O. Schwardt and B. Ernst, FimH antagonists for the oral treatment of urinary tract infections: from design and synthesis to in vitro and in vivo evaluation, *J. Med. Chem.*, 2010, **53**, 8627–8641; (i) C. K. Cusumano, J. S. Pinkner, Z. Han, S. E. Greene, B. A. Ford, J. R. Crowley, J. P. Henderson, J. W. Janetka and S. J. Hultgren, Treatment and prevention of urinary tract infection with orally active FimH inhibitors, *Sci. Transl. Med.*, 2011, **3**, 109–115; (j) Z. Han, J. S. Pinkner, B. Ford, E. Chorell, J. M. Crowley, C. K. Cusumano, S. Campbell, J. P. Henderson, S. J. Hultgren and J. W. Janetka, Lead optimization studies on FimH antagonists: discovery of potent and orally bioavailable *ortho*-substituted biphenyl mannosides, *J. Med. Chem.*, 2012, **55**, 3945–3959; (k) L. Pang, S. Kleeb, K. Lemme, S. Rabbani, M. Scharenberg, A. Zalewski, F. Schädler, O. Schwardt and B. Ernst, FimH antagonists: structure-activity and structure-property relationships for biphenyl  $\alpha$ -D-mannopyranosides, *ChemMedChem*, 2012, **7**, 1404–1422; (l) X. Jiang, D. Abgottspon, S. Kleeb, S. Rabbani, M. Scharenberg, M. Wittwer, M. Haug, O. Schwardt and B. Ernst, Anti-adhesion therapy for urinary tract infections – a balanced PK/PD profile



- proved to be key for success, *J. Med. Chem.*, 2012, **55**, 4700–4713; (m) O. Schwaradt, S. Rabbani, M. Hartmann, D. Abgottspon, M. Wittwer, S. Kleeb, A. Zalewski, M. Smiesko, B. Cutting and B. Ernst, Design, synthesis and biological evaluation of mannosyl triazoles as FimH antagonists, *Bioorg. Med. Chem.*, 2011, **19**, 6454–6473; (n) S. Brument, A. Sivignon, T. I. Dumych, N. Moreau, G. Roos, Y. Guérardel, T. Chalopin, D. Deniaud, R. O. Bilyy, A. Darfeuille-Michaud, J. Bouckaert and S. G. Gouin, Thiazolylamino-mannosides as potent antiadhesives of type 1 piliated *Escherichia coli* isolated from Crohn's disease patients, *J. Med. Chem.*, 2013, **56**, 5395–5406; (o) S. Kleeb, L. Pang, K. Mayer, D. Eris, A. Sigl, R. C. Preston, P. Zihlmann, T. Sharpe, R. P. Jakob, D. Abgottspon, A. S. Hutter, M. Scharenberg, X. Jiang, G. Navarra, S. Rabbani, M. Smiesko, N. Lüdin, J. Bezençon, O. Schwaradt, T. Maier and B. Ernst, FimH antagonists: bioisosteres to improve the in vitro and in vivo PK/PD profile, *J. Med. Chem.*, 2015, **58**, 2221–2239.
- 9 (a) T. K. Lindhorst, C. Kieburg and U. Krallmann-Wenzel, Inhibition of the type 1 fimbriae-mediated adhesion of *Escherichia coli* to erythrocytes by multiantennary D-mannosyl clusters: The effect of multivalency, *Glycoconjugate J.*, 1998, **15**, 605–613; (b) N. Nagahori, R. T. Lee, S.-L. Nishimura, S. Pagé, R. Roy and Y. C. Lee, Inhibition of adhesion of type 1 fimbriated *Escherichia coli* to highly mannosylated ligands, *ChemBioChem*, 2002, **3**, 836–844; (c) C. C. M. Appeldoorn, J. A. F. Joosten, F. A. Maate, U. Dobrindt, J. Hacker, R. M. J. Liskamp, A. S. Khan and R. J. Pieters, Novel multivalent mannose compounds and their inhibition of the adhesion of type 1 fimbriated uropathogenic *E. coli*, *Tetrahedron: Asymmetry*, 2005, **16**, 361–372; (d) A. Patel and T. K. Lindhorst, A modular approach for the synthesis of oligosaccharide mimetics, *Carbohydr. Res.*, 2006, **341**, 1657–1668; (e) M. Touaibia, A. Wellens, T. C. Shiao, Q. Wang, S. Sirois, J. Bouckaert and R. Roy, Mannosylated G(0) dendrimers with nanomolar affinities to *Escherichia coli* FimH, *ChemMedChem*, 2007, **2**, 1190–1201; (f) M. Durka, K. Buffet, J. Iehl, M. Holler, J.-F. Nierengarten, J. Taganna, J. Bouckaert and S. P. Vincent, The functional valency of dodecamannosylated fullerenes with *Escherichia coli* FimH – towards novel bacterial antiadhesives, *Chem. Commun.*, 2011, **47**, 1321–1323; (g) J. Bouckaert, Z. Li, C. Xavier, M. Almant, V. Caveliers, T. Lahoutte, S. D. Weeks, J. Kovensky and S. G. Gouin, Heptyl  $\alpha$ -D-mannosides grafted on a  $\beta$ -cyclodextrin core to interfere with *Escherichia coli* adhesion: An *in vivo* multivalent effect, *Chem. – Eur. J.*, 2013, **19**, 7847–7855.
- 10 (a) C. A. Lipinski, Drug-like properties and the causes of poor solubility and poor permeability, *J. Pharmacol. Toxicol. Methods*, 2000, **44**, 235–249; (b) H. van de Waterbeemd, D. Smith, K. Beaumont and D. Walker, Property-based design: Optimization of drug absorption and pharmacokinetics, *J. Med. Chem.*, 2001, **44**, 1313–1333.
- 11 (a) M. Ishikawa and Y. Hashimoto, Improvement in aqueous solubility in small molecule drug discovery programs by disruption of molecular planarity and symmetry, *J. Med. Chem.*, 2011, **54**, 1539–1554; (b) A.-E. F. Nassar, A. M. Kamel and C. Clarimont, Improving the decision-making process in the structural modification of drug candidates: enhancing metabolic stability, *Drug Discovery Today*, 2004, **9**, 1020–1028.
- 12 N. A. Meanwell, Synopsis of some recent tactical application of bioisosteres in drug design, *J. Med. Chem.*, 2011, **54**, 2529–2591.
- 13 I. L. Scott, R. V. Market, R. J. DeOrazio, H. Meckler and T. P. Kogan, Stereospecific  $\alpha$ -D-mannosylation, *Carbohydr. Res.*, 1999, **317**, 210–216.
- 14 A. Titz, Z. Radic, O. Schwaradt and B. Ernst, A safe and convenient method for the preparation of triflyl azide, and its use in diazo transfer reactions to

- primary amines, *Tetrahedron Lett.*, 2006, **47**, 2383–2385; R. Yan, F. Yang, Y. Wu, L. Zhang and X. Ye, An efficient and improved procedure for preparation of triflyl azide and application in catalytic diazotransfer reaction, *Tetrahedron Lett.*, 2005, **46**, 8993–8995.
- 15 V. Rostovtsev, L. Green, V. Fokin and K. Sharpless, A stepwise Huisgen cycloaddition process: Copper(I)-catalyzed regioselective “ligation” of azides and terminal alkynes, *Angew. Chem., Int. Ed.*, 2002, **41**, 2596–2599.
- 16 J. Antilla, J. Baskin, T. Barder and S. Buchwald, Copper-diamine-catalyzed *N*-arylation of pyrroles, pyrazoles, indazoles, imidazoles, and triazoles, *J. Org. Chem.*, 2004, **69**, 5578–5587.
- 17 (a) M. Node, K. Nishide, K. Fuji and E. Fujita, Hard acid and soft nucleophile system. 2. Demethylation of methyl esters of alcohol and phenol with an aluminum halide-thiol system, *J. Org. Chem.*, 1980, **45**, 4275–4277; (b) M. Node, K. Kumar, K. Nishide, S. Ohsugi and T. Miyamoto, Odorless substitutes for foul-smelling thiols: Syntheses and applications, *Tetrahedron Lett.*, 2001, **42**, 9207–9210.
- 18 B. Le Bourdonnec, R. Windh, L. Leister, Q. Zhou, C. Ajello, M. Gu, G. Chu, P. Tuthill, W. Barker, M. Koblish, D. Wiant, T. Graczyk, S. Belanger, J. Cassel, M. Feschenko, B. Brogdon, S. Smith, M. Derelanko, S. Kutz, P. Little, R. DeHaven, D. DeHaven-Hudkins and R. Dolle, Spirocyclic delta opioid receptor agonists for the treatment of pain: Discovery of *N,N*-diethyl-3-hydroxy-4-(spiro[chromene-2,4'-piperidine]-4-yl) benzamide (ADL5747), *J. Med. Chem.*, 2009, **52**, 5685–5702.
- 19 A. Katritzky, D. Cheng and R. Musgrave, Syntheses of imidazoles and pyrroles: BetMIC and TosMIC as complementary reagents, *Heterocycles*, 1997, **44**, 67–70.
- 20 M. Prieto, E. Zurita, E. Rosa, L. Munoz, P. Lloyd-Williams and E. Giralt, Arylboronic acids and arylpinacolboronate esters in Suzuki coupling reactions involving indoles. Partner role swapping and heterocycle protection, *J. Org. Chem.*, 2004, **69**, 6812–6820.
- 21 J. C. Dearden and G. M. Bresnen, The measurement of partition coefficients, *Quant. Struct. – Act. Relat.*, 1988, **7**, 133–144.
- 22 A. Avdeef, High-throughput measurements of solubility profiles, in *Pharmacokinetic Optimization in Drug Research; Biological, Physicochemical and Computational Strategies*, ed. B. Testa, H. van de Waterbeemd, G. Folkers and R. Guy, Verlag Helvetica Chimica Acta, Zurich, 2001, pp. 305–326.
- 23 M. Kansy, F. Senner and K. Gubernator, Physicochemical high throughput screening: Parallel artificial membrane permeation assay in the description of passive absorption processes, *J. Med. Chem.*, 1998, **41**, 1007–1010.
- 24 P. Artursson and J. Karlsson, Correlation between oral-drug absorption in humans and apparent drug permeability coefficients in human intestinal epithelial (Caco-2) cells, *Biochem. Biophys. Res. Commun.*, 1991, **175**, 880–885.
- 25 A. Avdeef, S. Bendels, L. Di, B. Faller, M. Kansy, K. Sugano and Y. Yamauchi, PAMPA – critical factors for better predictions of absorption, *J. Pharm. Sci.*, 2007, **96**, 2893–2909.
- 26 T. Hou, J. Wang, W. Zhang and X. Xu, ADME evaluation in drug discovery. 7. Prediction of oral absorption by correlation and classification, *J. Chem. Inf. Model.*, 2007, **47**, 208–218.
- 27 M. Taketani, M. Shii, K. Ohura, S. Ninomiya and T. Imai, Carboxylesterase in the liver and small intestine of experimental animals and human, *Life Sci.*, 2007, **81**, 924–932.
- 28 S. Rabbani, X. H. Jiang, O. Schwardt and B. Ernst, Expression of the carbohydrate recognition domain of FimH and development of a competitive binding assay, *Anal. Biochem.*, 2010, **407**, 188–195.

- 
- 29 I. Hubatsch, E. G. Ragnarsson and P. Artursson, Determination of drug permeability and prediction of drug absorption in Caco-2 monolayers, *Nat. Protoc.*, 2007, **2**, 2111–2119.
  - 30 MacroModel, version 9.9, Schrödinger, LLC, New York, NY, 2012. Torsion angle measurements are based on the lowest-energy conformers.
  - 31 (a) R. M. Wadkins, C. L. Morton, J. K. Weeks, L. Oliver, M. Wierdl, M. K. Danks and P. M. Potter, Structural constraints affect the metabolism of 7-ethyl-10-[4-(1-piperidino)-1-piperidino]carbonyloxycamptothecin (CPT-11) by carboxylesterases, *Mol. Pharmacol.*, 2001, **60**, 355–362; (b) J. M. Hatfield, M. Wierdl, R. M. Wadkins and P. M. Potter, Modifications of human carboxylesterase for improved prodrug activation, *Expert Opin. Drug Metab. Toxicol.*, 2008, **4**, 1153–1165; (c) G. Vistoli, A. Pedretti, A. Mazzolari and B. Testa, In silico prediction of human carboxylesterase-1 (hCES1) metabolism combining docking analyses and MD simulations, *Bioorg. Med. Chem.*, 2010, **18**, 320–329; T. Satoh and M. Hosokawa, Structure, function and regulation of carboxylesterases, *Chem. Biol. Interact.*, 2006, **162**, 195–211.
  - 32 J. H. Lin, Drug-drug interaction mediated by inhibition and induction of P-glycoprotein, *Adv. Drug Delivery Rev.*, 2003, **21**, 53–81.
  - 33 Glide, version 5.7, Schrödinger, LLC, New York, NY, 2011; 3D representations were made by the PyMOL Molecular Graphics System, Version 1.6 Schrödinger, LLC.
  - 34 D. A. Smith, B. C. Jones and D. K. Walker, Design of drugs involving the concepts and theories of drug metabolism and pharmacokinetics, *Med. Res. Rev.*, 1996, **16**, 243–266.
  - 35 M. V. Varma, B. Feng, R. S. Obach, M. D. Troutman, J. Chupka, H. R. Miller and A. El-Kattan, Physicochemical determinants of human renal clearance, *J. Med. Chem.*, 2009, **52**, 4844–4852.

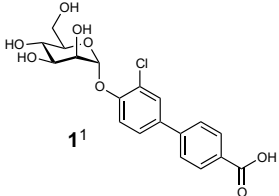
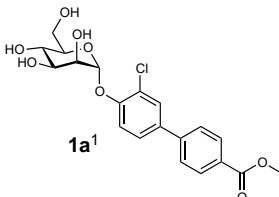
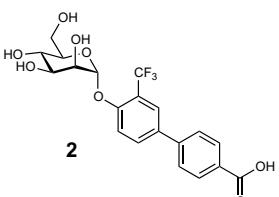


#### 4.4 Stability of FimH Antagonists in Gastro and Intestinal Fluids

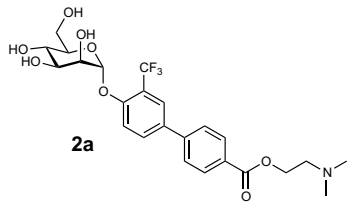
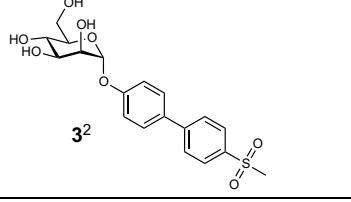
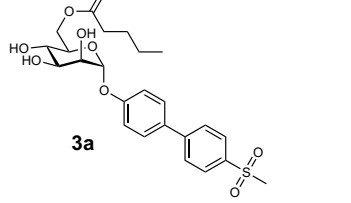
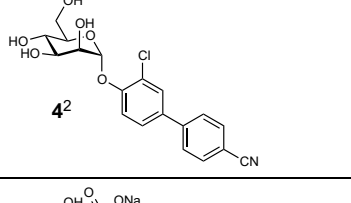
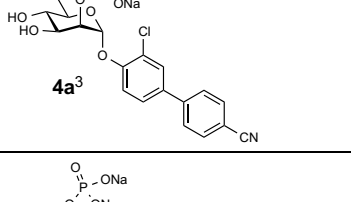
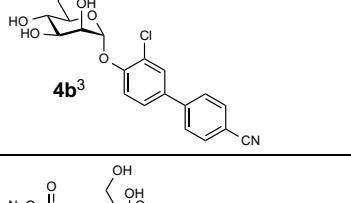
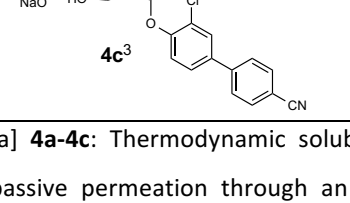
This chapter illustrates the stability of FimH antagonists in gastrointestinal fluids. These data originate from the master thesis of Karen Bamberger supervised by Jacqueline Bezençon.

The physicochemical properties permeability, solubility, and stability are key for good oral absorption. In previous studies, insufficient permeability (Caco-2 and PAMPA) and aqueous solubility were improved by ester and phosphate prodrug approaches, respectively (Table 4.5). To complete the evaluation of oral absorption, stability of two prodrugs with an ester on the terminal ring of the biphenyl aglycone ( $\rightarrow$ **1a**<sup>1</sup> and **2a**, Table 4.5), the *p*-sulfone biphenyl mannoside **3**<sup>2</sup> (Table 4.5 and Paper 3, page 133) with poor permeability and with an acylation at the C-6 position of mannose ( $\rightarrow$ **3a**, Table 4.5), and three different phosphate prodrugs (**4a** – **4c**<sup>3</sup>, Table 4.5 and Paper 4, page 153) of the *p*-cyano biphenyl mannoside **4**<sup>2</sup> (Table 4.5 and Paper 3) was analyzed in gastrointestinal fluids (biorelevant media).

**Table 4.5.** Physicochemical properties (solubility, permeability  $\log P_e$  and  $\log P_{app}$ ) of the active compounds **1**<sup>1</sup>, **2**, and **3**<sup>2</sup> with their ester prodrugs **1a-3a** and the active compound **4**<sup>2</sup> with its various phosphate prodrugs **4a-4c**<sup>3</sup>.

Compounds	Solubility <sup>[a]</sup> [ $\mu\text{g/mL}$ ] /pH	PAMPA <sup>[b]</sup> $\log P_e$ [cm/s]	Caco-2 <sup>[c]</sup> $P_{app}$ [ $10^{-6}$ cm/s]	
			a $\rightarrow$ b	b $\rightarrow$ a
 <b>1</b>	> 3000	-10	0.23	0.38
 <b>1a</b>	16.9	-4.6	5.3	17.5
 <b>2</b>	> 200	-8.6	n.d.	n.d.

#### 4 Results and Discussion: FimH Antagonists

Compounds	Solubility <sup>[a]</sup> [μg/mL] /pH	PAMPA <sup>[b]</sup> log $P_e$ [cm/s]	Caco-2 <sup>[c]</sup> $P_{app}$ [ $10^{-6}$ cm/s]	
			a→b	b→a
 <b>2a</b>	296	-6.4	1.6	36.7
 <b>3<sup>2</sup></b>	246	-7.2	0.36	1.76
 <b>3a</b>	145	-4.7	17.3	23.5
 <b>4<sup>2</sup></b>	192	-5.2	4.3	21.1
 <b>4a<sup>3</sup></b>	> 3000	n.d.	n.d.	n.d.
 <b>4b<sup>3</sup></b>	> 3000	n.d.	n.d.	n.d.
 <b>4c<sup>3</sup></b>	> 3000	n.d.	n.d.	n.d.

[a] **4a-4c**: Thermodynamic solubility, **1-3**, **1a-3a**, and **4**: Kinetic solubility;<sup>4</sup> [b]  $P_e$  = effective permeability: passive permeation through an artificial membrane was determined by the parallel artificial membrane permeability assay (PAMPA) at pH 7.4;<sup>5,6</sup> [c]  $P_{app}$  = apparent permeability: permeation through a Caco-2 cell monolayer was assessed in the absorptive (a→b) and secretory (b→a) directions in triplicate.<sup>7,8</sup> n.d. = not determined.

Different media were selected to mimic pre- and post-prandial conditions in the stomach and the small intestine. The compositions of these biorelevant media are listed in the supporting information of Paper 4 (page 153).

To mimic gastric fluids, the following fluids were used:

- Simulated gastric fluid (*sGF*)
- Fasted state simulated gastric fluid (*FaSSGF*)
- Fed state simulated gastric fluid (*FeSSGF*)

The intestinal fluids were represented by:

- Simulated intestinal fluid (*sIF*)
- Fasted state simulated intestinal fluid (*FaSSIF*)
- Fed state simulated intestinal fluid (*FeSSIF*)

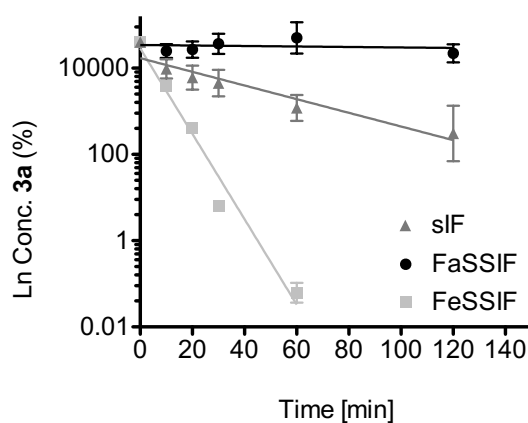
Additionally, two buffer solutions (*buffer sGF* and *buffer sIF*) were prepared the same way as *sGF* and *sIF*, but without pepsin and pancreatin, respectively. Water was used as a reference solution. The compounds were incubated for two hours and their time-dependent concentrations were measured. In earlier *in vivo* studies,  $C_{\max}$  (urine) of the FimH antagonists was reached within 1.5 hours.<sup>1, 2, 9</sup> Therefore, we assumed that compounds with moderate to good permeability with a stability of > 75% after two hours of incubation do not have an influence on oral absorption of a drug.

### Stability of Ester Prodrugs in Gastrointestinal Fluids

Ester prodrugs enhance permeability of the biphenyl  $\alpha$ -D-mannosides (Paper 2, page 107).<sup>1</sup> However, the prodrug approach is only successful if the ester is not cleaved in the gastrointestinal tract (GIT) prior to permeation. Therefore, stability of ester prodrugs **1a** - **3a** was tested in various simulated gastrointestinal fluids at 37 °C (Figure 4.33). Concentrations of the ester prodrugs **1a** and **2a** remained constant over 120 min in all simulated gastrointestinal fluids, as well as in the buffer solutions (> 75%). The measured values of the ester prodrug **1a** in *buffer sIF* and in *FaSSIF* show high standard deviations. However, stability in *sIF* and *FeSSIF* with additional pancreatin was higher than 75% after 120 min. Ester prodrug **3a** decomposed rapidly in *sIF* and *FeSSIF*, probably due to pancreatin, a component present only in these two fluids. Pancreatin is a combination of several digestive enzymes produced by the exocrine cells of the pancreas, such as amylase, lipases, and proteases. Pancreatic  $\alpha$ -amylases are known to digest carbohydrates present in food.<sup>10</sup> The

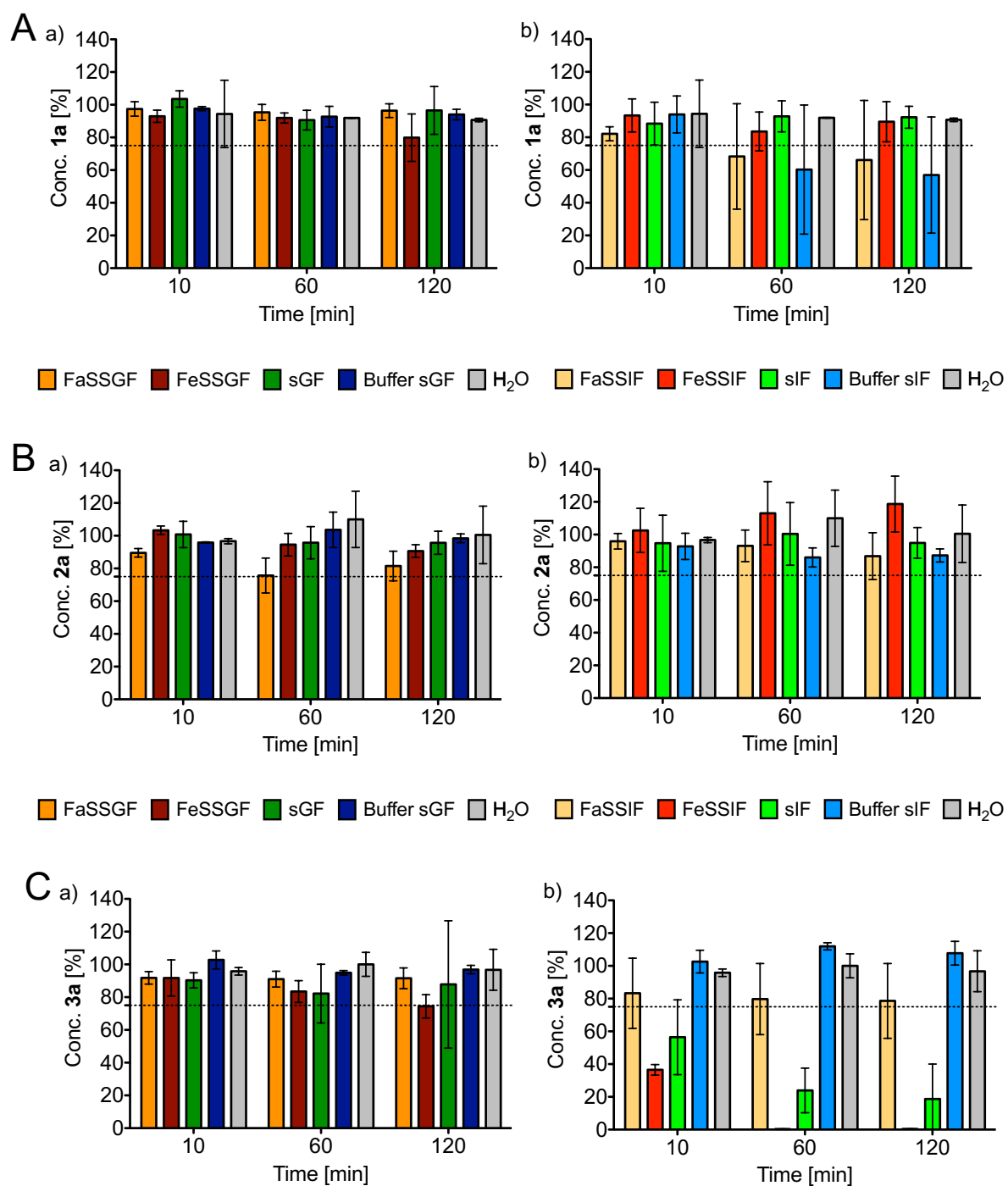
difference between the three FimH antagonists are the position of their ester, whereas compound **3a** have an acylation at C-6 position of the mannose moiety and compounds **1a** and **2a** have an ester bond attached at the biphenylic aglycone residue (Table 4.5). Degradation of ester prodrug **3a** was faster in *FeSSIF* with a  $t_{1/2}$  of 7 min compared to *sIF* with a  $t_{1/2}$  of 46 min (Figure 4.34), although *sIF* and *FeSSIF* contain the same amount of pancreatin.

This indicates that additional ingredients in *FeSSIF* promote the degradation of ester prodrug **3a** by pancreatin. This media contains additional surfactants, such as bile salts and lecithin, and maleic acid - which retard rancidity of fats and oils - and glycerides (oleate-based components, which reflect lipolysis products in the media).<sup>11</sup>



**Figure 4.34.** Stability of the ester prodrug **3a** in various simulated intestinal fluids. Degradation of compound **3a** in *FaSSIF* (black, without pancreatin), in *sIF* (dark grey, with pancreatin), and in *FeSSIF* (light grey, with pancreatin) over time is shown. Data represent mean ( $n = 3$ ) with the standard deviation.



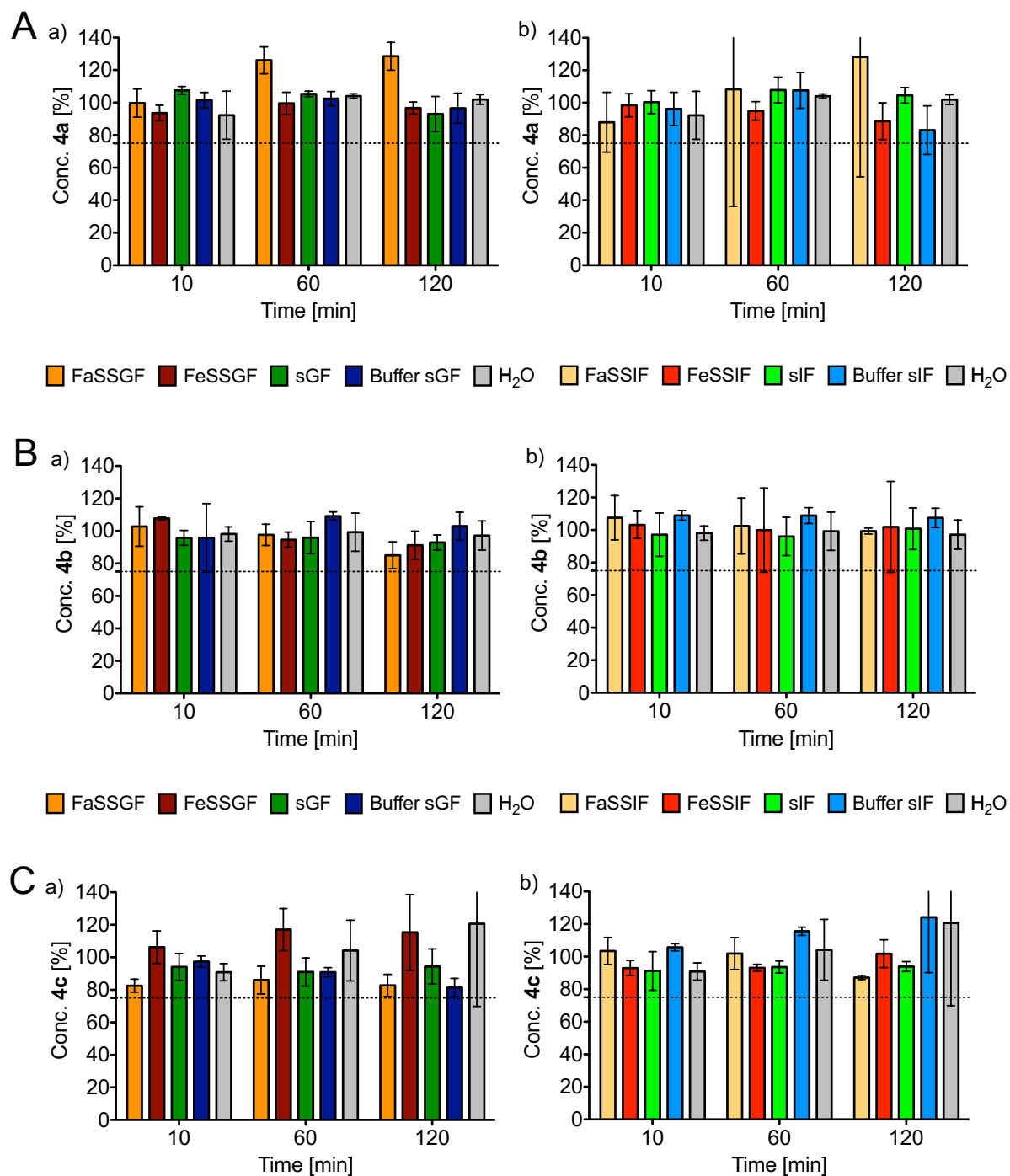


**Figure 4.33.** Stability of the ester prodrugs A) 1, B) 2, and C) 3 in biorelevant media. Percentage of the remaining compound concentration relative to the initial concentration ( $t = 0$  min) after 10, 60, and 120 min of incubation in a) simulated gastric fluids (*FaSSGF*, *FeSSGF*, *sGF*, *buffer sGF*) and b) simulated intestinal fluids (*FaSSIF*, *FeSSIF*, *sIF*, *buffer sIF*) are shown. Water was used as a control. Data represent the mean ( $n = 3$ ) with the standard deviation.

### Stability of Phosphate Prodrugs in Gastrointestinal Fluids

As a further approach to improve oral absorption of FimH antagonists, phosphate prodrugs were synthesized to improve solubility (cf. Paper 4, page 153). Phosphate prodrugs cannot permeate across the lipophilic lipid bilayer of the intestinal membrane due to the highly polar phosphate moiety. For this reason, cleavage of the phosphate prodrugs by alkaline phosphatase (ALP) in the small intestine is required.<sup>3</sup> To reach a controlled release and to avoid fast degradation including the risk of precipitation of the compound, no further degradation in the GIT is desired. Therefore, the stability of the phosphate prodrugs **4a** - **4c** in various simulated gastrointestinal fluids at 37 °C was tested (Figure 4.35). All three phosphate prodrugs are stable under simulated gastrointestinal conditions. Neither *pH* nor the presence of digestive enzymes, such as pepsin or pancreatin, had an influence on their stability. There was no difference between fasted and fed state. In addition, there is no difference between the positions of the phosphate moiety (2-, 4-, or 6-phosphate) in terms of stability in the gastrointestinal fluids.

In conclusion, ester prodrugs at the aglycone and phosphate prodrugs at the mannose moiety were stable in gastrointestinal fluids, whereas ester prodrugs in terms of acylation at the C-6 position of the mannose moiety exhibit fast degradation in the intestinal fluids due to the enzyme pancreatin. Further studies concerning the mechanism of degradation of antagonist **3a** and analogues thereof are required.



**Figure 4.35.** Stability of the phosphate prodrugs A) **4a**, B) **4b**, and C) **4c** in biorelevant media. Percentage of the remaining compound concentration relative to the initial concentration ( $t = 0$  min) after 10, 60, and 120 min of incubation in a) simulated gastric fluids (*FaSSGF*, *FeSSGF*, *sGF*, *buffer sGF*) and b) simulated intestinal fluids (*FaSSIF*, *FeSSIF*, *sIF*, *buffer sIF*) are shown. Water was used as a control. Data represent the mean ( $n = 3$ ) with the standard deviation.

### References

1. Klein, T.; Abgottspon, D.; Wittwer, M.; Rabbani, S.; Herold, J.; Jiang, X.; Kleeb, S.; Luethi, C.; Scharenberg, M.; Bezencon, J.; Gubler, E.; Pang, L.; Smiesko, M.; Cutting, B.; Schwardt, O.; Ernst, B. FimH Antagonists for the Oral Treatment of Urinary Tract Infections: From Design and Synthesis to *in Vitro* and *in Vivo* Evaluation. *J. Med. Chem.* **2010**, *53*, 8627-8641.
2. Kleeb, S.; Pang, L.; Mayer, K.; Eris, D.; Sigl, A.; Preston, R. C.; Zihlmann, P.; Sharpe, T.; Jakob, R. P.; Abgottspon, D.; Hutter, A. S.; Scharenberg, M.; Jiang, X.; Navarra, G.; Rabbani, S.; Smiesko, M.; Ludin, N.; Bezencon, J.; Schwardt, O.; Maier, T.; Ernst, B. FimH Antagonists: Bioisosteres To Improve the *in Vitro* and *in Vivo* PK/PD Profile. *J. Med. Chem.* **2015**, *58*, 2221-39.
3. Kleeb, S.; Jiang, X.; Frei, P.; Sigl, A.; Bezençon, J.; Bamberger, K.; Schwardt, O.; Ernst, B. FimH Antagonists: Phosphate Prodrugs Improve Oral Bioavailability. *J. Med. Chem.* **2016**, *59*, 3163-3182.
4. Alsenz, J.; Kansy, M. High throughput solubility measurement in drug discovery and development. *Adv. Drug. Deliv. Rev.* **2007**, *59*, 546-67.
5. Kansy, M.; Senner, F.; Gubernator, K. Physicochemical high throughput screening: Parallel artificial membrane permeation assay in the description of passive absorption processes. *J. Med. Chem.* **1998**, *41*, 1007-1010.
6. Avdeef, A.; Bendels, S.; Di, L.; Faller, B.; Kansy, M.; Sugano, K.; Yamauchi, Y. PAMPA - Critical factors for better predictions of absorption. *J. Pharm. Sci.* **2007**, *96*, 2893-2909.
7. Hubatsch, I.; Ragnarsson, E. G. E.; Artursson, P. Determination of drug permeability and prediction of drug absorption in Caco-2 monolayers. *Nat. Protoc.* **2007**, *2*, 2111-2119.
8. Artursson, P.; Karlsson, J. Correlation between oral drug absorption in humans and apparent drug permeability coefficients in human intestinal epithelial (Caco-2) cells. *Biochem. Biophys. Res. Commun.* **1991**, *175*, 880-5.
9. Jiang, X.; Abgottspon, D.; Kleeb, S.; Rabbani, S.; Scharenberg, M.; Wittwer, M.; Haug, M.; Schwardt, O.; Ernst, B. Antiadhesion therapy for urinary tract infections--a balanced PK/PD profile proved to be key for success. *J. Med. Chem.* **2012**, *55*, 4700-13.
10. Bencharit, S.; Morton, C. L.; Hyatt, J. L.; Kuhn, P.; Danks, M. K.; Potter, P. M.; Redinbo, M. R. Crystal structure of human carboxylesterase 1 complexed with the Alzheimer's drug tacrine: from binding promiscuity to selective inhibition. *Chem. & Biol.* **2003**, *10*, 341-349.
11. Jantratid, E.; Janssen, N.; Reppas, C.; Dressman, J. B. Dissolution media simulating conditions in the proximal human gastrointestinal tract: an update. *Pharm. Res.* **2008**, *25*, 1663-76.

---

## 5 Results and Discussion: Cyclic Hexapeptides

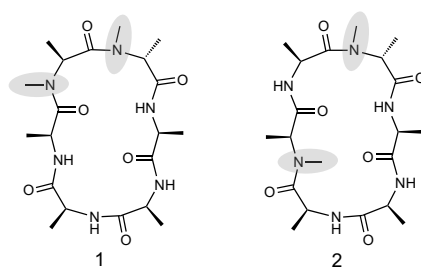
---

In this chapter, the *in vitro* permeability of cyclic hexapeptides derivatives is discussed. The cyclic hexapeptides were synthesized by Florian Rechenmacher, Udaya Kiran Marelli, and Eduard Puig in the research group of Prof. H. Kessler (Technical University of Munich, Institute for Advanced Study) and the *in vitro* pharmacokinetic experiments and evaluation of the results described in this chapter were performed in our laboratory. Parts of the data originate from the internship student Aleksandra Djekic supervised by Jacqueline Bezençon.

At the beginning of the subchapter 5.1, unpublished results are presented followed by a paper, accepted by *Chemistry - A European Journal*. My specific contribution is mentioned at the beginning of this paper.

### 5.1 *In Vitro* Permeability Evaluation of Cyclic Hexapeptides

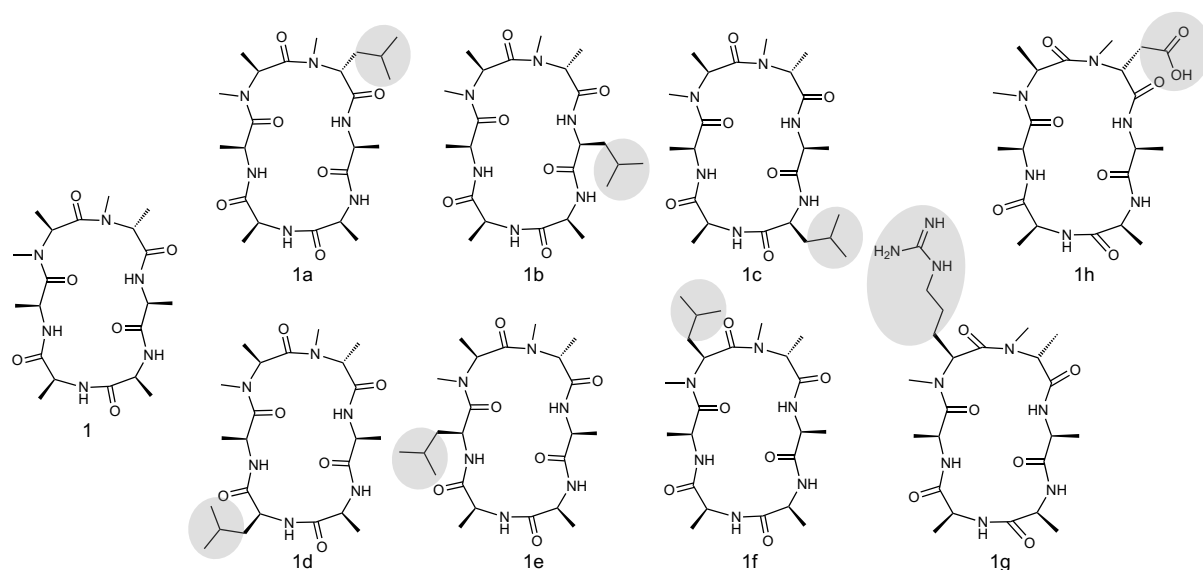
According to a previous study of Ovadia *et al.*,<sup>1</sup> it was suggested that multiple *N*-methylation (a naturally occurring chemical modification) of peptides improves intestinal permeability. In their study, a library of cyclic polyalanine hexapeptides, consisting of five L-ala and a single D-ala as well as *N*-methylation varying in numbers and position were synthesized and evaluated for intestinal permeability *in vitro*. Two of the di-*N*-methylated peptides (Figure 5.1, **1** and **2**) of this library had exceptional high permeability in the Caco-2 cell permeability experiment ( $\log P_{app} > -5.0$  cm/s).<sup>1</sup>



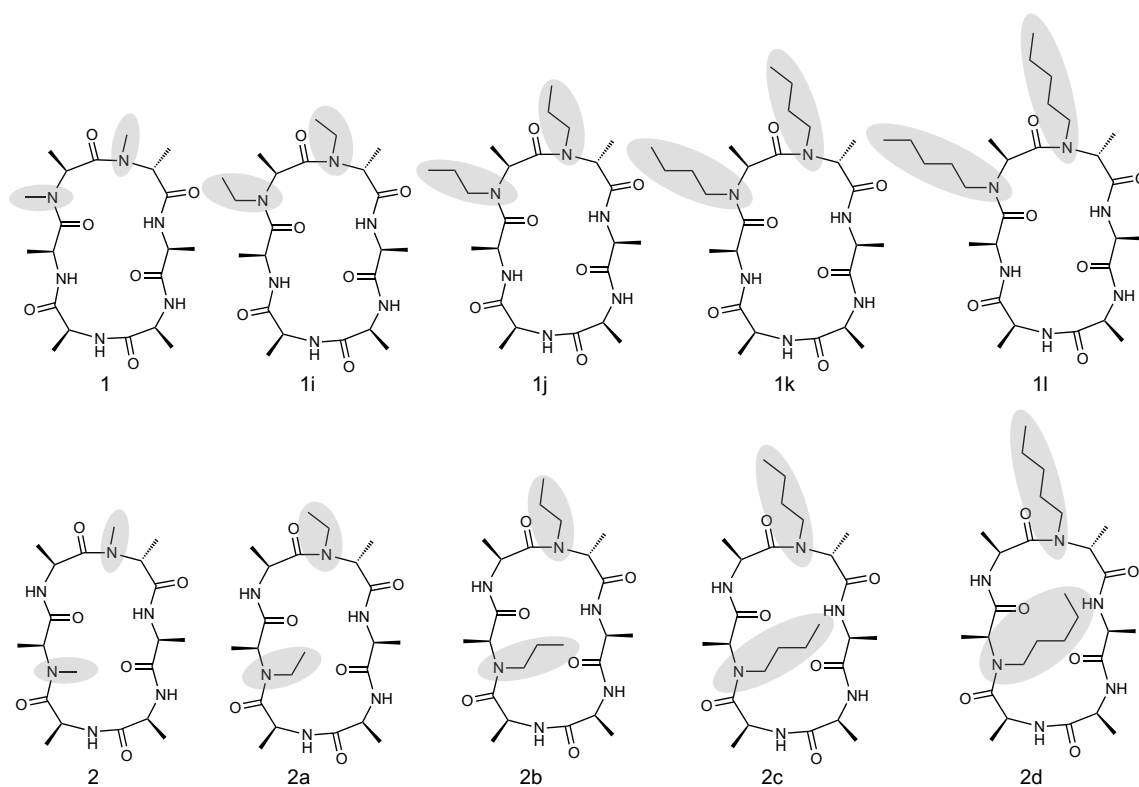
**Figure 5.1.** Di-*N*-methylated peptides **1** and **2**. The framework consists of two *N*-methylated residues (highlighted in grey), 5 amino acid residues in (L)-configuration and one residue in (D)-configuration.<sup>1</sup>

Based on the hexapeptides **1** and **2** showing high permeability, different derivatives were synthesized. First, eight derivatives of the hexapeptide **1** containing different amino acids (one leucine or arginine or aspartic acid residue and five alanine residues) were synthesized (Figure 5.2). One alanine residue has (D)-configuration as opposed to the remaining amino acids, which are all in the natural (L)-configuration. Six of the eight di-*N*-methylated cyclic hexapeptides differ only in the position of the leucine residue. In a second attempt, eight derivatives of the hexapeptides **1** and **2** containing *N*-alkylations of different chain lengths were synthesized (Figure 5.3).

To evaluate oral bioavailability of these cyclic peptides, physiochemical parameters, i.e. lipophilicity ( $\log D_{7.4}$ ), permeability through an artificial membrane (PAMPA) and a cell monolayer (Caco-2) were determined. Experimental details are described in the supporting information of Paper 6 (page 237).



**Figure 5.2.** Structures of the cyclic hexapeptide **1**<sup>1</sup> and its derivatives differing in position or kind of amino acids (highlighted in grey are the alanine replacement with another amino acid). The main chain framework consists of two *N*-methylated residues, 5 amino acid residues in (L)-configuration and one residue in (D)-configuration.



**Figure 5.3.** Structures of the hexapeptides **1**<sup>1</sup> and **2**<sup>1</sup> and its derivatives (**1i-1l**, **2a-2d**) containing different *N*-alkylations (highlighted in grey). The main chain framework consists of two *N*-methylated residues, 5 amino acid residues in (L)-configuration and one residue in (D)-configuration.

**Cyclic Hexapeptides Including Different Amino Acids**

Table 5.1 summarizes the physicochemical parameters determined for the first eight derivatives differing in position or kind of amino acids (Figure 5.2). They were all assessed as hydrophilic, since the predicted  $\log P$  values were estimated to be  $< -0.8$ . For the compounds **1**, **1g**, and **1h**  $\log D_{7.4}$  values  $< -1.5$  were obtained, whereas the remaining five hexapeptides, containing leucine, showed  $\log D_{7.4}$  values around 0 and were therefore classified as rather moderately lipophilic.

The peptides were further evaluated for passive transcellular permeability in the PAMPA model, in which phospholipids are used as an artificial cell membrane.<sup>2</sup> For PAMPA  $\log P_e > -5.7$  cm/s good permeability can be expected, whereas PAMPA  $\log P_e > -6.3$  cm/s are expected to show only moderate passive permeability.<sup>3</sup> Based on the  $\log P_e$  values of the eight cyclic peptides ( $\log P_e$  of  $< -6.5$  cm/s) only low passive permeability is measured. Therefore, only low passive absorption in the small intestine is suggested. Nevertheless, the rather moderate lipophilic peptides containing leucine could improve  $\log P_e$  in comparison to the more hydrophilic peptides (**1**, **1g**, and **1h**). Testosterone (T) was used as a control compound for transcellular permeability and behaves as expected showing high permeability ( $\log P_e$  of  $-4.3$  cm/s). Atenolol (A) was used as a positive control for paracellular permeability and exhibited a  $\log P_e$  of  $-8.2$  cm/s, which indicates only low transcellular permeability.

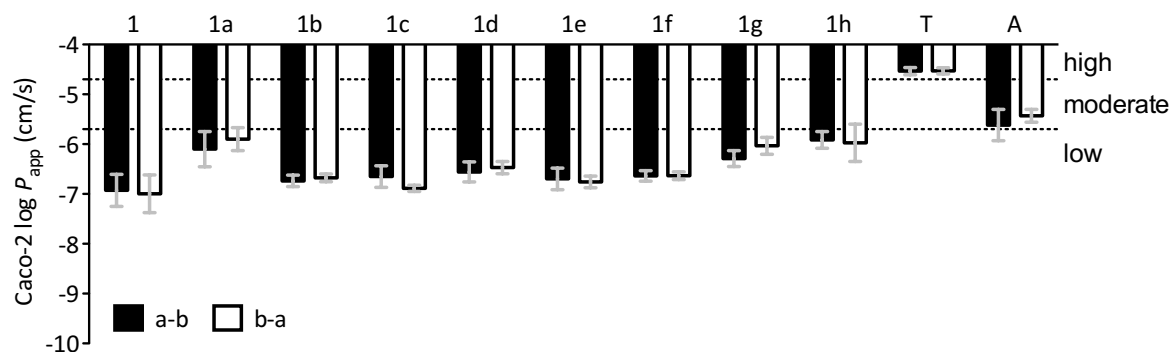
The Caco-2 permeabilities ( $\log P_{app}$ ) of the eight cyclic hexapeptides are illustrated in Figure 5.4. All eight peptides were poorly absorbed, with  $\log P_{app}$  values  $> -5.7$  cm/s, similar as for the cyclic hexapeptide **1**. In contrast to the measured effective permeability and to the  $\log D_{7.4}$  values for the peptides containing leucine, only small differences are observed within the Caco-2 results. With  $\log P_{app}$  values  $-4.5$  cm/s testosterone (T) showed the expected high permeability. Furthermore, atenolol (A) showed  $\log P_{app}$  value between  $-5.6$  and  $-5.4$  cm/s. One of the characteristics of carrier-mediated transport is the imbalance between measured apical to basolateral (a-b) and basolateral to apical (b-a) permeability. Ratios  $> 1.5 - 2$  indicate a possible efflux transport. Therefore, these differences were examined using the Caco-2 cell monolayer model. Compound **1g** showed a ratio  $> 1.5$ , all other peptides and the reference testosterone were found to result in similar ratios below 1.5.



**Table 5.1.** Physicochemical properties of the first eight derivatives of peptide **1** differing in position or kind of amino acids ( $\rightarrow$ **1a-1h**).

Compounds	MW [Da]	PAMPA $\log P_e$ [cm/s] <sup>a</sup>	Caco-2 $\log P_{app}$ [cm/s] <sup>b</sup>		$\log D_{7.4}$ <sup>c</sup>	
			a-b	b-a		
<b>1 (16-CHA)<sup>1</sup></b>	454	-8.3 ± 0.1	-6.9 ± 0.3	-7.0 ± 0.4	1.0	< -1.5
<b>1a</b>	496	-6.8 ± 0.1	-6.1 ± 0.4	-5.9 ± 0.2	1.0	0.1 ± 0.1
<b>1b</b>	496	-7.0 ± 0.1	-6.7 ± 0.1	-6.7 ± 0.1	1.0	-0.1 ± 0.1
<b>1c</b>	496	-6.9 ± 0.0	-6.7 ± 0.2	-6.9 ± 0.1	0.5	0.0 ± 0.1
<b>1d</b>	496	-6.6 ± 0.0	-6.6 ± 0.2	-6.5 ± 0.1	1.1	-0.3 ± 0.1
<b>1e</b>	496	-7.2 ± 0.1	-6.7 ± 0.2	-6.8 ± 0.1	0.8	-0.3 ± 0.0
<b>1f</b>	496	-6.8 ± 0.0	-6.6 ± 0.1	-6.6 ± 0.1	1.0	0.0 ± 0.0
<b>1g</b>	540	-10 ± 0.0	-6.3 ± 0.2	-6.0 ± 0.2	1.9	< -1.5
<b>1h</b>	499	-10 ± 0.0	-5.9 ± 0.2	-6.0 ± 0.4	1.1	< -1.5
<b>Controls</b>						
<b>testosterone<sup>d</sup></b>	288	-4.3 ± 0.0	-4.5 ± 0.1	-4.5 ± 0.1	1.0	3.4 ± 0.0
<b>atenolol<sup>e</sup></b>	266	-8.2 ± 0.2	-5.6 ± 0.3	-5.4 ± 0.1	1.3	< -1.5

a)  $P_e$  = effective permeability: passive permeability through an artificial membrane was determined by the parallel artificial membrane permeability assay (PAMPA) at pH 7.4; values represent the mean with its standard deviation (n = 4); b)  $P_{app}$  = apparent permeability: permeability through cell monolayers was assessed by a Caco-2 assay in the absorptive (a-b) and secretory (b-a) directions after 15, 30, and 60 min; values represent the mean with its corresponding standard deviation (n = 3). Ratios were calculated with the  $P_{app}$  mean values; c) Partition coefficients ( $\log D_{7.4}$ ) were measured by a miniaturised shake-flask procedure at pH 7.4; values represent the mean with its corresponding standard deviation (n = 6); d) A marker of transcellular permeability; e) A marker for paracellular permeability.



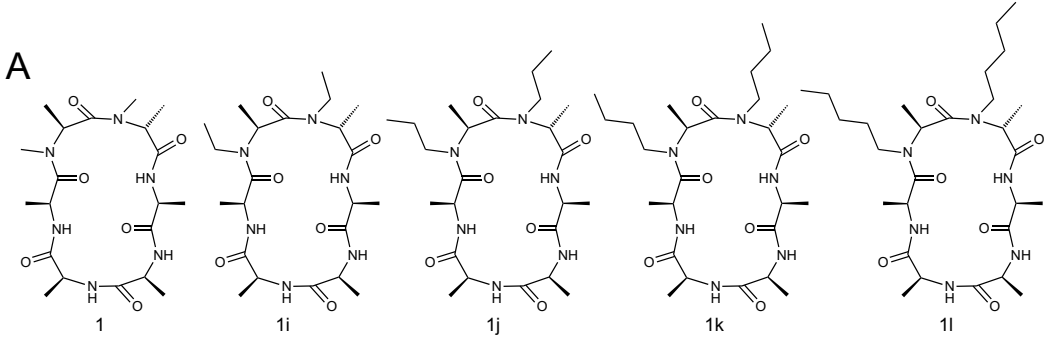
**Figure 5.4.** Caco-2 permeability  $\log P_{app}$  of cyclic hexapeptide **1** (remeasured in-house) and its eight derivatives. Apical to basolateral (a-b, black) compared to basolateral to apical (b-a, white) permeability, values of measurements taken after 15, 30, and 60 min, depicted as permeability coefficient,  $\log P_{app}$  (cm/s) with its corresponding standard deviation. Additionally, two reference compounds testosterone (**T**, a marker of transcellular permeability) and atenolol (**A**, a marker for paracellular permeability) are shown. Dashed lines on the y-axis represent the permeability thresholds from low to moderate ( $\log P_{app} > -5.7$  cm/s) and from moderate to high ( $\log P_{app} > -4.7$  cm/s).<sup>4</sup>

#### Cyclic Hexapeptides with Different N-Alkylations Lengths

Table 5.2 and 5.3 lists the results of the physicochemical and *in vitro* pharmacokinetic properties of the second eight cyclic hexapeptides derivatives with N-alkylations of different chain lengths. The longer the alkyl chain of the N-alkylated hexapeptides (**1** < **1i** < **1j** < **1k** < **1l** and **2** < **2a** < **2b** < **2c** < **2d**) the higher is the  $\log D_{7,4}$ , and the  $\log P_{app}$  b-a Caco-2 permeability, and the better is the effective permeability. However, the Caco-2  $\log P_{app}$  a-b of the two compounds with N-pentyl substituents (**1l** and **2d**) was low ( $\log P_{app} < -5.7$  cm/s), due to their efflux transport potential. Their  $P_{app}$  b-a/a-b ratio is > 2, which indicates an active efflux transport (e.g. P-glycoprotein, P-gp).<sup>5</sup> When **2d** was applied at different concentration (62.5  $\mu$ M, 125  $\mu$ M, and 300  $\mu$ M) saturation of the efflux transport ( $P_{app}$  b-a/a-b ratio 20, 10, 9.1 respectively) could be shown, confirming the involvement of an active efflux transporter. Figure 5.5 illustrate the  $\log P_{app}$  from the Caco-2 experiment in both directions for these cyclic hexapeptides. The Caco-2 permeability experiment was performed with two positive controls, namely testosterone, a marker of transcellular permeability [with  $\log P_{app}$  values around -4.5 cm/s (a-b and b-a)] and atenolol, a marker for paracellular permeability [with  $\log P_{app}$  values around -5.6 cm/s (a-b) to -5.4 cm/s (b-a)] (Table 5.4).

**Table 5.2.** Physiochemical properties of the derivatives of peptide **1** containing different N-alkylation lengths (→**1**, **1i-1l**).

**A**



Compounds	MW	PAMPA $\log P_e$	Caco-2 $\log P_{app}$		$\log D_{7.4}^c$	
	[Da]	[cm/s] <sup>a</sup>	a-b	b-a		
<b>1 (16-CHA)<sup>1</sup></b>	454	-8.3 ± 0.1	-6.9 ± 0.3	-7.0 ± 0.4	1.0	< -1.5
<b>1i</b>	482	-7.8 ± 0.1	-6.9 ± 0.7	-6.6 ± 0.4	1.8	-0.8 ± 0.0
<b>1j</b>	510	-6.9 ± 0.0	-6.3 ± 0.7	-6.0 ± 0.4	1.3	0.3 ± 0.1
<b>1k</b>	538	-6.1 ± 0.1	-5.8 ± 0.1	-5.7 ± 0.2	1.4	1.1 ± 0.1
<b>1l</b>	566	-5.1 ± 0.0	-6.4 ± 0.3	-5.0 ± 0.1	20.7	2.4 ± 0.1

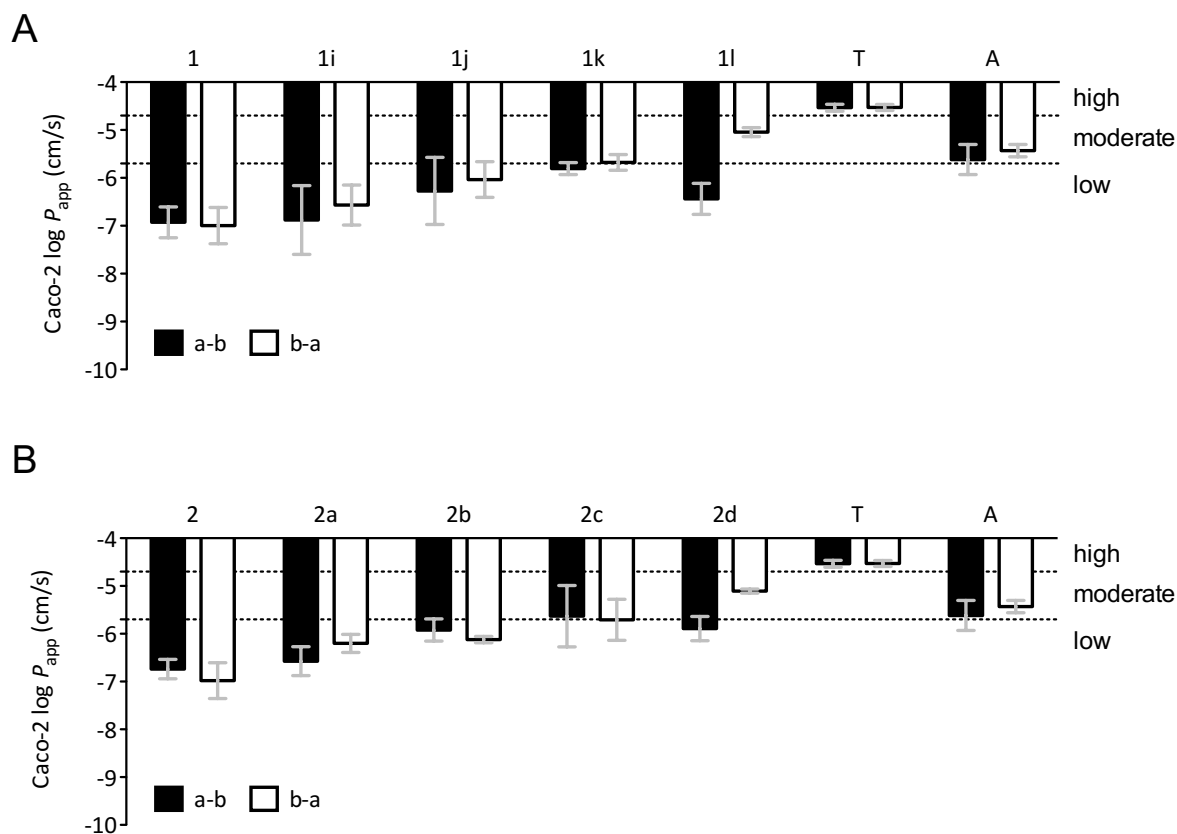
a)  $P_e$  = effective permeability: passive permeability through an artificial membrane was determined by the parallel artificial membrane permeability assay (PAMPA) at pH 7.4; values represent the mean with its standard deviation (n = 4); b)  $P_{app}$  = apparent permeability: permeability through cell monolayers was assessed by a Caco-2 assay in the absorptive (a-b) and secretory (b-a) directions after 15, 30, and 60 min; values represent the mean with its corresponding standard deviation (n = 3). Ratios were calculated with the  $P_{app}$  mean values; c) Partition coefficients ( $\log D_{7.4}$ ) were measured by a miniaturised shake-flask procedure at pH 7.4; values represent the mean with its corresponding standard deviation (n = 6).

**Table 5.3.** Physicochemical properties of the derivatives of peptide **2** containing different N-alkylation lengths ( $\rightarrow$ **2**, **2a-2d**).

**B**

Compounds	MW	PAMPA $\log P_e$	Caco-2 $\log P_{app}$		$\log D_{7.4}^c$	
	[Da]	[cm/s] <sup>a</sup>	a-b	b-a		
<b>2 (15-CHA)<sup>1</sup></b>	454	$-8.2 \pm 0.2$	$-6.7 \pm 0.2$	$-7.0 \pm 0.4$	0.8	$-1.0 \pm 0.1$
<b>2a</b>	482	$-8.3 \pm 0.0$	$-6.6 \pm 0.3$	$-6.2 \pm 0.2$	2.0	$-0.3 \pm 0.1$
<b>2b</b>	510	$-7.3 \pm 0.0$	$-5.9 \pm 0.2$	$-6.1 \pm 0.1$	0.6	$0.7 \pm 0.1$
<b>2c</b>	538	$-6.4 \pm 0.1$	$-5.6 \pm 0.6$	$-5.7 \pm 0.4$	0.5	$1.5 \pm 0.3$
<b>2d</b>	566	$-5.2 \pm 0.0$	$-5.9 \pm 0.3$	$-5.1 \pm 0.0$	5.2	$2.9 \pm 0.1$
			$-6.6 \pm 0.1^*$	$-5.3 \pm 0.0^*$	20	
			$-6.3 \pm 0.0^A*$	$-5.3 \pm 0.0^A*$	10	
			$-6.4 \pm 0.1^B*$	$-5.4 \pm 0.1^B*$	9.5	

a)  $P_e$  = effective permeability: passive permeability through an artificial membrane was determined by the parallel artificial membrane permeability assay (PAMPA) at pH 7.4; values represent the mean with its standard deviation ( $n = 4$ ); b)  $P_{app}$  = apparent permeability: permeability through cell monolayers was assessed by a Caco-2 assay in the absorptive (a-b) and secretory (b-a) directions after 15, 30, and 60 min; values represent the mean with its corresponding standard deviation ( $n = 3$ , \*one point measurements were performed,  $n = 1$ ). Ratios were calculated with the  $P_{app}$  mean values. If not otherwise mentioned the applied concentration was 62.5  $\mu$ M, A) 125  $\mu$ M, and B) 300  $\mu$ M; c) Partition coefficients ( $\log D_{7.4}$ ) were measured by a miniaturised shake-flask procedure at pH 7.4; values represent the mean with its corresponding standard deviation ( $n = 6$ ).



**Figure 5.5.** Caco-2 permeability  $\log P_{app}$  of cyclic hexapeptides A) **1** (remeasured in-house), **1i**, **1j**, **1k**, **1l**. B) **2** (remeasured in house), **2a**, **2b**, **2c**, and **2d**. Apical to basolateral (a-b, black) compared to basolateral to apical (b-a, white) permeability, values of measurements taken after 15, 30, and 60 min, depicted as permeability coefficient,  $P_{app}$  (cm/s) with its corresponding standard deviation ( $n = 3$ ). Additionally, two reference compounds testosterone (**T**, a marker of transcellular permeability) and atenolol (**A**, a marker for paracellular permeability) are shown. Dashes lines on the y-axis represent the permeability thresholds from low to moderate ( $\log P_{app} > -5.7$  cm/s) and from moderate to high ( $\log P_{app} > -4.7$  cm/s).<sup>4</sup>

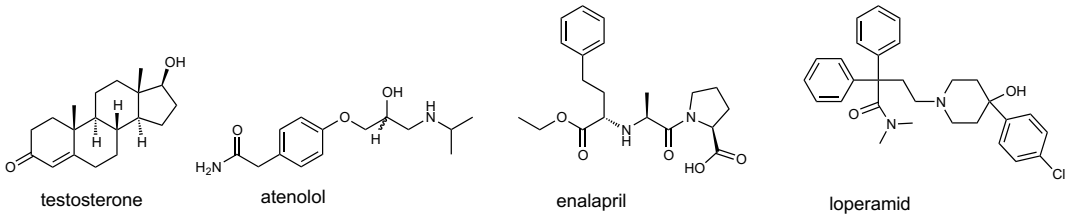
As reported by Ovadia *et al.* (2011), the di-*N*-methylated hexapeptide **1**, showed exceptionally high permeability in their Caco-2 permeation assay ( $\log P_{app} > -5.0$  cm/s), whereas in our Caco-2 permeation assay only low permeability ( $\log P_{app}$  of  $< -5.7$  cm/s) could be detected. Caco-2 results from different laboratories or from different cell batches have to be compared carefully. Culture conditions, such as passage number, seeding density, or post-seeding time before the experiment, can influence transporter expression and therefore Caco-2 permeability results.<sup>6</sup> For this reason, control compounds, e.g. markers for transcellular (testosterone) and paracellular (atenolol) permeability or specific substrates for carrier-mediated transporters (e.g. enalapril for PepT1-mediated transport and loperamide for the *mdr1*-mediated transport) are suggested to be applied in the Caco-2 cell model. Table 5.4 shows various levels of saturation of the transporter *mdr 1* (P-gp), when different concentrations of the substrate loperamide are applied. For enalapril, no uptake with

the PepT1 transporter could be shown, instead efflux transport could be observed, probably masking the uptake. Caco-2 experiments are important to confirm transcellular permeabilities, but not to evaluate paracellular transport or carrier-mediated transport.<sup>7,8</sup> For carrier-mediated transport evaluation overexpressing transporter cell lines studies should be performed.

In conclusion, exchanging an alanine residue in the hexapeptides by a more lipophilic or hydrophilic amino acid does not improve *in vitro* permeability. However, with increasing length of the *N*-alkylation permeability through the membrane is improving. Low to moderate Caco-2  $\log P_{app}$  a-b and high effective permeability is obtained for compound **1l** and **2d**, both with two *N*-pentyl alkylations. For compound **2d**, it was shown that Caco-2  $\log P_{app}$  a-b can be increased by saturation of the efflux transporter.

Finally, before performing *in vivo* pharmacokinetic experiments with **1l** and **2d**, the thermodynamic solubility of these compounds should be determined to show the highest possible dose for oral administration. Furthermore, stability in simulated gastrointestinal fluids, plasma and liver microsomes should be determined.

**Table 5.4.** Physicochemical properties of the control compound testosterone, atenolol, loperamid, and enalapril.

H						
						
Compounds	MW	PAMPA $\log P_e$	Caco-2 $\log P_{app}$			$\log D_{7.4}^c$
	[Da]	[cm/s] / pH <sup>a</sup>	a-b	b-a	b-a/a-b	
testosterone <sup>d</sup>	288	-4.3 ± 0.0 / 7.4	-4.5 ± 0.1	-4.5 ± 0.1	1.0	3.4 ± 0.0
atenolol <sup>e</sup>	266	-8.2 ± 0.2 / 7.4	-5.6 ± 0.3	-5.4 ± 0.1	1.3	< -1.5
loperamid <sup>f,*</sup>	477	-4.2 ± 0.0 / 7.4	-5.0 <sup>A</sup>	-4.5 <sup>A</sup>	3.5	3.6 ± 0.0
			-4.8 <sup>B</sup>	-4.6 <sup>B</sup>	1.3	
			-4.5 <sup>C</sup>	-4.6 <sup>C</sup>	0.8	
enalapril <sup>g,*</sup>	376	-5.9 ± 0.1 / 3.0	-8.1 <sup>D</sup>	-7.0 <sup>D</sup>	39	-1.1 ± 0.1
			-8.1 <sup>E</sup>	-7.0 <sup>E</sup>	18	
			-7.1 ± 0.0 / 7.4	-7.2 <sup>F</sup>	-6.0 <sup>F</sup>	

a)  $P_e$  = effective permeability: passive permeability through an artificial membrane was determined by the parallel artificial membrane permeability assay (PAMPA) at pH 7.4 (if not mentioned otherwise); values represent the mean with its standard deviation (n = 4); b)  $P_{app}$  = apparent permeability: permeability through cell monolayers was assessed by a Caco-2 assay in the absorptive (a-b) and secretory (b-a) directions after 15, 30, and 60 min; values represent the mean with its corresponding standard deviation (n = 3, \*one point measurements were performed, n = 1). Ratios were calculated with the  $P_{app}$  mean values. If not otherwise mentioned the applied concentration was 62.5  $\mu$ M, A) 5  $\mu$ M, and B) 20  $\mu$ M, C) 60  $\mu$ M, D) 80  $\mu$ M, E) 160  $\mu$ M, F) 300  $\mu$ M; c) Partition coefficients ( $\log D_{7.4}$ ) were measured by a miniaturised shake-flask procedure at pH 7.4; values represent the mean with its corresponding standard deviation (n = 6); d) A marker of transcellular permeability; e) A marker for paracellular permeability; f) Substrate of mdr1 transporter; g) Substrate of PepT1 transporter.

### References

1. Ovadia, O.; Greenberg, S.; Chatterjee, J.; Laufer, B.; Opperer, F.; Kessler, H.; Gilon, C.; Hoffman, A. The effect of multiple N-methylation on intestinal permeability of cyclic hexapeptides. *Mol. Pharm.* **2011**, *8*, 479-87.
2. Kansy, M.; Senner, F.; Gubernator, K. Physicochemical high throughput screening: Parallel artificial membrane permeation assay in the description of passive absorption processes. *J. Med. Chem.* **1998**, *41*, 1007-1010.
3. Avdeef, A.; Bendels, S.; Di, L.; Faller, B.; Kansy, M.; Sugano, K.; Yamauchi, Y. PAMPA - Critical factors for better predictions of absorption. *J. Pharm. Sci.* **2007**, *96*, 2893-2909.
4. Hou, T.; Wang, J.; Zhang, W.; Xu, X. ADME evaluation in drug discovery. 7. Prediction of oral absorption by correlation and classification. *J. Chem. Inf. Model* **2007**, *47*, 208-18.
5. Hubatsch, I.; Ragnarsson, E. G. E.; Artursson, P. Determination of drug permeability and prediction of drug absorption in Caco-2 monolayers. *Nat. Protoc.* **2007**, *2*, 2111-2119.
6. Hayashi, R.; Hilgendorf, C.; Artursson, P.; Augustijns, P.; Brodin, B.; Dehertogh, P.; Fisher, K.; Fossati, L.; Hovenkamp, E.; Korjamo, T.; Masungi, C.; Maubon, N.; Mols, R.; Mullertz, A.; Monkkonen, J.; O'Driscoll, C.; Oppers-Tiemissen, H. M.; Ragnarsson, E. G.; Rooseboom, M.; Ungell, A. L. Comparison of drug transporter gene expression and functionality in Caco-2 cells from 10 different laboratories. *Eur. J. Pharm. Sci.* **2008**, *35*, 383-96.
7. Yu, J.; Carrier, R. L.; March, J. C.; Griffith, L. G. Three dimensional human small intestine models for ADME-Tox studies. *Drug Discov. Today* **2014**, *19*, 1587-94.
8. Artursson, P.; Palm, K.; Luthman, K. Caco-2 monolayers in experimental and theoretical predictions of drug transport. *Adv. Drug Deliv. Rev.* **2001**, *46*, 27-43.



### 5.1.1 Paper 6:

#### **Enantiomeric cyclic peptides with different Caco-2 permeability suggest carrier-mediated transport**

This paper addresses the involvement of carrier-mediated transporters in oral uptake of enantiomeric cyclic peptides. The evaluation of lipophilicity ( $\log D$ ) and permeability (Caco-2 cell and PAMPA) was performed to characterize physicochemical properties of cyclic hexapeptide enantiomers.

#### **Contribution to the project:**

Jacqueline Bezençon was responsible for all experiments regarding the physicochemical properties of cyclic hexapeptides. Moreover, she contributed to the writing of the physicochemical part and edited the experimental section on the determination of the physicochemical properties in the supporting information.

The paper was published in the peer-reviewed *Chemistry - A European Journal* in 2015.

U. K. Marelli,\* **J. Bezençon**,\* E. Puig, B. Ernst, H. Kessler, Enantiomeric cyclic peptides with different Caco-2 permeability suggest carrier-mediated transport. *Chem. Eur. J.* **2015**, *21*, 8023-8027.

\*contributed equally.

## ■ Cyclic Peptides

# Enantiomeric Cyclic Peptides with Different Caco-2 Permeability Suggest Carrier-Mediated Transport

Udaya Kiran Marelli,<sup>[a]</sup> Jacqueline Bezençon,<sup>[b]</sup> Eduard Puig,<sup>[a]</sup> Beat Ernst,<sup>\*,[b]</sup> and Horst Kessler<sup>\*,[a]</sup>

**Abstract:** Recently, oral absorption of cyclic hexapeptides was improved by *N*-methylation of their backbone amides. However, the number and position of *N*-methylations or of solvent exposed NHs did not correlate to intestinal permeability, measured in a Caco-2 model. In this study, we investigate enantiomeric pairs of three polar and two lipophilic peptides to demonstrate the participation of carrier-mediated transporters. As expected, all the enantiomeric peptides exhibited identical lipophilicity ( $\log D_{7.4}$ ) and passive transcellular permeability determined by the parallel artificial membrane permeability assay (PAMPA). However, the enantiomeric polar peptides exhibited different Caco-2 permeability ( $P_{app}$ ) in both directions a–b and b–a. The same trend was observed for one of the lipophilic peptide, whereas the second lipophilic enantiomer pair showed identical Caco-2 permeability (within the errors). These findings provide the first evidence for the involvement of carrier-mediated transport for peptides, especially for those of polar nature.

Achieving oral bioavailability in peptides is still a bottleneck in successful peptide-based drug design.<sup>[1]</sup> It has been established that the usual instability of peptides against enzymatic degradation can be overcome by cyclization,<sup>[2]</sup> use of *D*-amino acids<sup>[3]</sup> and/or *N*-methylation.<sup>[4]</sup> However, for the development of new orally available peptides<sup>[5]</sup> and macrocycles<sup>[6]</sup> beyond Lipinski's "rule of 5",<sup>[7]</sup> elucidation of the pathway by which such molecules cross the intestinal epithelia<sup>[8]</sup> is indispensable. Encouraged by the currently accelerating market for peptide drugs,<sup>[1]</sup> efforts to develop orally available peptides attracts considerable attention.<sup>[5,6]</sup> In our previous studies on a library of *N*-methylated Veber–Hirschmann peptides (VHP), *N*-methylation improved permeability was demonstrated by developing

a biologically active and orally bioavailable tri-*N*-methylated VHP.<sup>[9]</sup> Later, some members of a library of 54 *N*-methylated cyclic hexaalanines (CHA) of the general structure cyclo(-*D*-Ala-*L*-Ala-*S*-)<sup>[10]</sup> were shown to be highly permeable. A comprehensive conformational analysis of all these peptides revealed some common backbone structural motifs (Figure 1) being key for promoting intestinal permeability.<sup>[11]</sup> The identified conformations also matched the structural features<sup>[11]</sup> of the orally available peptide drug Cyclosporin A (CsA).<sup>[12]</sup>

Interestingly, several parameters that are usually considered to be crucial for oral availability, such as lipophilicity, number of solvent exposed NHs or number and position of *N*-methyl groups did not correlate to intestinal permeability of the above peptides and the other peptides in the cyclic hexaalanine series.<sup>[9–11]</sup> Although the conformation of peptides was highlighted as a controlling factor for permeability,<sup>[11]</sup> the exact contribution of the various parameters as well as their transport pathway remains to be answered.

In the recent times, *N*-methylation of solvent exposed NHs is projected as the key for achieving permeability in peptides.<sup>[13,14]</sup> For the permeable lipophilic peptide (PLP) cyclo(-*N*Me-*D*-Leu-*N*Me-*L*-Leu-*D*-Pro-*N*Me-*L*-Tyr-*L*-Leu) and analogues thereof there is a correlation between the number of solvent exposed NHs and permeability.<sup>[13,14]</sup> However, in disagreement to these findings, our studies on CHAs exhibited several contradicting cases (Figure 2).<sup>[11]</sup> To highlight it, two cases, *N*Me (1,5) CHA and *N*Me (1,6) CHA, are shown in Figure 2. Both these peptides are highly permeable despite each of them possess two solvent exposed NHs.<sup>[10,11]</sup> Starting from *N*Me (1,5) CHA, further *N*-methylation of any one of the solvent exposed NHs ( $\rightarrow$  *N*Me(1,4,5) or *N*Me(1,2,5) CHA) abrogated permeability, whereas *N*-methylation of both solvent exposed NHs ( $\rightarrow$  *N*Me(1,2,4,5)) restored permeability. On the other hand, for *N*Me (1,6) CHA, even the *N*-methylation of one or both solvent exposed NHs destroyed the permeability. Considering these contradictory observations on CHA peptides, it is evident that the structural properties as solvent exposed NHs, lipophilicity, number and position of *N*-methyl groups alone are unlikely to define the permeability of polar as well as non-polar peptides.

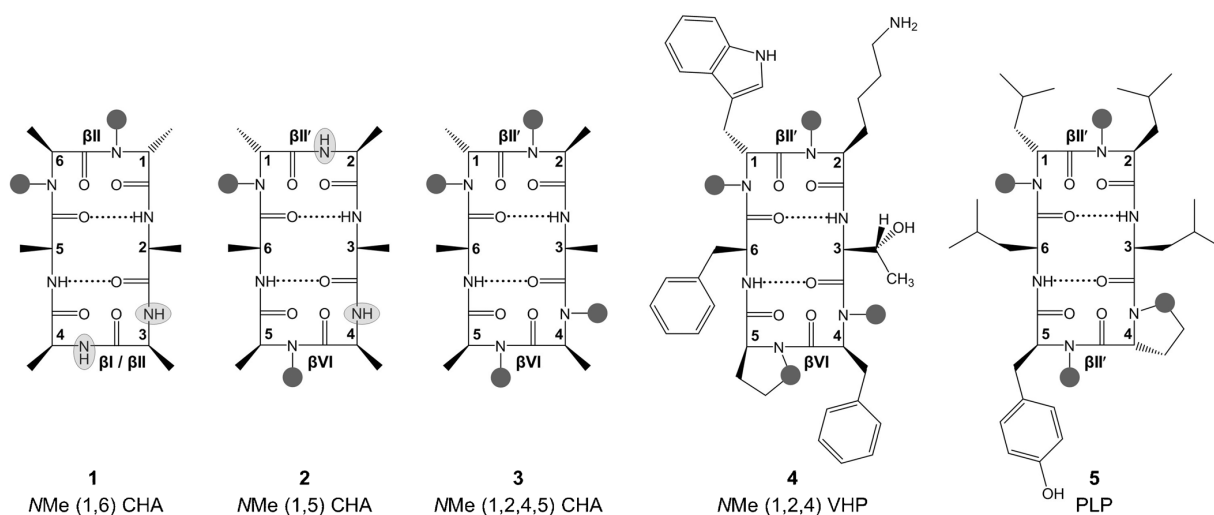
It is well known that the transport of molecules from the small intestine to the portal vein is controlled by cumulative effects of various physicochemical properties of a molecule<sup>[8b,15]</sup> as well as by the biochemical features of the intestinal layers.<sup>[8b,16]</sup> There are two alternative routes—the transcellular and the paracellular—by which a peptide can passively permeate the intestinal walls.<sup>[17]</sup> Whereas the paracellular pathway is

[a] Dr. U. K. Marelli,<sup>+</sup> B. Sc. E. Puig, Prof. Dr. H. Kessler  
Institute for Advanced Study and Center for Integrated Protein Science at the Technische Universität München, Department Chemie  
Lichtenbergstrasse 4, 85747 Garching (Germany)  
E-mail: kessler@tum.de

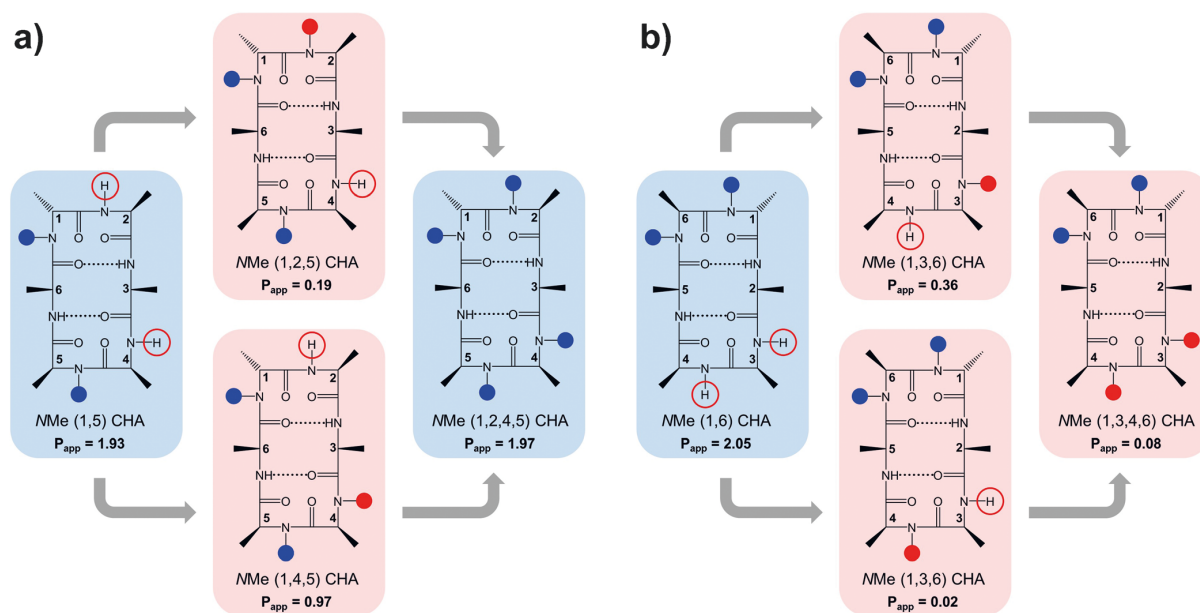
[b] M. Sc. J. Bezençon,<sup>+</sup> Prof. Dr. B. Ernst  
Institute of Molecular Pharmacy, University of Basel  
Klingelbergstrasse 50, 4056 Basel (Switzerland)  
E-mail: beat.ernst@unibas.ch

[\*] Contributed equally to this work.

Supporting information for this article is available on the WWW under <http://dx.doi.org/10.1002/chem.201501270>.



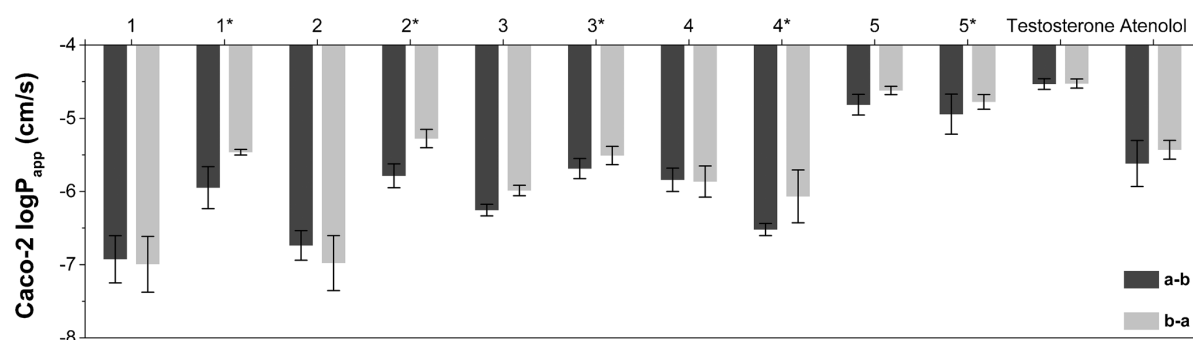
**Figure 1.** Schematic representation of the studied permeable stem peptides.<sup>[9–11,13]</sup> Constituent amino acids of each peptide are numbered in conventional N to C direction starting from the residue in “*d*” configuration. *N*-Methyl groups are labeled with grey dots. The  $\beta$ -turns, hydrogen bonding (shown in dashed lines) and solvent exposed NHs (enclosed in ellipses) as observed in the respective NMR derived conformations are indicated.<sup>[9,11,13]</sup> In the name of each peptide, the positions of *N*-methylated amino acids are indicated in parenthesis. While all peptides shown here exhibit a double  $\beta$ -turn conformation, peptides 2, 3 and 4 exhibit even the identical  $\beta$ -turn subtypes ( $\beta$ I' and  $\beta$ VI).<sup>[9,11]</sup> For stereo views of the NMR derived structures of peptides, please see Supporting Information.



**Figure 2.** Scheme to show the effect of sequential *N*-methylation of solvent exposed NHs (encircled in red, please see Supporting Information for temperature coefficients and conformation) on the Caco-2 permeability of a) NMe (1,5) CHA and b) NMe (1,5) CHA. *N*-Methyl groups that are favoring or prohibiting permeability are labeled with blue or red dots, respectively. Caco-2  $P_{app}$  values are in units of  $10^{-6} \text{ cm s}^{-1}$ . While peptides with high Caco-2 permeability are in blue background, the others are in red background. Except for NMe (1,2,4,5) CHA, which is derived by *N*-methylation of both the solvent exposed NHs in NMe (1,5) CHA, in all other cases, converting the solvent exposed NHs to *N*-methyl groups destroyed the permeability of the parent peptides NMe (1,5) CHA and NMe (1,6) CHA.<sup>[10,11]</sup>

dependent on molecular size, the transcellular pathway can be mimicked by the parallel artificial membrane permeability assay (PAMPA).<sup>[17]</sup> Since there is a rough correlation between

lipophilicity and passive transcellular transport,<sup>[17b,18]</sup> some lipophilic peptides may exhibit intestinal absorption by this route. In contrast, a subset of biologically active peptides with do-



**Figure 3.**  $\log_{10}$  of apparent permeabilities ( $P_{app}$ )  $\pm$  standard deviation from the Caco-2 permeability assay for the pairs of enantiomers and the controls atenolol (a marker for paracellular permeability) and testosterone (a marker for transcellular permeability).

mains of non-lipophilic amino acids might benefit from a paracellular uptake through the tight junctions or from active carrier-mediated transport systems.<sup>[8b, 19, 20]</sup>

To prove the stereospecific as well as conformation specific transport of peptides and therefore the involvement of chiral biological transport systems, we have analyzed enantiomeric pairs of peptides (Figure 1, Table 1), that is, three polar *N*-methylated CHAs (1–3),<sup>[10, 11]</sup> the oral available and lipophilic tri-*N*-methylated VHP (4),<sup>[9]</sup> and the lipophilic PLP (5).<sup>[13]</sup> In case chiral biological transport systems are involved, it is expected that the pairs of peptide enantiomers will behave differently.

Table 1 and Figure 3 summarize the experimental distribution coefficients ( $\log D_{7.4}$ ) and permeabilities of the studied peptides, determined by a miniaturized shake-flask  $\log D_{7.4}$  assay,<sup>[21]</sup> the PAMPA assay<sup>[17a]</sup> and the Caco-2 cell permeation assay (see Supporting Information for experimental details).<sup>[22]</sup>

As expected, the  $\log D_{7.4}$  values for pairs of enantiomers are identical. However, conformational differences or the number of *N*-methylations slightly influence their lipophilicity. Thus, among the enantiomer pairs 1 & 1\* and 2 & 2\* (Figure 1), which have identical molecular weights, equal numbers of *N*-methyl groups and solvent exposed NHs, show different  $\log D_{7.4}$  values, probably as a result of their conformational differences. For the peptides 3 & 3\*

**Table 1.**  $\log D_{7.4}$ ,<sup>[21]</sup> PAMPA<sup>[17a]</sup> permeability ( $\log P_e$ ) and Caco-2 permeability ( $P_{app}$ )<sup>[22a]</sup> values of the enantiomer pairs of the *N*-methylated CHAs 1 & 1\*, 2 & 2\*, 3 & 3\*, the tri-*N*-methylated VHP 4 & 4\* and PLPs 5 & 5\*. While single letter codes of amino acids are used to give the peptide sequence, the *D*- and *L*-amino acids are represented by lower case and upper case letters, respectively. \* implies the enantiomers, CHA=cyclic hexalanine, VHP=Veber–Hirschmann peptide and PLP=permeable lipophilic peptide; in peptide sequences, code letters shown in bold font indicate *N*-methylated amino acids.

Peptide number, name, sequence, position of amino acid and position of <i>N</i> -methylation	No.	Name	1 2 3 4 5 6						$\log D_{7.4}$ <sup>[a]</sup>	PAMPA $\log P_e$ <sup>[b]</sup> [ $\text{cm s}^{-1}$ ]/pH	Caco-2 $P_{app}$ <sup>[c]</sup> [ $10^{-6} \text{ cm s}^{-1}$ ]		
			a	A	A	A	A	A			a–b	b–a	b–a/a–b
1	<i>N</i> Me (1,6) CHA	<b>a</b>	A	A	A	A	A	<–1.5	–8.3 $\pm$ 0.1/7.4	0.15 $\pm$ 0.10	0.15 $\pm$ 0.15	1.0	
1*	<i>N</i> Me (1,6) CHA*	<b>A</b>	a	a	a	a	a	<–1.5	–8.2 $\pm$ 0.0/7.4	1.34 $\pm$ 0.76	3.45 $\pm$ 0.30	2.6	
2	<i>N</i> Me (1,5) CHA	<b>a</b>	A	A	A	A	A	–1.0 $\pm$ 0.1	–8.2 $\pm$ 0.2/7.4	0.20 $\pm$ 0.09	0.15 $\pm$ 0.13	0.8	
2*	<i>N</i> Me (1,5) CHA*	<b>A</b>	a	a	a	a	a	–1.1 $\pm$ 0.1	–8.3 $\pm$ 0.1/7.4	1.75 $\pm$ 0.69	5.48 $\pm$ 1.44	3.1	
3	<i>N</i> Me (1,2,4,5) CHA	<b>a</b>	<b>A</b>	<b>A</b>	<b>A</b>	<b>A</b>	<b>A</b>	–0.8 $\pm$ 0.1	–7.0 $\pm$ 0.0/7.4	0.56 $\pm$ 0.10	1.04 $\pm$ 0.17	1.9	
3*	<i>N</i> Me (1,2,4,5) CHA*	<b>A</b>	<b>a</b>	<b>a</b>	<b>a</b>	<b>a</b>	<b>a</b>	–0.7 $\pm$ 0.1	–7.1 $\pm$ 0.0/7.4	2.15 $\pm$ 0.70	3.22 $\pm$ 0.94	1.5	
4	<i>N</i> Me (1,2,4) VHP	<b>w</b>	<b>K</b>	<b>T</b>	<b>F</b>	<b>P</b>	<b>F</b>	2.0 $\pm$ 0.2	–7.1 $\pm$ 0.7/5.0	1.53 $\pm$ 0.56	1.51 $\pm$ 0.72	1.0	
4*	<i>N</i> Me (1,2,4) VHP*	<b>W</b>	<b>k</b>	<b>t</b>	<b>f</b>	<b>p</b>	<b>f</b>	2.1 $\pm$ 0.2	–10 $\pm$ 0.0/7.4	0.31 $\pm$ 0.06	1.14 $\pm$ 0.87	3.7	
5	PLP	<b>l</b>	<b>L</b>	<b>L</b>	<b>p</b>	<b>Y</b>	<b>L</b>	>3.0	–4.6 $\pm$ 0.0/5.0	16 $\pm$ 4.6	24 $\pm$ 3.2	1.5	
5*	PLP*	<b>L</b>	<b>l</b>	<b>l</b>	<b>P</b>	<b>y</b>	<b>l</b>	>3.0	–4.3 $\pm$ 0.1/3.0	13 $\pm$ 5.6	17 $\pm$ 3.6	1.3	
testosterone	–	–	–	–	–	–	–	3.4 $\pm$ 0.0	–4.3 $\pm$ 0.0/7.4	29.6 $\pm$ 4.70	30.0 $\pm$ 4.15	1.0	
atenolol	–	–	–	–	–	–	–	<–1.5	–8.2 $\pm$ 0.2/7.4	2.91 $\pm$ 1.69	3.87 $\pm$ 1.20	1.3	

[a] Octanol–water distribution coefficients ( $\log D_{7.4}$ ) were determined by a miniaturized shake-flask procedure at pH 7.4, values represent the mean  $\pm$  standard deviation of sexuplicate measurements.<sup>[21]</sup> [b]  $P_e$ =effective permeability: passive permeation through an artificial membrane was determined by the parallel artificial membrane permeability assay (PAMPA), values represent the mean  $\pm$  standard deviation of quadruplicate measurements performed at the indicated pH.<sup>[17a]</sup> [c]  $P_{app}$ =apparent permeability: permeation through a Caco-2 cell monolayer was assessed in the absorptive apical to basolateral (a–b) and secretory basolateral to apical (b–a) directions in triplicates at three different time points, values represent the mean  $\pm$  standard deviation.<sup>[22a]</sup>

(Figure 1) that exhibit identical conformations to 2 & 2\*<sup>[11]</sup> the two additional *N*-methylations present in the tetra-*N*-methylated CHA peptide increase lipophilicity ( $\log D_{7.4}$ ). Furthermore, the addition of amino acids with hydrophobic side chains as present in 4 & 4\* and 5 & 5\* substantially increase lipophilicity even in the presence of a lysine residue (4 & 4\*).

Similar to the distribution coefficients  $\log D_{7.4}$ , two additional *N*-methylations (**3** & **3\***) or the introduction of amino acids with lipophilic side chains (**4** & **4\***) also improved the PAMPA permeability  $\log P_e$  values. However, a comparison of the  $\log P_e$  values with the guidelines for PAMPA permeability<sup>[23]</sup> predict their low absorption potential ( $\log P_e < -6.3 \text{ cm s}^{-1}$ , membrane retention  $< 0.8$ ). Because somatostatin derivative **4** and its enantiomer **4\*** contain the primary amine of a lysine, PAMPA permeability was measured at different pH (3.0, 5.0 and 7.4) to take account for the pH-dependent protonation states. However, different pH of the solvent did not change their low PAMPA absorption potential. Nevertheless, at pH 7.4, a membrane retention of 70 and 60% was measured for enantiomers **4** and **4\***, respectively. In addition, at pH 3.0 and 5.0, a membrane retention of 30% was detected for compound **4**. The enantiomer pair **5** & **5\*** show good PAMPA permeability ( $\log P_e > -4.6 \text{ cm s}^{-1}$ ) due to their high lipophilicity.

Despite the various pairs of enantiomers having identical lipophilicities ( $\log D_{7.4}$ ) and PAMPA permeabilities ( $\log P_e$ ), their Caco-2  $P_{app}$  values showed differences (Table 1, Figure 3) except for **5** & **5\***. For the CHA peptides, the enantiomers (**1\***, **2\*** and **3\***) containing one *L*-alanine and five *D*-alanines exhibited higher  $P_{app}$  values in the Caco-2 assay compared to their corresponding parent enantiomers (**1**, **2** and **3**). The increased  $P_{app}$  values for **1\***, **2\*** and **3\*** can be observed for the apical to basolateral (a–b) as well as for basolateral to apical (b–a) direction. Whereas **1\*** and **2\*** showed an approximately nine-fold higher a–b permeability than their corresponding enantiomers **1** and **2**, the a–b permeability for **3\*** is approximately four-fold higher than that of **3**. Similarly, the b–a permeabilities for **1\***, **2\*** and **3\*** are ~23-, ~36- and ~3-fold higher than **1**, **2** and **3**, respectively. The efflux transport of the peptides has been analyzed from the Caco-2  $P_{app}$  ratio, (RO) = (b–a)/(a–b). Overall, **1\*** (RO = 2.6), **2\*** (RO = 3.1), and **3** (RO = 1.9) show a possible efflux transport (RO > 1.5),<sup>[22e]</sup> whereas **1** (RO = 1.0), **2** (RO = 0.8), and **3\*** (RO = 1.5) showed no indication for an efflux transport.

Similar to the pairs of enantiomeric CHA peptides, the enantiomers of VHP **4** & **4\*** also exhibited differential Caco-2 permeability. However, in contrast to the polyalanine peptides, peptide **4\*** consisting of six different amino acids, one with *L*- and five with *D*-configuration, has a lower Caco-2  $P_{app}$  (in both a–b and b–a directions) compared with the parent tri-*N*-methylated peptide **4**. For peptide **4\*** (RO = 3.7) an efflux transport can be assumed compared to **4** (RO = 1.0). In contrast, peptides **5** & **5\*** exhibited very marginal differences in their Caco-2  $P_{app}$  values. Both (a–b) and (b–a)  $P_{app}$  values for **5** & **5\*** are almost identical within the error bar limits. Furthermore, the RO values 1.5 and 1.3 for **5** and **5\*** do not indicate a carrier-mediated transport involved.

In summary, the present study suggests carrier-mediated transport through Caco-2 cell membranes for polar CHA peptides. This transport is associated with the recognition of their spatial structures. While the identification of distinct conformations as a necessary condition for high permeability<sup>[11]</sup> gave indirect evidence for receptor participation, the present results provide unequivocal proof for the participation of an active transport pathway for these peptides.<sup>[8b]</sup> Further we demon-

strated in this communication that configurational issues, that is, a cyclic peptide should exhibit the “right” chirality, can have an influence on permeability.

In the case of **4**, although different Caco-2 permeability of its enantiomer supports a carrier mediated transport, its much higher  $\log D_{7.4}$  value of 2 and PAMPA membrane retention might also contribute partially to its oral availability.<sup>[9]</sup> On the other hand, in the case of the high lipophilic ( $\log D_{7.4} > 3$ ) and high PAMPA permeable ( $\log P_e > -4.6 \text{ cm s}^{-1}$ ) peptides **5** and **5\*** the dominant transport pathway was shown to be the passive transcellular permeation.

Further proof for the interpretation on the crucial role of conformation comes from our previous study on the library of *N*-methylated VHPs.<sup>[9]</sup> There, we also reported an epimeric analogue of **4** (a diastereomer in which one of the many chiral centers is inverted, called here as **4<sub>ep</sub>**).<sup>[9]</sup> In **4<sub>ep</sub>**, the configuration of the *L*-phenylalanine at position 4 has been switched to *D*-phenylalanine. This resulted not only in loss of biological activity but it also exhibited very poor permeability compared to **4**.<sup>[9]</sup> It has to be noted that the backbone conformation of the epimer (**4<sub>ep</sub>**) is similar to that in **4** (two  $\beta$  turns about the same amino acids, all solvent exposed NH protons *N*-methylated, Figure 1) except that the  $\beta$ VI turn containing a *cis* peptide bond about *L*-Phe<sup>4</sup>*L*-Pro<sup>5</sup> in **4** is replaced by a  $\beta$ II' turn about *D*-Phe<sup>4</sup>*L*-Pro<sup>5</sup> in **4<sub>ep</sub>**.

In conclusion, the spatial structure—conformation and configuration—of peptides has a significant influence not only on their biological activity but also on their intestinal permeability through carrier-mediated transporters.

## Acknowledgement

Financial support by the Deutsche Forschungsgemeinschaft (Reinhart Koselleck grant KE 147/42-1 and CIPSM) is gratefully acknowledged.

**Keywords:** conformation · cyclic peptides · enantioselectivity · intestinal permeability · oral availability

- [1] a) L. Otvos, Jr, *Methods Mol. Biol.* **2008**, *494*, 1–8; b) S. R. Gracia, K. Gaus, N. Sewald, *Future Med. Chem.* **2009**, *1*, 1289–1310; c) A. A. Kaspar, J. M. Reichert, *Drug Discovery Today* **2013**, *18*, 807–817.
- [2] H. Kessler, *Angew. Chem. Int. Ed. Engl.* **1982**, *21*, 512–523; *Angew. Chem.* **1982**, *94*, 509–520.
- [3] a) H. Kessler, B. Kutscher, A. Klein, *Liebigs Ann. Chem.* **1986**, 893–913; b) M. Aumailley, M. Gurrath, G. Müller, J. Calvete, R. Timpl, H. Kessler, *FEBS Lett.* **1991**, *291*, 50–54.
- [4] a) J. Chatterjee, C. Gilon, A. Hoffman, H. Kessler, *Acc. Chem. Res.* **2008**, *41*, 1331–1342; b) J. Chatterjee, B. Laufer, H. Kessler, *Nat. Protoc.* **2012**, *7*, 432–444; c) J. Chatterjee, F. Rechenmacher, H. Kessler, *Angew. Chem. Int. Ed.* **2013**, *52*, 254–269; *Angew. Chem.* **2013**, *125*, 268–283.
- [5] a) M. Morishita, N. A. Peppas, *Drug Discovery Today* **2006**, *11*, 905–910; b) D. J. Craik, D. P. Fairlie, S. Liras, D. Price, *Chem. Biol. Drug Des.* **2013**, *81*, 136–147; c) J. E. Bock, J. Gavenonis, J. A. Kritzer, *ACS Chem. Biol.* **2013**, *8*, 488–499; d) J. Renukuntla, A. D. Vadlapudi, A. Patel, S. H. Boddu, A. K. Mitra, *Int. J. Pharm.* **2013**, *447*, 75–93; e) A. T. Bockus, C. M. McEwen, R. S. Lokey, *Curr. Top. Med. Chem.* **2013**, *13*, 821–836.
- [6] a) F. Giordanetto, J. Kihlberg, *J. Med. Chem.* **2014**, *57*, 278–295; b) C. Heinis, *Nat. Chem. Biol.* **2014**, *10*, 696–698; c) A. K. Yudin, *Chem. Sci.* **2015**, *6*, 30–49.

- [7] a) C. A. Lipinski, *J. Pharmacol. Toxicol. Methods* **2000**, *44*, 235–249; b) C. A. Lipinski, F. Lombardo, B. W. Dominy, P. J. Feeney, *Adv. Drug Delivery Rev.* **2001**, *46*, 3–26.
- [8] a) L. Di, E. H. Kerns, K. Fan, O. J. McConnell, G. T. Carter, *Eur. J. Med. Chem.* **2003**, *38*, 223–232; b) K. Sugano, M. Kansy, P. Artursson, A. Avdeef, S. Bendels, L. Di, G. F. Ecker, B. Faller, H. Fischer, G. Gerebtzoff, H. Lennernaes, F. Senner, *Nat. Rev. Drug Discovery* **2010**, *9*, 597–614.
- [9] E. Biron, J. Chatterjee, O. Ovadia, D. Langenegger, J. Brueggen, D. Hoyer, H. A. Schmid, R. Jelinek, C. Gilon, A. Hoffman, H. Kessler, *Angew. Chem. Int. Ed.* **2008**, *47*, 2595–2599; *Angew. Chem.* **2008**, *120*, 2633–2637.
- [10] O. Ovadia, S. Greenberg, J. Chatterjee, B. Laufer, F. Opperer, H. Kessler, C. Gilon, A. Hoffman, *Mol. Pharm.* **2011**, *8*, 479–487.
- [11] J. G. Beck, J. Chatterjee, B. Laufer, M. U. Kiran, A. O. Frank, S. Neubauer, O. Ovadia, S. Greenberg, C. Gilon, A. Hoffman, H. Kessler, *J. Am. Chem. Soc.* **2012**, *134*, 12125–12133.
- [12] a) A. Ruegger, M. Kuhn, H. Lichti, H. R. Loosli, R. Huguenin, C. Quiquerez, A. von Wartburg, *Helv. Chim. Acta* **1976**, *59*, 1075–1092; b) J. F. Tjia, I. R. Webber, D. J. Back, *Br. J. Clin. Pharmacol.* **1991**, *31*, 344–346; c) J. C. Kolars, W. M. Awani, R. M. Merion, P. B. Watkins, *Lancet* **1991**, *338*, 1488–1490; d) J. F. Borel, *Wien Klin. Wochenschr.* **2002**, *114*, 433–437.
- [13] T. R. White, C. M. Renzelman, A. C. Rand, T. Rezai, C. M. McEwen, V. M. Gelev, R. A. Turner, R. G. Linington, S. S. Leung, A. S. Kalgutkar, J. N. Bauman, Y. Zhang, S. Liras, D. A. Price, A. M. Mathiowetz, M. P. Jacobson, R. S. Lokey, *Nat. Chem. Biol.* **2011**, *7*, 810–817.
- [14] a) T. Rezai, J. E. Bock, M. V. Zhou, C. Kalyanaraman, R. S. Lokey, M. P. Jacobson, *J. Am. Chem. Soc.* **2006**, *128*, 14073–14080; b) T. Rezai, B. Yu, G. L. Millhauser, M. P. Jacobson, R. S. Lokey, *J. Am. Chem. Soc.* **2006**, *128*, 2510–2511; c) T. A. Hill, R. J. Lohman, H. N. Hoang, D. S. Nielsen, C. C. Scully, W. M. Kok, L. Liu, A. J. Lucke, M. J. Stoermer, C. I. Schroeder, S. Chaousis, B. Colless, P. V. Bernhardt, D. J. Edmonds, D. A. Griffith, C. J. Rotter, R. B. Ruggeri, D. A. Price, S. Liras, D. J. Craik, D. P. Fairlie, *ACS Med. Chem. Lett.* **2014**, *5*, 1148–1151; d) D. S. Nielsen, H. N. Hoang, R. J. Lohman, T. A. Hill, A. J. Lucke, D. J. Craik, D. J. Edmonds, D. A. Griffith, C. J. Rotter, R. B. Ruggeri, D. A. Price, S. Liras, D. P. Fairlie, *Angew. Chem. Int. Ed.* **2014**, *53*, 12059–12063; e) C. K. Wang, S. E. Northfield, B. Colless, S. Chaousis, I. Hamernig, R. J. Lohman, D. S. Nielsen, C. I. Schroeder, S. Liras, D. A. Price, D. P. Fairlie, D. J. Craik, *Proc. Natl. Acad. Sci. USA* **2014**, *111*, 17504–17509; f) W. M. Hewitt, S. S. Leung, C. R. Pye, A. R. Ponkey, M. Bednarek, M. P. Jacobson, R. S. Lokey, *J. Am. Chem. Soc.* **2015**, *137*, 715–721.
- [15] G. M. Pauletti, S. Gangwar, G. T. Knipp, M. M. Nerurkar, F. W. Okumu, K. Tamura, T. J. Siahhan, R. T. Borchardt, *J. Controlled Release* **1996**, *41*, 3–17.
- [16] M. Boegh, H. M. Nielsen, *Basic Clin. Pharmacol. Toxicol.* **2015**, *116*, 179–186.
- [17] a) M. Kansy, F. Senner, K. E. Gubernator, *J. Med. Chem.* **1998**, *41*, 1007–1010; b) A. Avdeef, *Expert Opin. Drug Metab. Toxicol.* **2005**, *1*, 325–342; c) E. H. Kerns, L. Di, S. Petusky, M. Farris, R. Ley, P. Jupp, *J. Pharm. Sci.* **2004**, *93*, 1440–1453; d) B. Faller, *Curr. Drug Metab.* **2008**, *9*, 886–892.
- [18] a) J. M. Reis, B. Sinkó, C. H. Serra, *Mini-Rev. Med. Chem.* **2010**, *10*, 1071–1076; b) E. Rutkowska, K. Pajak, K. Józwiak, *Acta Pol. Pharm.* **2013**, *70*, 3–18.
- [19] a) G. M. Pauletti, F. W. Okumu, R. T. Borchardt, *Pharm. Res.* **1997**, *14*, 164–168; b) P. D. Ward, T. K. Tippin, D. R. Thakker, *Pharm. Sci. Technology Today* **2000**, *3*, 346–358.
- [20] a) A. Tsuji, I. Tamai, *Pharm. Res.* **1996**, *13*, 963–977; b) P. D. Dobson, D. B. Kell, *Nat. Rev. Drug Discovery* **2008**, *7*, 205–220; c) D. B. Kell, P. D. Dobson, S. G. Oliver, *Drug Discovery Today* **2011**, *16*, 704–714.
- [21] M. Kah, C. D. Brown, *Chemosphere* **2008**, *72*, 1401–1408; b) M. J. Waring, *Expert Opin. Drug Discovery* **2010**, *5*, 235–248.
- [22] a) G. Wilson, I. F. Hassan, C. J. Dix, I. Williamson, R. Shah, M. Mackay, *J. Comput. Chem.* **1990**, *11*, 25–40; b) P. Artursson, J. Karlsson, *Biochem. Biophys. Res. Commun.* **1991**, *175*, 880–885; c) P. Artursson, K. Palm, K. Luthman, *Adv. Drug Delivery Rev.* **2001**, *46*, 27–43; d) R. B. van Breemen, Y. Li, *Expert Opin. Drug Metab. Toxicol.* **2005**, *1*, 175–185; e) I. Hubatsch, E. G. Ragnarsson, P. Artursson, *Nat. Protoc.* **2007**, *2*, 2111–2119; f) B. Press, D. Di Grandi, *Curr. Drug Metab.* **2008**, *9*, 893–900; g) D. A. Volpe, *Future Med. Chem.* **2011**, *3*, 2063–2077.
- [23] A. Avdeef, S. Bendels, L. Di, B. Faller, M. Kansy, K. Sugano, Y. Yamauchi, *J. Pharm. Sci.* **2007**, *96*, 2893–2909.

Received: March 31, 2015  
Published online on April 27, 2015



# CHEMISTRY

## A **European** Journal

### Supporting Information

#### **Enantiomeric Cyclic Peptides with Different Caco-2 Permeability Suggest Carrier-Mediated Transport**

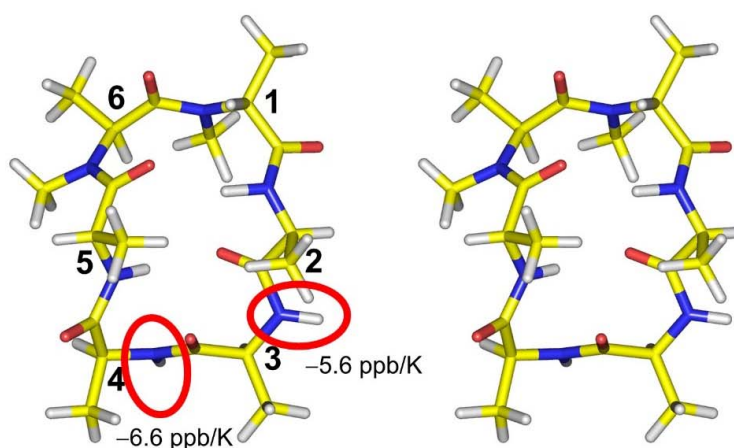
Udaya Kiran Marelli,<sup>[a]</sup> Jacqueline Bezençon,<sup>[b]</sup> Eduard Puig,<sup>[a]</sup> Beat Ernst,<sup>\*,[b]</sup> and Horst Kessler<sup>\*,[a]</sup>

chem\_201501270\_sm\_miscellaneous\_information.pdf

**Synthesis:** Synthesis of the stem peptides is described previously [see main text references 9,10 and 13]. All enantiomeric compounds were synthesized as described for the stem peptides but using enantiomeric amino acid precursors. All (achiral) physicochemical properties between enantiomeric pairs are identical.

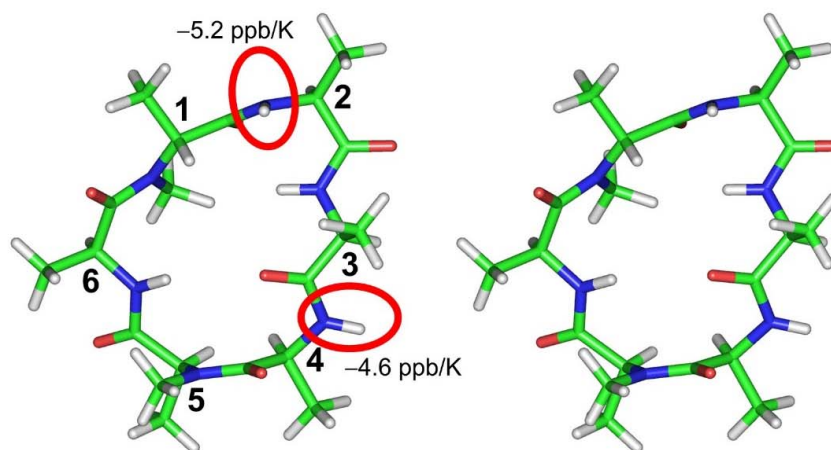
**Conformation of the compounds:** Conformational characterization of the cyclic peptides was done by solution state NMR in DMSO- $d_6$  and MD, and was described in the literature [see main text references 9 and 11]. For convenience, here we are providing the stereo views of the structures determined by us for the four stem peptides **1**, **2**, **3** and **4**. Furthermore, solvent exposed NHs are enclosed in ellipses (red color) and the corresponding NMR temperature coefficients are indicated [see main text reference 11].

**Supporting Figure 1:** Stereo view of the NMR derived conformation of **1**. Backbone amide NHs of the Ala<sup>3</sup> and Ala<sup>4</sup> residues are solvent exposed.

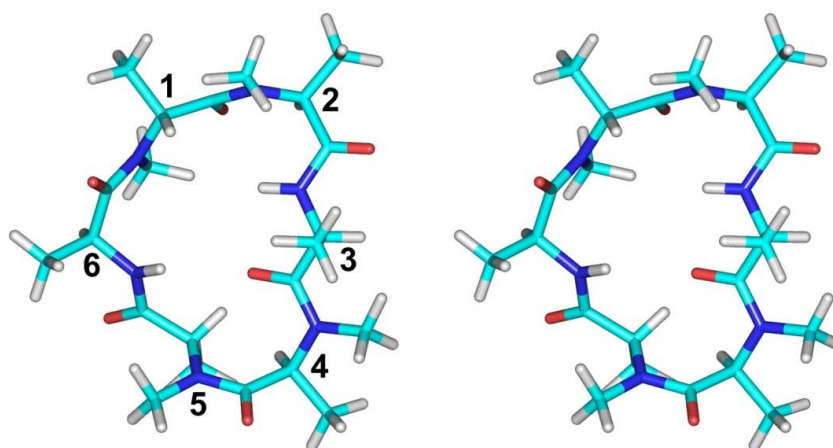


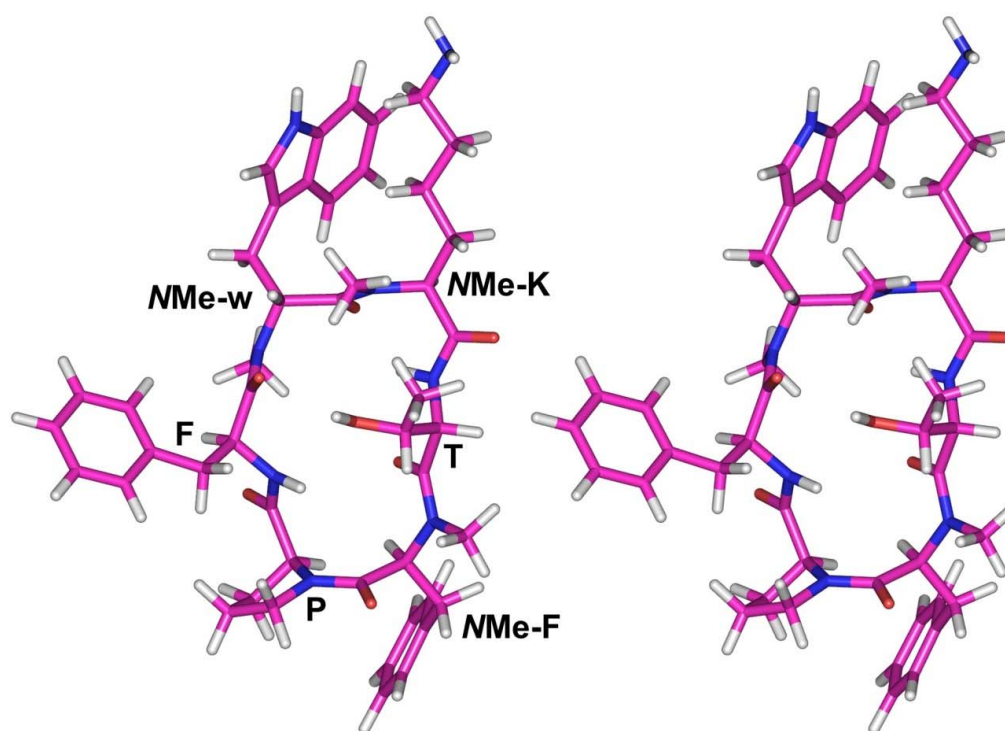


**Supporting Figure 2:** Stereo view of the NMR derived conformation of **2**. Backbone amide NHs of the Ala<sup>2</sup> and Ala<sup>4</sup> residues are solvent exposed.



**Supporting Figure 3:** Stereo view of the NMR derived conformation of **3**.



**Supporting Figure 4:** Stereo view of the NMR derived conformation of **4**.**Determination of physicochemical and in vitro pharmacokinetic parameters.**

**Materials:** Dimethyl sulfoxide (DMSO), 1-octanol, Dulbecco's modified Eagle's medium (DMEM) high glucose, L-glutamine solution, penicillin-streptomycin solution, Dulbecco's phosphate-buffered saline (DPBS), trypsin-EDTA solution and atenolol were purchased from Sigma-Aldrich. MEM nonessential amino acid (MEM-NEAA) solution, fetal bovine serum (FBS), and DMEM without sodium pyruvate and phenol red were bought from Invitrogen (Basel, Switzerland). PAMPA System Solution, GIT-0 Lipid solution, and Acceptor Sink Buffer were ordered from plon (Woburn, MA) and acetonitrile (MeCN) was from Acros Organics (Geel, Belgium). Testosterone is from P. H. Stehelin & Co (Basel, Switzerland). The Caco-2 cells were kindly provided by

Prof. G. Imanidis, FHNW, Muttenz, Switzerland and originated from the American Type Culture Collection (Rockville, MD, USA).

**Parallel artificial membrane permeability assay (PAMPA):** Values of  $\log P_e$  were determined in a 96-well format with the PAMPA permeability assay. For each compound, measurements were performed in quadruplicate at pH value 7.4 (for compound **4**, **4\***, **5**, and **5\*** pH 3.0 and 5.0 were measured additionally). For this purpose, wells of a deep-well plate were filled with 650  $\mu\text{L}$  System Solution. Samples (150  $\mu\text{L}$ ) were withdrawn from each well to determine the blank spectra by UV spectroscopy (SpectraMax 190). Then, analyte dissolved in DMSO was added to the remaining System Solution to yield 50  $\mu\text{M}$  solutions. To exclude precipitation, the optical density was measured at 650 nm, with 0.01 being the threshold value. Solutions exceeding this threshold were filtered. Afterwards, samples (150  $\mu\text{L}$ ) were withdrawn to determine the reference spectra. Further 200  $\mu\text{L}$  were transferred to each well of the donor plate of the PAMPA sandwich P/N 110 163 (plon, Woburn MA, USA). The filter membranes at the bottom of the acceptor plate were impregnated with 5  $\mu\text{L}$  of GIT-0 Lipid Solution each, and 200  $\mu\text{L}$  of Acceptor Sink Buffer were filled into each acceptor well. The sandwich was assembled, placed in the Gut-Box, and left undisturbed for 16 h. It was then disassembled, and samples (150  $\mu\text{L}$ ) were transferred from each donor and acceptor well to 96 well plates. Quantification was performed by LC-MS;  $\log P_e$  values were calculated with the aid of the PAMPA Explorer Software (plon, version 3.5 and 3.7).

**Log P determination:** The *in silico* prediction tool ALOGPS (VCCLAB, Virtual Computational Chemistry Laboratory, <http://www.vcclab.org>, 2005) was used to estimate the  $\log P$  values of the compounds. Depending on these values, the compounds are classified into three categories: hydrophilic compounds ( $\log P < 0$ ),

moderately lipophilic compounds ( $0 \leq \log P \leq 1$ ) and lipophilic compounds ( $\log P > 1$ ). As listed in Table S1, for the hydrophilic category, two different ratios (volume of 1-octanol : volume of buffer) were defined as experimental parameters for hydrophilic  $\log P < 0$ ; ratios: (1-octanol) : (buffer) 30:140 and 40:130.

Compound Type	log P	Ratio = (1-octanol) : (buffer) [ $\mu\text{L}$ ]
hydrophilic	$< 0$	30:140, 40:130
moderately lipophilic	$0 - 1$	70:110; 110:70
lipophilic	$> 1$	3:180; 4:180

Equal amounts of phosphate buffer (0.1 mM, pH 7.4) and 1-octanol were mixed and shaken vigorously for 5 min to saturate the phases. The mixture was left until separation of the two phases occurred, and the buffer was retrieved. Stock solutions of the test compounds were diluted with buffer to a concentration of 1 or 10  $\mu\text{M}$ . For each compound, six determinations, i.e., three determinations per 1-octanol : buffer ratio, were performed in different wells of a 96-well plate. The respective volumes of buffer containing analyte (1 or 10  $\mu\text{M}$ ) were pipetted to the wells and covered by saturated 1-octanol according to the volume ratio. The plate was sealed with aluminium foil, shaken (1350 rpm, 25 °C, 2h) on a Heidolph Titramax 1000 plate shaker (Heidolph instruments GmbH & Co. KG, Schwabach, Germany) and centrifuged (2000 rpm, 25 °C, 5 min, 5804 R Eppendorf centrifuge, Hamburg Germany). The aqueous phase was transferred to a 96-well plate for analysis by LC-MS.

Log P was calculated from the 1-octanol/buffer ratio (o : b), the initial concentration of the analyte in buffer (1 or 10  $\mu$ M) and the concentration of the analyte in the aqueous phase ( $c_B$ ) with equation:

$$\text{Log}P = \log\left(\frac{1 \mu\text{M} - c_B}{c_B} \times \frac{1}{o : b}\right)$$

**Colorectal adenocarcinoma (Caco-2) cell permeability assay:** Caco-2 cells were cultivated in tissue culture flasks (BD Biosciences, Franklin Lakes, NJ, USA) with DMEM high-glucose medium containing L-glutamine (2 mM), nonessential amino acids (0.1 mM), penicillin (100 U/mL), streptomycin (100  $\mu$ g/mL), and FBS (10%). The cells were kept at 37 °C in humidified air containing 5% CO<sub>2</sub>, and the medium was changed every second day. When ca. 90% confluence was reached, the cells were split in a 1:10 ratio and distributed to new tissue culture flasks. At passage numbers between 60 and 65, they were seeded at a density of 5.3x10<sup>5</sup> cells per well to Transwell 6-well plates (Corning, NY, USA) with 2.5 mL culture medium in the basolateral and 1.5 mL in the apical compartment. The medium was renewed on alternate days (2 mL apical, 2.5 mL basolateral). Permeation experiments were performed between days 19 and 21 post-seeding. Prior to the experiment, the integrity of the Caco-2 monolayers was evaluated by measuring the transepithelial electrical resistance (TEER) with an Endohm tissue resistance instrument (WORLD Precision Instruments Inc., Sarasota, FL, USA). Only wells with TEER values > 250  $\Omega$ cm<sup>2</sup> were used. Experiments were performed in the apical-to-basolateral (absorptive) and basolateral-to-apical (secretory) directions in triplicate at a compound concentration of 62.5  $\mu$ M. Transport medium (DMEM without sodium pyruvate and phenol red) was withdrawn from the donor compartments and the compound solution was added. The Transwell plate was then shaken (600 rpm) in

the incubator. Samples (40  $\mu\text{L}$ ) were withdrawn after 15, 30, and 60 min from the donor and acceptor compartments. The concentrations were determined by LC-MS. Apparent permeability coefficients ( $P_{app}$ ) were calculated according to the equation:

$$P_{app} = \frac{dQ}{dt} \times \frac{l}{A \times c_0}$$

where  $dQ/dt$  is the permeability rate,  $A$  the surface area of the monolayer, and  $c_0$  the initial concentration in the donor compartment. After the experiment, TEER values were assessed again for each well and results from wells with values  $< 250 \Omega\text{cm}^2$  were discarded.

**LC-MS measurements:** A 1100/1200 Series HPLC System coupled to a 6410 Triple Quadrupole mass detector (Agilent Technologies, Inc., Santa Clara, CA, USA) equipped with electrospray ionization was used for analysis. The system was controlled with the Agilent MassHunter Workstation Data Acquisition software (version B.01.04). The column used was an Atlantis T3 C18 column (2.1x50 mm) with a 3  $\mu\text{m}$  particle size (Waters Corp., Milford, MA, USA). The mobile phases (A, water; B, MeCN) contained 0.1% formic acid (v/v) and were delivered at 0.6 ml/min. The gradient was ramped from 95% A/5% B to 5% A/95% B over 1 min, and then held at 95% A/5% B for 0.1 min. The system was then brought back to 95%A/5% B, resulting in a total duration of 4 min. For compounds **5** and **5\*** the gradient was ramped from 60% A/40% B to 5% A/95% B over 1 min, and then held at 5% A/95% B for 0.5 min before the gradient was brought back to 60% A/40% B, resulting in a total duration of 6 min. MS parameters such as fragmentor voltage, collision energy and polarity were optimized individually for each analyte and the molecular ions were followed for each compound in the multiple reaction monitoring mode. The

concentrations of the analytes were quantified by the Agilent MassHunter Quantitative Analysis software (version B.01.04 and B.03.01).





---

## Summary and Outlook

---

The aim of the present Ph.D. thesis was to develop *in vitro* assays which would provide information on glycomimetics (FimH antagonists) and cyclic hexapeptides, in order to better understand the factors that influence their pharmacokinetic properties and as well as prediction of oral bioavailability.

Besides *in vitro* assays to determine solubility and potential passive permeability, assays predictive for  $pK_a$ ,<sup>1</sup> carrier-mediated permeability, stability in gastrointestinal fluids were implemented into the PADMET platform. In order to select specific compound classes and to avoid attrition in a late pre-clinical stage,<sup>2</sup> a decision tree (Figure 4.10, page 84) with illustrated trends for different classes of FimH antagonists and published thresholds was established for the prediction of potential oral bioavailability of FimH antagonists. Based on the nanomolar affinities of FimH antagonists, a minimum solubility of at least 50  $\mu\text{g/mL}$  was required before other assays were performed. Concerning lipophilicity, compounds with a  $\log D_{7.4} > 1$  were more likely to show passive permeation. For issues such as insufficient passive permeability ( $\log P_e < -6.3$  cm/s) and/or insufficient solubility ( $< 520$   $\mu\text{g/ml}$  for an oral dose of 10 mg/kg,  $< 52$   $\mu\text{g/ml}$  for an oral dose of 1 mg/kg) several approaches were applied and are summarized in the next sections.<sup>3,4</sup>

A biphenyl  $\alpha$ -D-mannopyranoside FimH antagonist with a *para*-carboxylate on the terminal aromatic ring of the aglycone with high solubility ( $> 3000$   $\mu\text{g/mL}$ ) but poor permeability ( $\log P_e < -6.3$  cm/s) was the starting point for permeability enhancing strategies.<sup>5</sup>

One of the strategies was to analyze the interaction potential of the FimH antagonists with the active transporters (e.g. OATP, OAT1, and OCT2) to improve drug delivery. Interactions of various classes of FimH antagonists (e.i. biphenyl, indoliny- and indolyphenyl, pyrrolylphenyl and

guanidinylphenyl  $\alpha$ -D-mannoside) could be illustrated with the transporters OATP2B1 and OATP1B3. Small structural differences within a compound class could be observed. Whereas a chloro- or trifluoromethyl-substitution at the aromatic ring adjacent to the anomeric oxygen of biphenyl and indolinyphenyl increased inhibition of the OATP2B1-mediated  $E_1S^+$  uptake, substitution at the outer aromatic ring of biphenyl with cyanide, sulfonamide, sulfone, carboxylic acid, N,N-dimethylaminoethyl ester or the N,N-dimethylaminoethyl amide or *o*-methoxy-substitution of indolinyphenyl mannoside did not show any inhibition (> 80%). Furthermore, compounds with  $\log D_{7.4} > 1$  and with  $\log P_e < -6.3$  cm/s were more prone to show an inhibitory effect on the  $E_1S^+$  uptake. However, only for two FimH antagonists of the biphenyl and guanidinylphenyl classes, which did not show any interactions with OATP2B1 transporter in the inhibition screening, OATP2B1-mediated uptake could be observed. For this reason, multiple binding sites on the OATP2B1 transporter need to be evaluated in more detail. Contrary to the OATP2B1 transporter, the biphenyl containing a triazolyl amine substitution and the indolinyphenyl containing an *o*-methoxy substitution showed an increase in inhibition of the OAT1B3-mediated  $E_2G^+$  uptake.

In a subsequent study, when the polar carboxylate on the terminal ring of the biphenyl aglycone was masked as ester prodrug, membrane permeability could be improved. However, aqueous solubility suffered and dropped to the low  $\mu\text{g/mL}$  range (< 50  $\mu\text{g/mL}$ ).<sup>5</sup>

For this purpose, approaches to improve solubility were studied. Replacement of the carboxylate with bioisosteres improved solubility as compared to the ester prodrugs.<sup>6</sup> However, only *para*-cyano analogues were found to be passively permeable with increased, but still insufficient, solubility (< 520  $\mu\text{g/mL}$ ). Acylation at the C-6 position of mannose on the poorly permeable bioisostere FimH antagonists was applied (prodrug approach) to improve permeability; however, fast degradation in pancreatin-containing intestinal fluids was observed and needs further investigation.

For this reason, phosphate promoieties were introduced to the mannose moiety at the 2-, 3-, 4-, or 6- position of the passively permeable *p*-cyanobiphenyl derivative, leading to an increased solubility of > 3000  $\mu\text{g/mL}$ .<sup>7</sup> This solubility allows the application of higher doses (up to 10 mg/kg), leading to higher intestinal concentrations and to saturation of the efflux transporter. As a result, an increase of  $P_{app}$  permeability in the *in vitro* and *in vivo* models can be expected. Furthermore, hydrolysis of the phosphate promoieties was confirmed in the Caco-2 cell model with alkaline phosphatases, where phosphate esters at positions 2- and 3- of the mannose were rapidly hydrolyzed, and phosphate esters at positions 4- and 6- were more stable with  $t_{1/2}$  exceeding 40 min. In addition, phosphate prodrugs were stable in gastrointestinal fluids.

Furthermore, the replacement of the outer ring of the biphenyl aglycone with a heteroaromatic ring (e.g. triazoles, pyrazoles, or pyridines) was considered an alternative strategy to improve aqueous solubility.<sup>8</sup> However, whereas FimH affinity could be maintained, no improvement of permeability could be detected. With ester prodrugs of the heteroaromatic FimH antagonists moderate to good permeability were achieved, which were similar than for the biphenyl ester prodrugs. Slow enzyme-mediated hydrolysis of esters on the heteroaromatic prodrugs turned out to be a major drawback. Nevertheless, affinities of the pyrrolylphenyl prodrugs were high and therefore hydrolysis is not necessary after reaching systemic circulation. However, insufficient solubility (< 520 µg/mL) for a dose of 10 mg/kg was detected.

Finally, various preformulations using appropriate co-solvents, surfactants, and complexing agents were tested. With the surfactant Tween 80 at 1% (w/w), solubility could be improved significantly (> 520 µg/ml) for the *p*-cyanobiphenyl and the pyrrolylphenyl mannosides. With *in vivo* PK studies high urine concentration over an extended period of time (> 3 h) could be achieved. Even though the solubility issue for some selected FimH antagonists could be addressed by appropriate preformulations, further structural modifications to improve solubility are necessary.

For the cyclic hexapeptides, di-*N*-pentyl alkylation improved passive permeability ( $\log P_e < 6.3$  cm/s). Because enantiomers of polar cyclic hexapeptides showed different permeation, the involvement of carrier-mediated transporters in the Caco-2 cell model can be assumed.<sup>9</sup> Further studies regarding gastrointestinal stability and metabolic stability as well as investigations of the active uptake mechanisms are required.

In conclusion, our PADMET platform with its various structural, physicochemical, and biochemical properties assays is essential for predicting oral bioavailability and for selecting specific compound classes for further *in vivo* studies. Furthermore, several successful strategies to enhance oral absorption were studied. For insufficient solubility, the introduction of a phosphate promoiety at the mannose moiety, replacement of the *para*-carboxylate on the terminal ring of the biphenyl aglycone with bioisosteres (e.g. a cyano substituent), or preformulation (e.g. 1% surfactant Tween 80) allowed the successful improvement of solubility. For insufficient permeability, the introduction of an ester improved passive permeability (prodrug approach) and active transport with the uptake transporter OATP2B1 was illustrated. However, further investigations are required for the active drug transport.

### Outlook PADMET Platform

Further work should focus on active uptake and efflux mechanism in the intestine (e.g. PEPT1 and P-gp transporters), on stability in the gastrointestinal fluids (i.e. pancreatin), and on metabolism in the liver (e.g. phase II metabolism). Toxicity is not fully covered in the PADMET platform. Besides cytotoxicity, other *in vitro* toxicity assays, e.g. cardiotoxicity (i.e. hERG K<sup>+</sup> channel blocking), genetic toxicity, or drug-drug interactions needs to be implemented into the platform.

### References

1. Bezençon, J.; Wittwer, M. B.; Cutting, B.; Smiesko, M.; Wagner, B.; Kansy, M.; Ernst, B. pKa determination by (1)H NMR spectroscopy - an old methodology revisited. *J. Pharm. Biomed. Anal.* **2014**, *93*, 147-55.
2. Kola, I.; Landis, J. Can the pharmaceutical industry reduce attrition rates? *Nat. Rev. Drug Discov.* **2004**, *3*, 711-715.
3. Avdeef, A.; Bendels, S.; Di, L.; Faller, B.; Kansy, M.; Sugano, K.; Yamauchi, Y. PAMPA - Critical factors for better predictions of absorption. *J. Pharma. Sci.* **2007**, *96*, 2893-2909.
4. Lipinski, C. A. Drug-like properties and the causes of poor solubility and poor permeability. *J. Pharmacolo. Toxicolo. Methods* **2000**, *44*, 235-249.
5. Klein, T.; Abgottspon, D.; Wittwer, M.; Rabbani, S.; Herold, J.; Jiang, X.; Kleeb, S.; Luethi, C.; Scharenberg, M.; Bezençon, J.; Gubler, E.; Pang, L.; Smiesko, M.; Cutting, B.; Schwaradt, O.; Ernst, B. FimH Antagonists for the Oral Treatment of Urinary Tract Infections: From Design and Synthesis to *in Vitro* and *in Vivo* Evaluation. *J. Med. Chem.* **2010**, *53*, 8627-8641.
6. Kleeb, S.; Pang, L.; Mayer, K.; Eris, D.; Sigl, A.; Preston, R. C.; Zihlmann, P.; Sharpe, T.; Jakob, R. P.; Abgottspon, D.; Hutter, A. S.; Scharenberg, M.; Jiang, X.; Navarra, G.; Rabbani, S.; Smiesko, M.; Ludin, N.; Bezençon, J.; Schwaradt, O.; Maier, T.; Ernst, B. FimH Antagonists: Bioisosteres To Improve the *in Vitro* and *in Vivo* PK/PD Profile. *J. Med. Chem.* **2015**, *58*, 2221-2239.
7. Kleeb, S.; Jiang, X.; Frei, P.; Sigl, A.; Bezençon, J.; Bamberger, K.; Schwaradt, O.; Ernst, B. FimH Antagonists: Phosphate Prodrugs Improve Oral Bioavailability. *J. Med. Chem.* **2016**, *59*, 3163-3182.
8. Pang, L.; Bezençon, J.; Kleeb, S.; Rabbani, S.; Sigl, A.; Smiesko, M.; Sager, C.P.; Eris, D.; Schwaradt, O.; Ernst, B. FimH Antagonists – Solubility vs. Permeability. *Carbohydrate Chemistry*, **2017**, *42*, 248-273.
9. U. K. Marelli, J. Bezençon, E. Puig, B. Ernst, H. Kessler, Enantiomeric cyclic peptides with different Caco-2 permeability suggest carrier-mediated transport. *Chem. Eur. J.* **2015**, *21*, 8023-8027.

